

NASA Contractor Report 3959

(NASA-CR-3959) DEVELOPMENT OF A GLOBAL
MODEL FOR ATMOSPHERIC BACKSCATTER AT CO₂
WAVELENGTHS Final Report, 7 Dec. 1983 - 6
Apr. 1985 (Institute for Atmospheric Optics
and Remote) 388 p HC A17/MF A01

N86-24089

Unclas

CSCL 04B H1/47 04169

Development of a Global Model for Atmospheric Backscatter at CO₂ Wavelengths

G. S. Kent, P. H. Wang,
U. Farrukh, A. Deepak,
and E. M. Patterson

CONTRACT NAS8-35594
FEBRUARY 1986



NASA

NASA Contractor Report 3959

Development of a Global Model for Atmospheric Backscatter at CO₂ Wavelengths

G. S. Kent, P. H. Wang,
U. Farrukh, and A. Deepak
*Institute for Atmospheric Optics and Remote Sensing
Hampton, Virginia*

E. M. Patterson
*Georgia Technology Research Institute
Atlanta, Georgia*

Prepared for
George C. Marshall Space Flight Center
under Contract NAS8-35594



National Aeronautics
and Space Administration

**Scientific and Technical
Information Branch**

1986

ACKNOWLEDGMENTS

The Institute for Atmospheric Optics and Remote Sensing (IFAORS) is pleased to submit the final report on NASA Contract NAS8-35594. We take pleasure in acknowledging the assistance and interest of Dr. D. E. Fitzjarrald, NASA-MSFC, at all stages of this work, as well as that shown by Dr. M. P. McCormick and Mr. L. E. McMaster, NASA-LRC, in the analysis of the satellite occultation data.

PRECEDING PAGE BLANK NOT FILMED

PRECEDING PAGE BLANK NOT FILMED

PAGE 11 INTENTIONALLY BLANK

11 11 11 11

SUMMARY

This is the final report on NASA-MSFC Contract No. NAS8-35594. The objective of this work was to improve our understanding of the variation of the aerosol backscattering at $10.6\text{ }\mu\text{m}$ within the free troposphere and to develop a model to describe this. The analysis combines theoretical modeling with the results contained within three independent data sets. The data sets used are those obtained by the SAGE I/SAM II satellite experiments, the GAMETAG flight series and by direct backscatter measurements. The theoretical work includes use of a bimodal, two component aerosol model, and the study of the microphysical and associated optical changes occurring within an aerosol plume. A consistent picture is obtained, which describes the variation of the aerosol backscattering function in the free troposphere with altitude, latitude, and season. Most data are available and greatest consistency is found inside the northern hemisphere. The scarcity of data and lesser agreement within the southern hemisphere indicates the need for further experimental and theoretical studies.

PRECEDING PAGE BLANK NOT FILMED

PAGE IV INTENTIONALLY BLANK

TABLE OF CONTENTS

Acknowledgments	iii
Summary	v
List of Figures	ix
List of Tables.	xv
1. INTRODUCTION	1-1
2. ANALYSIS OF THE SAGE I/SAM II DATA SET.	2-1
2.1 SAGE I AND SAM II TROPOSPHERIC OBSERVATIONS.	2-1
2.2 EXTINCTION PROBABILITY DISTRIBUTIONS AND USE OF THE MEDIAN EXTINCTION	2-5
2.3 VARIATION WITH LATITUDE, ALTITUDE, AND SEASON.	2-12
2.4 VARIATION WITH SURFACE TYPE	2-20
2.5 VOLCANIC EFFECTS	2-27
3. ANALYSIS OF THE GAMETAG DATA SET.	3-1
3.1 INTRODUCTION	3-1
3.2 GAMETAG FLIGHT PROFILES.	3-2
3.3 INSTRUMENTATION.	3-5
3.4 DATA ANALYSIS.	3-8
3.5 DAILY FLIGHT DATA.	3-12
3.6 LATITUDINAL PROFILES ALONG AIRCRAFT FLIGHT TRACKS	3-17
3.7 CONCLUSIONS.	3-29
4. MICROPHYSICAL PROCESSES IN AN AEROSOL PLUME	4-1
4.1 BACKGROUND	4-1
4.2 NUMERICAL MODEL.	4-1
4.2.1 Coagulation.	4-3
4.2.2 Theory of Differential Settling - Sedimentation.	4-7
4.2.3 Vertical Diffusion	4-7
4.2.4 Backscattering Coefficient	4-9
4.3 NUMERICAL RESULTS AND DISCUSSION	4-10
4.4 DISCUSSION AND REMARKS	4-23
5. CONVERSION OF SAGE I/SAM II EXTINCTION TO 10.6 μ m BACKSCATTER	5-1
5.1 INTRODUCTION	5-1
5.2 BIMODAL SIZE DISTRIBUTION AND FITTING TO THE GAMETAG DATA	5-3
5.3 BIMODAL OPTICAL MODEL AND COMPARISON OF SAGE I/SAM II AND GAMETAG DATA	5-7
5.4 DERIVATION OF A CONVERSION FACTOR AND ITS APPLICATION.	5-11

TABLE OF CONTENTS (cont'd)

6.	CO ₂ LIDAR MEASUREMENTS OF $\beta_{10.6}$	6-1
6.1	PUBLISHED MEASUREMENTS	6-1
6.2	VARIATION OF $\beta_{10.6}$ WITH ALTITUDE AND SEASON	6-2
6.3	PROBABILITY DISTRIBUTIONS FOR $\beta_{10.6}$	6-7
7.	DATA INTERCOMPARISON	7-1
7.1	VARIATION WITH LATITUDE AND SEASON	7-1
7.2	VARIATION WITH ALTITUDE	7-3
7.3	PROBABILITY DISTRIBUTIONS	7-5
7.4	VOLCANIC EFFECTS	7-6
8.	CONCLUSIONS	8-1
9.	REFERENCES	9-1
APPENDIX A		A1 - A220
APPENDIX B		B1 - B21

LIST OF FIGURES

- Figure 2.1. SAGE 1 μm extinction profiles showing penetration into the troposphere. 2-4
 (a) No high-altitude cloud present
 (b) High-altitude cloud present
- Figure 2.2. Scatter plots showing the distribution of SAGE 1 μm extinction values at different altitudes. Superimposed on the scatter plot are lines showing the 20%, 50%, and 80% cumulative probability levels for the extinction. 2-7 - 2-8
 (a) Northern hemisphere, 20 - 60 N, March - May, 1979
 (b) Southern hemisphere, 20 - 60 S, March - May, 1979
- Figure 2.3. Cumulative probability distributions for SAGE I and SAM II extinction, March - May, 1979 2-9 - 2-11
 (a) SAM II 60 - 90 S
 (b) SAGE I 20 - 90 S
 (c) SAGE I 20 S - 20 N
 (d) SAGE I 20 N - 60 N
 (e) SAM II 60 N - 90 N
- Figure 2.4. Median 1 μm aerosol extinction profiles for SAGE I data shown as a function of latitude band 2-15 - 2-17
 (a) March - May, 1979
 (b) June - August, 1979
 (c) September - November, 1979
 (d) December 1979 - February 1980
- Figure 2.5. Median 1 μm aerosol extinction profiles for SAM II data shown as a function of latitude band 2-18
 (a) March - May, 1979
 (b) September - November, 1979
- Figure 2.6. SAGE I/SAM II median 1 μm aerosol extinction profiles at an altitude of 6 km. 2-19
 (a) Equinoxes
 (b) Solstices

LIST OF FIGURES (cont'd)

Figure 2.7.	Contour plots of free tropospheric aerosol extinction at 1 μm from SAGE I and SAM II.	2-21
	(a) March - May, 1979	
	(b) September - November, 1979	
Figure 2.8.	Division of the global surface area by surface type.	2-24
Figure 2.9.	Median 1 μm aerosol extinction profiles over different types of surfaces. . . .	2-25
	(a) 20 - 60 N	
	(b) 20 - 60 S	
Figure 2.10.	(a) Histograms of percentage departures from the zonal mean for four surface classes, 20 S - 20 N. Values used are three-month median levels, the eleven points within each histogram covering the entire 33-month SAGE I data set.	2-26
	(b) Variation of the time-averaged zonal wind with latitude (Lorenz, 1967) .	2-26
Figure 2.11.	Median 1 μm aerosol extinction profiles for SAGE I data at a time of volcanic activity.	2-29
	(a) March - May, 1980	
	(b) June - August, 1980	
	(c) September - November, 1980	
	(d) December 1980 - February 1981	
Figure 3.1.	Flight tracks for the NCAR Electra aircraft during 1977 (solid line) and 1978 (dashed line)	3-3
Figure 3.2.	A representative size distribution measured during the GAMETAG flights . .	3-9
Figure 3.3.	A plot of total aerosol volume inferred from the optical particle data for the May 3, 1978 flight	3-15
Figure 3.4.	A plot of particulate extinction calculated for $\lambda = 0.63 \mu\text{m}$ for the May 2, 1978 data set	3-16
Figure 3.5.	A plot of the ratio of backscatter to extinction at 0.63 μm for the May 2, 1978 data set	3-18

LIST OF FIGURES (cont'd)

Figure 3.6.	Latitudinal profile along the GAMETAG flight tracks for the $0.63 \mu\text{m}$ extinction determined in the marine boundary layer during the 1977 GAMETAG flights.	3-19
Figure 3.7.	As in Fig. 3.6, except for the 1978 oceanic data	3-20
Figure 3.8.	As in Fig. 3.6, except for the 1978 continental data	3-21
Figure 3.9	Latitudinal profile along the GAMETAG flight tracks in the free troposphere for the $\lambda = 0.63 \mu\text{m}$ extinction data determined during the 1977 flights	3-23
Figure 3.10.	As in Fig. 3.9 except for the 1978 continental data	3-24
Figure 3.11.	As in Fig. 3.9 except for the 1978 oceanic data	3-25
Figure 3.12.	Free tropospheric latitudinal profiles along GAMETAG flight tracks for the $\lambda = 10.6 \mu\text{m}$ extinction data	3-28
Figure 4.1.	Schematic diagram shows the 10-layer model used for numerical study of the aerosol transport. The arrows indicate the interaction of aerosol size distribution between successive layers through the effect of gravitational sedimentation.	4-2
Figure 4.2.	Time evolution of the aerosol size distribution in layer no. 1. The initial distribution is given by the solid line, and ----- is the distribution at $2\Delta t$ ---- " " " " $4\Delta t$ --- " " " " $6\Delta t$ ---- " " " " $8\Delta t$ - - - " " " " $10\Delta t$. . .	4-14
Figure 4.3.	As Fig. 4.2, but for layer no. 2	4-14
Figure 4.4.	As Fig. 4.2, but for layer no. 3	4-15
Figure 4.5.	As Fig. 4.2, but for layer no. 4	4-15
Figure 4.6.	As Fig. 4.2, but for layer no. 5	4-17

LIST OF FIGURES (cont'd)

Figure 4.7.	As Fig. 4.2, except that the size distribution curves are derived from model size distribution parameters obtained by fitting to the curves in Fig. 4.2.	4-17
Figure 4.8.	As Fig. 4.7, but corresponding to Fig. 4.3.	4-20
Figure 4.9.	As Fig. 4.7, but corresponding to Fig. 4.4.	4-20
Figure 4.10.	As Fig. 4.7, but corresponding to Fig. 4.5.	4-21
Figure 4.11.	As Fig. 4.7, but corresponding to Fig. 4.6.	4-21
Figure 4.12.	Time evolution of the 10.6 μm back-scattering function in the model analysis.	4-22
Figure 5.1.	Backscatter to extinction ratios $\beta_{10.6}/\sigma_{1.00}$ shown as a function of log-normal mode radius.	5-2
Figure 5.2.	Example of the application of the bi-modal log-normal fitting program to a simulated experimental size distribution.	5-4
Figure 5.3.	Histograms of the log-normal parameters obtained from the bimodal fitting program (a) σ_{g1} : accumulation mode (b) r_{g1} : accumulation mode (c) σ_{g2} : coarse particle mode (d) r_{g2} : coarse particle mode	5-6
Figure 5.4.	1 μm extinction values calculated from size distributions measured during the GAMETAG flights	5-10
Figure 5.5.	Scatter plot of values of $\beta_{10.6}/\sigma_{1.00}$ as a function of $\sigma_{1.00}$. Data is for an altitude of 5-7 km and taken from the 1977-78 GAMETAG flights. The figure also shows the best fit regression line for $\beta_{10.6}/\sigma_{1.00}$ upon $\sigma_{1.00}$	5-12

LIST OF FIGURES (cont'd)

Figure 5.6.	Contour plots of the free tropospheric backscatter function at 10.6 μm derived from the SAGE I/SAM II data set.	5-15
	(a) March - May, 1979	
	(b) September - November, 1979	
Figure 6.1.	Measured values for $\beta_{10.6}$ in the free troposphere.	6-3 - 6-4
	(a) NOAA seasonal averages	
	(b) JPL seasonal averages, spring-summer, 1983-84	
	(c) NASA-MSFC, 1981 individual profiles	
	(d) NASA-MSFC, 1982 individual profiles	
Figure 6.2.	Cumulative probability distributions for $\beta_{10.6}$ measured at NOAA	6-8
Figure 7.1	Comparison of modeled and directly measured values of $\beta_{10.6}$ for altitudes between 5 and 7 km	7-2
	(a) Northern hemisphere, Spring-Summer	
	(b) Northern hemisphere, Fall-Winter	
Figure 7.2.	Composite diagram showing modeled and directly measured vertical profiles for $\beta_{10.6}$	7-4

LIST OF TABLES

Table 2.1.	Relative Frequency of SAGE Observations in the Troposphere (March-May 1979)	2-3
Table 2.2.	Latitude Bands Used in the Analysis of SAGE I and SAM II Data.	2-14
Table 2.3.	Set of Surface Types Used	2-23
Table 3.1.	Detailed Flight Tracks During the 1977 and 1978 GAMETAG Flight Series.	3-4
Table 3.2.	Optical Constants Used in Calculations.	3-10
Table 4.1.	Terminal Velocity V_t	4-8
Table 4.2.	Initial Aerosol Size Distribution	4-12
Table 4.3.	Results of Curve Fitting at the Tenth Time Step	4-18
Table 5.1.	Refractive Indices Used for Mie Scattering Calculations	5-8
Table 5.2.	Conversion Factors Used with the SAGE I/ SAM II Free Tropospheric Data Sets	5-14
Table 6.1.	Royal Signal and Radar Establishment β_{CO_2} Measurements (D. M. Vaughn, 1983).	6-5
Table 7.1.	Range of Observed Extinction and Backscatter Values (SAGE I and NOAA Data from Figs. 2.3(d) and 6.2).	7-7

~~PRECEDING PAGE BLANK NOT FILMED~~

~~PRECEDING PAGE BLANK NOT FILMED~~

PRECEDING PAGE BLANK NOT FILMED

1. INTRODUCTION

The increased interest, in recent years, in the development and deployment of a Global Wind Measurement Satellite System (WINDSAT) (NOAA 1981), has led to an awareness of our lack of knowledge of the global characteristics of the free tropospheric aerosol. WINDSAT, as presently proposed, would use CO₂ doppler shift lidar to measure wind velocity from the boundary layer to the lower stratosphere. It would rely on backscattering from the atmospheric aerosol for its signal and thus a knowledge of the global behavior of the aerosol backscattering function, β_{CO_2} , is essential for the system design. In a previous study (Deepak et al., 1982), a broad survey was made of the problems associated with modeling the aerosol backscattering function and the principal characteristics of its global variation were determined. These included a decrease in β_{CO_2} from the boundary layer to the upper free troposphere and a strong latitudinal gradient with minimum values occurring over the southern oceans.

The present study focusses on the use of three data sets to develop a global model for β_{CO_2} , including variation with latitude, altitude, and season. Although present experimental work is exploring the use of alternative wavelengths between 9 and 11 μm , the work in this report concentrates on the use of the standard wavelength, $\lambda = 10.6 \mu\text{m}$. The data sets will include

those obtained from the Stratospheric Aerosol and Gas Experiment I (SAGE I) and Stratospheric Aerosol Measurement II (SAM II) satellite systems, the GAMETAG experimental series, and CO₂ lidar measurements. Individually, each data set has important limitations as far as the present objectives are concerned. Viewed collectively, as a data set which must be made self-consistent, they enable a significant advance to be made on previous global models. The SAGE I/SAM II data set is the result of a direct global measurement of aerosol extinction at a wavelength of 1 μm , $\sigma_{1.00}$ (McCormick et al., 1979). The satellites were designed for measurement of the stratospheric aerosol extinction but significant penetration of the troposphere down to an altitude of about 5 km is found, enabling the latitudinal and seasonal characteristics of the upper free tropospheric aerosol to be mapped. This information is for a wavelength of 1 μm and to obtain the equivalent map for the aerosol backscatter function at 10.6 μm , $\beta_{10.6}$, assumptions concerning the aerosol size distribution and composition must be made so that a conversion factor can be calculated. The GAMETAG data set consists of previously unanalyzed data obtained during two latitudinal flight surveys over the Pacific Ocean in 1977 and 1978 (Patterson et al., 1980). Its analysis has been carried out under subcontract by the Georgia Institute of Technology under the direction of Dr. E. Patterson. These surveys measured the aerosol size distribution and composition and the data has been used to calculate the aerosol optical properties at 10.6 μm and

other wavelengths. Its limitations are in terms of the small range in flight altitude (boundary layer or 5-7 km for the majority of the data) and the fact that these flights represent single time and space cross-sections. Uncertainties also exist because of the limited sampling volumes of the instruments used, resulting in significant statistical fluctuations in some of the particle counts. The direct lidar measurements of $\beta_{10.6}$ appear to offer the most accurate input into a global model. Unfortunately, the amount of published data is very small; this situation may be expected to improve as several groups are currently making or planning to make measurements. All of the published data is confined to the northern hemisphere, and, although experiments are planned for the southern hemisphere, data for that hemisphere are not yet available. In addition, all these measurements have been made during or following a period of significant volcanic activity. Since 1979, several volcanoes have injected material into the stratosphere (Kent & McCormick, 1984) and the recent eruption of El Chichon (McCormick et al., 1984) is still profoundly influencing the stratospheric aerosol content. As will be shown later in this report, this volcanic influence extends into the upper troposphere as well as the stratosphere. WINDSAT cannot rely upon volcanic aerosol for its operation and present CO_2 lidar measurements are thus not representative of the conditions under which it may have to operate.

In addition to the use of the above data sets, this report contains the results of further theoretical studies. In the first of these, modeling has been carried out of the microphysical processes and changes in optical properties occurring in long-distance transport of an aerosol plume. The aerosol in the free troposphere over the remote oceans originates mainly from long-distance transport of aerosol injected over the continents. Changes in the aerosol size distribution, particularly for the larger particles which sediment, occur during this transport, resulting in corresponding changes in $\beta_{10.6}$. The other modeling which has been done is of an improved optical model in which a bimodal aerosol size distribution is used in conjunction with a two component aerosol. The main application of this model has been to the calculation of conversion factors to derive $\beta_{10.6}$ from the SAGE I/SAM II extinction at 1 μm .

The organization of this report is as follows: Sections 2 and 3 present, respectively, the results of the analysis of the SAGE I/SAM II and GAMETAG data sets. As the latter contains a large number of plots representing the results of the analysis for individual stages of the 1977/1978 flights, these have been removed from Section 3 and placed in the Appendix to this report. Section 4 contains the results of the microphysical modeling study and Section 5 presents the results of the bimodal size distribution modeling, and its use in the conversion of the

SAGE/SAM II 1 μm extinction to the 10.6 μm backscattering function. Section 6 describes the available CO₂ lidar data set and Section 7 is an intercomparison of the results of the previous sections. Section 8 summarizes the main results, indicating the areas where further development is needed.

2. ANALYSIS OF THE SAGE I/SAM II DATA SET

2.1 SAGE I AND SAM II TROPOSPHERIC OBSERVATIONS

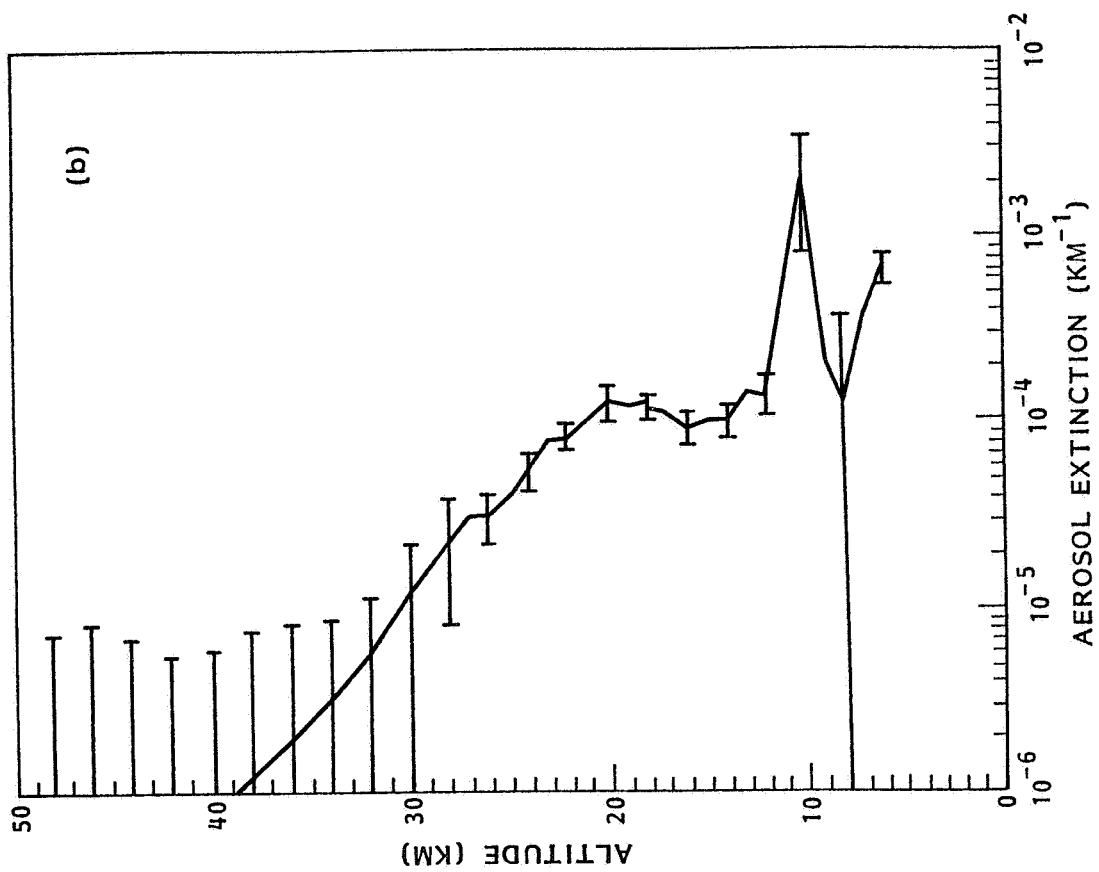
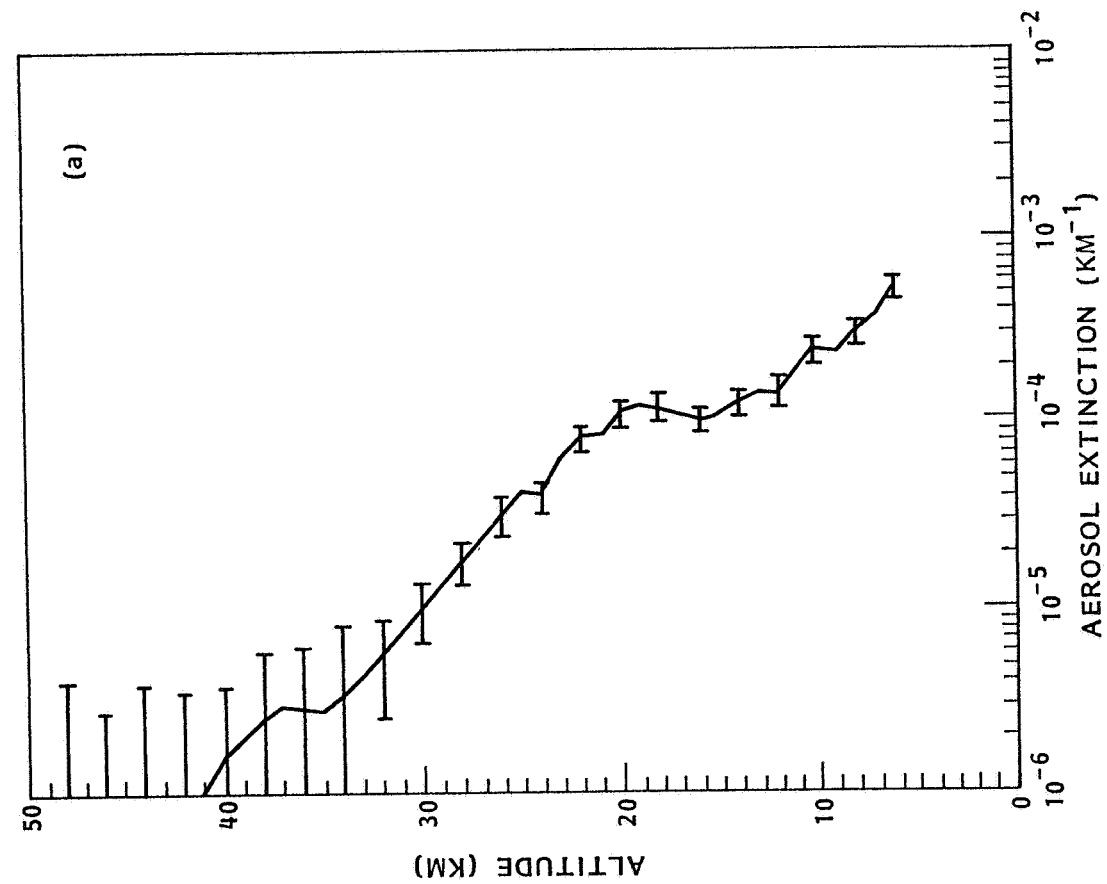
The SAGE I (Stratospheric Aerosol and Gas Experiment I) and SAM II (Stratospheric Aerosol Measurement II) satellite experiments contain sun photometers designed to measure the extinction produced by stratospheric aerosols at a wavelength of $1 \mu\text{m}$ (McCormick et al., 1979). SAM II, which was launched in October 1978, and which is still operational, consists of a single channel sun photometer only. The orbit of SAM II is such that its observations, which are made at satellite sunrise and sunset, occur between latitudes of 64°S and 81°S and 65°N and 83°N , two measurements being made on each orbit. SAGE I commenced its observations in February 1979 and, owing to a faulty satellite power supply, these were terminated in November 1981. In contrast to SAM II, the SAGE I coverage is nearly global, the latitude of observation moving during a six-week period through about 120° of latitude, the latitude extremes being approximately 74°N & 74°S . SAGE I also contains an aerosol channel at a wavelength of $0.45 \mu\text{m}$ in addition to the $1 \mu\text{m}$ channel. Useful data on the former channel is limited to altitudes above 10 km and, in this report, our analysis has been confined to the $1 \mu\text{m}$ data only. The SAGE I data set is also limited by the fact that observations were confined to sunsets only, after the first few months of observation, in order to conserve satellite power.

As noted above, SAGE I and SAM II were designed for the

measurement of stratospheric aerosols and it was anticipated that tropospheric measurements would be hindered or possibly prevented by the presence of high altitude cloud. The former is indeed the case but significant tropospheric penetration does occur. An example of a SAGE I profile showing penetration down to an altitude of 6 km is shown in Fig. 2.1.(a). It may be noted that the aerosol extinction increases smoothly with decreasing altitude, no apparent discontinuity occurring at the tropopause. Fig. 2.1(b) shows a different profile with a strong enhancement at an altitude of 10 km, presumed to be due to high altitude cloud. Table 2.1 shows the total number of observations made by SAGE I over a 3-month period and the frequency of penetration to various tropospheric altitudes for different latitude bands. It can be seen that good penetration ($\geq 50\%$) is obtained down to an altitude of 8 kilometers or less. Greatest frequency of penetration occurs in the southern hemisphere and, as might be expected, least occurs in the equatorial zone with its higher tropopause. This table shows that one might expect to obtain a reasonable description of the free troposphere aerosol, on an average basis, down to an altitude of perhaps 5 or 6 km. Below this altitude, individual profiles, when available, will be accurate but average values, which represent only 20% - 30% of the total potential data set, may be expected to be biased toward more transparent atmospheres and lower extinction.

Table 2.1. Relative Frequency of SAGE Observations in the Troposphere (March - May 1979)

Altitude (km)	Relative Frequency (%)		
	60°S - 20°S	20°S - 20°N	20°N - 60°N
20	100	100	100
18	100	96	100
16	100	78	99
14	98	61	98
12	89	53	89
10	73	48	68
8	58	45	52
6	44	36	34
4	30	17	15
2	6	0	4
TOTAL OBSERVATIONS	827	290	455



(a) No high-altitude cloud present.

(b) High-altitude cloud present.

Figure 2.1. SAGE $1\text{ }\mu\text{m}$ extinction profiles showing penetration into the troposphere.

2.2 EXTINCTION PROBABILITY DISTRIBUTIONS AND USE OF THE MEDIAN EXTINCTION

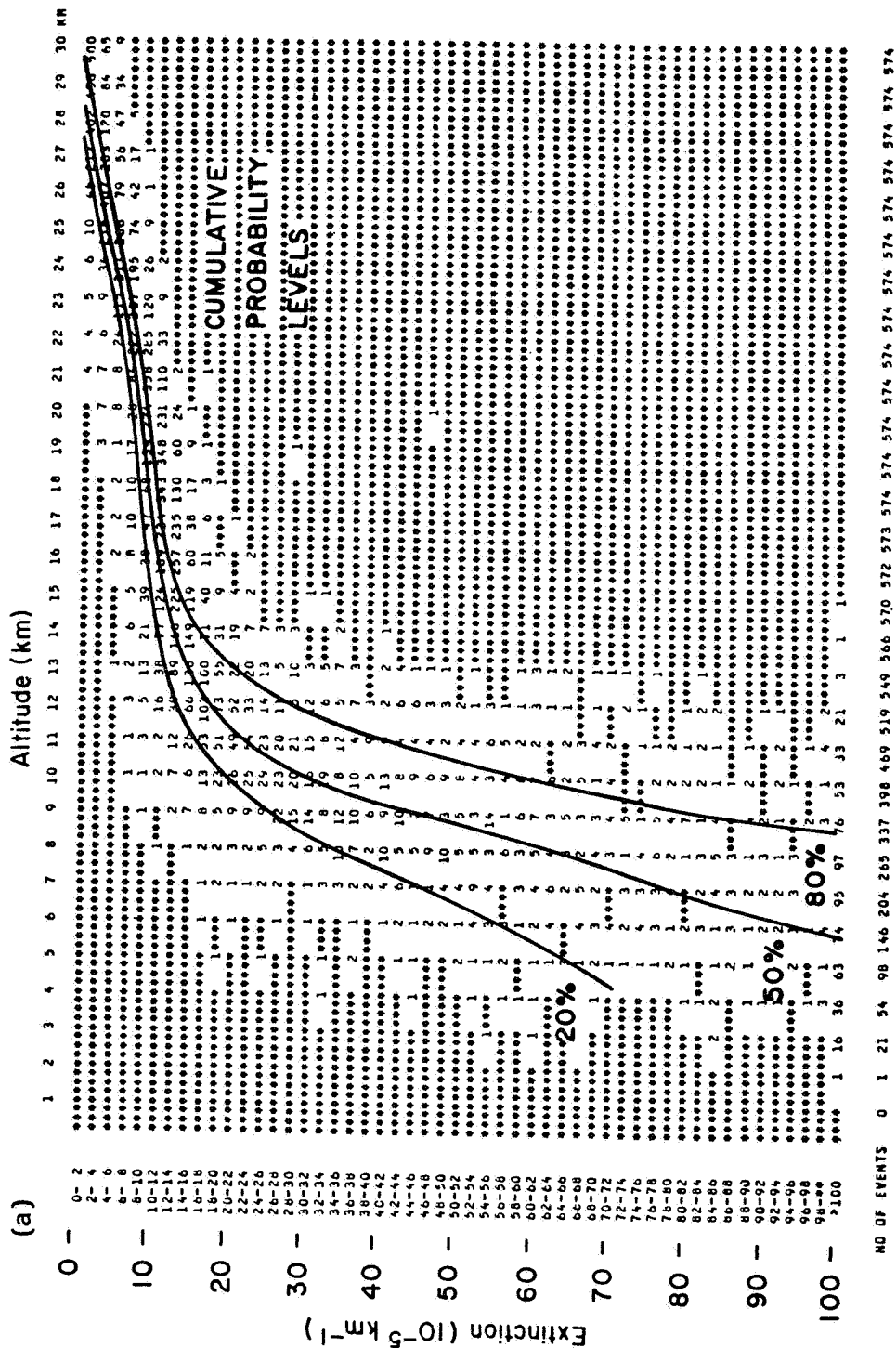
Examination of the SAGE I and SAM II data shows that whereas, in the stratosphere, extinction values at a given altitude and latitude are fairly tightly concentrated about a mean level, the same is not true in the troposphere. In the latter case, extinction values may vary over several orders of magnitude, the higher values probably being due to attenuation by thin (sub-visible) cloud. Under such conditions, the use of the mean extinction as a measure of central tendency is of doubtful value. In order to obtain a better description, we have examined, in some detail, the extinction probability distribution.

Figure 2.2(a) shows the result of binning three months of SAGE I data by altitude and extinction. The data has been taken over the latitude band 20° - 60° N, between March and May 1979, and the numbers on the diagram represent the numbers of observations falling into each $(1 \text{ km}) \times (2 \times 10^{-5} \text{ km}^{-1})$, altitude-extinction bin. In the stratosphere, the extinction values are tightly bunched at a given altitude and there is no problem about defining and using a mean level. In contrast, in the troposphere below about 12 km, the values are widely separated and there is a significant number of very high values ($\text{Extinction} > 10^{-3} \text{ km}^{-1}$) which are shown in the bins at the bottom of the diagram. These values probably represent attenuation by sub-visible cloud (Rao, 1975; Uthe & Russell,

1977). Superimposed on the diagram are lines showing the cumulative probability levels for the extinction. In the stratosphere they are close together, in the troposphere, they are quite widely separated. Rather than averaging the extinction values at a given altitude to form a mean value, we have chosen to use the 50% probability level, or the median, as our measure of central tendency. In the stratosphere, it approximates very well to the mean level. In the troposphere, it defines an aerosol level which is both useful and meaningful. The numerical value of the median is not appreciably affected by the inclusion of very high extinctions due to cloud and its relationship to the extinction probability distribution makes it compatible with published CO₂ lidar backscatter observations, e.g. (Post et al., 1982). A second example of binned aerosol data and the associated probability levels is shown in Fig. 2.2(b). This is for the same time period as Fig. 2.2(a) and for the same latitude band in the southern hemisphere. The marked difference between the two diagrams with less extinction occurring in the southern hemisphere is a systematic feature of the SAGE I and SAM II data.

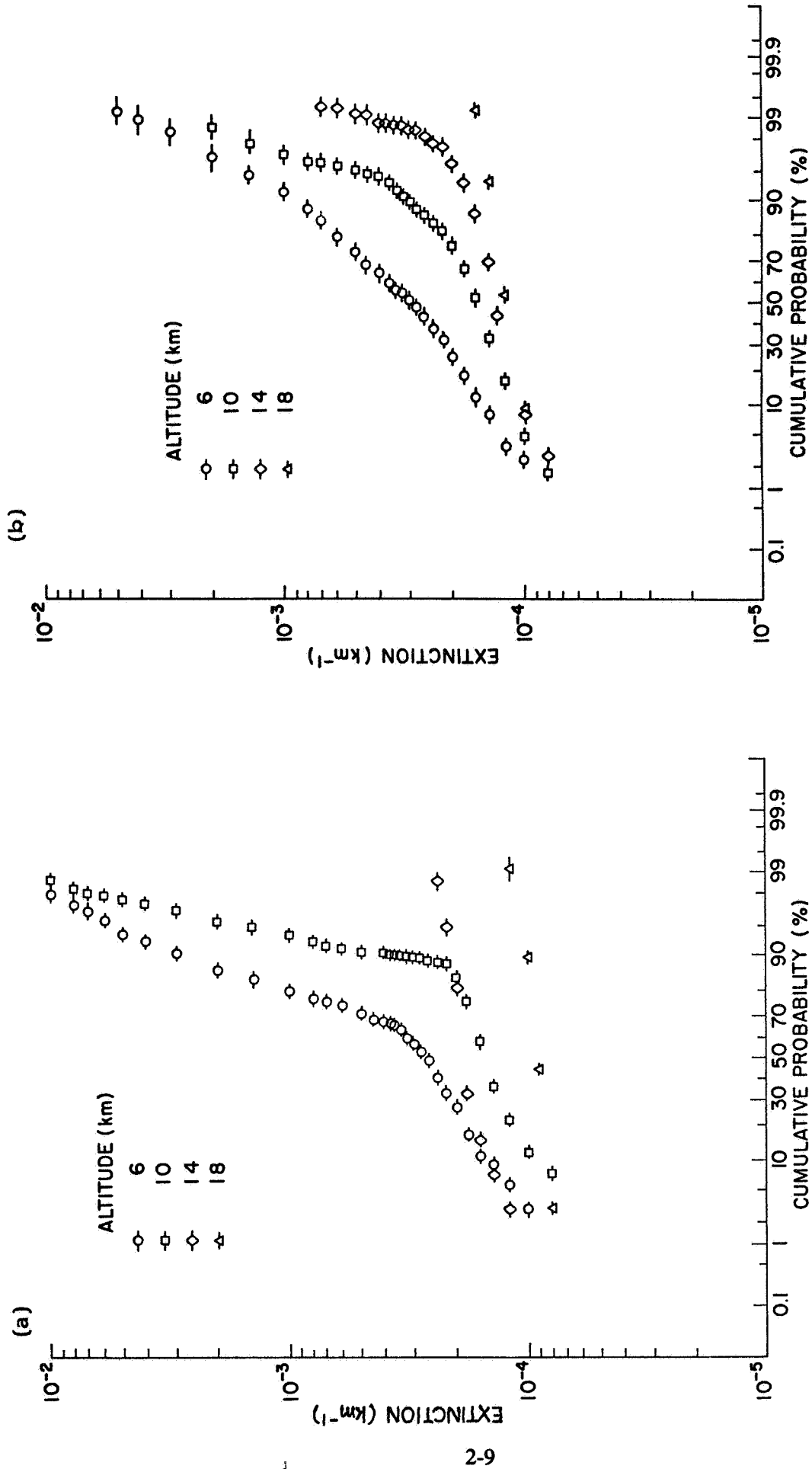
Figure 2.3(a-e) shows cumulative extinction probability distributions for five latitude bins and various altitudes. The data is for the period March-May 1979 and is for both SAGE I and SAM II. The choice of axes and scales on these figures is such that log normal probability distributions appear as straight

ORIGINAL PAGE IS
OF POOR QUALITY



(a) Northern hemisphere, 20 - 60 N, March - May, 1979.

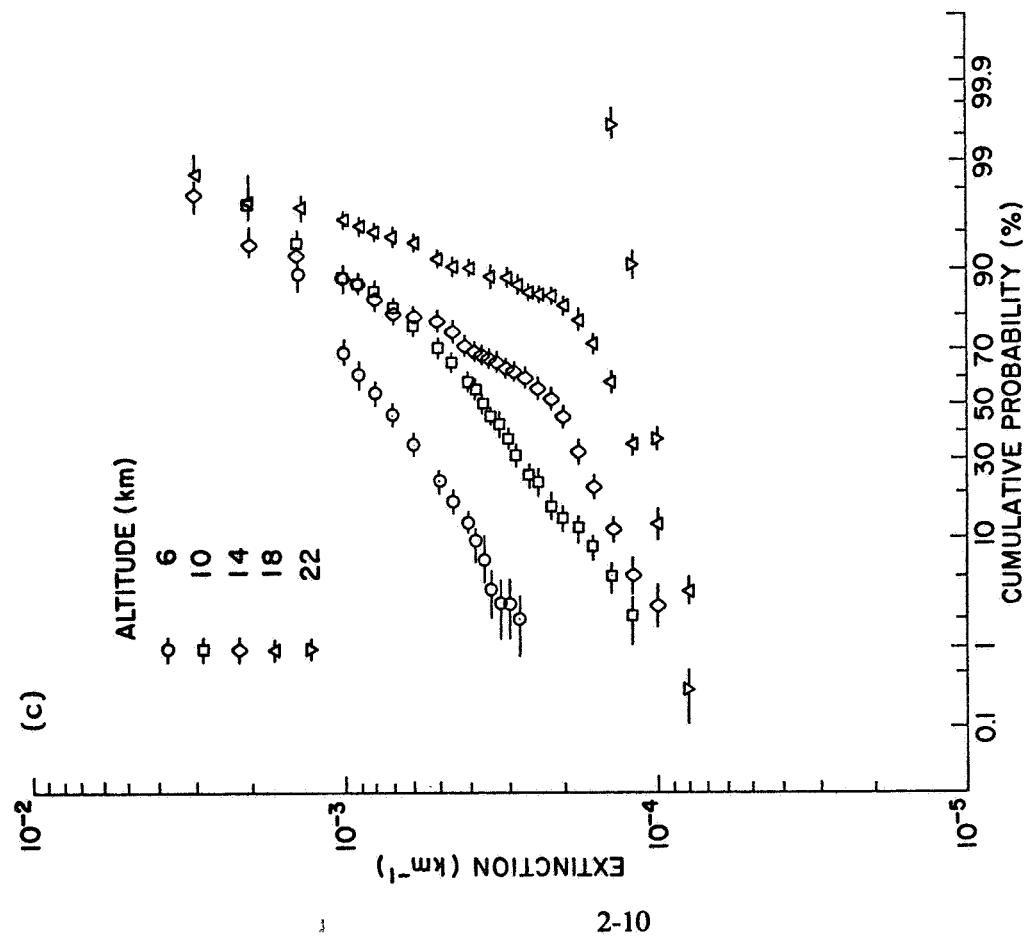
Figure 2.2. Scatter plots showing the distribution of SAGE $1 \mu\text{m}$ extinction values at different altitudes. Superimposed on the scatter plot are lines showing the 20%, 50%, and 80% cumulative probability levels for the extinction.



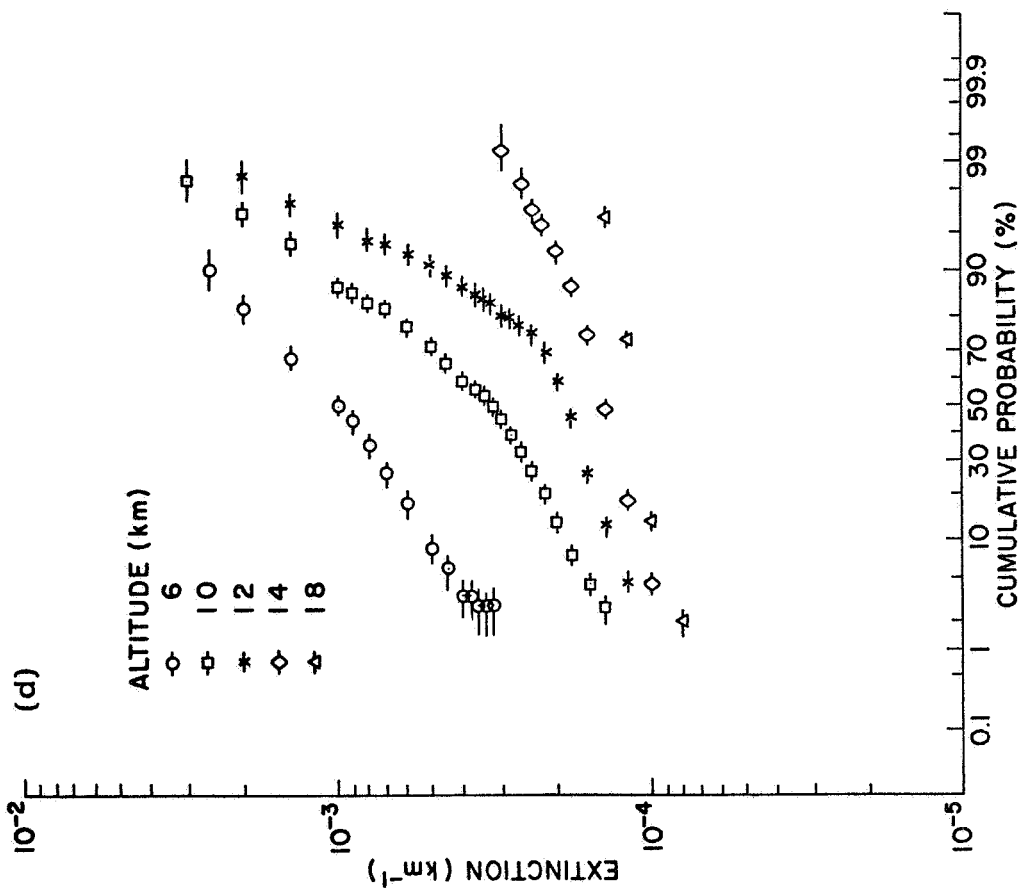
(a) SAM II 60 - 90 S

(b) SAGE I 20 - 90 S

Figure 2.3. Cumulative probability distributions for SAGE I and SAM II extinction, March - May, 1979.

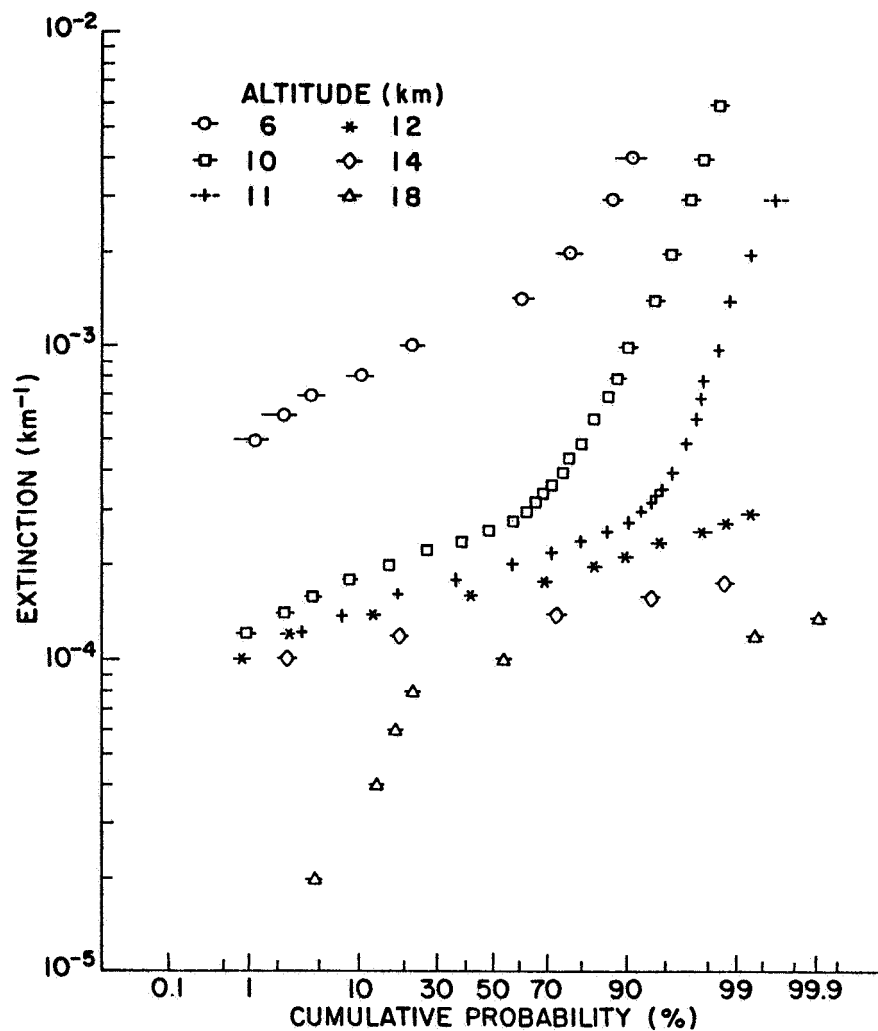


(c) SAGE I 20S - 20 N



(d) SAGE I 20 N - 60 N

Figure 2.3. Cumulative probability distributions for SAGE I and SAM II extinction, March - May, 1979.



(e) SAM II 60 N - 90 N

Figure 2.3. Cumulative probability distributions for SAGE I and SAM II extinction, March - May 1979.

lines. Although no detailed study has been made of these distributions, several interesting points emerge.

(1) In the stratosphere, the probability distribution appears to be log-normal. The only exception to this is the distribution for an altitude of 18 km shown in Fig. 2.3(e). At this time of year, the stratospheric aerosol at this altitude is strongly differentiated depending upon whether it is observed inside or outside the polar vortex (McCormick et al., 1983). The two slope nature of the probability distribution reflects this division in the data, which includes measurements made both inside and outside the vortex.

(2) Near the tropopause [e.g., at altitudes 14 and 18 km in Fig. 2.3(c)], the distribution shows a strong discontinuity in slope. The lower section of the distribution is believed to be due to aerosol, the higher and steeper section to the presence of sub-visible cloud.

(3) The steeper slope and vague linearity of the probability distributions at lower altitude in the troposphere indicates the wide range of aerosol conditions included in the data set.

2.3 VARIATION WITH LATITUDE, ALTITUDE, AND SEASON

In order to study the variation of the aerosol extinction with latitude and season, the SAGE I data was grouped into seven latitude bands and the SAM II data in four latitude bands, as

shown in Table 2.2. Figure 2.4(a) shows the altitude variation of the median SAGE I extinction for the six latitude bands covered during the period March-May 1979. Apart from data in the 60 N - 75 N latitude band, there is a general decrease in aerosol extinction with increasing altitude. In examining these and other data presented in this section, it should be remembered that below an altitude of 5 or 6 km, the fractional penetration is less than 50% and the data may have a systematic bias. This is particularly so when the extinction is high, as in the 60 N - 75 N latitude band, and it is doubtful if in this case the decrease in median extinction for altitudes below 5 km is representative. It is more likely that observations are being made down to these altitudes only when the atmosphere is relatively clean of both aerosol and cloud. A secondary feature of the variation with altitude is the greater extinction observed in the upper free troposphere within the equatorial belt (20 S - 20 N) as compared to the other latitude bands. This reflects the higher tropopause level (~16 km against ~12 km for mid-latitude) and must indicate the effects of convection in raising the aerosol to the higher levels.

Apart from the variation with altitude, the most important feature is the marked latitude asymmetry. At an altitude of 6 km, the variation in extinction between 60 N - 75 N and 40 - 60 S is approximately one order of magnitude. Although this asymmetry is present at all times of the year, it is at a maximum in

**TABLE 2.2. Latitude Bands Used in the Analysis of
SAGE I and SAM II Data**

(a) SAGE I

60 N - 75 N
40 N - 60 N
20 N - 40 N
20 S - 20 N
40 S - 20 S
60 S - 40 S
75 S - 60 S

(b) SAM II

75 N - 90 N
60 N - 75 N
75 S - 60 S
90 S - 75 S

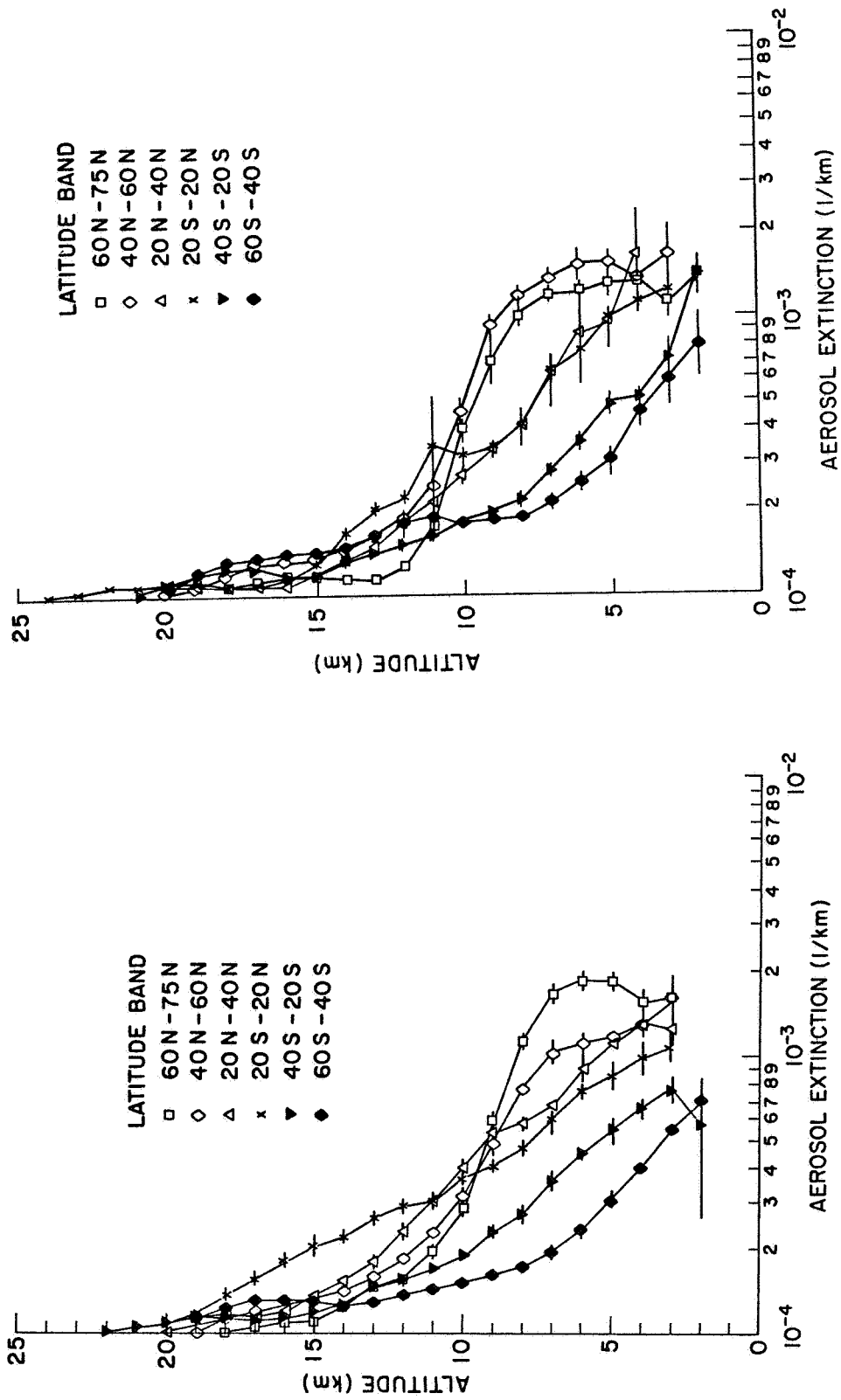
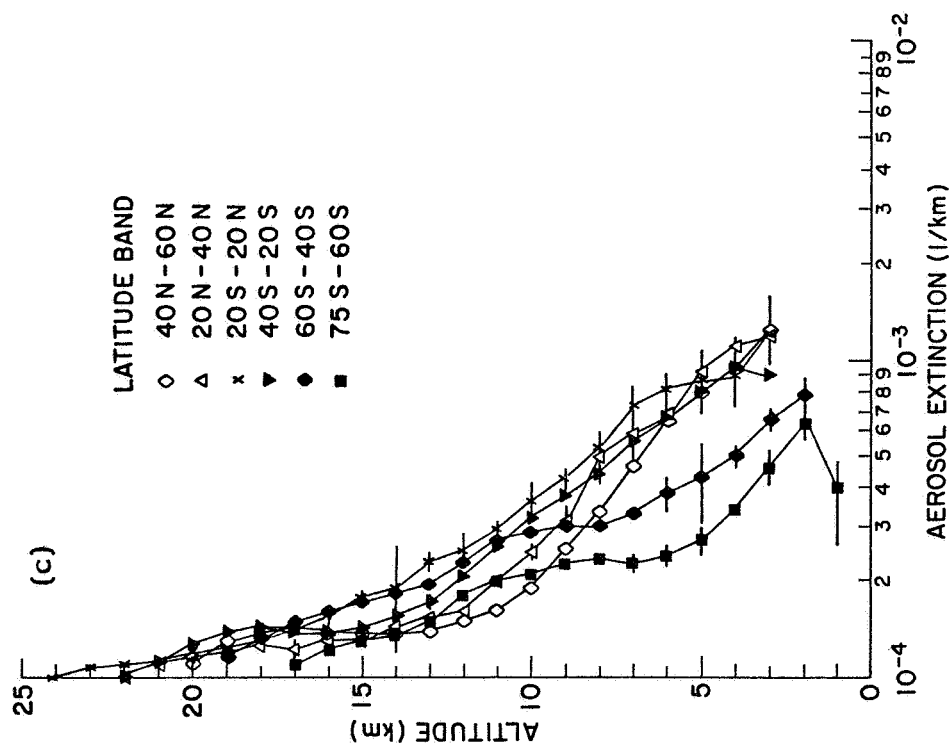


Figure 2.4. Median 1 μ m aerosol extinction profiles for SAGE I data shown as a function of latitude band.

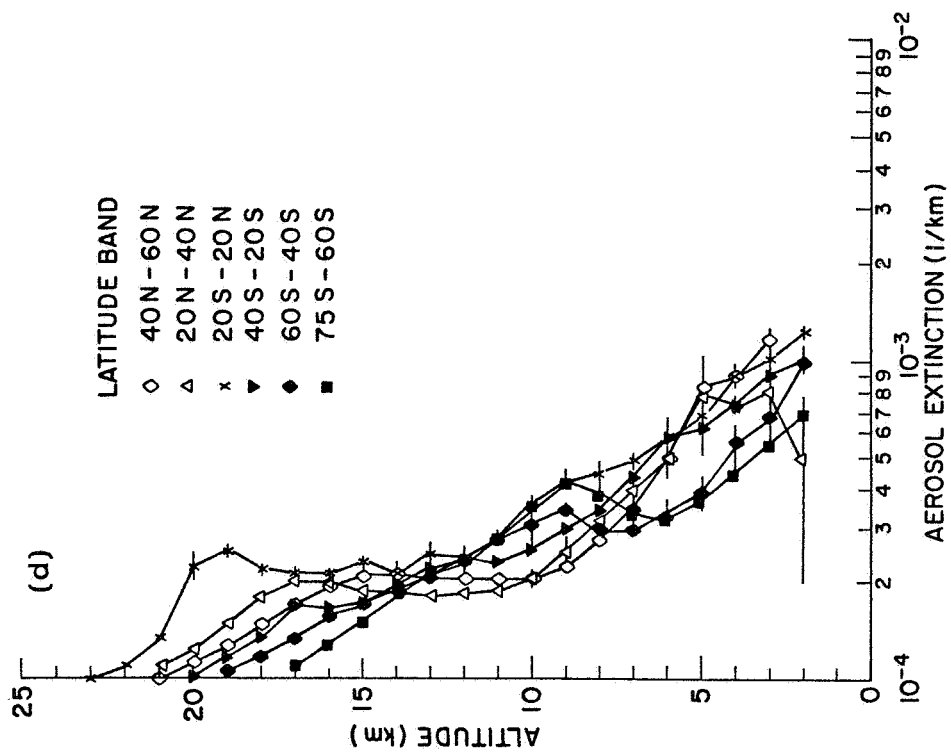
March-May, both in 1979 and in the following years. It seems possible that the occurrence of particularly strong extinction in high northern latitudes at this time of year may be connected with the observation of arctic haze (Schnell, 1984) at somewhat lower altitudes.

Figures 2.4(b)-(d) show the equivalent aerosol extinction plots for June-August 1979, September-November 1979, and December 1979-February 1980. The features noted above are present in all these plots, the latitude asymmetry is, however, less in Figs. 2.4(c) and (d). The peak in aerosol extinction visible in the 20 S - 20 N latitude band in Fig. 2.4(d) at an altitude of 19 km is caused by the injection of material from the eruption of the Sierra Negra volcano on November 13, 1979 (Kent & McCormick, 1984). Figures 2.5(a) and (b) show the high latitude aerosol extinction as measured by SAM II during March-May 1979 and September-November 1979. The tropopause altitude is lower (~10 km) and colder temperatures in the antarctic stratosphere have produced an enhancement in the median aerosol extinction. In the troposphere, the hemispheric asymmetry observed at lower latitudes is still very evident.

Figures 2.4 and 2.5 may be used to study the seasonal changes which occur in the aerosol extinction. An alternative way of displaying this which shows the seasonal variation very clearly is given in Fig. 2.6(a) and (b). In these figures, the SAGE 1/SAM II extinction at an altitude of 6 km has been plotted



(c) September - November, 1979.



(d) December 1979 - February 1980.

Figure 2.4. Median $1\ \mu\text{m}$ aerosol extinction profiles for SAGE I data shown as a function of latitude band.

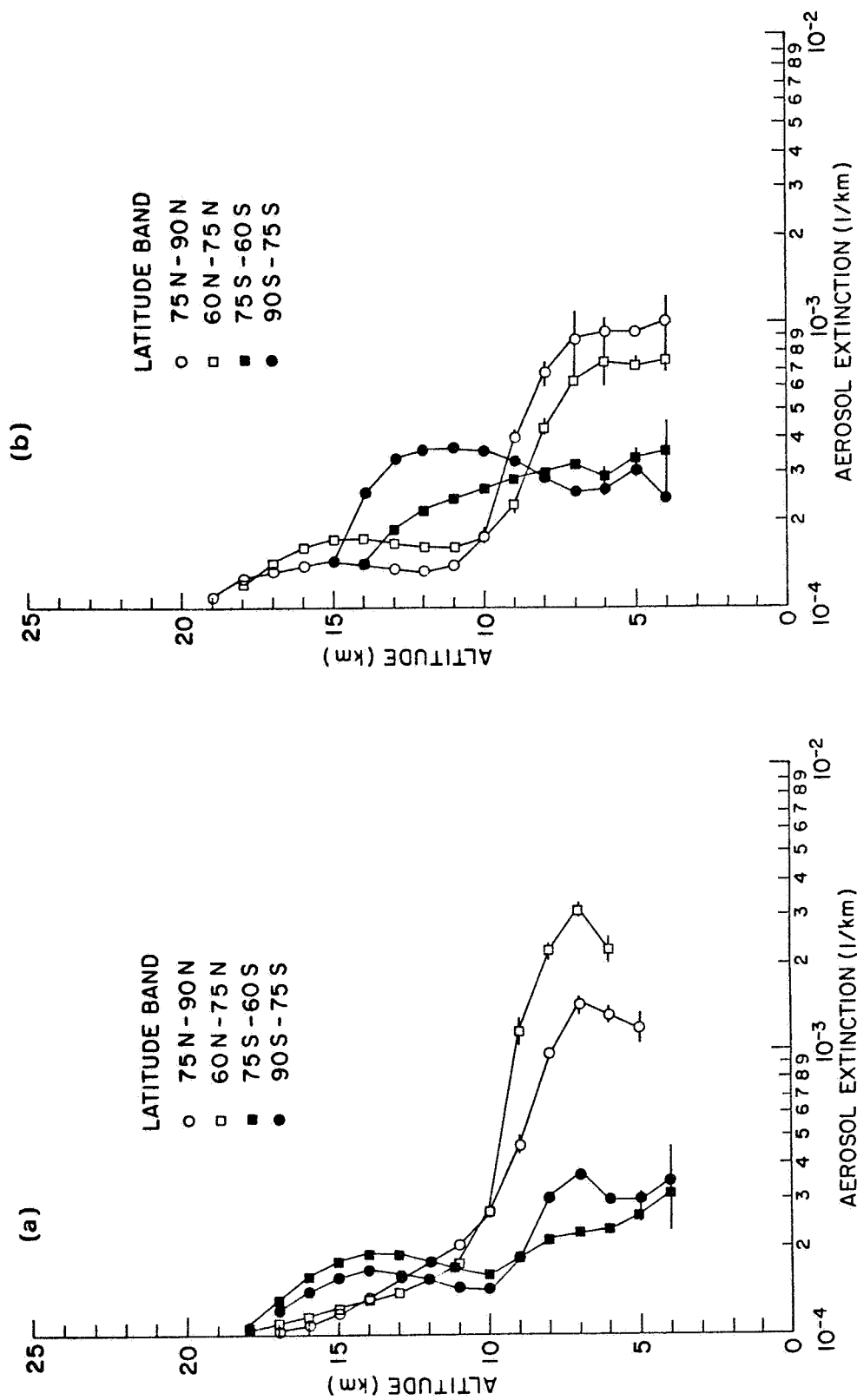


Figure 2.5. Median 1 μ m aerosol extinction profiles for SAM II data shown as a function of latitude band.

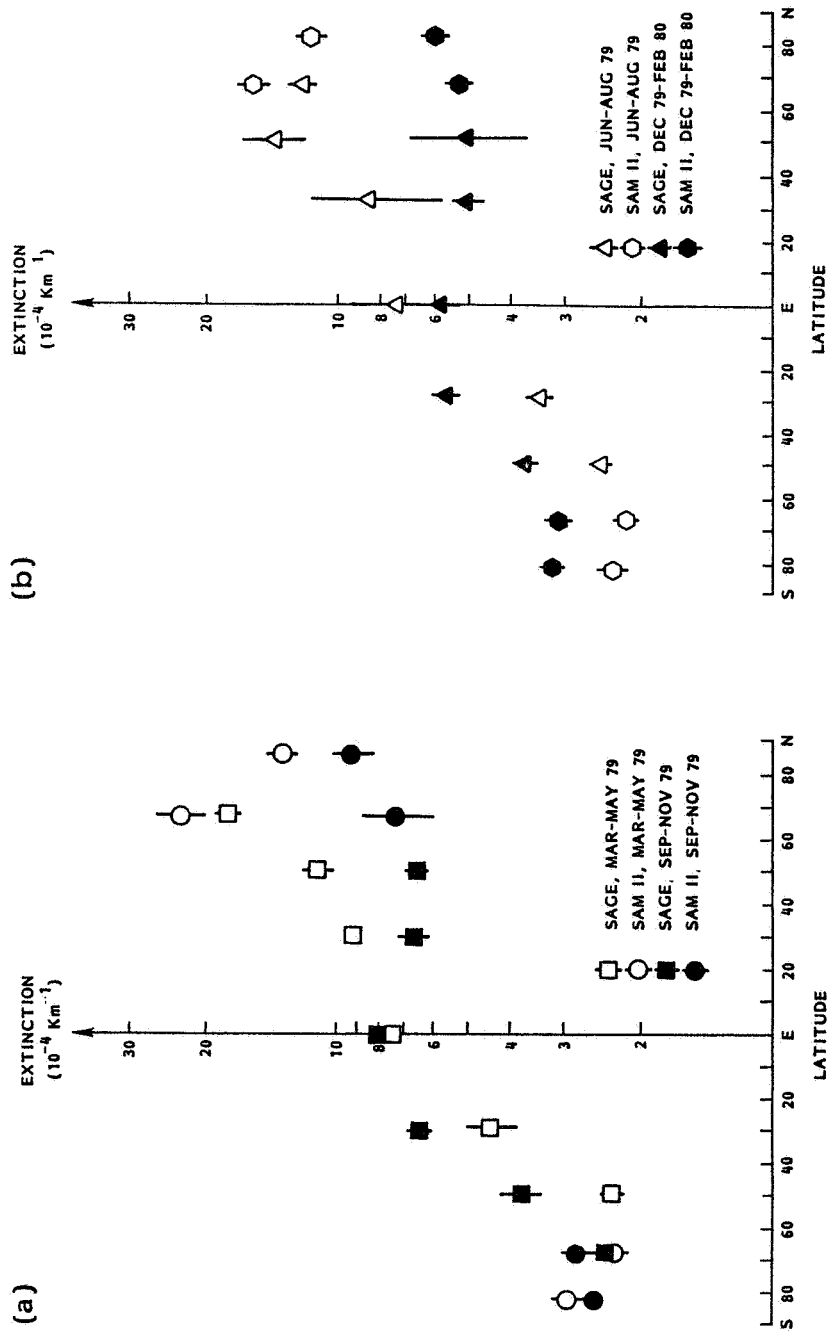


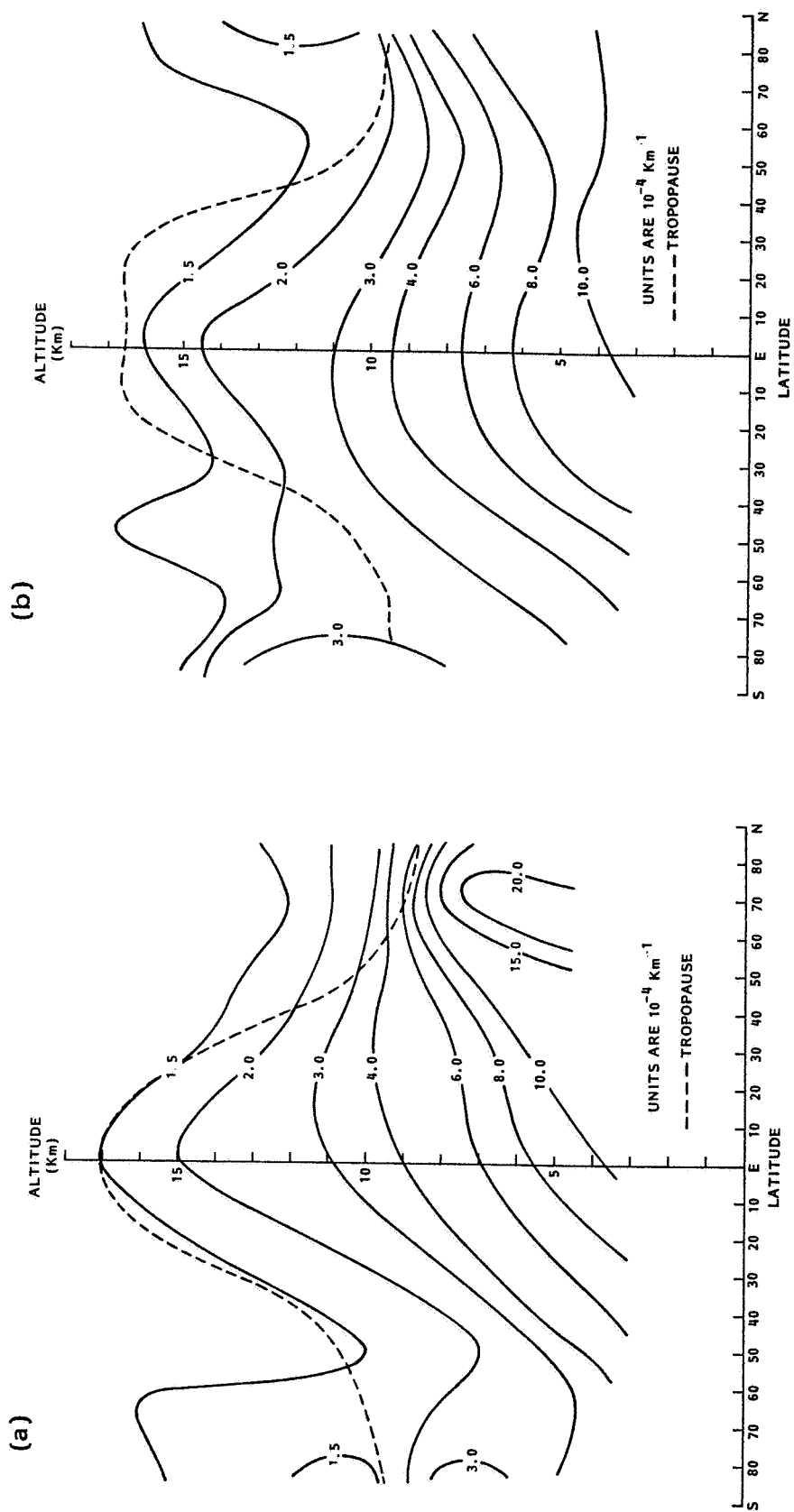
Figure 2.6. SAGE I/SAM II median 1 μm aerosol extinction profiles at an altitude of 6 km.

against latitude for the same four seasons as shown in Fig. 2.4 and 2.5. Both figures show the hemispheric asymmetry; in addition, they show a clear superimposed seasonal variation. In both hemispheres, maximum aerosol extinction is found in local Spring-Summer and minimum extinction in local Fall-Winter. As most aerosol at this altitude is derived from continental sources, the higher values in the northern hemisphere most likely reflect the greater land surface as compared to the southern hemisphere. The Spring-Summer maximum is most probably related to the increased convection over land at that time of year.

Another way of displaying the data in Figs 2.4 and 2.5 is shown in Fig. 2.7(a) and (b). In these figures, the aerosol extinction is plotted in the form of a contour diagram as a function of latitude and altitude. These figures will later be converted to equivalent plots for the backscatter function at $10.6\text{ }\mu\text{m}$.

2.4 VARIATION WITH SURFACE TYPE

Most of the aerosol in the free troposphere over the remote oceans is derived, not by convection from the ocean surface, but by long-range transport of aerosol from over the continental land masses. Some modification of the aerosol optical properties might be expected to occur during this transport and in Section 4 a microphysical model is presented which investigates this variation theoretically. In the present section, we report the



results of an examination of the SAGE I data set for experimental evidence of such a variation. For the purposes of this study, the global surface has been divided into 10-degree latitude-longitude squares and each square categorized according to one of the five classes shown in Table 2.3. Two classes of remote ocean have been defined as it was felt that the antarctic continent was unlikely to be a major source of aerosols. A global map showing the classification of each 10-degree latitude-longitude square on the surface of the globe is given in Fig. 2.8.

Each SAGE I observation has been classified according to the surface type beneath the observation position, as well as for season and latitude. Median extinction values have been calculated for each altitude. The analysis shows very little variation of aerosol extinction with sub-surface type, typical results of this analysis being shown in Fig. 2.9(a) and (b). In these figures, it can be seen that any systematic difference between the extinction over land or ocean is less than the error in the median values as shown by the error bars in the figures. The only positive result to be obtained from the analysis is for the equatorial region ($20^{\circ}\text{S} - 20^{\circ}\text{N}$). Figure 2.10(a) shows histograms of percentage departures from the zonal mean extinction at an altitude of 6 km for the four surface classes found in the equatorial region. Individual data points in the histograms are for the medians of 3-month data sets and the

TABLE 2.3. Set of Surface Types Used

Type	Symbol Used	Definition
Land	L	More than 50% of the area within the 10 degrees square to be land.
Coastal	C	Mixed land and ocean, with more than 50% ocean within the square.
Ocean	O	Includes no land (other than small islands) and lying not more than 3000 km from the nearest land.
Remote 1	R1	Ocean lying more than 3000 km from the nearest land excepting the antarctic continent.
Remote 2	R2	Ocean lying more than 3000 km from the nearest land.

ORIGINAL PAGE IS
OF POOR QUALITY

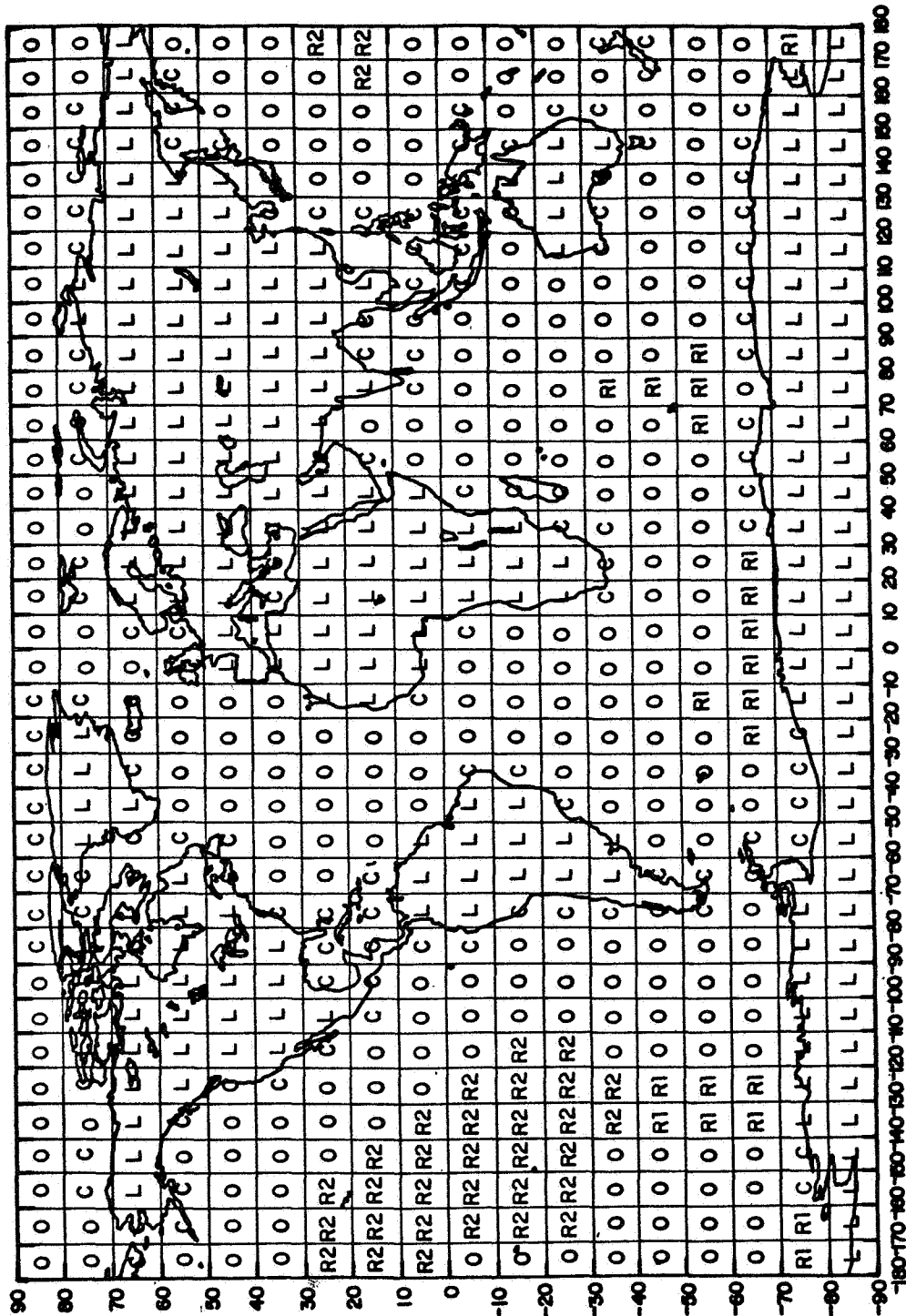
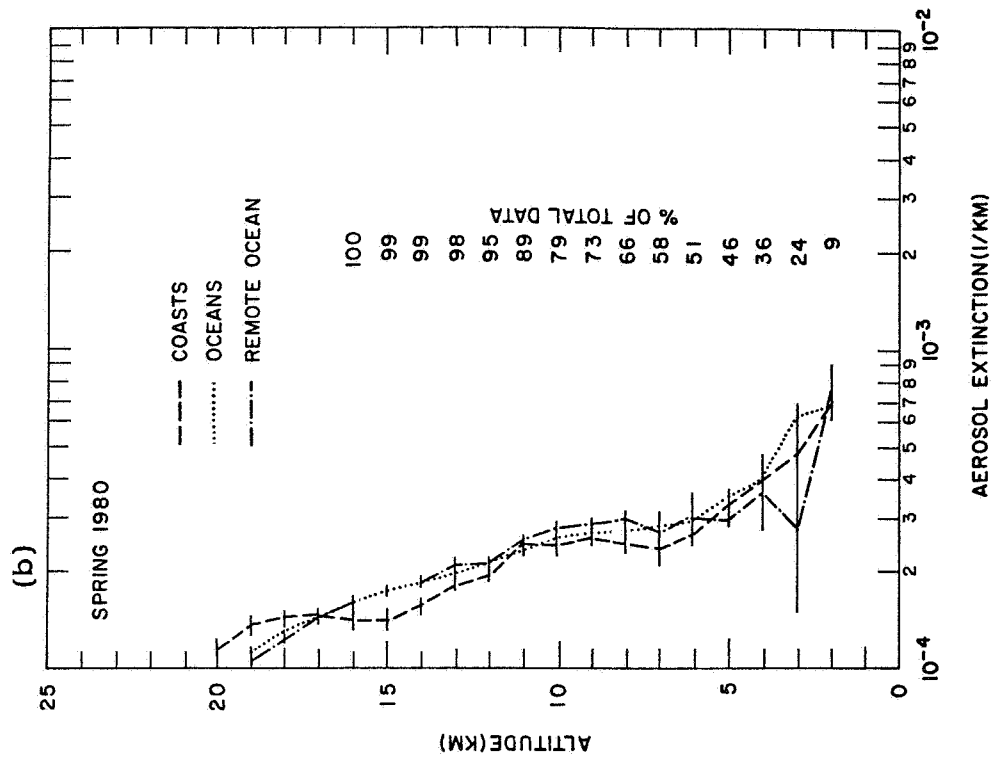


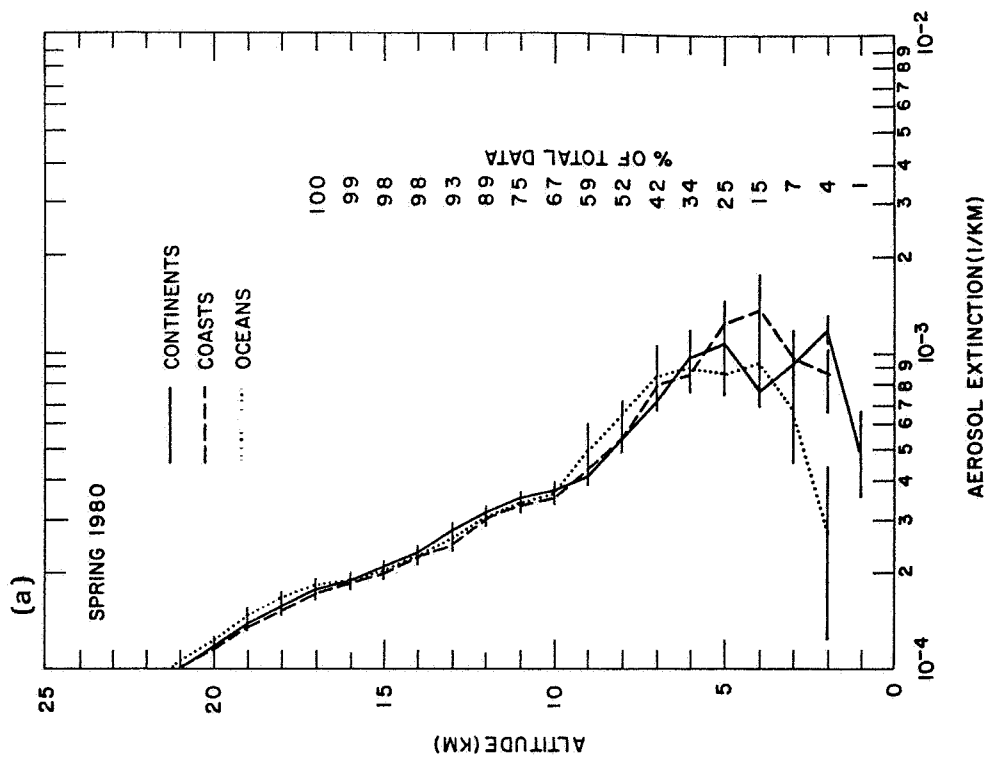
Figure 2.8. Division of the global surface area by surface type:

- L - Land
- C - Coastal
- O - Ocean
- R1 - Remote Ocean I
- R2 - Remote Ocean II

ORIGINAL PAGE IS
OF POOR QUALITY



(b) 20 - 60 S.



(a) 20 - 60 N.

Figure 2.9. Median 1 μ m aerosol extinction profiles over different types of surface.

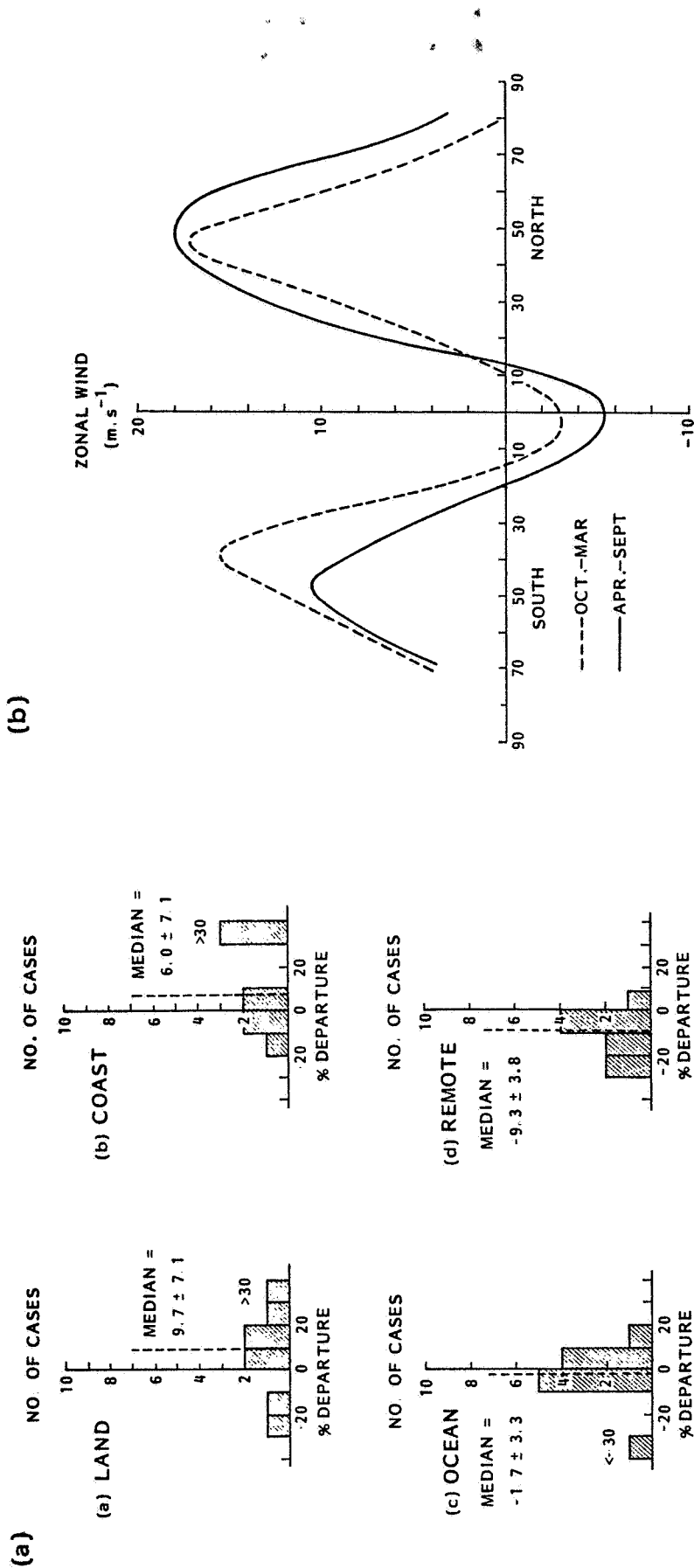


Figure 2.10 (a). Histograms of percentage departures from the zonal mean for four surface classes, 20 S - 20 N. Values used are three-month median levels, the eleven points within each histogram covering the entire 33-month SAGE I data set.

Figure 2.10 (b). Variation of the time-averaged zonal wind with latitude (Lorenz, 1967).

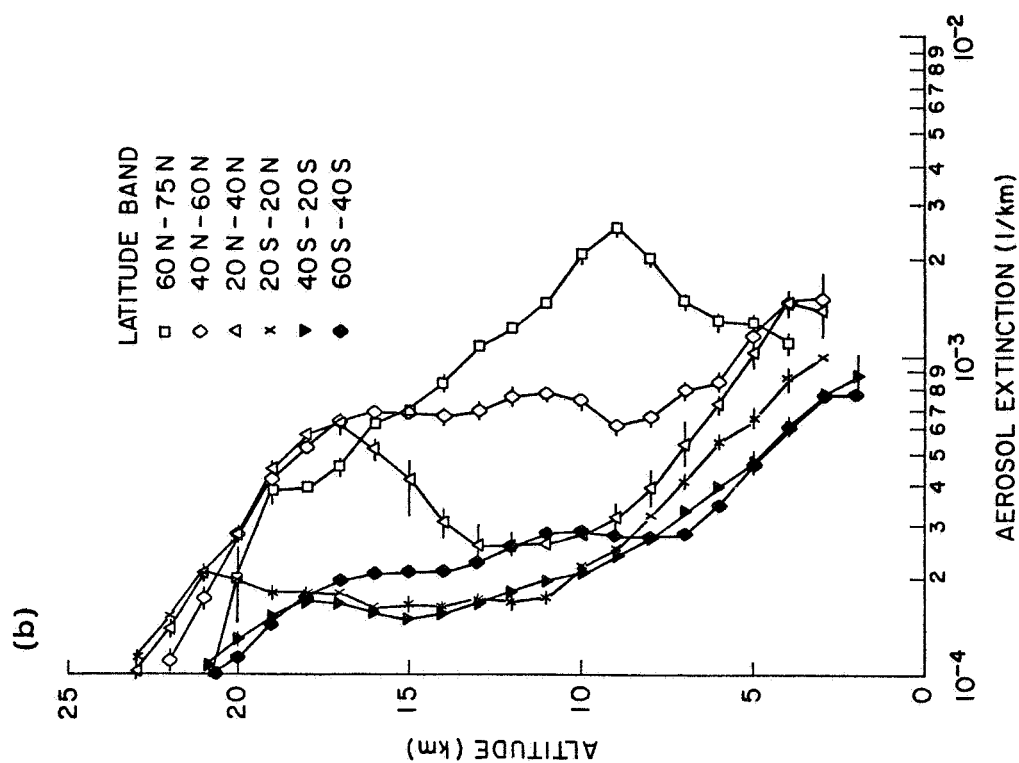
eleven points within each histogram represent the entire 33-month SAGE I operational period. The median values of all the data within each histogram shows a small but steady shift from +9.7% for land to -9.3% for remote ocean. This very small change is in the expected direction and is indeed comparable to the statistical errors. At other latitudes, no such systematic variation is observed and it is likely that this difference is related to the magnitude of the zonal wind velocity. Figure 2.10(b) shows the time averaged zonal wind at the 500 mb level as a function of latitude (Lorenz, 1967). The lowest velocities are observed within the equatorial belt giving greater transport times for movement of aerosol from over land to over ocean. Correspondingly, greater changes in microphysical properties and related optical extinction are thus likely to occur.

2.5 VOLCANIC EFFECTS

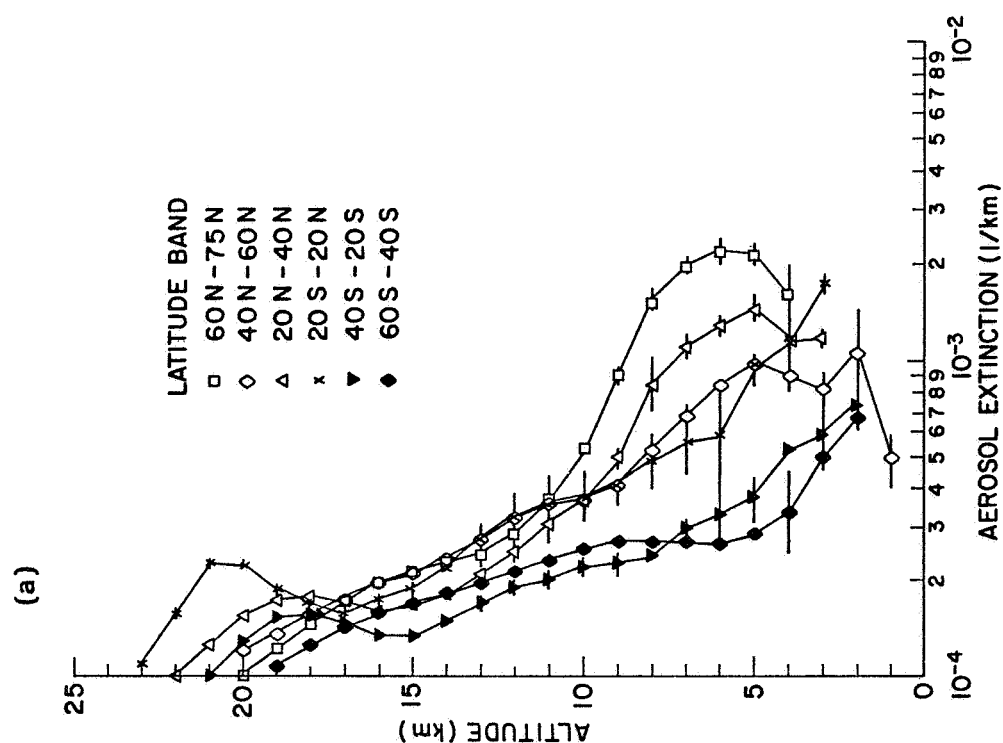
It is well known that volcanic eruptions inject solid and gaseous materials into the stratosphere and that aerosols formed and deposited there have lifetime of months or years (Deirmendjian, 1973; Deepak, 1982; Kent and McCormick, 1984). Solid particles are also injected in the troposphere where the majority of them are presumed to be fairly quickly removed by sedimentation and washout. Examination of the SAGE I and SAM II data set show that the upper troposphere, as well as the stratosphere, has a long-lived enhancement in aerosol extinction. Examples of this enhancement are presented in Figs.

2.11 (a) thru (d), which shows vertical median extinction profiles for the four seasons between March 1980 and February 1981. In 1979 the only volcanic eruption of significance was that of Sierra Negra on November 13, 1979, for which the major stratospheric effects were not felt until early in 1980. The stratosphere (and upper troposphere) in 1980 was affected not only by the after-effects of the Sierra Negra eruption but also by the eruptions of St. Helens (46 N, May 18, 1980) and Uluwun (5 S, October 7, 1980). The 1980-81 seasonal extinction profiles (Fig. 2.11) may be compared with their equivalents for 1979 (Fig. 2.4). Those for March thru May are similar, except for the stratospheric enhancement produced by Sierra Negra and visible in the 20 S - 20 N latitude belt in March thru May, 1980. Those for June thru August are very different. In 1980, the free troposphere between 40 N - 60 N and 60 N - 75 N is profoundly modified following the eruption of St. Helens. In the case of the 60 N - 75 N band, the 1980 increase is visible down to an altitude of about 5 km, well beneath the tropopause altitude. Similar differences are observed within the same latitude bands for September-November and in the 40 - 60 N latitude band for December-February (no data is available for the 60 N - 75 N latitude band during northern winter); in all cases the enhancement appears to occur in the free troposphere down to an altitude of about 5 km. The stratospheric enhancement during this period and within these latitude bands is produced by the injection of material from the St. Helens eruption which was the

ORIGINAL PAGE IS
OF POOR QUALITY

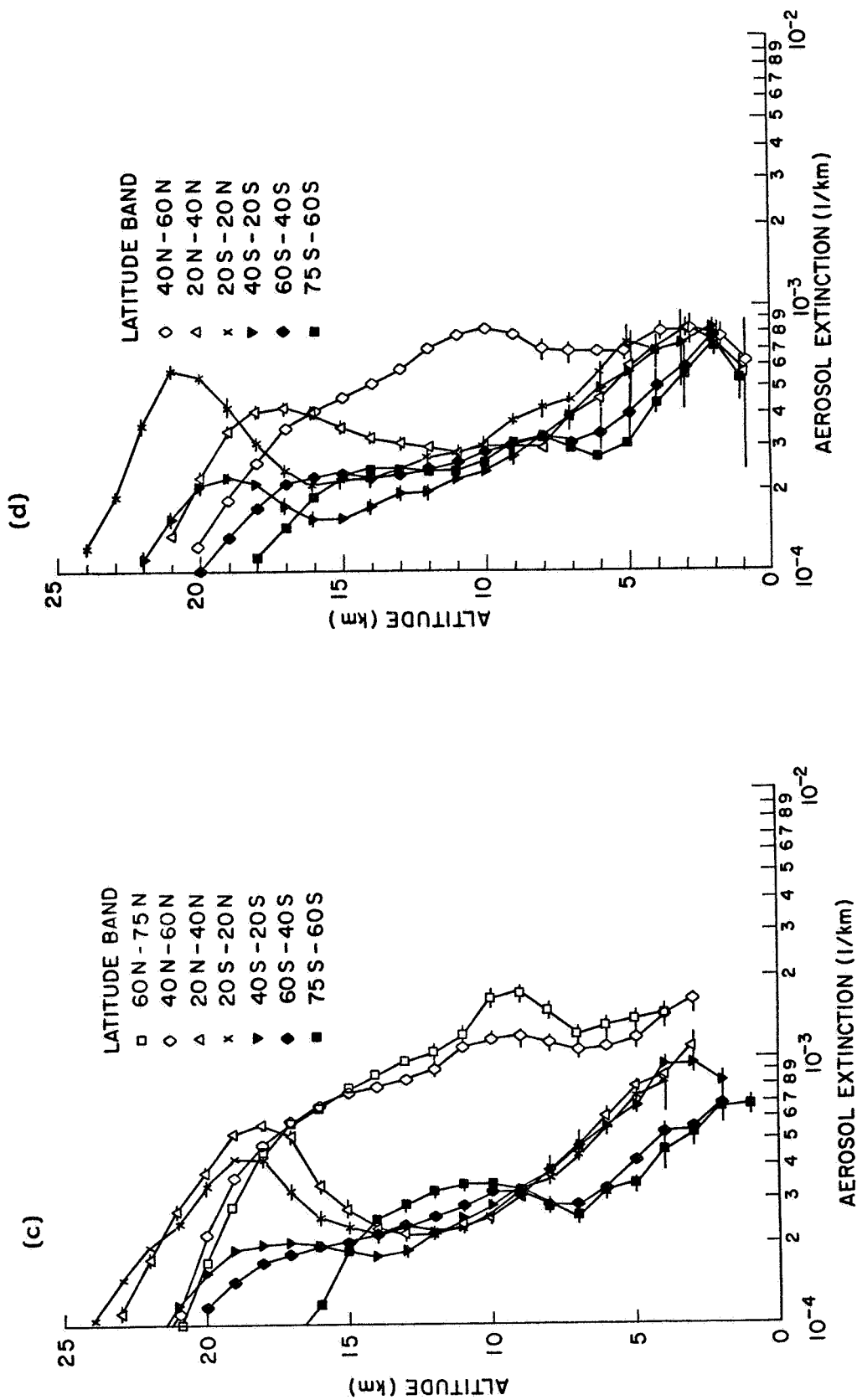


(b) June - August, 1980.



(a) March - May, 1980.

Figure 2.11. Median $1 \mu\text{m}$ aerosol extinction profiles for SAGE I data at a time of volcanic activity.



largest of the four eruptions discussed above. There seems little doubt, therefore, that the free tropospheric enhancement is related to the same source. It is noticeable that the enhancement reaches to maximum amplitude close to the tropopause (~10 km at 60° N, see Fig. 2.7) and it is possible that the aerosol in the stratosphere is acting as a reservoir from which material is being fed into the upper troposphere by sedimentation and stratospheric-tropospheric exchange processes. The data shows many interesting and puzzling features which will be the object of future study. For example, the data shows that the maximum transfer of aerosol from the stratosphere to the troposphere occurs at high latitudes, whereas no such transfer is evident at low latitudes, although volcanic material is clearly present in the stratosphere (Fig. 2.11(a), (b), and (d)). These differences may help resolve the relative importance of sedimentation, stratospheric-tropospheric exchange and general circulation as mechanisms for transfer of material from stratosphere to troposphere or vice-versa.

3. ANALYSIS OF THE GAMETAG DATA SET

3.1 INTRODUCTION

Section 3, along with Appendices A and B, are based on the Final Report submitted by Georgia Institute of Technology, Principal Investigator, Dr. E. M. Patterson, under IFAORS sub-contract F-520.

The Global Atmospheric Measurement Experiment of Tropospheric Aerosols and Gases (GAMETAG) has as its objective the coordinated measurement of those atmospheric trace species (gases and aerosols) that are necessary to gain an understanding of atmospheric chemical properties and processes. In particular, the aerosol measurements of the phase I GAMETAG program were designed to measure the levels and types of tropospheric aerosols both in the planetary boundary layer and at mid-tropospheric altitudes in the free troposphere under a variety of remote conditions, to study aerosol chemical processes, and to study the optical effects of the aerosols as an indication of possible climatic impact.

The aerosol measurements during the GAMETAG program have provided the most extensive data set available for mid-tropospheric remote area measurements. A detailed description of these aerosol measurements, emphasizing the aerosol chemistry, has been reported by Patterson et al. (1980), but only a limited analysis of the optical properties has been reported.

It is the purpose of this chapter to present in considerably greater detail some calculated visible and infrared optical properties of the measured aerosol in both the free troposphere and the boundary layer. The visible wavelength calculations were made for $\lambda = 0.63 \mu\text{m}$ for comparison with on-board in-situ scattering instruments. Since one of the major aims of this work is the determination of aerosol properties in the $10 \mu\text{m}$ wavelength range for the analysis of the expected signal from an orbiting doppler lidar, the infrared calculations were made for $\lambda = 10.6 \mu\text{m}$. Calculations were made of extinction and backscatter coefficients for each of these two wavelengths; ratios of backscatter to extinction were also calculated for each of these wavelengths.

3.2 GAMETAG FLIGHT PROFILES

There were two series of GAMETAG flights. One took place in August and September of 1977; the other occurred in April, May, and June of 1978. The GAMETAG flight patterns for the 1977 and 1978 operations are shown in Figure 3.1. A listing of the data and location for each flight is given in Table 3.1; analysis was done for those days marked with +'. Generally, the two flight series consisted of flights over continental and adjacent marine areas of North America and flights across the Pacific Ocean that were designed to cover as wide a latitude range as possible. In general, the flights consisted of sampling legs in both the mid-tropospheric region (5-6 km altitude) of the free troposphere

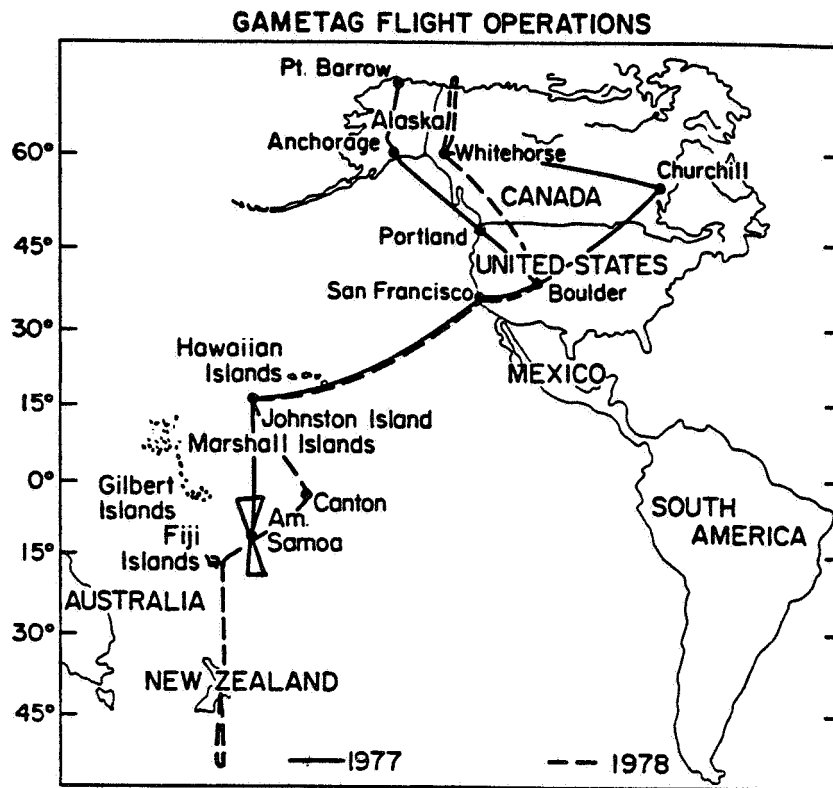


Figure 3.1. Flight tracks for the NCAR Electra aircraft during 1977 (solid line) and 1978 (dashed line). (From Patterson et al., 1980.)

**TABLE 3.1. Detailed Flight Tracks During the 1977 and 1978
GAMETAG Flight Series**

DATE	INITIATION	DESTINATION
1977		
Aug. 7 +	Denver	Portland
Aug. 8 +	Portland	Anchorage
Aug. 9	Anchorage	Anchorage
Aug. 11	Anchorage	Churchill
Aug. 12	Churchill	Denver
Aug. 22 +	Denver	San Francisco
Aug. 23 +	San Francisco	Hilo, Hawaii
Aug. 25 +	Hilo, Hawaii	Johnston Island
Aug. 26 +	Johnston Island	Pago Pago
Aug. 28 +	Pago Pago	Pago Pago
Aug. 31 +	Pago Pago	Pago Pago
Sept. 1 +	Pago Pago	Johnston Island
Sept. 2 +	Johnston Island	Hilo, Hawaii
Sept. 5	Hilo, Hawaii	San Francisco
Sept. 6	San Francisco	Denver
1978		
April 27 +	Denver	San Francisco
April 28	San Francisco	Hilo, Hawaii
May 2 +	Hilo, Hawaii	Johnston Island
May 3	Johnston Island	Canton Island
May 4 +	Canton Island	Fiji Island
May 6	Fiji Islands	Christchurch, N.Z.
May 10 +	Christchurch, N.Z.	Christchurch, N.Z.
May 11 +	Christchurch, N.Z.	Fiji Islands
May 12 +	Fiji Islands	Canton Island
May 13	Canton Island	Johnston Island
May 14 +	Johnston Island	Hilo, Hawaii
May 17	Hilo, Hawaii	San Francisco
May 18 +	San Francisco	Denver
May 27 +	Denver	Great Falls
May 28 +	Great Falls	Whitehorse
May 30	Whitehorse	Whitehorse
May 31 +	Whitehorse	Great Falls
June 1 +	Great Falls	Denver

(that portion of the troposphere not directly influenced by the surface) and in the planetary boundary layer (0-2 km altitude) with sounding data taken on the ascents and descents available to link the measurements in the two regions. The detailed flight tracks for each flight are shown in Appendix A.

The data were taken during two seasons, with most of the flights centered around local noon for maximum photochemical activity. Because of the scientific objectives of the program, the flights were planned to avoid regions of strong convective activity and to avoid cloud penetration as much as possible. Thus the measurements emphasized clear air data.

3.3 INSTRUMENTATION

The size distributions discussed here were determined by means of single particle optical counters. As discussed in Patterson et al. (1980) the inferences from these optical particle counters were tested by comparison with filter and cascade impactor measurements.

Two optical particle counters manufactured by Particle Measurements Systems (PMS) of Boulder, Colorado, were used on the National Center for Atmospheric Research (NCAR) Electra aircraft during GAMETAG. A combination active scattering aerosol spectrometer and classical scattering spectrometer probe (ASAS-CSSP) was mounted within the aircraft, and it sampled air from an aerosol inlet manifold, which also supplied the sample

air for the filter samples. The aerosol inlet manifold was designed to sample air isokinetically from the outside of the aircraft, to have a diffuser section to reduce the air speed within the sample tube, and to have a series of intakes for each of the aerosol measurement devices. All intakes were operated approximately isokinetically, and the entire system was wind-tunnel tested for sampling efficiency. Such testing showed sampling efficiencies of ~ 1 for particles with $r \leq 0.75 \mu\text{m}$. Sampling efficiency decreased for the larger particles, and so an externally mounted probe, the forward scatter spectrometer probe (FSSP), was used to measure the larger particles. Each of the probes has been extensively calibrated by the manufacturer and by the GAMETAG experimenters by using polystyrene latex spheres and glass spheres for the particle ranges used. Our determination of sizes from the optical particle counter data is based on the polystyrene and glass sphere calibration, with no explicit use of calculations for the differing response of the instruments to particles with differing refractive indices. Our calculations of the Mie scattering functions appropriate to the PMS optical geometry, as well as those reported by Pinnick and Auvermann (1979), indicate that for the range of sizes and refractive indices encountered in this experiment, the differing instrumental response characteristics will have no significant effect on our measured size distribution.

The data from the PMS probes were transferred to the Electra

Electronic Data Management system tape every 2 s, but for analysis, these second-by-second averages were converted to longer time averages to reduce statistical fluctuations. One minute accumulations were used as the standard archived output from the particle probes.

Although each probe is a multi range device (for a complete description see the ASAS and FSSP manuals, available from PMS), only one of the ranges for each probe was used in the analysis of the size data: the nominal $0.25 \mu\text{m} \leq r < 3.0 \mu\text{m}$ for the FSSP and nominal $0.15 \mu\text{m} \leq r < 0.75 \mu\text{m}$ for the ASAS-CSSP.

The response calculations for these optical particle counters exhibit double valuedness, and so the ASAS and the FSSP size data were combined into a smaller number of larger intervals. Nine combined size ranges were used in the calculations, six ASAS size ranges and three FSSP size ranges.

The same ASAS size ranges were used for both the 1977 and the 1978 data sets. The FSSP data for the two data sets was handled somewhat differently, however. For the 1977 data, the FSSP data was combined into three ranges consisting of Channel 1 (FSSP Range 7), Channels 2 - 9 (FSSP Range 8), and the rest of the FSSP Channels (FSSP Range 9). Range 7, which overlapped the ASAS data, was not used and Range 7 consisted of Channels 2 - 5, Range 8 consisted of Channels 6 - 9, while Range 9 consisted of the rest. These ranges, size limits, and mean radii are shown in

Table I of Appendix B.

3.4 DATA ANALYSIS

The earlier analyses by Patterson et al showed that the typical size distribution exhibited a bimodal nature as shown in Fig. 3.2. Analysis of the filter and cascade impactor samples showed that these modes had different composition over land, with the submicron mode composed of sulfate and other secondary and combustion aerosols, and the supermicron mode composed of soil-derived aerosol particles. The marine free tropospheric aerosol was similar to the continental aerosol; the marine boundary layer aerosol, by contrast, was dominated by a sea salt aerosol.

Consequently, we have used more than one set of optical constants to describe the aerosol. Over continental areas, and in the marine free troposphere the particles with $r > 0.5 \mu\text{m}$ were described by optical constants appropriate to soil aerosols, while the smaller particles with $r < 0.5 \mu\text{m}$ were described by optical constants appropriate to ammonium sulfate. Optical constraints appropriate to a wetted sea salt aerosol were used for the total size distribution in the marine boundary layer. The optical constants used in these calculations are shown in Table 3.2.

Calculations of the extinction coefficient σ_E (expressed in

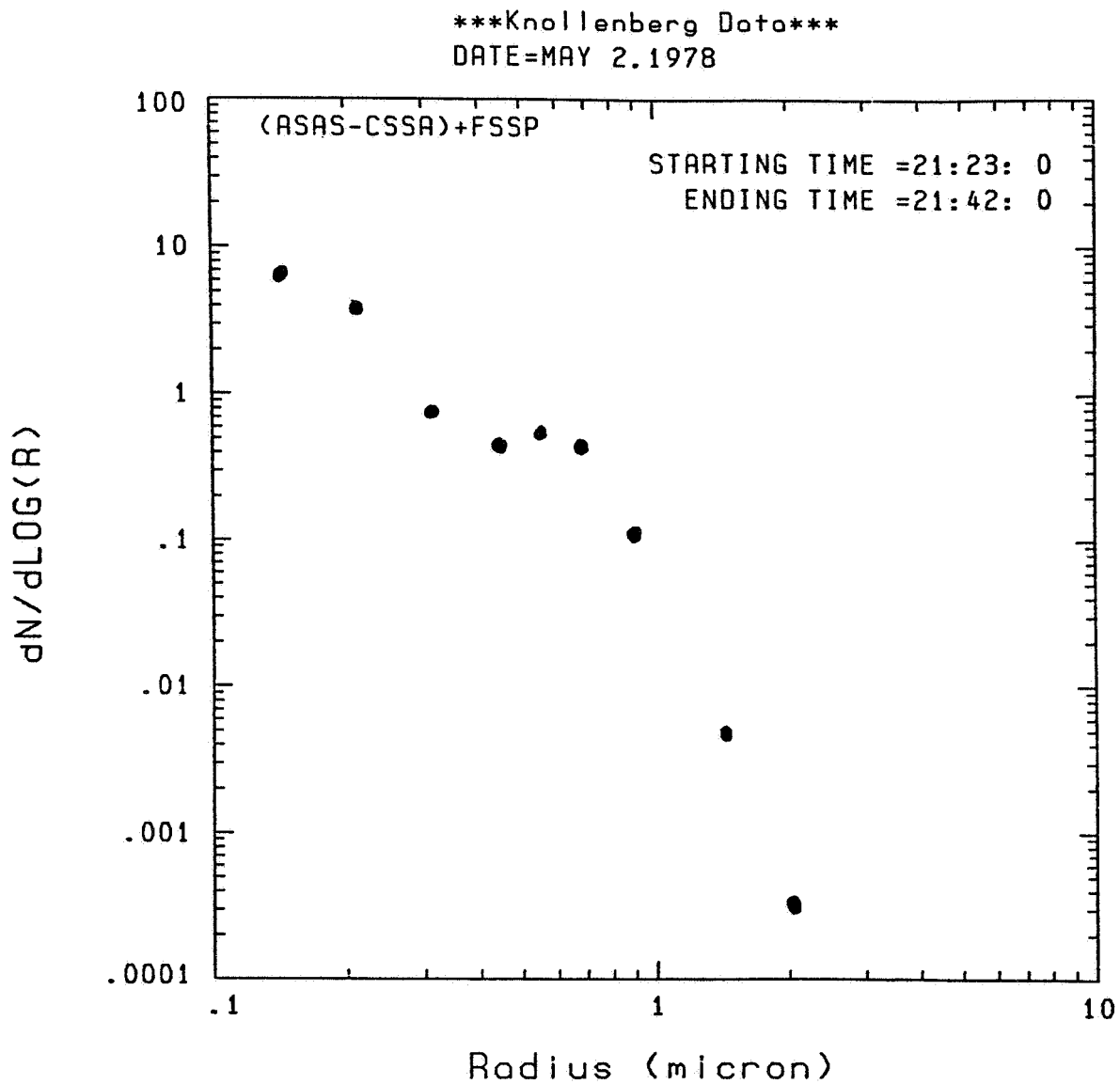


Figure 3.2. A representative size distribution measured during the GAMETAG flights.

Table 3.2. Optical Constants Used in Calculations

Wavelength	0.63 μm	10.6 μm
$(\text{NH}_4)_2 \text{SO}_4$	1.5 - 0.005i	1.98 - 0.06i
Soil-Aerosol	1.9 - 0.005i	1.74 - 0.4i
Sea Salt (Wetted)	1.4 - 0.0i	1.38 - 0.057i

m^{-1}) and the backscatter coefficient β (in units of $\text{m}^{-1} \text{sr}^{-1}$) were made for $0.63 \mu\text{m}$ and $10.6 \mu\text{m}$. A Mie scattering routine available at Georgia Tech was used for the calculations. The calculation procedure involved a calculation of the optical quantity of interest using appropriate optical constants for each size range. These average efficiency factors were multiplied by the average particle cross sectional area for the interval and by the number density of the particles to determine σ_{ϵ} or β for each size interval. Values for the individual size intervals were then summed to determine σ_{ϵ} or β for the entire distribution.

Calculations were made for the basic one-minute data set that consists of counts/cm³ in each one of the nine channels. These one-minute averages were combined into five minute averages which are plotted, together with the standard deviation calculated for each set. These one-minute and five-minute data are plotted for each of the days analyzed.

The time averaging corresponds to a spatial averaging along the aircraft flight ²²tracks as well. A one-minute average corresponds to a distance of ~ 9 km at high altitudes and ~ 7 km at low altitudes. Five minute averages correspond to a spatial averaging over ~ 50 km at high altitudes and ~ 35 km at low altitudes.

In addition, longer time averaging was also done. The

one-minute particle averages were combined into 20 minute averages to produce a series of size distributions which are presented in Appendix B. The one-minute optical data were also averaged over flight legs or portions of flight legs (generally 100-200 km) and plotted as a function of latitude to determine latitudinal profiles along our flight tracks.

We will discuss the calculated optical properties in terms of the daily flight data and the latitude profiles. We will not further discuss the size distribution data.

3.5 DAILY FLIGHT DATA

Detailed optical calculations were made for twelve of the 1978 flights and ten of the 1977 flights. These calculations were made as described above for the optical properties of interest: extinction coefficients at visible and infrared wavelengths, backscatter coefficients at these wavelengths, and backscatter-extinction ratios. These quantities have been plotted against time into the flight for each of the days analyzed. This data set is shown in Appendix A, arranged by flight days. In this Appendix, each data set consists of ten pages including a table and nine figures (Figures a-i) arranged as follows:

1. An initial table giving date and location of the day's flight with a list of significant points keyed to a detailed altitude

and location plot for the flight.

2. A detailed plot of altitudes and locations as a function of time after takeoff, with significant points indicated on the plot.
3. A plot of the extinction, calculated for $\lambda = 0.63 \mu\text{m}$ using the assumed optical properties for the particles discussed above for the one-minute optical particle data. These and other optical data are plotted against time after takeoff for each flight.
4. A plot of the extinction, calculated for $\lambda = 0.63 \mu\text{m}$ as above except for the five-minute optical particle counter data.
5. A plot of the backscatter coefficient in $\text{m}^{-1} \text{sr}^{-1}$ calculated for $\lambda = 0.63 \mu\text{m}$ based on the measured size distribution with five -minute resolution and assumed refractive indices.
6. A plot of the ratio of the calculated backscattering coefficient to the calculated extinction coefficient for $\lambda = 0.63 \mu\text{m}$.
7. A plot of the extinction coefficient calculated for $\lambda = 10.6 \mu\text{m}$ using the measured size distribution (one-minute averages) and assumed refractive indices.
8. A plot of the extinction coefficient calculated for $\lambda = 10.6 \mu\text{m}$ as above for the five-minute averages.
9. A plot of the backscatter coefficient calculated for $\lambda = 10.6 \mu\text{m}$ using the measured size distribution (five-minute averages) and assumed refractive indices.
10. A plot of the ratio of the calculated backscattering coefficient to the calculated extinction coefficient

for $\lambda = 10.6 \text{ } \mu\text{m}$.

In addition, a numerical listing of the dN values (in cts/cm) for each size interval, presented as 20 minute averages, is shown in Appendix B. Although the complete series of plots is shown in Appendix A, we will discuss some points of interest in the data.

A representative comparison of the total distribution volume, calculated in a manner analogous to that of β and σ_{ϵ} , with the extinction is shown in Figures 3.3 and 3.4. This comparison indicates that the variation in particle volume is quite comparable to the variation for σ_{ϵ} . Although no formal statistical tests have been made, the variation within flight legs that is shown in the figure appears to be separable into a random variation that is a statistical fluctuation due to the small number of particles sampled and a larger scale variation that reflects differences in aerosol concentrations on time scales of the order of 30 minutes, which correspond to distance scales of 200-300 km. There is also, of course, the large variation in concentration that is seen in going from the troposphere to the boundary layer; this concentration variation results in different calculated optical properties for the free troposphere and the boundary layer.

The calculated β values also show a variation that is similar to that shown by the σ_{ϵ} values; a consideration of extinction to backscatter ratios for these distributions, such as

Knollenberg Data

DATE=MAY 2, 1978

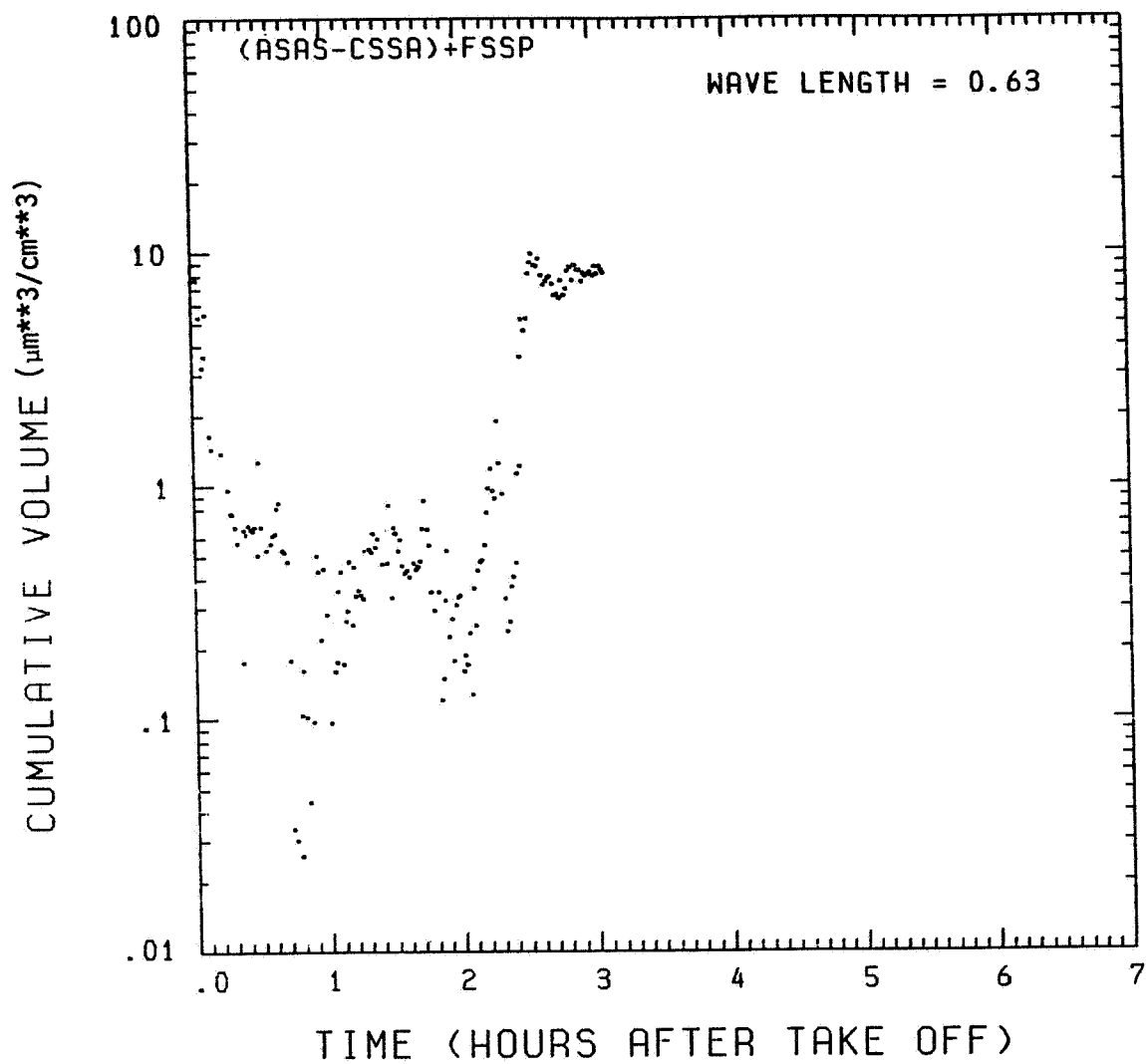


Figure 3.3. A plot of total aerosol volume inferred from the optical particle data for the May 2, 1978 flight.

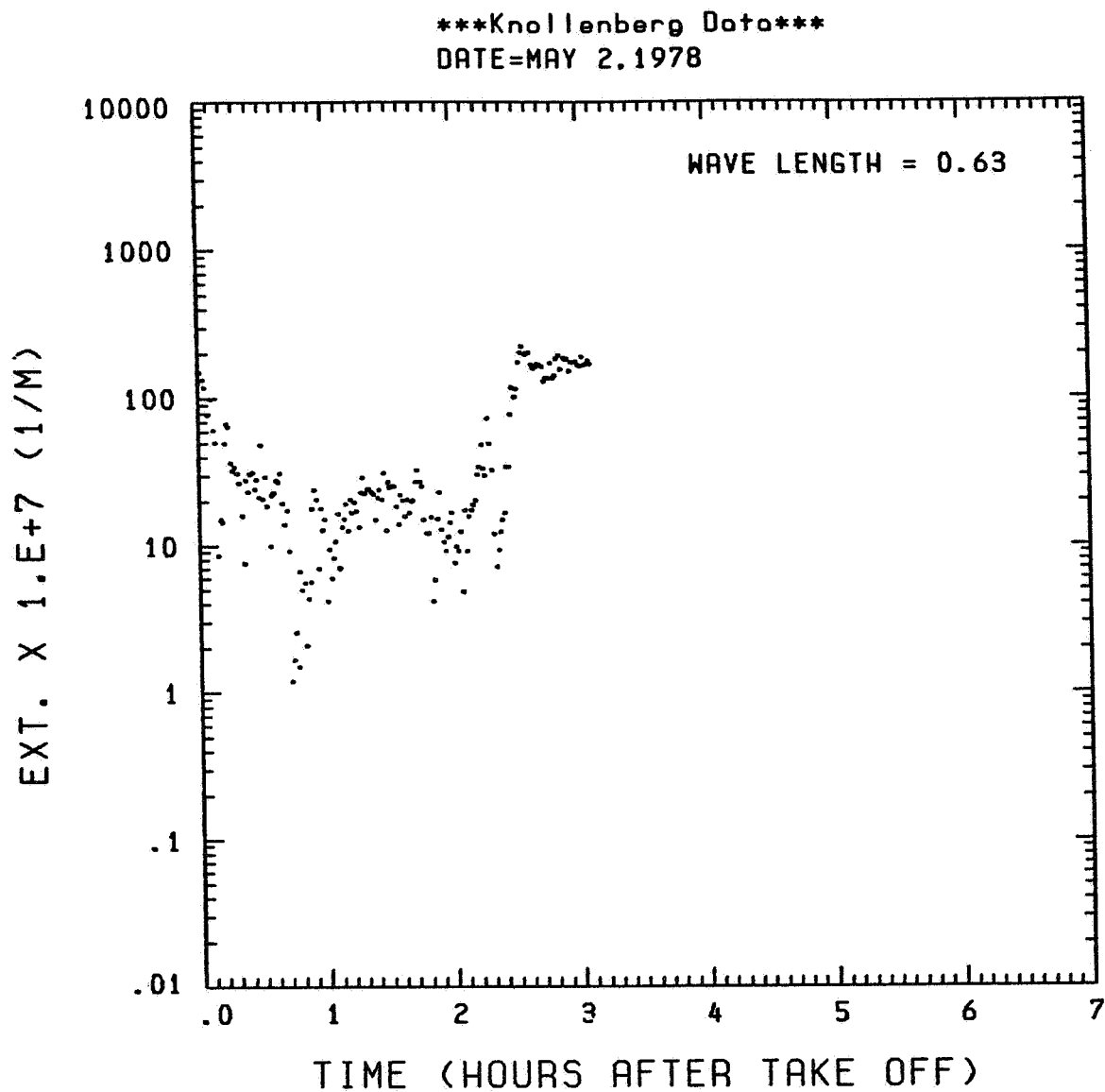


Figure 3.4. A plot of particulate extinction calculated for $\lambda = 0.63 \mu\text{m}$ for the May 2, 1978 data set.

the calculations shown in Figure 3.5, shows much less variation in calculated ratios. This relative uniformity is due to the similar variation of each of these quantities with particle size, and to the importance of the submicron particles in all of our measured distributions. The major difference that is seen is associated with the transition between boundary layer and free troposphere. The 10.6 μm values of β and σ_{ϵ} are generally significantly lower than the 0.63 values, as expected. Calculated $\beta / \sigma_{\epsilon}$ ratios for 10.6 μm are near 0.01 and are generally somewhat less than those calculated for visible wavelength data.

3.6 LATITUDINAL PROFILES ALONG AIRCRAFT FLIGHT TRACKS

The $\lambda = 0.63 \mu\text{m}$ extinction data from the individual flights were grouped into boundary layer and free tropospheric data and plotted against latitude for each of the flight series (1977 and 1978). The 1978 data were further divided into marine and continental data. We note, however, that the separation into boundary layer and free troposphere was not always as well defined over the continental areas as over the ocean areas.

The boundary layer data is shown in Figures 3.6 (1977 data), 3.7 (1978 oceanic data), and 3.8 (1978 continental data). The 1977 boundary layer data consists entirely of oceanic data. for these figures, the symbol 0 represents data between 100 and 200 m, Δ data between 200 and 300 m, + data between 300 and 400 m, *

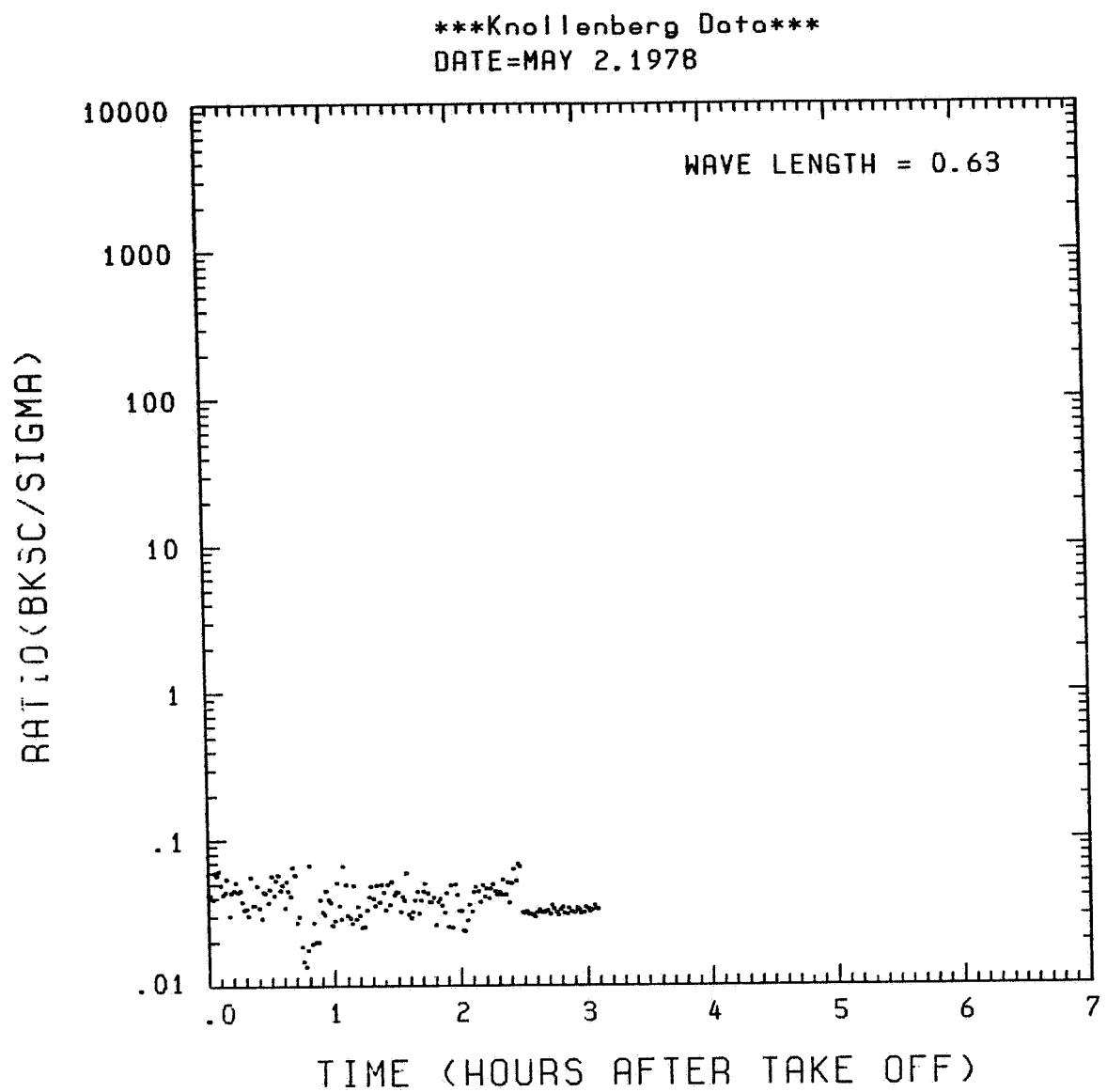


Figure 3.5. A plot of the ratio of backscatter to extinction at $0.63 \mu\text{m}$ for the May 2, 1978 data set.

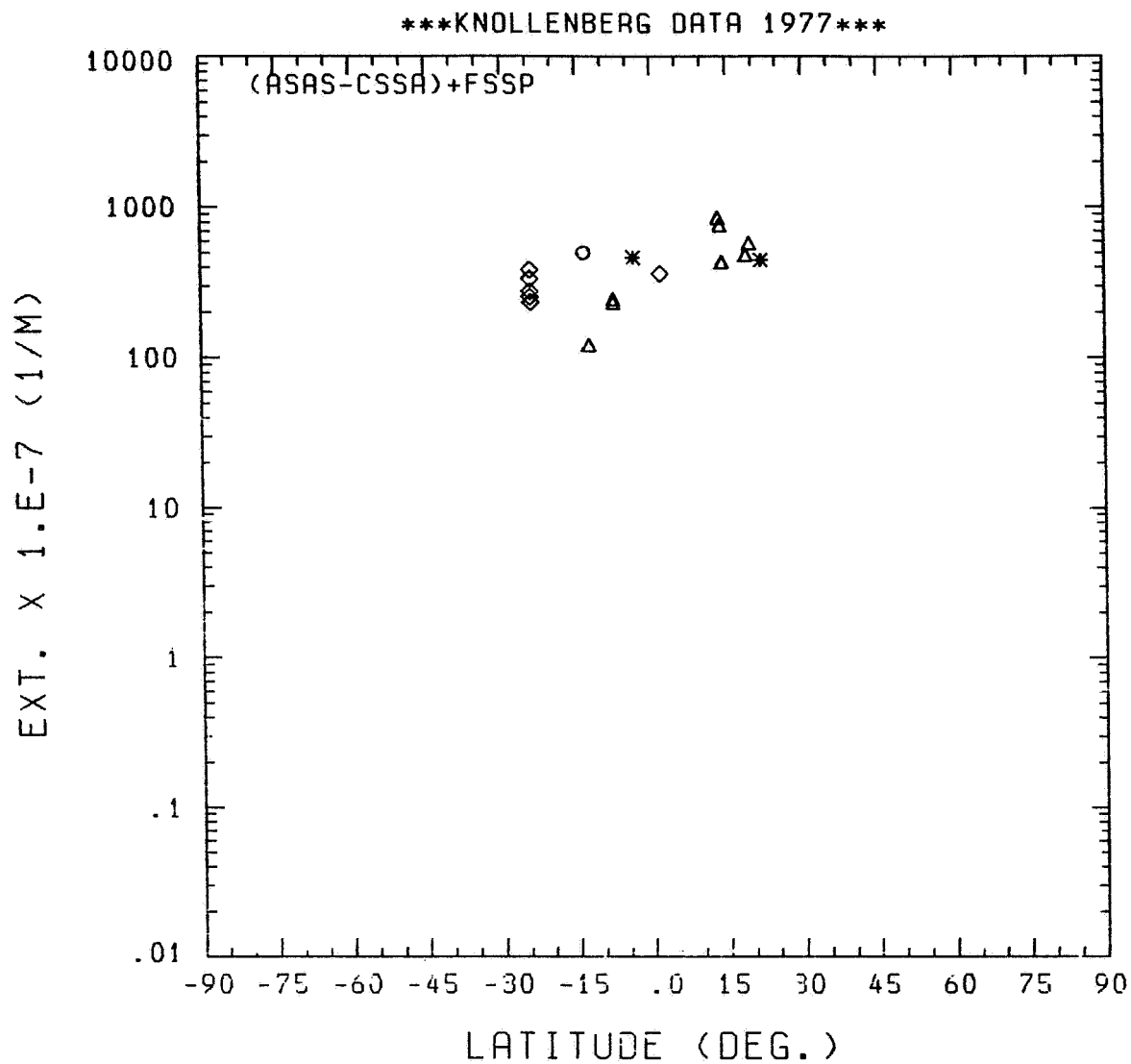


Figure 3.6. Latitudinal profile along the GAMETAG flight tracks for the $0.63 \mu\text{m}$ extinction determined in the marine boundary layer during the 1977 GAMETAG flights.

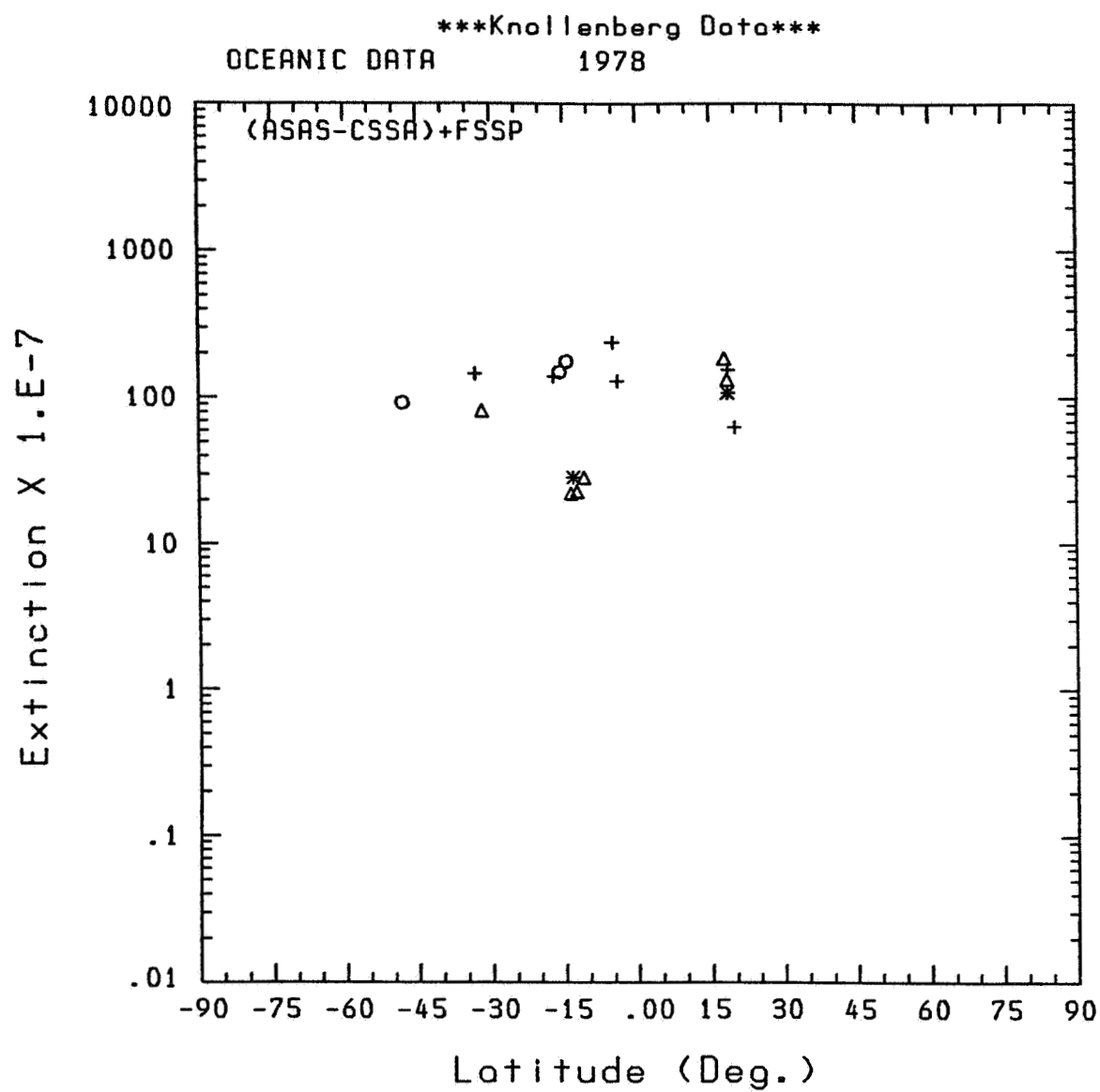


Figure 3.7. As in Fig. 3.6, except for the 1978 oceanic data.

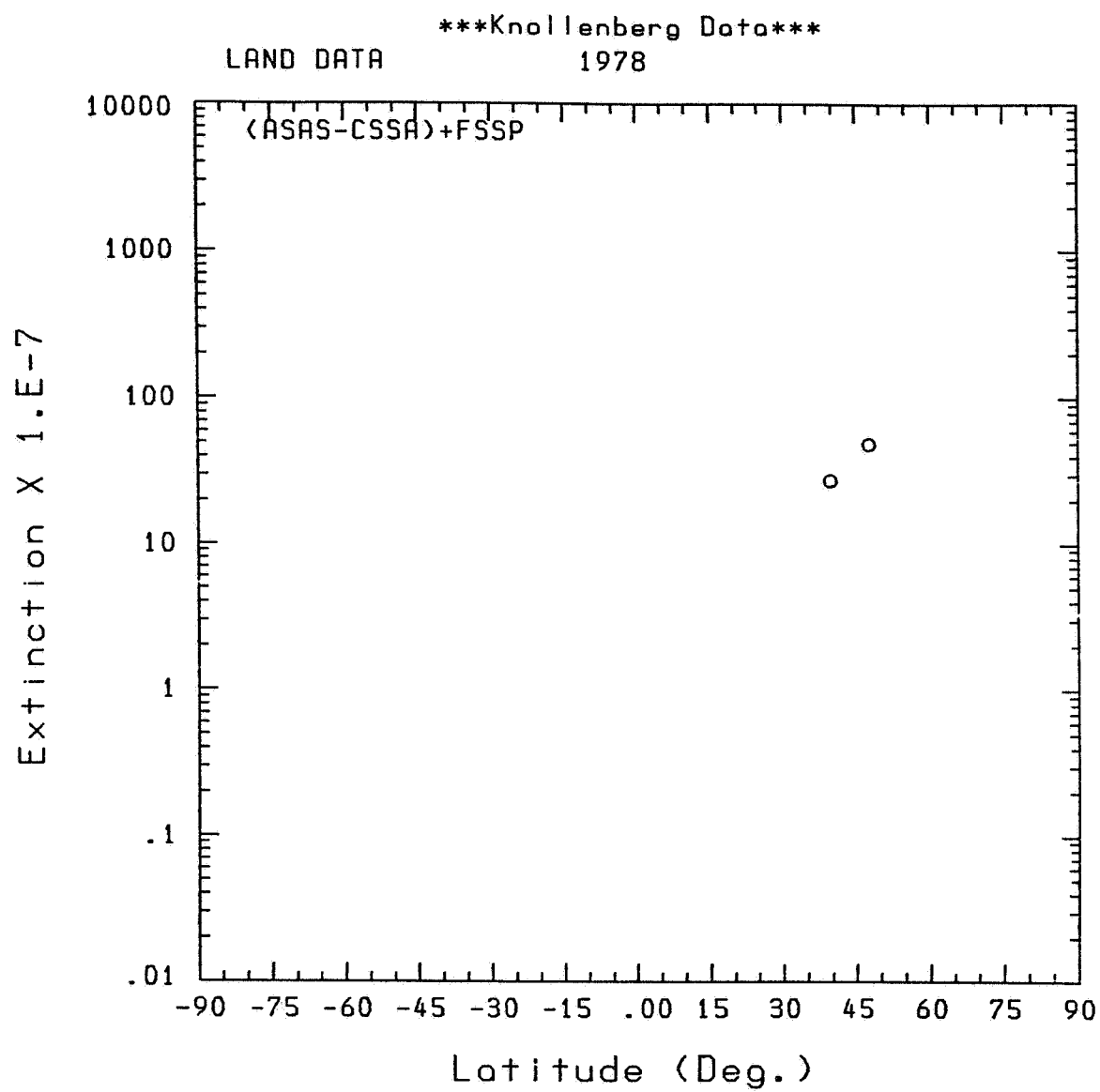


Figure 3.8. As in Fig. 3.6, except for the 1978 continental data.

data between 400 and 500 m, and \diamond data between 500 and 1000 m. The 1977 and the 1978 data are consistent; each suggests a marine boundary layer extinction somewhat greater than 10^{-5} m^{-1} at 0.63 μm , with slight decrease south of ITCZ (which was about 5-10 N for both of the flight series. There are no clear differences in the northern and southern hemisphere data, there are, however, a few data points in which the extinction is very low, $\sim 2-3 \times 10^{-6} \text{ m}^{-1}$, which corresponds to very low concentrations of sea salt aerosol.

The free tropospheric data is shown in Figures 3.9, 3.10, and 3.11. The 1977 free tropospheric data is shown in Fig. 3.9. For this data set, the data for latitudes north of $\sim 35^{\circ}$ represent data collected over continental areas; the data for latitudes south of 35° are oceanic data. The 1978 free tropospheric data is separated into continental data (Fig. 3.10) and marine data (Fig. 3.11). The lack of data for latitudes north of 20° N in Fig. 3.11 corresponds to missing data between San Francisco and Hawaii ($20-30^{\circ}$ N) which a separate analysis has shown to be similar to that measured in 1977.

For this free tropospheric data, the Δ 's represent data at all altitudes between 2 and 3 km, the + 's between 3 and 4 km, the * 's between 4 and 5 km, and the \diamond 's for altitudes greater than 5 km.

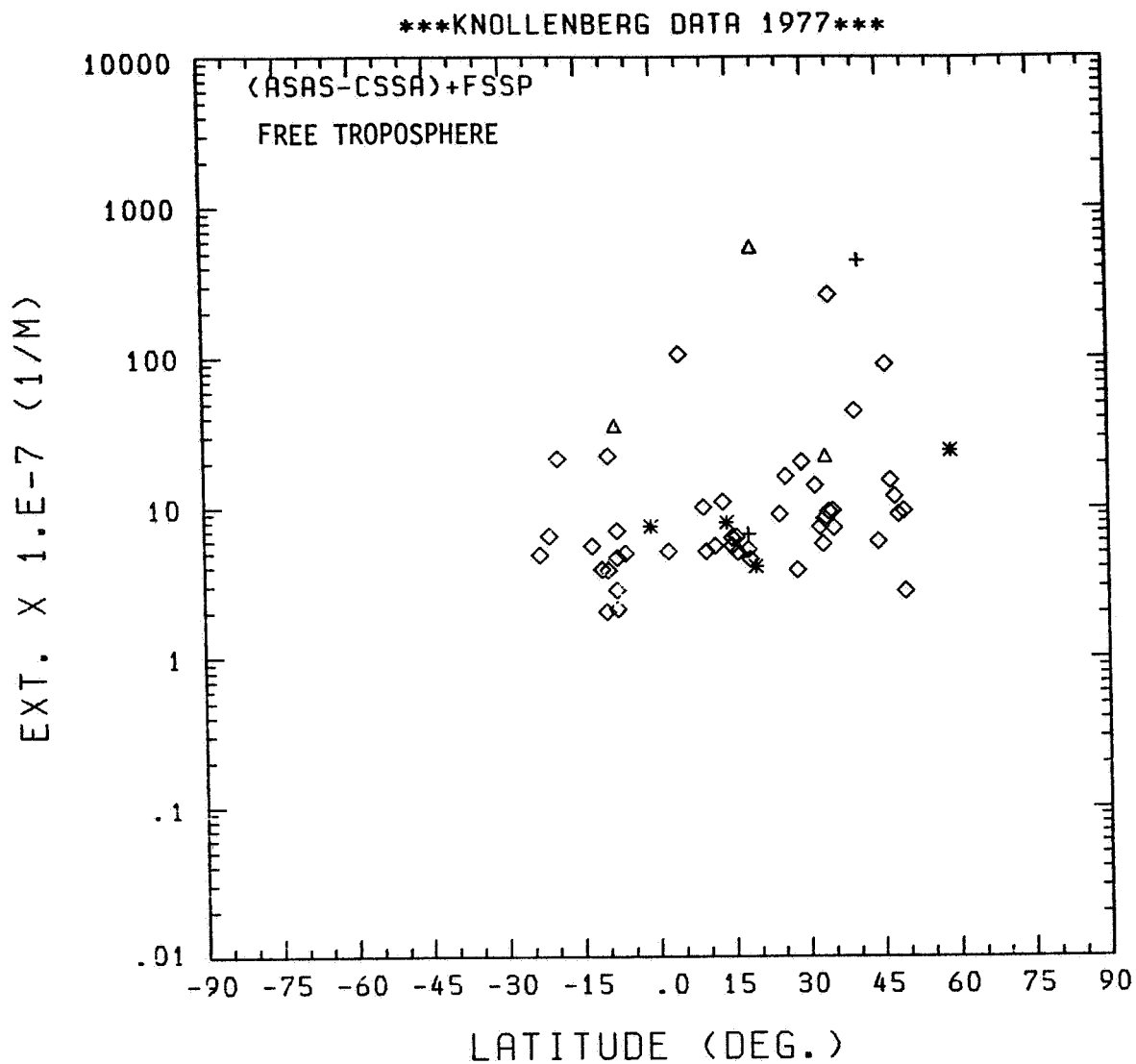


Figure 3.9. Latitudinal profile along the GAMETAG flight tracks in the free troposphere for the $\lambda = 0.63 \mu\text{m}$ extinction data determined during the 1977 flights.

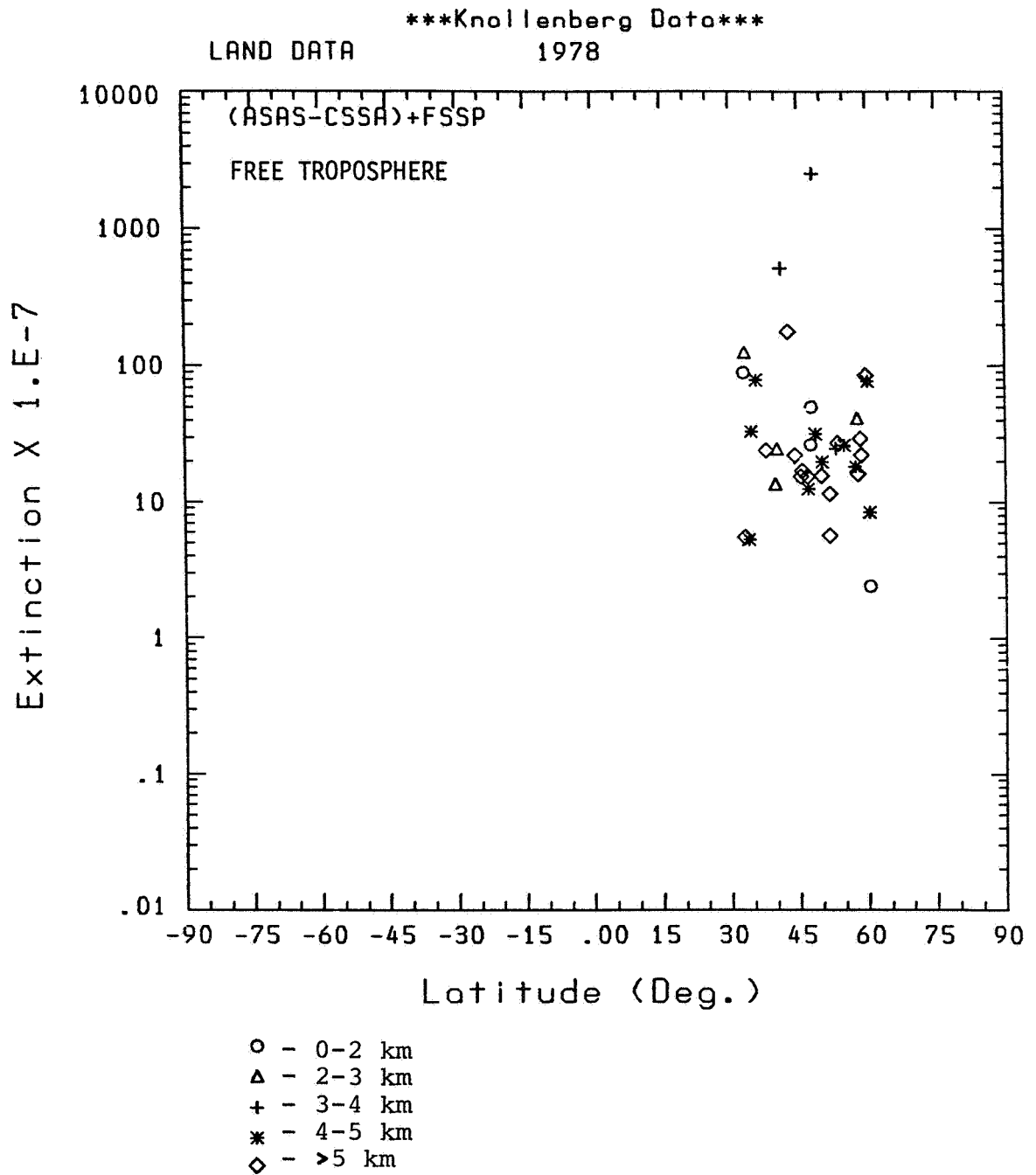


Figure 3.10. As in Fig. 3.9, except for 1978 continental data.

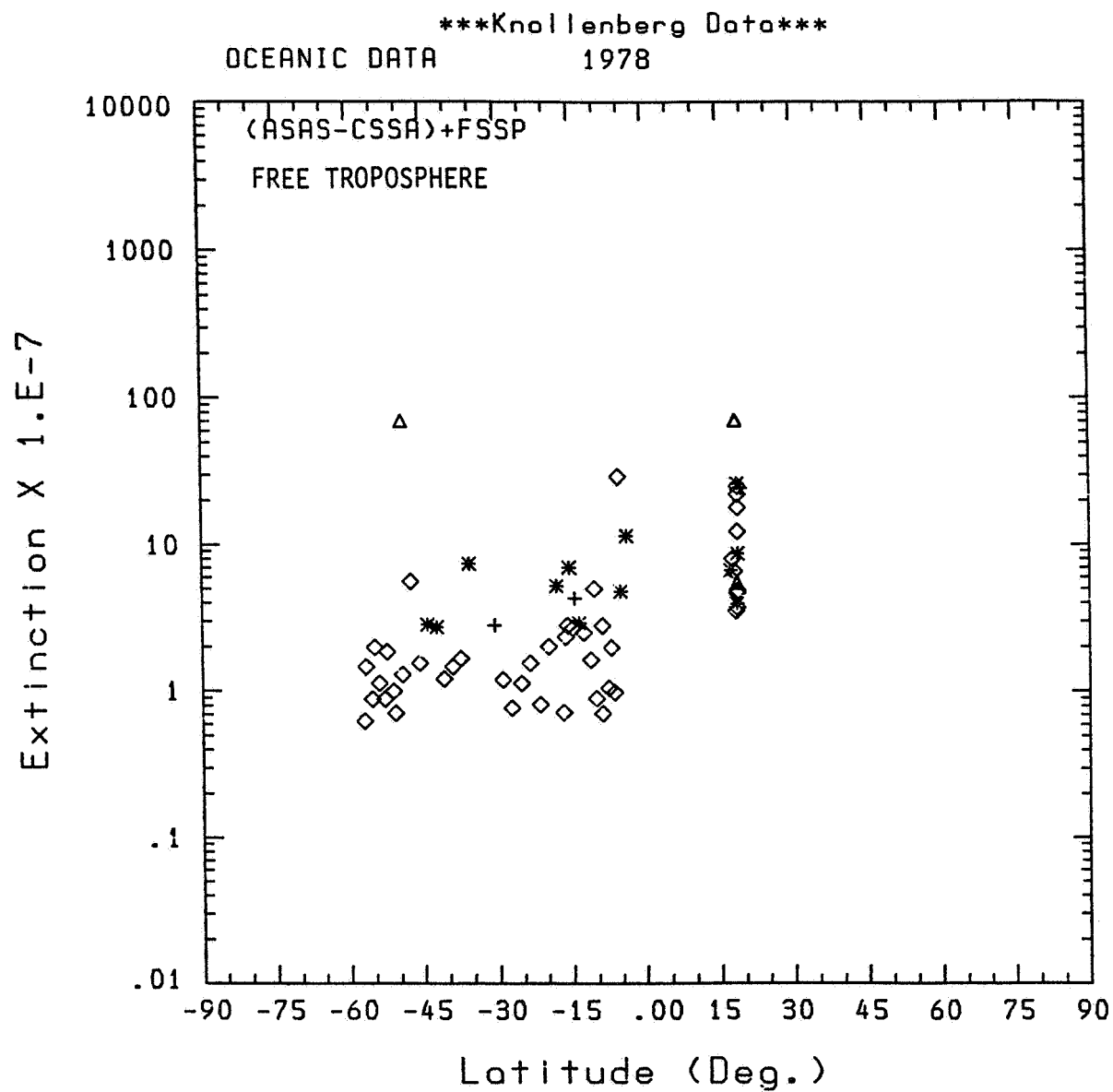


Figure 3.11. As in Fig. 3.9, except for the 1978 oceanic data.

A comparison of the free tropospheric data for the 1977 and the 1978 flights indicates that the continental data for each of the two years are consistent, with each exhibiting a similar (though wide) range of observed values between $\sim 2 \times 10^{-7}$ and $1 \times 10^{-4} \text{ m}^{-1}$. Both of the marine free tropospheric data sets show a decrease in extinction from north to south. Looked at in detail, however, there are some significant differences in the two data sets. In the latitude region where there is considerable overlap of data (25° S to the equator), there appears to be a greater extinction in the fall of 1977 than in the spring of 1978 by a factor of ~ 2 . The 1977 data also show more very high values of extinction. While some of these north of the equator may be influenced by clouds, others are associated only with increases in the submicron aerosol population. The marine data north of the equator appear to be consistent for the two years.

The lowest values of extinction measured in the southern hemisphere are lower than the corresponding northern hemisphere low values. The 1978 data for latitudes south of 20° S suggest that we are measuring a mid-tropospheric background aerosol. The average for σ_{ϵ} for latitudes south of 20° S is $\sim 1 \times 10^{-7} \text{ m}^{-1}$. If we look at the variation about this average, we see that the

lowest values measured in the southern hemisphere are $6-7 \times 10^{-8-1}$ m with the 200 - 300 km spatial integration of Fig. 3.11, decreasing to $4 \times 10^{-8-1}$ m for the 50 km data set and $4 \times 10^{-9-1}$ m for the 9 km data sets.

As an additional comparison, we have calculated similar latitudinal averages of σ_e for the 1977 data set for $\lambda = 10.6$ μ m. These values, shown in Fig. 3.12, are significantly lower than the visible wavelength extinction data. The continental 10.6 μ m data range between $1 \times 10^{-8-1}$ m and 10^{-5-1} m with the majority less than 10^{-6-1} m. The oceanic data shown on this figure ranges from $4 \times 10^{-9-1}$ m to 10^{-5-1} m, although almost all of the oceanic values are less than $6 \times 10^{-8-1}$ m. The average for the oceanic data south of about 15° N appears to be in the range of 10^{-8-1} m. Because of the greater dependence of the 10.6 μ m data on the larger particles, and the greater variability of these particles, there is more variation in this IR data than in the visible data. Based on the data, however, we can estimate that the 10.6 μ m extinction is lower than the 0.63 μ m extinction by a factor of about 30. For the more southerly latitudes measured in 1978, the 10.6 μ m mid-tropospheric extinction is $\sim 10^{-9-1}$ m with

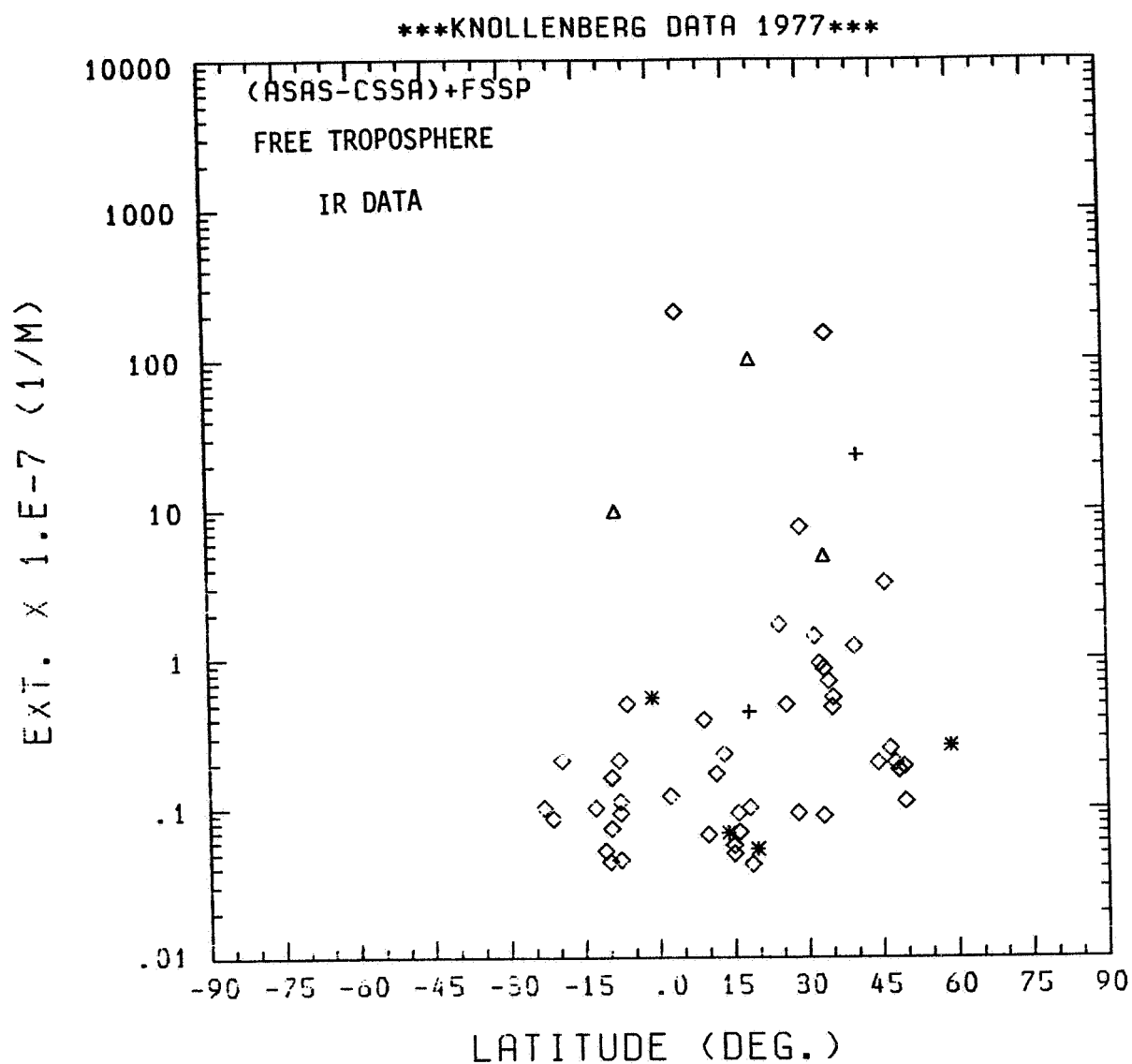


Figure 3.12. Free tropospheric latitudinal profiles along GAMETAG flight tracks for the $\lambda = 10.6 \mu\text{m}$ extinction data.

lowest values (50 km averages) of the order of $3 \times 10^{-10} \text{ m}^{-1}$. The corresponding $0.63 \text{ } \mu\text{m}$ extinction is $\sim 1 \times 10^{-7} \text{ m}^{-1}$, roughly 2 orders of magnitude higher. For the average free tropospheric β/σ_{ϵ} ratio of less than 0.01 calculated for the $10.6 \text{ } \mu\text{m}$ data, a average β 's will be approximately 10^{-11} m^{-1} and lower.

3.7 CONCLUSIONS

We have used measured particle size information and assumed refractive indices to calculate the aerosol extinction and backscatter coefficients along aircraft flight tracks for $\lambda = 0.63 \text{ } \mu\text{m}$ and $\lambda = 10.6 \text{ } \mu\text{m}$. These calculations show that mid-tropospheric extinctions over the Pacific are significantly higher in the northern hemisphere than the southern hemisphere. The data indicate that the average $\lambda = 0.63 \text{ } \mu\text{m}$ extinction is $\sim 1 \times 10^{-7} \text{ m}^{-1}$ in the southern hemisphere at the mid-tropospheric flight altitudes. The $10.6 \text{ } \mu\text{m}$ extinction is between 1 and 2 orders of magnitude less, decreasing to $\sim 1 \times 10^{-9}$ at the southernmost latitudes of the GAMETAG measurements. Corresponding calculations of β show that the ratio of β to σ_{ϵ} is in the range of 0.01 to 0.1 for the $0.63 \text{ } \mu\text{m}$ data and in the range of 0.01 and lower for the $10.6 \text{ } \mu\text{m}$ data. The ratios appear to decrease at southern latitudes over the Pacific due to the decreased importance of particles with $r > 1 \text{ } \mu\text{m}$.

4. MICROPHYSICAL PROCESSES IN AN AEROSOL PLUME

4.1 BACKGROUND

A moving aerosol plume may spontaneously undergo different microphysical processes. These microphysical processes, in addition to condensation and evaporation, include coagulation, sedimentation, and diffusion. In our previous work we examined the possible effects of growth and evaporative processes on the backscatter of radiation traversing an aerosol medium (Deepak et al., 1982). In this report, the analysis is focused on the effects of coagulation, sedimentation, and diffusion on the aerosol size distribution and backscattering coefficient at 10.6 μm wavelength. In general, a discussion of these microphysical processes in an aerosol plume requires a time dependent 3-D model. Detailed modeling like this is beyond the scope of this analysis. Instead, we will use a 1-D model in this study. This simplification allows us to examine these microphysical processes in considerable detail.

4.2 NUMERICAL MODEL

To achieve the objective of this investigation, a ten-layer model has been developed for study of the effect of coagulation, sedimentation, and diffusion processes on aerosol size distribution and backscattering at 10.6 μm wavelength. Figure 4.1 shows schematically the model layers. It includes ten 1 km

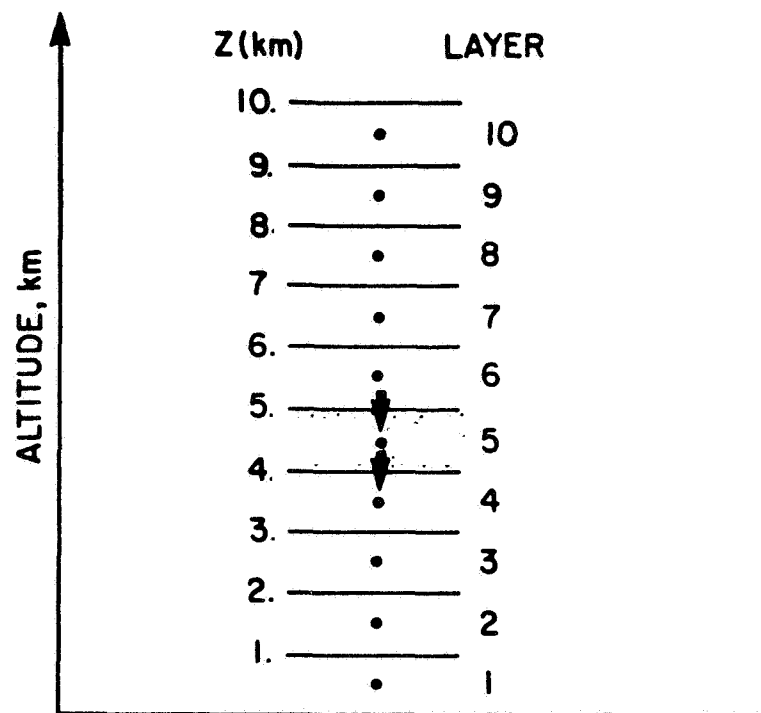


Figure 4.1. Schematic diagram shows the 10-layer model used for numerical study of the aerosol transport. The arrows indicate the interaction of aerosol size distribution between successive layers through the effect of gravitational sedimentation.

thick layers above the earth's surface. A description of the basic equations governing the microphysical processes are given below.

4.2.1 Coagulation

Coagulation is the process under which aerosol particles come into contact and coalesce or adhere to one another. In other words, coagulation leads to the increase in the number of large particles at the expense of the number of smaller particles. Coagulation can arise as a result of Brownian motion of the aerosol particles--the so-called thermal coagulation. In addition, it can be also produced by hydrodynamic, electrical, gravitational, or other forces (Fuchs, 1964). In this investigation, we shall assume that the Brownian motion is the major cause of the coagulation processes and only the thermal coagulation is considered in the analysis. A brief theory of this coagulation is given as follows:

The coagulation equation can be written as

$$\begin{aligned} \frac{\partial}{\partial t} n(V,t) = & - \int_0^\infty K(V,u) n(V,t) n(u,t) du \\ & + \frac{1}{2} \int_0^V K(u_i, u_j) n(u_i,t) n(u_j,t) dV \end{aligned} \quad (4.1)$$

where $K(V,u)$ is the coagulation kernel, which is the frequency of collisions per unit volume between particles of volume V and particles of volume u , $n(V,t)$ is defined so that the number of

particles per unit volume with volume between u and $u+du$ at an instant t is given by

$$\int_u^{u+du} n(u, t) du.$$

The first term on the right-hand side of Eq. 4.1 describes the reduction in number of particles with volume V by coagulation processes between particles of this particular size with all particles of other sizes. The second term on the right-hand side of Eq. 4.1 gives the production of new particles with volume V by coagulation processes between particles with volumes u_i and u_j , so that u_i and u_j are related by the equation

$$u_i + u_j = V.$$

To calculate the coagulation kernel $K(V, u)$, we have employed the formulation derived by Fuchs (1964), which is given by

$$K(u_i, u_j) = 4\pi r_{ij} D_{ij} \left(\frac{r_{ij}}{r_{ij} + \delta_{ij}} + \frac{4D_{ij}}{G_{ij} r_{ij}} \right)^{-1} \quad (4.2)$$

with r_{ij} , D_{ij} , δ_{ij} , and G_{ij} defined as

$$\begin{aligned} r_{ij} &= r_i + r_j \\ D_{ij} &= D_i + D_j \\ G_{ij} &= (G_i^2 + G_j^2)^{1/2} \end{aligned}$$

and

$$\delta_{ij} = (\delta_i^2 + \delta_j^2)^{1/2}$$

where r_i and r_j are the radii of i th and j th particles with volume u_i and u_j respectively; D_i is the diffusion coefficient, and can be determined from the Einstein relation. That is, $D_i = kTB_i$, where k is the Boltzmann constant, T is the absolute temperature, and B_i is the mobility that can be calculated by

$$B_i = \frac{1}{6\pi \eta_m r_i} \left[1 + 1.246 K_n + 0.24 K_n \exp \left(-\frac{0.87}{K_n} \right) \right]$$

where η_m is the viscosity of air; and K_n is the Knudson number and is defined as the ratio of the effective mean free path of air molecules (ℓ) to the radius r_i . G_i is the average kinetic velocity of a particle,

$$G_i = \left(\frac{\delta k T}{\pi m_i} \right)^{1/2}$$

where m_i is the mass of the particle of volume u_i . δ_i is a correction factor given by

$$\delta_i = \frac{1}{6r_i \ell_b} \left[(2r_i + \ell_b)^3 - (4r_i^2 + \ell_b^2)^{3/2} \right] - 2r_i$$

where $\ell_b = 8D_i / (\pi G_i)$

The analytic solution of Eq. 4.1 is very difficult. In this

modelling analysis, it is solved numerically. The approach is given as follows.

First, the integration on the right-hand side of Eq. 4.1 is achieved by binning the particle volume spectrum into discrete bins. In this analysis, the bins are chosen so that the volume of a bin is twice that of the preceding bin. To assure the conservation of mass as coagulation takes place, it is assumed that,

$$u_i + u_j = f_{ij} u_i + (1 - f_{ij}) u_{i+1} \quad , \quad j \leq i \quad (4.3)$$

Note, $f_{ij} = 0$, in the case $i = j$.

Equation 4.1 can now be rewritten in the form

$$\begin{aligned} \frac{\Delta N_i}{\Delta t} = & - \sum_{j \neq i} K_{ij} N_i N_j - \frac{1}{2} K_{ii} N_i^2 \\ & + \sum_{j < i} f_{ij} K_{ij} N_i N_j + \frac{1}{2} K_{i-1,i-1} N_{i-1}^2 + \sum_{j < i-1} (1-f_{i-1,j}) K_{i-1} N_{i-1} N_j \end{aligned} \quad (4.4)$$

By applying Eq. 4.4, the rate of change of aerosol concentration with time in each bin can be calculated, and the change in the aerosol size distribution with time can then be determined. In the model, the volume range corresponds to a radius range of .01 μm to 1.29 μm . The number of bins used in the calculation is 32.

4.2.2 Theory of Differential Settling - Sedimentation

Assume the aerosol particles are spherical in shape. The terminal velocity v_t is governed by the Stokes law

$$v_t = \frac{2}{9} \frac{g}{\eta_m} (\rho_p - \rho_m) r^2 \quad (4.5)$$

where ρ_p and ρ_m are densities of the particle and air, respectively, and r is the radius of the particle. Since the terminal velocity is a function of particle size, sedimentation results in differential settling, and thus in changes of the aerosol particle size distribution. Furthermore, the settling of the particles leads to interaction between different levels. In the present analysis, the fraction of the total number of the same size of particles falling out of a given layer is determined by

$$f_r = \frac{\Delta t}{\tau} \quad (4.6)$$

where τ is the mean time required for a particle of a given size to fall out of the layer and is given by

$$\tau = \frac{1}{v_t} \quad (4.7)$$

and Δt is the time interval used in the numerical integration.

In the model computation, we have specified $\rho_p = 1.001 \text{ gm/cm}^3$,

and used U.S. Standard Atmosphere (1976) as the background atmosphere. Table 4.1 gives the terminal velocity as a function of the particle size.

4.2.3 Vertical Diffusion

In one-dimensional models, the vertical movement of

Table 4.1. Terminal Velocity V_t

	$\gamma (\mu\text{m})$	$V_t (\text{in/sec})$
1	1.00E-02	1.48E-06
2	1.26E-02	2.35E-06
3	1.59E-02	3.72E-06
4	2.00E-02	5.91E-06
5	2.52E-02	9.38E-06
6	3.17E-02	1.49E-05
7	4.00E-02	2.36E-05
8	5.04E-02	3.75E-05
9	6.35E-02	5.96E-05
10	8.00E-02	9.45E-05
11	1.01E-01	1.50E-04
12	1.27E-01	2.38E-04
13	1.60E-01	3.78E-04
14	2.02E-01	6.00E-04
15	2.54E-01	9.53E-04
16	3.20E-01	1.51E-03
17	4.03E-01	2.40E-03
18	5.08E-01	3.81E-03
19	6.40E-01	6.05E-03
20	8.06E-01	9.61E-03
21	1.02E+00	1.52E-02
22	1.28E+00	2.42E-02
23	1.61E+00	3.84E-02
24	2.03E+00	6.10E-02
25	2.56E+00	9.08E-02
26	3.23E+00	1.54E-01
27	4.06E+00	2.44E-01
28	5.12E+00	3.87E-01
29	6.45E+00	6.15E-01
30	8.13E+00	9.76E-01
31	1.02E+01	1.55E+00
32	1.29E+00	2.46E+00

stratospheric minor constituents is generally described by eddy diffusion processes. For small particles this can be an important transport mechanism. However, for relative large particles the gravitational sedimentation is perhaps the dominant transport mode. Generally, the vertical flux at the k th level of the aerosol particles due to eddy diffusion can be written as

$$\phi_k = -D n_m \frac{\partial}{\partial z} \left(\frac{n_p}{n_m} \right) \quad (4.8)$$

where n is the concentration, and n_m and n_p denote the air and aerosol, respectively; D is the eddy diffusion coefficient. In the model analysis, the set of diffusion coefficients given by Liu et al. (1984) is adopted for the computation. They derived the vertical diffusion coefficients for tropospheric application based on the results of Radon 222 tracer observations. They also showed the seasonal dependence of the diffusion coefficients. With the vertical flux given by Eq. (4.8), the increase of the aerosol particles with size u_i in the layer between the k th and

$(k-1)$ th levels in a time step Δt can then simply be calculated by

$$\Delta n_i = (\phi_k - \phi_{k-1}) \Delta t \quad (4.9)$$

In the calculation, the profile of n_m is adopted from the U.S. Standard Atmosphere (1976).

4.2.4 Backscattering Coefficient

The general expression for the volume backscattering coefficient β of aerosol particles illuminated with light of

wavelength λ is

$$\beta(180^\circ) = \int_0^\infty \sigma(\lambda, r, m, 180^\circ) f(r) dr \quad (4.10)$$

where r is the radius of the particle, $m = (n-ik)$ the complex refractive index, $f(r)dr$ the number of particles per unit volume with radius between r and $r+dr$, and $\sigma(\lambda, r, m, 180^\circ)$ is the backscattering cross section

$$\sigma = \frac{\lambda^2}{4\pi^2} \cdot \frac{i_1(\lambda, r, m, 180^\circ) + i_2(\lambda, r, m, 180^\circ)}{2} \quad (4.11)$$

where i_1 and i_2 are the Mie intensity distribution functions for light scattered at 180° . In the model, the integration over the particle size in Eq. 4.10 is carried out numerically. In doing this, the computed size spectrum is first fitted by a single log-normal or a bimodel aerosol distribution depending on the size spectrum. Then, the backscattering coefficient is determined with the size parameters obtained from the fitting processes. It will be shown later that a bimodel aerosol distribution is a better description in many cases, especially when the mixing of aerosol particles of two quite different size distributions is taking place.

4.3 NUMERICAL RESULTS AND DISCUSSION

The model described in the preceding section has been used to examine the evolution of aerosol size distribution and the backscattering of an aerosol plume involving coagulation,

sedimentation, and diffusion processes. The plume is assumed to extend from an altitude of 2 km to 4 km. In the regions below 1 km and between 4 km and 10 km, only the background aerosol particles are introduced in the model. The initial aerosol size distributions in various layers are given in terms of parameters of log-normal size distributions (Table 4.2).

In the analysis, it is assumed that the top layer (10th layer) is steady. In other words, the aerosol size distribution in the top layer does not change with time. In the calculation, a time step of 0.05 day is used. The solution from this time step has been compared with that of a time step of 0.1 day. It is found that the differences between the results obtained with $\Delta t = 0.1$ day and that with $\Delta t = 0.05$ day are less than 0.5% in all the layers considered. The discussion on the computed results of the first ten time steps using a 0.05 day increment are given below.

The time evolution of the aerosol size distribution in the first layer is given in Figure 4.2. In the figure, the initial size distribution is given by the solid line. Only the results of every other time step computations are shown. It is interesting to note that the concentration of the aerosol particles with size greater than about 0.05 μm show a sequential increase during the calculated ten steps. On the other hand, a decrease in the concentration of particles with size less than 0.05 μm is also noticeable. This decrease in the concentration

Table 4.2. Initial Aerosol Size Distribution

No. (particles/cm³), r_g (mode radius), σ (width of log-normal curve)

Layer No.	Altitude (km)	No.	r_g (μm)	σ
1	0 - 1	7.0	0.3	2.512
2	1 - 2	10.0	1.0	2.0
3	2 - 3	10.0	1.0	2.0
4	3 - 4	10.0	1.0	2.0
5	4 - 5	3.1	0.151	1.5
6	5 - 6	3.1	0.151	1.5
7	6 - 7	3.1	0.151	1.5
8	7 - 8	3.1	0.151	1.5
9	8 - 9	3.1	0.151	1.5
10	9 - 10	3.1	0.151	1.5

of smaller size particles can be attributed to coagulation, sedimentation, and diffusion processes. As to the increase in the number concentration of larger particles in the first layer, sedimentation and diffusion must be the main mechanisms since there is a dust layer right above this first model layer. The time evolution of the size distribution of the second layer is shown in Fig. 4.3. The main feature of this figure is the increase in number concentration of particles with radius smaller than $0.05\text{ }\mu\text{m}$. Very little change is found for larger particles. The increase in concentration of smaller particles is mainly due to diffusion processes which bring in these smaller particles from the layer immediately below. The corresponding time evolution of the size distributions of layer No. 3 is given in Fig. 4.4. It shows that little change has occurred in the first ten time steps. However, a slightly increase in the number concentration of small particles is noticeable. Fig. 4.5 shows the time variations of the size distributions for the layer No. 4, which is the upper part of the entire dust layer of this model computation. The noticeable features of Fig. 4.5 are the enrichment of small particles ($< 0.03\text{ }\mu\text{m}$), and reduction of larger particles. These features can only arise through sedimentation and diffusion processes; not aerosol coagulation processes, since the latter will cause the changes in opposite directions. By inspection, one may find that the increase in the number of small particle in the layer No. 4 can be linked with the background aerosol particles in the layer No. 5 (Fig. 4.6).

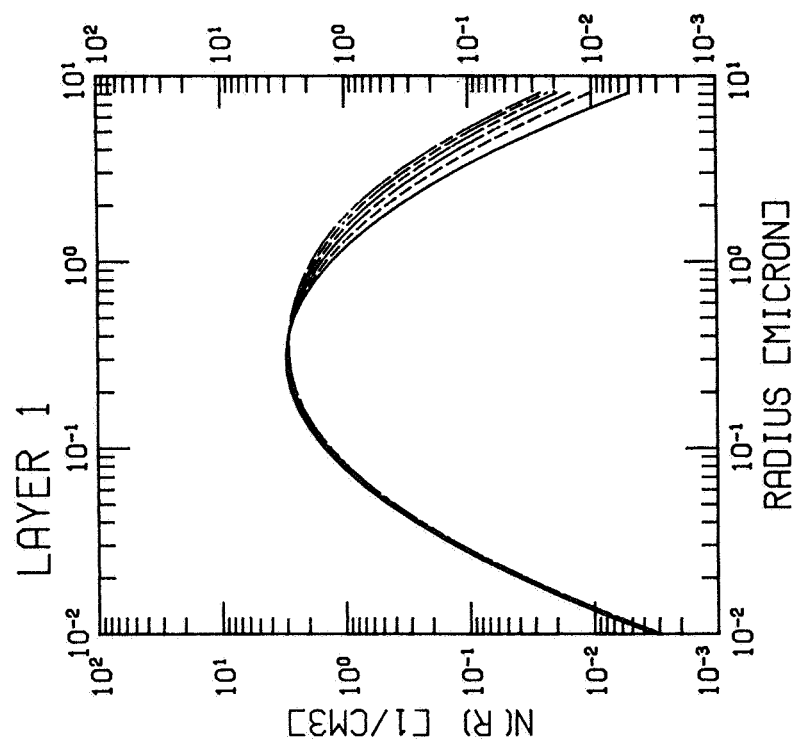


Figure 4.2. Time evolution of the aerosol size distribution in layer no. 1. The initial distribution is given by the solid line, and

-----	is the distribution at $2\Delta t$
-----	" " " at $4\Delta t$
-----	" " " at $6\Delta t$
-----	" " " at $8\Delta t$
-----	" " " at $10\Delta t$,
($t = 0.05$ day)	

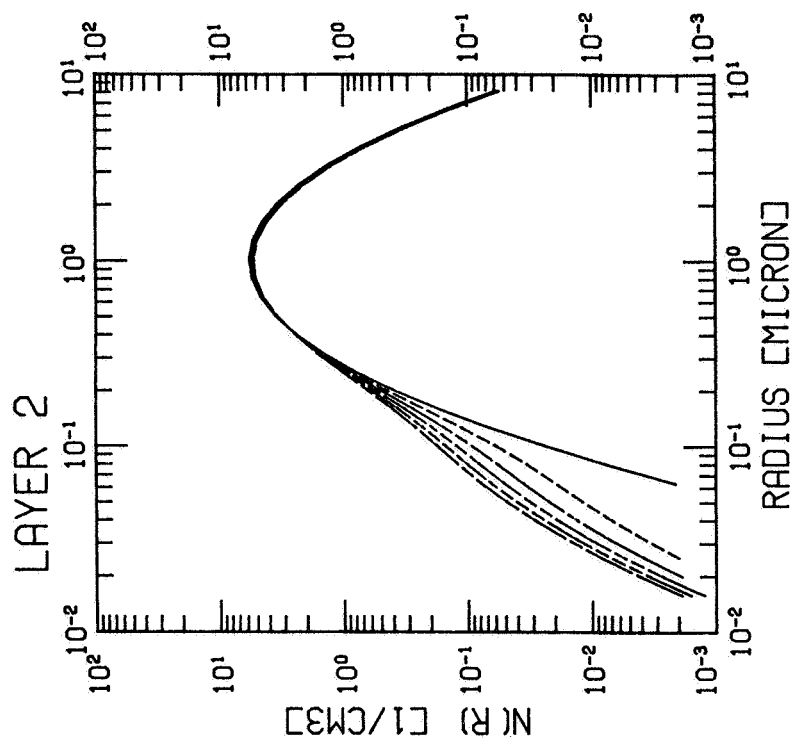


Figure 4.3. As Fig. 4.2, but for layer no. 2.

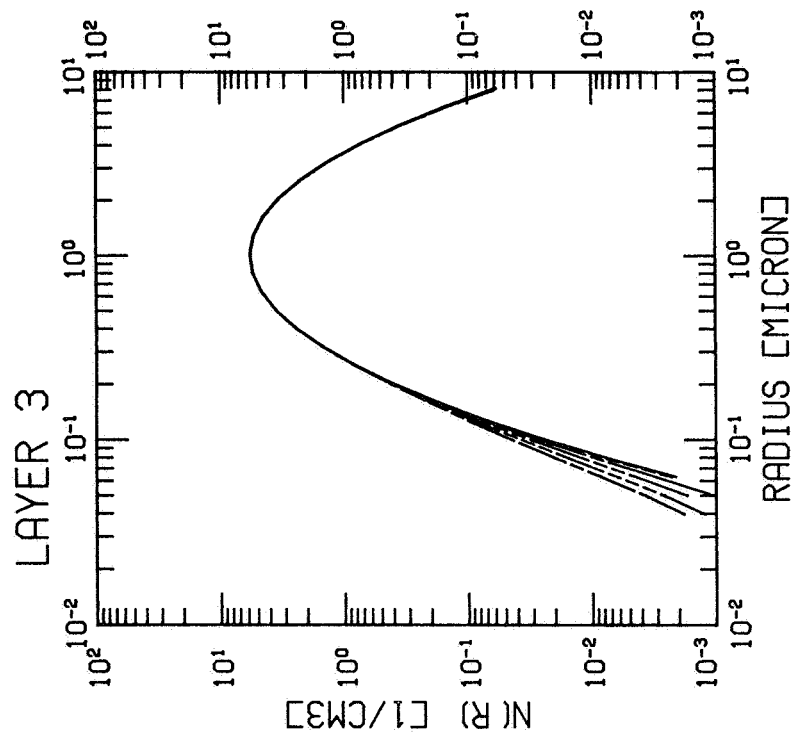


Figure 4.4. As Fig. 4.2, but for layer No. 3.

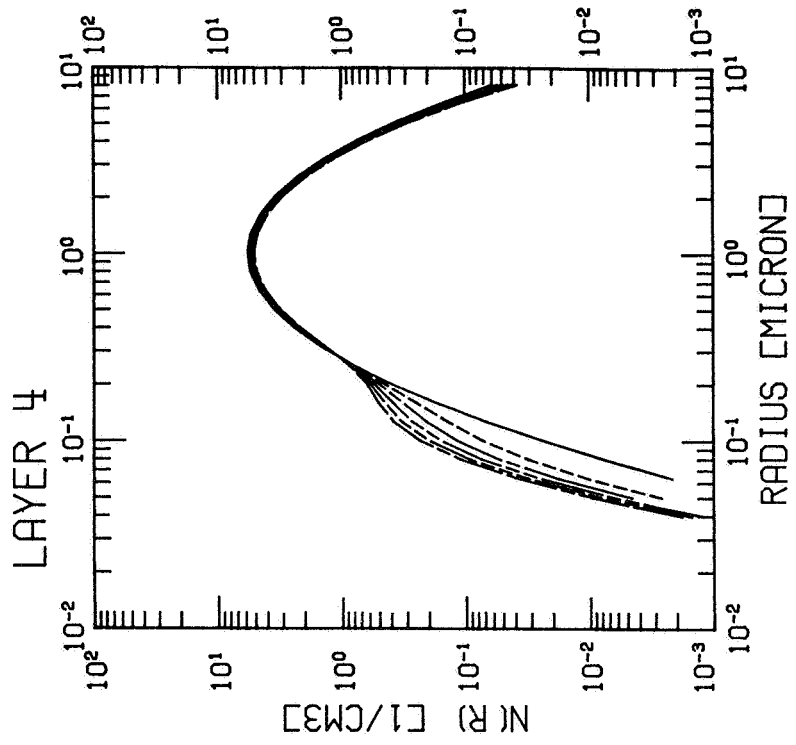


Figure 4.5. As Fig. 4.2, but for layer No. 4.

Fig. 4.6 displays the time variation of the aerosol size distribution in the layer No. 5. The increase in large size particles ($r > 0.04 \mu\text{m}$) are clearly shown. By inspection of the aerosol size distributions in the layer No. 4, it is clear that the appearance of the larger size particles is primarily due to diffusion processes which bring in these particles from the model dust layer. From Fig. 4.6, a slight reduction in the number of background aerosol particles is also noticeable, which can be linked to the increase of the number concentration of particles of the corresponding size in the layer No. 4. Since, like the layer No. 5, the aerosol particles in the layers above No. 5 are specified as background aerosols with the same size distribution, the behavior of their aerosol size distributions (not shown) are found to have similar features to those of layer No. 5, but of much less intensity. It should be mentioned that, as clearly shown in Figs. 4.5 and 4.6, there is mixing of aerosol particles with two quite different size distributions taking place in the layers No. 4 and 5 as a result of sedimentation and diffusion processes. For this reason, a bimodel fitting process is introduced in the model computation. This is done by fitting the aerosol size spectrum with a single log-normal mode first. Then the differences in the differential aerosol concentrations between the original size spectrum and the fitted curve at the assigned particle radii (Table 4.1) was determined. A scan procedure is then applied to search the maximum difference. A second curve fitting process is performed if this maximum

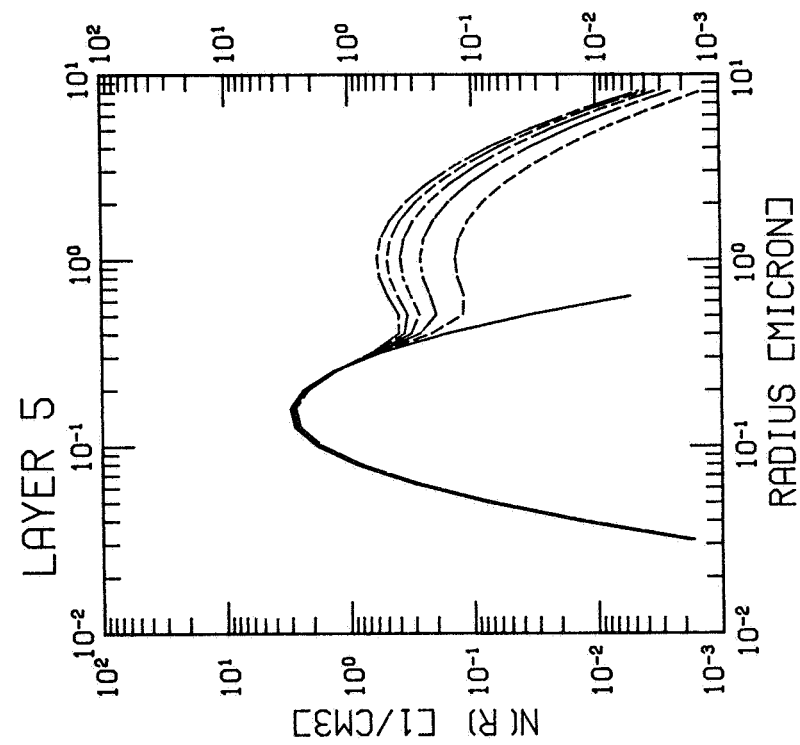


Figure 4.6. As Fig. 4.2, but for layer No. 5.

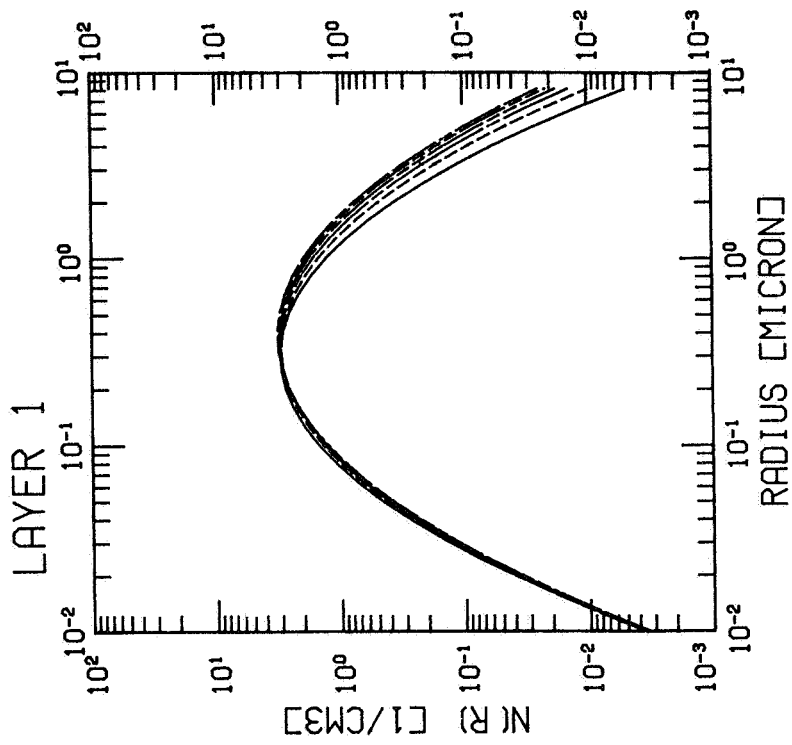


Figure 4.7. As Fig. 4.2, except that the size distribution curves are derived from model size distribution parameters obtained by fitting to the curves in Fig. 4.2.

Table 4.3. Results of Curve Fitting at the Tenth Time Step

Layer No.	n_o	r_g	σ	n_o	r_g	σ
1	7.85(0)	3.822(-1)	2.667(0)	--	--	--
2	9.36(0)	9.804(-1)	2.020(0)	3.65(-1)	1.876(-1)	1.906(0)
3	9.88(0)	9.986(-1)	1.999(0)	4.34(-2)	1.628(-1)	1.653(0)
4	8.73(0)	9.946(-1)	1.987(0)	3.76(-1)	1.532(-1)	1.519(0)
5	3.11(0)	1.491(-1)	1.652(0)	9.56(-1)	1.025(0)	1.904(0)
6	3.10(0)	1.508(-1)	1.509(0)	5.45(-2)	1.012(0)	1.939(0)
7	3.10(0)	1.510(-1)	1.500(0)	--	--	--
8	3.10(0)	1.510(-1)	1.509(0)	--	--	--
9	3.10(0)	1.510(-1)	1.500(0)	--	--	--
10	3.10(0)	1.510(-1)	1.500(0)	--	--	--

difference is greater than $5 \times 10^{-3} (\text{cm}^{-3})$. Table 4.3 presents the results of this fitting processes after ten steps of computation. Figs. 4.7 to 4.11 are the plots of the fitted size distributions for model layers from No. 1 to No. 5, respectively. By comparing them with the corresponding Figs. 4.2 to 4.6, one can see that the fitted size distributions correspond closely to the original size distributions.

As mentioned earlier, (Sec. 4.1), one of the objectives of this study is to examine the possible effects of the coagulation, sedimentation, and diffusion processes on the aerosol backscattering at CO₂ wavelengths (10.6 μm). The time evolution of the vertical profile of the aerosol backscattering coefficients is given in Fig. 4.12. In Fig. 4.12, the symbols \circ , \square , \diamond , \triangle , Δ , and ∇ correspond to the computed results at time steps of 0, 2, 4, 6, 8, and 10, respectively. It shows high values of the coefficients in the layers No. 2 to No. 4, corresponding to the model dust layer. In this dust layer, Fig. 4.12 shows no noticeable changes in the backscattering coefficients. On the other hand, changes can be found in the layers immediately below and above this dust layer. It is interesting to note that the layer No. 6 does not show any change until after the 4th time step of the computation. In addition, the changes taking place in layers No. 5 and No. 6 are mainly due to the vertical diffusion processes which bring up the large particles from the model dust layer.

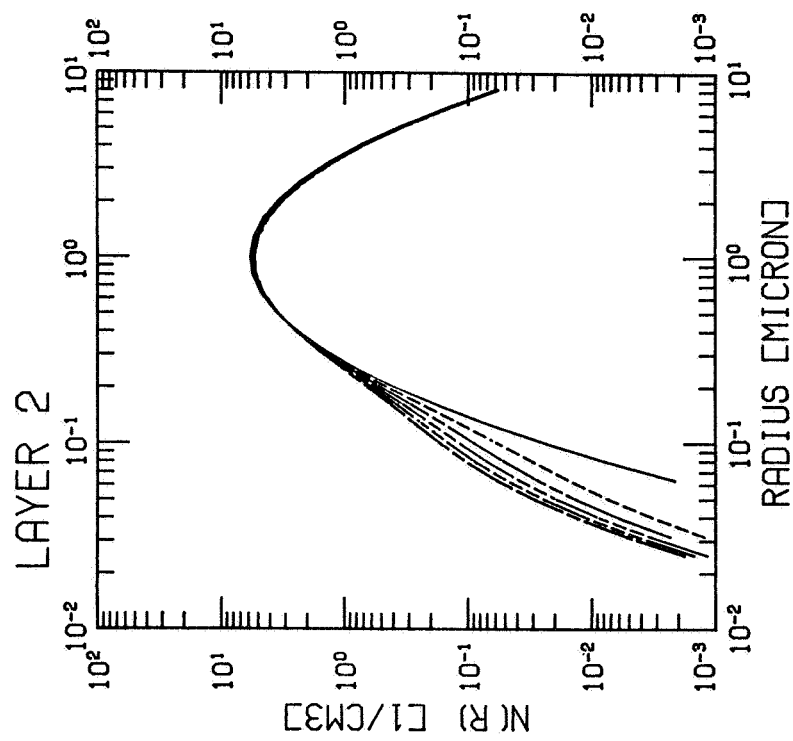


Figure 4.8. As Fig. 4.7, but corresponding to Fig. 4.3.

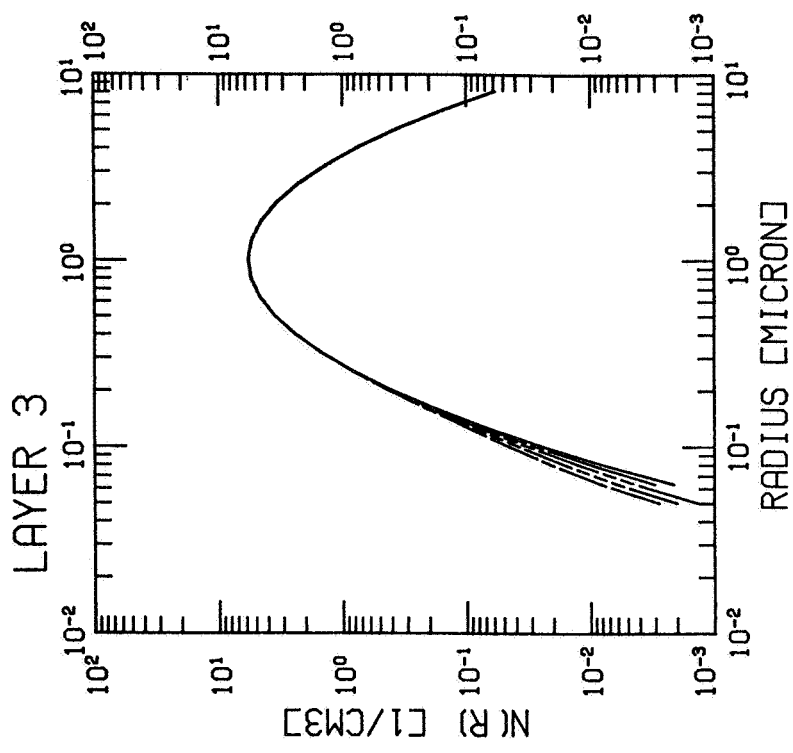


Figure 4.9. As Fig. 4.7, but corresponding to Fig. 4.4.

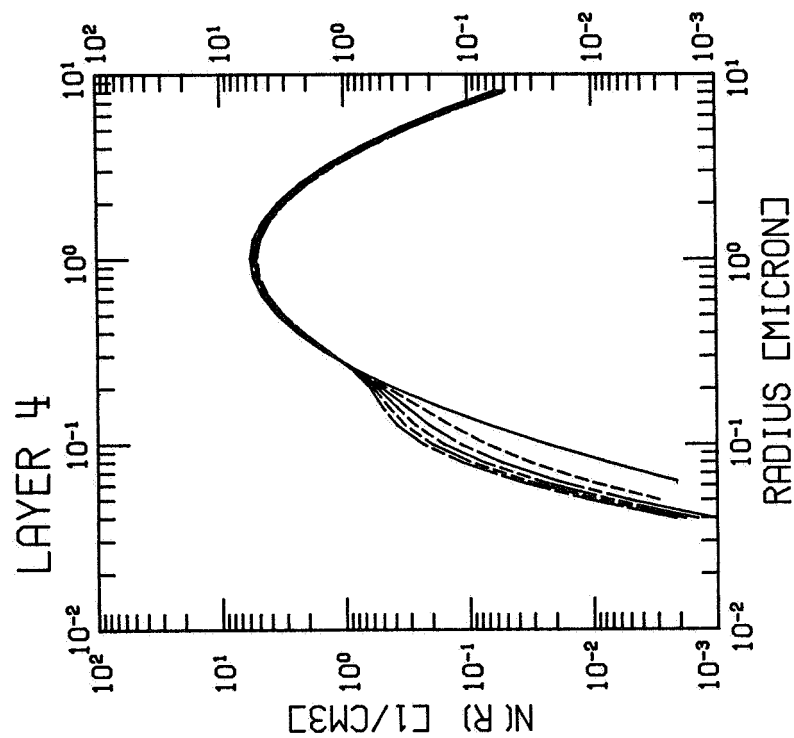


Figure 4.10. As Fig. 4.7, but corresponding to Fig. 4.5.

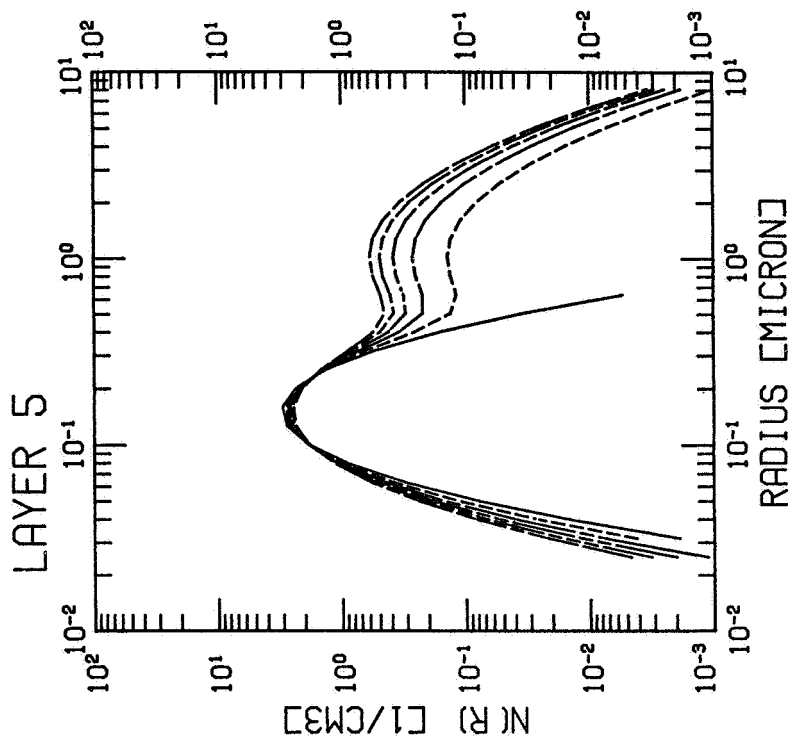


Figure 4.11. As Fig. 4.7, but corresponding to Fig. 4.6.

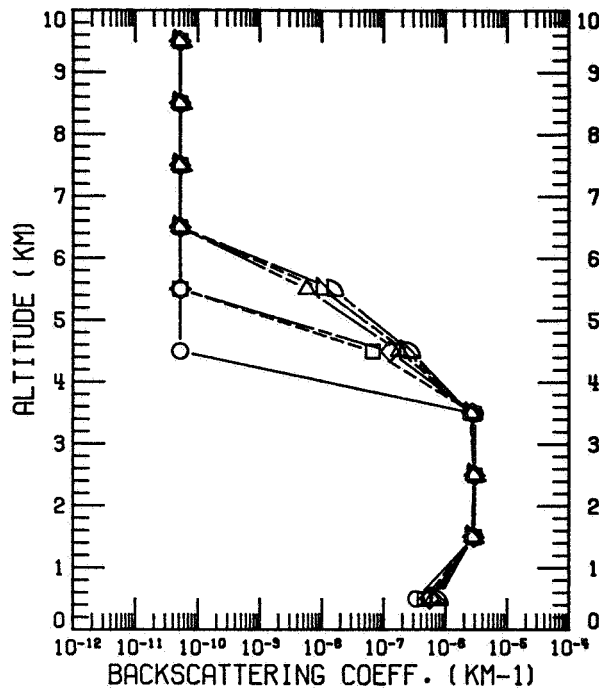


Figure 4.12. Time evolution of the $10.6 \mu\text{m}$ backscattering function in the model analysis.

- O initial profile,
- at $2 \Delta t$
- ◊ at $4 \Delta t$
- △ at $6 \Delta t$
- ▽ at $8 \Delta t$
- ◐ at $10 \Delta t$
- ($\Delta t = 0.05 \text{ day}$)

$n = 1.75 - 0.3i$ for both components of the aerosol

4.4 DISCUSSION AND REMARKS

The aerosol plume model described in this chapter is able to simulate the essential effect of the coagulation, sedimentation, and vertical transport, on the aerosol size distributions and the aerosol backscattering at CO₂ wavelength (10.6 μ m). Although the

model does not include the aerosol growth effect of condensation and evaporation processes (Deepak et al., 1982), an attempt has been made to apply the developed model to an observational case study. A transport of Asian desert aerosol during the spring of 1979 has been reported by Shaw (1980), based on observations over the Hawaiian Islands and trajectory analysis. A dust layer of 1 km thick was observed with the layer centered at 3.5 - 4 km altitude. SAGE sampling (sunrise measurements) swept gradually

over the Pacific Ocean from latitude about 12° to 44° N during the period from April 21 to 28, 1979 which coincides with the observed Asian dust event. SAGE profiles during this period have then been examined at altitudes 4 and 6 km. Unfortunately, it was found that many of the SAGE profiles stop at higher altitudes. As a result, there is not enough aerosol information to give an appropriate picture of this particular dust event.

5. CONVERSION OF SAGE I/SAM II EXTINCTION TO 10.6 μm BACKSCATTER

5.1 INTRODUCTION

Conversion of a 1 μm SAGE I/SAM II extinction cross section to the equivalent backscatter function at 10.6 μm requires knowledge or assumptions concerning the aerosol size distribution and composition, or alternatively of their general optical behavior. In an earlier report, Deepak et al (1982) modeled the ratio $\beta_{10.6} / \sigma_{1.00}$ as a function of aerosol composition for log-normal model of varying mode radii. A summary diagram, showing the results of this modeling is reproduced in Fig. 5.1. The range for the conversion factor $\beta_{10.6} / \sigma_{1.00}$ shown here is three orders of magnitude, sufficiently wide to make it of little practical value. This range may be reduced somewhat if we restrict ourselves to the free troposphere and take account of the fact that the bulk of the smaller aerosols are water soluble in composition and that the larger aerosols consist mainly of dust. We may then suppose $\beta_{10.6} / \sigma_{1.00}$ to lie between 10^{-4} and 10^{-2} sr^{-1} . To improve on this range of values, which is still too great, we have chosen to develop a bimodal model to describe the aerosol. This has been combined with the size distributions measured during the GAMETAG experiments and described in Chapter 3 of this report.

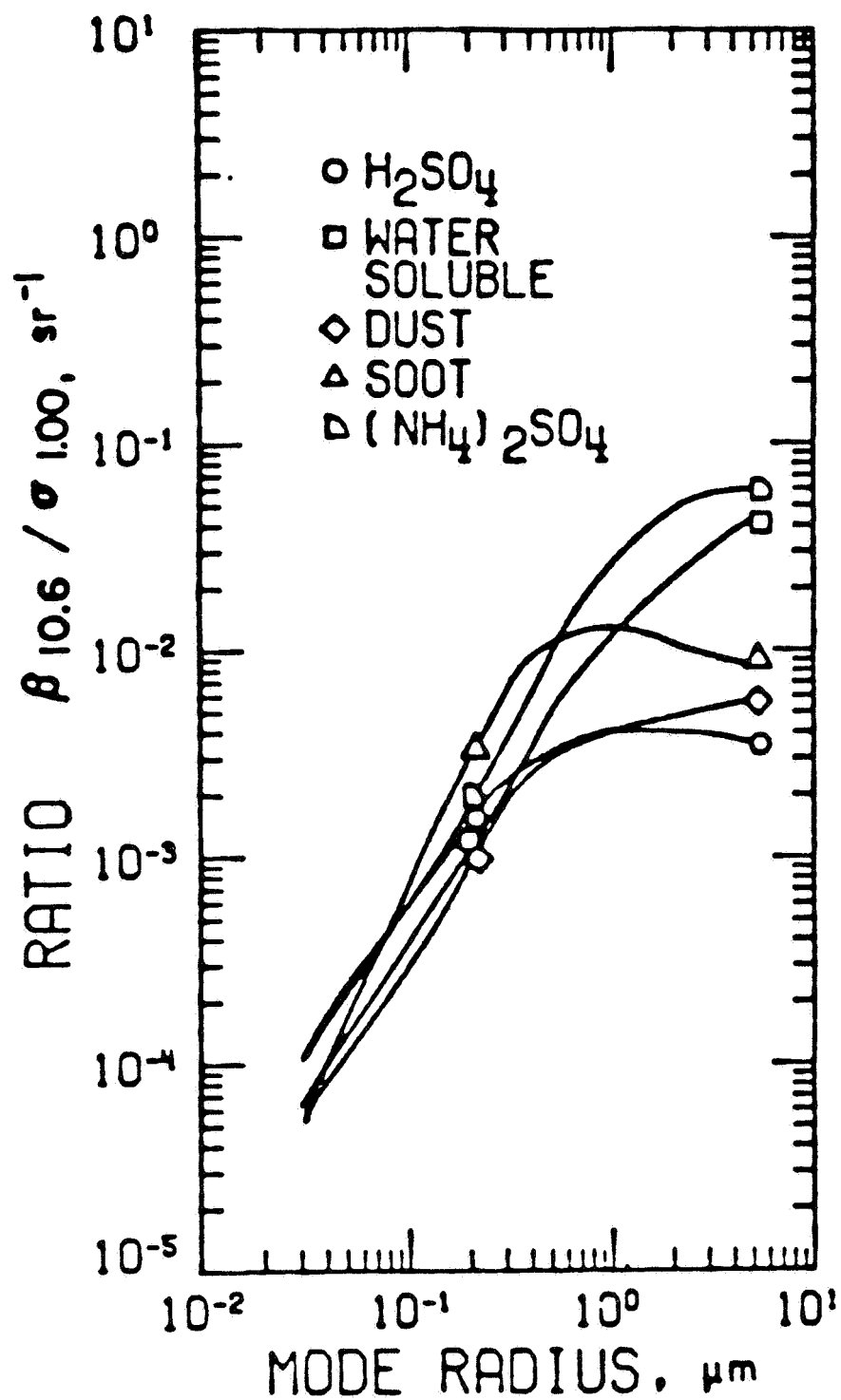


Figure 5.1. Backscatter to extinction ratios $\beta_{10.6}/\sigma_{1.00}$ shown as a function of log-normal mode radius.

5.2 BIMODAL SIZE DISTRIBUTION AND FITTING TO THE GAMETAG DATA

Aerosol size distributions measured during the GAMETAG flight series have been fitted to a bimodal model of the form

$$\begin{aligned} dN(r)/d \log(r) = & A_1 \exp(-k_1 \ln^2(r/r_{g1})) \\ & + A_2 \exp(-k_2 \ln^2(r/r_{g2})) \end{aligned} \quad (5.1)$$

where $k_1 = 1/(2 \ln^2 \sigma_{g1})$ and $k_2 = 1/(2 \ln^2 \sigma_{g2})$

In this equation, r is the particle radius and $N(r)$ the cumulative particle number. $A_1, A_2, r_{g1}, r_{g2}, \sigma_{g1}$ and σ_{g2} are constants describing the log normal distributions. Computer software has been written which will fit Eq. (5.1) exactly to six data points which may be in the form $dN(r)/d \log(r)$ as a function of r or $N(r)$ as a function of r . The program output contains the six constants that describe the bimodal distribution. An example of its application to simulated data is shown in Fig. 5.2 where the experimental points are shown by round dots, the individual fitted curves by dashed lines and the total fitted bimodal distribution by the solid line.

The experimental size distributions used are those listed in Appendix B and described in Chapter 3. They represent particle counts obtained for twenty-minute flight segments, the nine size intervals being as listed in Table B.1, covering the size range 0.128 - 2.34 μm . Forty-two flight segments were chosen,

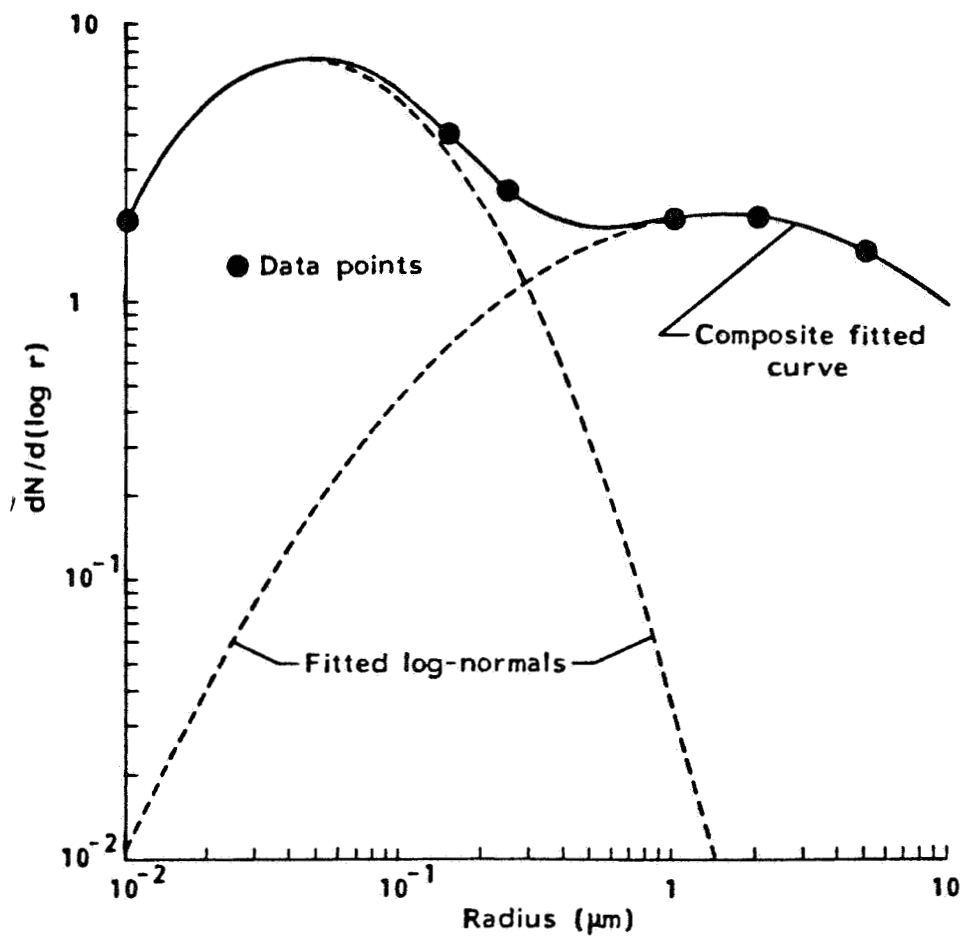


Fig.5.2. Example of the application of the bi-modal log-normal fitting program to a simulated experimental size distribution.

measurements being made at altitudes between approximately 5 and 7 kilometers and representative of the whole range of latitudes covered by the two flight series. Data segments where the particle counts were obviously enhanced due to the presence of haze or cloud were avoided. Three additional size distributions were added from earlier published data (Patterson et al., 1980). Size distribution data are available for these flight segments at a maximum of nine radii, although inspection of the data in Appendix B shows that the channels representing the largest particle sizes were frequently empty, particularly over the southern hemisphere. The remaining seven or eight data points are nevertheless still in excess of the number required to solve Eq. (5.1). In order to obtain the best estimate of the log-normal constants, the size distributions were plotted and the six data points (from the possible maximum of nine) most representative of the distribution were used as input to the fitting program. In almost all cases, an exact fit was either obtained directly or after making a small adjustment to the counts in one channel only. Two cases were rejected where reasonable fits could not be obtained. Figure 5.3 shows histograms of the resultant values of σ_{g1} , σ_{g2} , r_{g1} , and r_{g2} . It can be seen that, for the accumulation mode, values of σ_{g1} lie between 1.1 and 2.0 while r_{g1} lies between 0.06 and 0.20 μm . For the coarse particle mode, the distribution is somewhat narrower, most values of σ_{g2} lying between 1.0 and 1.5 with r_{g2} values peaking at around 0.6 μm . The somewhat greater imprecision for the accumulation mode is at

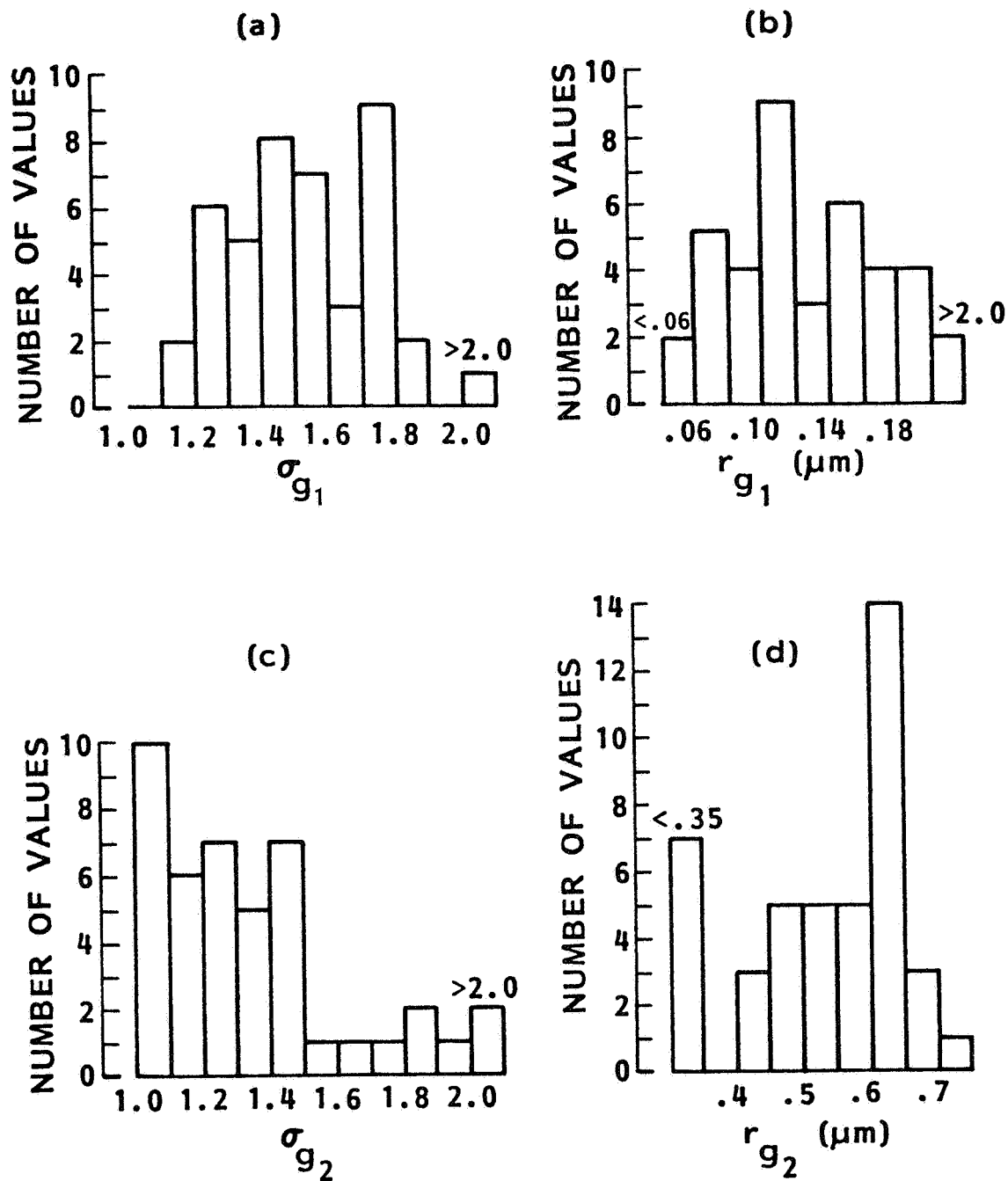


Figure 5.3. Histograms of the log-normal parameters obtained from the bimodal fitting program.

- (a) σ_{g1} : accumulation mode
- (b) r_{g1} : accumulation mode
- (c) σ_{g2} : coarse particle mode
- (d) r_{g2} : coarse particle mode

least partially due to the fact that the experimental size ranges did not cover particle sizes less than 0.126 μm .

5.3 BIMODAL OPTICAL MODEL AND COMPARISON OF SAGE I/SAM II AND GAMETAG DATA

The bimodal model described in the previous section has been used in conjunction with the AGAUS Mie scattering program to calculate the optical properties of the GAMETAG size distributions. We have assumed the log normal mode of smallest radius (accumulation mode) to consist entirely of water soluble aerosol and the mode of greatest radius (coarse particle mode) to consist entirely of a dust-type aerosol. The refractive indices at 1.00 μm and 10.6 μm are those used previously by Deepak et al. (1982) and are listed in Table 5.1. This model is very similar to, but not identical to, that used by Georgia Institute of Technology to calculate the optical data presented in Chapter 3 and Appendix A. In the latter case, a two-composition model is used, the division between the two components being made at a particle radius of 0.5 μm rather than in terms of independently-fitted log-normal functions. Comparison of optical properties calculated by the two alternative models shows good agreement, any differences being much less than observed changes due to natural aerosol variation.

In order to compare the GAMETAG and SAGE I/SAM II data sets, the forty-three size distributions described in Section 5.2 have

Table 5.1. Refractive Indices Used for Mie Scattering Calculations

<u>Aerosol Material</u>	Wavelength	
	<u>1.00 μm</u>	<u>10.6 μm</u>
Dust-like	1.520 - 0.008i	1.620 - 0.120i
Water Soluble	1.520 - 0.017i	1.760 - 0.070i

been used in conjunction with the above model to calculate corresponding equivalent extinction values at $1\ \mu\text{m}$. The results of these calculations are shown in Fig. 5.4(a) and (b) for the 1977 and 1978 flights, respectively. As the 1977 flights were made in May and June and the 1978 flights in August and September (September 1st and 2nd only), the data in these figures may be compared with that shown in Fig. 2.6(a) (March-May, 1979) and Fig. 2.6(b) (June-August, 1979). The $1\ \mu\text{m}$ extinction values calculated for the 1977 flight data (Fig. 5.4(a)) agree well with the direct SAGE I/SAM II measurements for June-August, 1979 (Fig. 2.6(b)). The absolute magnitudes of the extinction values are very close and a similar latitude variation occurs in both data sets. The 1978 GAMETAG flight data extends over a wider latitude range than the 1977 data and shows greater latitudinal variation. Among the calculated values for $\sigma_{1.00}$, the northern hemisphere values [Fig. 5.4(b)] agree well with the direct SAGE I/SAM II measurements [Fig. 2.6(a)]; the southern hemisphere values are somewhat lower than the direct measurements by about a factor of two. This difference between the two GAMETAG data sets for latitudes south of the equator has been noted in Chapter 3. It is believed to be due to a genuine variation in the aerosol characteristics observed in the two years and does not reflect any instrumental uncertainty.

Bearing in mind the fact that the GAMETAG data was obtained during two cross-sectional flights limited in time and longitude,

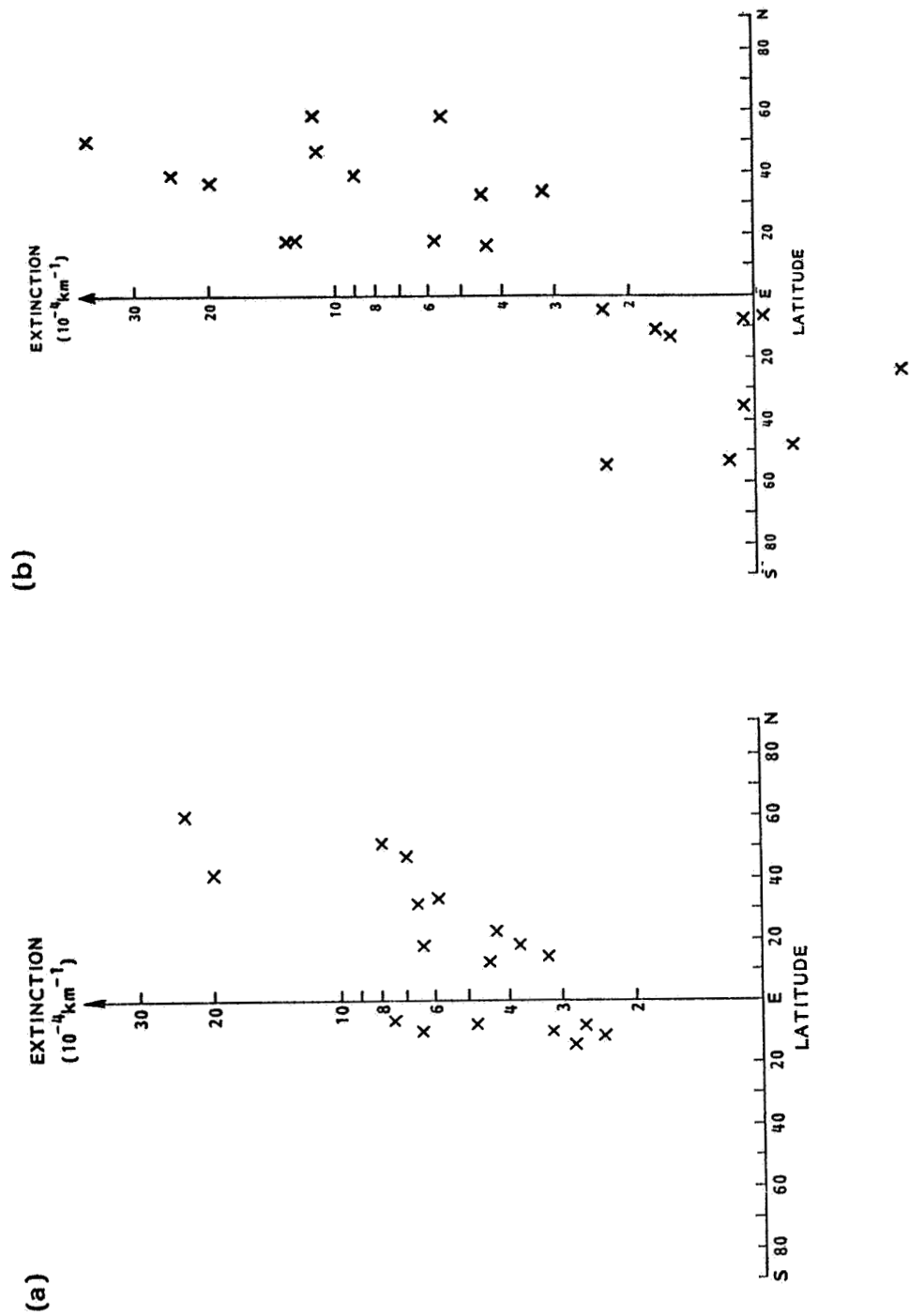


Figure 5.4. $1 \mu\text{m}$ extinction values calculated from size distributions measured during the GAMETAG flights.

the agreement between the calculated 1 μ m extinction values and the SAGE I/SAM II direct measurements must be considered to be within the range of expected variations. Based on this agreement, we have used conversion factors for $\beta_{10.6}/\sigma_{1.00}$ calculated from the GAMETAG data to correct the 1 μ m SAGE I/SAM II data to the equivalent backscatter at 10.6 μ m.

5.4 DERIVATION OF A CONVERSION FACTOR AND ITS APPLICATION

The forty-three bimodal size distributions taken from the GAMETAG data set, as described in the previous section, have been used to calculate values for the conversion factor $\beta_{10.6}/\sigma_{1.00}$. The calculated values are shown in the form of a scatter plot as a function of $\sigma_{1.00}$ in Fig. 5.5. The majority of the values lie between 10^{-4} and 10^{-3} sr^{-1} and there is a small but definite trend in the data, larger values of $\beta_{10.6}/\sigma_{1.00}$ being associated with larger values of $\sigma_{1.00}$. This is to be expected as distributions containing relatively more large particles will show increased values of both $\beta_{10.6}/\sigma_{1.00}$ and $\sigma_{1.00}$. A regression line for $\beta_{10.6}/\sigma_{1.00}$ (as the dependent variable) on $\sigma_{1.00}$ (as the independent variable), using logarithmic coordinates, has been calculated, and is shown in the figure. Seventy-five percent of the calculated values lie within a factor of two of this line.

The data shown in Fig. 5.5 has been obtained at altitudes of 5-7 km and is strictly applicable only to this altitude range. In spite of this, we have chosen to apply it to all SAGE I/SAM II

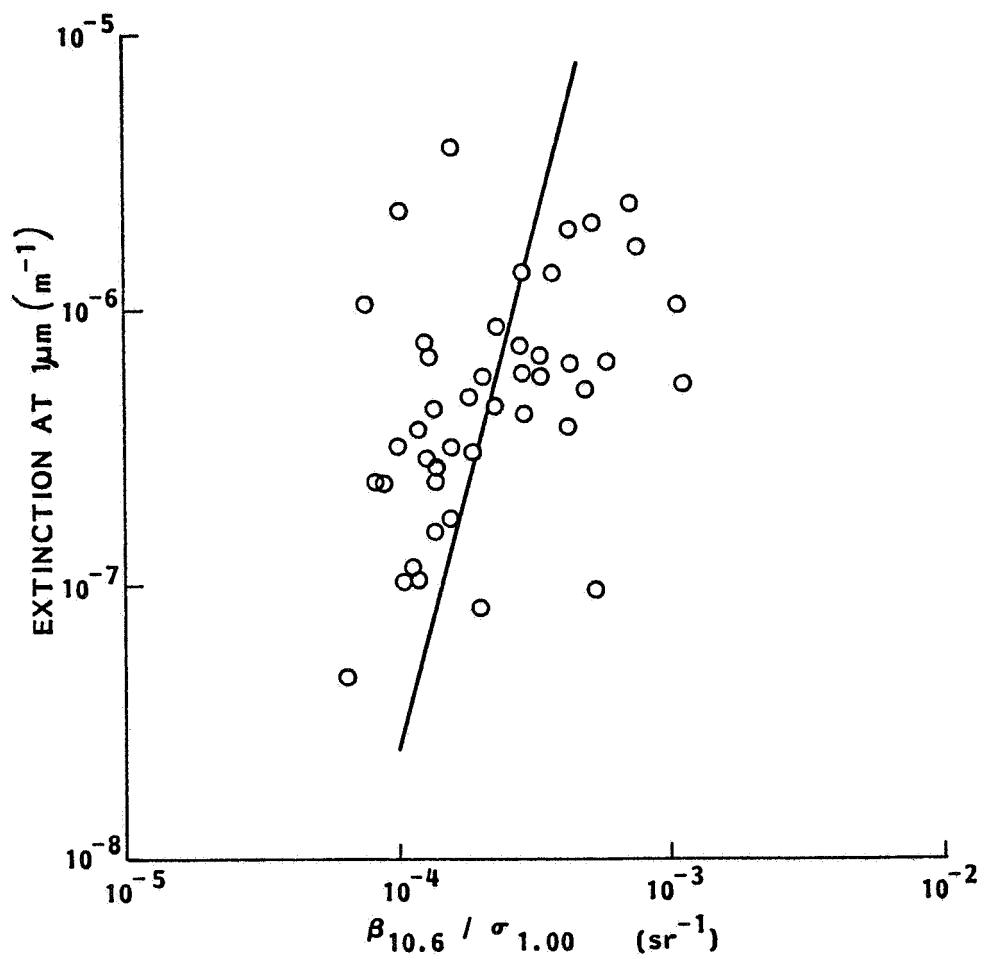


Figure 5.5. Scatter plot of values of $\beta_{10.6}/\sigma_{1.00}$ as a function of $\sigma_{1.00}$. Data is for an altitude of 5-7 km and taken from the 1977-78 GAMETAG flights. The figure also shows the best fit regression line for $\beta_{10.6}/\sigma_{1.00}$ upon $\sigma_{1.00}$.

tropospheric data above about 4 km. Some error may be expected at 4 km (and below) because of relatively increased numbers of large particles; these will increase $\beta_{10.6}/\sigma_{1.00}$ faster than they will increase $\sigma_{1.00}$. At the higher altitudes near the tropopause, the aerosol composition will most likely contain a high percentage of sulfuric acid and its optical properties will merge into those of the stratospheric aerosol. The size distribution will also be strongly dependent upon volcanic input and the conversion factor likewise highly variable (Kent et al., 1984). Despite these limitations, it is felt that the regression line shown in Fig. 5.5 is a good approximation for use, during a volcanically quiet period, in the middle and upper free troposphere.

Table 5.2 contains a list of conversion factors corresponding to the regression line in Fig. 5.5. This has been applied to the contour plots of 1 μm extinction shown in Fig. 2.8. The results of this are shown in Fig. 5.6(a) and (b) for the March-May and September-November, 1979 seasons, respectively. We see that, in the middle and upper free troposphere, southern hemisphere values for $\beta_{10.6}$ range between 3×10^{-11} and 2×10^{-10} . In the northern hemisphere, values are greater at all altitudes becoming as large as 7×10^{-10} in March-May, 1979 at 5 km and 70N. The latitudinal and seasonal variation is very pronounced, as is the variation with altitude. It must be emphasized that these are seasonal median values and daily values

**Table 5.2. Conversion Factors Used with the SAGE I/
SAM II Free Tropospheric Data Sets**

$\sigma_{1.00}$ (10^{-7} m^{-1})	$\beta_{10.6}/\sigma_{1.00}$ (10^{-4} sr^{-1})
1.0	1.34
1.5	1.53
2.0	1.67
3.0	1.89
4.0	2.07
5.0	2.22
6.0	2.35
8.0	2.57
10.0	2.75
15.0	3.12
20.0	3.42

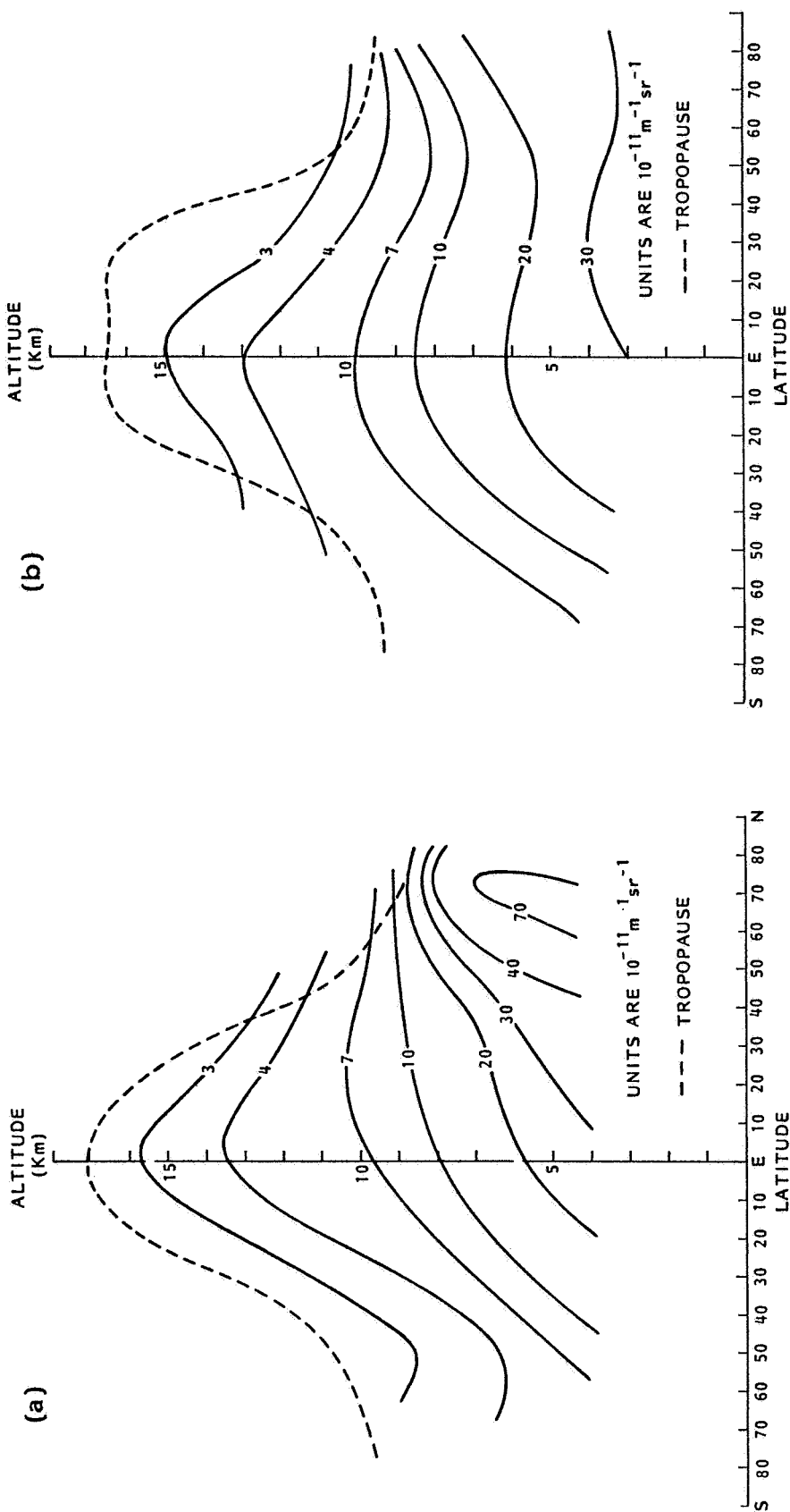


Figure 5.6. Contour plots of the free tropospheric backscatter function at $10.6 \mu\text{m}$ derived from the SAGE I/SAM II data set.

would be expected to depart considerably from them. In addition, they correspond to a volcanically quiet period; during the present, more volcanically active period, upper tropospheric values would be considerably increased.

6. CO₂ LIDAR MEASUREMENTS OF $\beta_{10.6}$

6.1 PUBLISHED MEASUREMENTS

Published measurements of aerosol backscatter cross sections in the free troposphere using CO₂ lidar systems are scarce. The most extensive data series is that made at NOAA in Boulder, Colorado (Post et al., 1982; Post, 1984a). Measurements have also been made at NASA-MSFC, Huntsville, Alabama (Weaver, 1983; Jones, 1983) and JPL, Pasadena, California (Menzies et al., 1984). Updates to these data sets have recently been presented at the Third NASA/NOAA Infrared Lidar Backscatter Workshop, Lake Tahoe, Nevada, January 14, 1985. These data sets have all been obtained over, or close to, the continental U.S.A. There is, in addition, an extensive unpublished data set obtained by the Royal Signals and Radar Establishment, United Kingdom over the United Kingdom and Europe (Vaughan, 1985).

The earliest published data that extends to altitudes above 4-5 km (Post et al., 1982) was taken in the Spring and Summer of 1981 when the atmosphere was affected by aerosol produced in recent volcanic eruptions. The only earlier data, which shows conditions prior to these eruptions is that of Schweisow et al. (1981). This data, taken in 1978, does not extend above 5 km (4 km for most of the data) and thus does not describe conditions in the middle and upper free troposphere. Data, since 1981, has

been very strongly affected by the eruption of El Chichon in April, 1982 and we therefore have no direct measurements of background non-volcanic aerosol scattering cross sections in the upper free troposphere.

6.2 VARIATION OF $\beta_{10.6}$ WITH ALTITUDE AND SEASON

Figure 6.1 summarizes the measured variation of $\beta_{10.6}$ with altitude. Figure 6.1(a) shows eight seasonal averages for $\beta_{10.6}$ measured by NOAA (Post, 1983; Post, 1984a), Figure 6.1(b) shows a single seasonal average obtained by JPL (Menzies, 1984) and Figure 6.1(c) and (d) show individual profiles measured by the NASA-MFC airborne system over California in 1981 and 1982, respectively (Jones, 1983). Table 6.1 summarizes the main characteristic of the RSRE measurements (Vaughan, 1983). Although these data have been obtained by several different instruments and at different times and locations, several general features may be identified.

1. Maximum values for $\beta_{10.6}$ occur in the boundary layer where $\beta_{10.6}$ is greater than 10^{-8}

2. Above the boundary layer, $\beta_{10.6}$ falls rapidly to a rather broad minimum between about 5 and 10 km altitude. Values in this minimum lie mainly in the range $3 \times 10^{-11} - 3 \times 10^{-10} \text{ m}^{-1} \text{ sr}^{-1}$.

3. Above the minimum, values rise into the stratosphere where peak values of the order of $10^{-9} \text{ m}^{-1} \text{ sr}^{-1}$ may be found

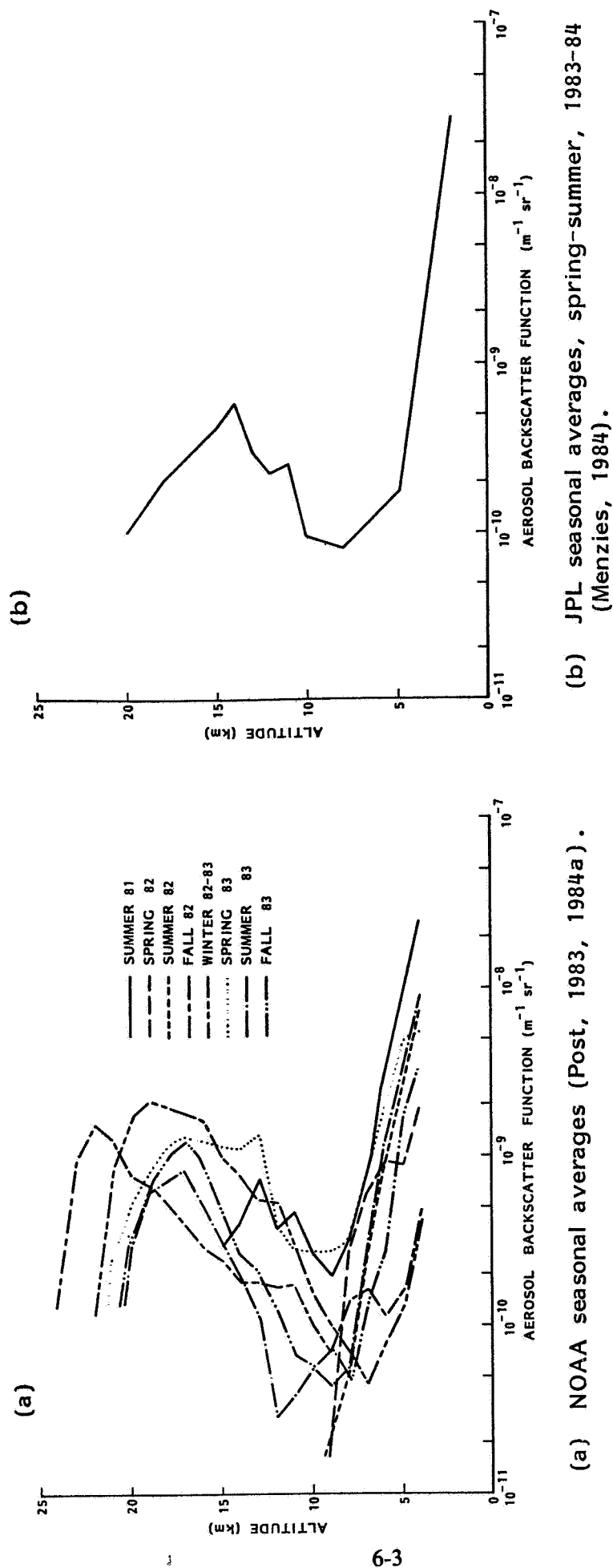
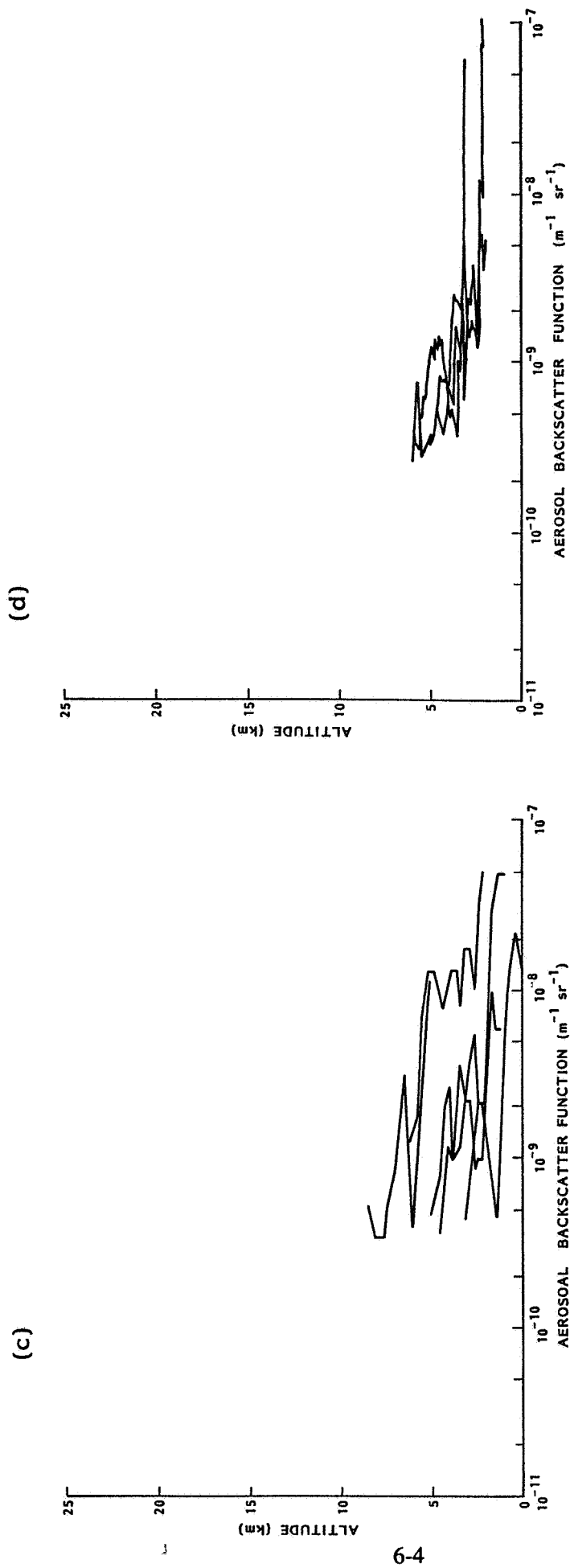


Figure 6.1. Measured values for $\beta_{10.6}$ in the free troposphere.



(c) NASA-MSFC, 1981 individual profiles
(Jones, 1983).

(d) NASA-MSFC, 1982 individual profiles
(Jones, 1983).

Figure 6.1. Measured values for $\beta_{10.6}$ in the free troposphere.

Table 6.1. Royal Signal and Radar Establishment
 β_{CO_2} Measurements (D. M. Vaughan, 1983)

<u>Location</u>	<u>Season</u>	<u>Altitude</u>	<u>β_{CO_2} ($m^{-1}sr^{-1}$)</u>
United Kingdom	Spring, Summer, Fall	Sea Level to 13 km	$> 3 \times 10^{-11}$ 95% of the time
United Kingdom	Winter	4.5 km to 13 km	$> 3 \times 10^{-11}$ 60% of the time
North Atlantic	June, July 1982		$> 4 \times 10^{-11}$ 100% of the time

(post-volcanic).

Apart from these general characteristics of the vertical profile, more specific characteristics of $\beta_{10.6}$, shown by one or more data sets are as follows.

1. There exists a day to day variation (up to 5 km at least) of an order of magnitude or more, combined with pronounced vertical stratification.

2. Geophysical differences exist between California and Colorado. Over the former, the decrease in $\beta_{10.6}$ occurs at a lower altitude than over the latter. This is most likely associated with the higher altitude of the Colorado plateau and greater vertical convection.

3. A seasonal variation is observed by NOAA and by RSRE. At an altitude of 6 km minimum values of $\beta_{10.6}$ are seen by NOAA in Fall and Winter ($\sim 10^{-10} \text{ m}^{-1} \text{ sr}^{-1}$), maximum values occur in Spring and Summer ($\sim 10^{-9} \text{ m}^{-1} \text{ sr}^{-1}$). RSRE observed minimum $\beta_{10.6}$ in Winter.

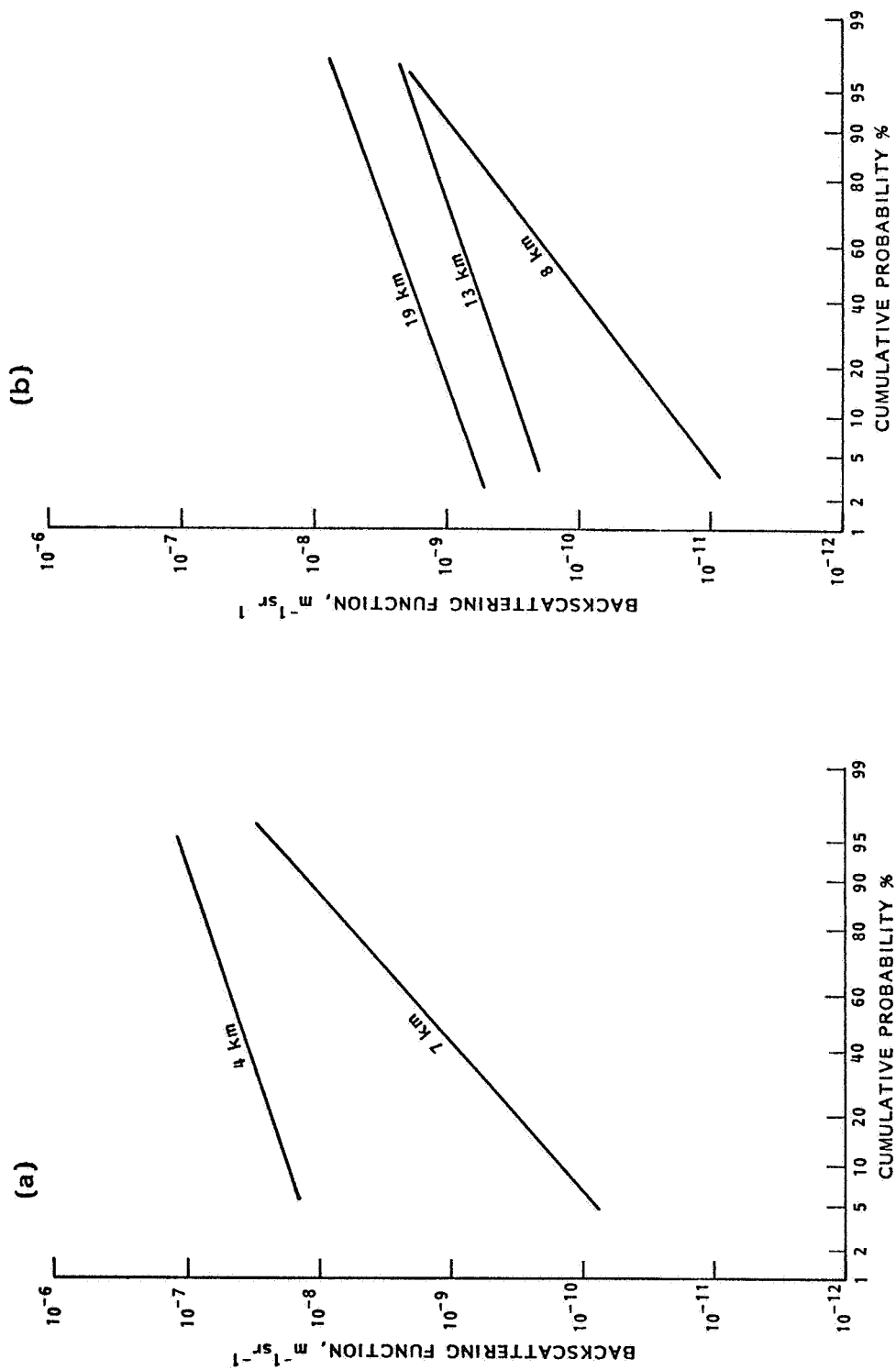
4. A decrease occurred in the peak altitude of the stratospheric volcanic layer over NOAA (from 23 km in Fall, 1982 to 17 km in Fall, 1983).

5. Lowest mean values for $\beta_{10.6}$ in the upper stratosphere ($2 \times 10^{-11} \text{ m}^{-1}$) were observed by NOAA in Spring and Summer of 1982. This was after the decay of material injected by the eruptions of

St. Helens and Alaid and before the arrival of material injected by El Chichon.

6.3 PROBABILITY DISTRIBUTIONS FOR $\beta_{10.6}$

Cumulative probability distributions for $\beta_{10.6}$ have been published by NOAA (Post et al., 1982; Post, 1984a). These show a good fit to log-normality and the best-fit straight lines to the data sets at five altitudes and on two occasions are reproduced in Fig. 6.2(a) and (b) (Post et al., 1982; Post, 1984a,b). The lower spread in $\beta_{10.6}$ values at stratospheric altitudes, as opposed to tropospheric altitudes is shown in Fig. 6.2(b) and is to be noted.



(a) 1981 data.

(b) 1983 data.

Figure 6.2. Cumulative probability distributions for $\beta_{10.6}$ measured at NOAA (Post et al., 1982; Post, 1984a).

7. DATA INTERCOMPARISON

7.1 VARIATION WITH LATITUDE AND SEASON

Figures 7.1(a) and (b) are composite figures on which theoretical and experimental values for $\beta_{10.6}$ at an altitude of about 6 km have been plotted as a function of latitude. The altitude of 6 km has been chosen for several reasons. It is close to the mean flight altitude for much of the GAMETAG measurement series and it is an altitude at which good (> 40%) SAGE I/SAM II penetration is found, and for which the median values may be considered to be without serious systematic bias. It is also close to the level at which minimum values for $\beta_{10.6}$ are found experimentally and it thus represents a compromise altitude that is not too affected by ground topography below and volcanic fallout from above.

Data for Spring and Summer have been plotted in Fig. 7.1(a), the much more limited data for Fall and Winter is plotted in Fig. 7.1(b). In Fig. 7.1(a), the GAMETAG data points represent median values for $\beta_{10.6}$ observed over flight segments for which the flight altitude was between 5 and 7 km. Data for 1977 and 1978 have been distinguished by different symbols. The lines representing the SAGE I data are the March-May and September-November median values in Fig. 7.1(a) and 7.1(b), respectively.

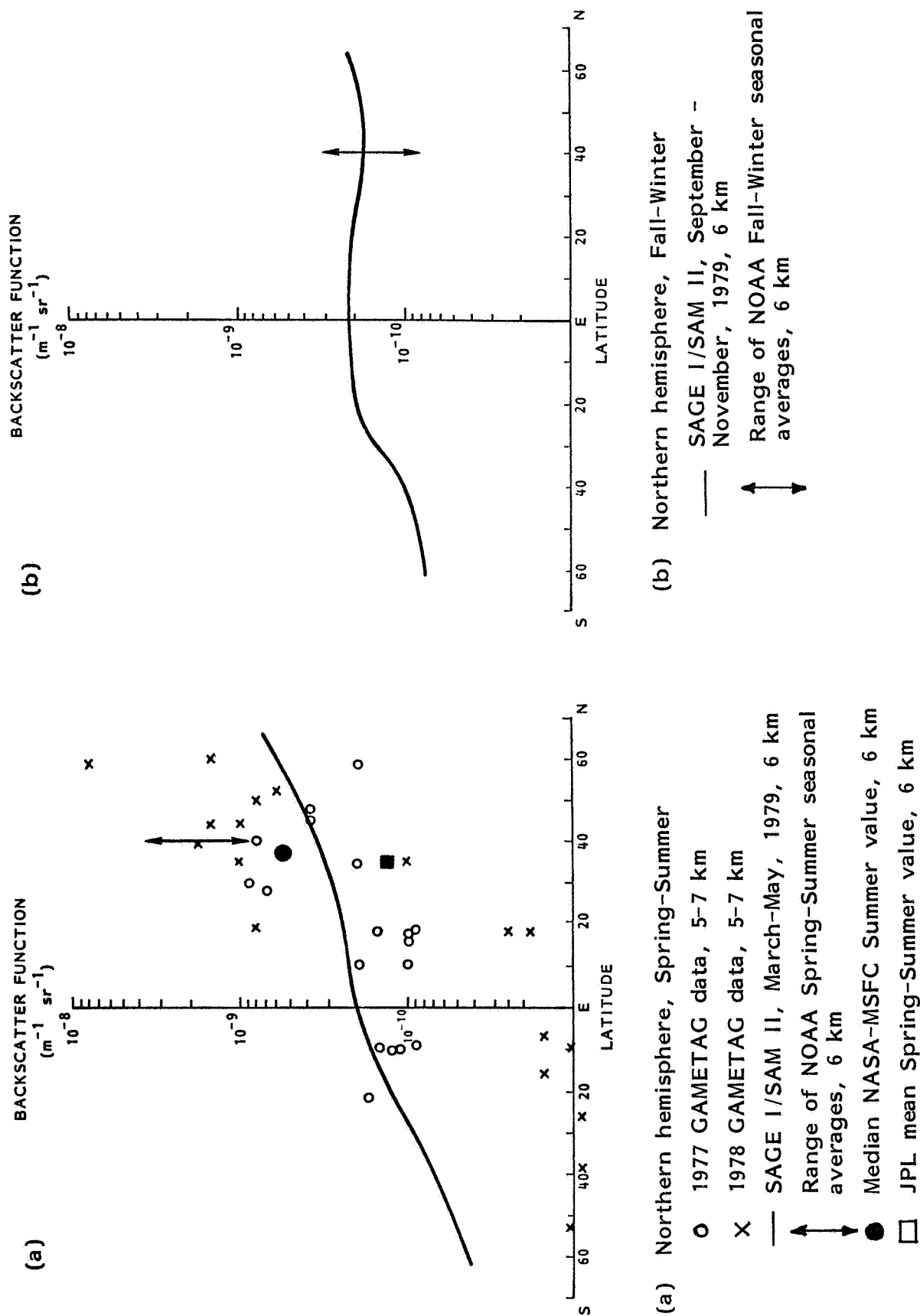


Figure 7.1. Comparison of modeled and directly measured values of $\beta_{10.6}$ for altitudes between 5 and 7 km.

Seasonal averages for JPL and NASA-MSU are shown by single symbols (no data is available for Fall-Winter). The larger amount of data from NOAA is shown by vertical lines in Figs. 7.1(a) and 7.1(b) which represent the range of seasonal mean values found [five Spring-Summer seasons in Fig. 7.1(a) and three Fall-Winter seasons in Fig. 7.1(b)].

Examination of these figures shows that, apart from the 1978 GAMETAG data in the southern hemisphere, agreement is quite good between the different data sets. Comment has already been made concerning the difference between the 1977 and 1978 GAMETAG data sets and without further evidence we must regard this as a sampling fluctuation. In the northern hemisphere, most of the measured and modeled values for $\beta_{10.6}$ lie between 10^{-10} and $2 \times 10^{-9} \text{ m}^{-1} \text{ sr}^{-1}$. When judging the goodness of fit between these data sets, it must be remembered that they refer to different years and geographical regions and to different degrees of stratospheric volcanic contamination. There is apparently still a very considerable need for direct measurements of $\beta_{10.6}$ in the southern hemisphere.

7.2 VARIATION WITH ALTITUDE

Figure 7.2 shows the altitude variation of $\beta_{10.6}$ for three early NOAA seasonal averages, the 1983-1984 JPL Spring-Summer average and the SAGE I modeled values for 40° N. One of the NOAA averages (Summer 1981) and the JPL average show a clear

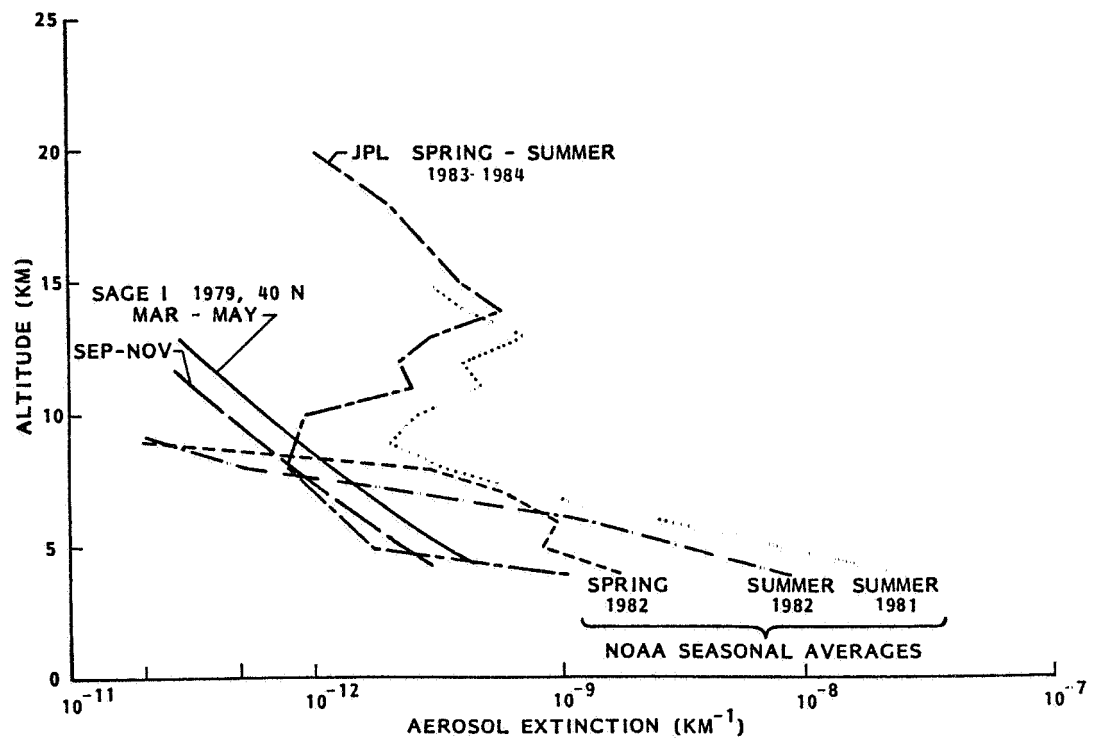


Figure 7.2. Composite diagram showing modeled and directly measured vertical profiles for $\beta_{10.6}$.

stratospheric volcanic enhancement which is not present in the other profiles. Between altitudes of 5 and 9 km, the agreement between SAGE I and JPL is good. The agreement between both of these and the NOAA data is quantitatively poor. It is quite possible that much of this difference may be due to the location of Boulder high on the continental plateau. There will be increased convective activity and the boundary layer will extend to a considerably greater altitude above sea-level. The low values observed by NOAA at a height of 9 km in Spring and Summer of 1982 do not fit well with the modeled data.

7.3 PROBABILITY DISTRIBUTIONS

Examples of the probability distribution for $\sigma_{1.00}$ and $\beta_{10.6}$ have been shown in Figs. 2.3 (a)-(e) and 6.2(a) and (b). Certain similarities exist in these figures. All the NOAA data shows clear log-normal characteristics. This is also shown by the SAGE I/SAM II data in the stratosphere. In the upper troposphere, the distribution is clearly two-component and we believe the higher estimation component to be sub-visible cirrus (cirrus returns have been omitted from the NOAA data). In the middle free troposphere, the SAGE I/SAM II data is once again approximately log-normal for some of the latitude bands. In order to make a more quantitative comparison of the distribution, Table 7.1 shows the extinction and backscatter changes corresponding to the 5% - 50% probability range, i.e., the departure of the 5% probability level from the median level. Values are shown for similar

latitudes (20 N - 60 N for SAGE I and 40 N for NOAA) and for altitudes above 5 km. The range of the optical parameter has been expressed as the ratio of its value at the 50% probability level to its value at the 5% level.

Table 7.1 shows that for both $\sigma_{1.00}$ and $\beta_{10.6}$, the ratio decreases with altitude by roughly comparable amounts. The absolute magnitude of the ratio in the two cases is nevertheless very different. Part of this difference can be accounted for by the fact that the conversion factor $\beta_{10.6}/\sigma_{1.00}$ itself depends upon the value of $\sigma_{1.00}$. This is, however, not sufficient to account for most of the observed difference. It is more likely that the explanation for this lies in the different geometry of the two measurements. The 10.6 μm backscatter function is measured over horizontal dimensions of a few meters only and the probability distribution will reflect all changes with horizontal scales greater than this. The 1 μm extinction function, on the other hand, is derived from a measurement made over a 200-300 km long horizontal path. Fluctuations with horizontal scales less than this will be smoothed. The major part of the difference in ratio observed in Table 7.1 almost certainly arise from these different measurement geometries.

7.4 VOLCANIC EFFECTS

Volcanic effects have already been discussed in Sections 2.5 and 6.2 and the details will not be presented again here. The

TABLE 7.1. Range of Observed Extinction and Backscatter Values
(SAGE I and NOAA Data from Figs. 2.3(d) and 6.2)

Altitude (km)	$1\ \mu\text{m}$ Extinction at 50% Level $1\ \mu\text{m}$ Extinction at 5 % Level	$10.6\ \mu\text{m}$ Backscatter at 50% Level $10.6\ \mu\text{m}$ Backscatter at 5 % Level
6	3.0	
7		13.0
8		12.7
10	2.1	
12	1.5	
13		3.2
14	1.3	
18	1.2	
19		3.2

most obvious point of comparison to note is the stratospheric enhancement observed in both cases (Figs. 2.11 and 6.1). A more subtle point of comparison is the enhancement in the upper troposphere. Figure 2.11 shows that the upper troposphere, following volcanic injection into the stratosphere, has a raised $1\ \mu\text{m}$ extinction which extends from the tropopause down to 5-6 km. Figure 6.1(a) shows similar effects, post-volcanic $10.6\ \mu\text{m}$ back-scattering, following volcanic injection, is enhanced from the tropopause down to an altitude of 7-8 km. The fact that this altitude is somewhat higher than that given above for SAGE I/SAM II is, as discussed earlier, most likely due to a geographic effort associated with the location of Boulder, Colorado.

8. CONCLUSIONS

In the work described in this report, the objective has been to improve our understanding of the global behavior of the aerosol backscatter function in the free troposphere at a wavelength of 10.6 μm . Three experimental data sets have been used, each with certain limitations in either wavelength or temporal and geographical coverage. In addition to the use of these data sets, modeling has been carried out on the microphysical and optical changes to be expected within an aerosol plume.

The SAGE I/SAM II data set has yielded a detailed picture of the variation of 1 μm aerosol extinction with latitude, season and altitude above 5 km. This shows pronounced hemispheric asymmetry, with minimum extinction occurring in high southern latitudes. In both hemispheres, the aerosol extinction in spring and summer is greater than that in fall and winter. Volcanic enhancement of the aerosol extinction above 5 km is also apparent at high latitudes in the 1980-81 data. The GAMETAG data sets for 1977 and 1978 have shown a latitude variation in aerosol concentration and optical properties, that is in overall qualitative agreement with the SAGE I/SAM II data, and in good quantitative agreement in the northern hemisphere. Direct measurements of $\beta_{10.6}$ using CO_2 lidar are confined to a limited latitude band in the northern hemisphere and have only been made

since 1980, during a period of volcanic activity.

Comparison has been made of the direct measurements with values for $\beta_{10.6}$ calculated from the other data sets. This comparison has particularly been carried out for an altitude of 6 km, which is close to the level at which minimum values for $\beta_{10.6}$ are currently observed. Median summer values for $\beta_{10.6}$ at this level, in the northern hemisphere, vary from $1 \times 10^{-10} \text{ m}^{-1} \text{ sr}^{-1}$ at the equator to $1 \times 10^{-9} \text{ m}^{-1} \text{ sr}^{-1}$ at 60 N. Median winter values at the same altitude are about 2×10^{-10} at all northern latitudes. In the southern hemisphere, the situation is less clear. There are no direct measurements and the 1977 and 1978 GAMETAG measurements yield significantly different values for $\beta_{10.6}$. SAGE I/SAM II median values at 6 km altitude lie between $3 \times 10^{-11} \text{ m}^{-1} \text{ sr}^{-1}$ and $2 \times 10^{-10} \text{ m}^{-1} \text{ sr}^{-1}$; the range for median GAMETAG values is between 1×10^{-11} and 2×10^{-10} . Both data sets show a decreasing aerosol concentration toward high southern latitudes. Intercomparison of vertical profiles for $\beta_{10.6}$ is difficult. GAMETAG data has been obtained mainly between 5 and 7 km altitude and it is not possible to derive a vertical profile with any precision. Almost all the direct measurements of $\beta_{10.6}$ are affected by volcanic input, which enhances the upper free troposphere. Reasonable agreement is obtained between the direct measurements of $\beta_{10.6}$ and values modeled from SAGE I/SAM II at altitudes between 5 and 10 km but any exact comparison is not at present possible.

It is clear, from the analysis carried out and the data comparisons made, that we now have a reasonable quantitative understanding of the principal features of free tropospheric aerosol concentrations and optical characteristics and their variation with latitude season and volcanic activity. We are, nevertheless, still a considerable distance from being able to supply a complete statistical description, particularly of the optical characteristics at the longer wavelengths. This is especially true in the southern hemisphere where there is a total lack of direct measurements at 10.6 μm .

9. REFERENCES

- Deepak, A., (Ed.), 1982: Atmospheric effects and potential climatic impact of the 1980 eruptions of Mount St. Helens, NASA Conference Publication 2240.
- Deepak, A., G. S. Kent, G. K. Yue, 1982: Atmospheric Backscatter Model Development for CO₂ Wavelengths, IFAORS Final Report for NASA Marshall Space Flight Center, Contract NAS8-34427.
- Deirmendjian, D., 1973: On volcanic and other particulate turbidity anomalies, Advan. Geophys. 16, 267-296.
- Fuchs, N. A., 1964: The Mechanics of Aerosols, Pergamon, New York.
- Jones, W. D., 1983. Beta System Test Results (1981 and 1982), Second Multi-Agency Workshop on Atmospheric Backscatter at IR Wavelengths, April 12-13, Workshop Notes, pp. 53-70.
- Kent, G. S. & M. P. McCormick, 1984: SAGE and SAM II measurements of global stratospheric aerosol optical depth and mass loading, J. Geophys. Res. 89, 5303-5314.
- Liu, S. C., J. R. McAfee, and R. J. Cicerone, 1984: Radon 222 and tropospheric vertical transport, J. Geophys. Res. 89, 7291-7297.
- Lorenz, E. N., 1967: The nature and theory of the general circulation of the atmosphere, WMO.
- McCormick, M. P., P. Hamill, T. J. Pepin, W. P. Chu, T. J. Swissler, and L. R. McMaster, 1979: Satellite studies of the stratospheric aerosol, Bull. of the Am. Meteor. Soc. 60, 1038-1046.
- McCormick, M. P., C. R. Trepte, and G. S. Kent, 1983: Spatial changes in the stratospheric aerosol associated with the north polar vortex, Geophys. Res. Lett. 10, 941-944.
- McCormick, M. P., T. J. Swissler, W. H. Fuller, W. H. Hunt, and M. T. Osborn, 1984: Airborne and ground-based lidar measurements of the El Chichon stratospheric aerosol from 90°N to 56°S, Geof. Int. 23-2, 187-221.

- Menzies, R. T., M. J. Kavaya, P. H. Flamant, and D. A. Haner, 1984: Atmospheric aerosol backscatter measurements using a tunable coherent CO₂ lidar, Appl. Opt. 23, 2510-2516.
- Menzies, R. T., 1984. Private communication.
- NOAA, 1981: Global Wind Measuring Satellite System-WINDSAT Final Report for NOAA Contract #NA 79RA C00127.
- Patterson, E. M., C. S. Kiang, A. C. Delany, A. F. Wartburg, A. C. D. Leslie and B. J. Huebert, 1980: Global measurements of aerosols in remote continental and marine regions: Concentrations, size distributions, and optical properties, J. Geophys. Res. 85, 7361-7376.
- Pinnick, R. G., and H. J. Auvermann, 1979: Response characteristics of Knollenberg light scattering aerosol counters, J. Aerosol. Sci. 10, 55-74.
- Post, M. J., F. F. Hall, R. A. Richter, and T. R. Lawrence, 1982: Aerosol backscattering profiles at $\lambda = 10.6 \mu\text{m}$, Appl. Opt. 21, 2442-2446.
- Post, M. J., 1983: Atmospheric aerosol profiles at CO₂ wavelengths, 2nd Topical Meeting on Coherent Laser Radar; Technology and Applications, August 1-4, 1983, Aspen, Colorado, Technical Digest, pp. Th B4-1 to Th B4-5.
- Post, M. J., 1984a: Lidar observations of the El Chichon Cloud at $\lambda = 10.6 \mu\text{m}$. Geophys. Res. Lett. 1, 846-849.
- Post, M. J., 1984b: Private communication.
- Rao, P. K., 1975: Invisible cirrus clouds in NOAA-2 VHRR imagery, Mon. Weather Rev. 103, 72-77.
- Schnell, R. C., 1984: Arctic haze and the arctic gas and aerosol sampling program (GASP), Geophys. Res. Lett. 11, 361-364.
- Schweisow, R. L., R. E. Cupp, V. E. Derr, E. W. Barrett, R. F. Pueschel, and P. C. Sinclair, 1981: Aerosol backscatter profiles measured at 10.6 μm . J. Appl. Meteor. 20, 184-194.
- Shaw, G. E., 1980. Transport of Asian desert aerosol to the Hawaiian Islands, J. Appl. Meteor. 19, 1254-1259.
- U. S. Standard Atmosphere, 1976: NOAA.

- Uthe, E. E. and P. B. Russell, 1977: Lidar Observations of Tropical High Altitude Cirrus Clouds. Proceedings of the Symposium on Radiation in the Atmosphere, Garmisch-Partenkirchen, FRG, 19-28 August 1976, H. J. Bolle (ed.) Science Press, 242-244.
- Vaughan, M., 1983. CO₂ β Measurement, Second Multi-Agency Workshop on Atmospheric Backscatter at IR Wavelengths, April 12-13, 1983. Workshop Notes, pp. 79-80.
- Vaughan, M., 1985: Private communication.
- Weaver, E., 1983. MSFC Beta System and Pulsed Doppler Lidar System. 2nd Multi-Agency Workshop on Atmospheric Backscatter at IR Wavelengths, April 12-13, 1983, Workshop Notes, pp. 83-96.

APPENDIX A

LIST OF TABLES

Table A1.	Significant times for August 7, 1977. Denver, Colorado to Portland, Oregon.	A1
Table A2.	Significant times for August 8, 1977. Portland, Oregon to Anchorage, Alaska	A11
Table A3.	Significant times for August 22, 1977. Denver, Colorado to Moffett Field, California.	A21
Table A4.	Significant times for August 23, 1977. Moffett Field, California to Hilo, Hawaii.	A31
Table A5.	Significant times for August 25, 1977. Hilo, Hawaii to Johnston Atoll	A41
Table A6.	Significant times for August 26, 1977. Johnston Atoll to American Samoa	A51
Table A7.	Significant times for August 28, 1977. Pago Pago, American Samoa and Return (North)	A61
Table A8.	Significant times for August 31, 1977. Pago Pago, American Samoa and Return (South)	A71
Table A9.	Significant times for September 1, 1977. Pago Pago, Ameircan Samoa to Johnston Atoll	A81
Table A10.	Significant times for September 2, 1977. Johnston Atoll to Hilo, Hawaii	A91
Table A11.	Significant times for April 27, 1978. Denver, Colorado to Moffett Field, California	A101
Table A12.	Significant times for May 2, 1978. Hilo, Hawaii to Johnston Atoll	A111
Table A13.	Significant times for May 4, 1978. Canton Island to Nandi, Fiji Islands	A121
Table A14.	Significant times for May 10, 1978. Christchurch, New Zealand to Christchurch, New Zealand	A131

PRECEDING PAGE BLANK NOT FILMED

LIST OF TABLES (cont'd)

Table A15. Significant times for May 11, 1978. Christchurch, New Zealand to Nandi, Fiji Islands.A141
Table A16. Significant times for May 12, 1978. Nandi, Fiji Islands to Canto IslandA151
Table A17. Significant times for May 14, 1978. Johnson Atoll to Hilo, Hawaii.A161
Table A18. Significant times for May 18, 1978. Moffett Field, California to Denver, ColoradoA171
Table A19. Significant times for May 27, 1978. Denver, Colorado to Great Falls, MontanaA181
Table A20. Significant times for May 28, 1978. Great Falls, Montana to White Horse, CanadaA191
Table A21. Significant times for May 31, 1978. White Horse, Canada to Great Falls, Montana.A201
Table A22. Significant times for June 1, 1978. Great Falls, Montana to Denver, ColoradoA211

LIST OF FIGURES

Figure A1 (a-i) GAMETAG flight data for August 7, 1977....A2-A10

- (a) Altitude and location flight track plotted as a function of time after takeoff
- (b) Calculated particulate extinction along the flight track for one-minute data sets for $\lambda = 0.63 \mu\text{m}$
- (c) Calculated particulate extinction along the flight track for five-minute data sets for $\lambda = 0.63 \mu\text{m}$
- (d) Calculated backscatter coefficient along the flight track for five-minute data sets for $\lambda = 0.63 \mu\text{m}$
- (e) Calculated ratios for backscatter to extinction for five-minute data sets for $\lambda = 0.63 \mu\text{m}$
- (f) Calculated particulate extinction along the flight track for one-minute data sets for $\lambda = 10.6 \mu\text{m}$
- (g) Calculated particulate extinction along the flight track for five-minute data sets for $\lambda = 10.6 \mu\text{m}$
- (h) Calculated backscatter coefficient along the flight track for five-minute data sets for $\lambda = 10.6 \mu\text{m}$
- (i) Calculated ratios for backscatter to extinction for five-minute data sets for $\lambda = 10.6 \mu\text{m}$

Figure A2(a-i) GAMETAG flight data for August 8, 1977..... A12-A20

Figure A3(a-i) GAMETAG flight data for August 22, 1977..... A22-A30

Figure A4(a-i) GAMETAG flight data for August 23, 1977..... A32-A40

Figure A5(a-i) GAMETAG flight data for August 25, 1977..... A42-A50

Figure A6(a-i) GAMETAG flight data for August 26, 1977..... A52-A60

Figure A7(a-i) GAMETAG flight data for August 28, 1977..... A62-A70

Figure A8(a-i) GAMETAG flight data for August 31, 1977..... A72-A80

Figure A9(a-i) GAMETAG flight data for September 1, 1977... A82-A90

Figure A10(a-i) GAMETAG flight data for September 2, 1977... A92-A100

Figure A11(a-i) GAMETAG flight data for April 27, 1978..... A102-A110

Figure A12(a-i) GAMETAG flight data for May 2, 1978..... A112-A120

Figure A13(a-i) GAMETAG flight data for May 4, 1978..... A122-A130

LIST OF FIGURES (cont'd)

Figure A14(a-i)	GAMETAG flight data for May 10, 1978.....	A132-A140
Figure A15(a-i)	GAMETAG flight data for May 11, 1978.....	A142-A150
Figure A16(a-i)	GAMETAG flight data for May 12, 1978.....	A152-A160
Figure A17(a-i)	GAMETAG flight data for May 14, 1978.....	A162-A170
Figure A18(a-i)	GAMETAG flight data for May 18, 1978.....	A172-A180
Figure A19(a-i)	GAMETAG flight data for May 27, 1978.....	A182-A190
Figure A20(a-i)	GAMETAG flight data for May 28, 1978.....	A192-A200
Figure A21(a-i)	GAMETAG flight data for May 31, 1978.....	A202-A210
Figure A22(a-i)	GAMETAG flight data for June 1, 1978.....	A212-A220

**Table A1. Significant times for August 7, 1977.
Denver, Colorado to Portland, Oregon.**

Significant Points

<u>#</u>	<u>TIME</u>	
1	16:30	Denver
2	16:52	
3	18:04	
4	18:18	
5	18:57	
6	19:01	
7	19:13	
8	19:20	
9	19:25	
10	20:12	
11	20:39	
12	21:00	
13	21:10	Portland

ORIGINAL PAGE IS
OF POOR QUALITY

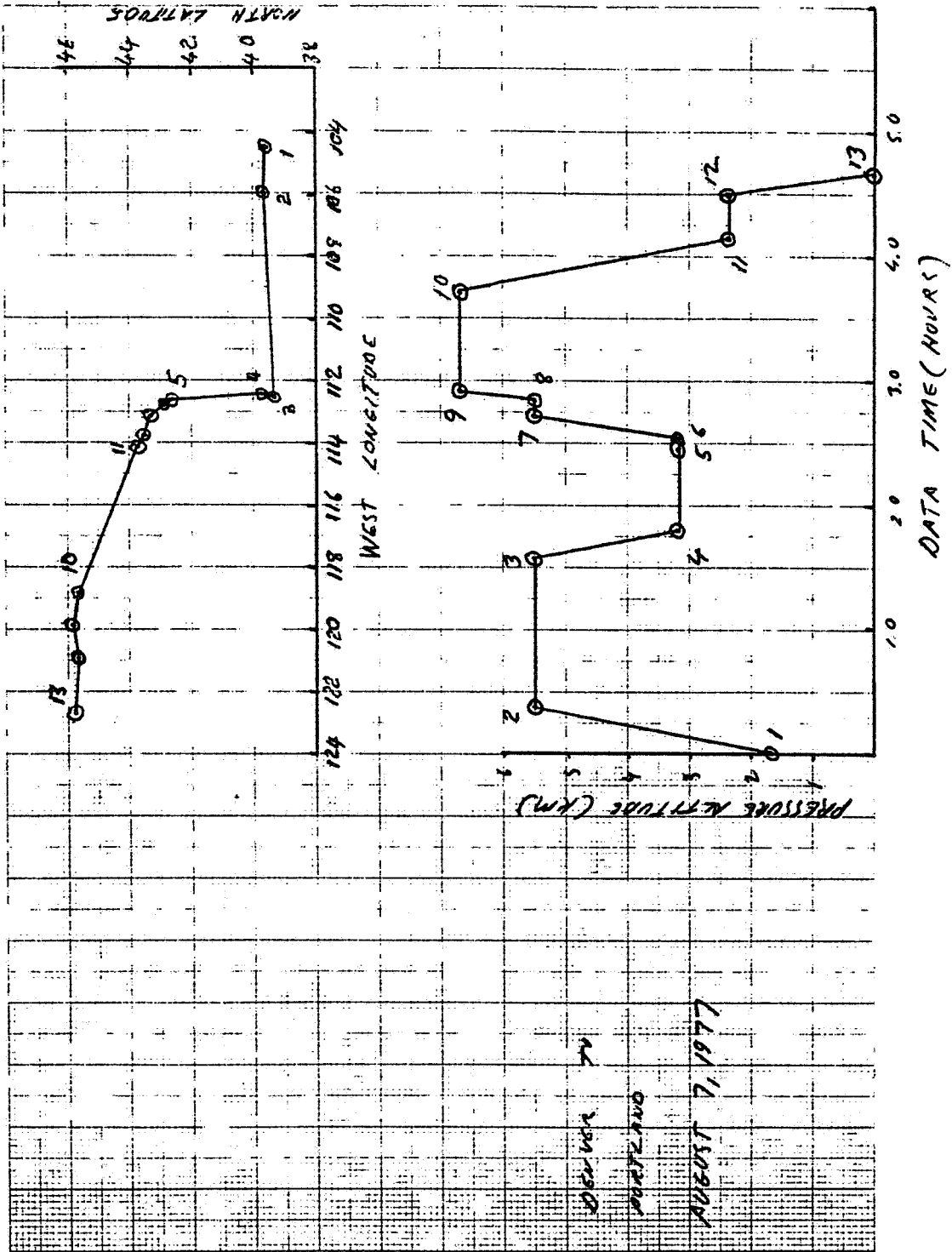


Fig. A 1 (a). GAMETAG flight data for August 7, 1977.
Altitude and location flight track plotted as a
function of time after takeoff.

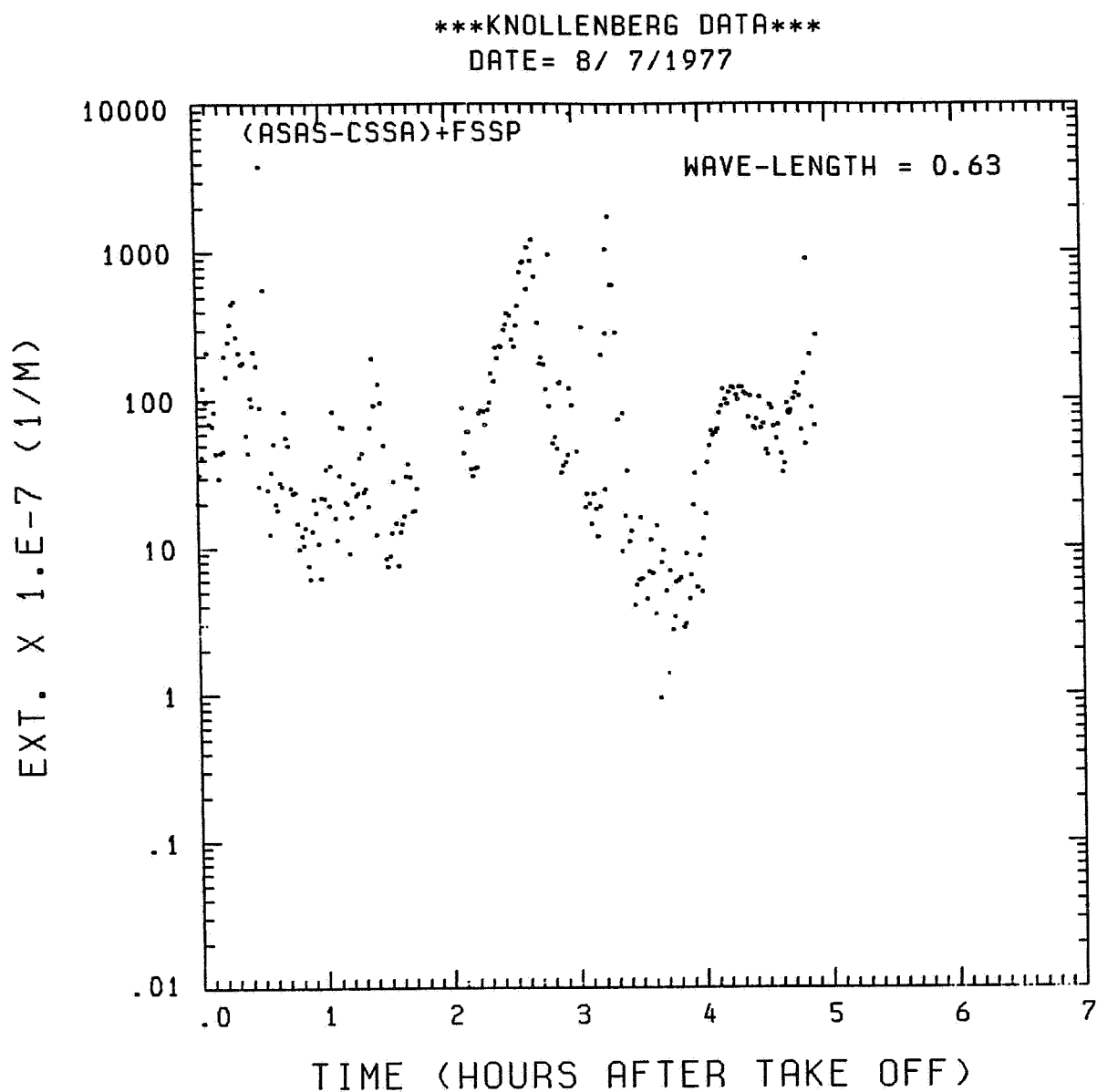


Fig. A 1 (b). GAMETAG flight data for August 7, 1977.
Calculated particulate extinction along the flight
track for one-minute data sets for $\lambda = 0.63 \mu\text{m}$.

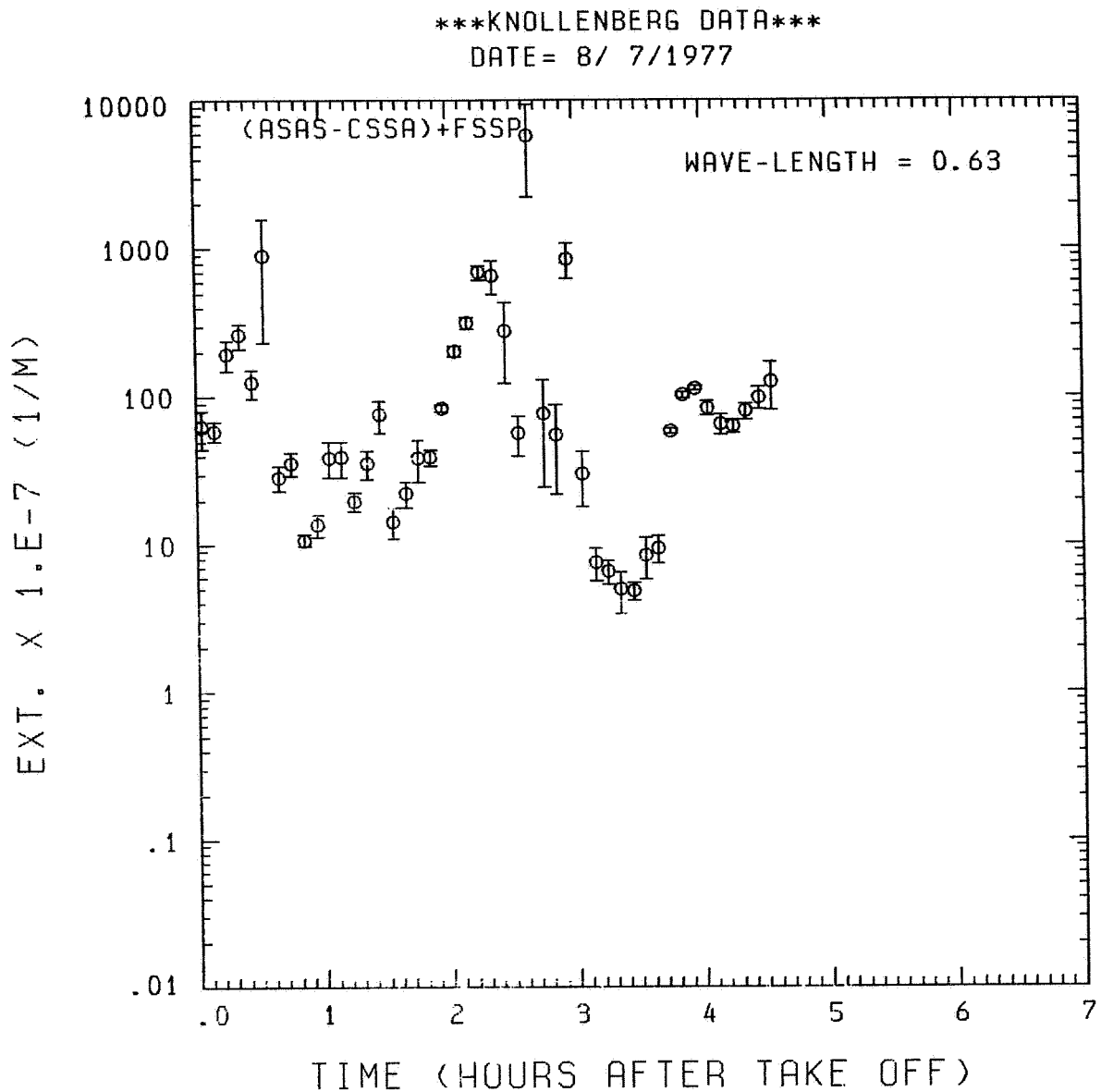


Fig. A1(c). GAMETAG flight data for August 7, 1977.
Calculated particulate extinction along the flight
track for five-minute data sets for $\lambda = 0.63 \mu\text{m}$.

KNOLLENBERG DATA

DATE= 8/ 7/1977

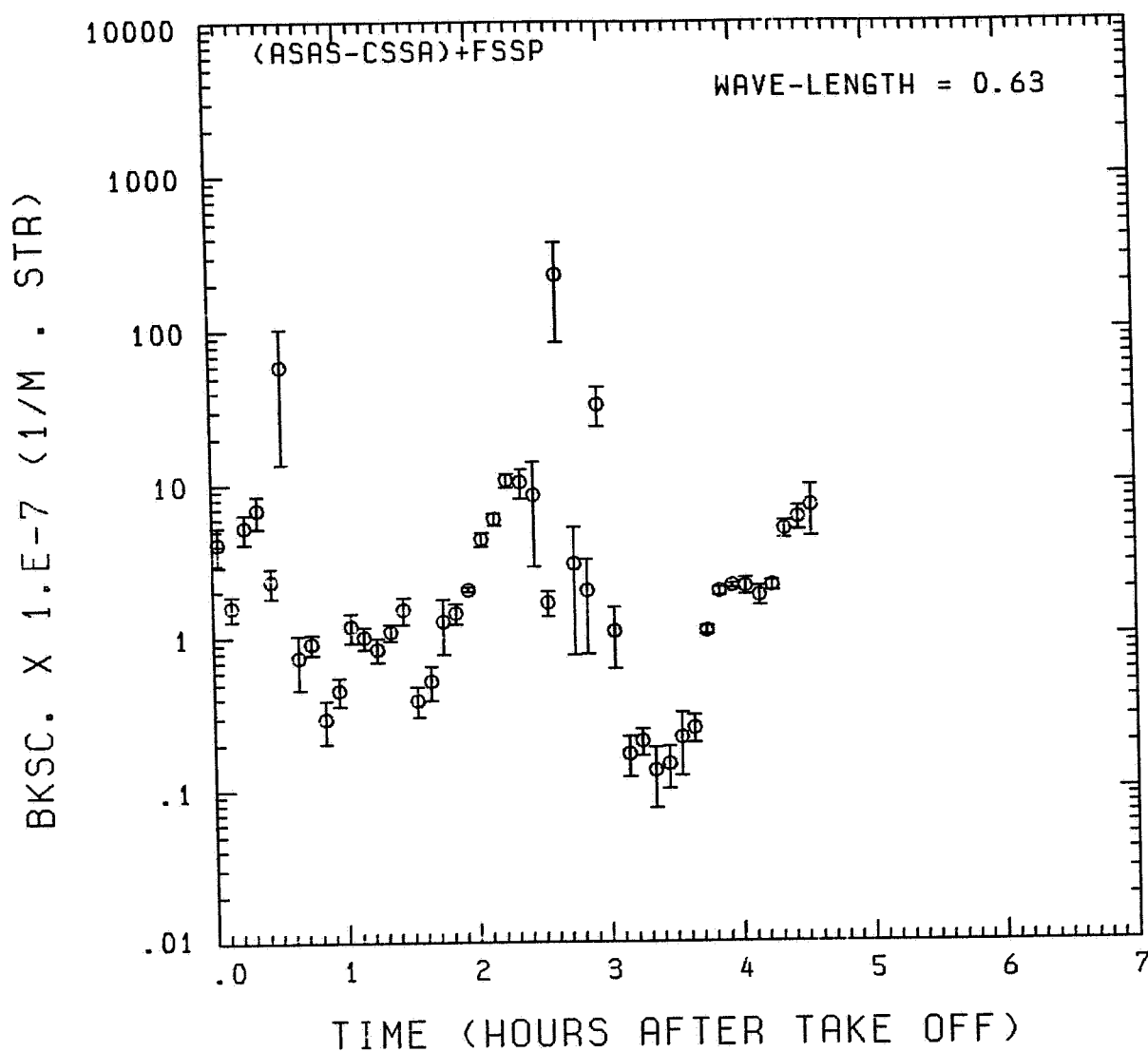


Fig. A 1 (d). GAMETAG flight data for August 7, 1977.

Calculated backscatter coefficient along the flight track for five-minute data sets for $\lambda = 0.63 \mu\text{m}$.

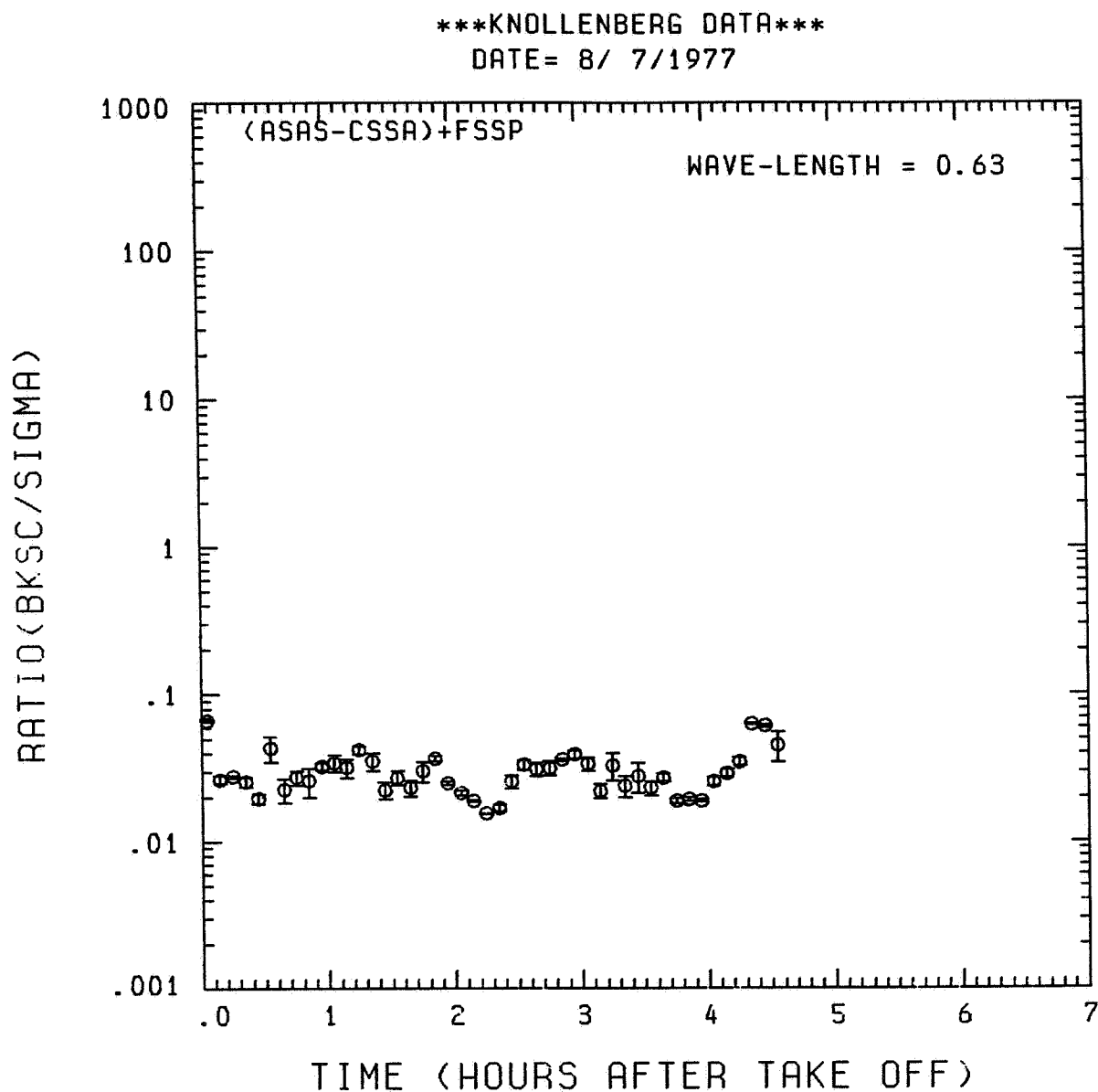


Fig. A 1 (e). GAMETAG flight data for August 7, 1977.
Calculated ratios for backscatter to extinction for
five-minute data sets for $\lambda = 0.63 \mu\text{m}$.

KNOLLENBERG DATA

DATE= 8/ 7/1977

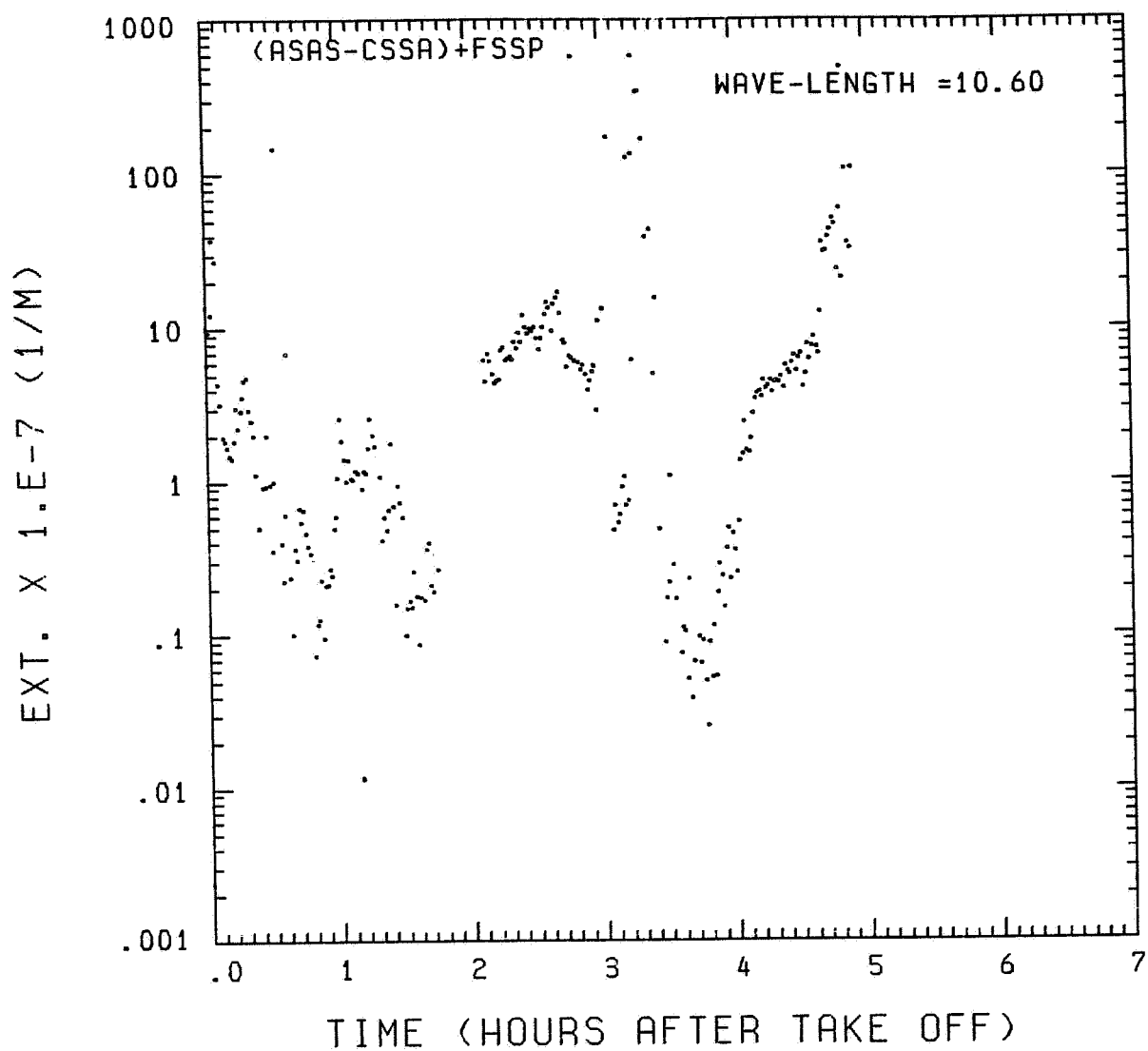


Fig. A 1 (f). GAMETAG flight data for August 7, 1977.

Calculated particulate extinction along the flight track for one-minute data sets for $\lambda = 10.6 \mu\text{m}$.

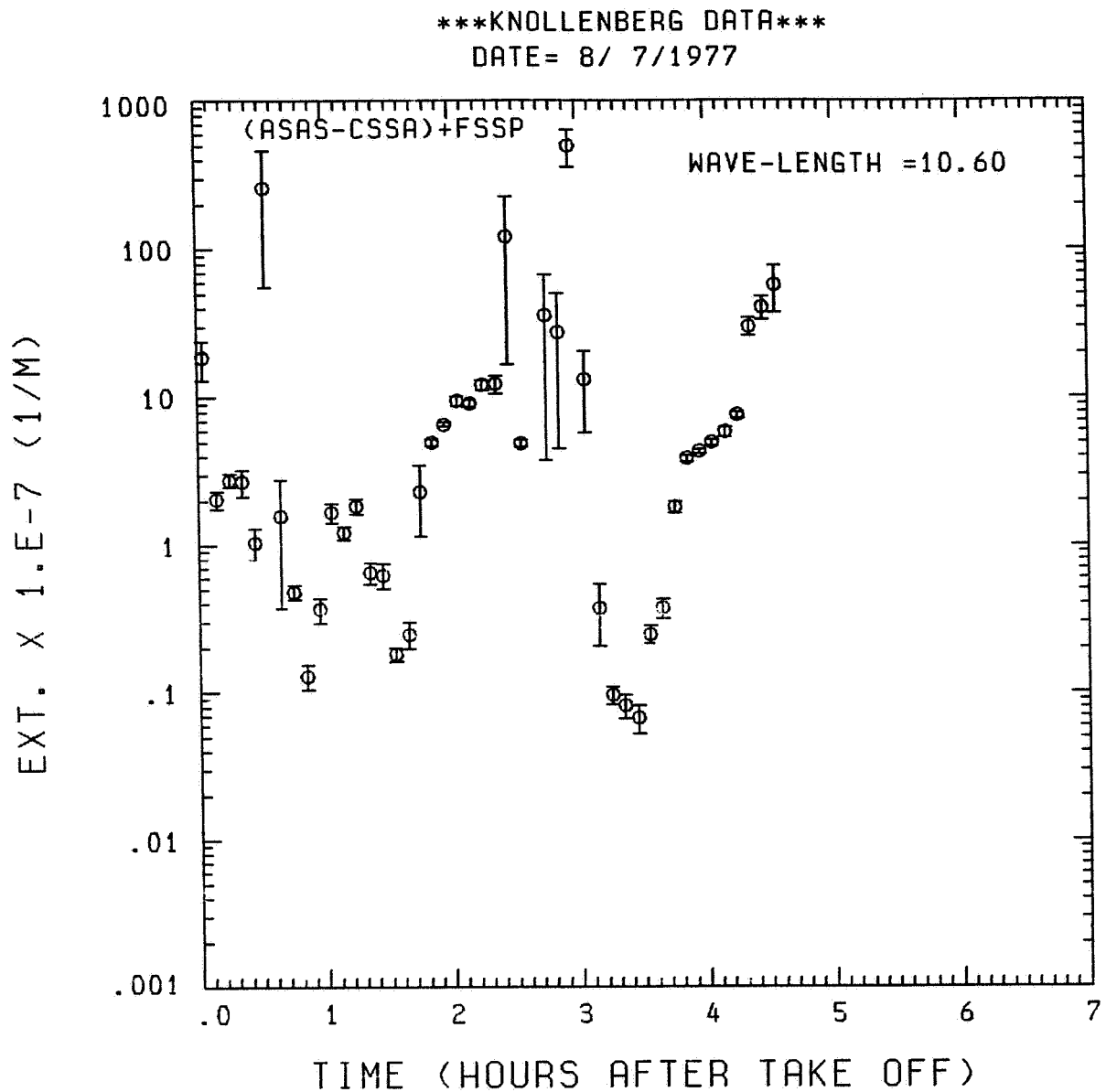


Fig. A 1 (g). GAMETAG flight data for August 7, 1977.
Calculated particulate extinction along the flight
track for five-minute data sets for $\lambda = 10.6 \mu\text{m}$.

KNOLLENBERG DATA

DATE= 8/ 7/1977

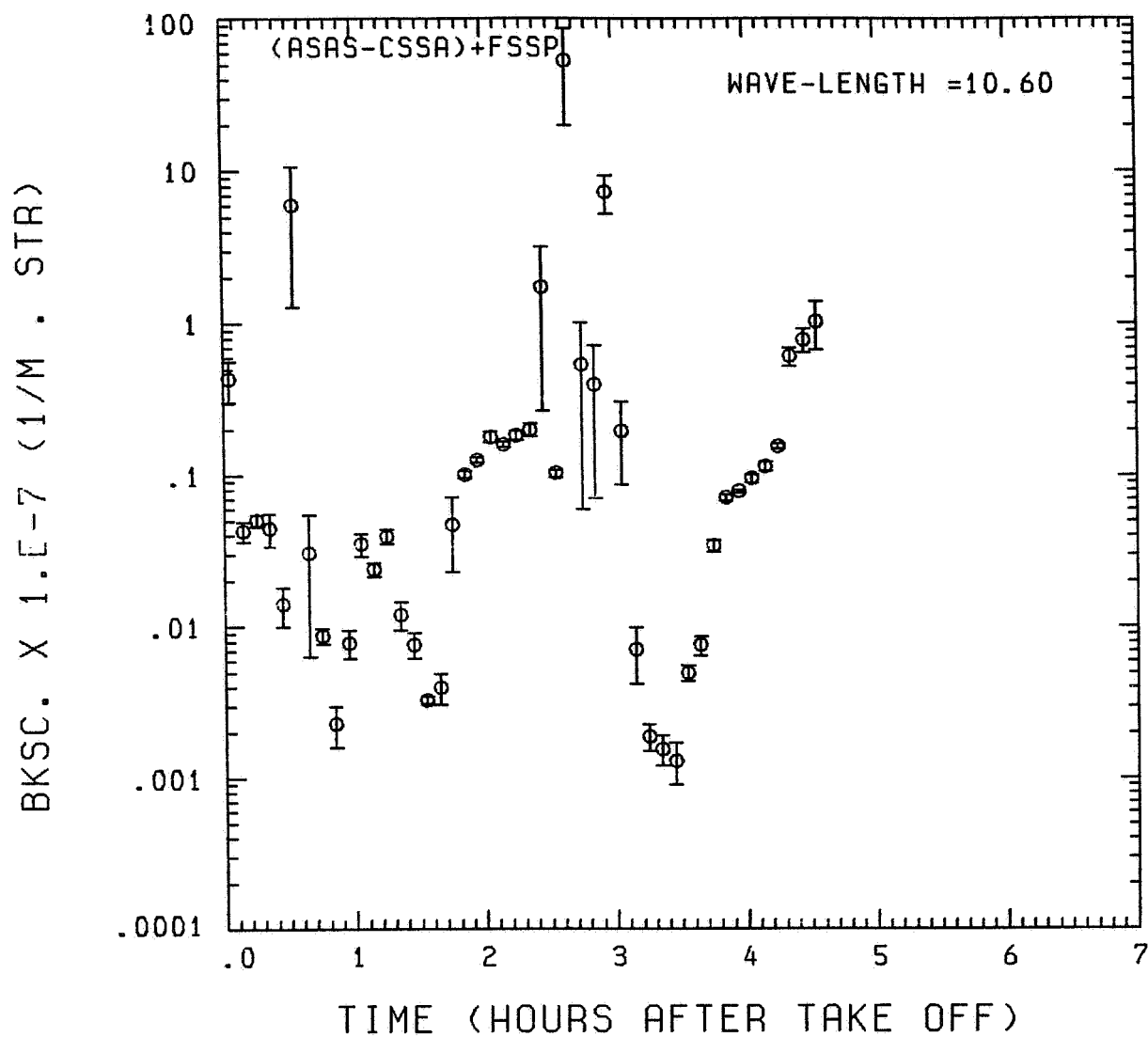


Fig. A 1 (h). GAMETAG flight data for August 7, 1977.

Calculated backscatter coefficient along the flight track for five-minute data sets for $\lambda = 10.6 \mu\text{m}$.

KNOLLENBERG DATA

DATE= 8/ 7/1977

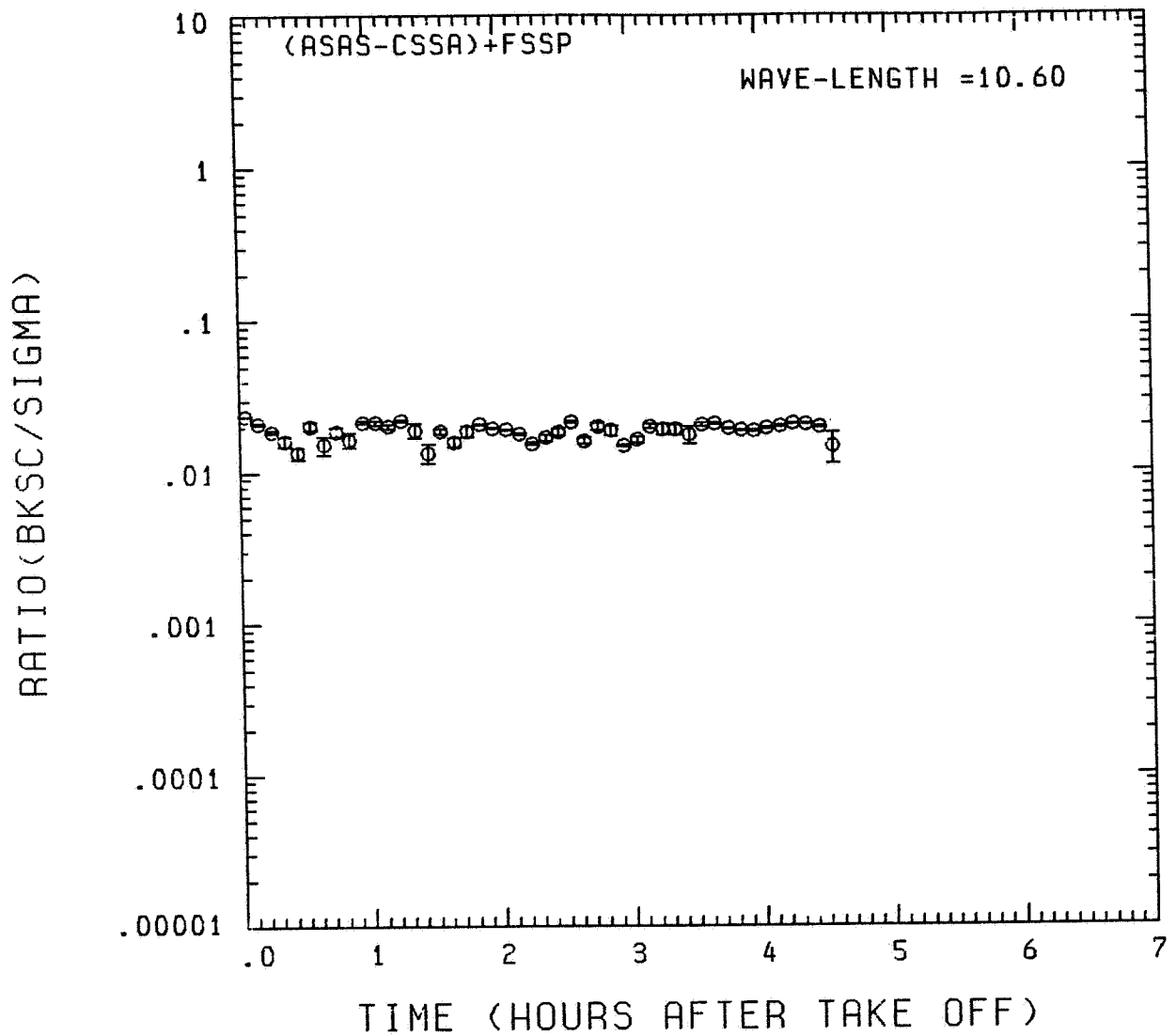


Fig. A 1 (i). GAMETAG flight data for August 7, 1977.

Calculated ratios for backscatter to extinction for
five-minute data sets for $\lambda = 10.6 \mu\text{m}$.

Table A2. Significant times for August 8, 1977.
Portland, Oregon to Anchorage, Alaska.

Significant Points

<u>#</u>	<u>TIME</u>	
1	18:54	Portland
2	19:22	
3	21:40	
4	21:56	
5	22:10	
6	22:15	
7	22:24	
8	22:38	
9	23:08	
10	23:33	
11	23:39	
12	23:52	
13	00:02	
14	00:35	
15	00:55	Anchorage

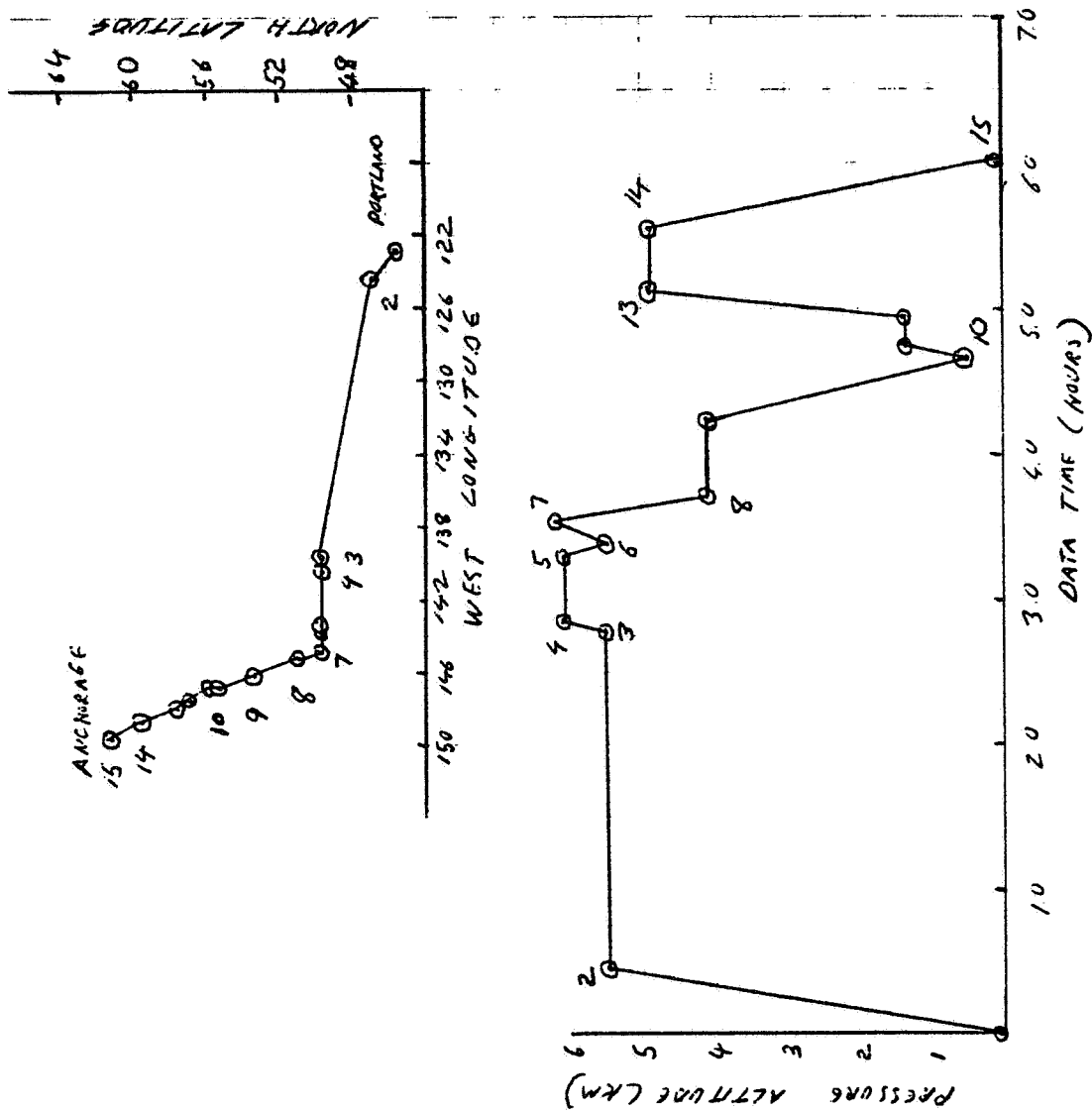


Fig. A2 (a). GAMETAG flight data for August 8, 1977.
Altitude and location flight track plotted as a
function of time after takeoff.

KNOLLENBERG DATA

DATE= 8/ 8/1977

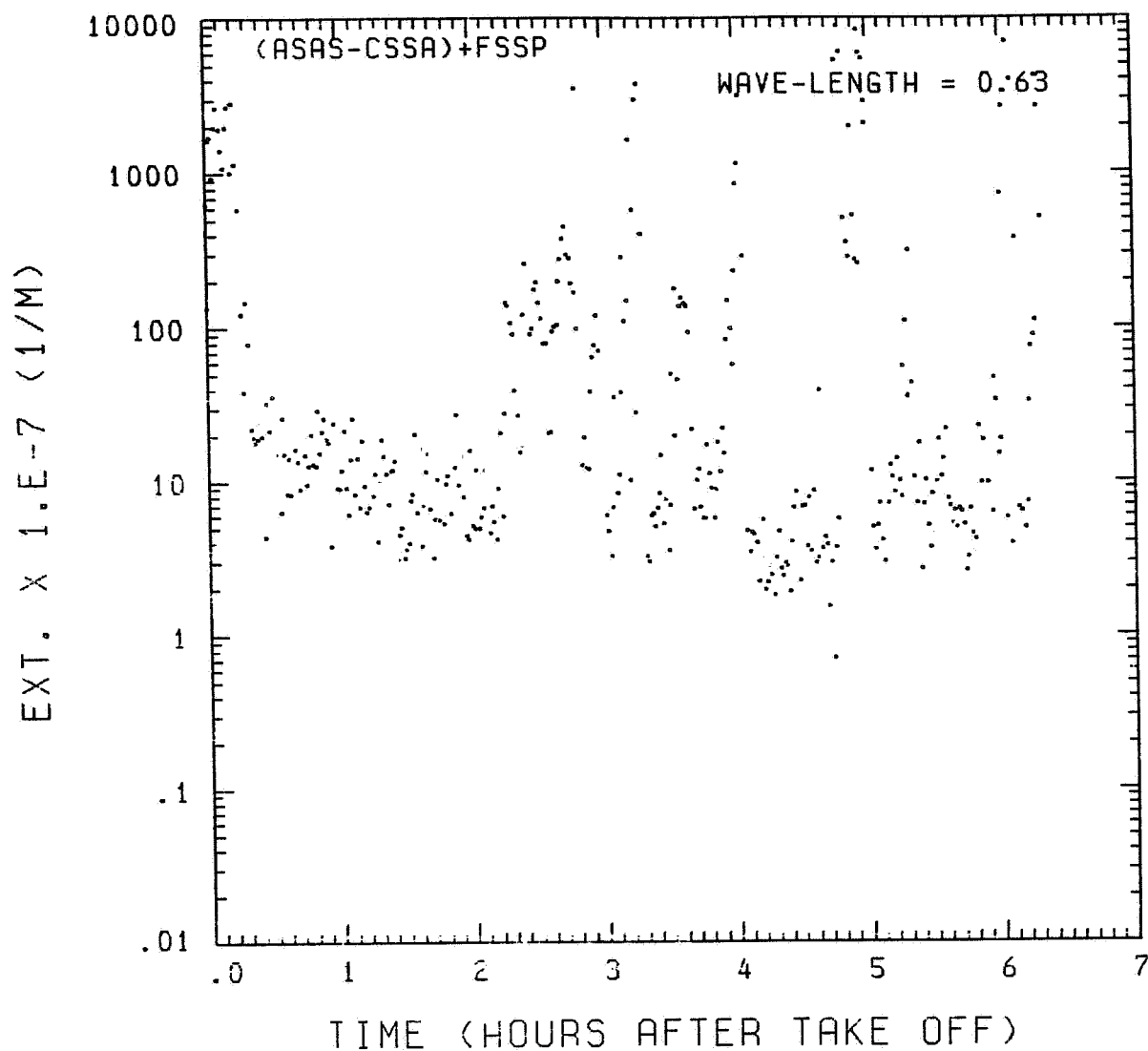


Fig. A2 (b). GAMETAG flight data for August 8, 1977.

Calculated particulate extinction along the flight track for one-minute data sets for $\lambda = 0.63 \mu\text{m}$.

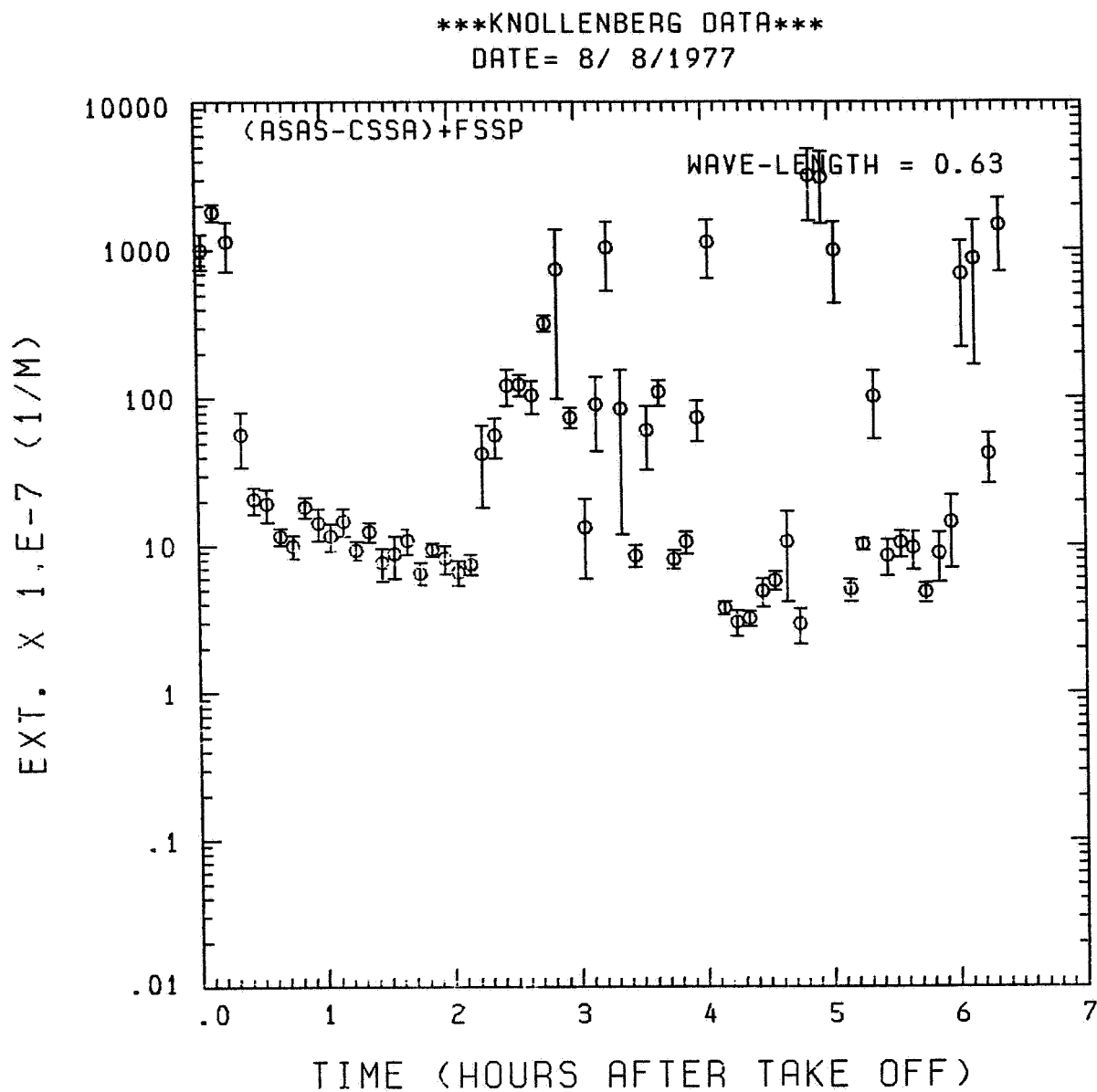


Fig. A2 (c). GAMETAG flight data for August 8, 1977.
Calculated particulate extinction along the flight
track for five-minute data sets for $\lambda = 0.63 \mu\text{m}$.

KNOLLENBERG DATA

DATE= 8/ 8/1977

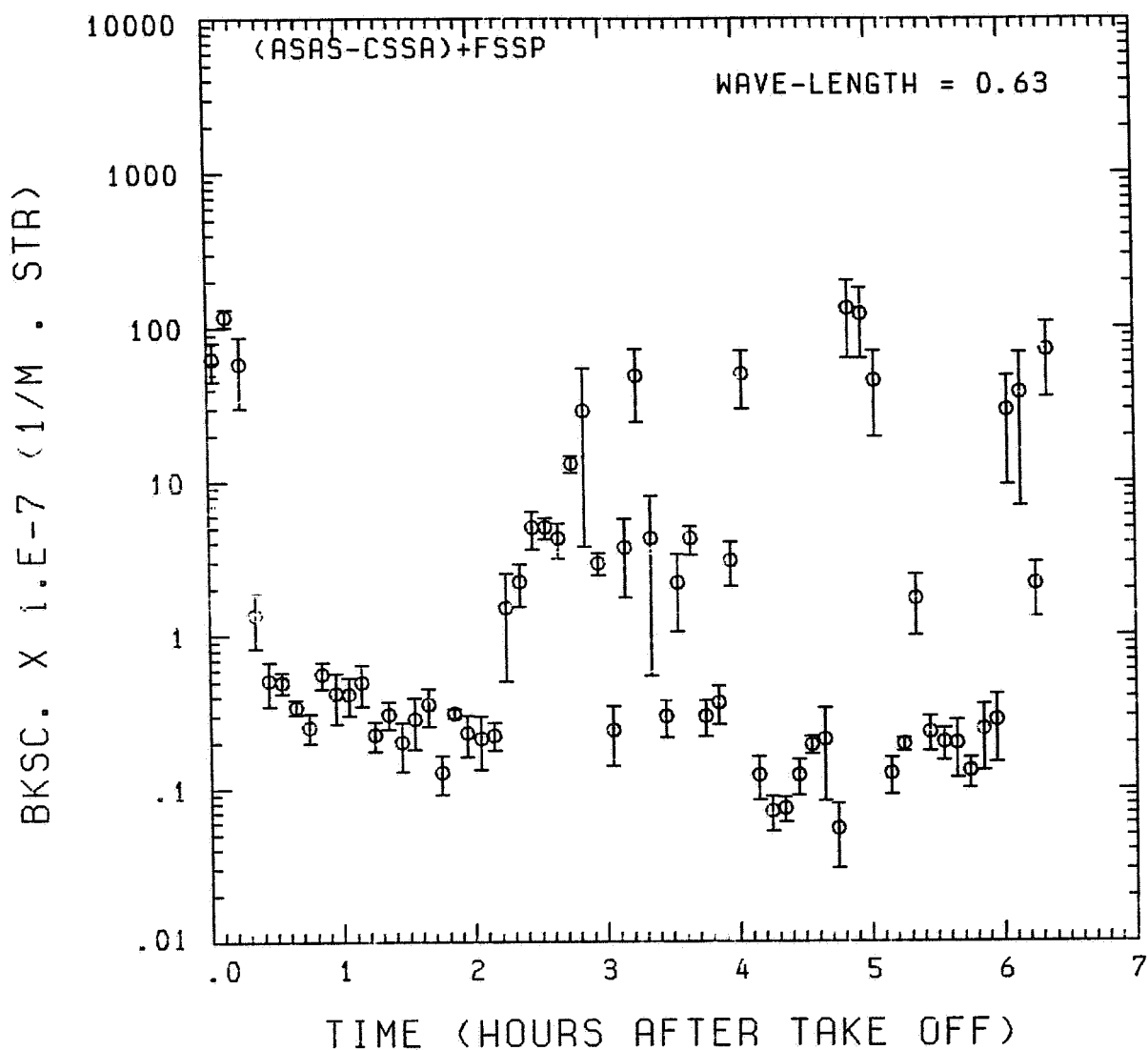


Fig. A2 (d). GAMETAG flight data for August 8, 1977.

Calculated backscatter coefficient along the flight track for five-minute data sets for $\lambda = 0.63 \mu\text{m}$.

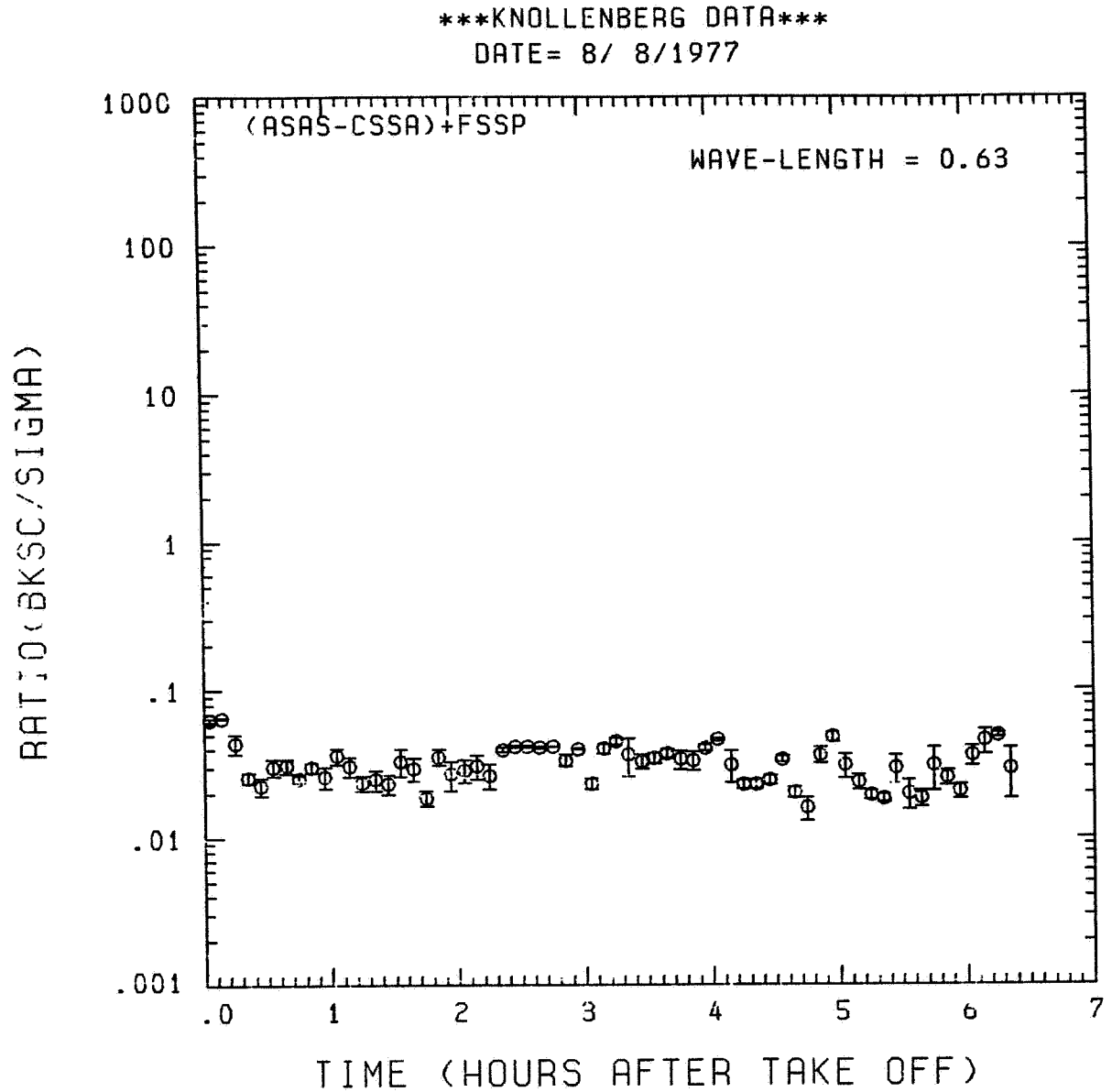


Fig. A 2 (e). GAMETAG flight data for August 8, 1977.
Calculated ratios for backscatter to extinction for
five-minute data sets for $\lambda = 0.63 \mu\text{m}$.

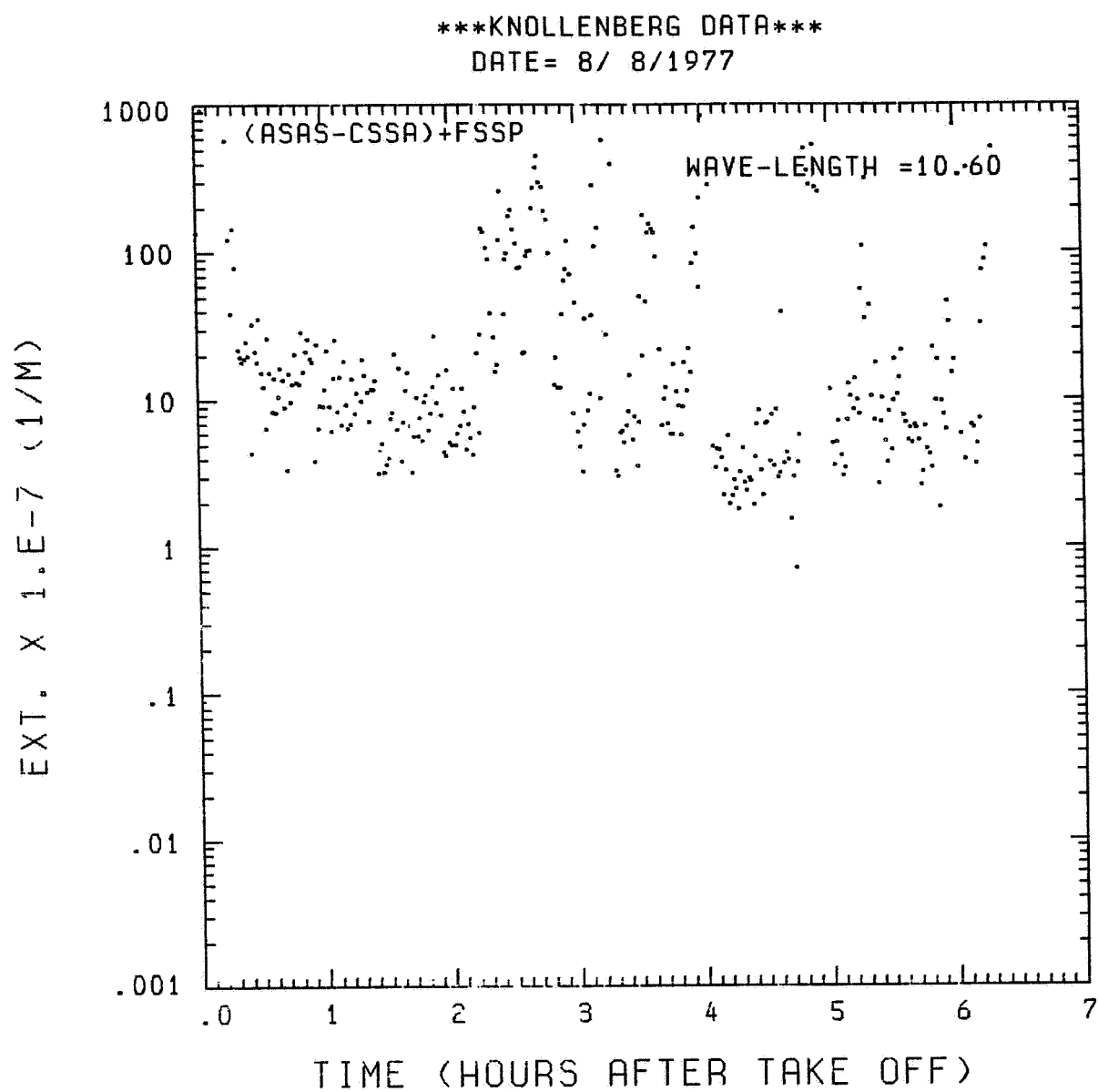


Fig. A 2 (f). GAMETAG flight data for August 8, 1977.
Calculated particulate extinction along the flight
track for one-minute data sets for $\lambda = 10.6 \mu\text{m}$.

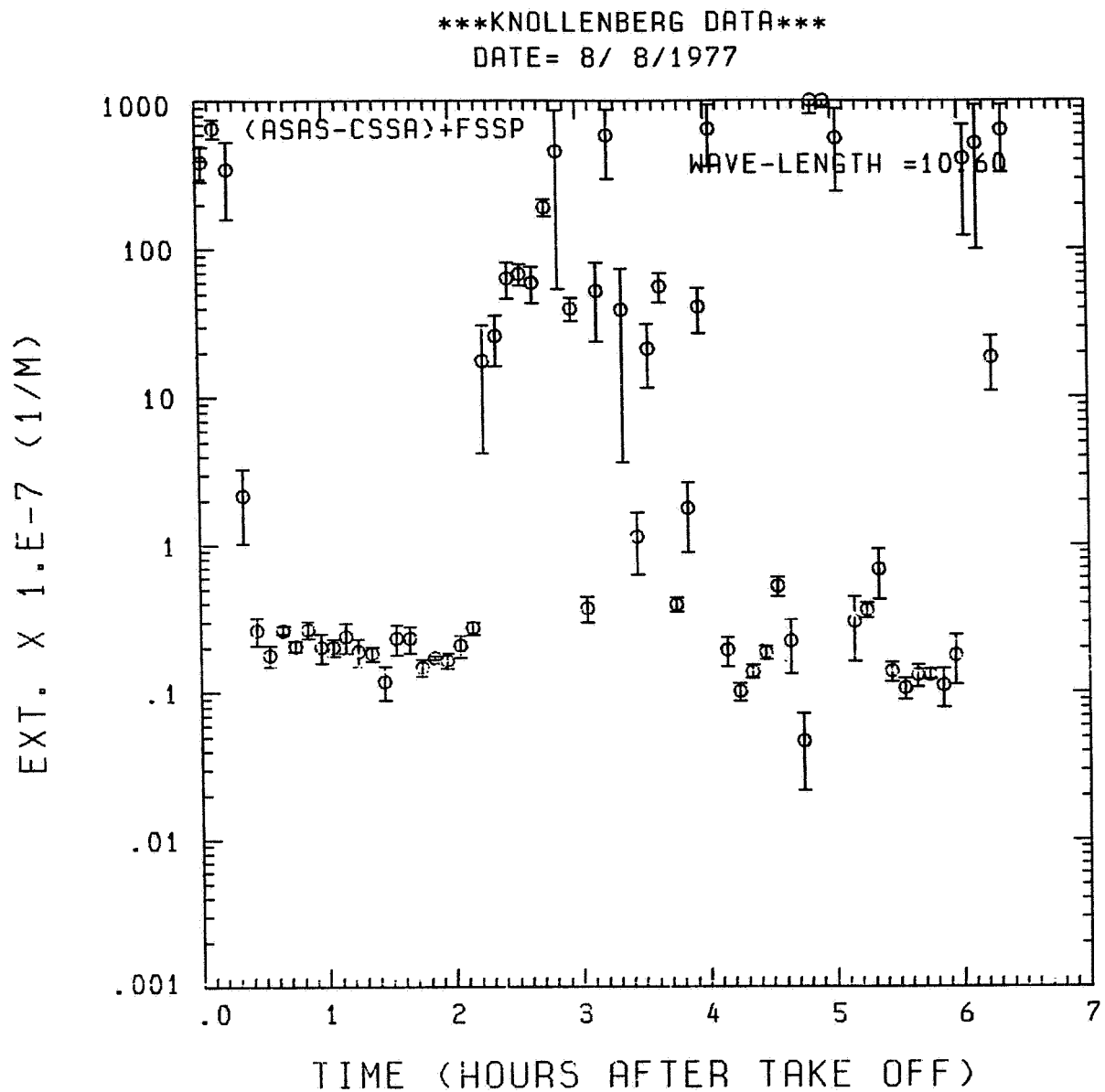


Fig. A 2 (g). GAMETAG flight data for August 8, 1977.
Calculated particulate extinction along the flight
track for five-minute data sets for $\lambda = 10.6 \mu\text{m}$.

ORIGINAL PAGE IS
OF POOR QUALITY

KNOLLENBERG DATA

DATE= 8/ 8/1977

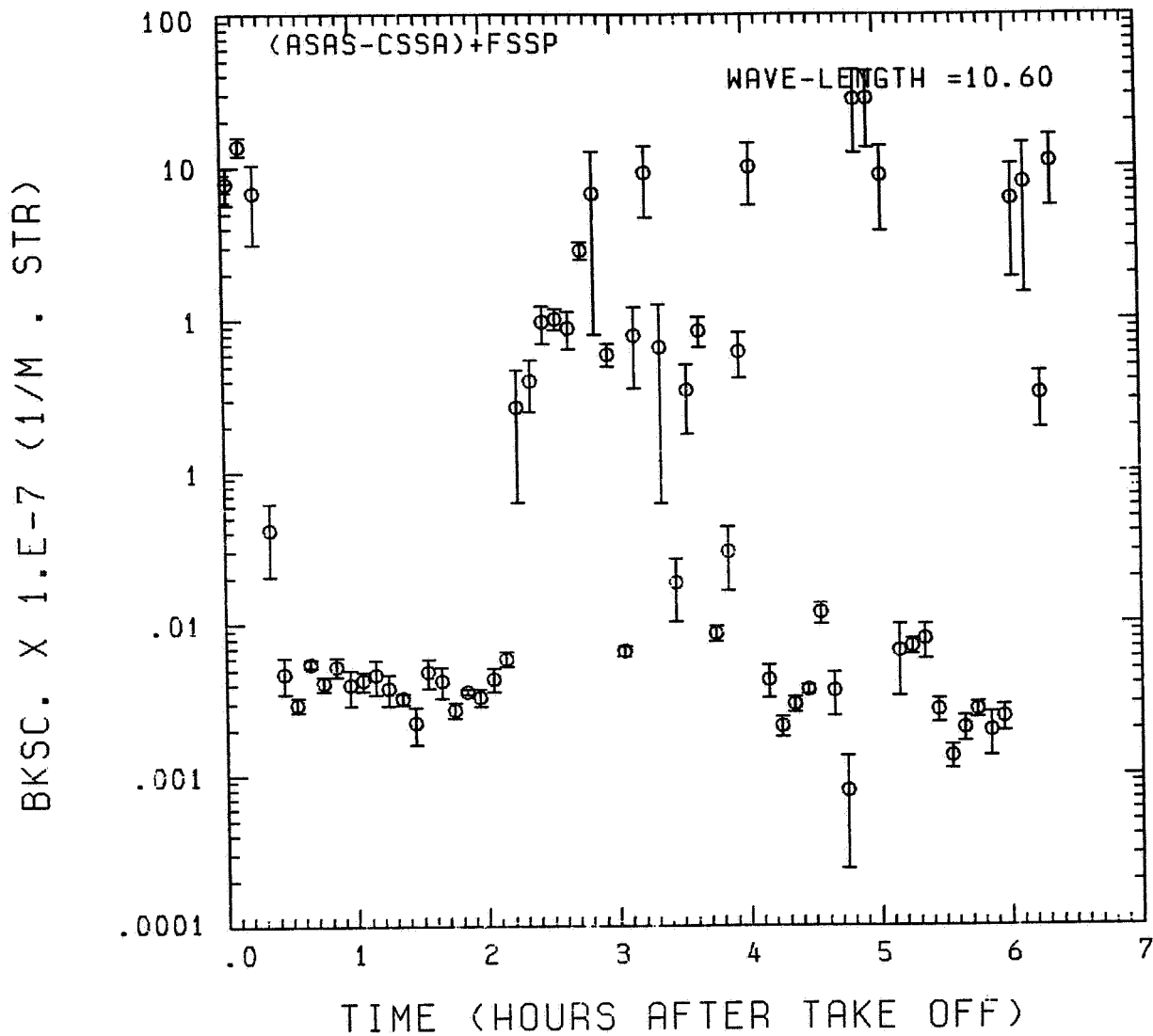


Fig. A2 (h). GAMETAG flight data for August 8, 1977.

Calculated backscatter coefficient along the flight
track for five-minute data sets for $\lambda = 10.6 \mu\text{m}$.

KNOLLENBERG DATA
 DATE= 8/ 8/1977

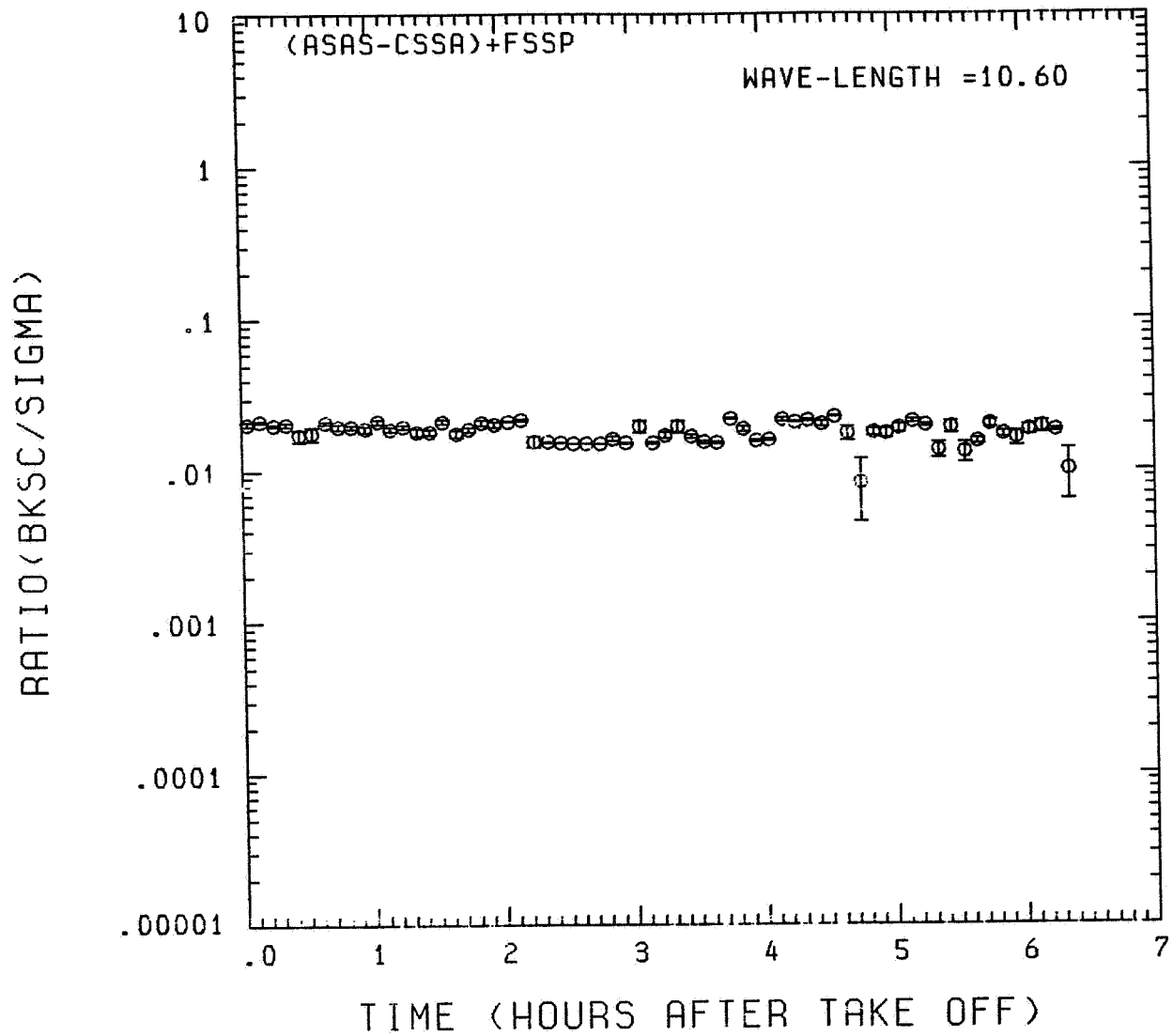


Fig. A2 (i). GAMETAG flight data for August 8, 1977.
 Calculated ratios for backscatter to extinction for
 five-minute data sets for $\lambda = 10.6 \mu\text{m}$.

Table A3. Significant times for August 22, 1977.
Denver, Colorado to Moffett Field,
California.

Significant Points

<u>#</u>	<u>TIME</u>	
1	18:22	Denver
2	19:12	
3	19:22	
4	20:21	
5	21:01	
6	21:15	
7	21:17	
8	21:38	
9	21:41	
10	21:51	
11	22:17	
12	22:26	
13	23:15	
14	23:34	Moffett Field

ORIGINAL PAGE IS
OF POOR QUALITY

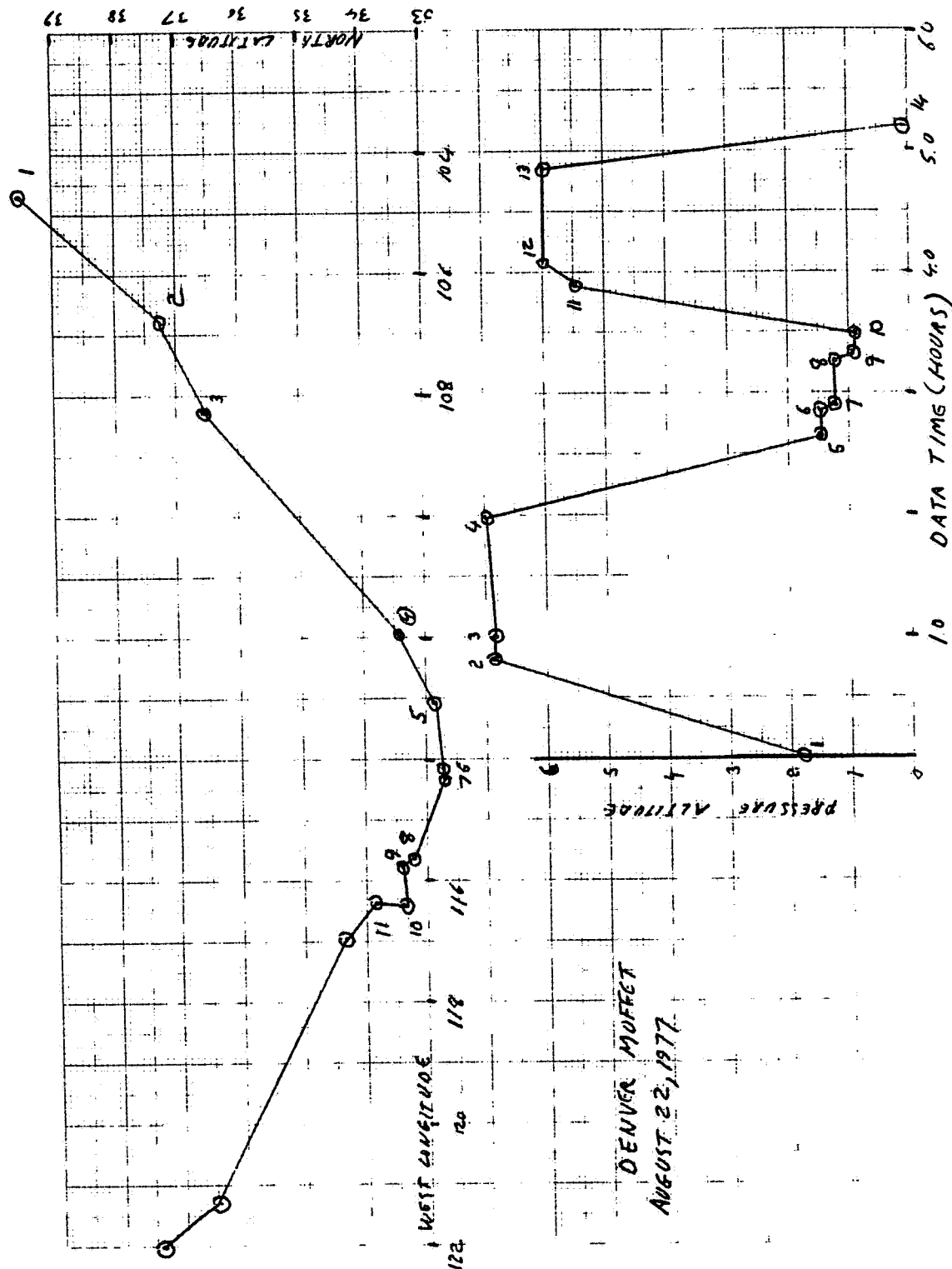


Fig. A 3 (a). GAMETAG flight data for August 22, 1977.
Altitude and location flight track plotted as a
function of time after takeoff.

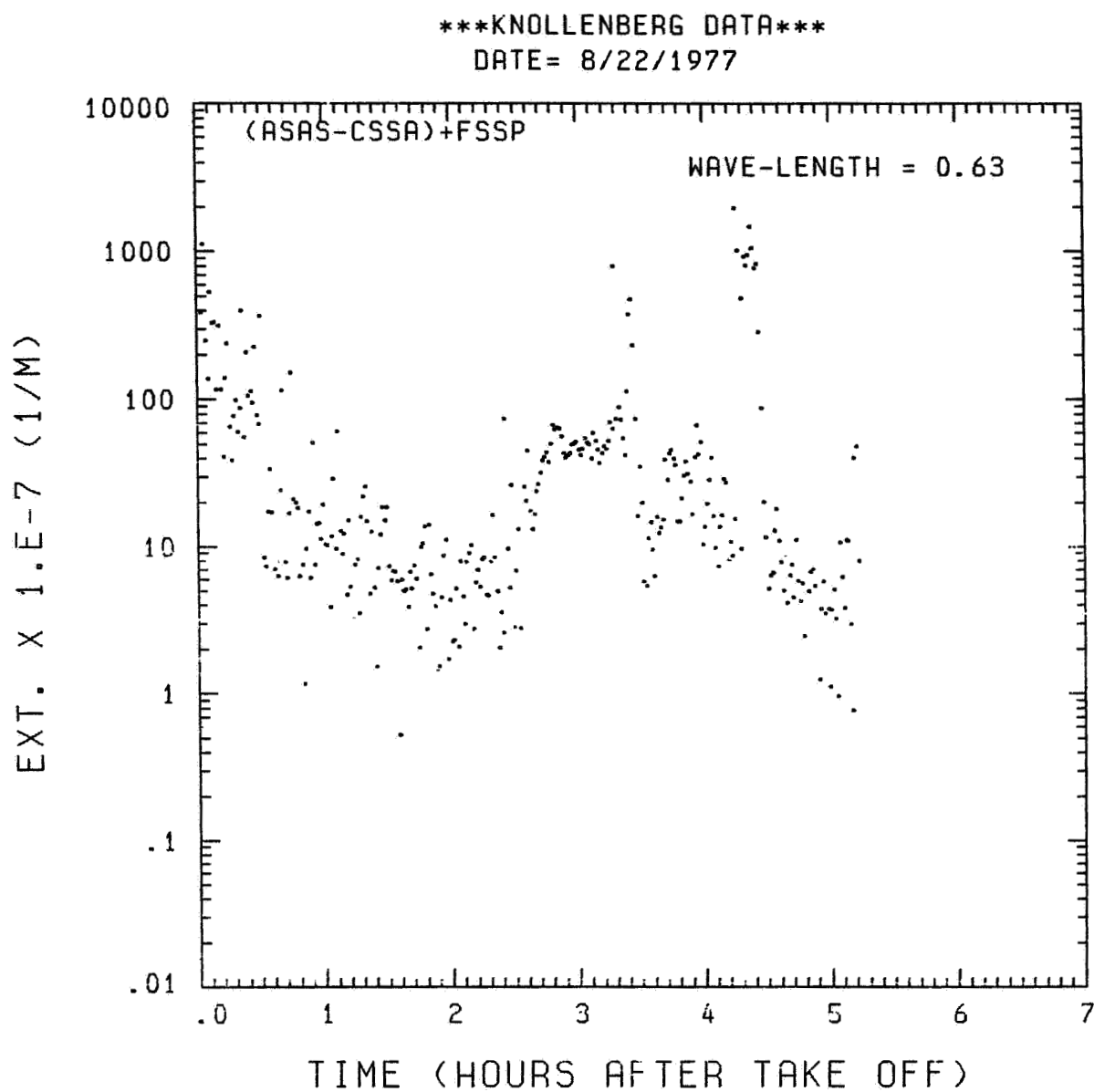


Fig. A 3 (b). GAMETAG flight data for August 22, 1977.
Calculated particulate extinction along the flight
track for one-minute data sets for $\lambda = 0.63 \mu\text{m}$.

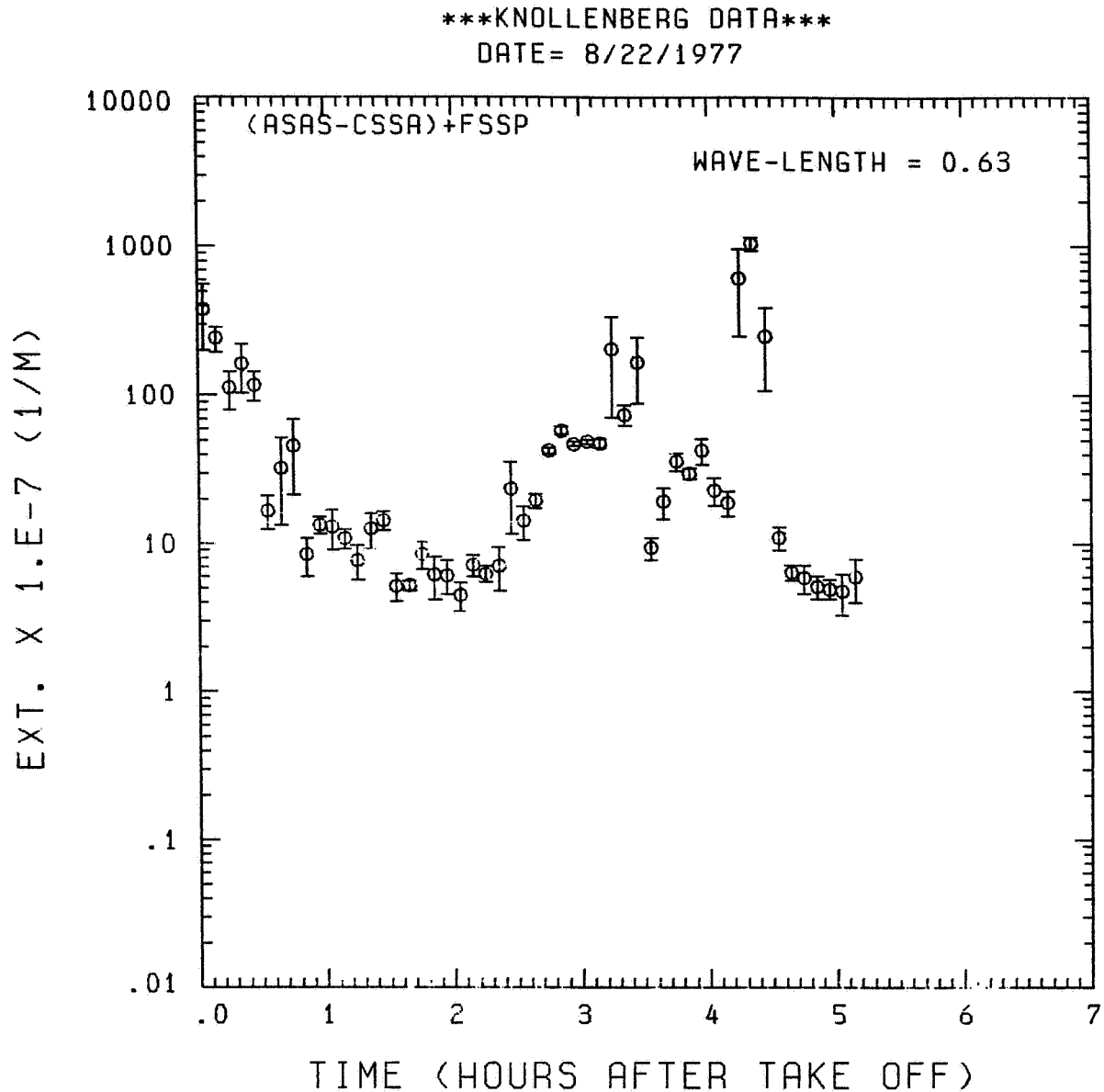


Fig. A3 (c). GAMETAG flight data for August 22, 1977.
Calculated particulate extinction along the flight
track for five-minute data sets for $\lambda = 0.63 \mu\text{m}$.

KNOLLENBERG DATA

DATE= 8/22/1977

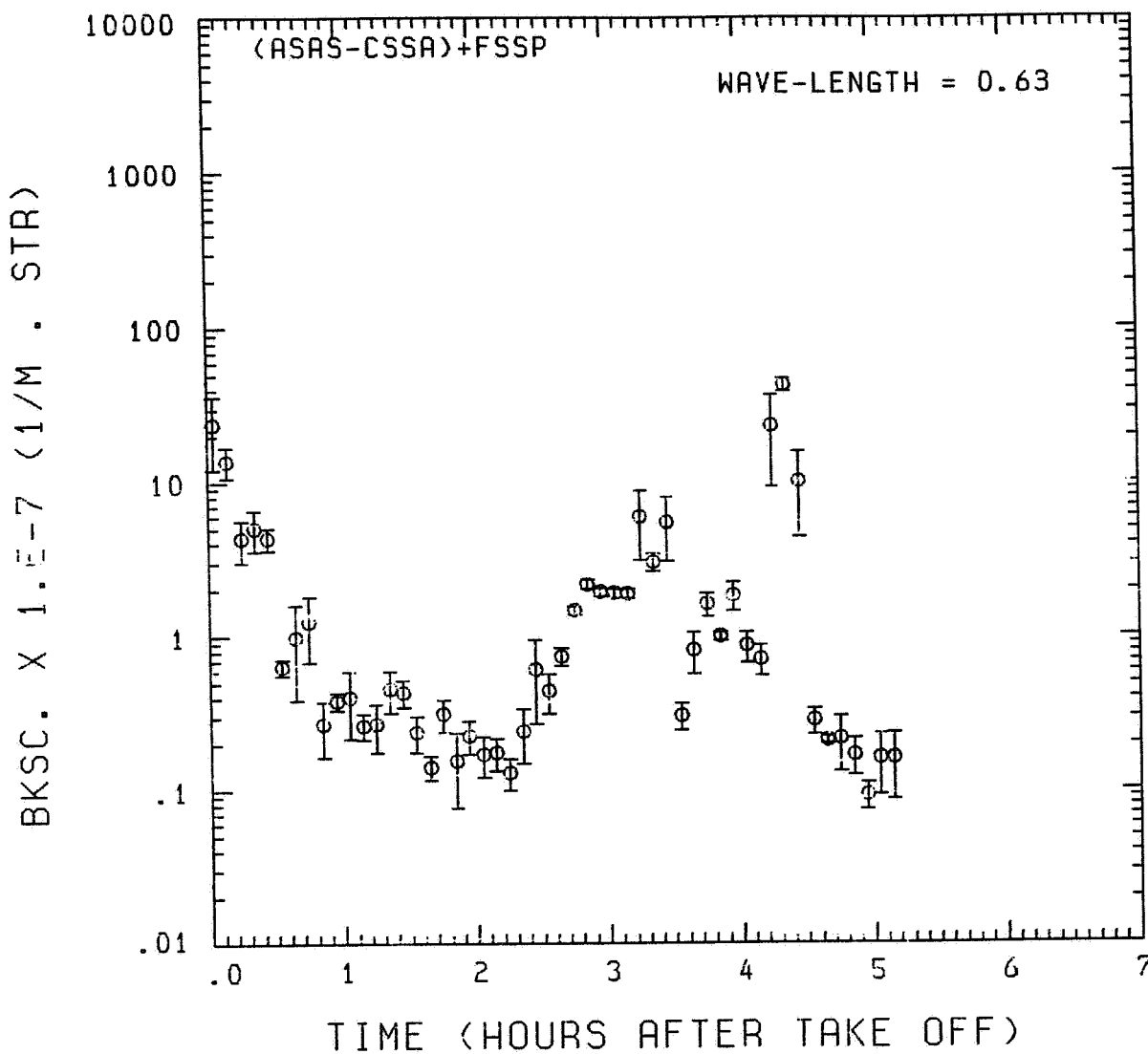


Fig. A3 (d). GAMETAG flight data for August 22, 1977.

Calculated backscatter coefficient along the flight track for five-minute data sets for $\lambda = 0.63 \mu\text{m}$.

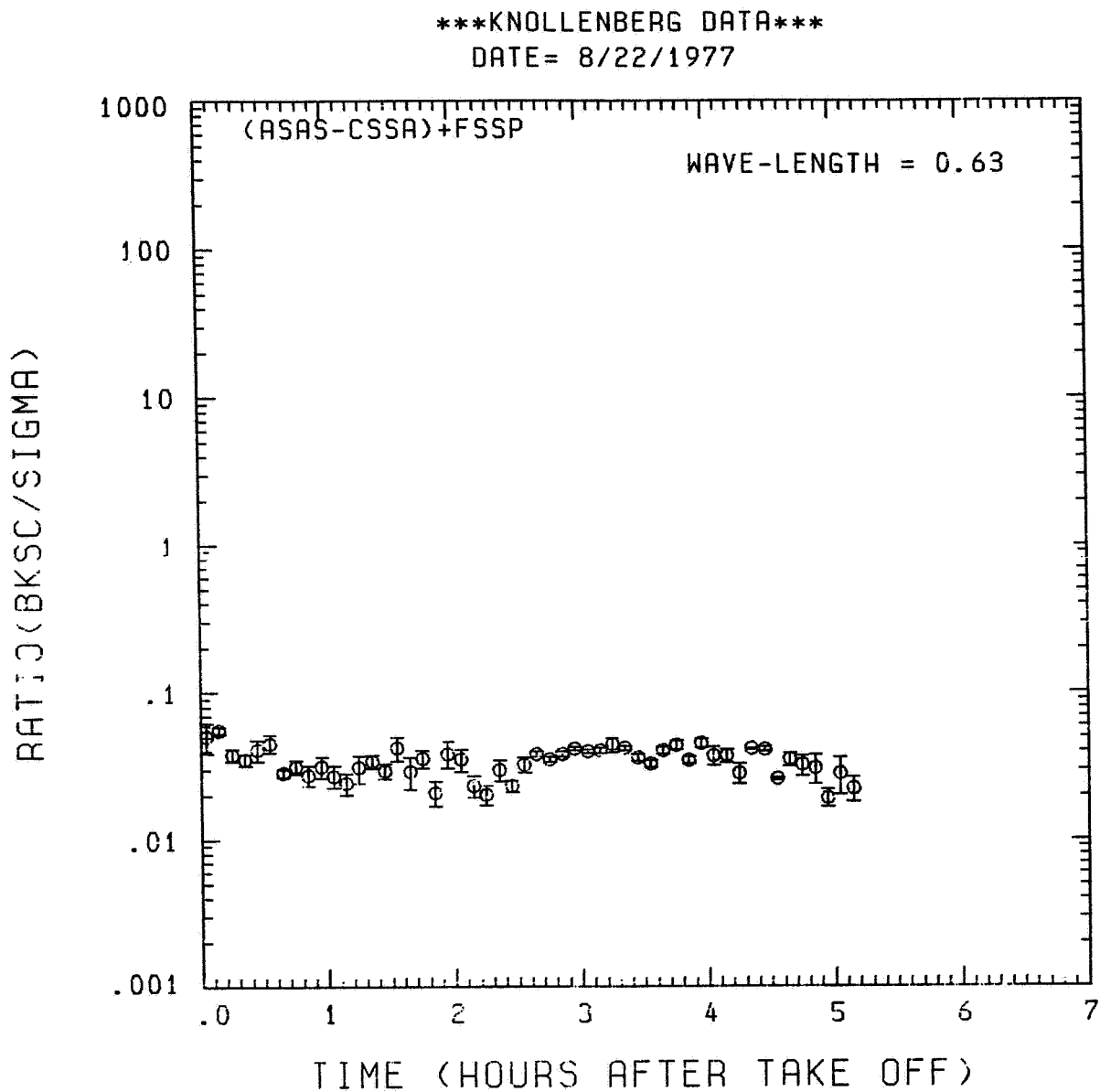


Fig. A 3 (e). GAMETAG flight data for August 22, 1977.
Calculated ratios for backscatter to extinction for
five-minute data sets for $\lambda = 0.63 \mu\text{m}$.

ORIGINAL PAGE IS
OF POOR QUALITY

KNOLLENBERG DATA

DATE= 8/22/1977

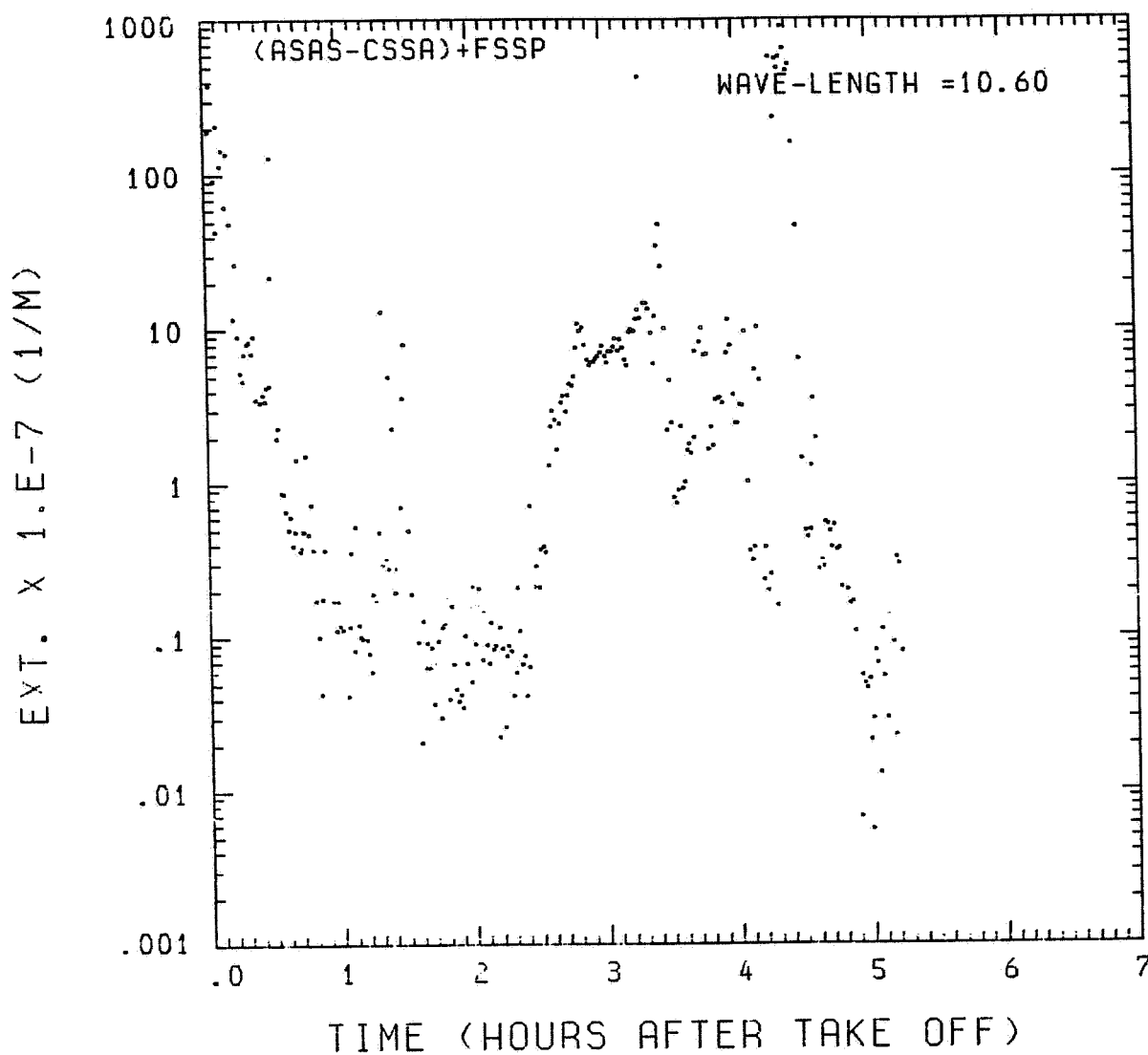


Fig. A3 (f). GAMETAG flight data for August 22, 1977.
Calculated particulate extinction along the flight
track for one-minute data sets for $\lambda = 10.6 \mu\text{m}$.

KNOLLENBERG DATA

DATE= 8/22/1977

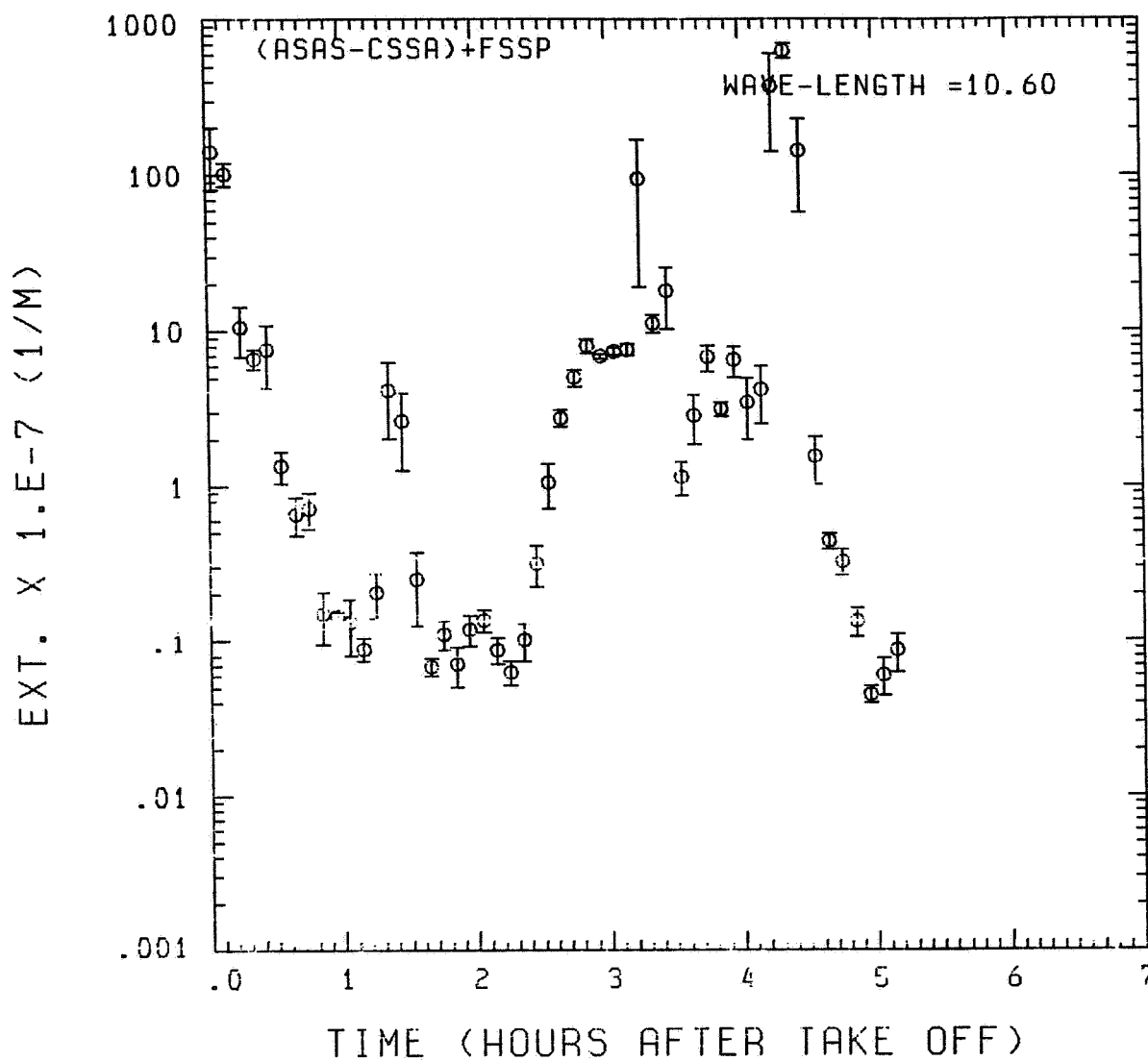


Fig. A3 (g). GAMETAG flight data for August 22, 1977.

Calculated particulate extinction along the flight track for five-minute data sets for $\lambda = 10.6 \mu\text{m}$.

KNOLLENBERG DATA

DATE= 8/22/1977

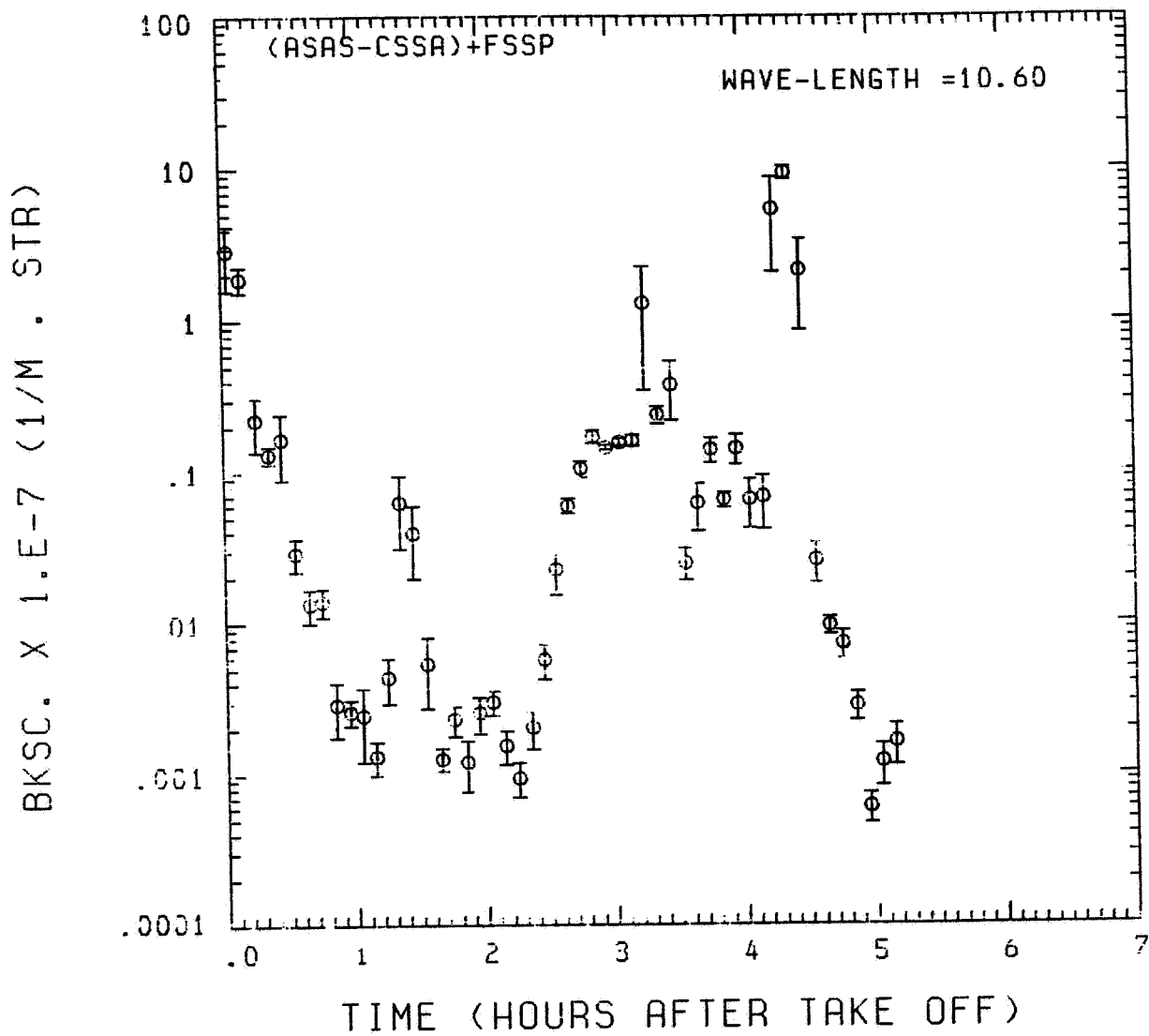


Fig. A3 (h). GAMETAG flight data for August 22, 1977.

Calculated backscatter coefficient along the flight track for five-minute data sets for $\lambda = 10.6 \mu\text{m}$.

KNOLLENBERG DATA

DATE= 8/22/1977

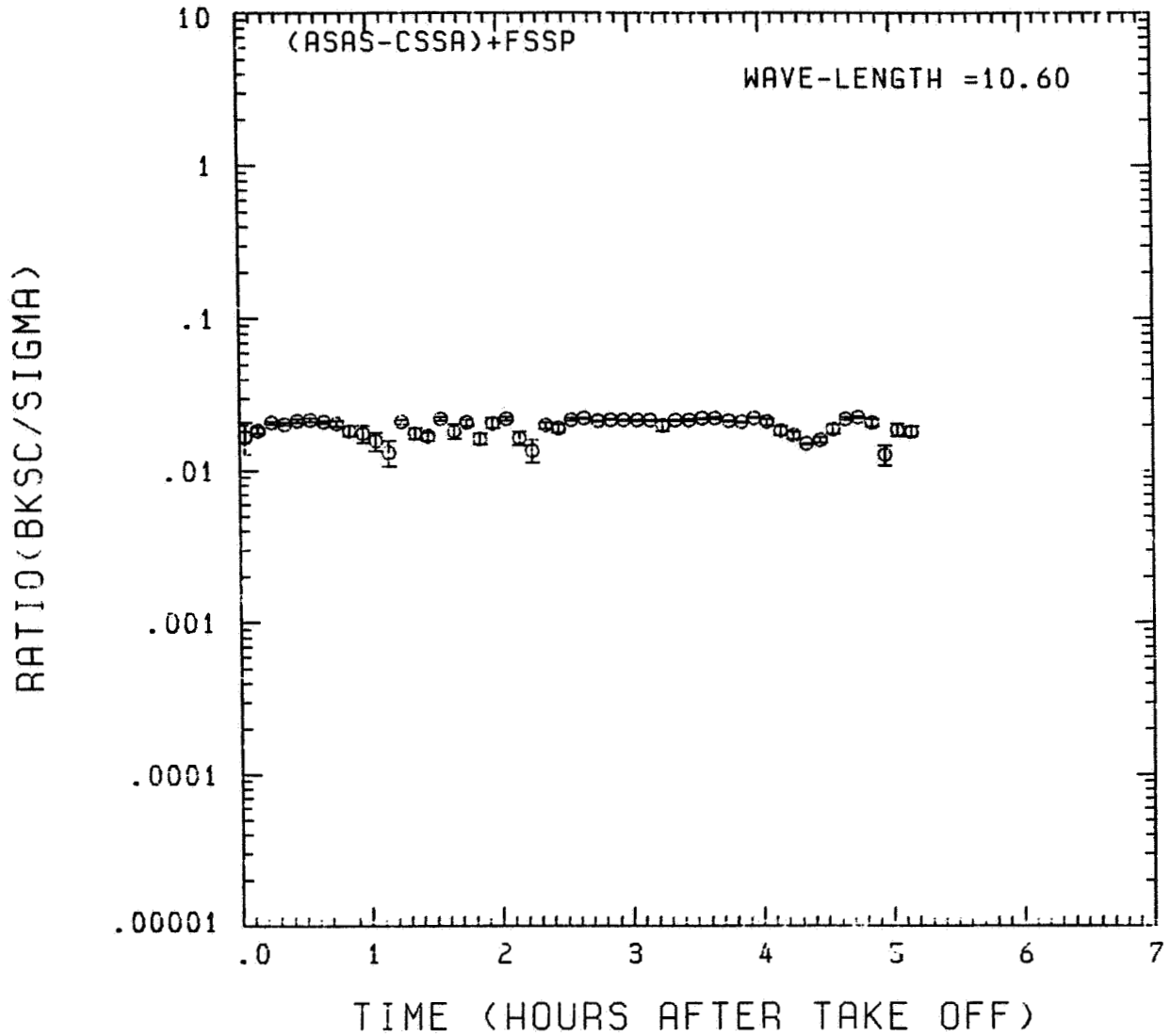


Fig. A3 (i). GAMETAG flight data for August 22, 1977.
Calculated ratios for backscatter to extinction for
five-minute data sets for $\lambda = 10.6 \mu\text{m}$.

Table A4. Significant times for August 23, 1977.
Moffett Field, California to Hilo, Hawaii.

Significant Points

<u>#</u>	<u>TIME</u>	
1	17:45	Moffett Field
2	18:20	
3	20:31	
4	20:40	
5	22:13	
6	22:19	
7	23:18	
8	23:28	
9	00:09	
10	00:26	
11	00:46	
12	00:59	Hilo

ORIGINAL PAGE IS
OF POOR QUALITY

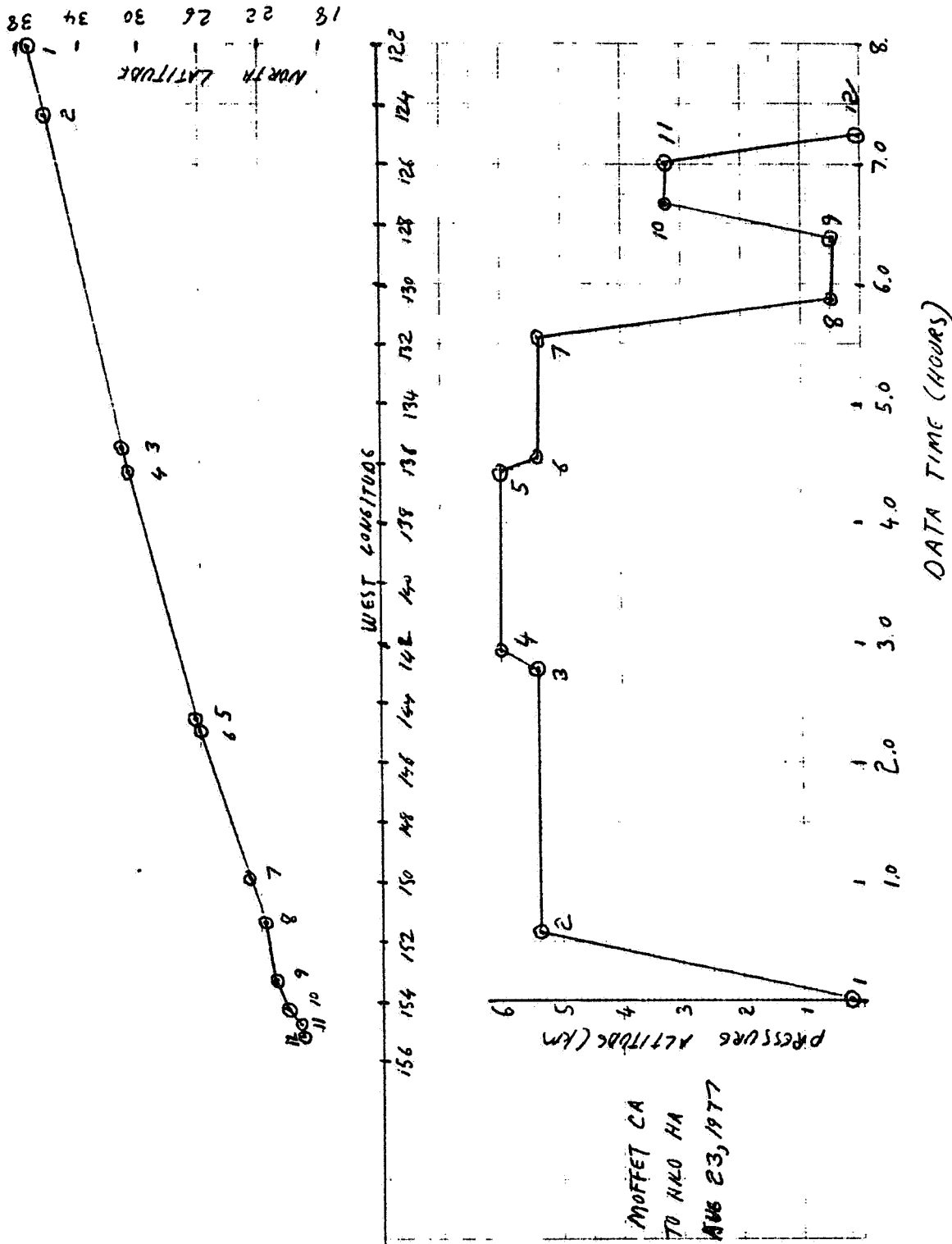


Fig. A4 (a). GAMETAG flight data for August 23, 1977.
Altitude and location flight track plotted as a
function of time after takeoff.

KNOLLENBERG DATA

DATE= 8/23/1977

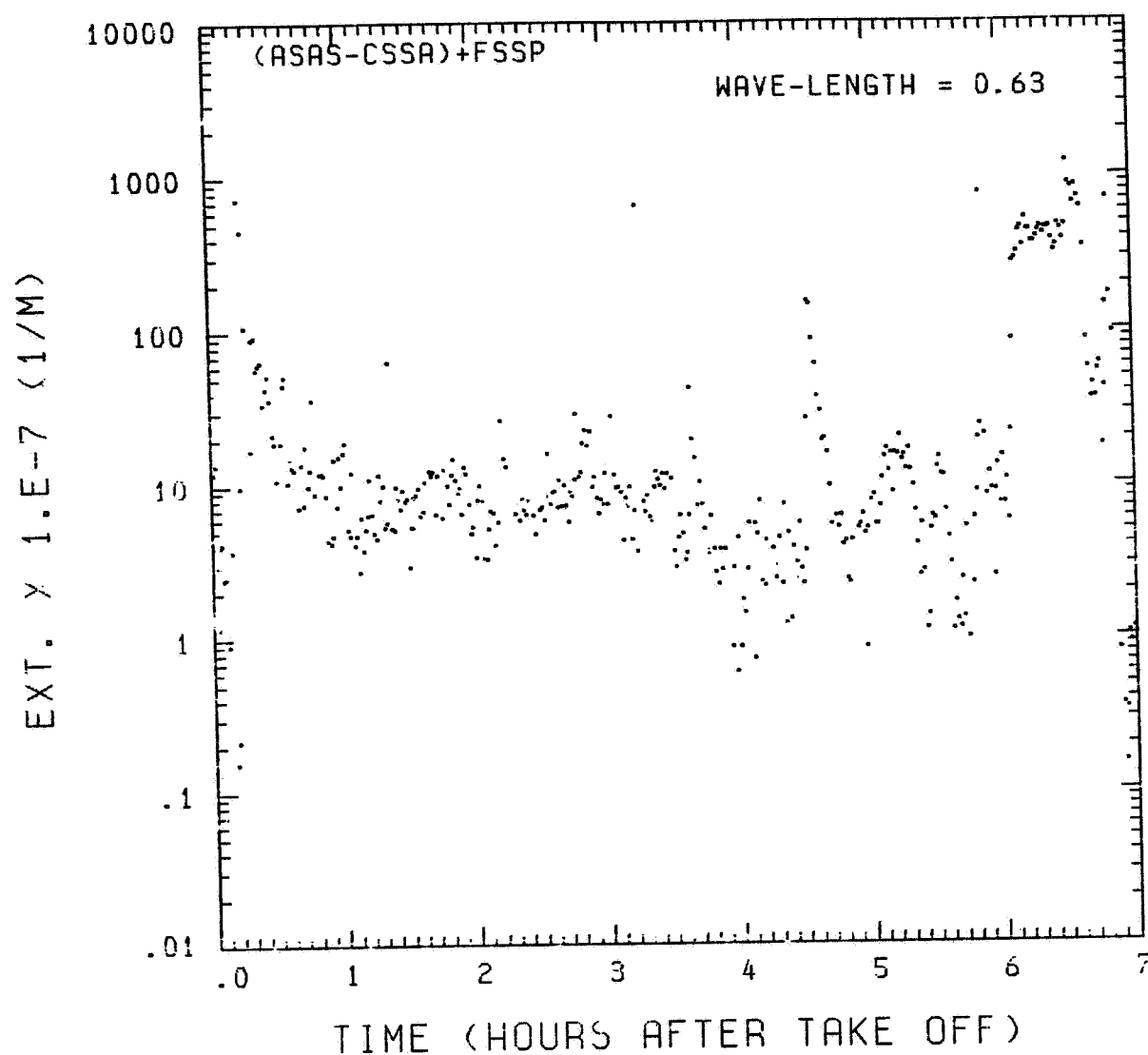


Fig. A4 (b). GAMETAG flight data for August 23, 1977.

Calculated particulate extinction along the flight track for one-minute data sets for $\lambda = 0.63 \mu\text{m}$.

KNOLLENBERG DATA

DATE= 8/23/1977

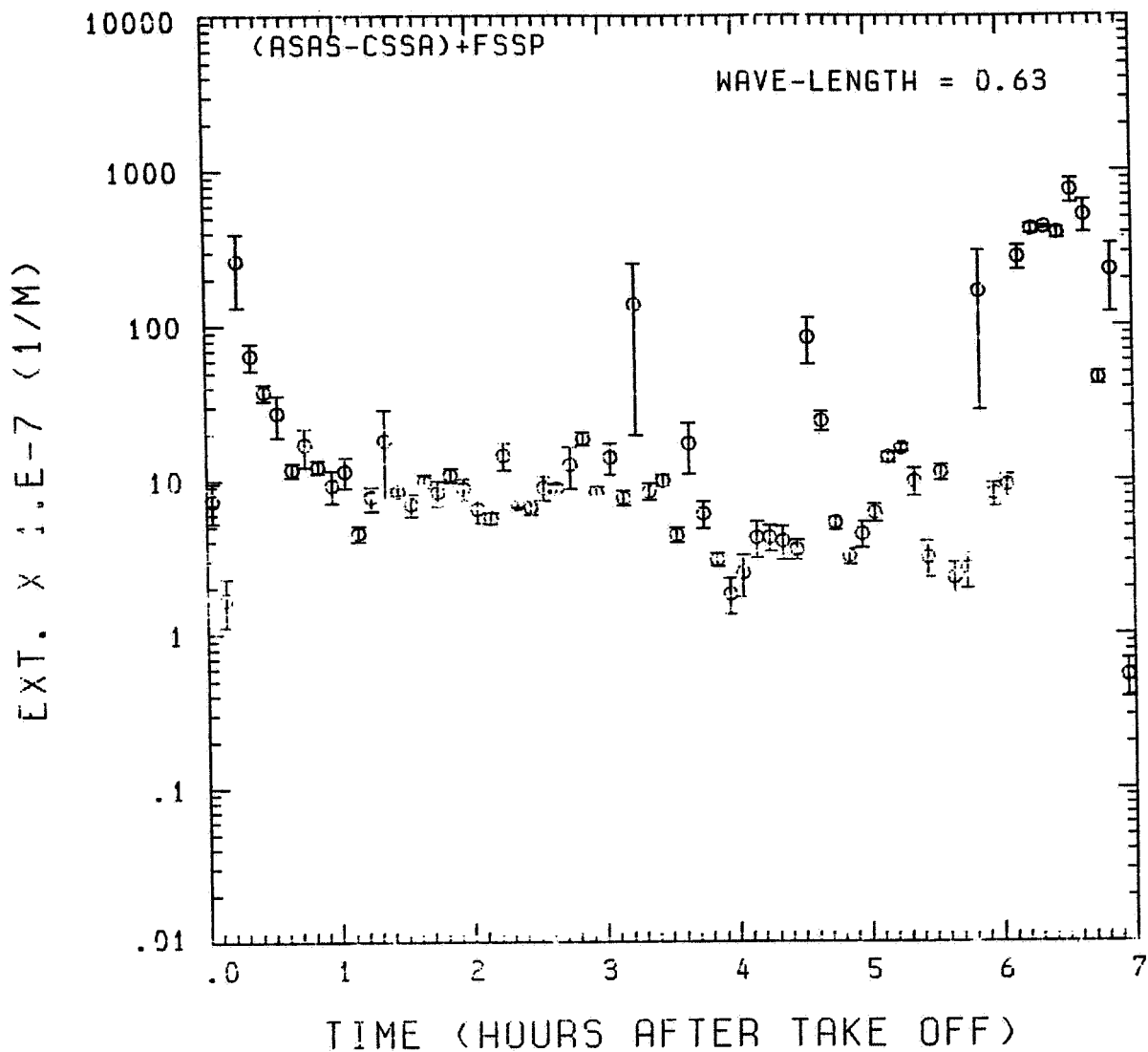


Fig. A4 (c). GAMETAG flight data for August 23, 1977.

Calculated particulate extinction along the flight track for five-minute data sets for $\lambda = 0.63 \mu\text{m}$.

KNOLLENBERG DATA

DATE= 8/23/1977

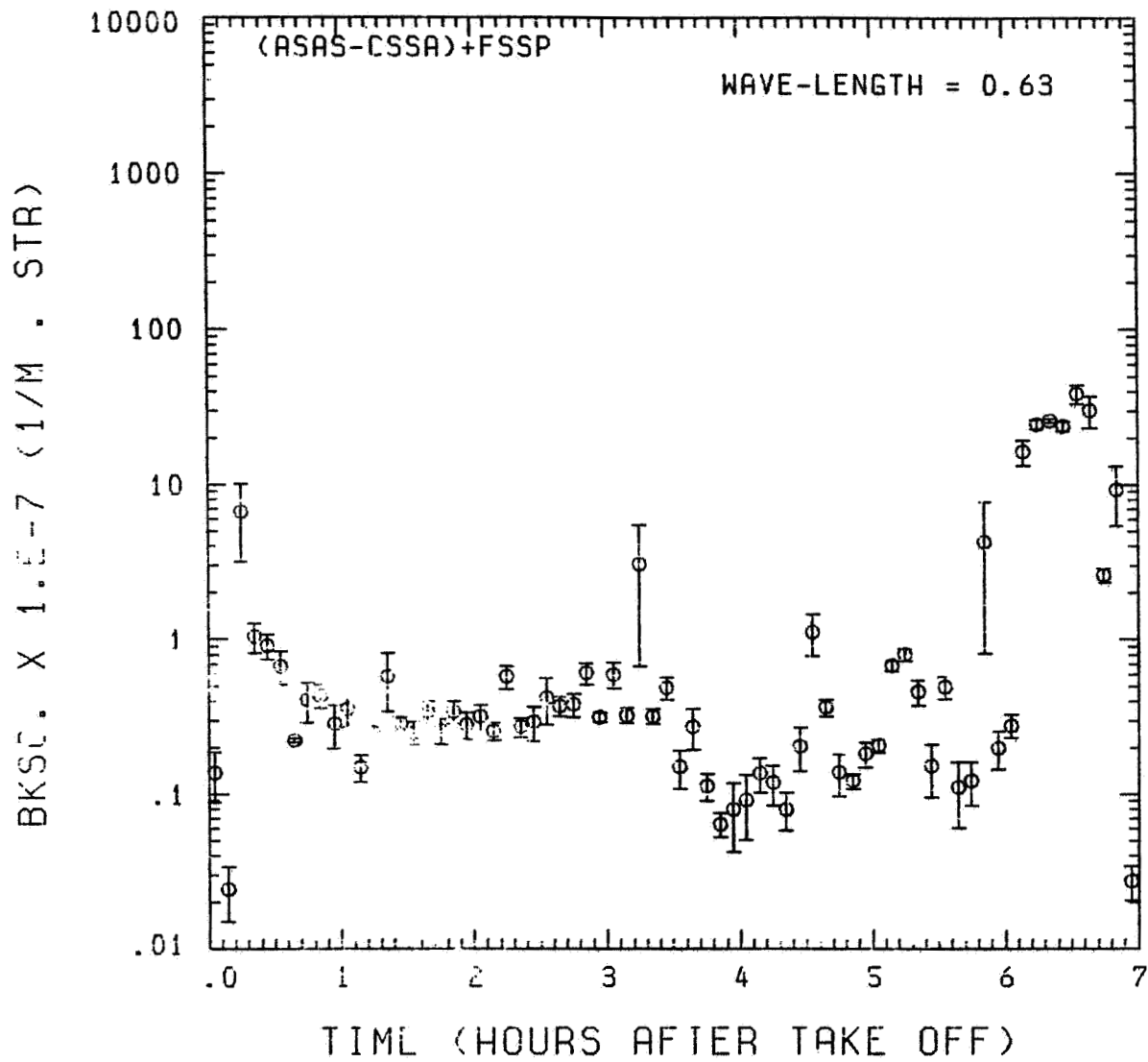


Fig. A4 (d). GAMETAG flight data for August 23, 1977.

Calculated backscatter coefficient along the flight track for five-minute data sets for $\lambda = 0.63 \mu\text{m}$.

KNOLLENBERG DATA

DATE= 8/23/1977

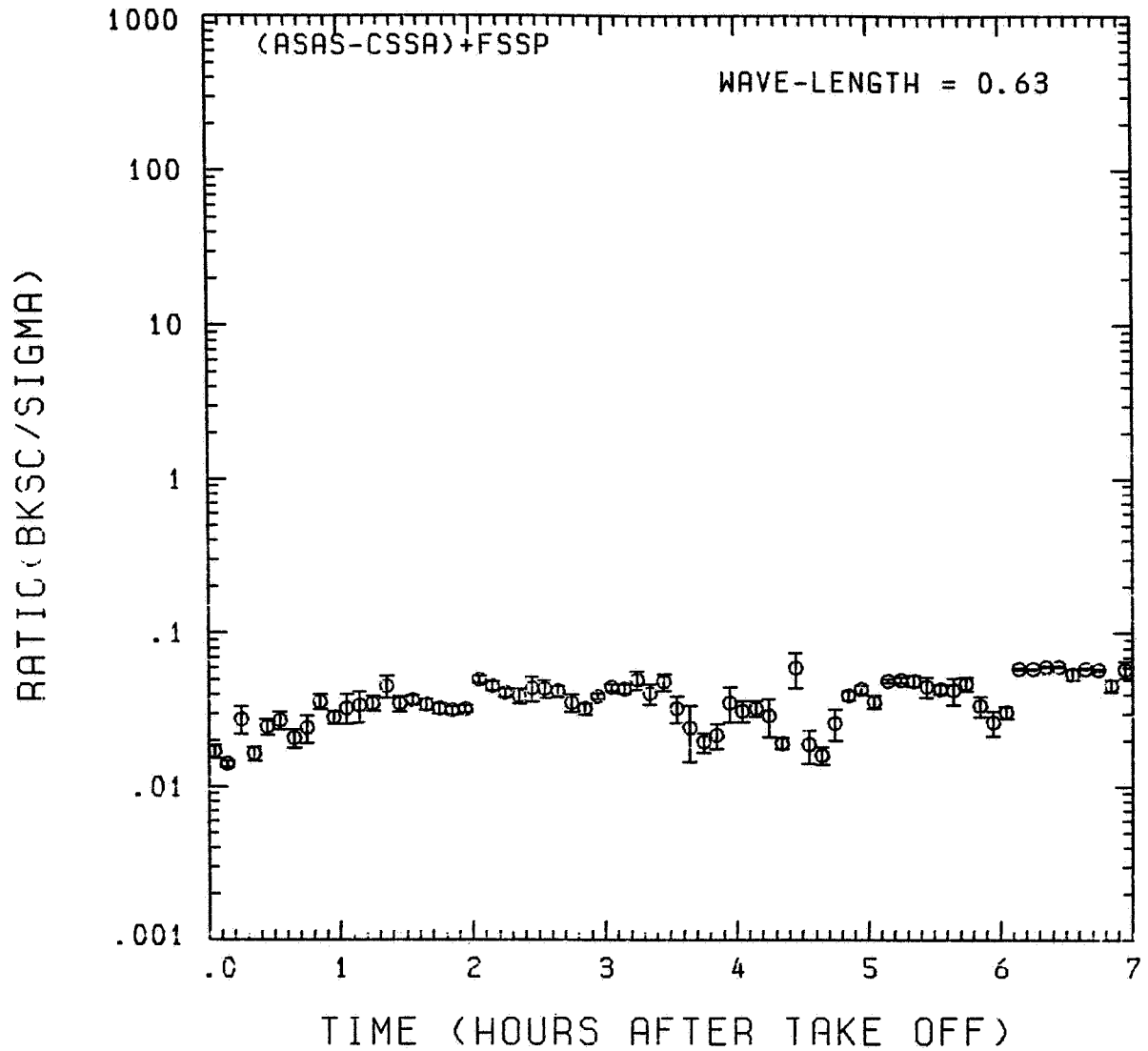


Fig. A4 (e). GAMETAG flight data for August 23, 1977.

Calculated ratios for backscatter to extinction for
five-minute data sets for $\lambda = 0.63 \mu\text{m}$.

KNOLLENBERG DATA

DATE= 8/23/1977

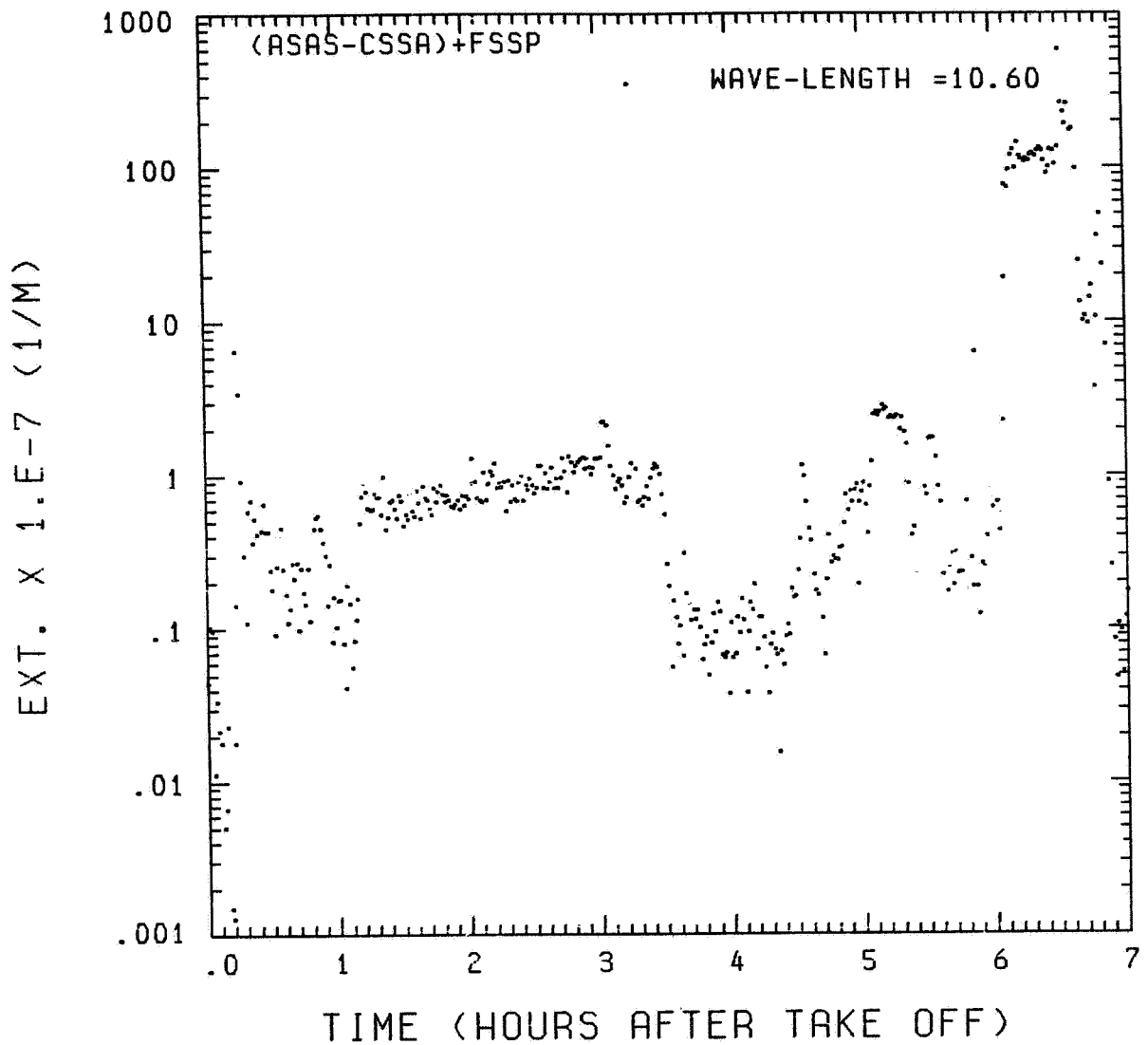


Fig. A4 (f). GAMETAG flight data for August 23, 1977.

Calculated particulate extinction along the flight track for one-minute data sets for $\lambda = 10.6 \mu\text{m}$.

KNOLLENBERG DATA

DATE= 8/23/1977

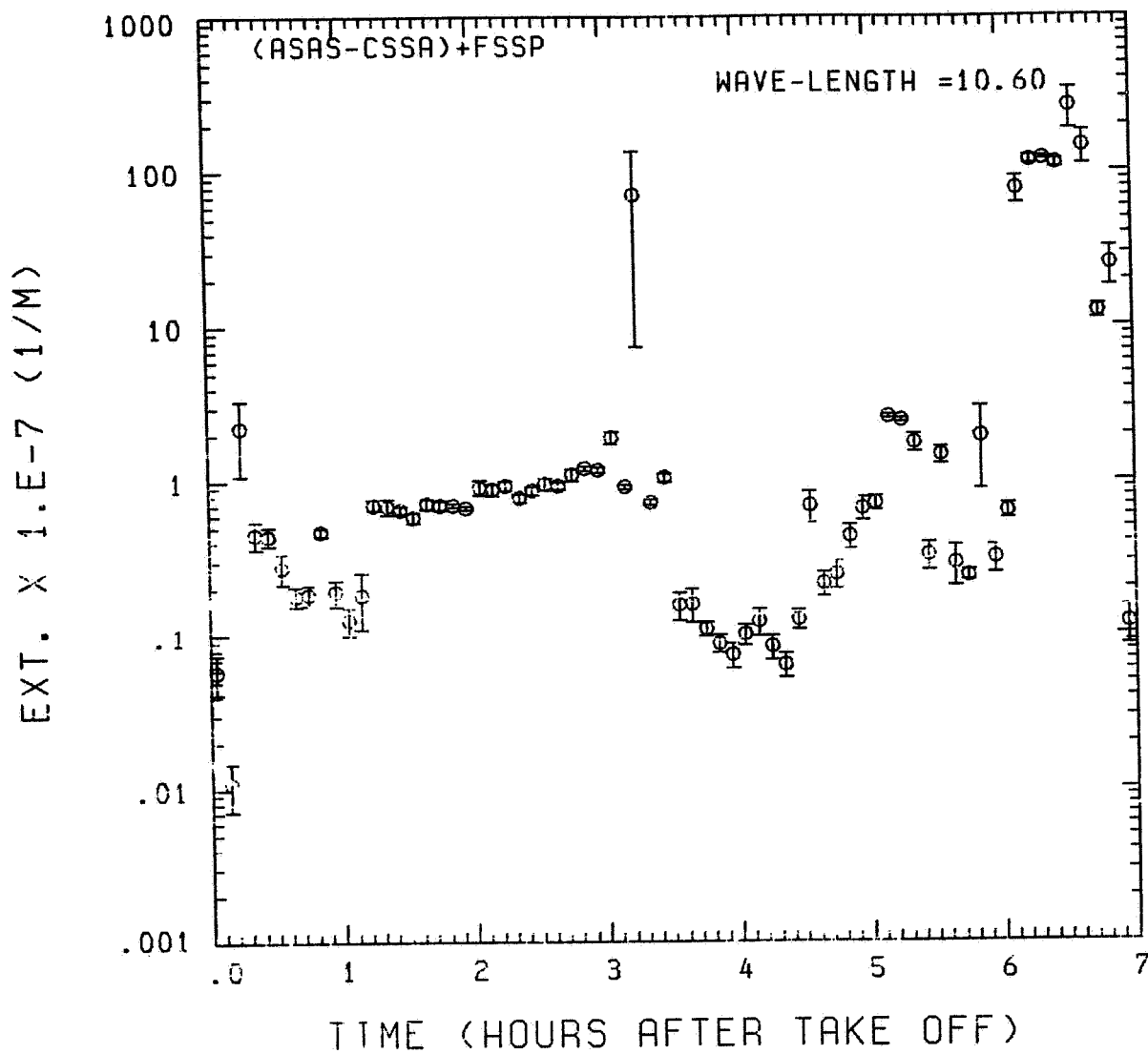


Fig. A4 (g). GAMETAG flight data for August 23, 1977.

Calculated particulate extinction along the flight track for five-minute data sets for $\lambda = 10.6 \mu\text{m}$.

ORIGINAL PAGE IS
OF POOR QUALITY

KNOLLENBERG DATA

DATE= 8/23/1977

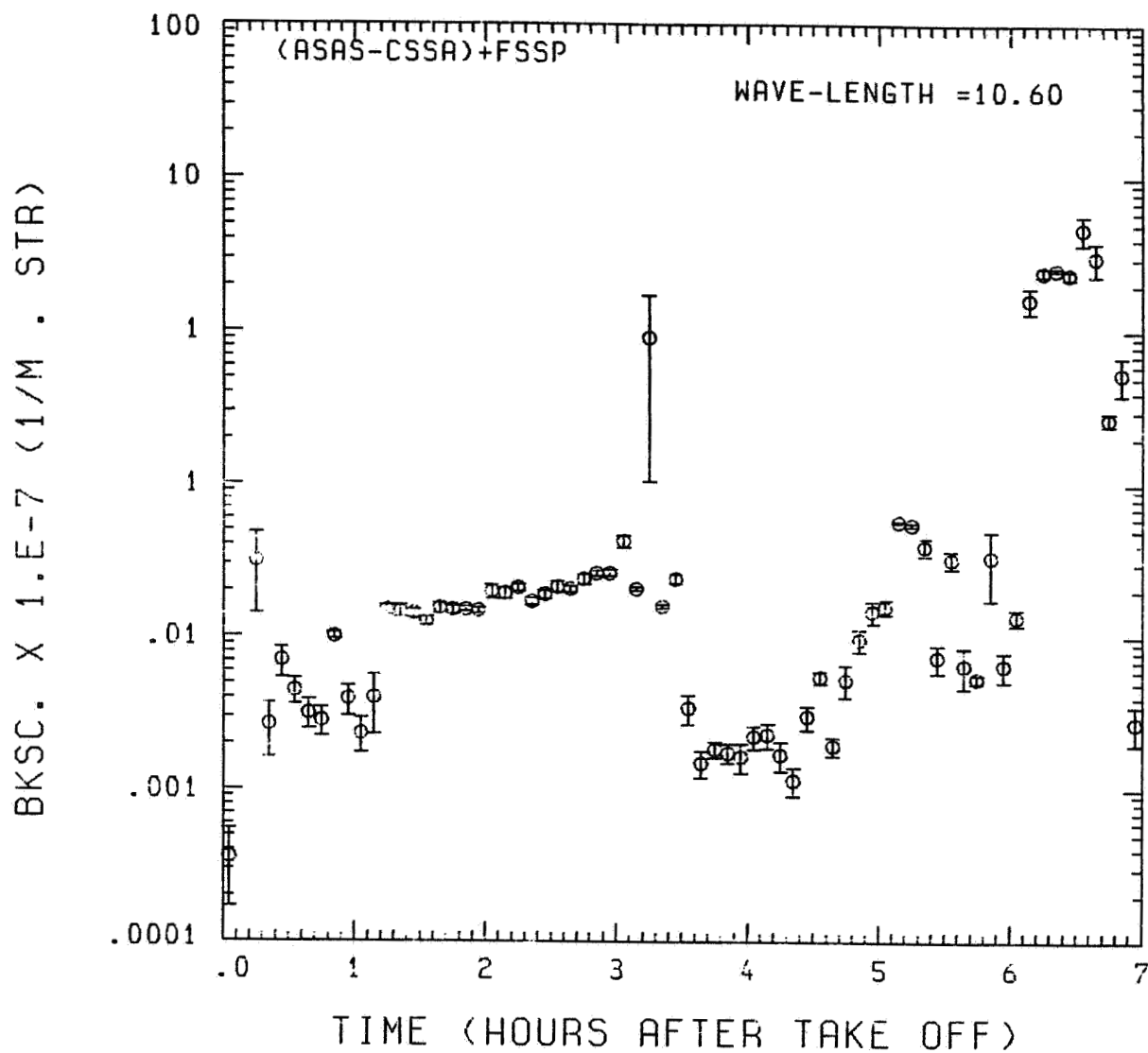


Fig. A4 (h). GAMETAG flight data for August 23, 1977.

Calculated backscatter coefficient along the flight
track for five-minute data sets for $\lambda = 10.6 \mu\text{m}$.

KNOLLENBERG DATA

DATE= 8/23/1977

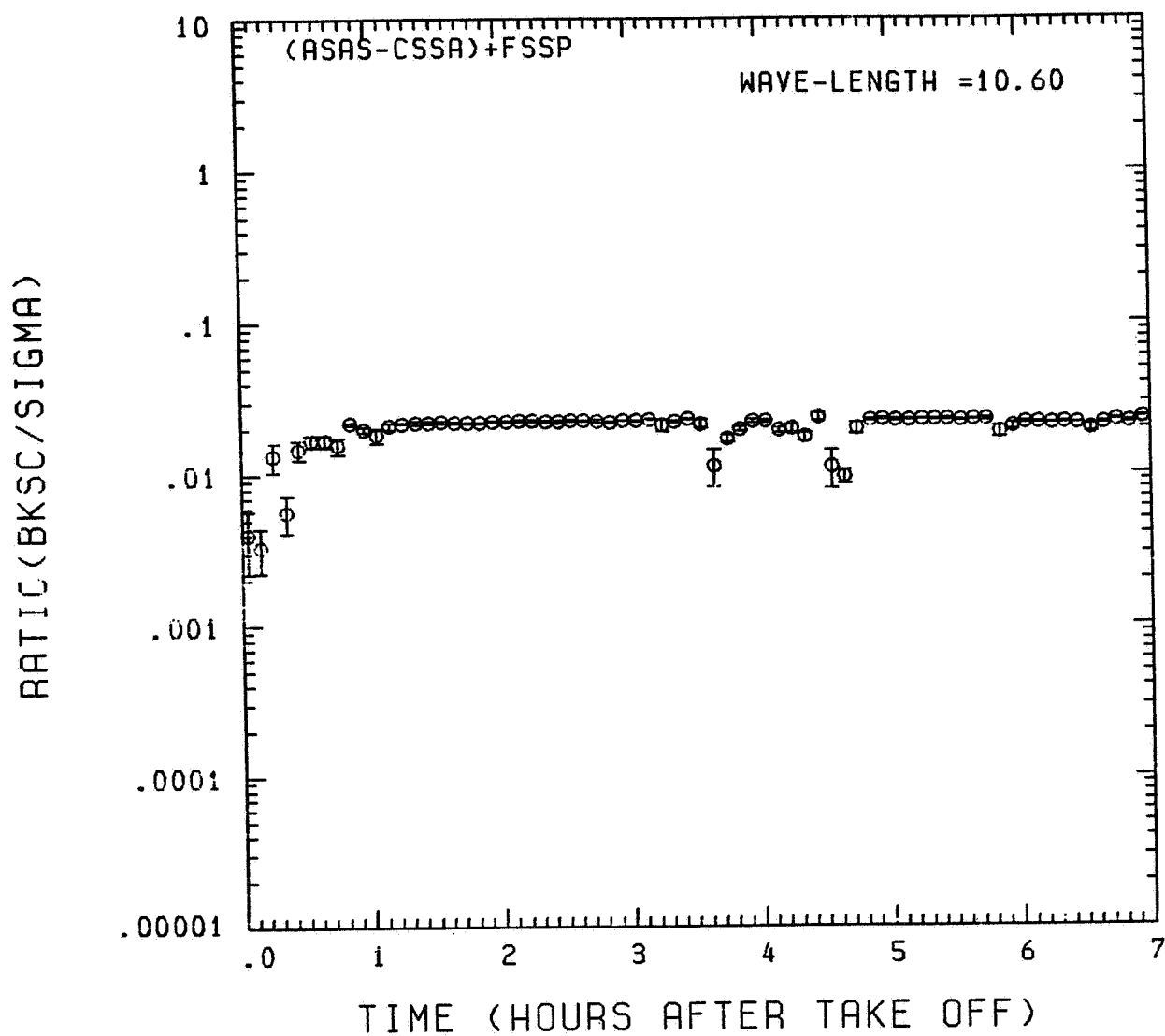
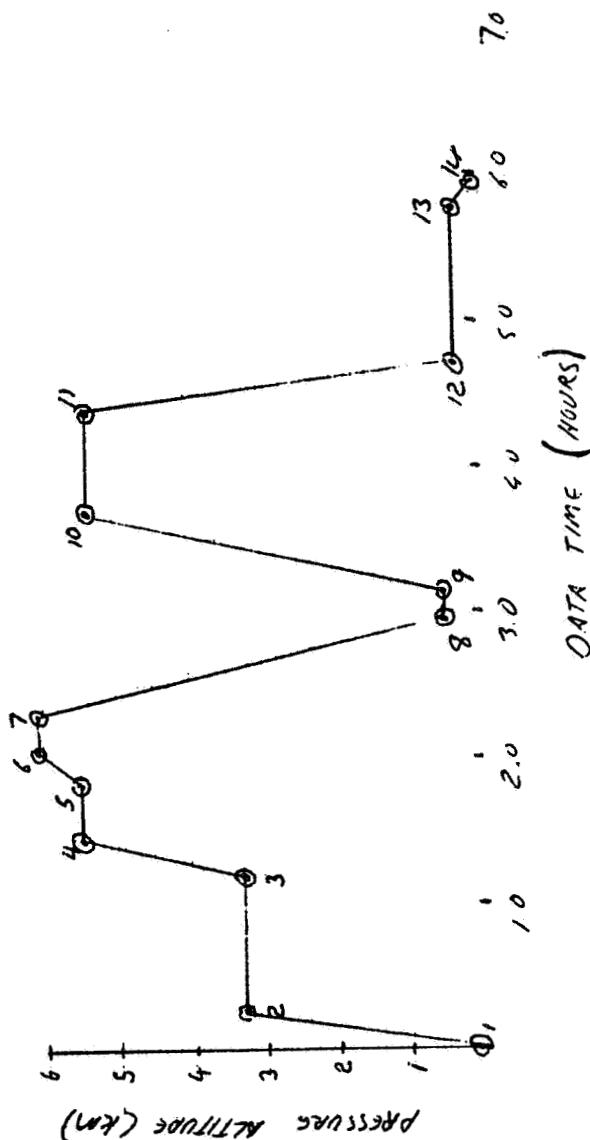
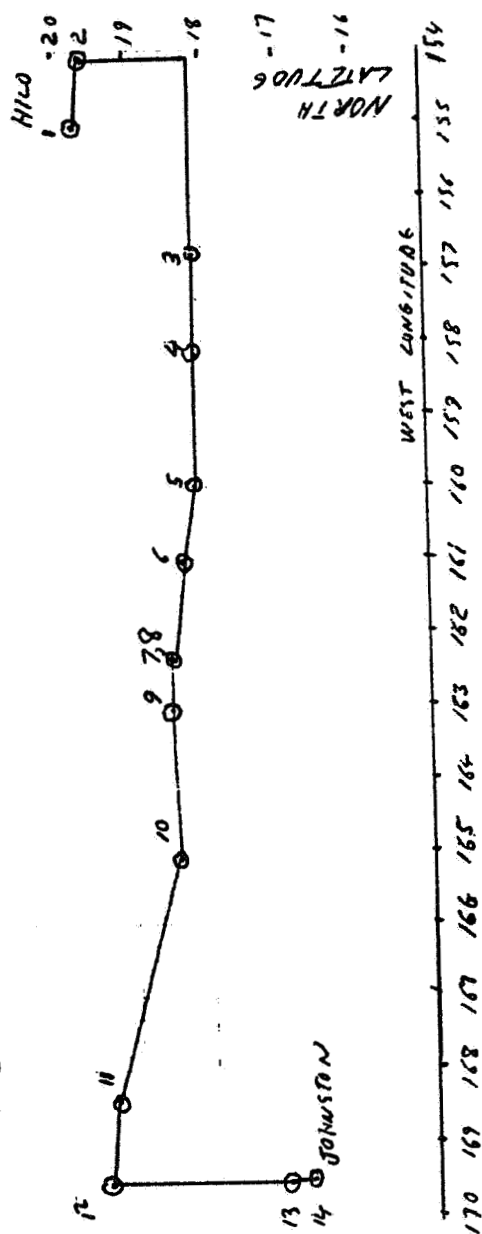


Fig. A4 (i). GAMETAG flight data for August 23, 1977.
Calculated ratios for backscatter to extinction for
five-minute data sets for $\lambda = 10.6 \mu\text{m}$.

Table A5. Significant times for August 25, 1977.
Hilo, Hawaii to Johnston Atoll.

Significant Points

<u>#</u>	<u>TIME</u>	
1	20:51	Hilo
2	21:07	
3	22:03	
4	22:19	
5	22:41	
6	22:54	
7	23:09	
8	23:47	
9	23:59	
10	00:32	
11	01:14	
12	01:33	
13	02:36	
14	02:48	Johnston Atoll



Hilo Hawaii
To Johnston Atoll
Aug 25, 1977

Fig. A 5 (a). GAMETAG flight data for August 25, 1977.
Altitude and location flight track plotted as a
function of time after takeoff.

KNOLLENBERG DATA

DATE= 8/25/1977

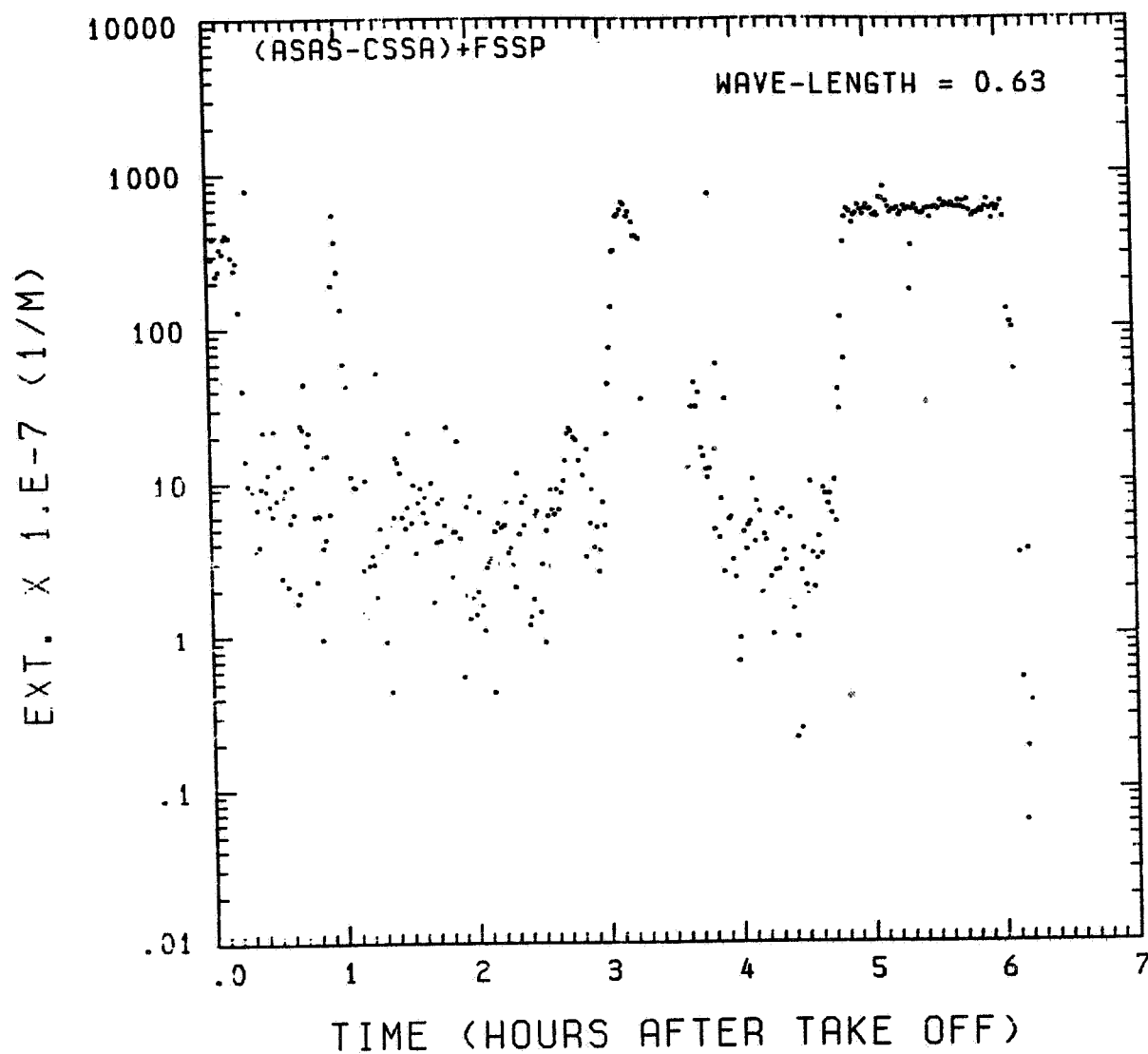


Fig. A 5 (b). GAMETAG flight data for August 25, 1977.
Calculated particulate extinction along the flight
track for one-minute data sets for $\lambda = 0.63 \mu\text{m}$.

KNOLLENBERG DATA

DATE= 8/25/1977

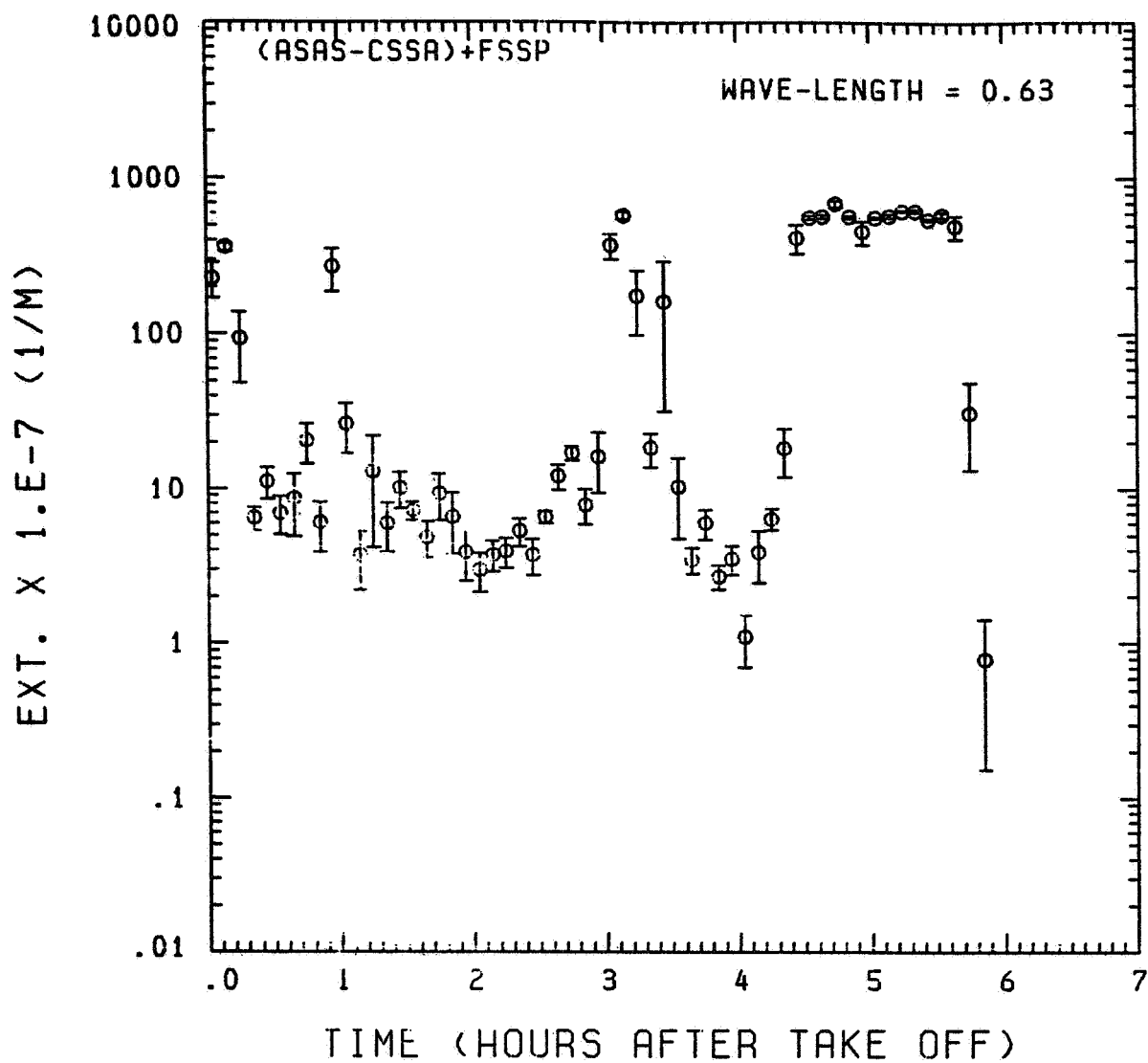


Fig. A 5 (c). GAMETAG flight data for August 25, 1977.

Calculated particulate extinction along the flight track for five-minute data sets for $\lambda = 0.63 \mu\text{m}$.

ORIGINAL PAGE IS
OF POOR QUALITY

KNOLLENBERG DATA

DATE= 8/25/1977

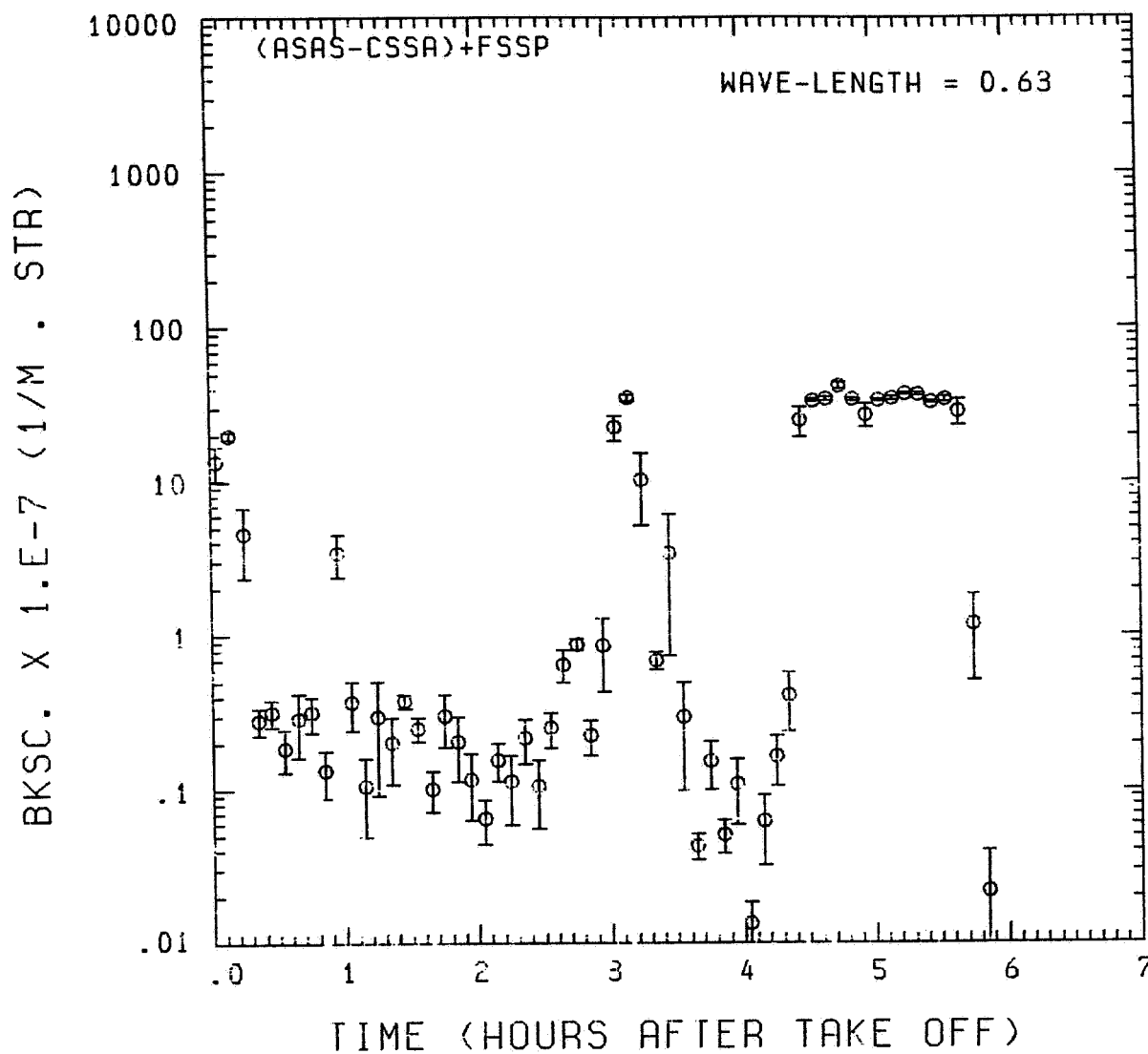


Fig. A 5 (d). GAMETAG flight data for August 25, 1977.

Calculated backscatter coefficient along the flight
track for five-minute data sets for $\lambda = 0.63 \mu\text{m}$.

KNOLLENBERG DATA

DATE= 8/25/1977

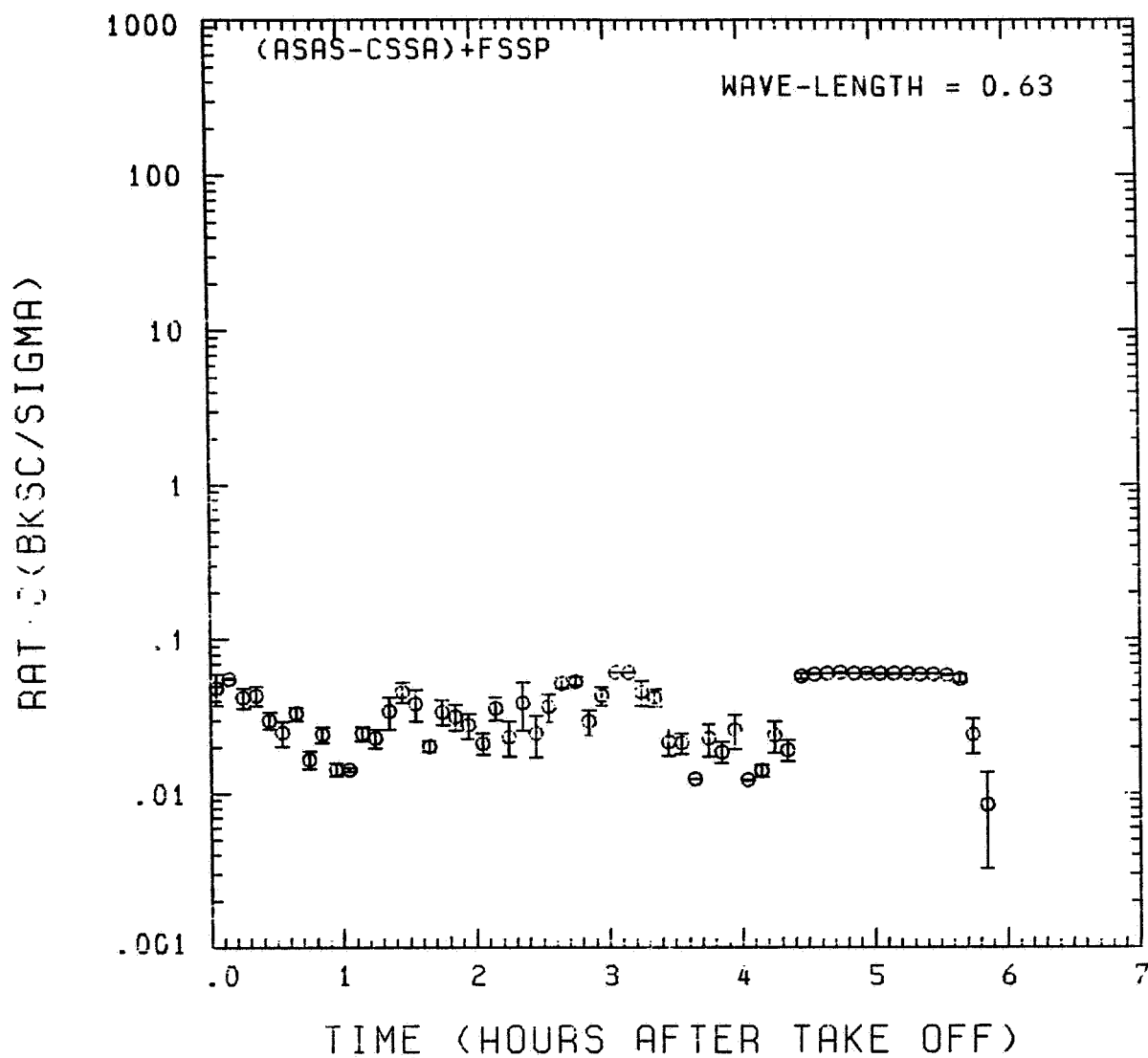


Fig. A 5 (e). GAMETAG flight data for August 25, 1977.

Calculated ratios for backscatter to extinction for
five-minute data sets for $\lambda = 0.63 \mu\text{m}$.

KNOLLENBERG DATA

DATE= 8/25/1977

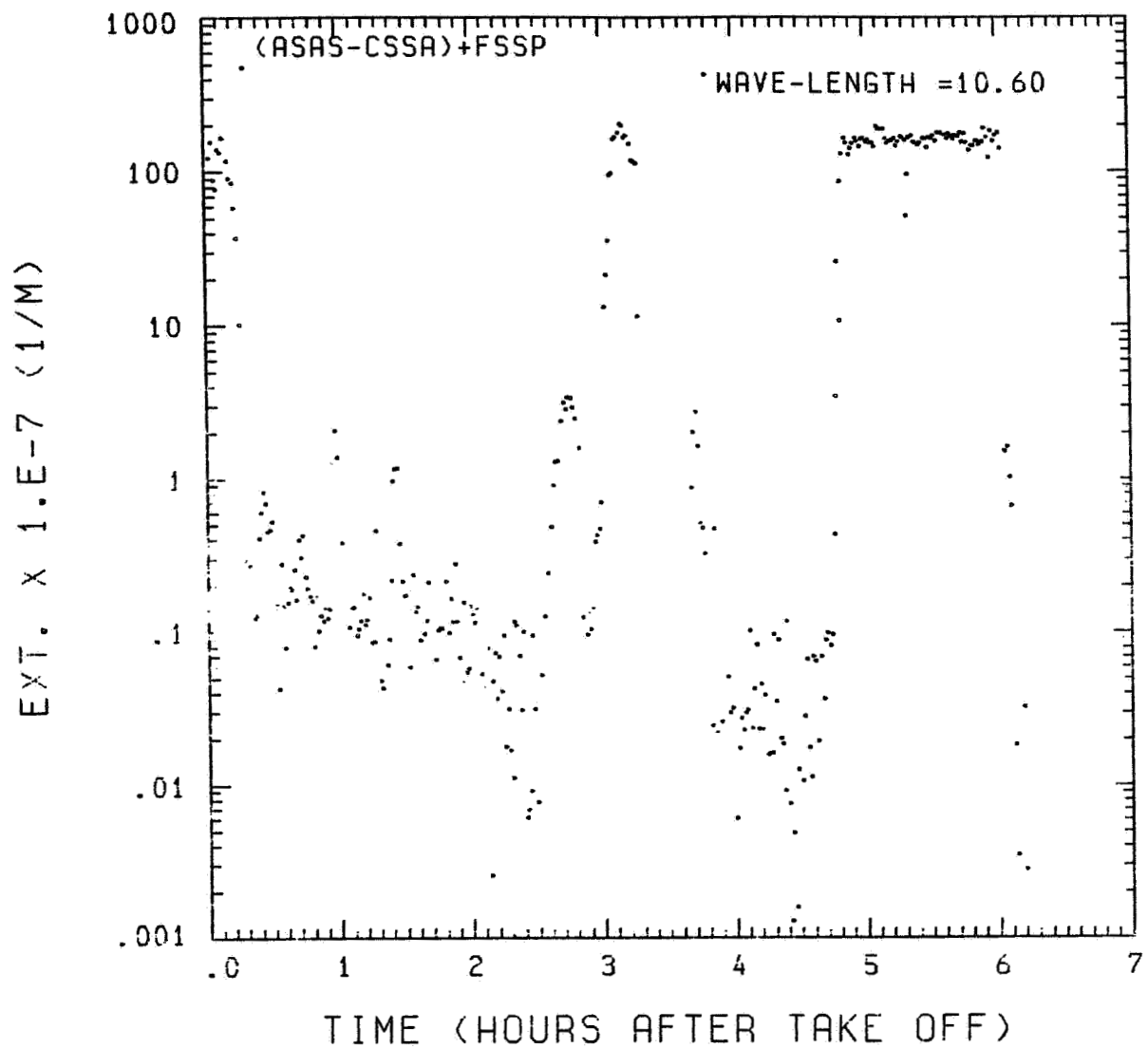


Fig. A 5 (f). GAMETAG flight data for August 25, 1977.

Calculated particulate extinction along the flight track for one-minute data sets for $\lambda = 10.6 \mu\text{m}$.

KNOLLENBERG DATA

DATE= 8/25/1977

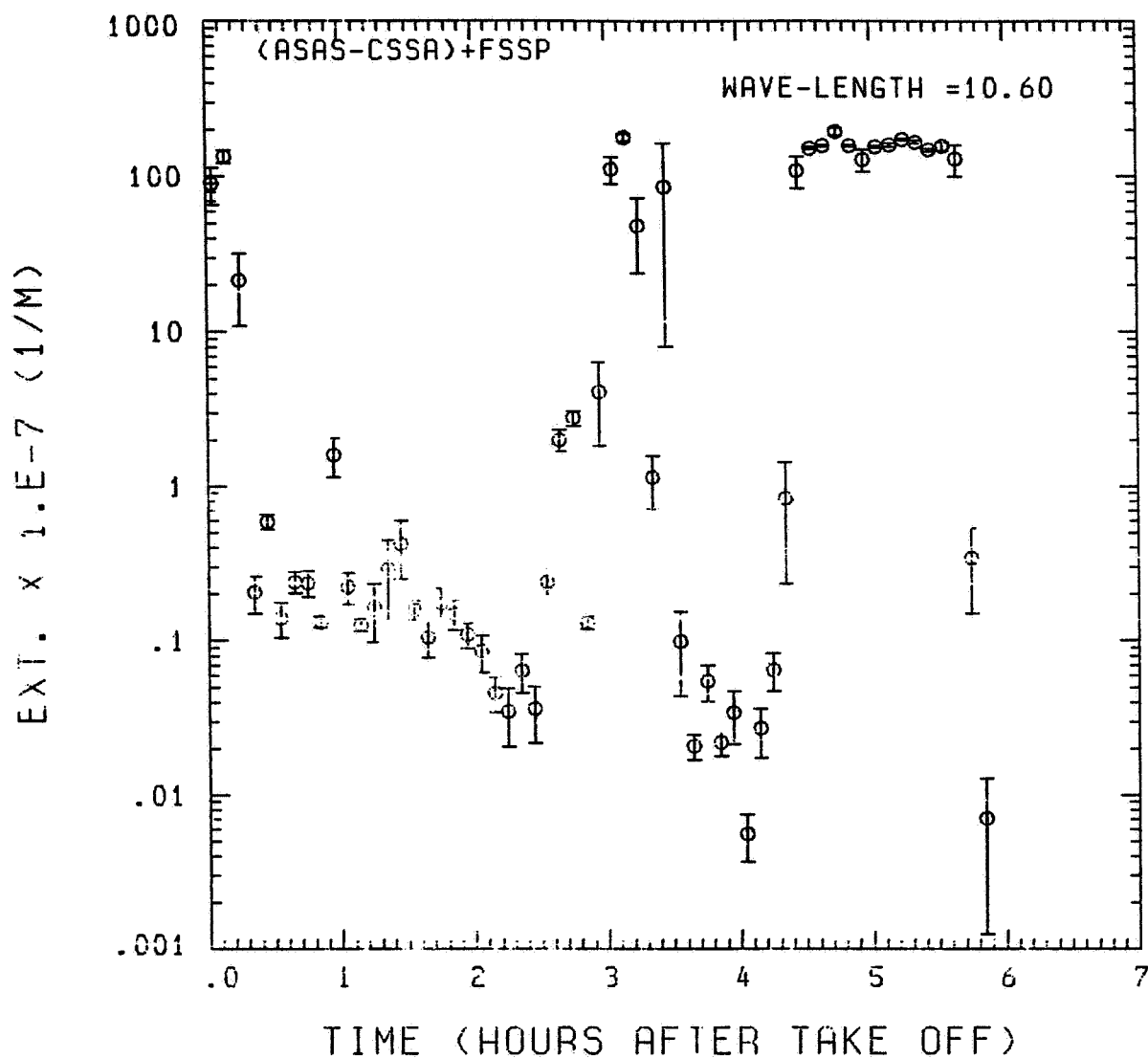


Fig. A 5 (g). GAMETAG flight data for August 25, 1977.

Calculated particulate extinction along the flight track for five-minute data sets for $\lambda = 10.6 \mu\text{m}$.

KNOLLENBERG DATA

DATE= 8/25/1977

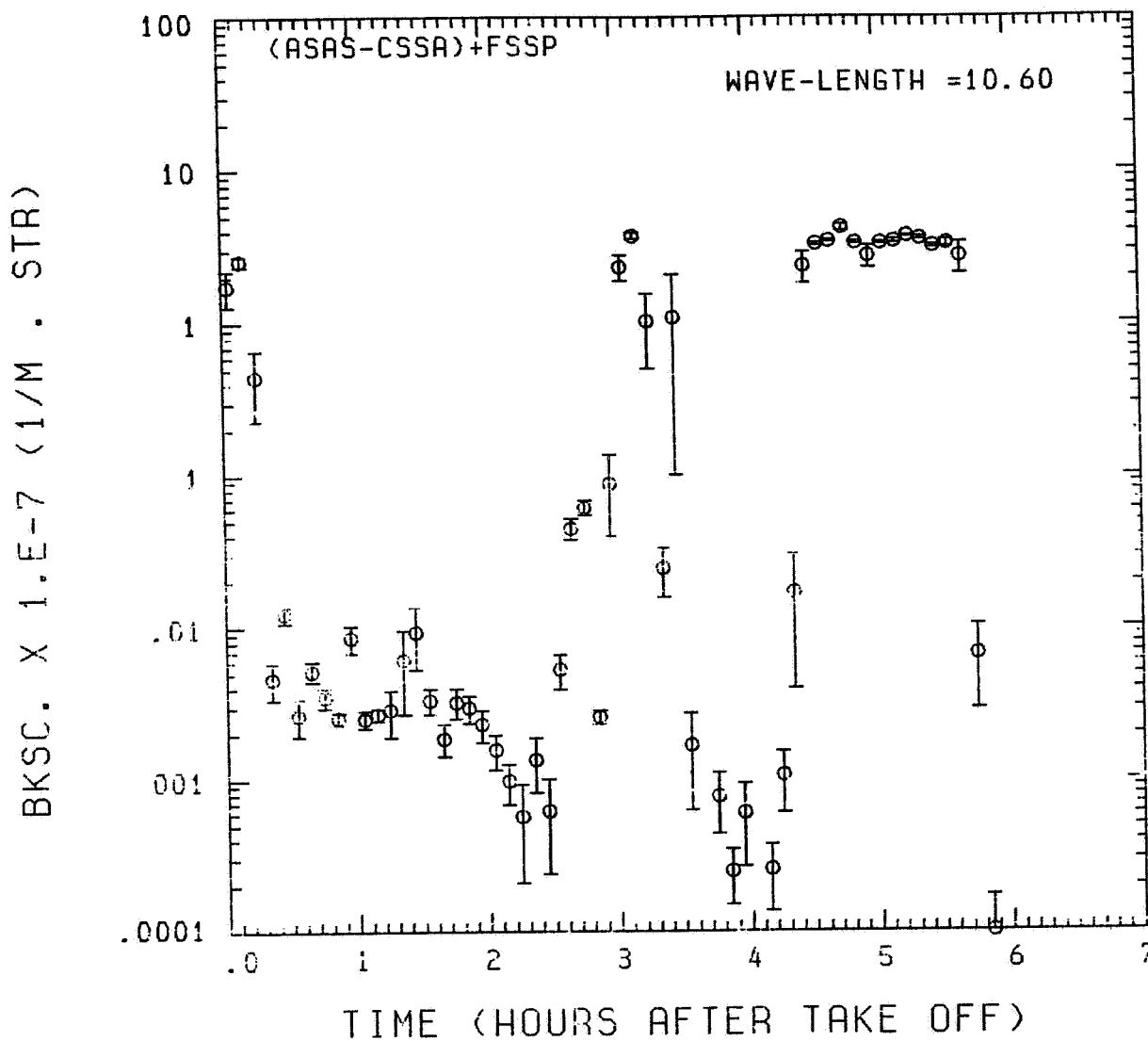


Fig. A 5 (h). GAMETAG flight data for August 25, 1977.

Calculated backscatter coefficient along the flight track for five-minute data sets for $\lambda = 10.6 \mu\text{m}$.

KNOLLENBERG DATA

DATE= 8/25/1977

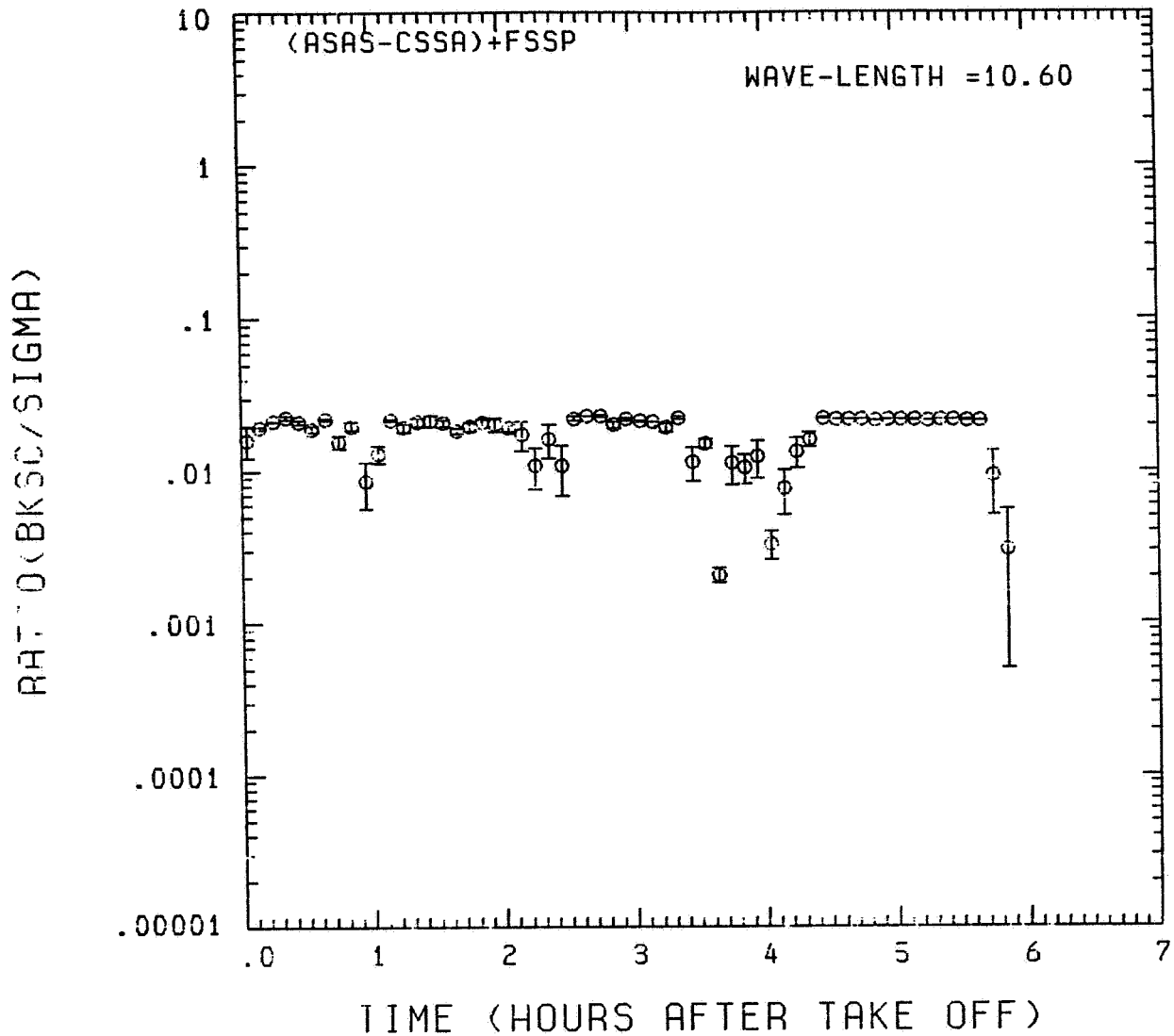


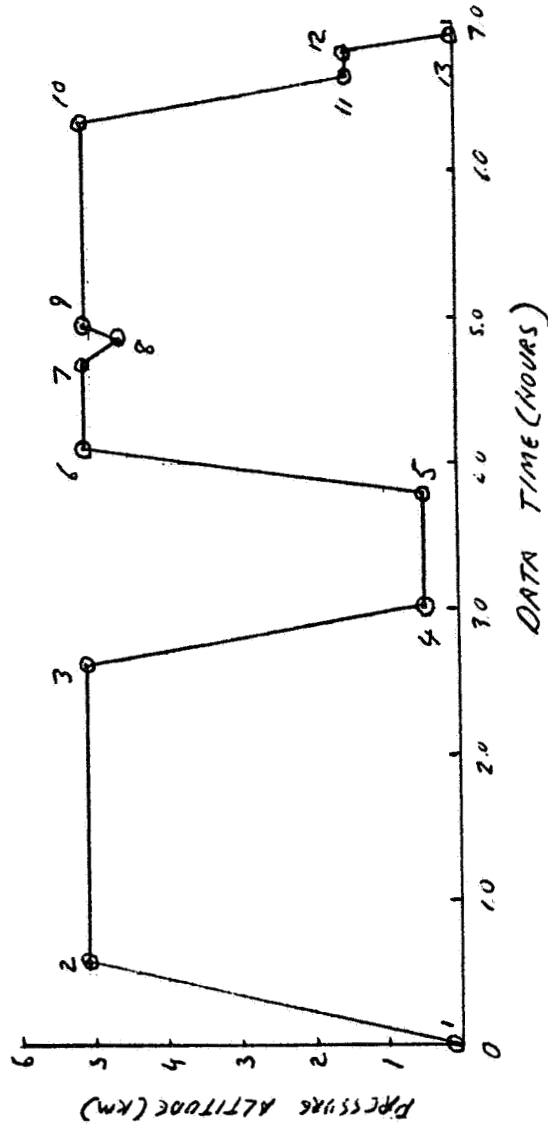
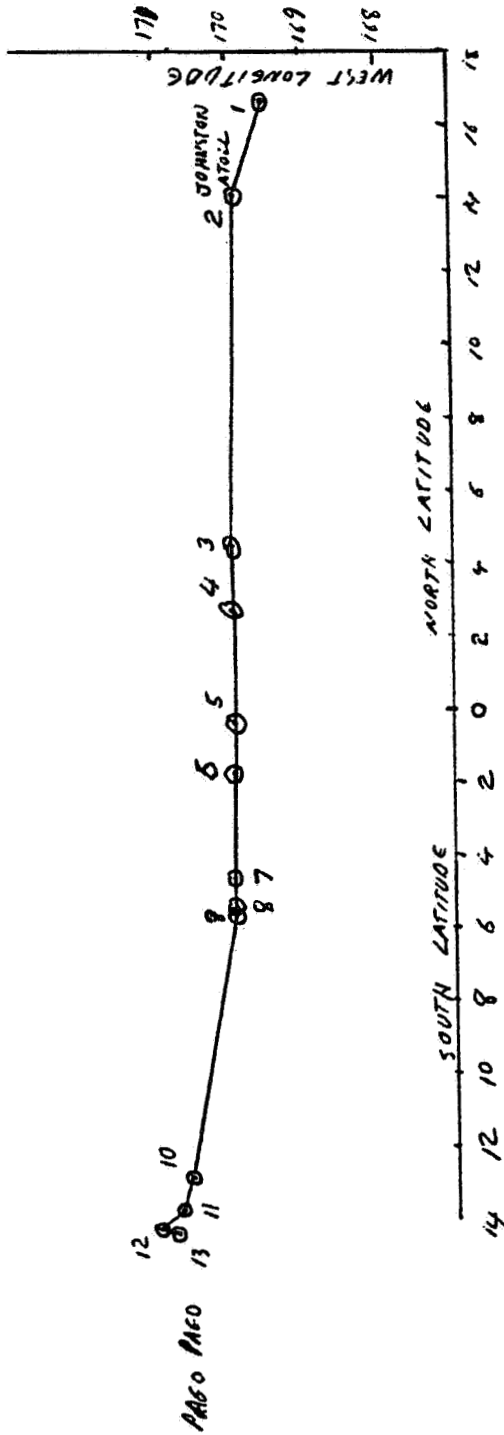
Fig. A 5 (i). GAMETAG flight data for August 25, 1977.
Calculated ratios for backscatter to extinction for
five-minute data sets for $\lambda = 10.6 \mu\text{m}$.

Table A6. Significant times for August 26, 1977.
Johnston Atoll to American Samoa.

Significant Points

<u>#</u>	TIME	
1	20:00	Johnston Atoll
2	20:35	
3	22:37	
4	23:01	
5	23:47	
6	00:06	
7	00:41	
8	00:50	
9	00:52	
10	02:20	
11	02:39	
12	02:48	
13	02:55	Pago Pago, American Samoa

ORIGINAL PAGE IS
OF POOR QUALITY



JOHNSTON ATOLL
TO PAGO PAGO (A.S.)
AUG 26, 1977

Fig. A 6 (a). GAMETAG flight data for August 26, 1977.
Altitude and location flight track plotted as a
function of time after takeoff.

KNOLLENBERG DATA

DATE= 8/26/1977

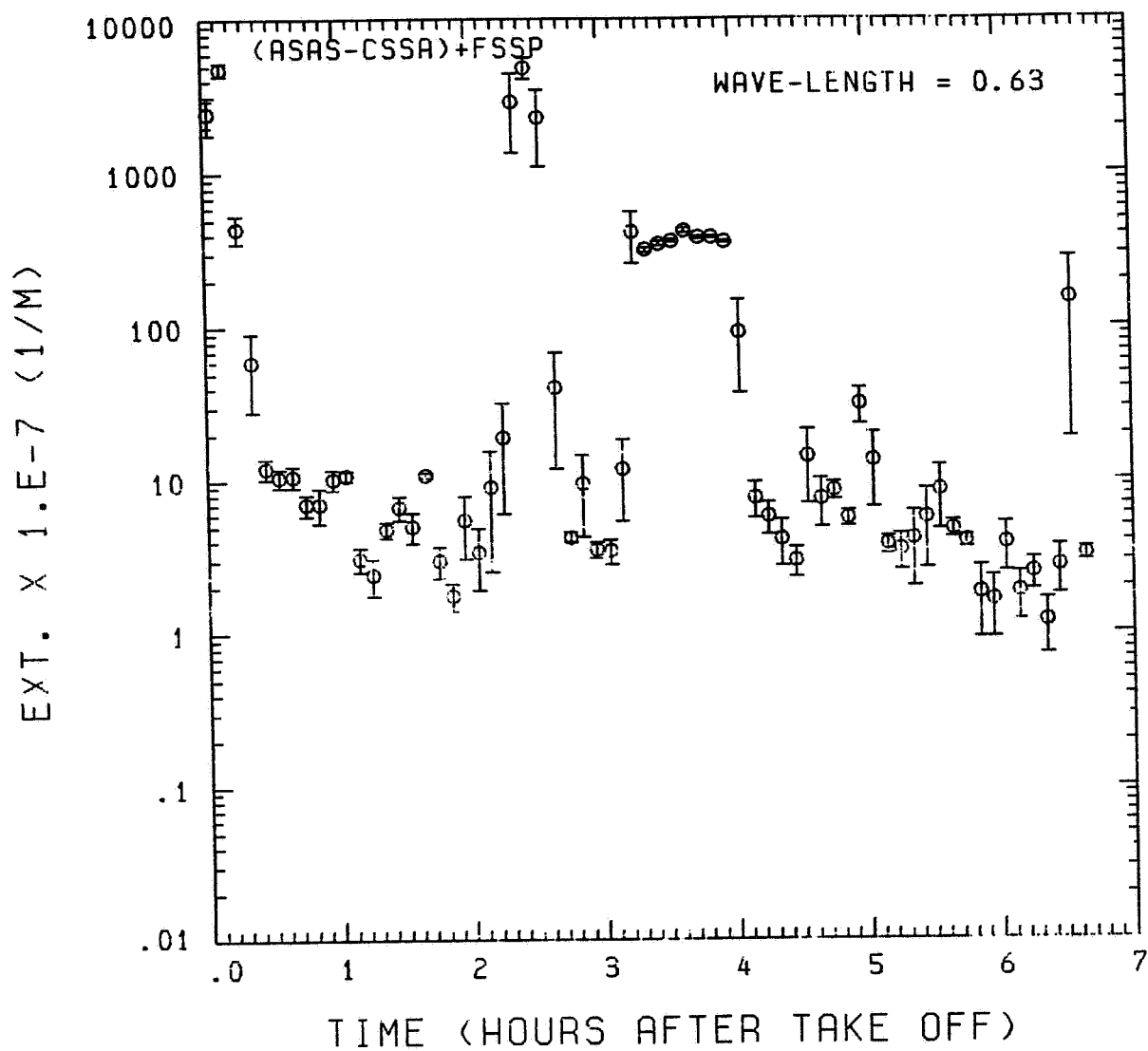


Fig. A 6 (b). GAMETAG flight data for August 26, 1977.

Calculated particulate extinction along the flight track for one-minute data sets for $\lambda = 0.63 \mu\text{m}$.

KNOLLENBERG DATA

DATE= 8/26/1977

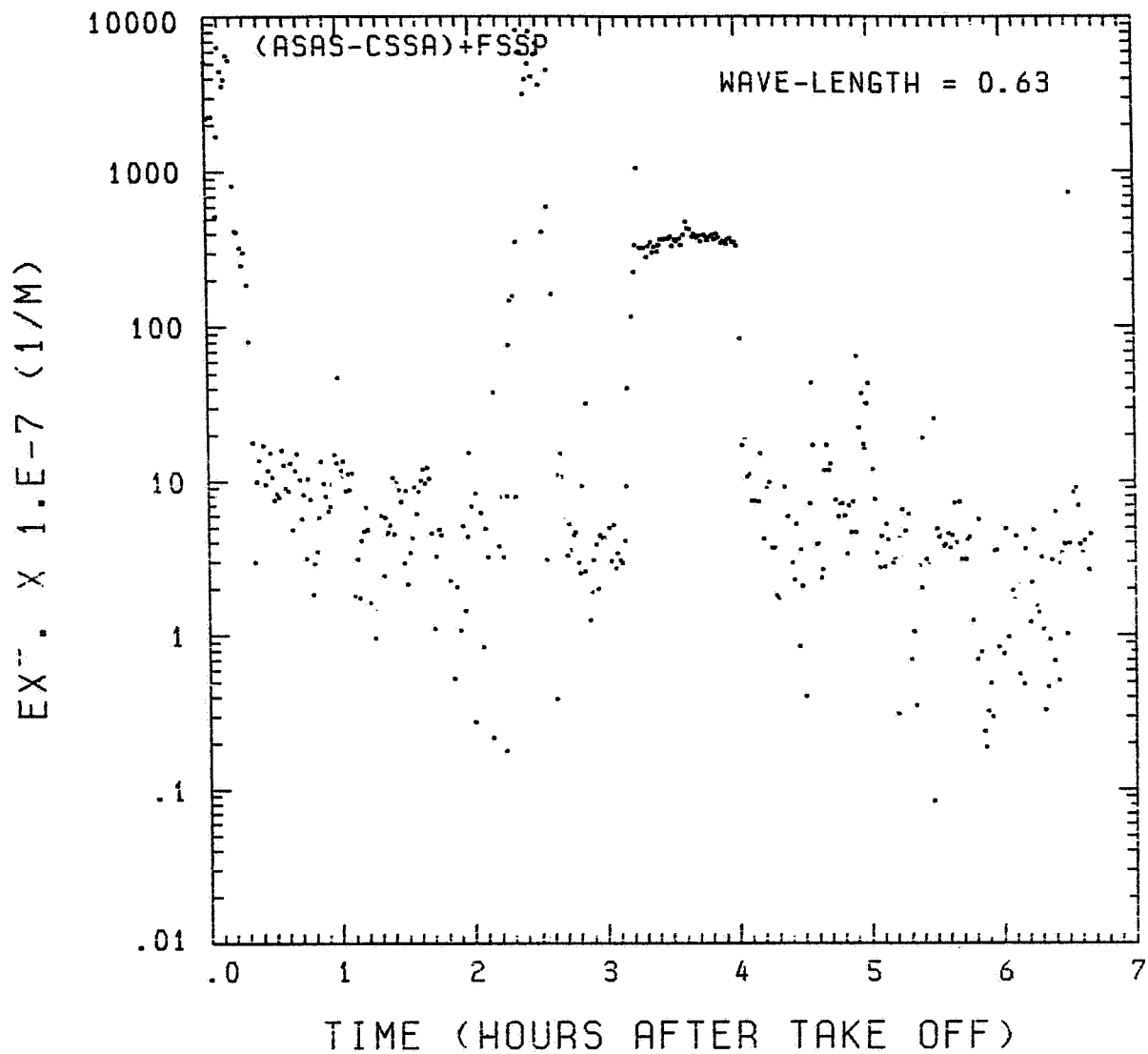


Fig. A 6 (c). GAMETAG flight data for August 26, 1977.

Calculated particulate extinction along the flight track for five-minute data sets for $\lambda = 0.63 \mu m$.

KNOLLENBERG DATA

DATE= 8/26/1977

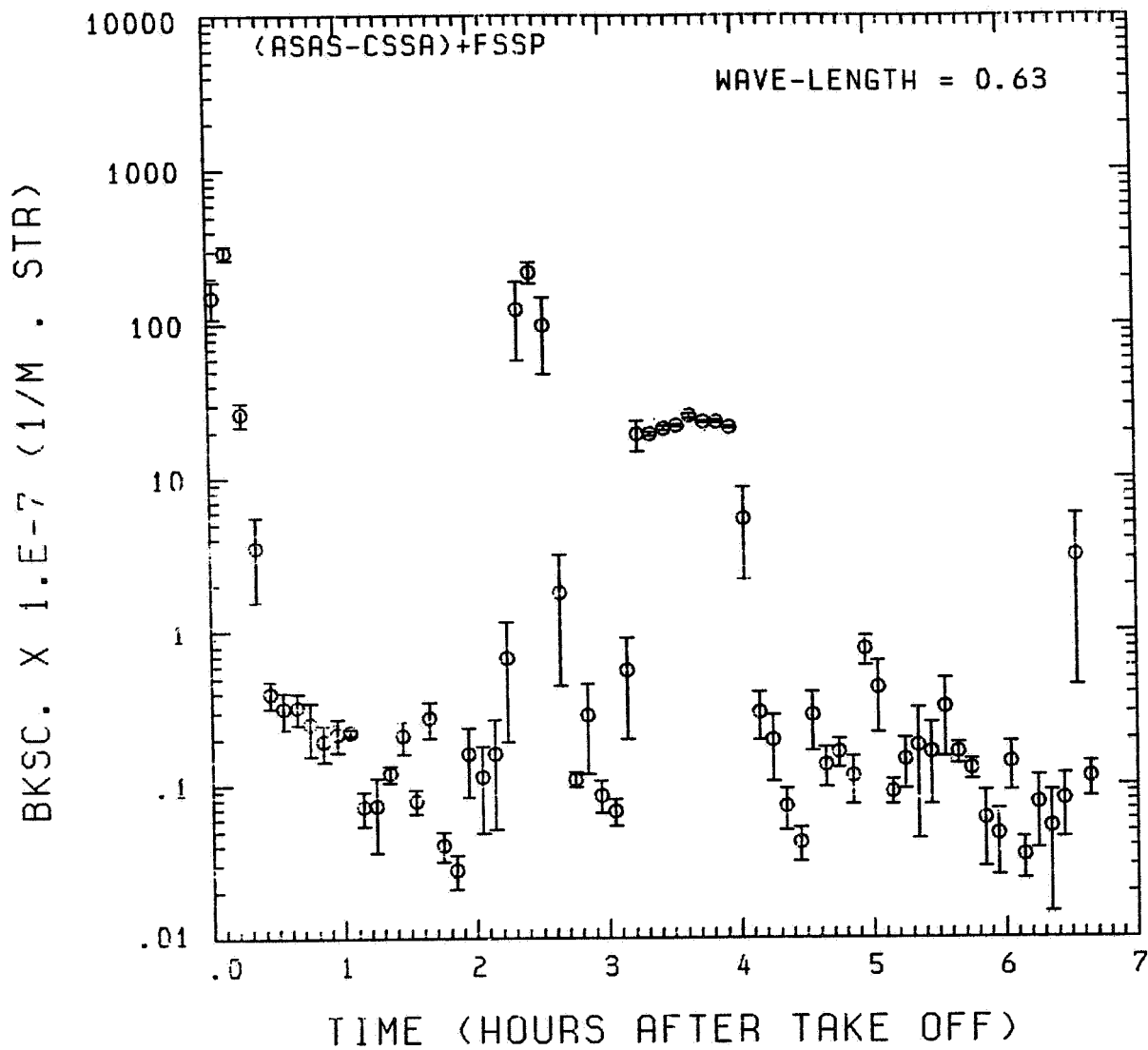


Fig. A6 (d). GAMETAG flight data for August 26, 1977.

Calculated backscatter coefficient along the flight
track for five-minute data sets for $\lambda = 0.63 \mu\text{m}$.

KNOLLENBERG DATA

DATE= 8/26/1977

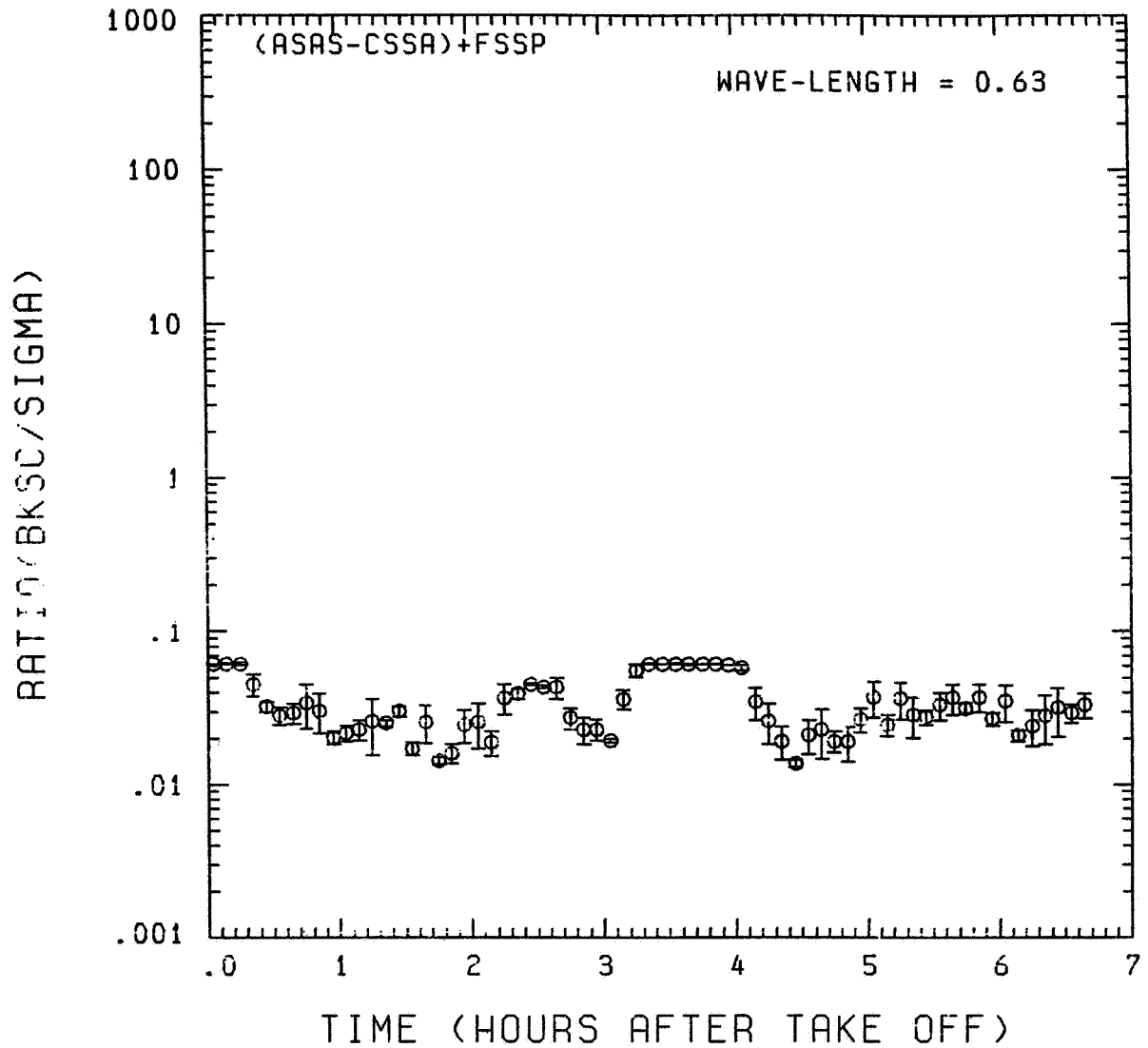


Fig. A6 (e). GAMETAG flight data for August 26, 1977.

Calculated ratios for backscatter to extinction for
five-minute data sets for $\lambda = 0.63 \mu\text{m}$.

KNOLLENBERG DATA

DATE= 8/26/1977

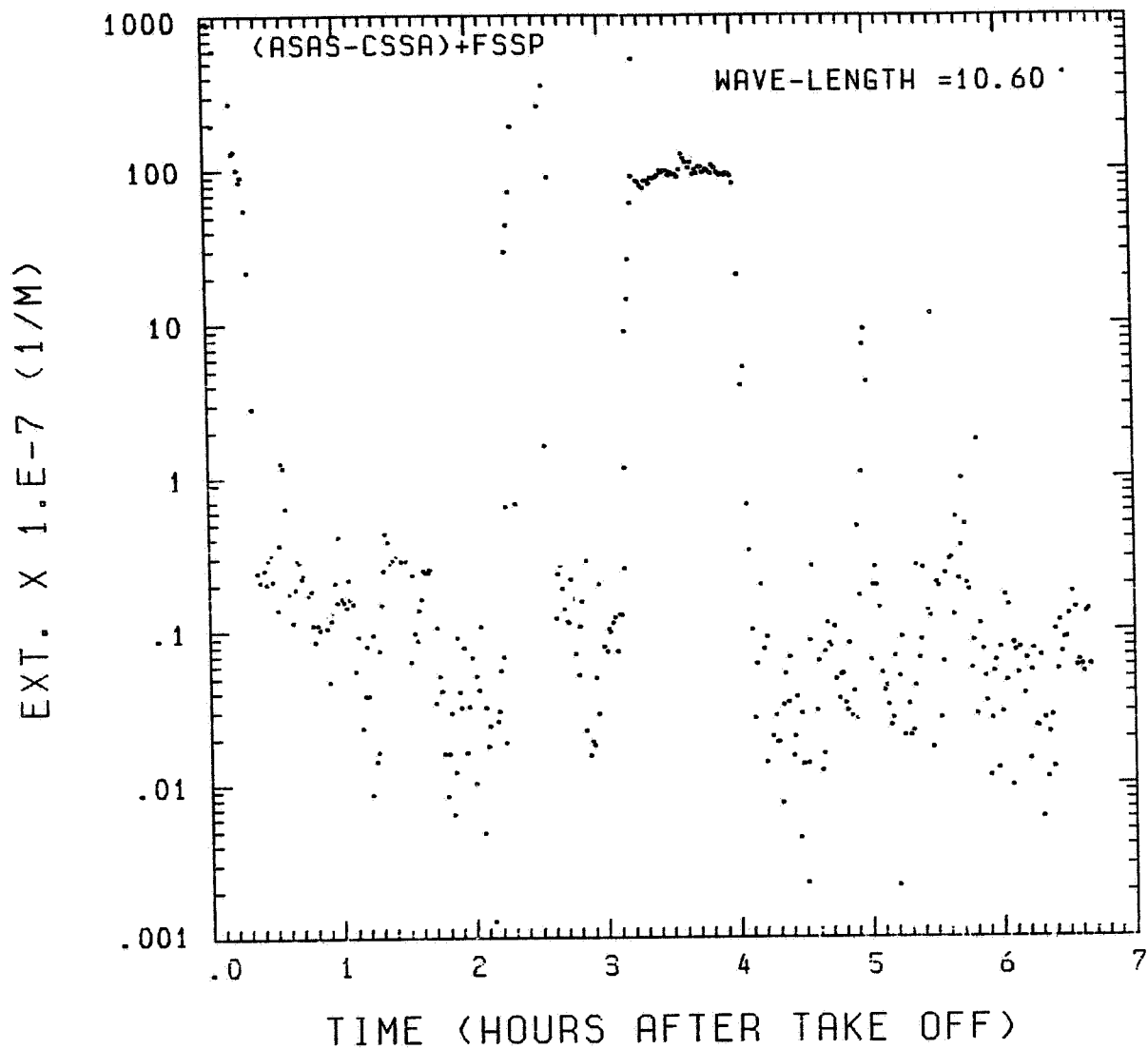


Fig. A6 (f). GAMETAG flight data for August 26, 1977.
Calculated particulate extinction along the flight
track for one-minute data sets for $\lambda = 10.6 \mu\text{m}$.

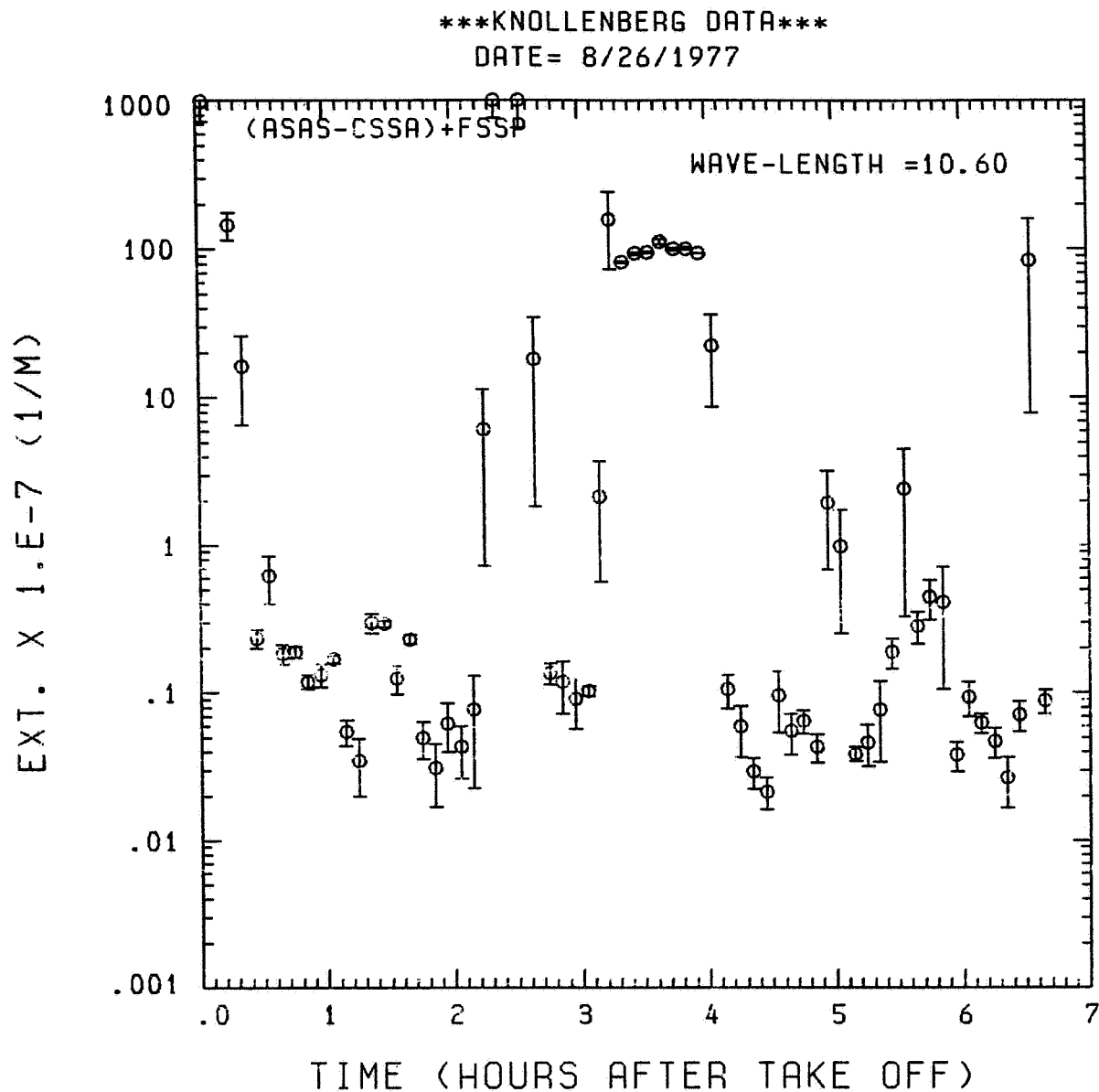


Fig. A6 (g). GAMETAG flight data for August 26, 1977.
Calculated particulate extinction along the flight
track for five-minute data sets for $\lambda = 10.6 \mu\text{m}$.

KNOLLENBERG DATA

DATE= 8/26/1977

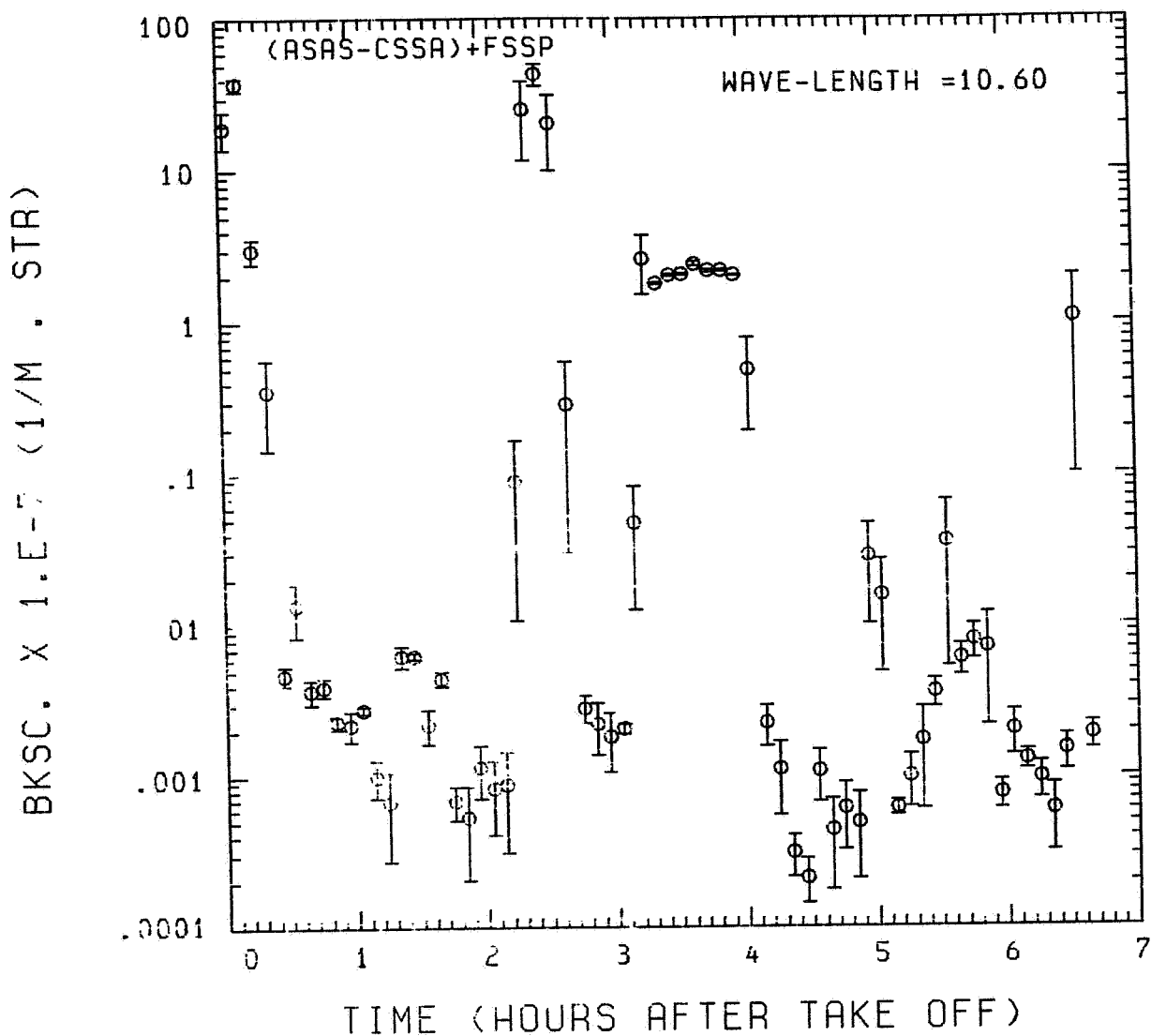


Fig. A 6 (h). GAMETAG flight data for August 26, 1977.

Calculated backscatter coefficient along the flight track for five-minute data sets for $\lambda = 10.6 \mu\text{m}$.

KNOLLENBERG DATA

DATE= 8/26/1977

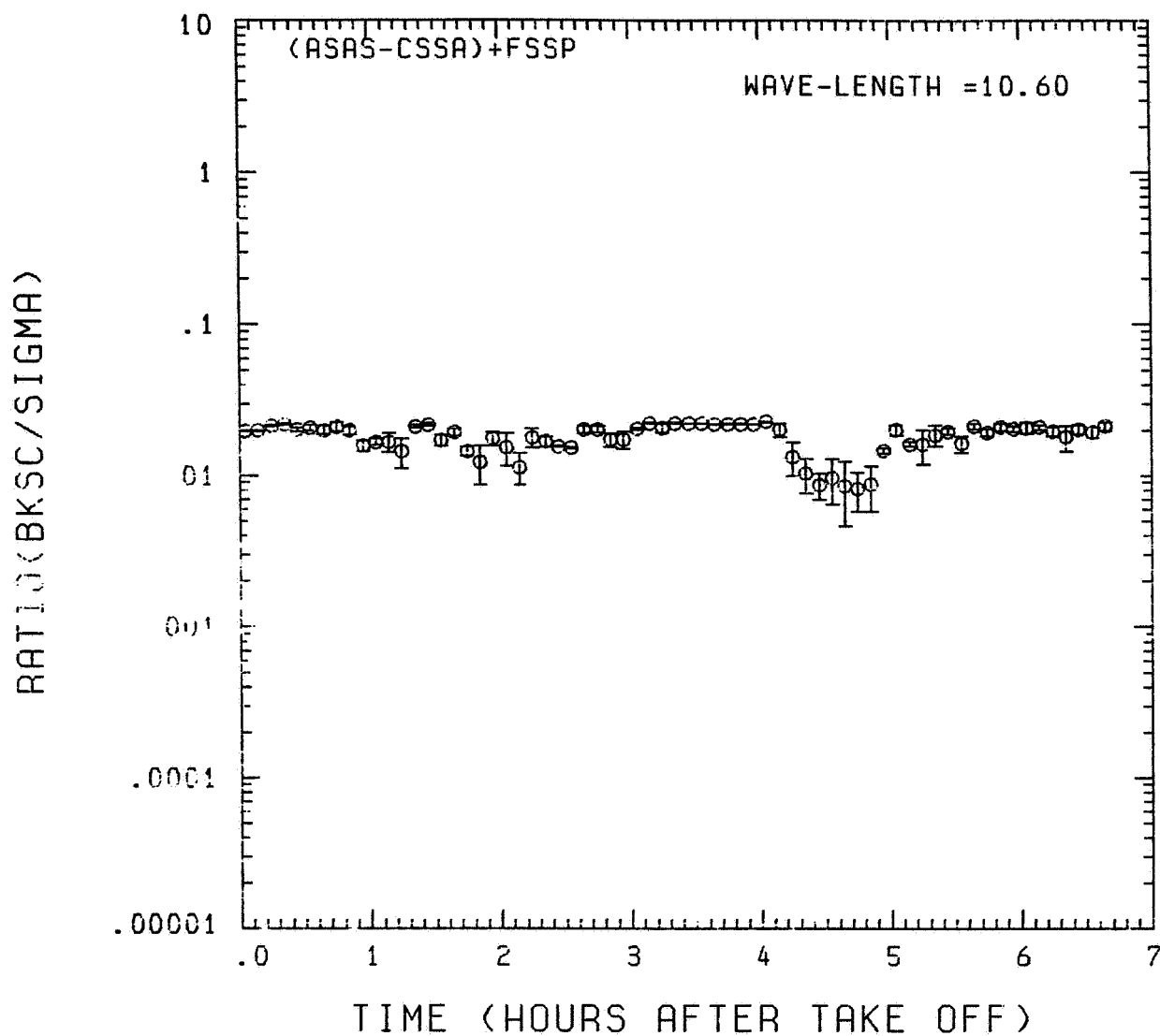


Fig. A6 (i). GAMETAG flight data for August 26, 1977.
Calculated ratios for backscatter to extinction for
five-minute data sets for $\lambda = 10.6 \mu\text{m}$.

**Table A7. Significant times for August 28, 1977.
Pago Pago, American Samoa and Return
(North).**

Significant Points

<u>#</u>	<u>TIME</u>	
1	21:02	Pago Pago
2	21:35	
3	22:30	
4	23:00	
5	23:45	
6	00:18	
7	01:24	
8	01:57	
9	02:18	
10	02:20	
11	02:36	
12	02:43	
13	02:55	Pago Pago

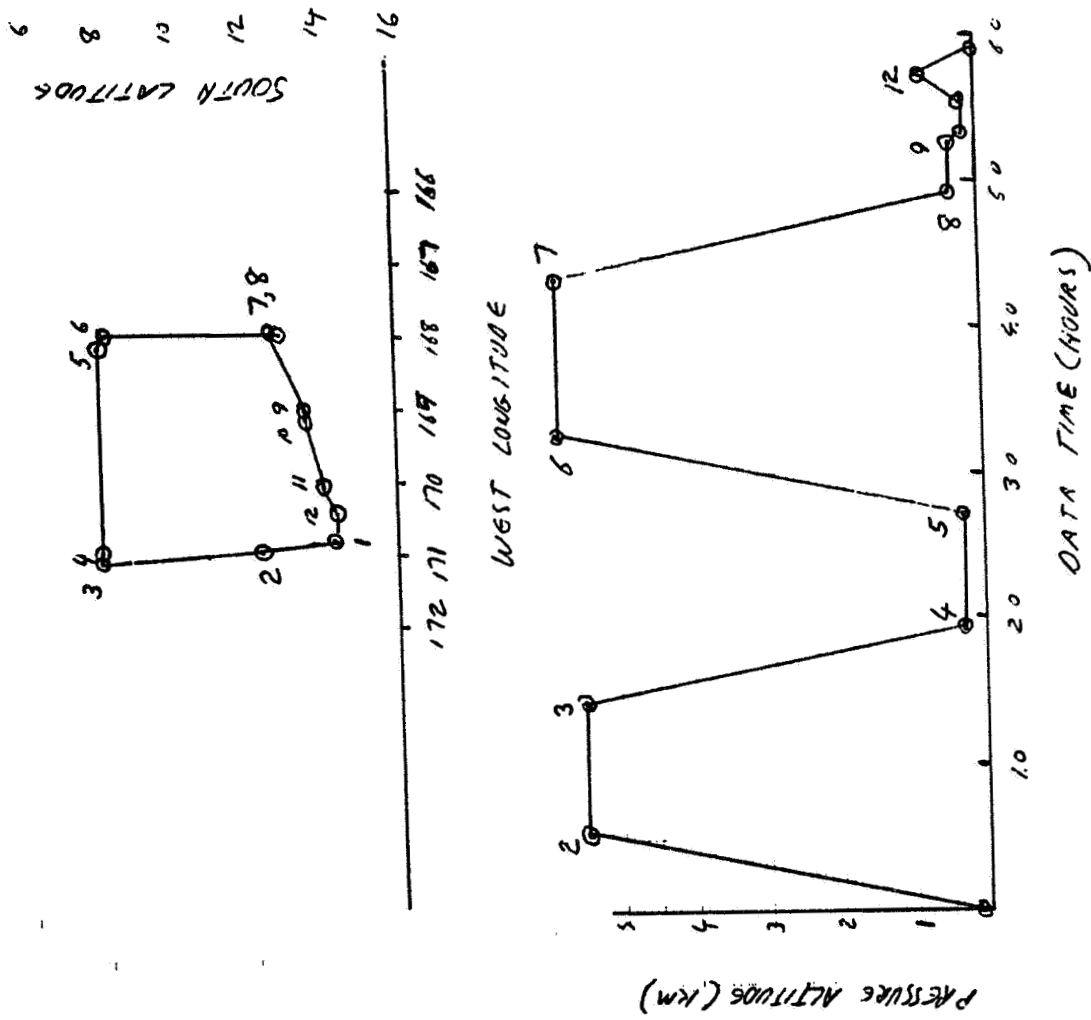


Fig. A7 (a). GAMETAG flight data for August 28, 1977.
Altitude and location flight track plotted as a
function of time after takeoff.

ORIGINAL PAGE IS
OF POOR QUALITY

KNOLLENBER DATA

DATE= 8/28/ 977

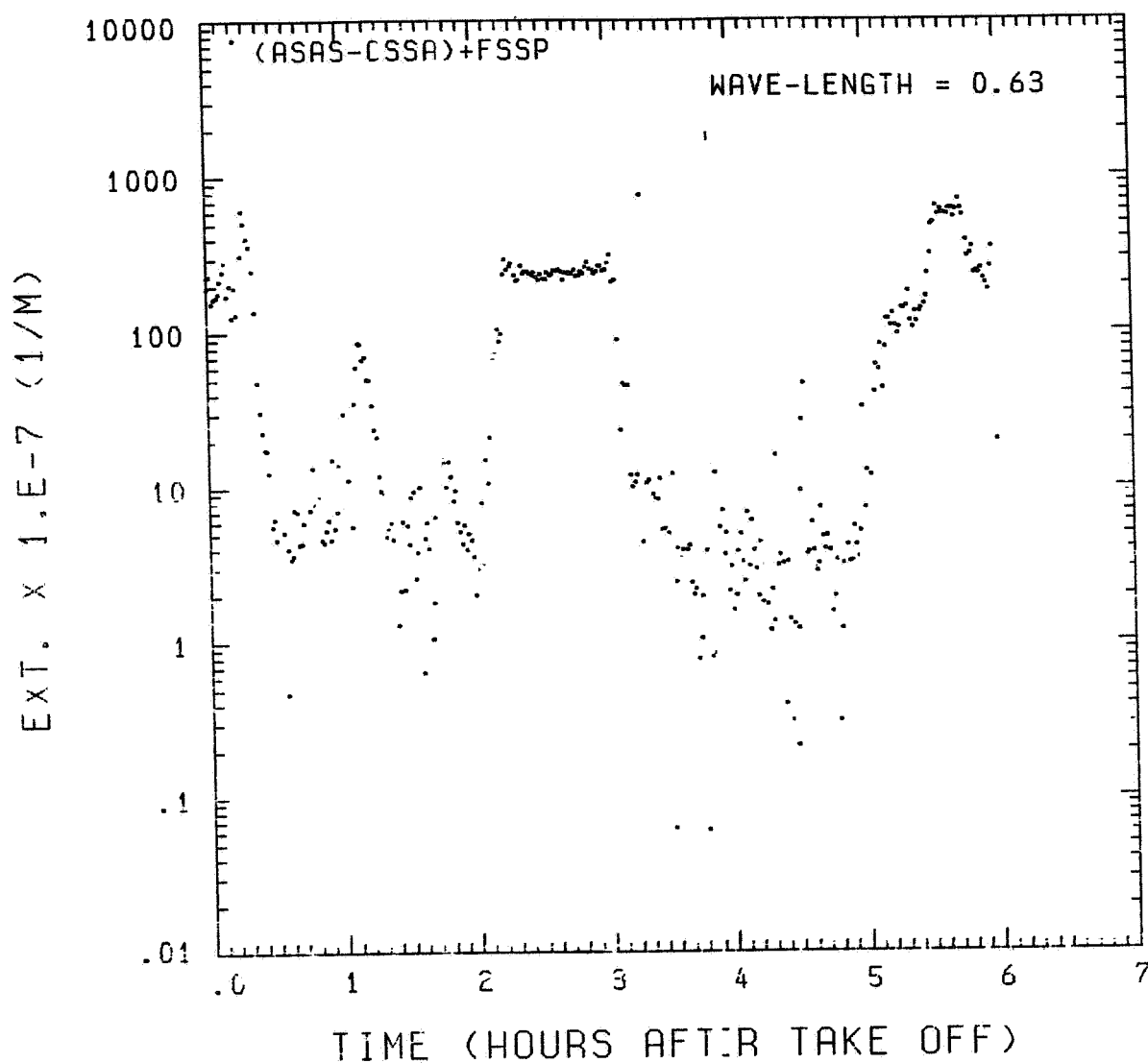


Fig. A7 (b). GAMETAG flight data for August 28, 1977.
Calculated particulate extinction along the flight
track for one-minute data sets for $\lambda = 0.63 \mu\text{m}$.

KNOLLENBERG DATA

DATE= 8/28/1977

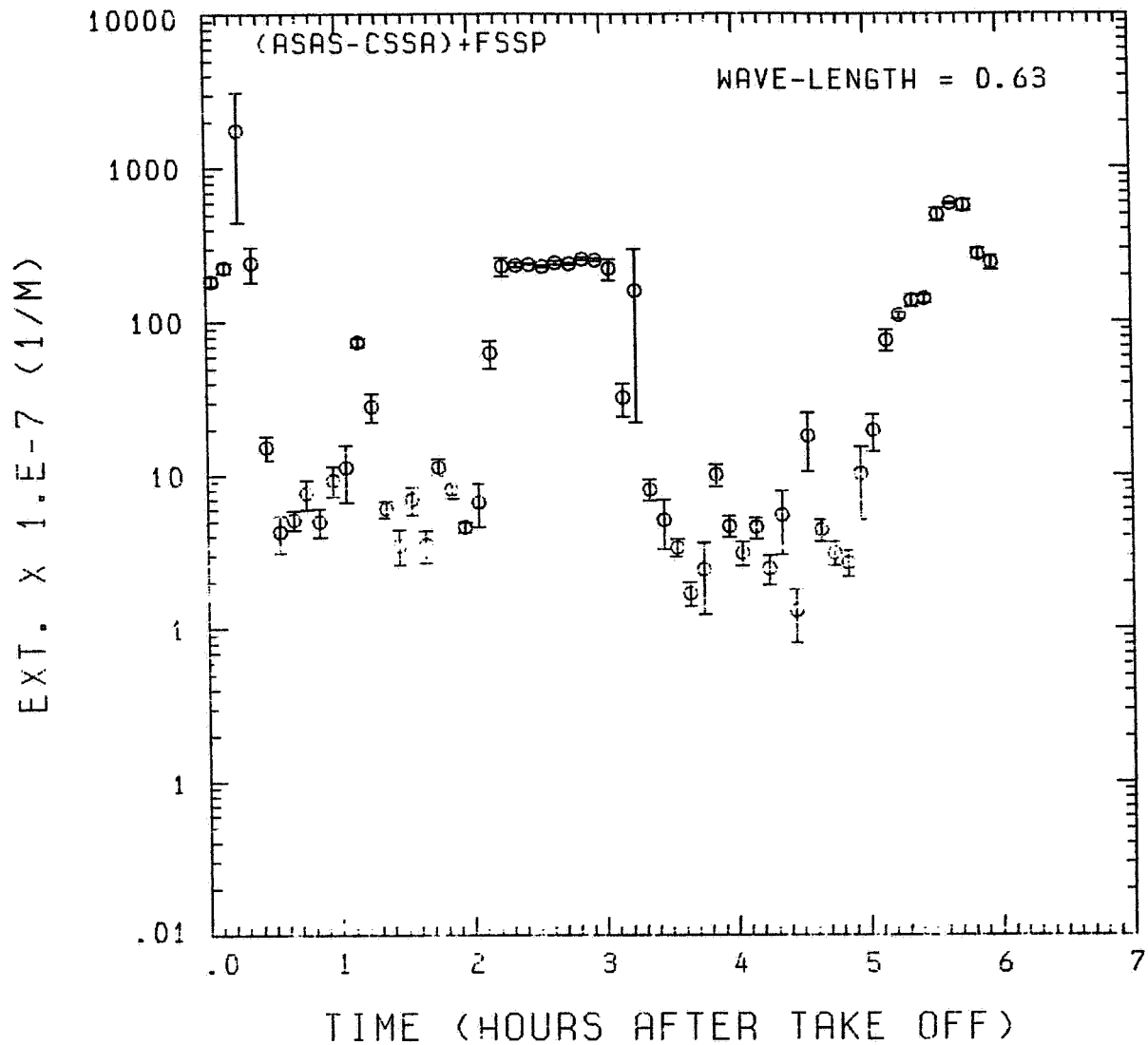


Fig. A7 (c). GAMETAG flight data for August 28, 1977.
Calculated particulate extinction along the flight
track for five-minute data sets for $\lambda = 0.63 \mu\text{m}$.

ORIGINAL PAGE IS
OF POOR QUALITY

KNOLLENBERG DATA

DATE= 8/28/1977

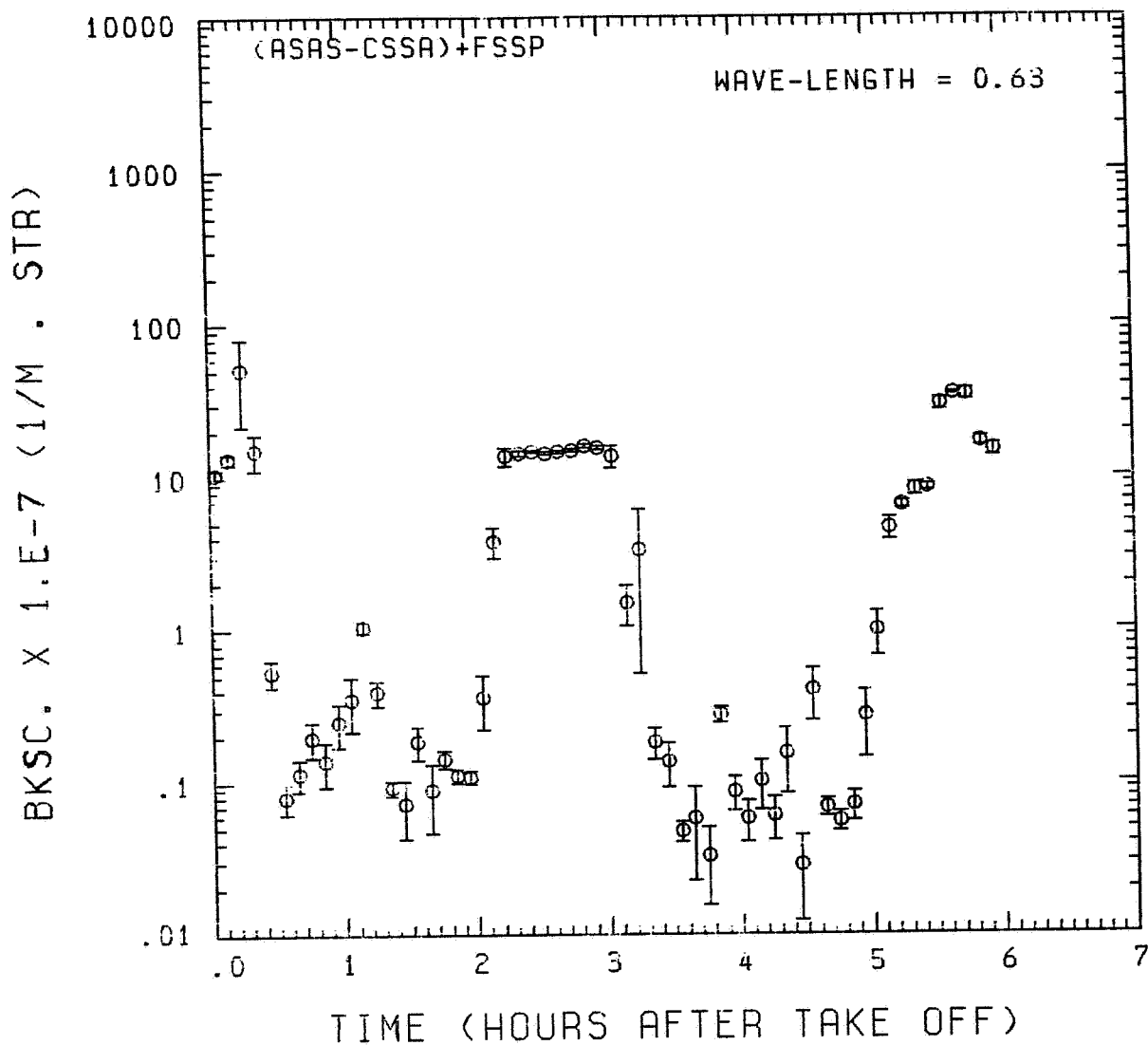


Fig. A7 (d). GAMETAG flight data for August 28, 1977.

Calculated backscatter coefficient along the flight
track for five-minute data sets for $\lambda = 0.63 \mu\text{m}$.

KNOLLENBERG DATA

DATE= 8/28/1977

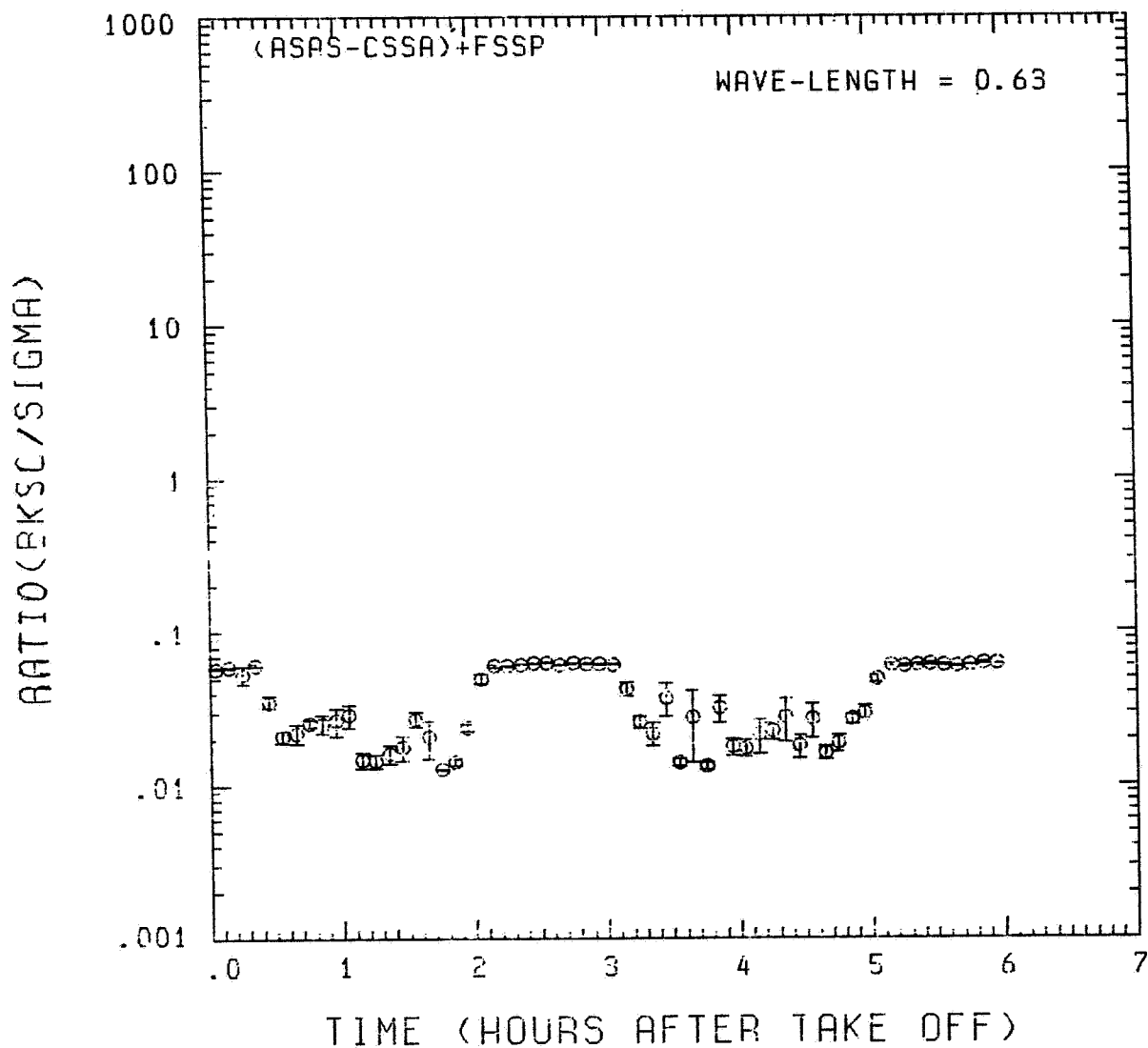


Fig. A 7 (e). GAMETAG flight data for August 28, 1977.

Calculated ratios for backscatter to extinction for five-minute data sets for $\lambda = 0.63 \mu\text{m}$.

KNOLLENBERG DATA

DATE= 8/28/1977

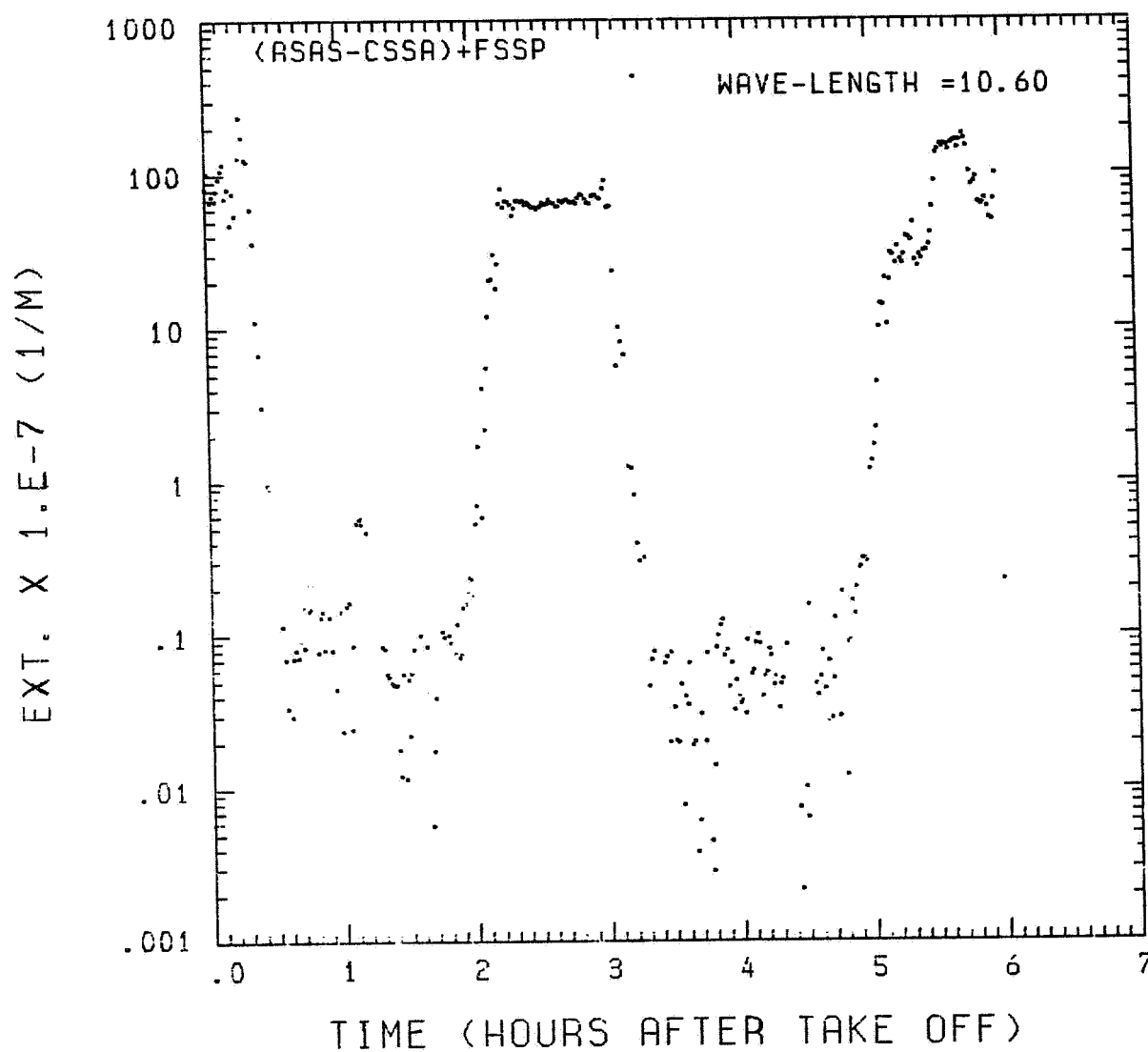


Fig. A 7 (f). GAMETAG flight data for August 28, 1977.
Calculated particulate extinction along the flight
track for one-minute data sets for $\lambda = 10.6 \mu\text{m}$.

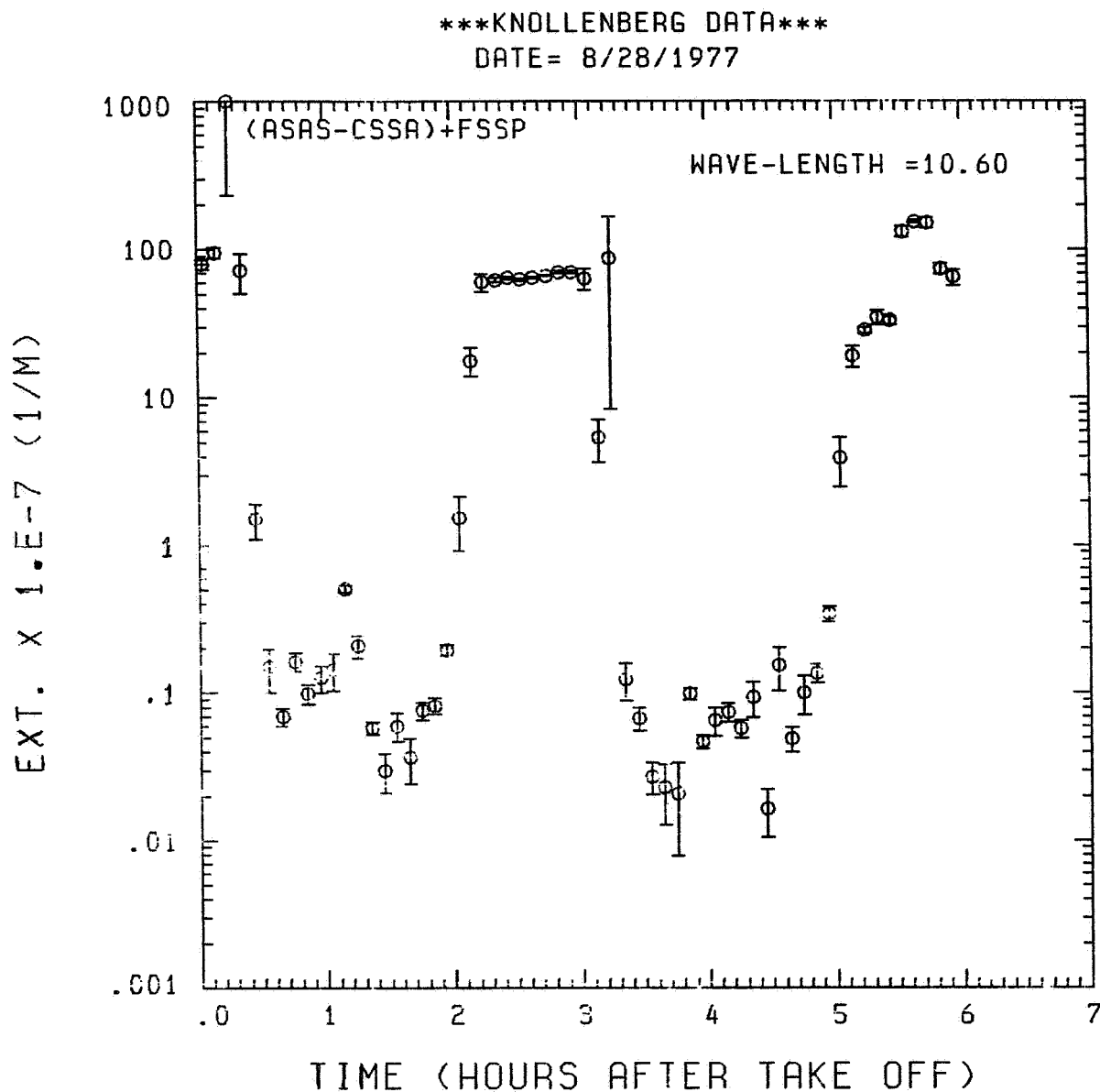


Fig. A7 (g). GAMETAG flight data for August 28, 1977.
Calculated particulate extinction along the flight
track for five-minute data sets for $\lambda = 10.6 \mu\text{m}$.

KNOLLENBERG DATA

DATE= 8/28/1977

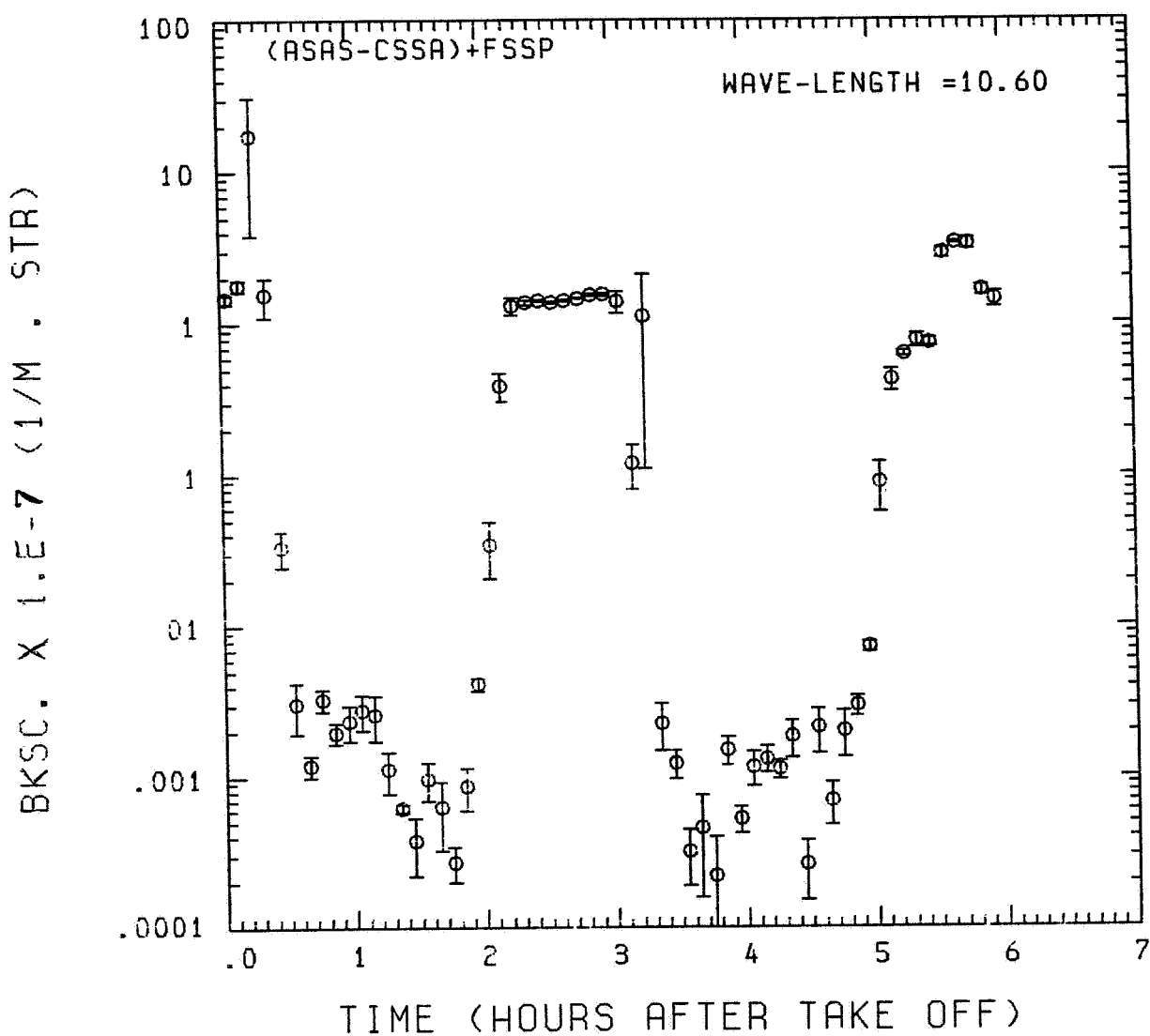


Fig. A 7 (h). GAMETAG flight data for August 28, 1977.

Calculated backscatter coefficient along the flight track for five-minute data sets for $\lambda = 10.6 \mu\text{m}$.

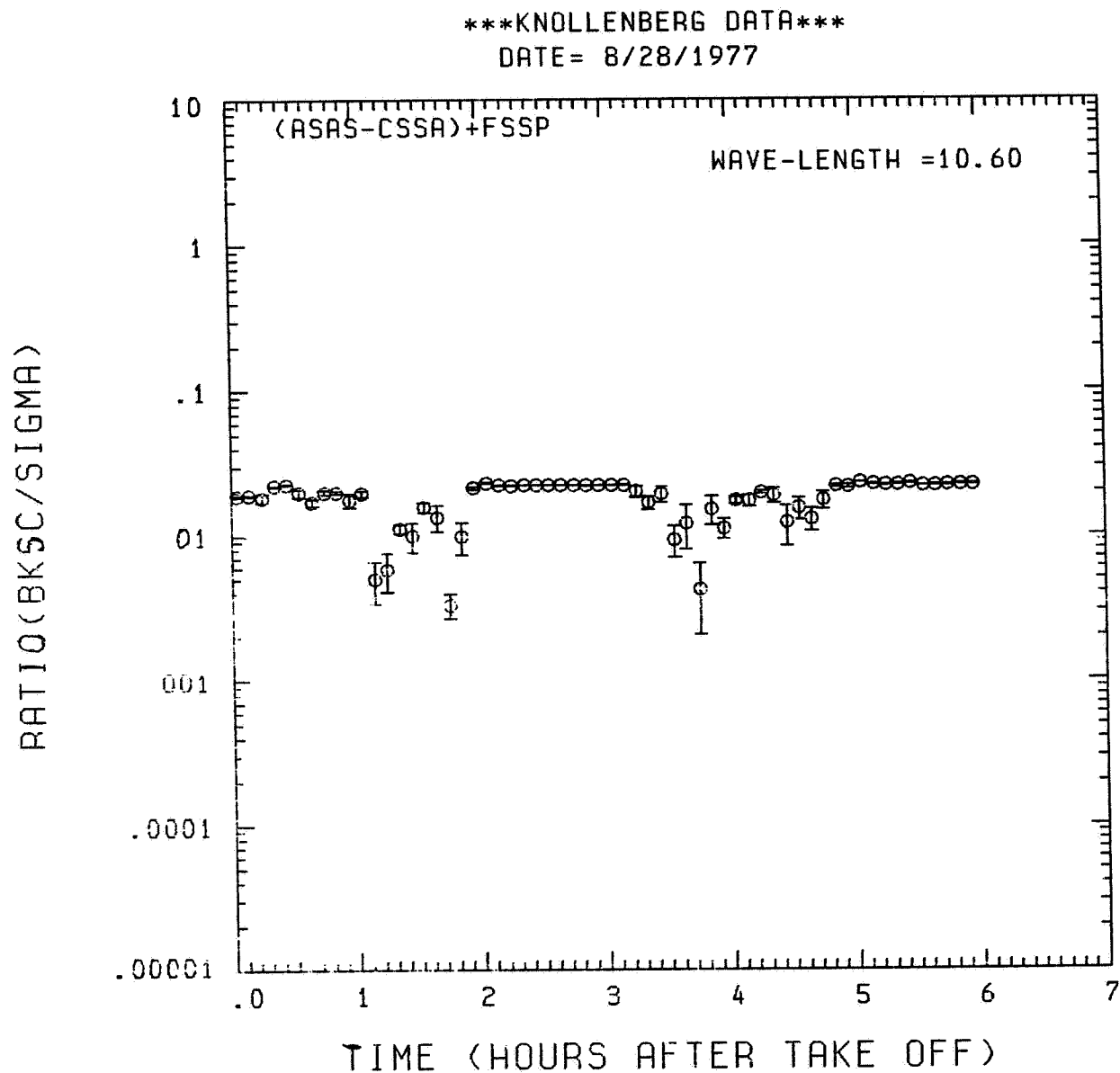


Fig. A 7 (i). GAMETAG flight data for August 28, 1977.
Calculated ratios for backscatter to extinction for
five-minute data sets for $\lambda = 10.6 \mu\text{m}$.

Table A8. Significant times for August 31, 1977.
Pago Pago, American Samoa and Return
(South).

Significant Points

<u>#</u>	TIME	
1	20:58	Pago Pago
2	21:30	
3	22:32	
4	22:38	
5	23:44	
6	23:53	
7	01:14	
8	01:35	
9	01:53	
10	02:07	
11	02:25	
12	02:33	
13	02:39	
14	02:45	
15	03:19	
16	03:24	
17	03:39	
18	03:49	Pago Pago

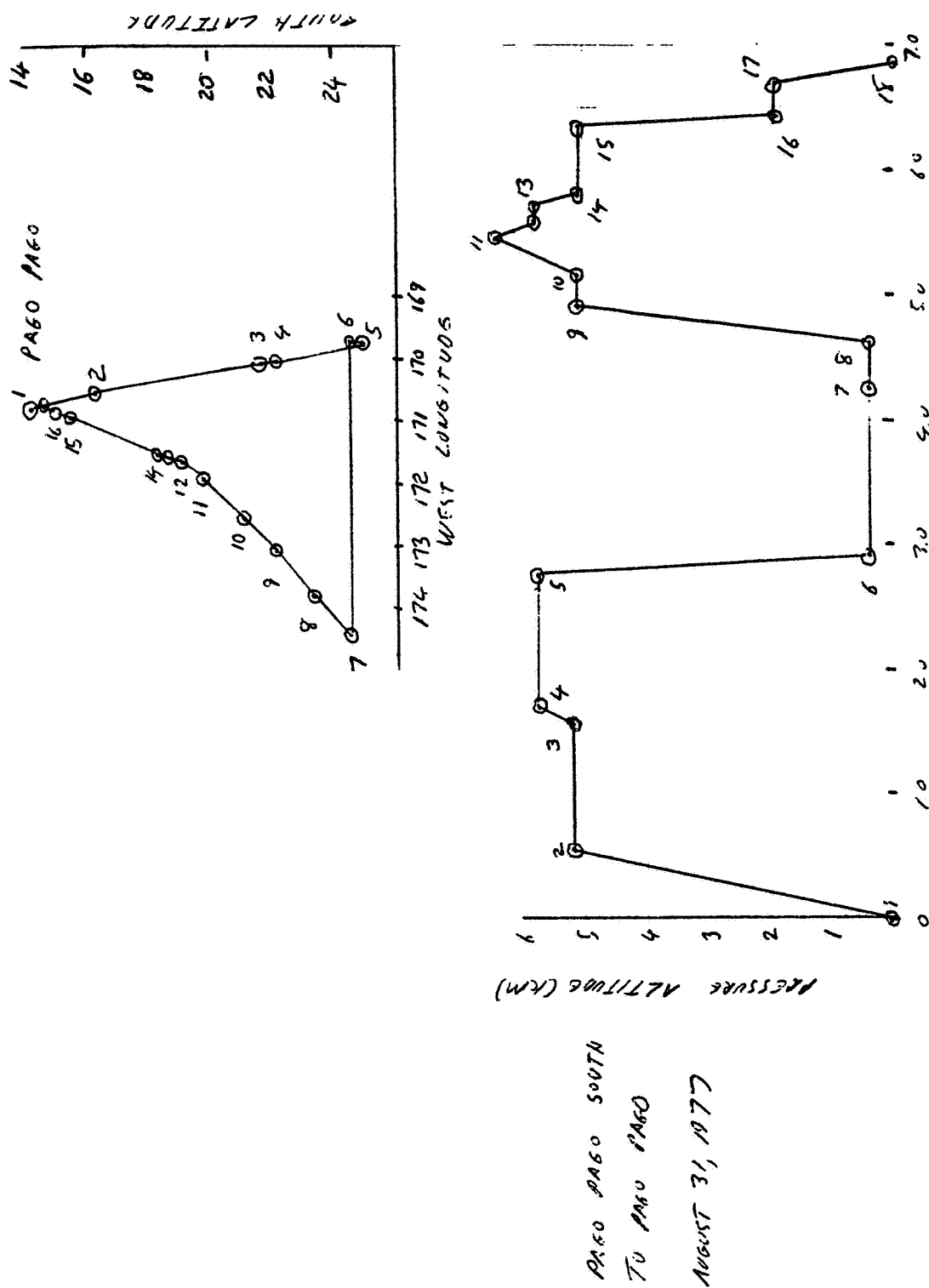


Fig. A 8 (a). GAMETAG flight data for August 31, 1977.
Altitude and location flight track plotted as a function of time after takeoff.

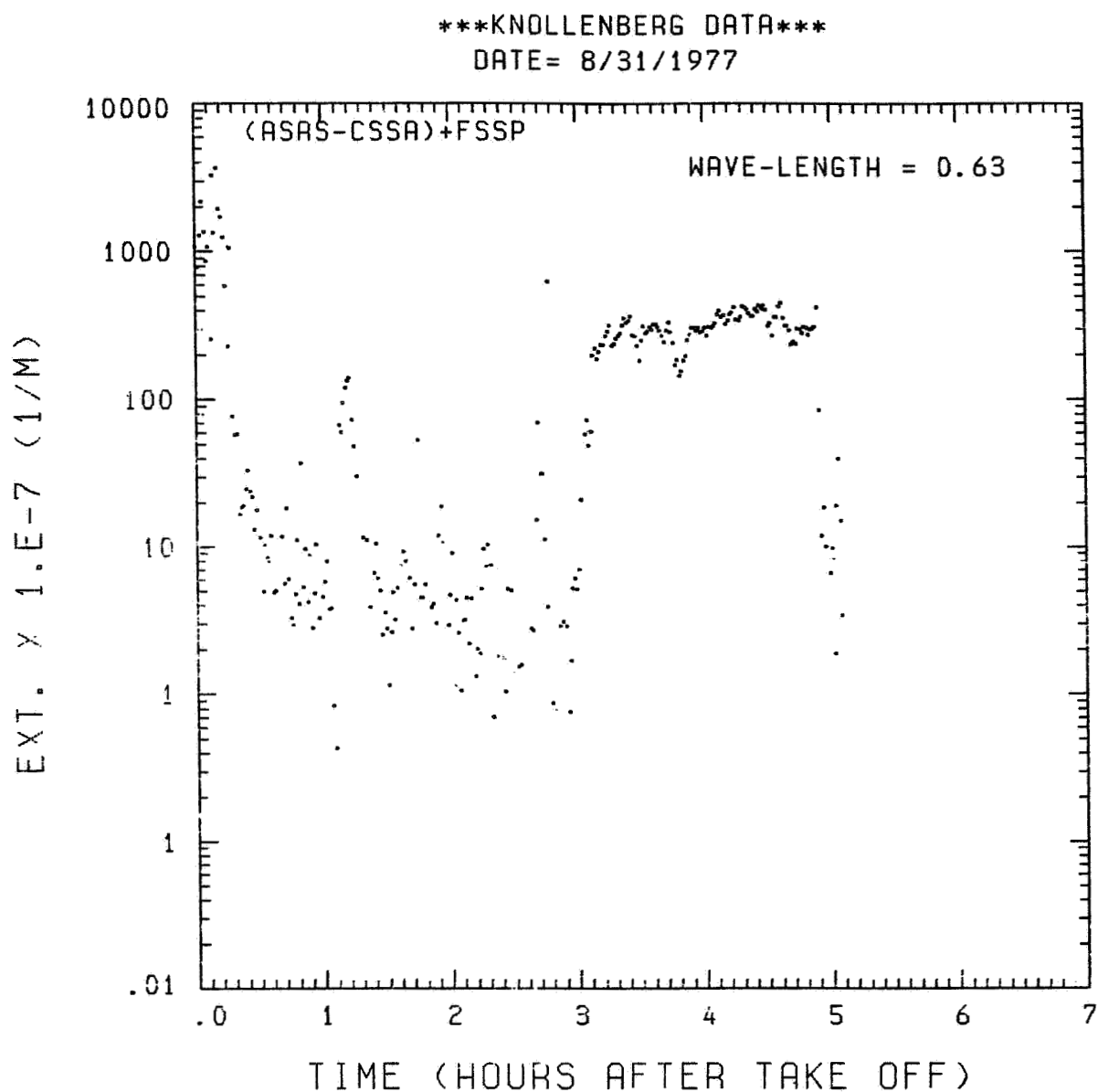


Fig. A8 (b). GAMETAG flight data for August 31, 1977.
Calculated particulate extinction along the flight track for one-minute data sets for $\lambda = 0.63 \mu\text{m}$.

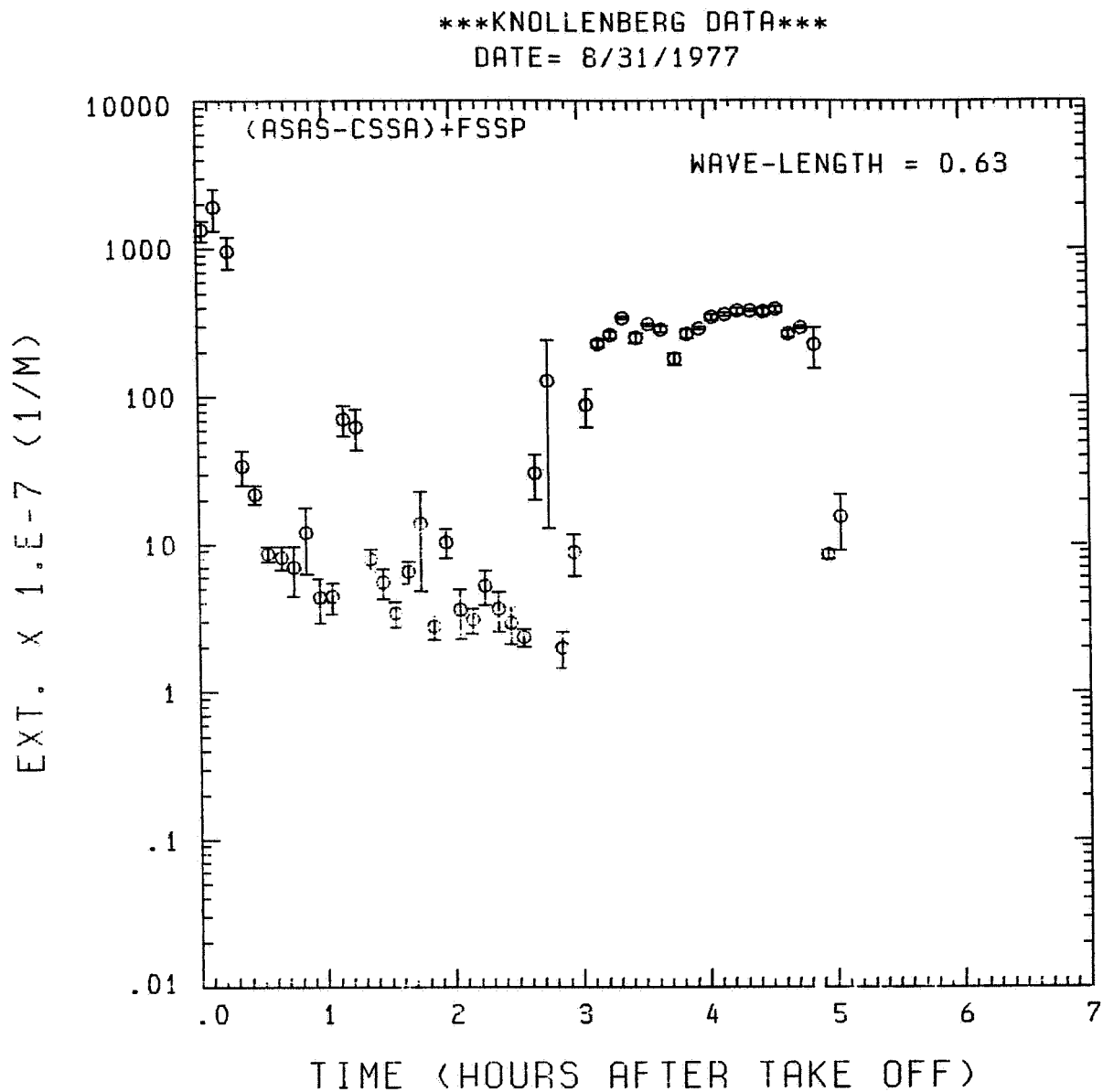


Fig. A 8 (c). GAMETAG flight data for August 31, 1977.
Calculated particulate extinction along the flight
track for five-minute data sets for $\lambda = 0.63 \mu\text{m}$.

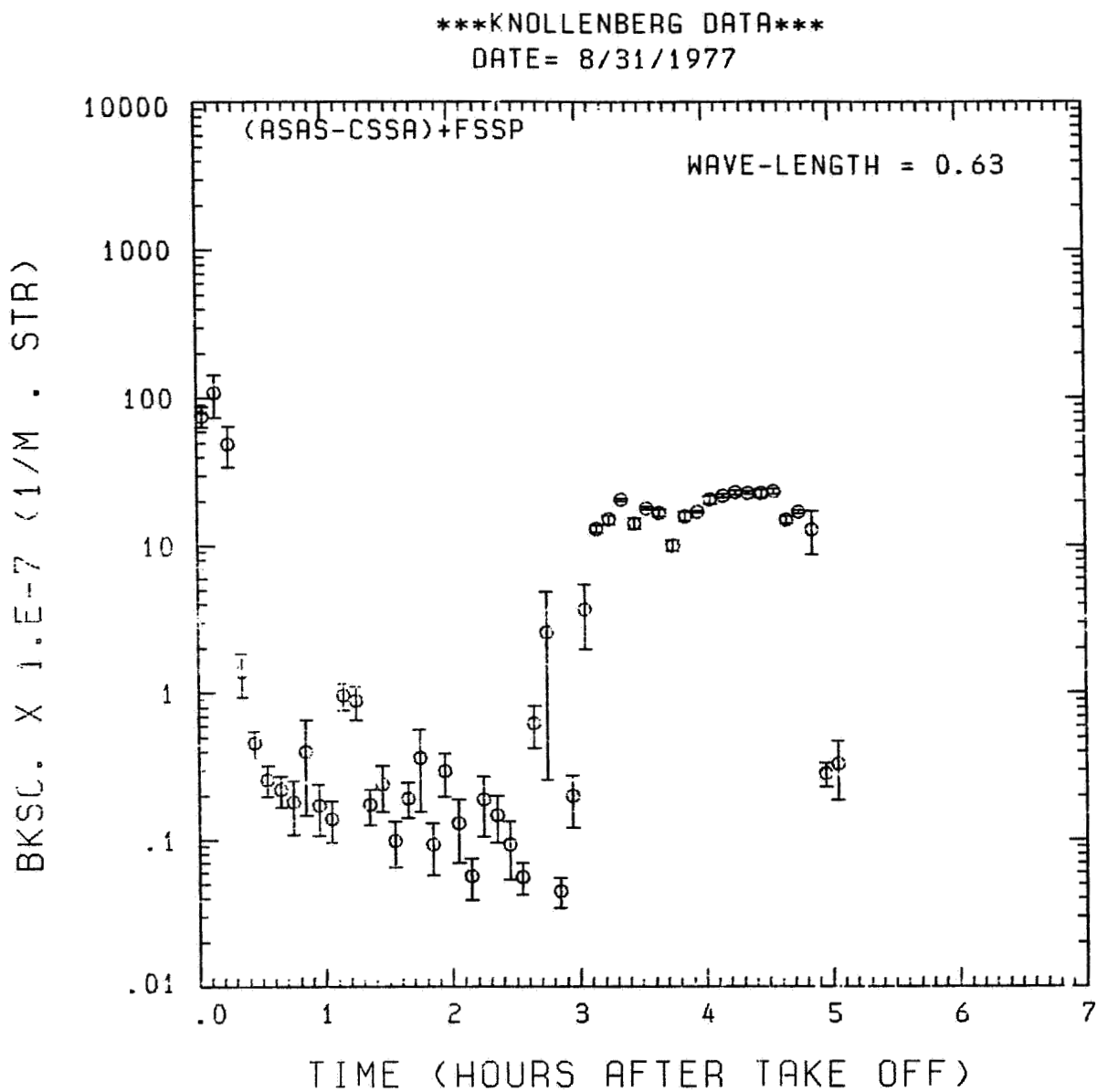


Fig. A8 (d). GAMETAG flight data for August 31, 1977.
Calculated backscatter coefficient along the flight track for five-minute data sets for $\lambda = 0.63 \mu\text{m}$.

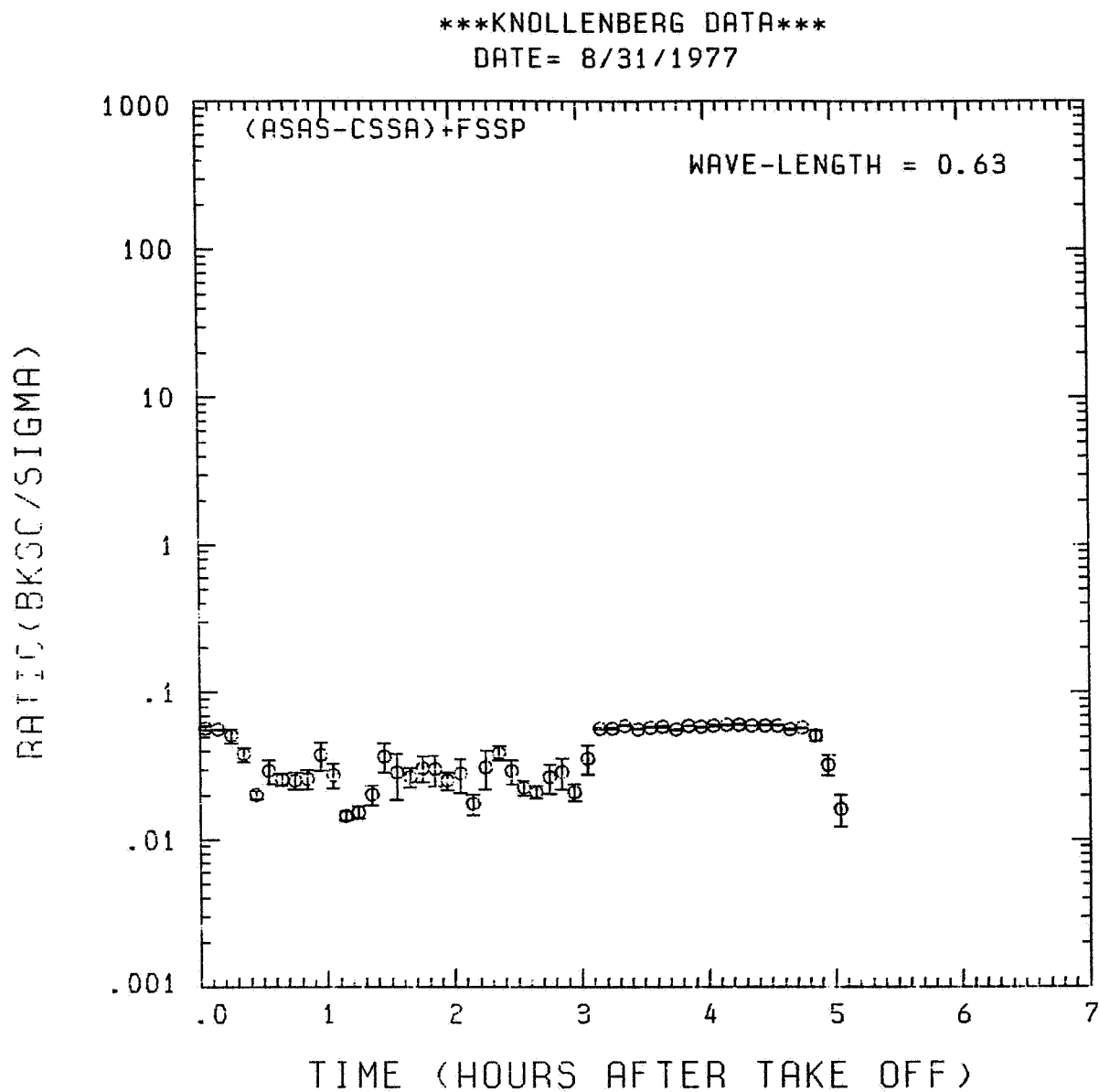


Fig. A 8 (e). GAMETAG flight data for August 31, 1977.
Calculated ratios for backscatter to extinction for
five-minute data sets for $\lambda = 0.63 \mu\text{m}$.

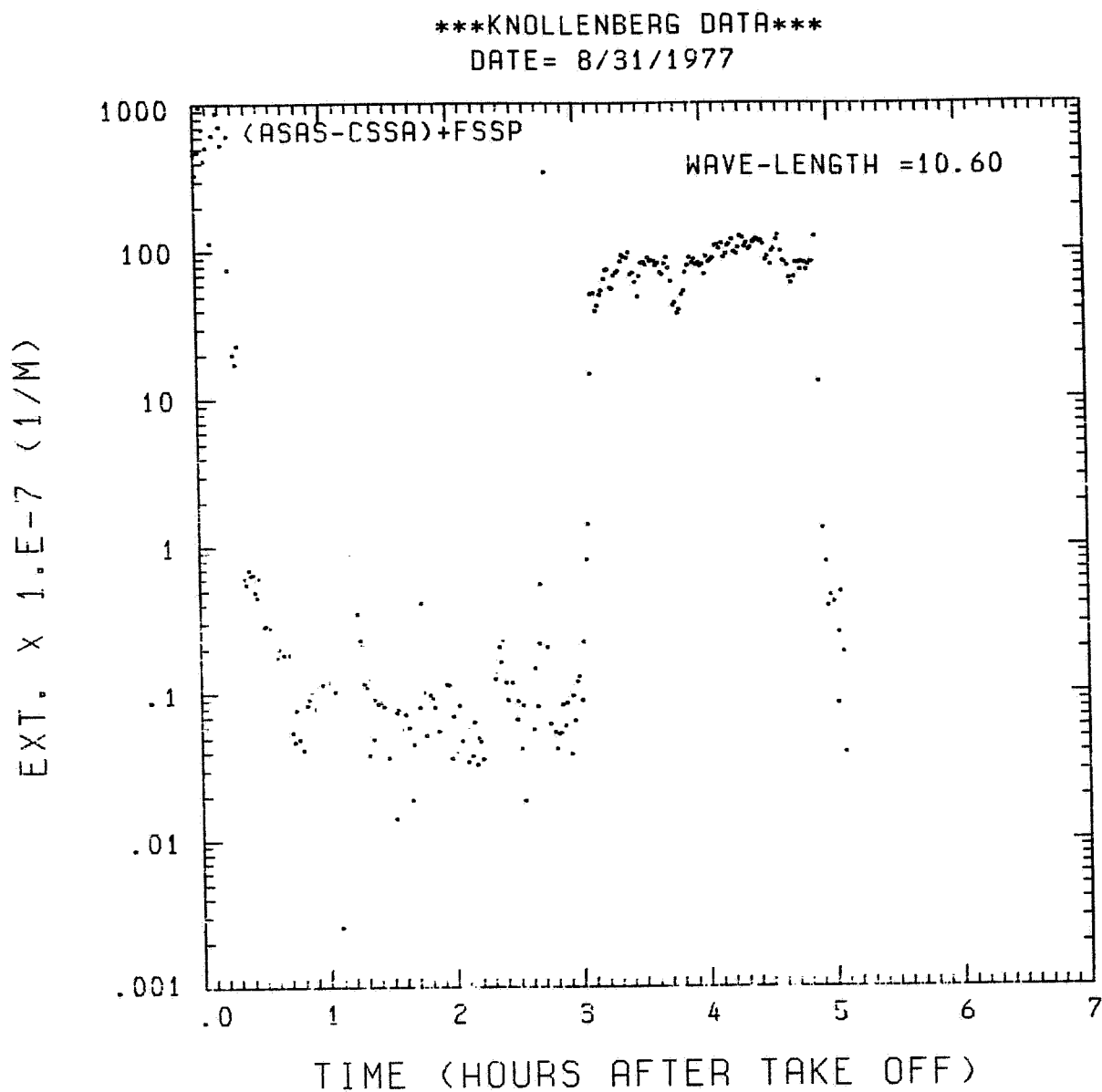


Fig. A8 (f). GAMETAG flight data for August 31, 1977.
Calculated particulate extinction along the flight
track for one-minute data sets for $\lambda = 10.6 \mu\text{m}$.

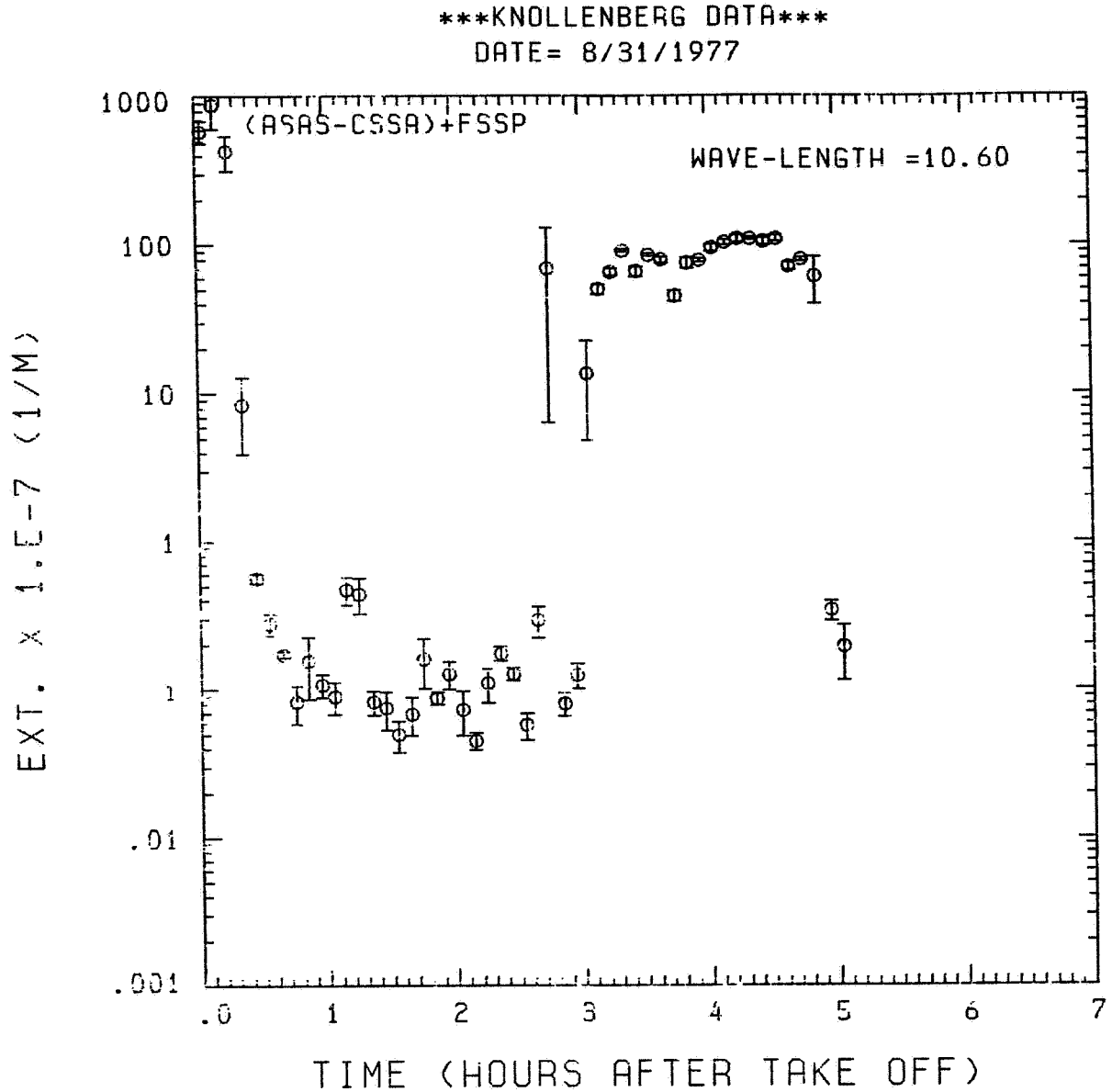


Fig. A8 (g). GAMETAG flight data for August 31, 1977.
Calculated particulate extinction along the flight
track for five-minute data sets for $\lambda = 10.6 \mu\text{m}$.

KNOLLENBERG DATA

DATE= 8/31/1977

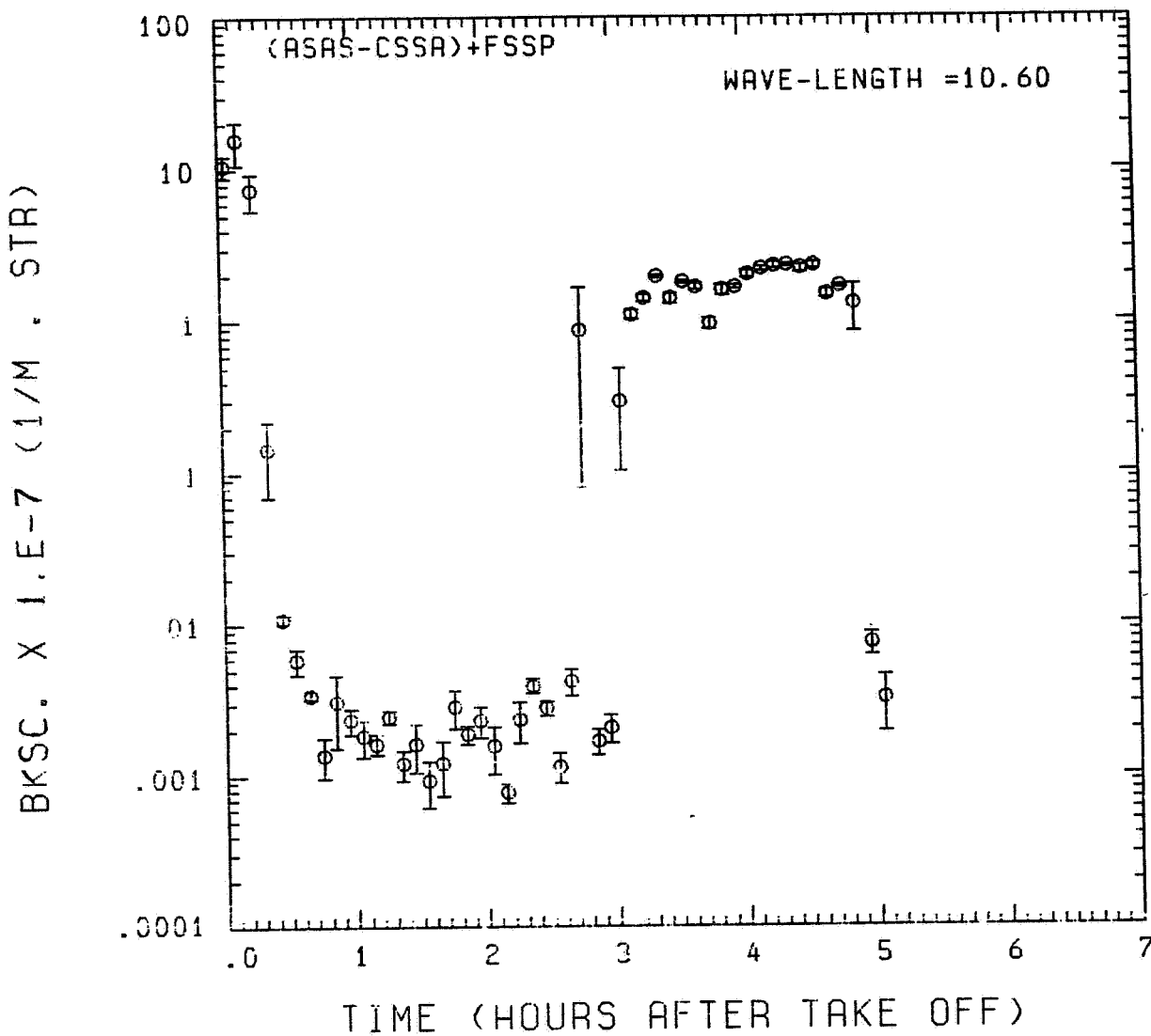


Fig. A 8 (h). GAMETAG flight data for August 31, 1977.

Calculated backscatter coefficient along the flight track for five-minute data sets for $\lambda = 10.6 \mu\text{m}$.

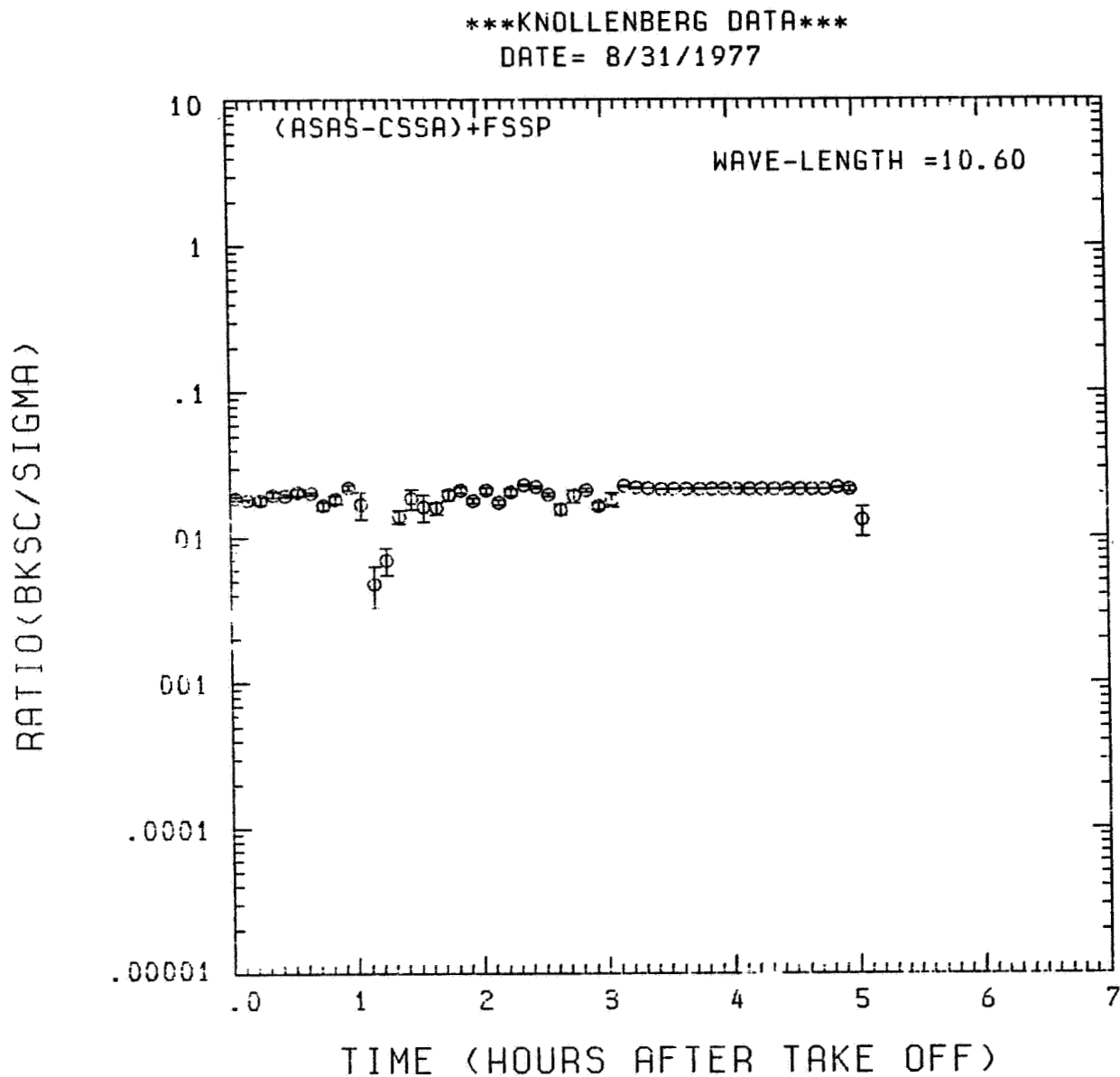


Fig. A 8 (i). GAMETAG flight data for August 31, 1977.
Calculated ratios for backscatter to extinction for
five-minute data sets for $\lambda = 10.6 \mu\text{m}$.

Table A9. Significant times for September 1, 1977.
Pago Pago, American Samoa to Johnston Atoll.

1 2 3

Significant Points

<u>#</u>	<u>TIME</u>	
1	19:57	Pago Pago
2	20:27	
3	21:57	
4	22:15	
5	22:42	
6	23:05	
7	00:49	
8	01:01	
9	01:19	
10	01:31	
11	01:32	
12	01:41	
13	02:01	
14	02:25	
15	02:40	
16	02:46	Johnston Atoll

ORIGINAL PAGE IS
OF POOR QUALITY

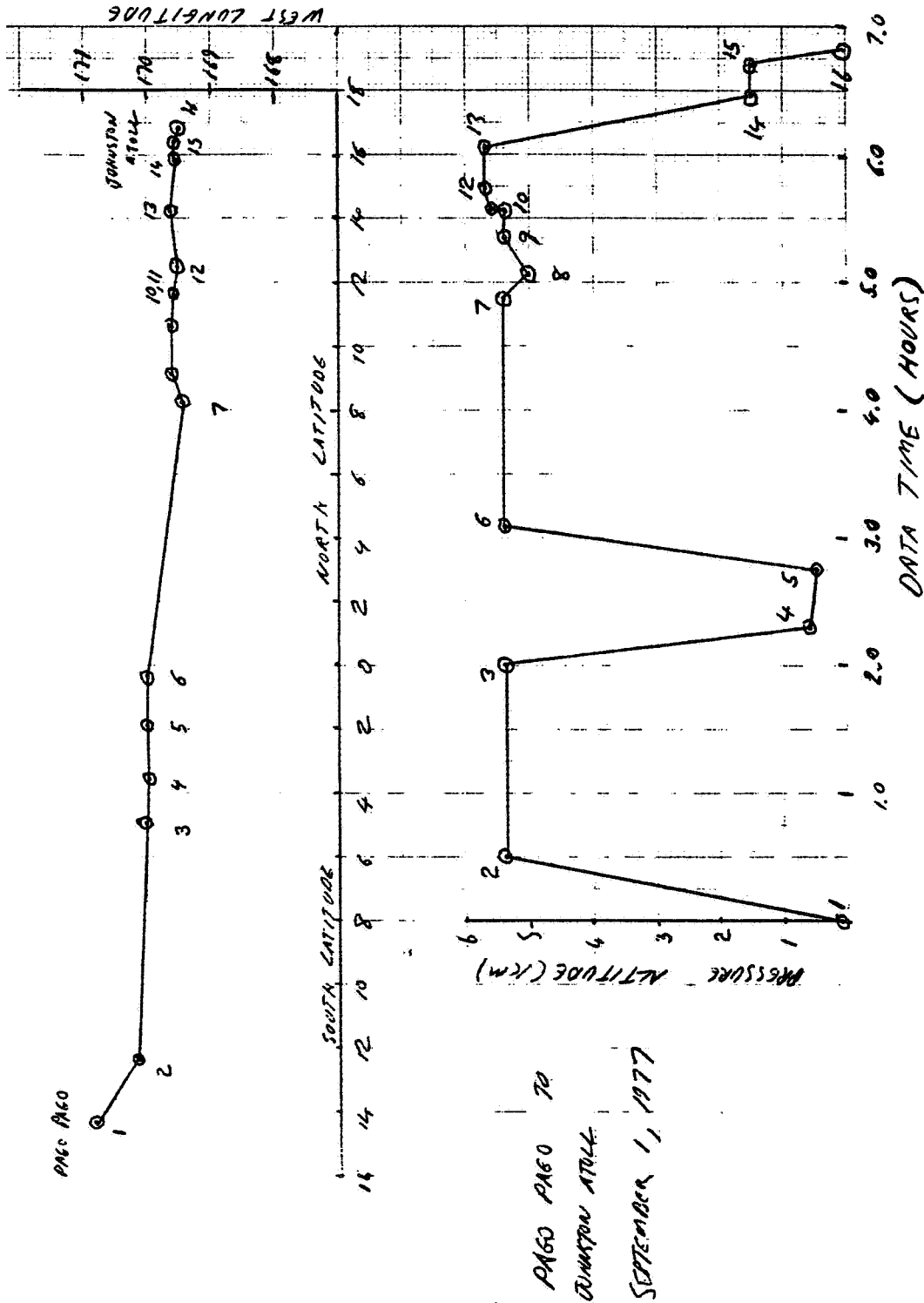


Fig. A 9 (a). GAMETAG flight data for September 1, 1977.
Altitude and location flight track plotted as a
function of time after takeoff.

KNOLLENBERG DATA

DFTE= 9/ 1/1977

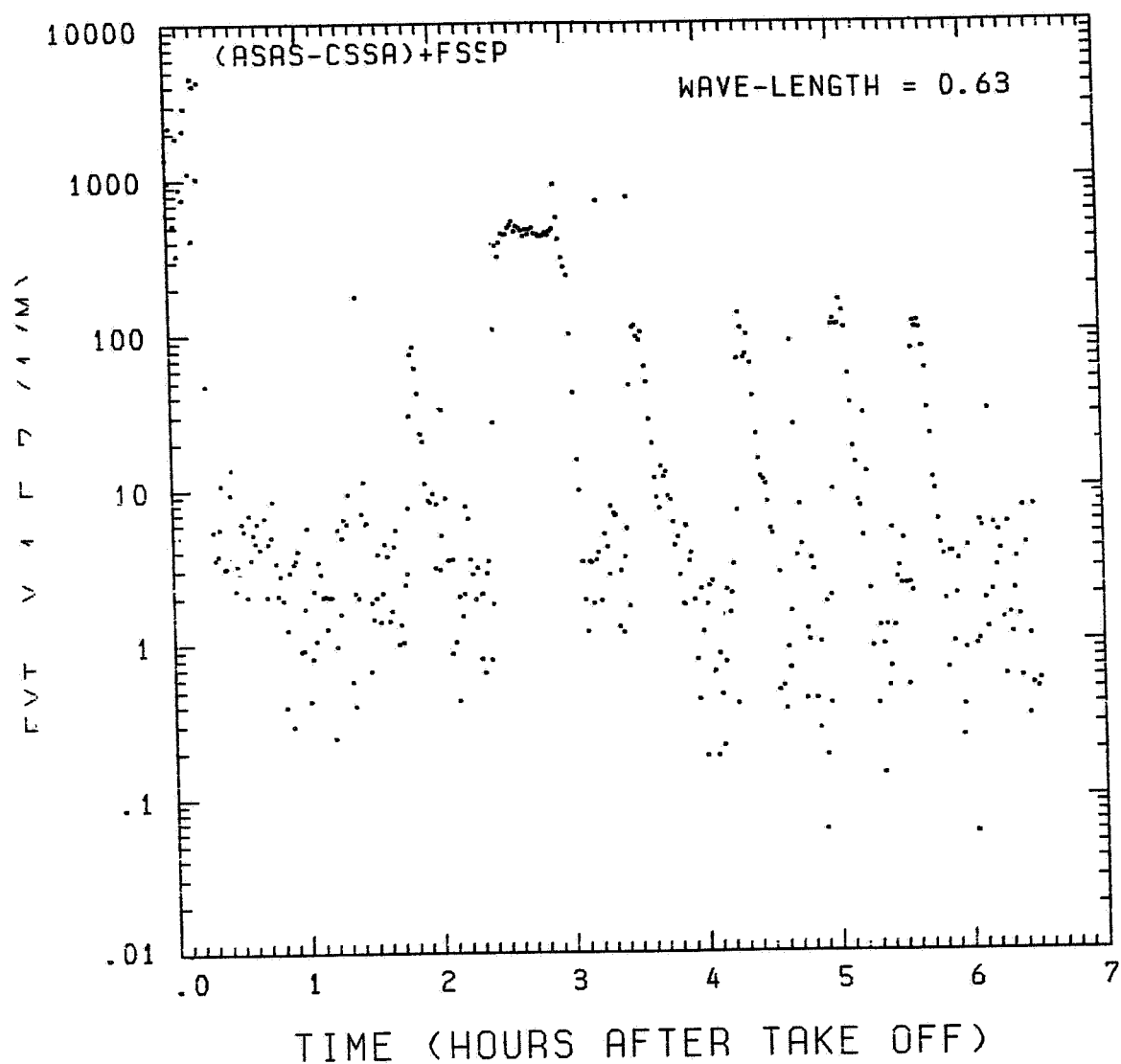


Fig. A9 (b). GAMETAG flight data for September 1, 1977.

Calculated particulate extinction along the flight track for one-minute data sets for $\lambda = 0.63 \mu\text{m}$.

KNOLLENBERG DATA

DATE= 9/ 1/1977

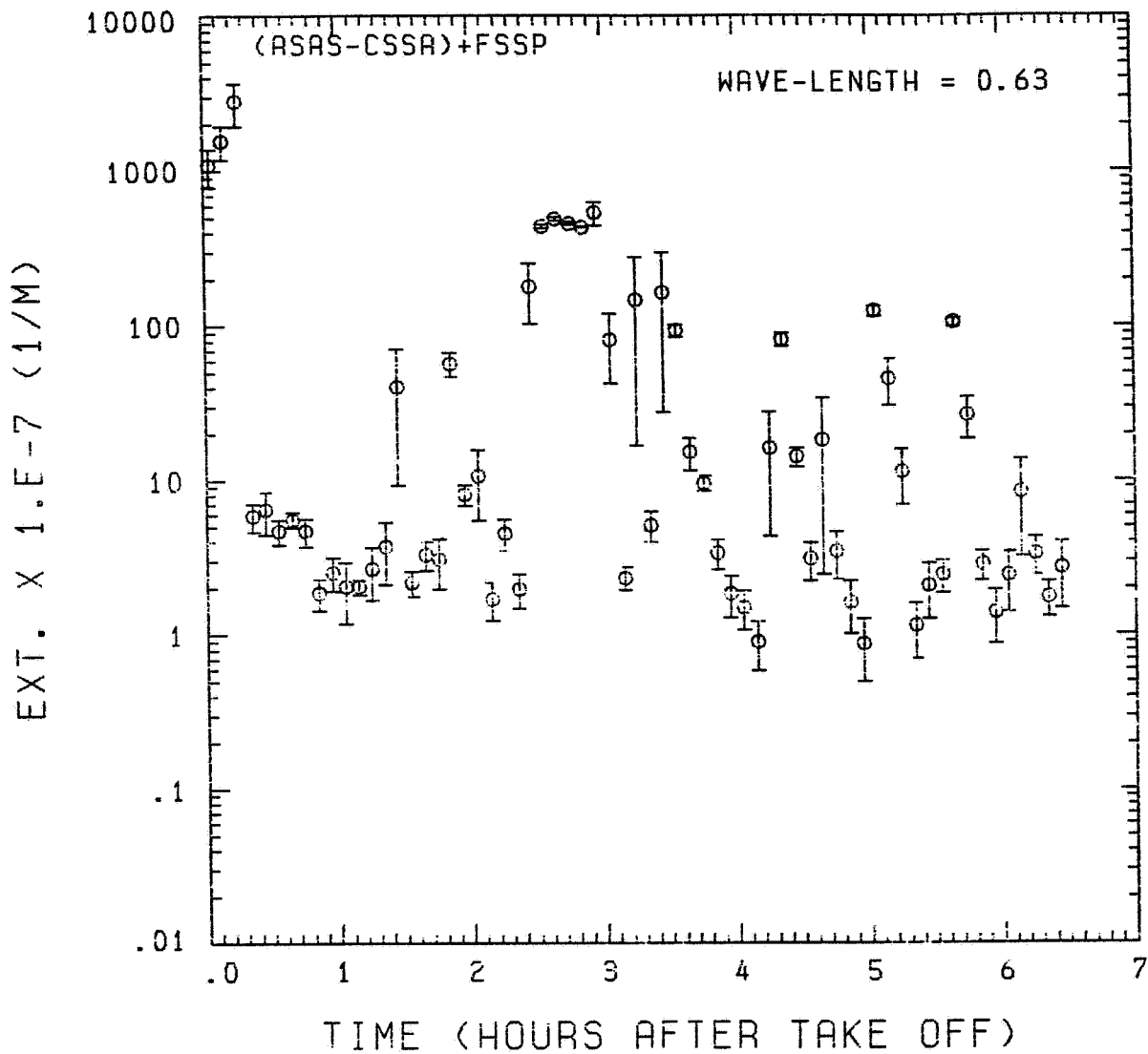


Fig. A9 (c). GAMETAG flight data for September 1, 1977.

Calculated particulate extinction along the flight track for five-minute data sets for $\lambda = 0.63 \mu\text{m}$.

KNOLLENBERG DATA

DATE= 9/ 1/1977

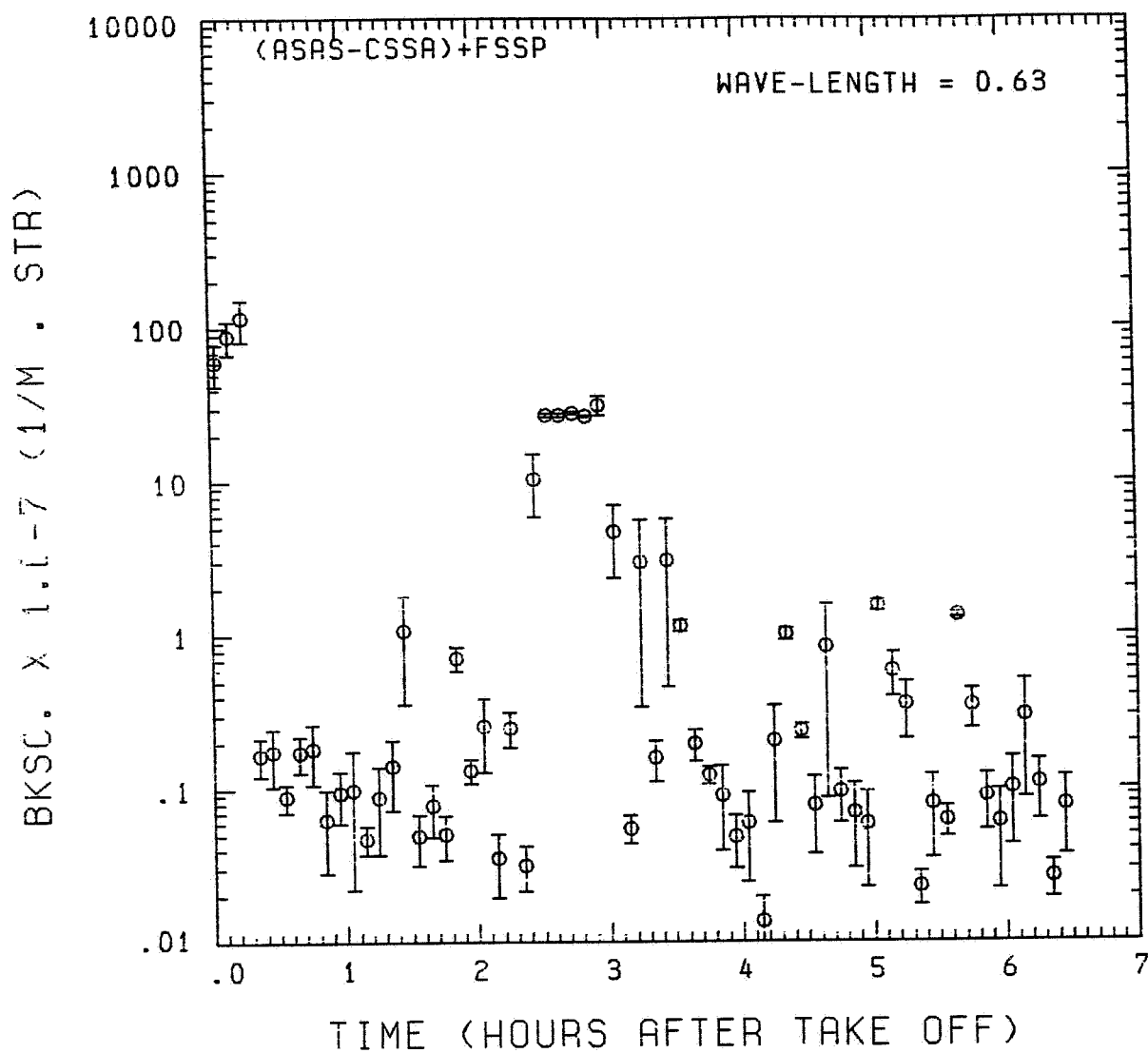


Fig. A9 (d). GAMETAG flight data for September 1, 1977.

Calculated backscatter coefficient along the flight track for five-minute data sets for $\lambda = 0.63 \mu\text{m}$.

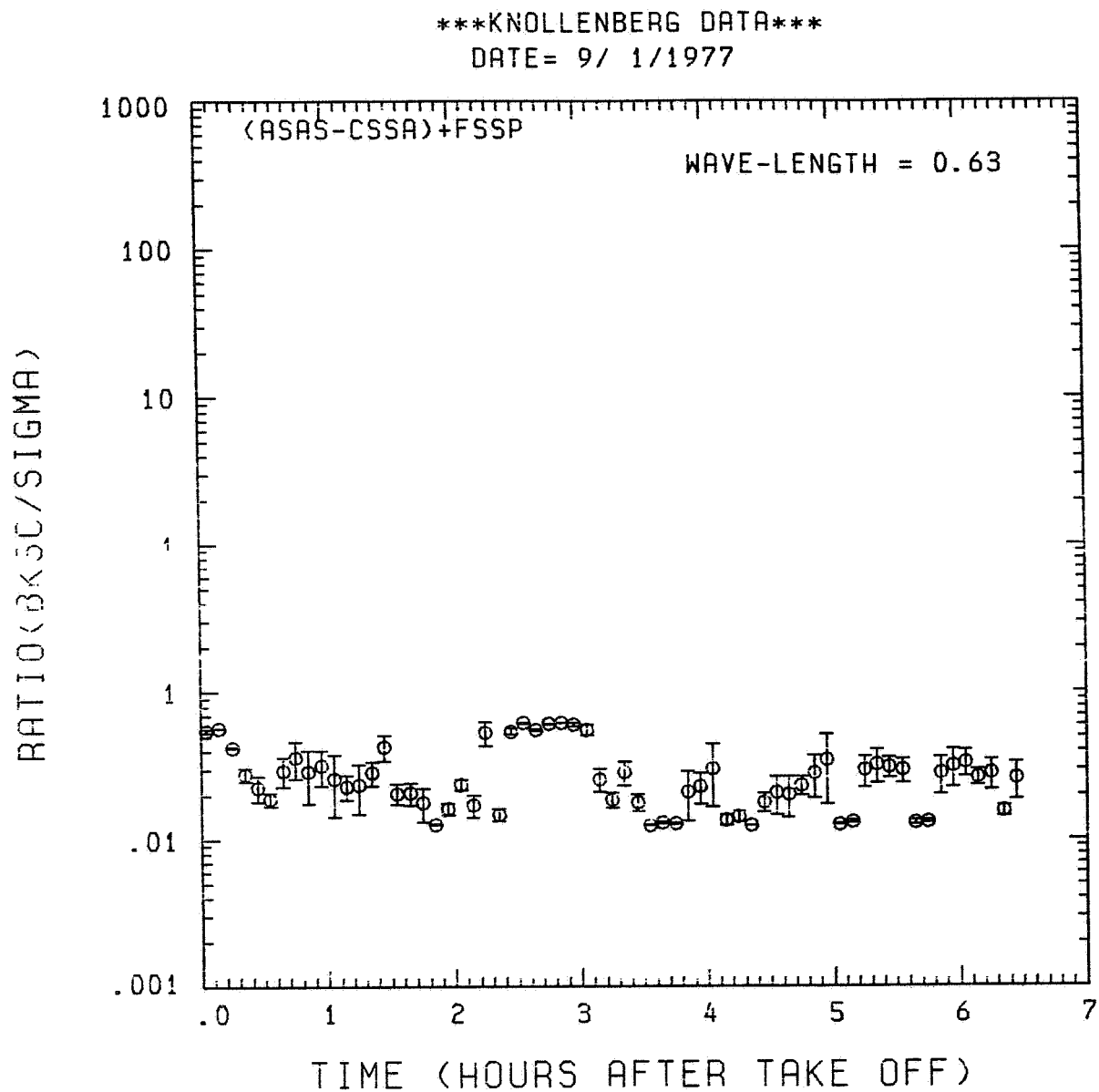


Fig. A9 (e). GAMETAG flight data for September 1, 1977.
Calculated ratios for backscatter to extinction for
five-minute data sets for $\lambda = 0.63 \mu\text{m}$.

KNOLLENBERG DATA

DATE= 9/ 1/1977

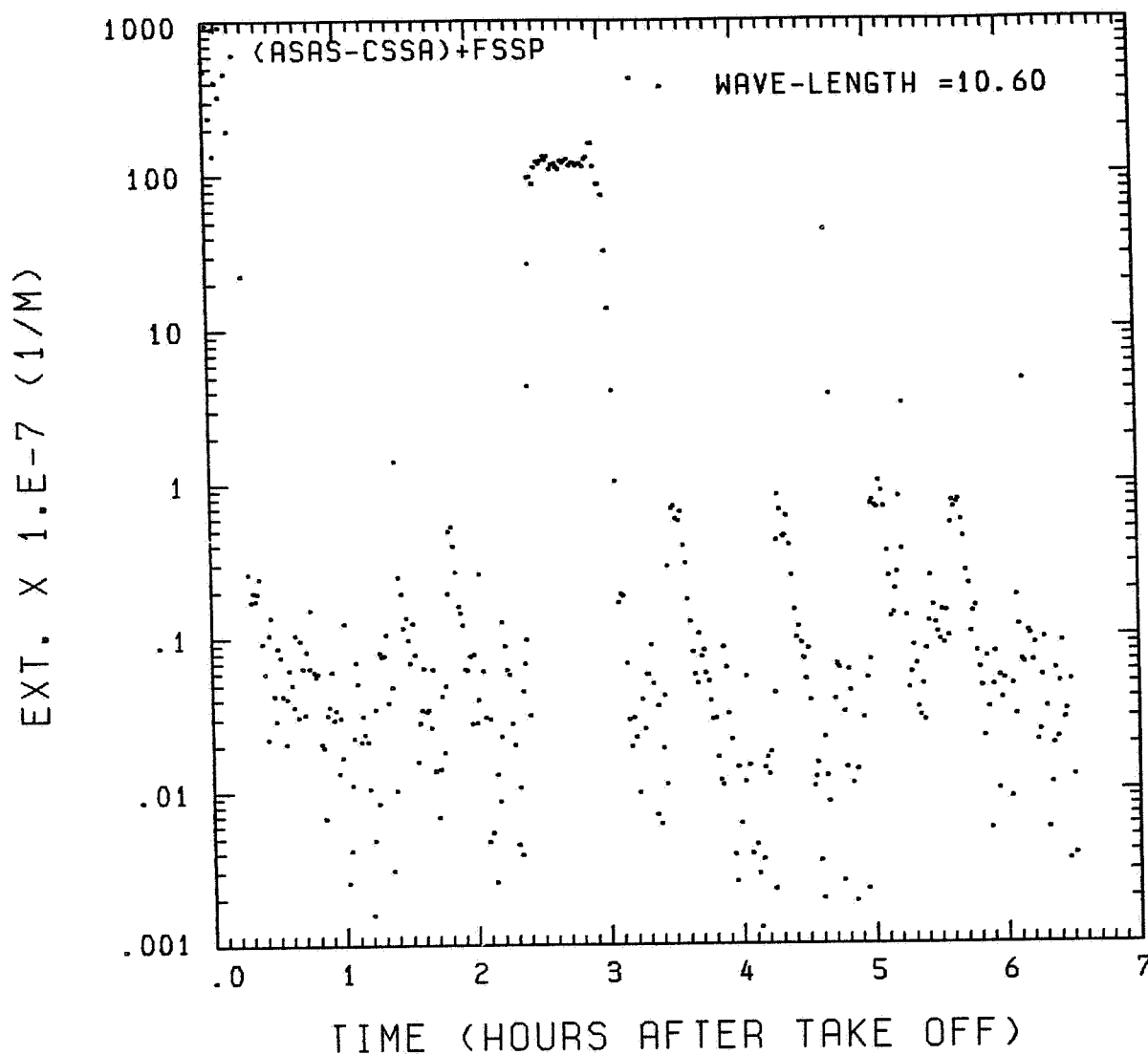


Fig. A 9 (f). GAMETAG flight data for September 1, 1977.
Calculated particulate extinction along the flight
track for one-minute data sets for $\lambda = 10.6 \mu\text{m}$.

KNOLLENBERG DATA

DATE= 9/ 1/1977

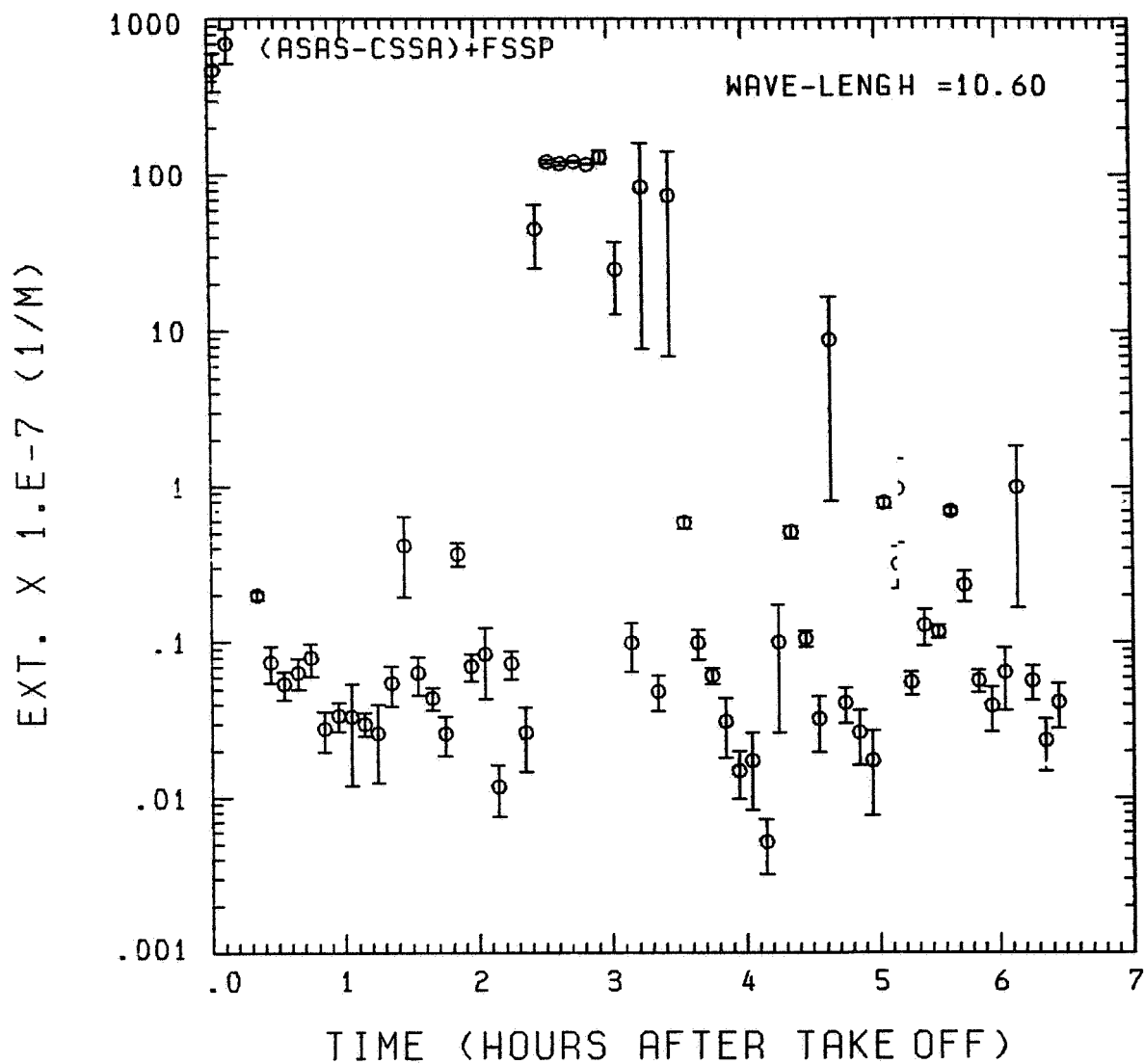


Fig. A9 (g). GAMETAG flight data for September 1, 1977.

Calculated particulate extinction along the flight track for five-minute data sets for $\lambda = 10.6 \mu\text{m}$.

ORIGINAL PAGE IS
OF POOR QUALITY

KNOLLENBERG DATA

DATE= 9/ 1/1977

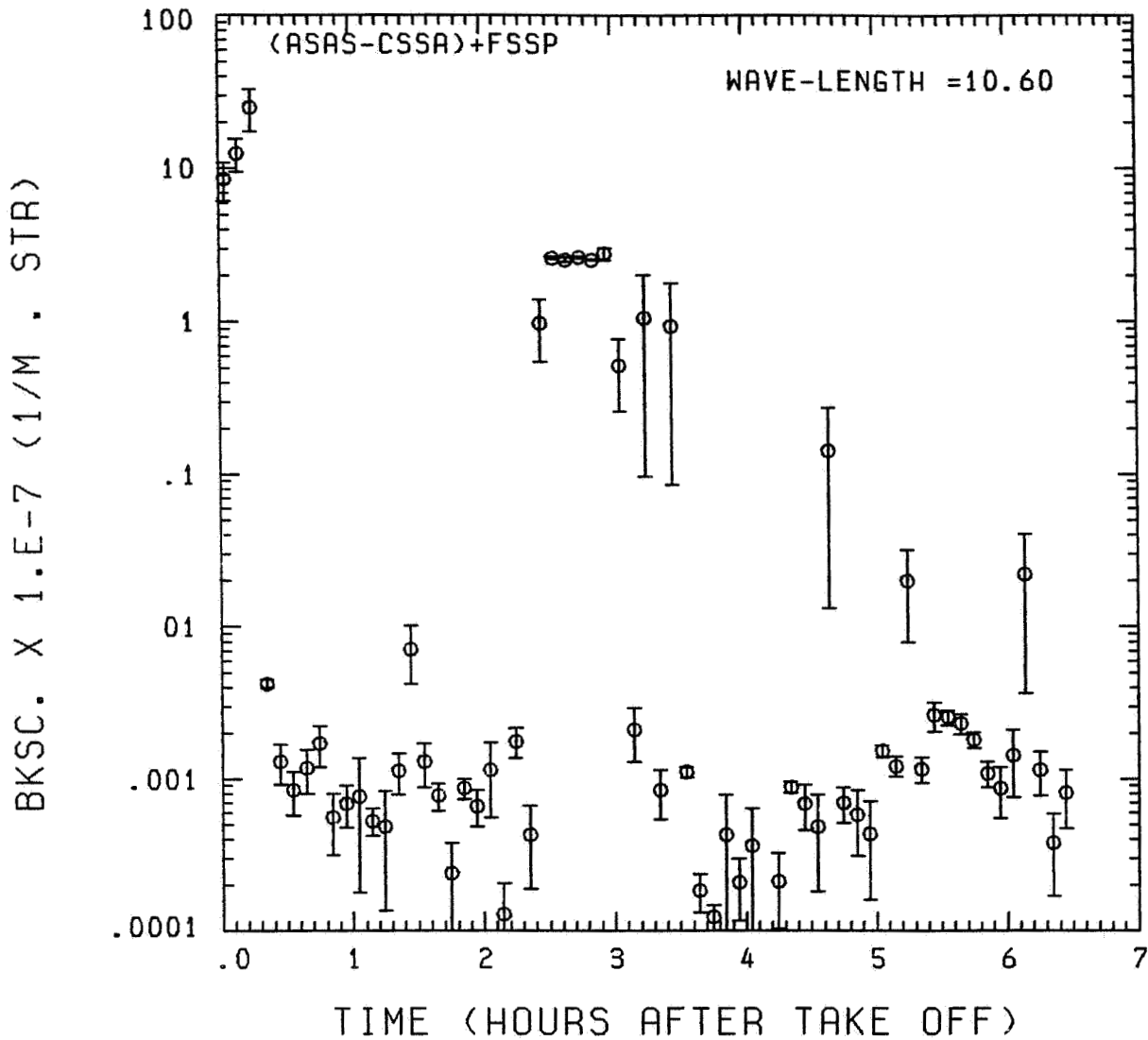


Fig. A 9 (h). GAMETAG flight data for September 1, 1977.

Calculated backscatter coefficient along the flight
track for five-minute data sets for $\lambda = 10.6 \mu\text{m}$.

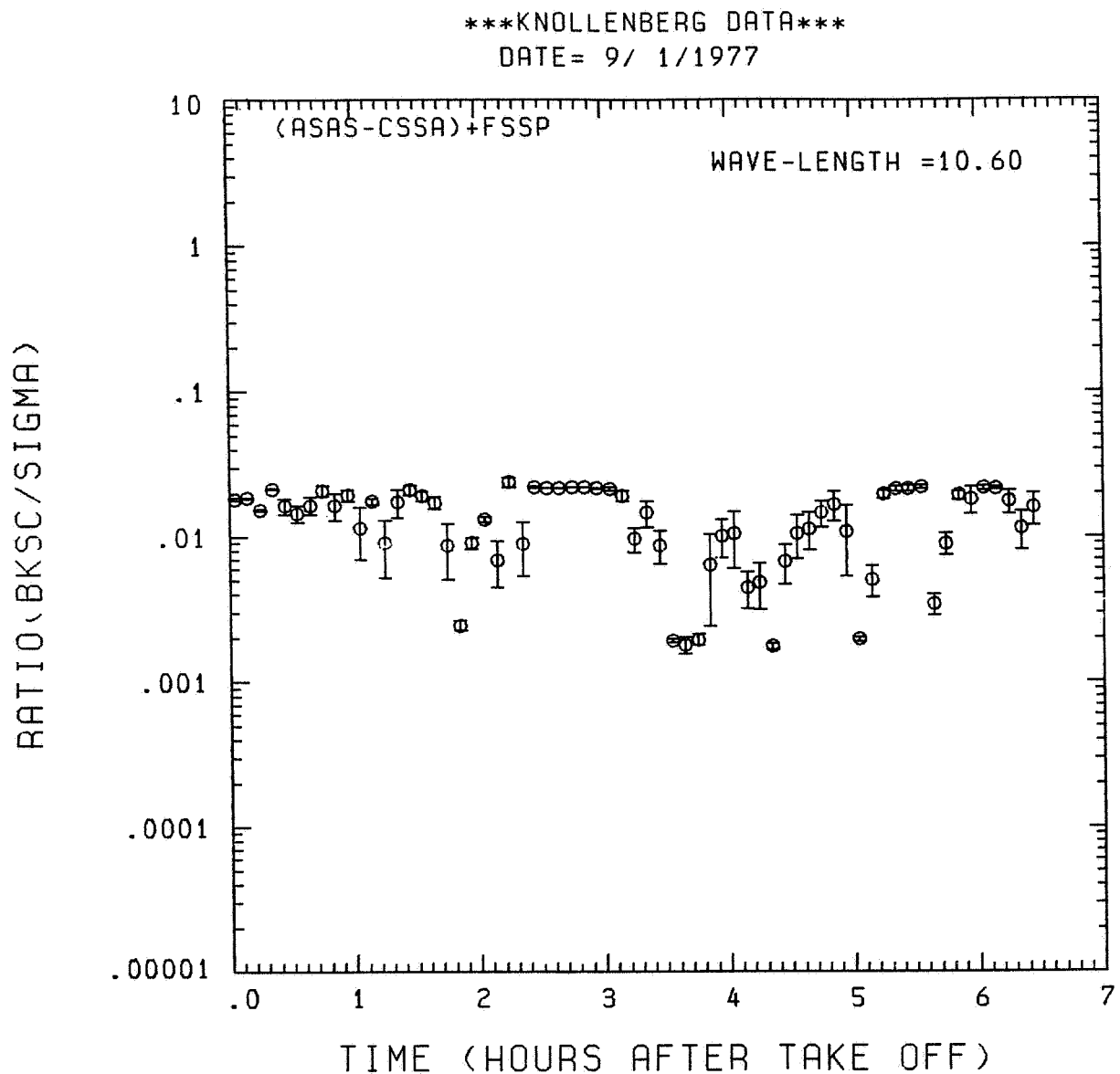


Fig. A9 (i). GAMETAG flight data for September 1, 1977.
Calculated ratios for backscatter to extinction for
five-minute data sets for $\lambda = 10.6 \mu\text{m}$.

Table A10. Significant times for September 2, 1977.
Johnston Atoll to Hilo, Hawaii.

Significant Points

<u>#</u>	<u>TIME</u>	
1	16.49	Johnston Atoll
2	17:13	
3	18:02	
4	18:30	
5	19:37	
6	19:48	
7	20:06	
8	20:16	
9	20:36	
10	21:18	
11	21:32	
12	21:47	
13	22:10	
14	22:27	
15	22:40	Hilo

ORIGINAL PAGE IS
OF POOR QUALITY

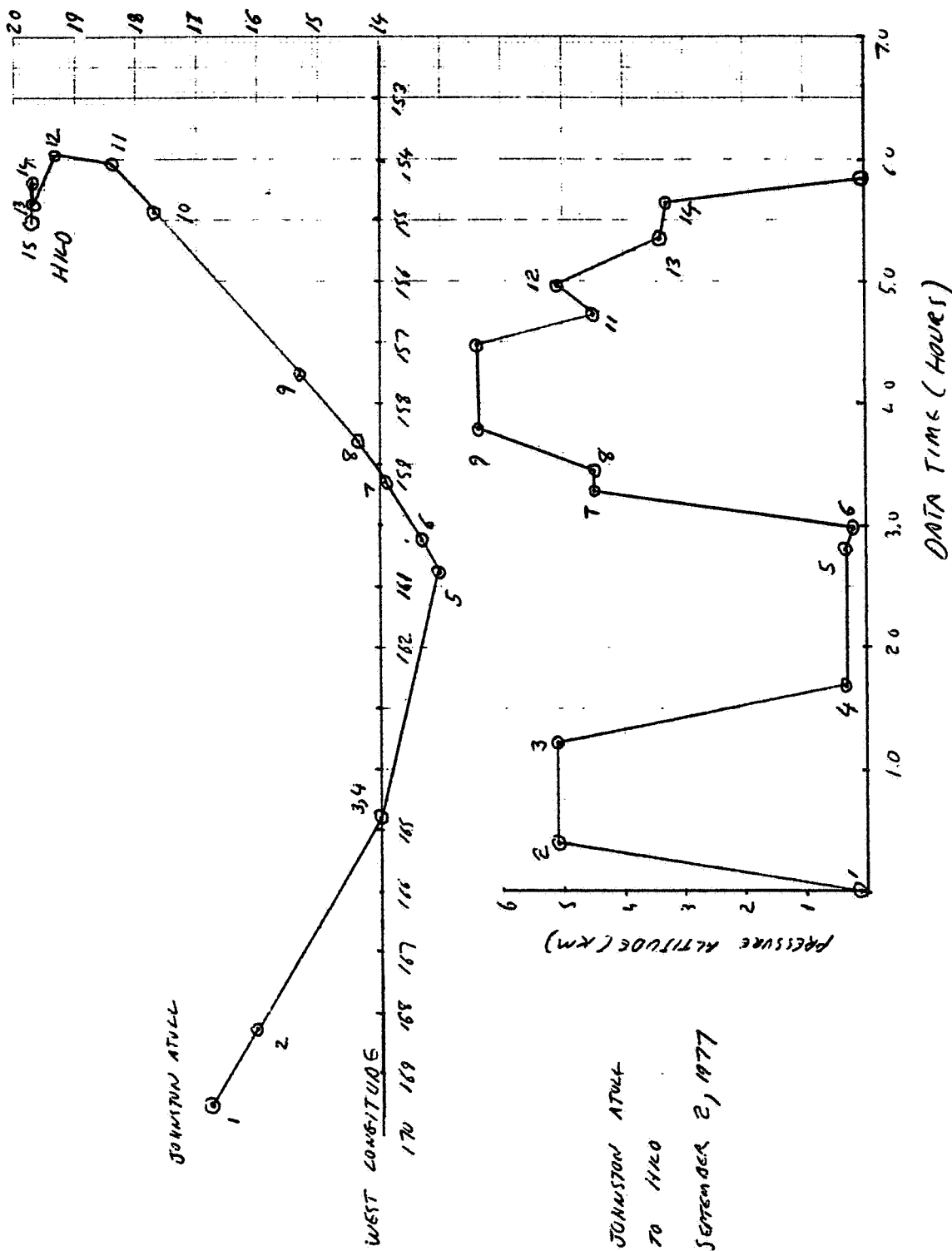


Fig. A 10 (a). GAMETAG flight data for September 2, 1977.
Altitude and location flight track plotted as a
function of time after takeoff.

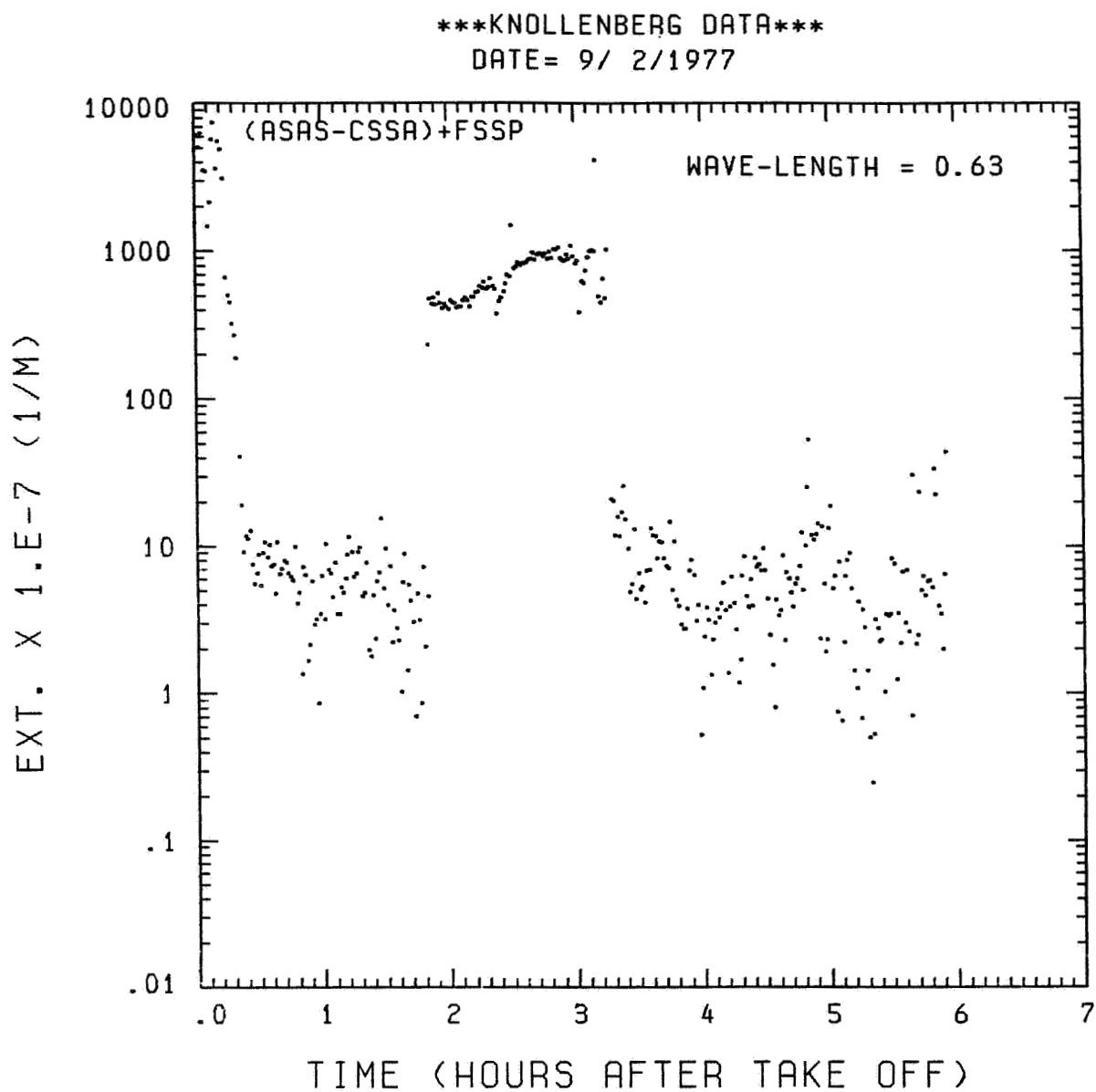


Fig. A10 (b). GAMETAG flight data for September 2, 1977.
Calculated particulate extinction along the flight
track for one-minute data sets for $\lambda = 0.63 \mu\text{m}$.

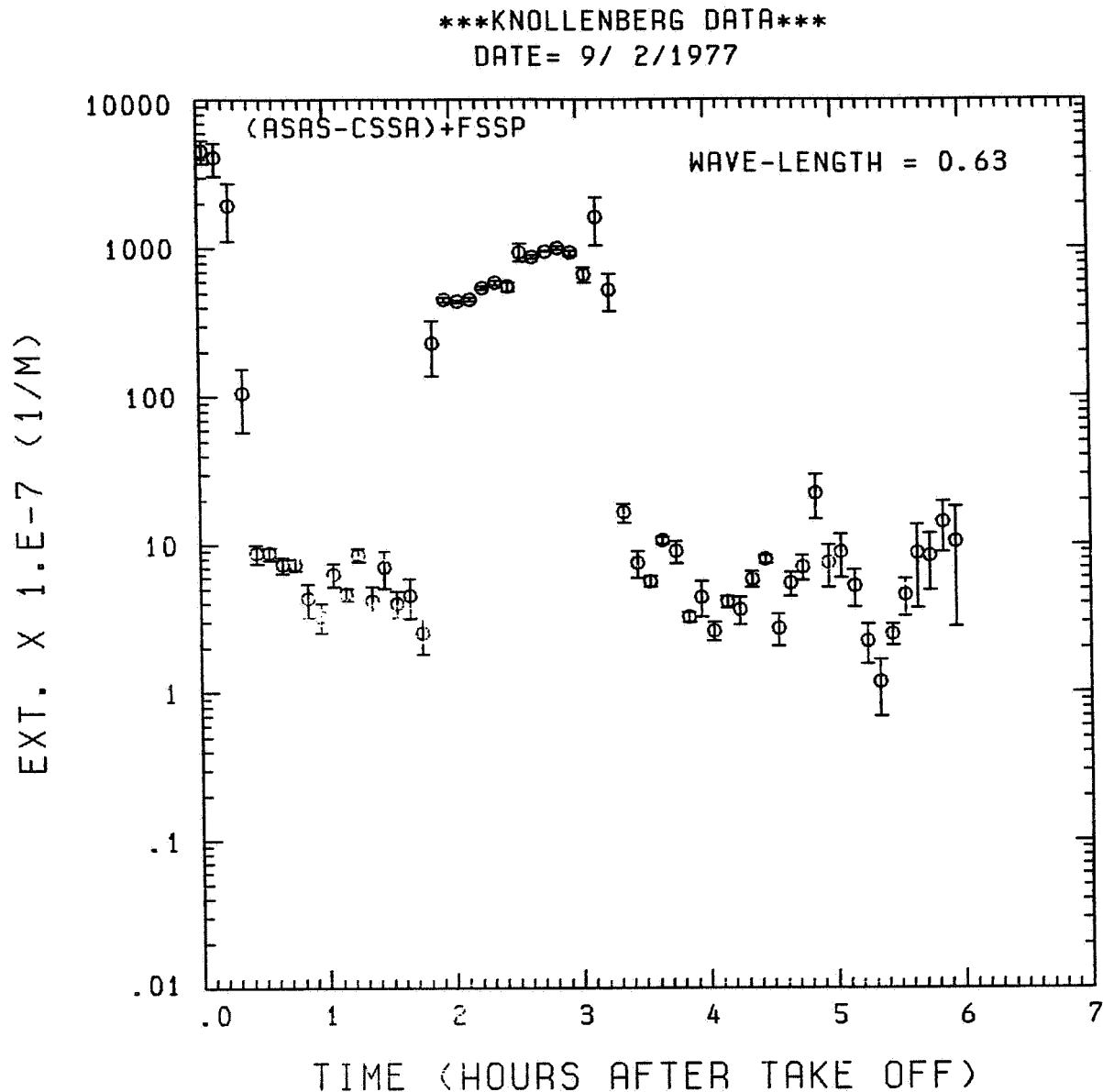


Fig. A10 (c). GAMETAG flight data for September 2, 1977.
Calculated particulate extinction along the flight
track for five-minute data sets for $\lambda = 0.63 \mu\text{m}$.

KNOLLENBERG DATA

DATE= 9/ 2/1977

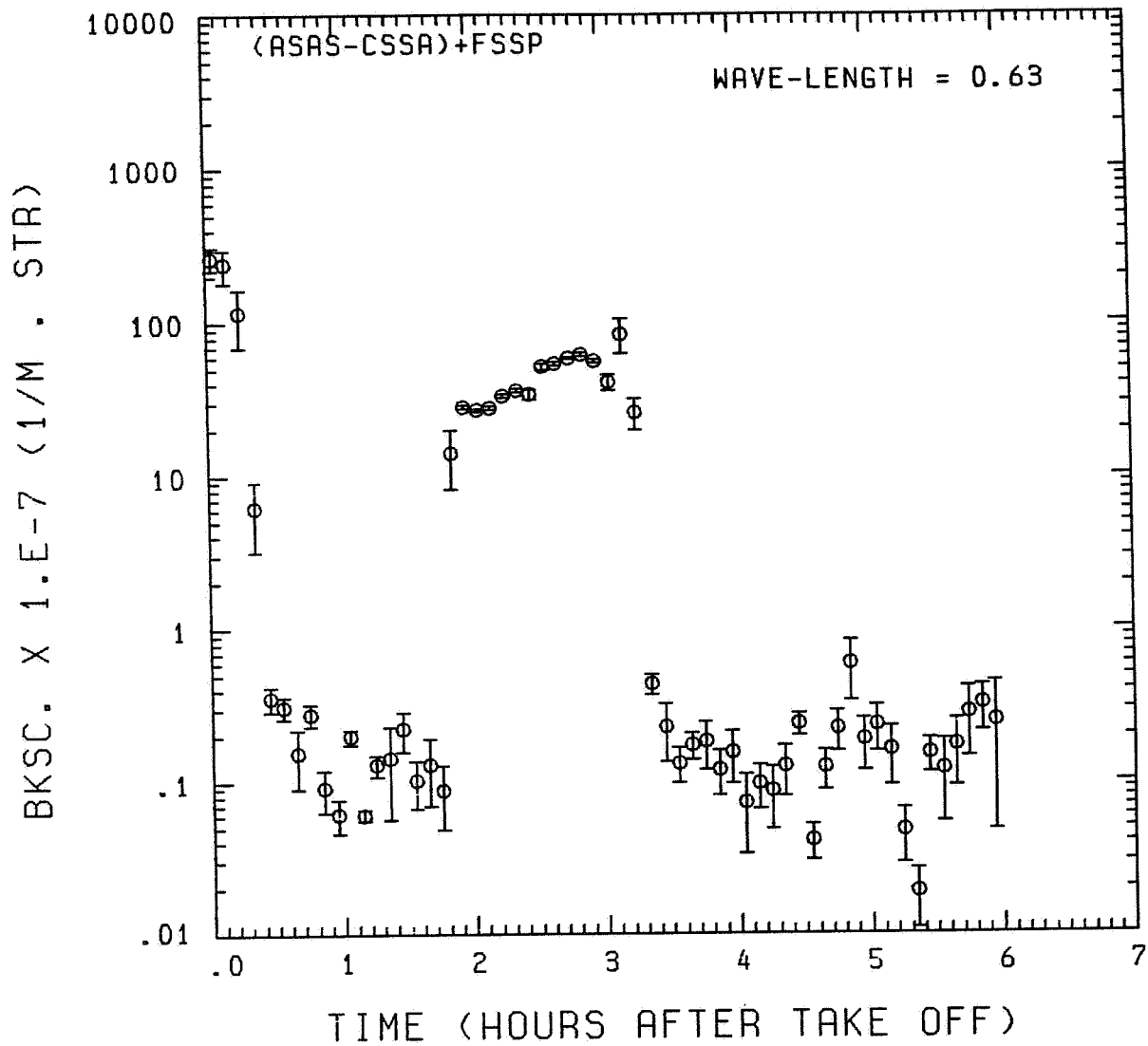


Fig. A10 (d). GAMETAG flight data for September 2, 1977.

Calculated backscatter coefficient along the flight track for five-minute data sets for $\lambda = 0.63 \mu\text{m}$.

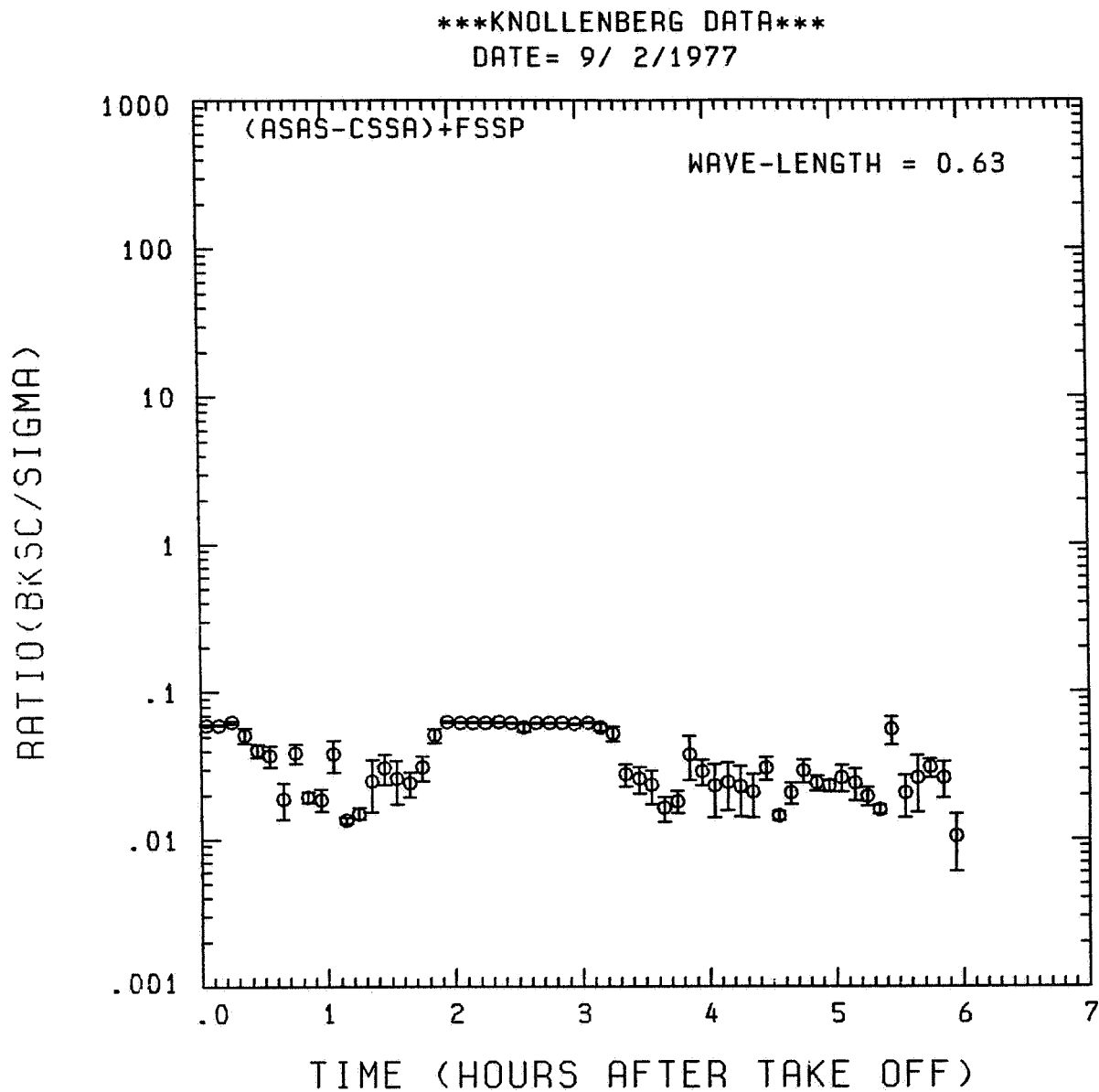


Fig. A10 (e). GAMETAG flight data for September 2, 1977.
Calculated ratios for backscatter to extinction for
five-minute data sets for $\lambda = 0.63 \mu\text{m}$.

KNOLLENBERG DATA

DATE= 9/ 2/1977

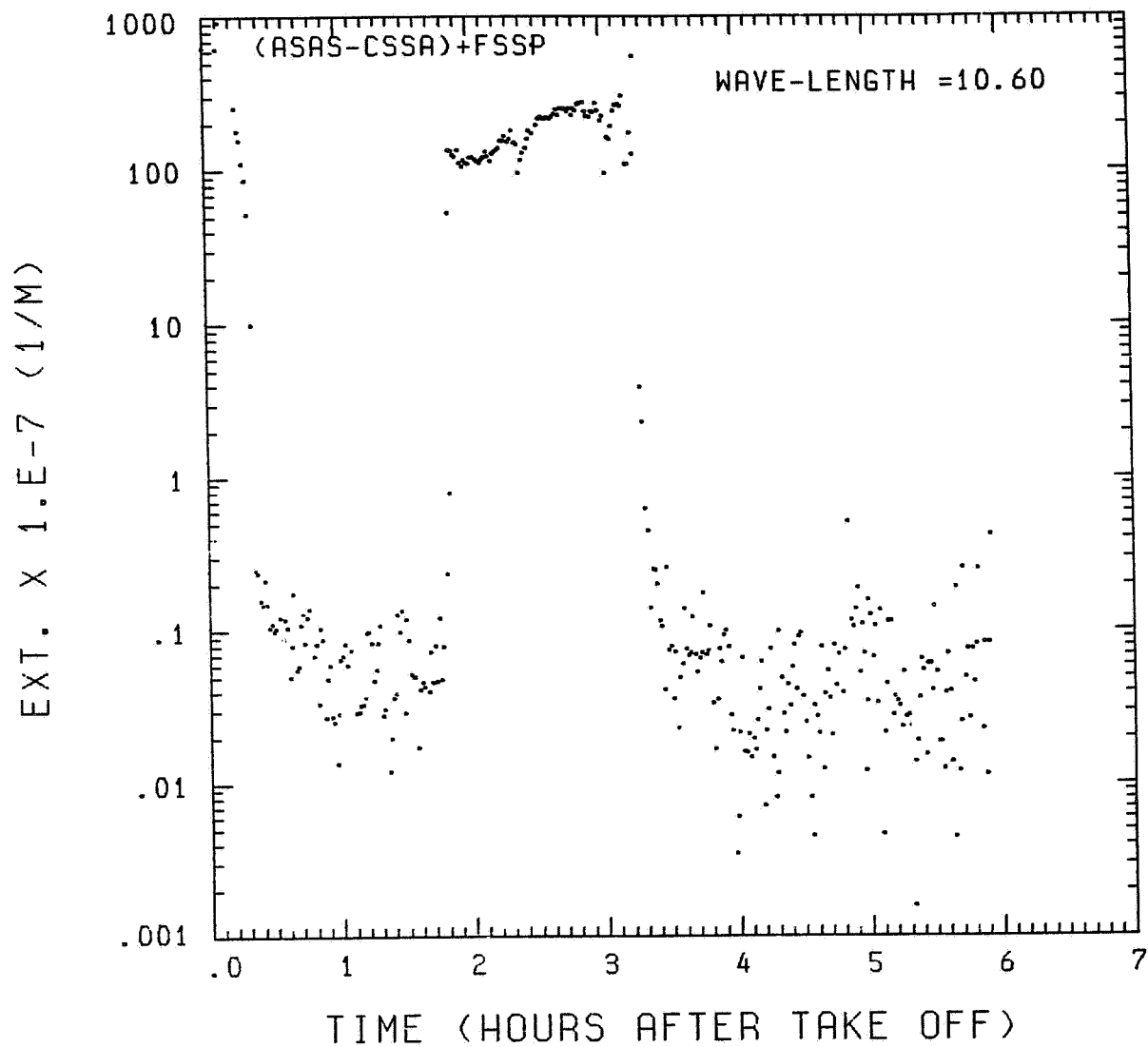


Fig. A10 (f). GAMETAG flight data for September 2, 1977.
Calculated particulate extinction along the flight
track for one-minute data sets for $\lambda = 10.6 \mu\text{m}$.

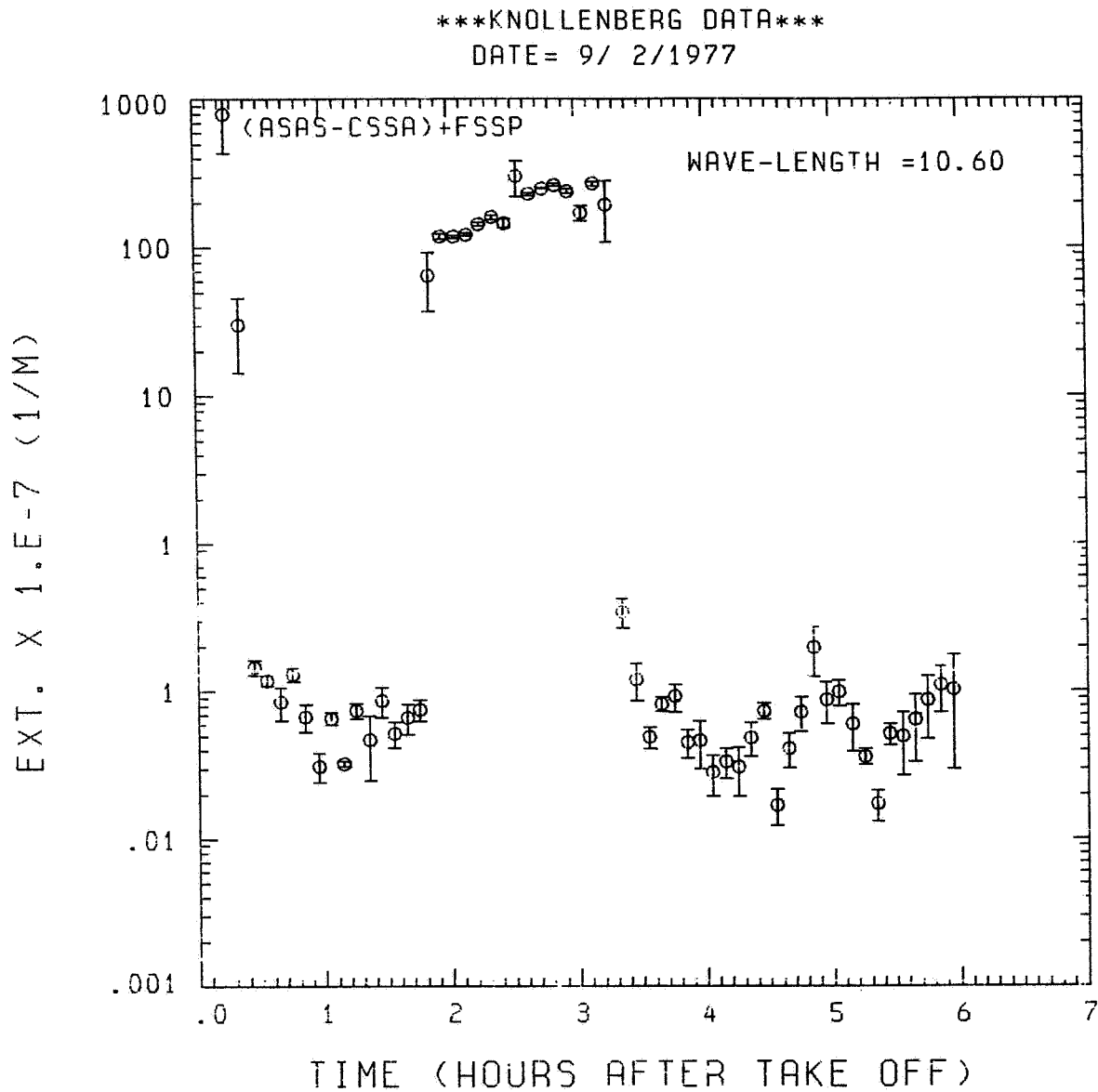


Fig. A10 (g). GAMETAG flight data for September 2, 1977.
Calculated particulate extinction along the flight
track for five-minute data sets for $\lambda = 10.6 \mu\text{m}$.

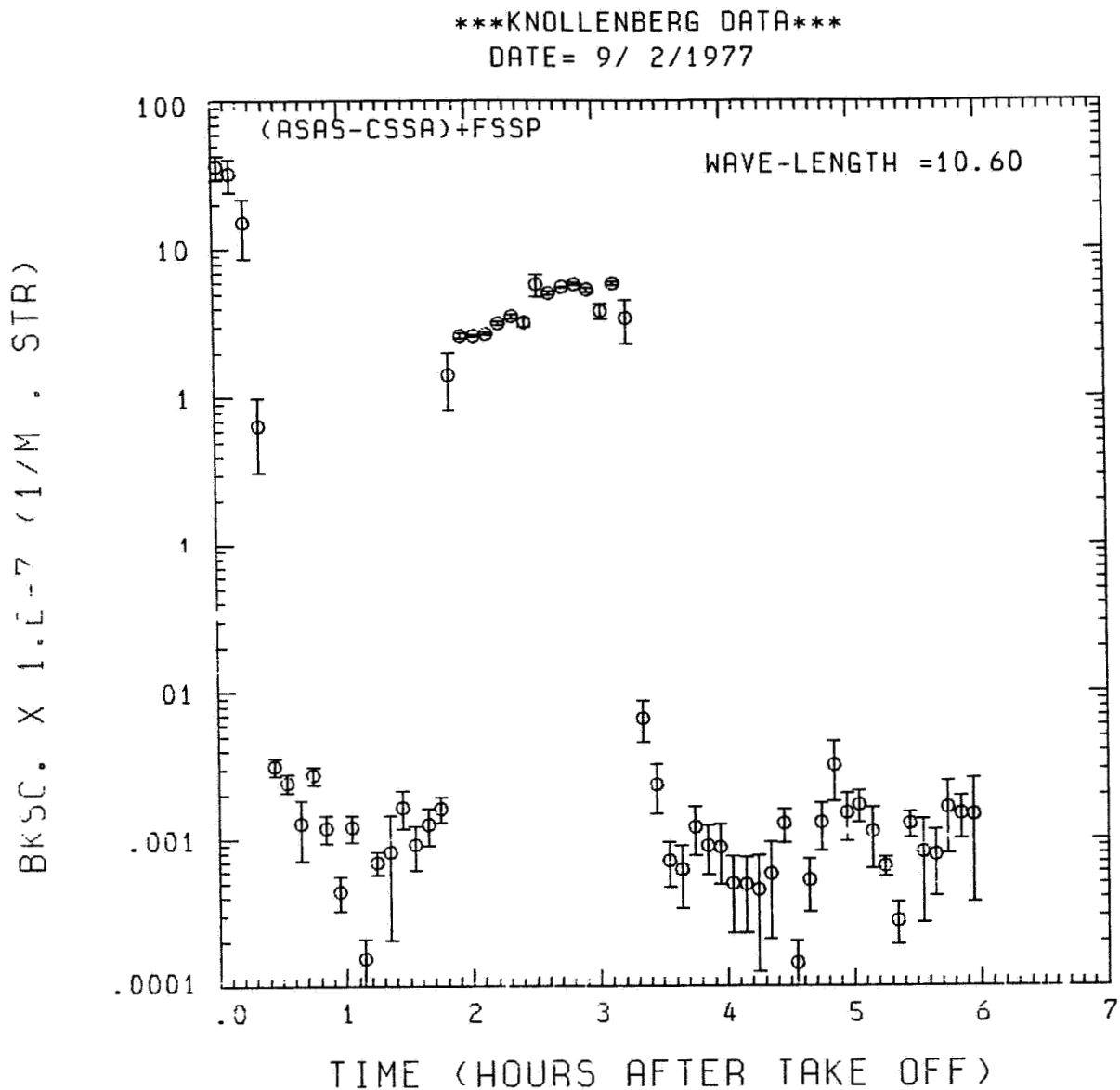


Fig. A10(h). GAMETAG flight data for September 2, 1977.
Calculated backscatter coefficient along the flight
track for five-minute data sets for $\lambda = 10.6 \mu\text{m}$.

KNOLLENBERG DATA

DATE= 9/ 2/1977

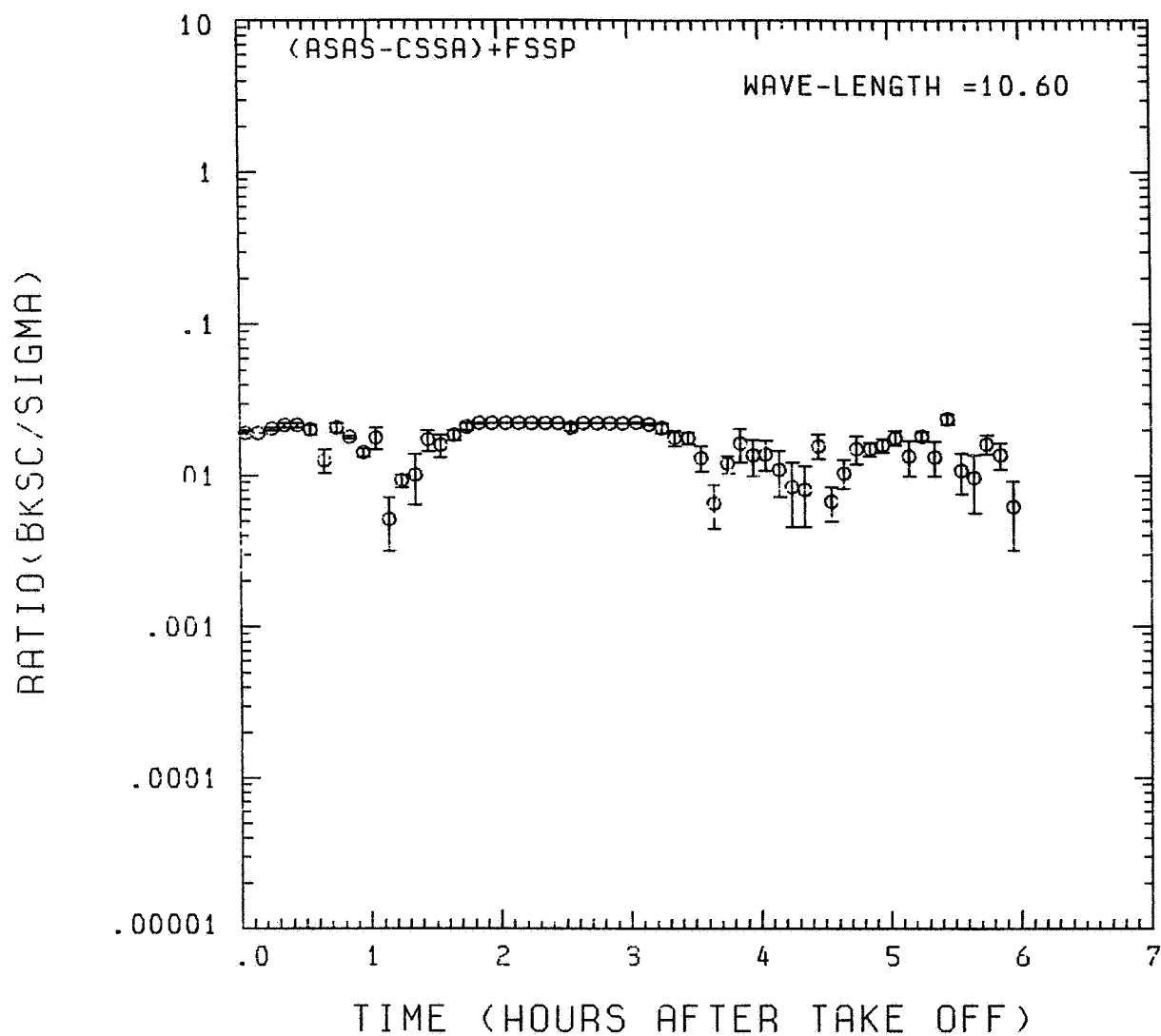


Fig. A 10 (i). GAMETAG flight data for September 2, 1977.
Calculated ratios for backscatter to extinction for
five-minute data sets for $\lambda = 10.6 \mu\text{m}$.

Table A11. Significant times for April 27, 1978.
Denver, Colorado to Moffett Field,
California.

Significant Points

<u>#</u>	<u>TIME</u>	
1	17:00	Denver
2	17:21	
3	19:23	
4	19:24	
5	19:54	
6	20:19	
7	20:25	
8	20:28	
9	20:52	
10	21:14	
11	22:36	
12	22:53	Moffett Field

ORIGINAL PAGE IS
OF POOR QUALITY

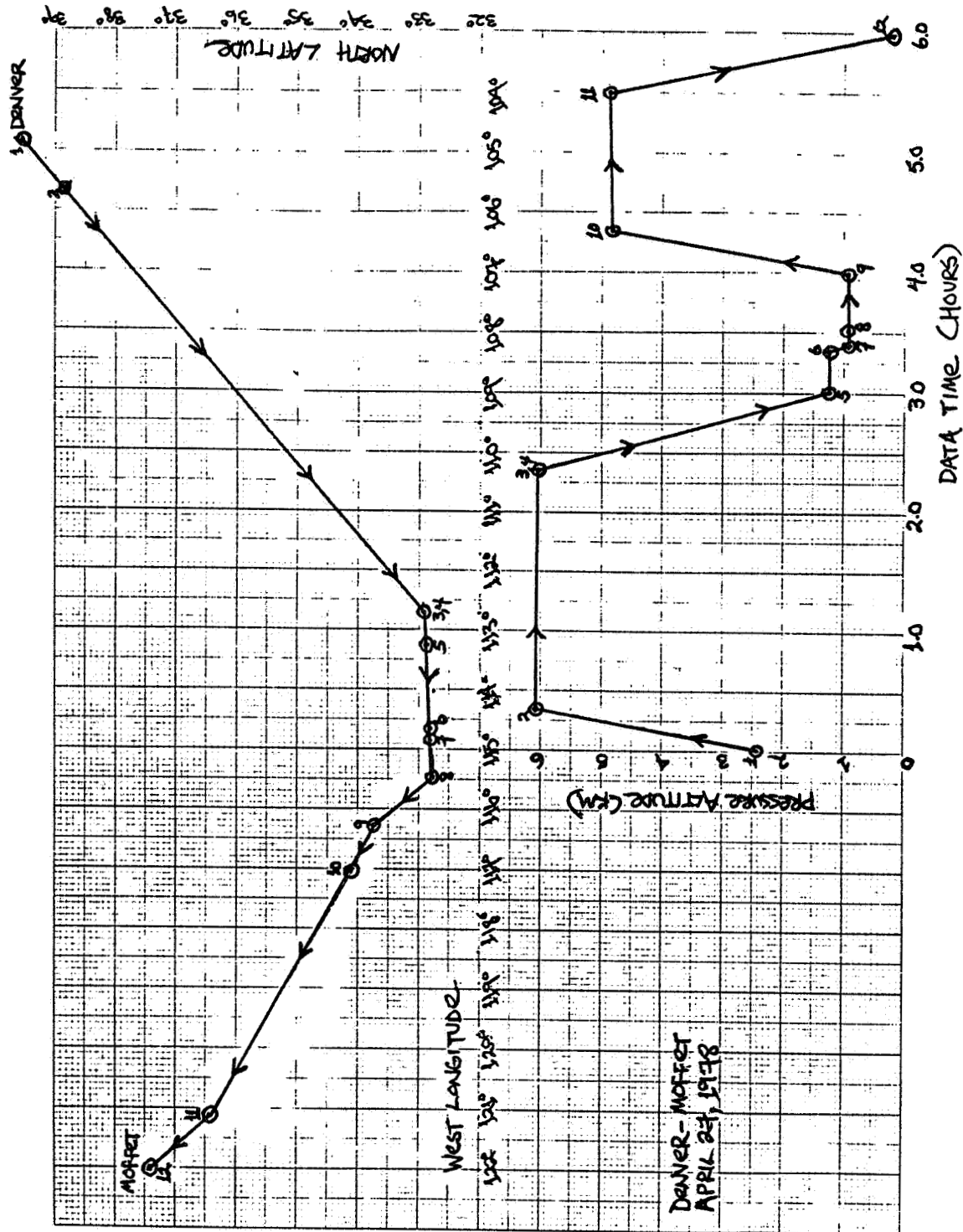


Fig. A 11 (a). GAMETAG flight data for April 27, 1978.

Altitude and location flight track plotted as a function of time after takeoff.

Knollenberg Data
DATE=APRIL 27,1978

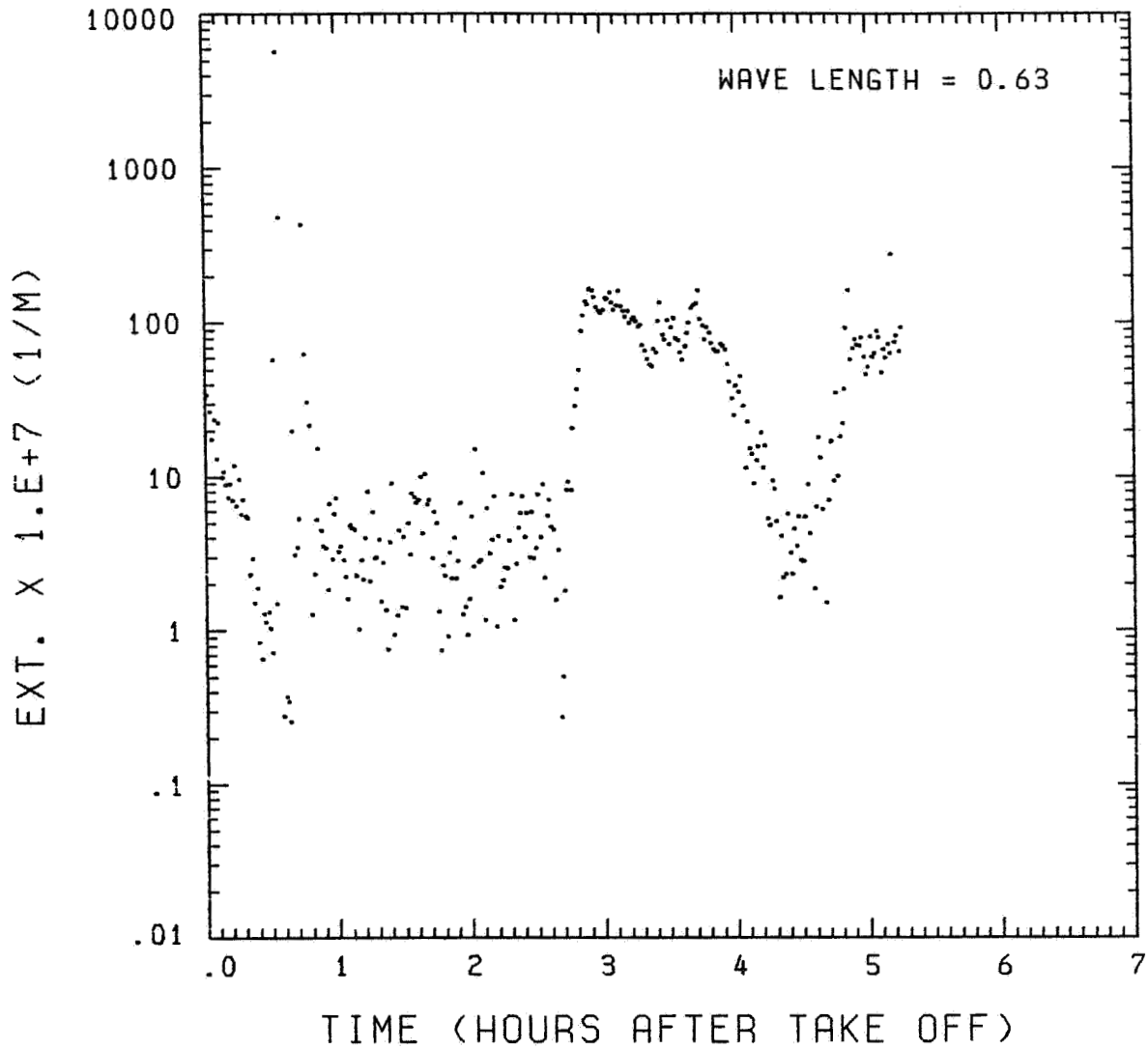


Fig. A11(b). GAMETAG flight data for April 27, 1978.
Calculated particulate extinction along the flight
track for one-minute data sets for $\lambda = 0.63 \mu\text{m}$.

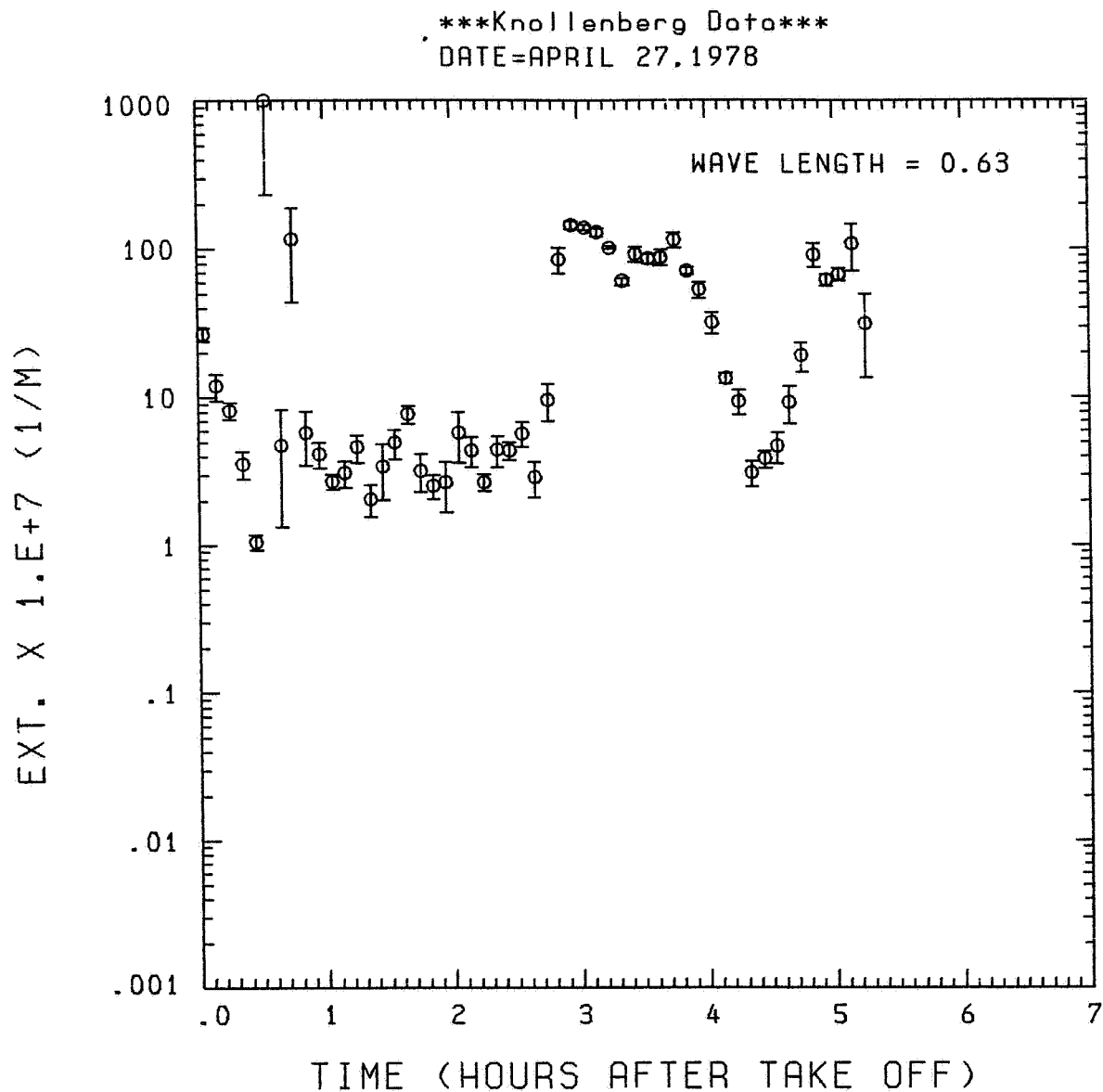


Fig. A11(c). GAMETAG flight data for April 27, 1978.
Calculated particulate extinction along the flight
track for five-minute data sets for $\lambda = 0.63 \mu\text{m}$.

ORIGINAL PAGE IS
OF POOR QUALITY

Knollenberg Data
DATE=APRIL 27,1978

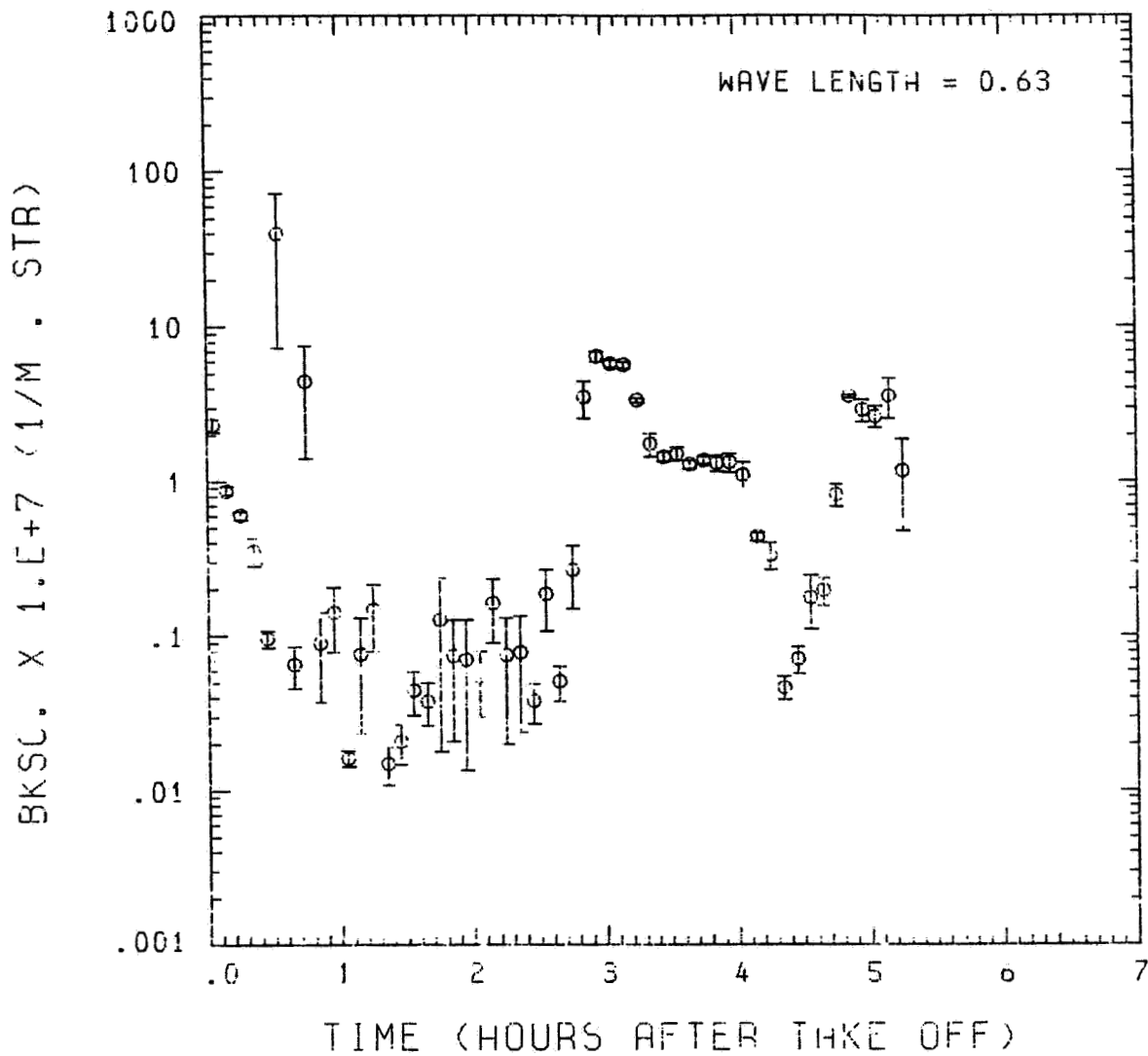


Fig. A11(d). GAMETAG flight data for April 27, 1978.

Calculated backscatter coefficient along the flight
track for five-minute data sets for $\lambda = 0.63 \mu\text{m}$.

Knollenberg Data
 DATE=APRIL 27,1978

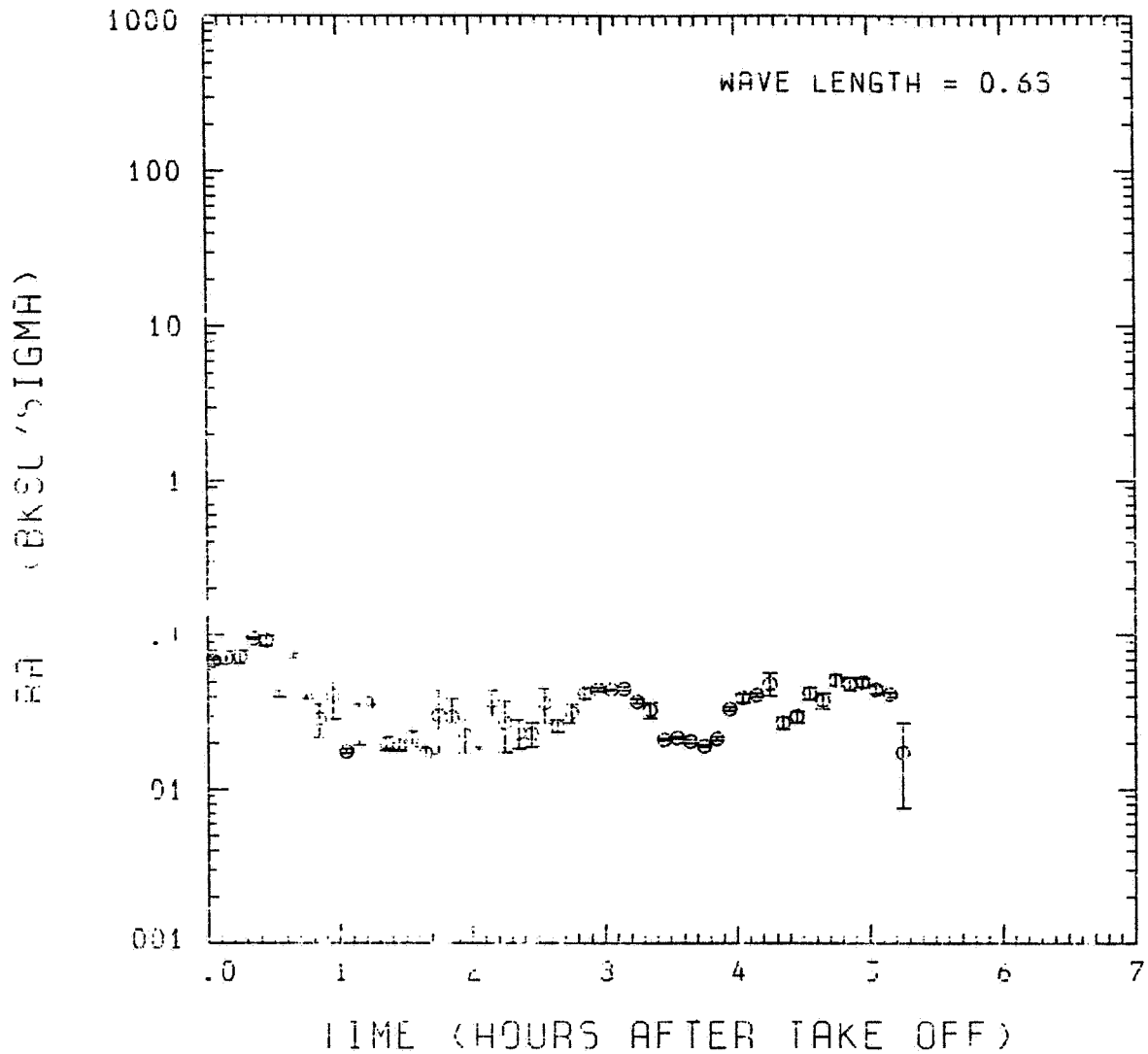


Fig. A11 (e). GAMETAG flight data for April 27, 1978.
 Calculated ratios for backscatter to extinction for
 five-minute data sets for $\lambda = 0.63 \mu\text{m}$.

ORIGINAL PAGE IS
OF POOR QUALITY

Knollenberg Data
DATE=APRIL 27, 1978

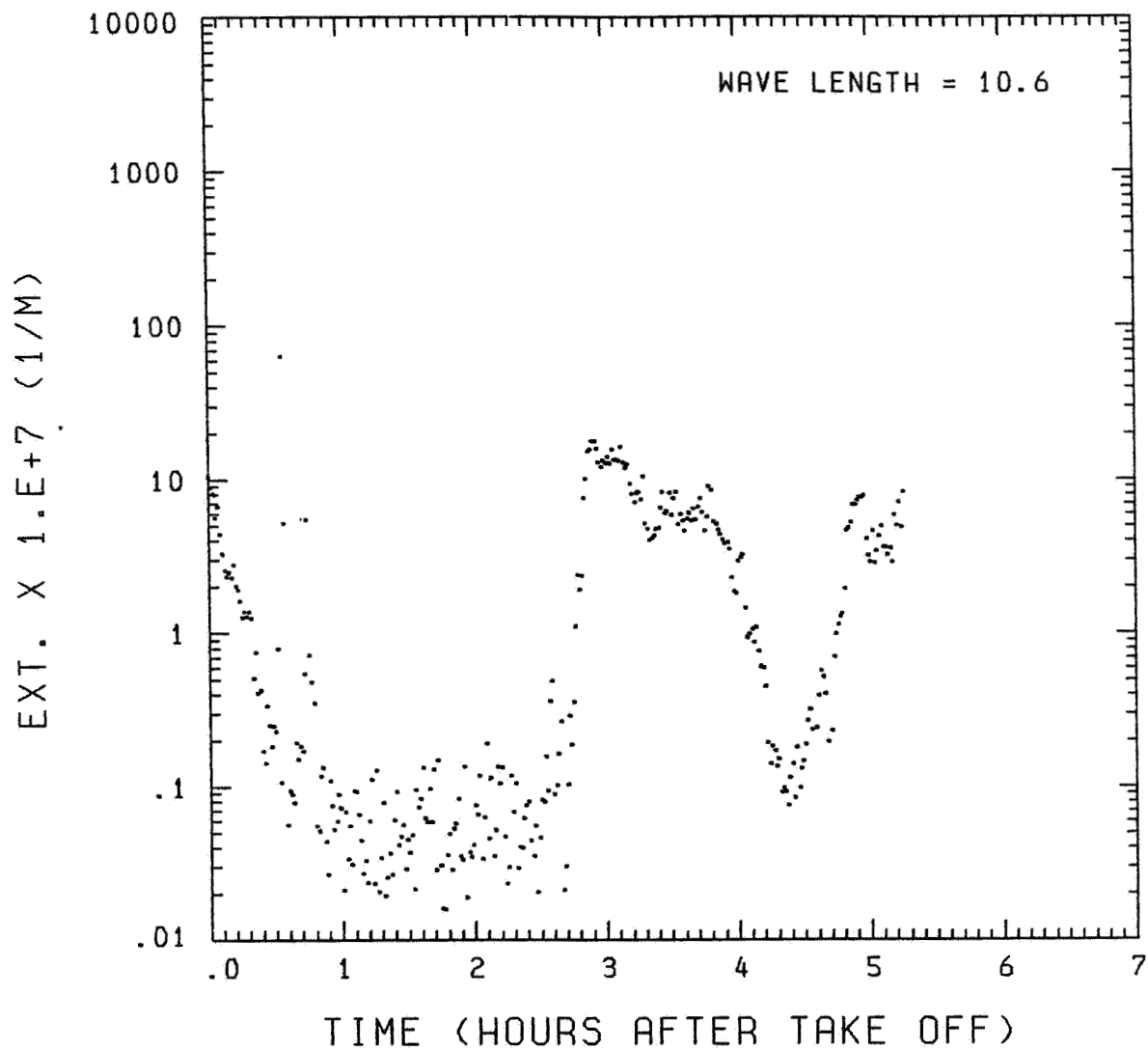


Fig. A 11 (f). GAMETAG flight data for April 27, 1978.
Calculated particulate extinction along the flight
track for one-minute data sets for $\lambda = 10.6 \mu\text{m}$.

Knollenberg Data
 DATE=APRIL 27, 1978

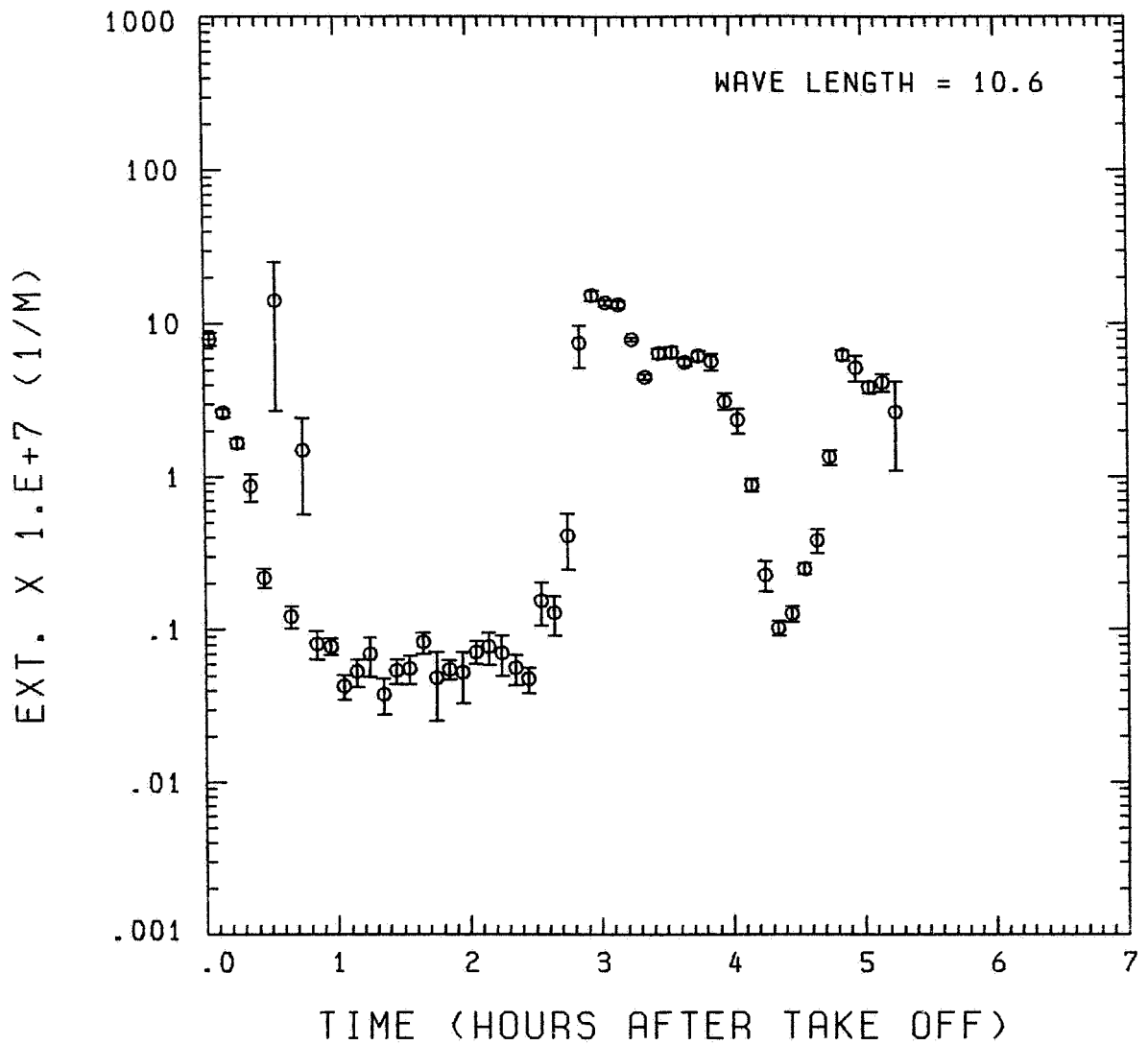


Fig. A11(g). GAMETAG flight data for April 27, 1978.
 Calculated particulate extinction along the flight
 track for five-minute data sets for $\lambda = 10.6 \mu\text{m}$.

Knollenberg Data
 DATE=APRIL 27,1978

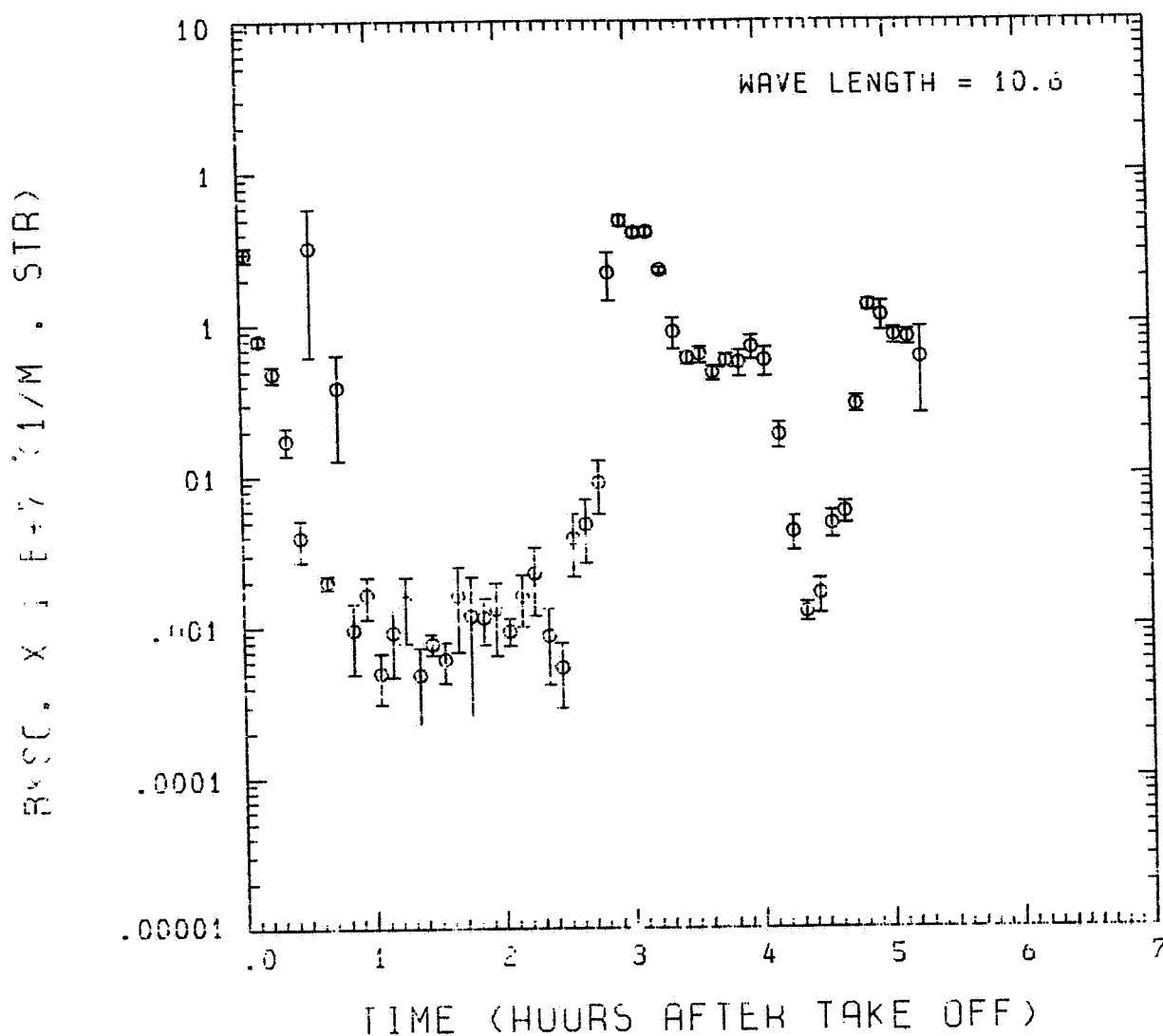


Fig. A11 (h). GAMETAG flight data for April 27, 1978.
 Calculated backscatter coefficient along the flight
 track for five-minute data sets for $\lambda = 10.6 \mu\text{m}$.

ORIGINAL PAGE IS
OF POOR QUALITY

Knollenberg Data
DATE=APRIL 27, 1978

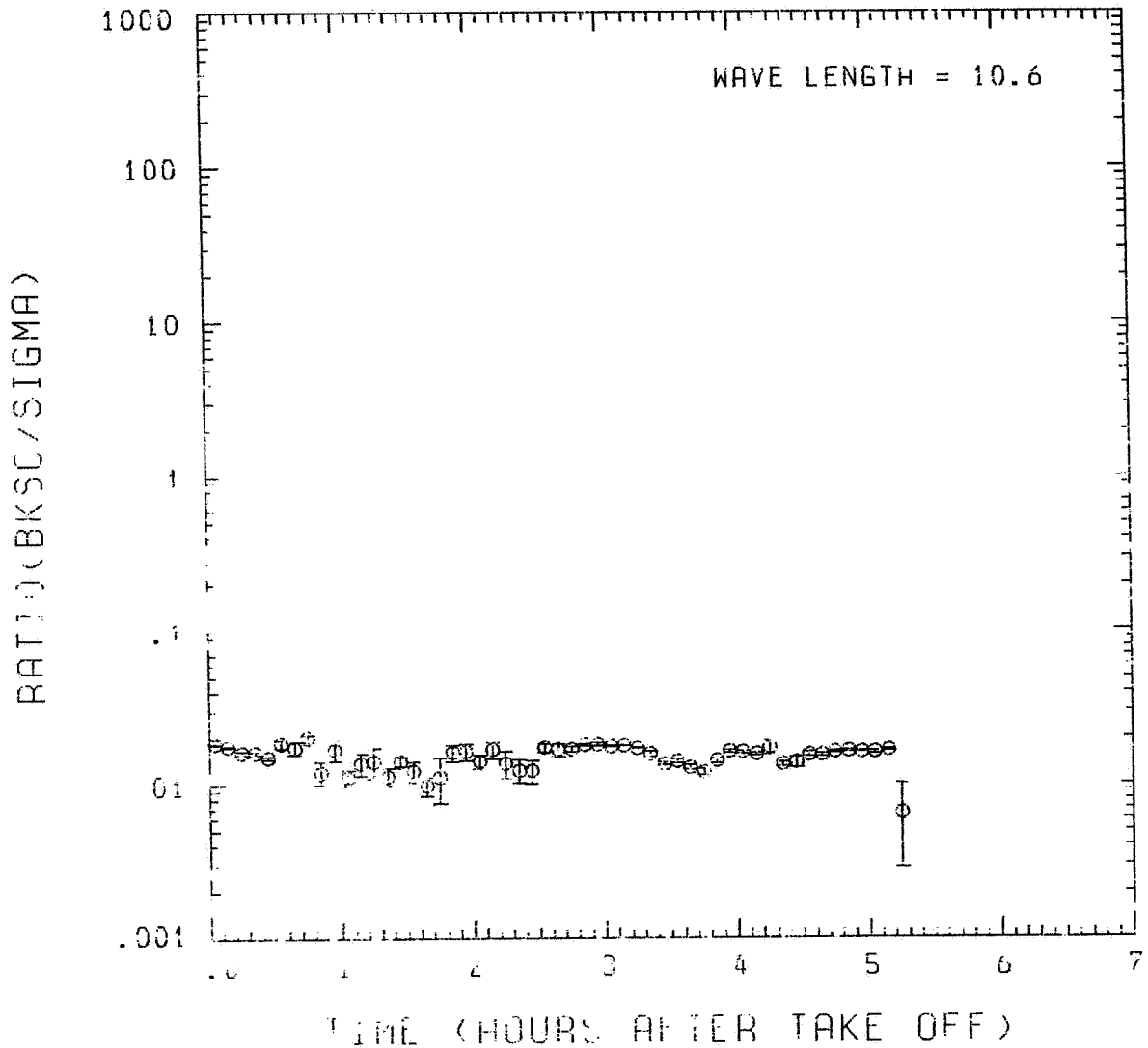


Fig. A11 (i). GAMETAG flight data for April 27, 1978.
Calculated ratios for backscatter to extinction for
five-minute data sets for $\lambda = 10.6 \mu\text{m}$.

Table A12. Significant times for May 2, 1978.
Hilo, Hawaii to Johnston Atoll.

Significant Points

<u>#</u>	<u>TIME</u>	
1	20:03	Hilo
2	20:19	
3	20:36	(Long.) = 20:42 (Alt.).
4	20:57	
5	22:05	
6	22:28	(Lat.) = 22:36 (Alt.)
7	23:17	
8	23:48	
9	00:47	
10	01:18	
11	02:21	Johnston Atoll

ORIGINAL PAGE IS
OF POOR QUALITY

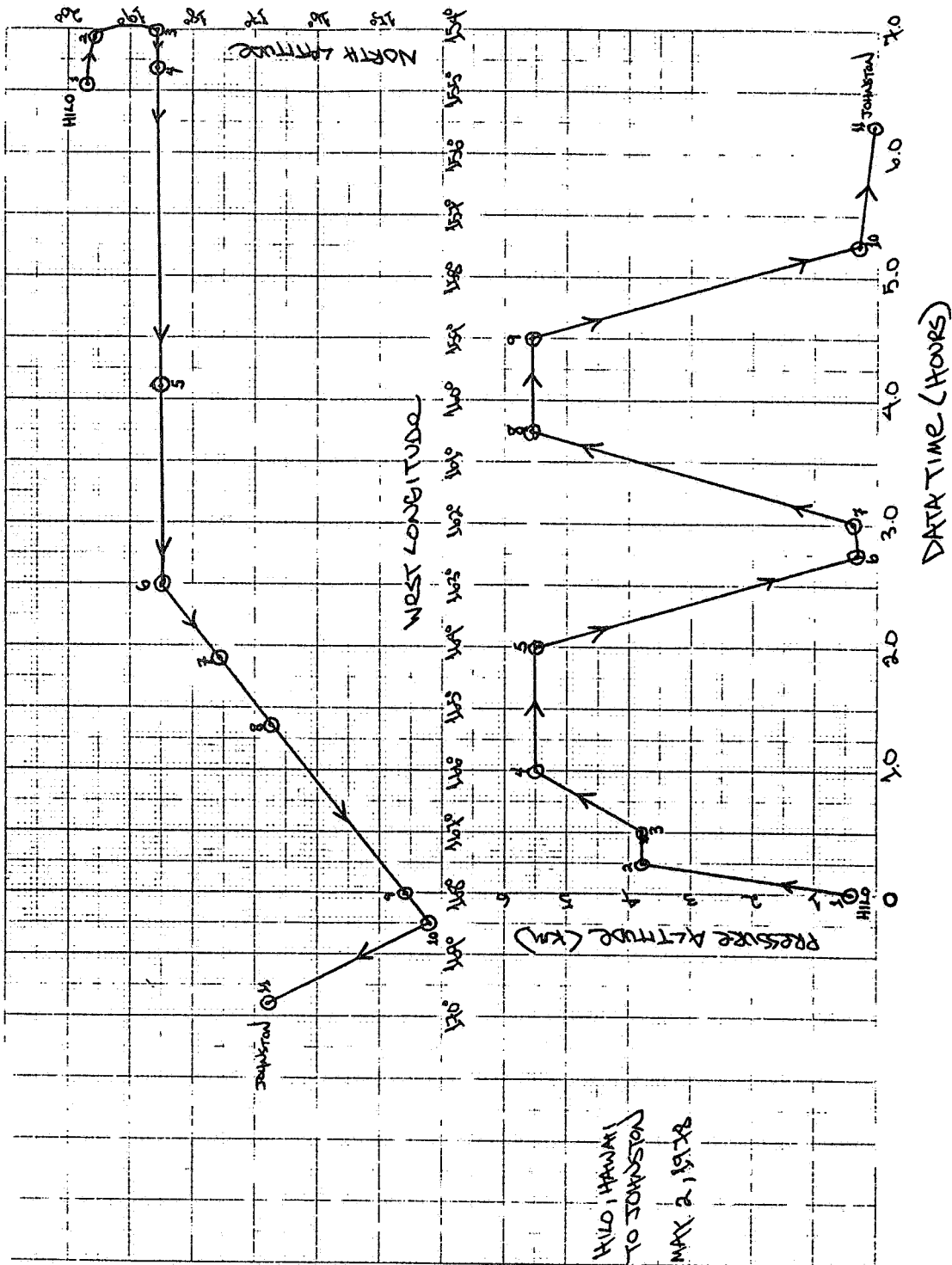


Fig. A12 (a). GAMETAG flight data for May 2, 1978.
Altitude and location flight track plotted as a
function of time after takeoff.

Knollenberg Data
DATE=MAY 2, 1978

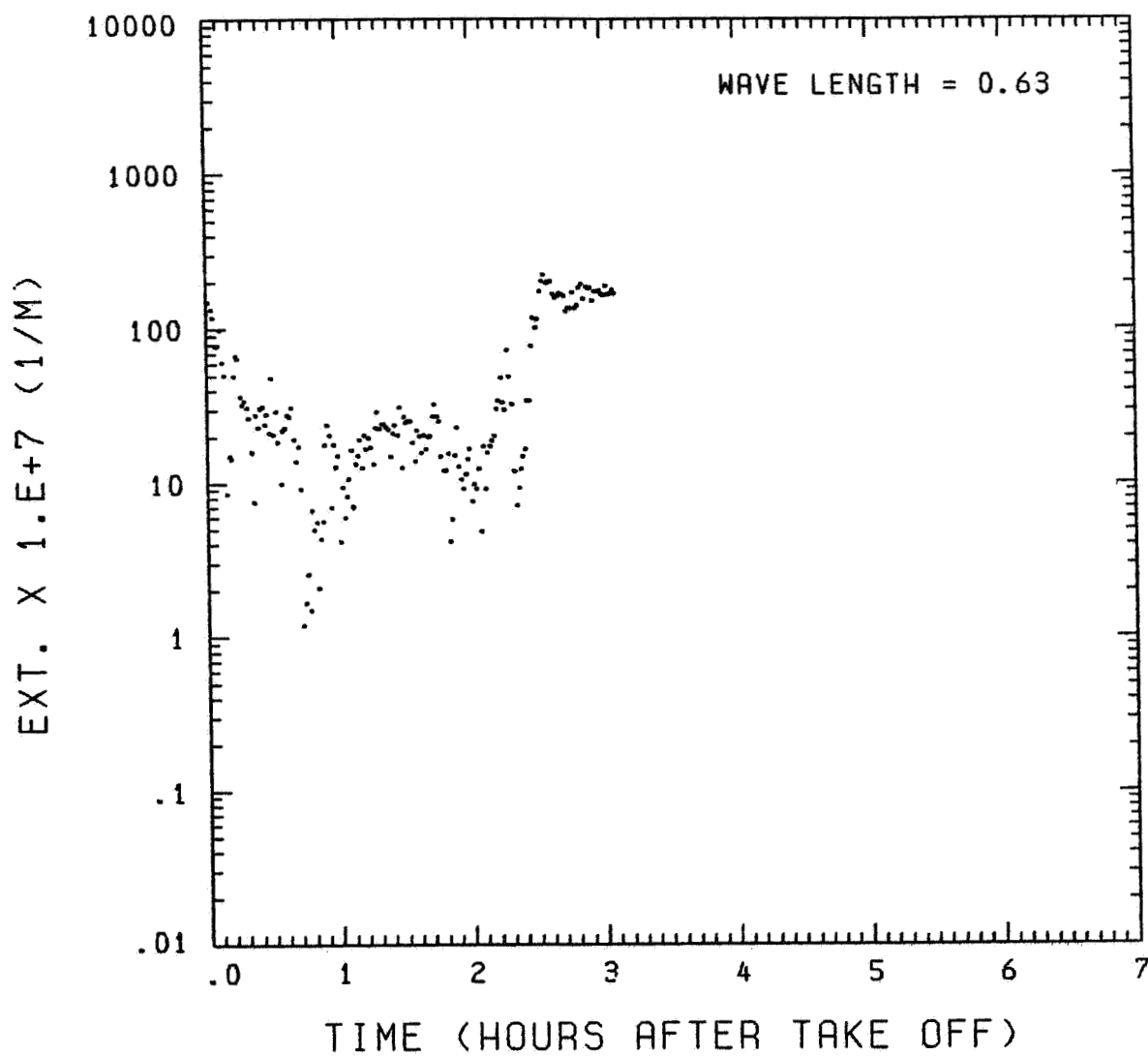


Fig. A12 (b). GAMETAG flight data for May 2, 1978.
Calculated particulate extinction along the flight
track for one-minute data sets for $\lambda = 0.63 \mu\text{m}$.

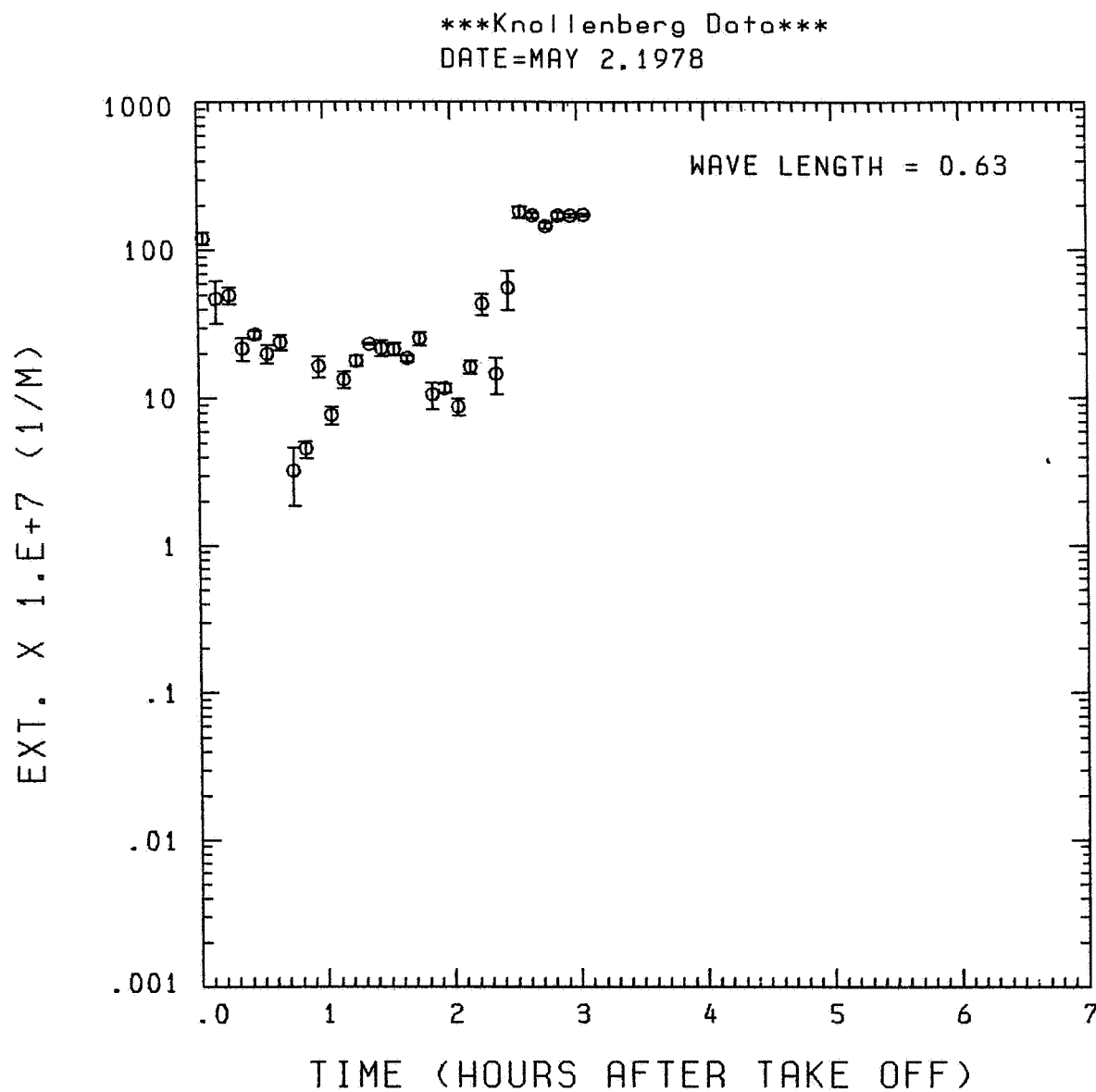


Fig. A12 (c). GAMETAG flight data for May 2, 1978.
Calculated particulate extinction along the flight
track for five-minute data sets for $\lambda = 0.63 \mu\text{m}$.

ORIGINAL PAGE IS
OF POOR QUALITY

Knollenberg Data
DATE=MAY 2.1978

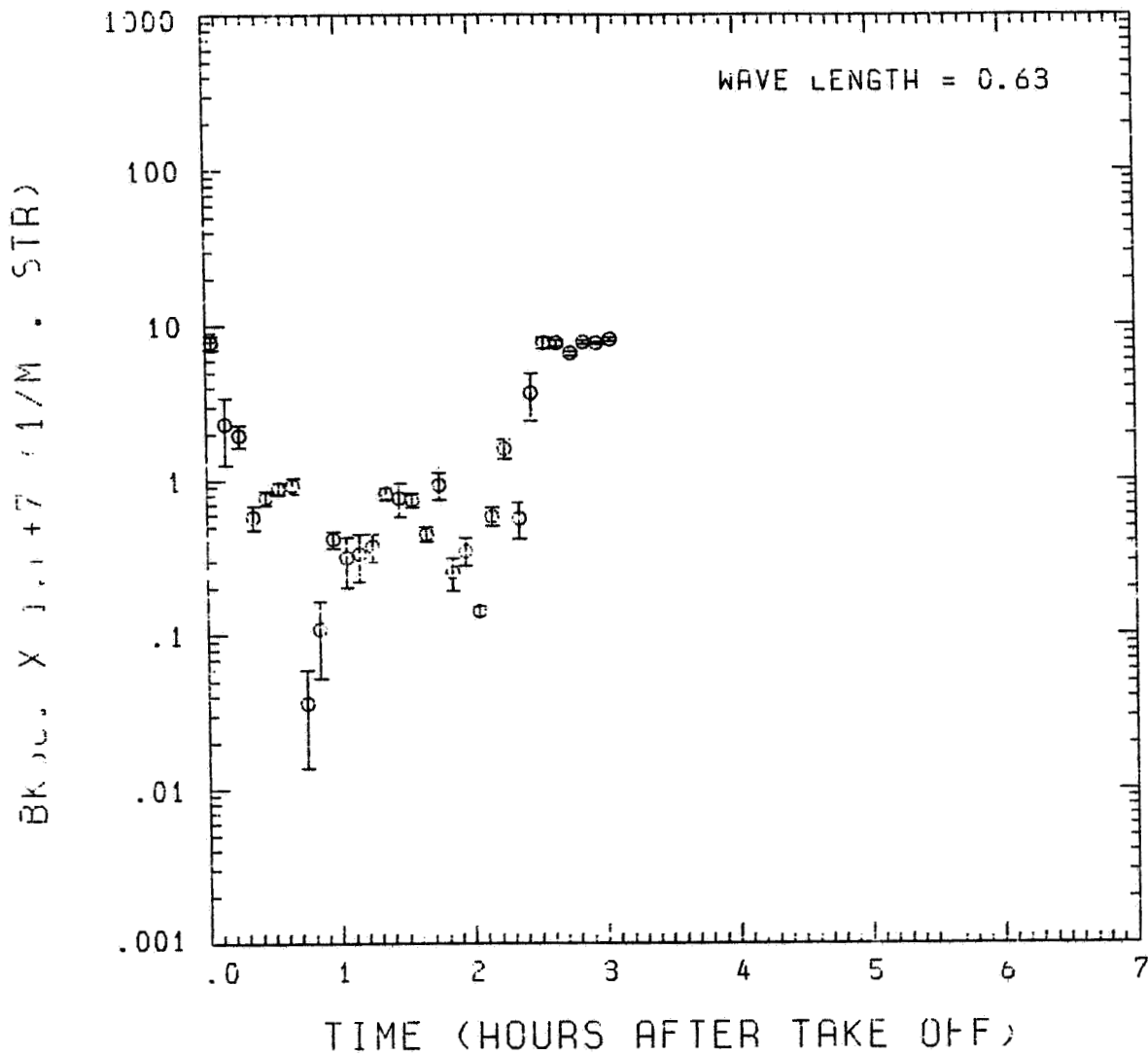


Fig. A12 (d). GAMETAG flight data for May 2, 1978.

Calculated backscatter coefficient along the flight
track for five-minute data sets for $\lambda = 0.63 \mu\text{m}$.

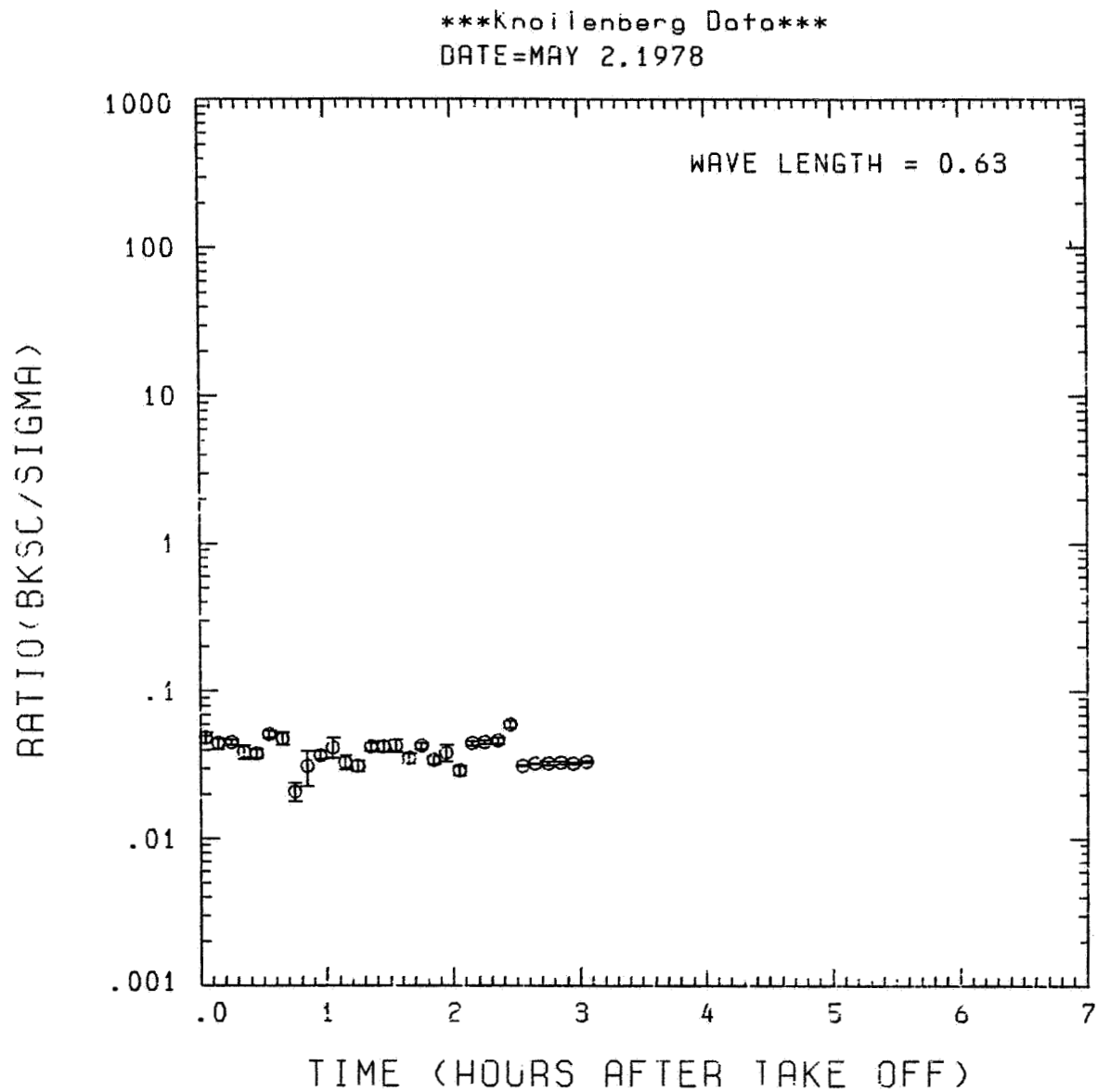


Fig. A12 (e). GAMETAG flight data for May 2, 1978.
Calculated ratios for backscatter to extinction for
five-minute data sets for $\lambda = 0.63 \mu\text{m}$.

Knollenberg Data
DATE=MAY 2, 1978

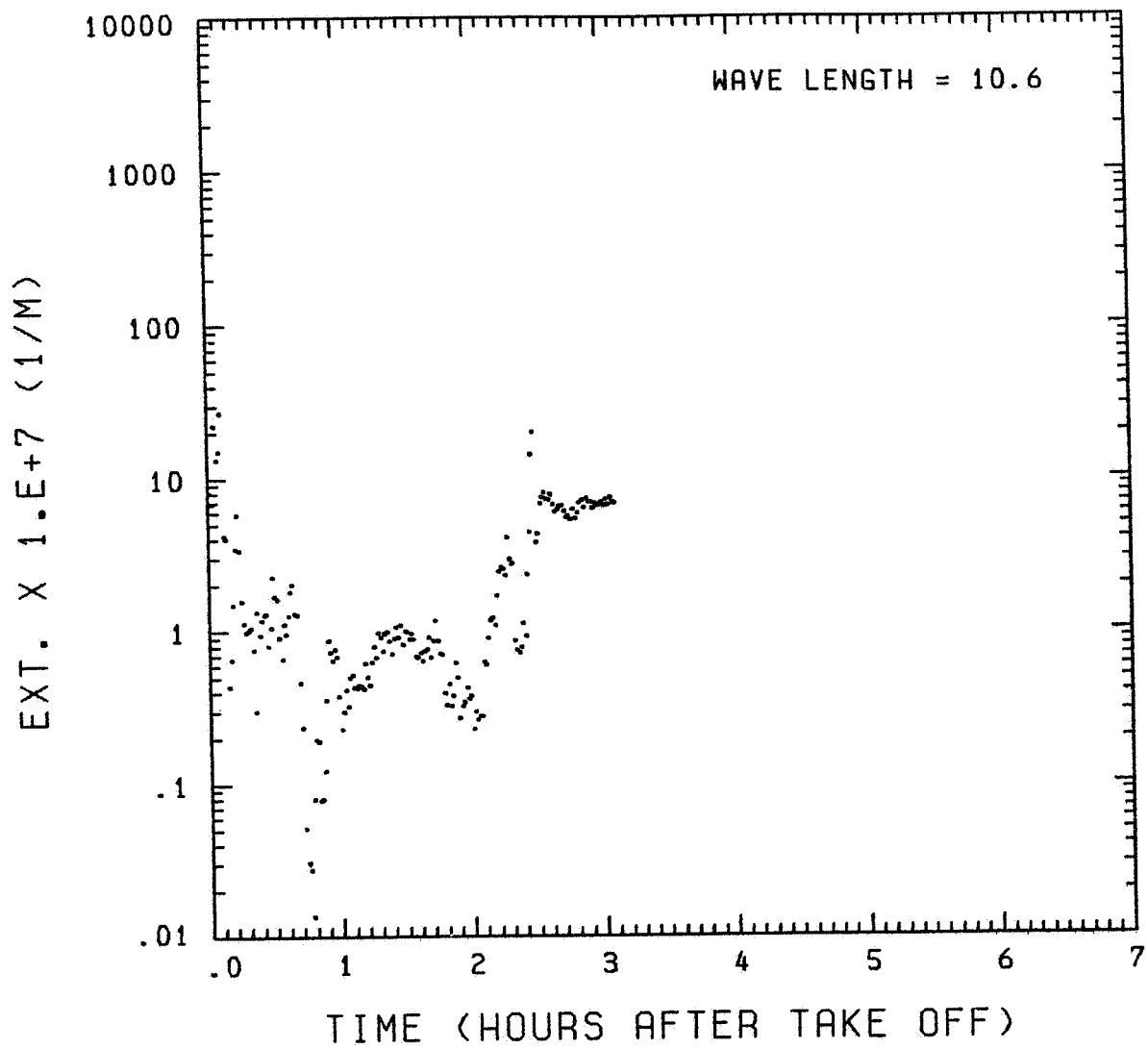


Fig. A12 (f). GAMETAG flight data for May 2, 1978.
Calculated particulate extinction along the flight
track for one-minute data sets for $\lambda = 10.6 \mu\text{m}$.

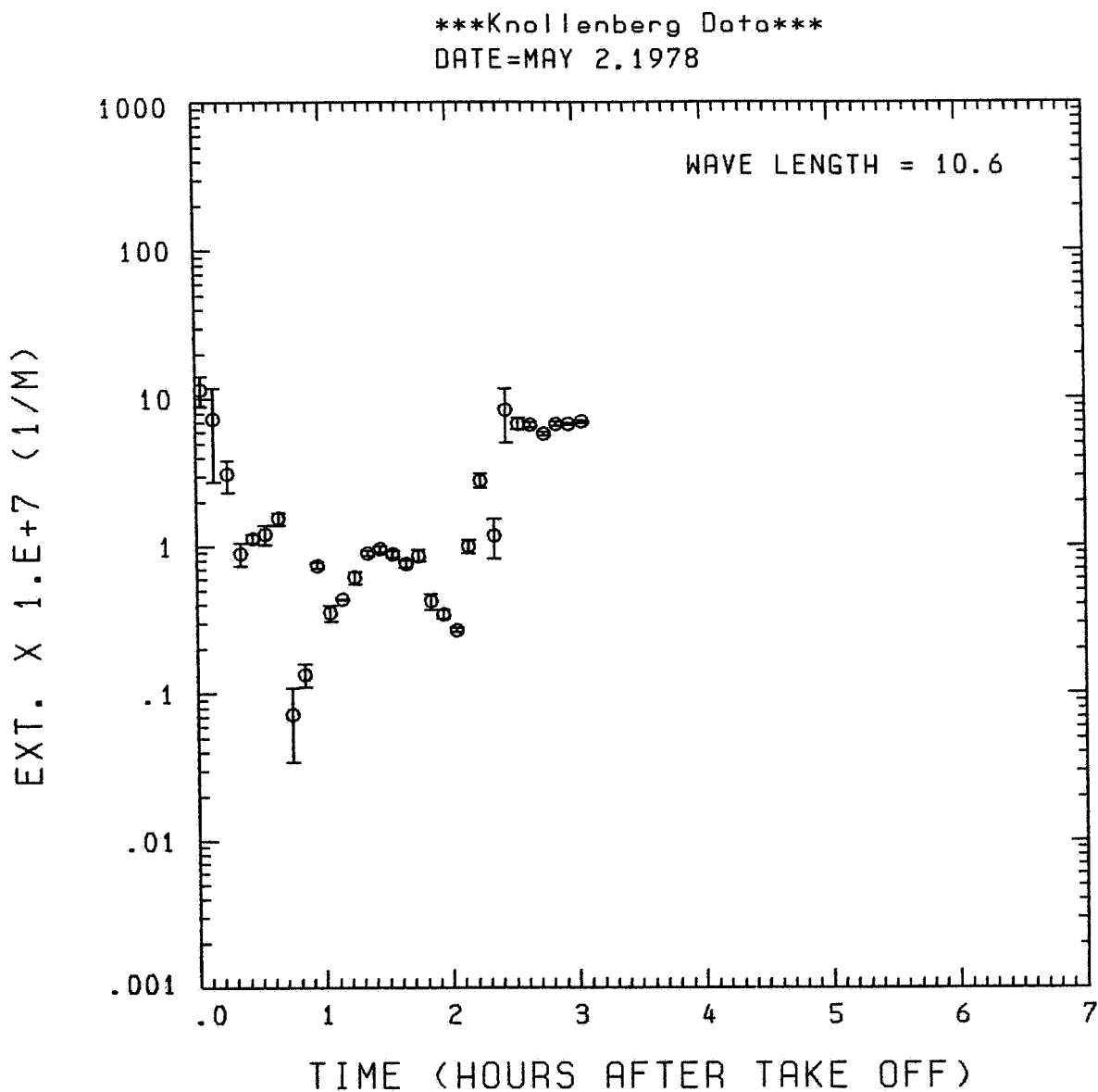


Fig. A12 (g). GAMETAG flight data for May 2, 1978.

Calculated particulate extinction along the flight track for five-minute data sets for $\lambda = 10.6 \mu\text{m}$.

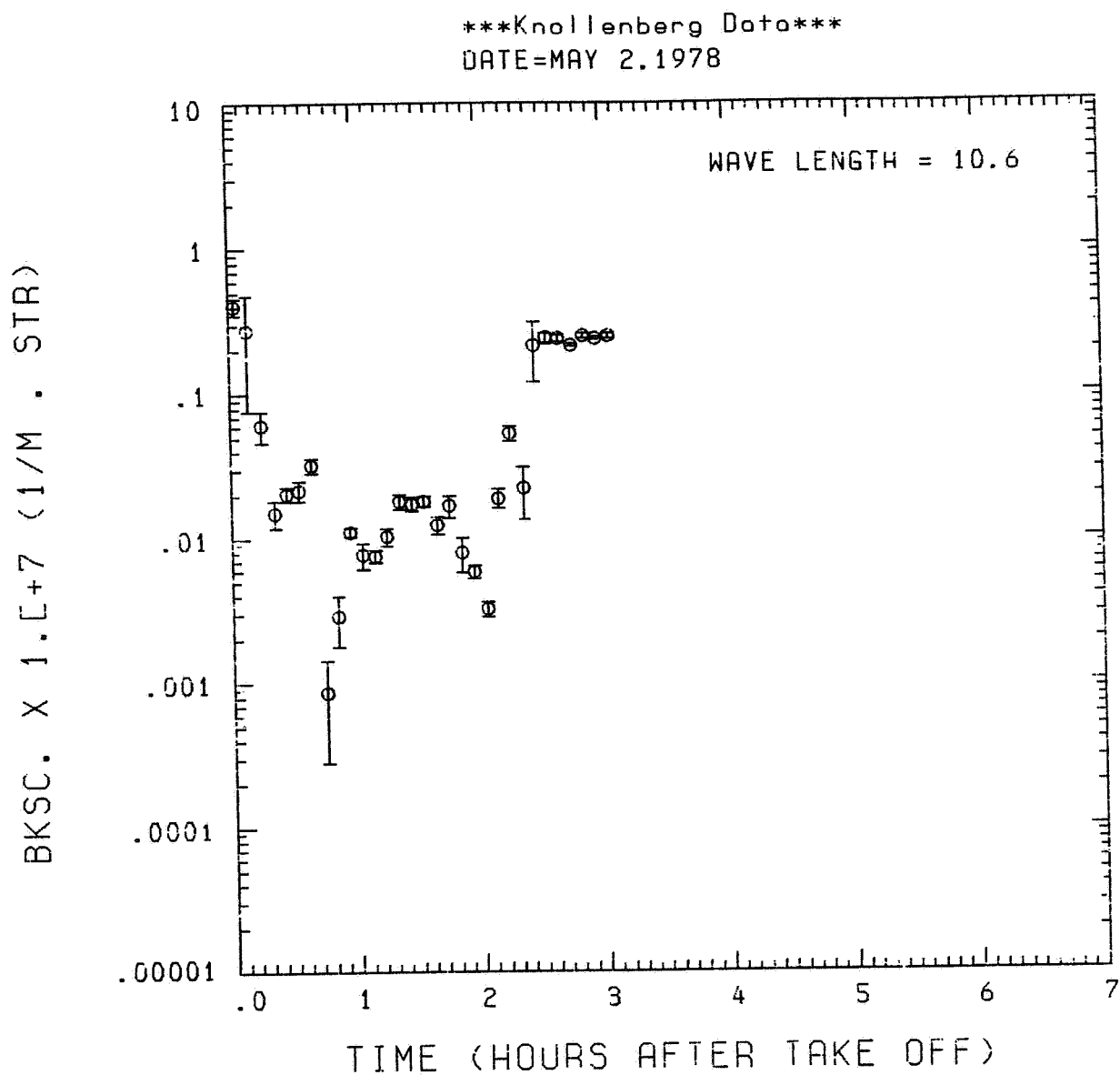


Fig. A 12(h). GAMETAG flight data for May 2, 1978.
Calculated backscatter coefficient along the flight
track for five-minute data sets for $\lambda = 10.6 \mu\text{m}$.

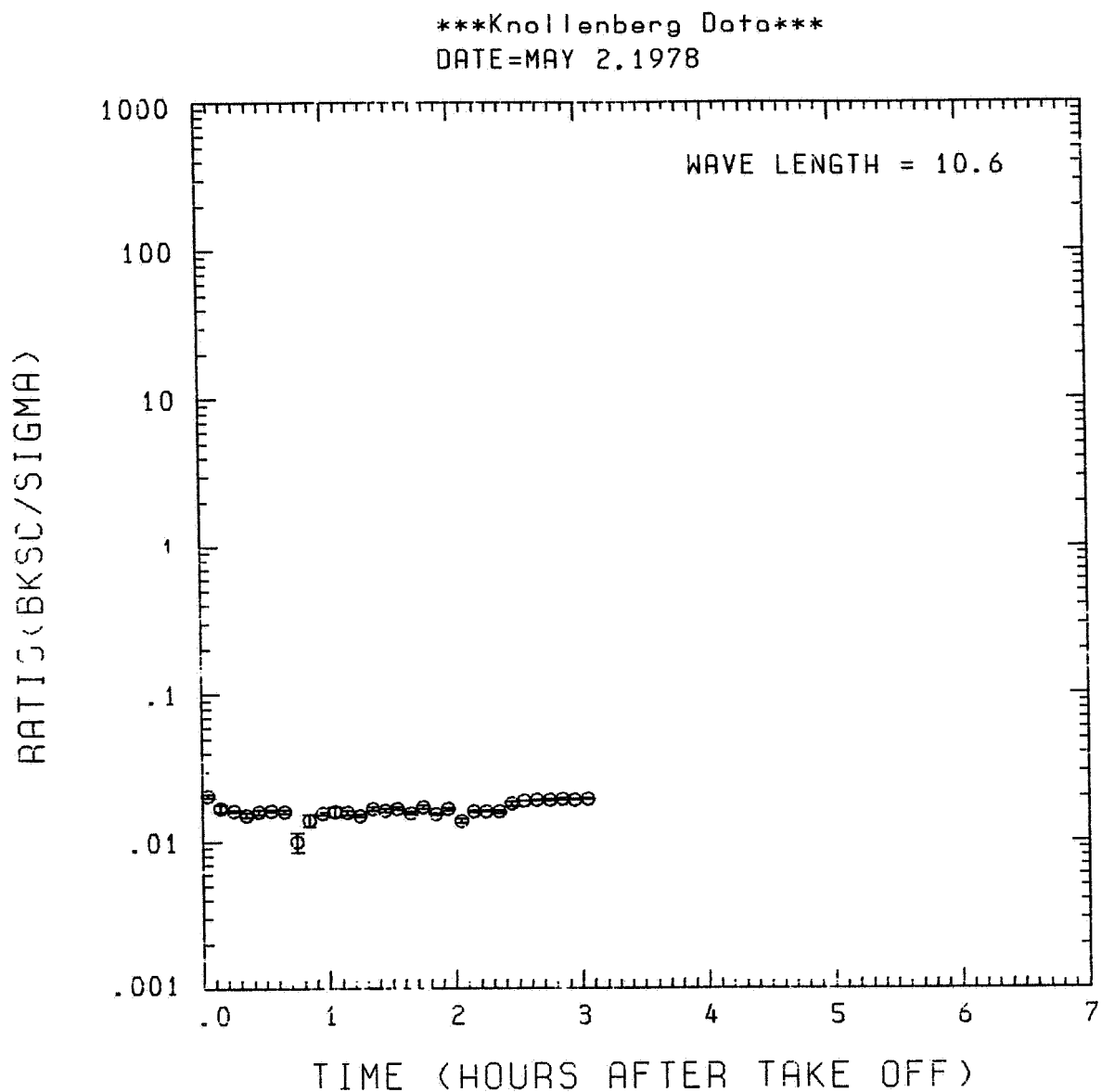


Fig. A12(i). GAMETAG flight data for May 2, 1978.
Calculated ratios for backscatter to extinction for
five-minute data sets for $\lambda = 10.6 \mu\text{m}$.

Table A13. Significant times for May 4, 1978.
Canton Island to Nandi, Fiji Islands.

Significant Points

<u>#</u>	<u>TIME</u>	
1	20:55	Canton Island
2	21:26	
3	22:37	
4	23:05	
5	23:18	
6	0:11 (Alt.) - 0:22 (Long.)	
7	0:41	
8	2:23	
9	2:45	
10	2:53	
11	3:10	
12	3:26	Nandi

ORIGINAL PAGE IS
OF POOR QUALITY

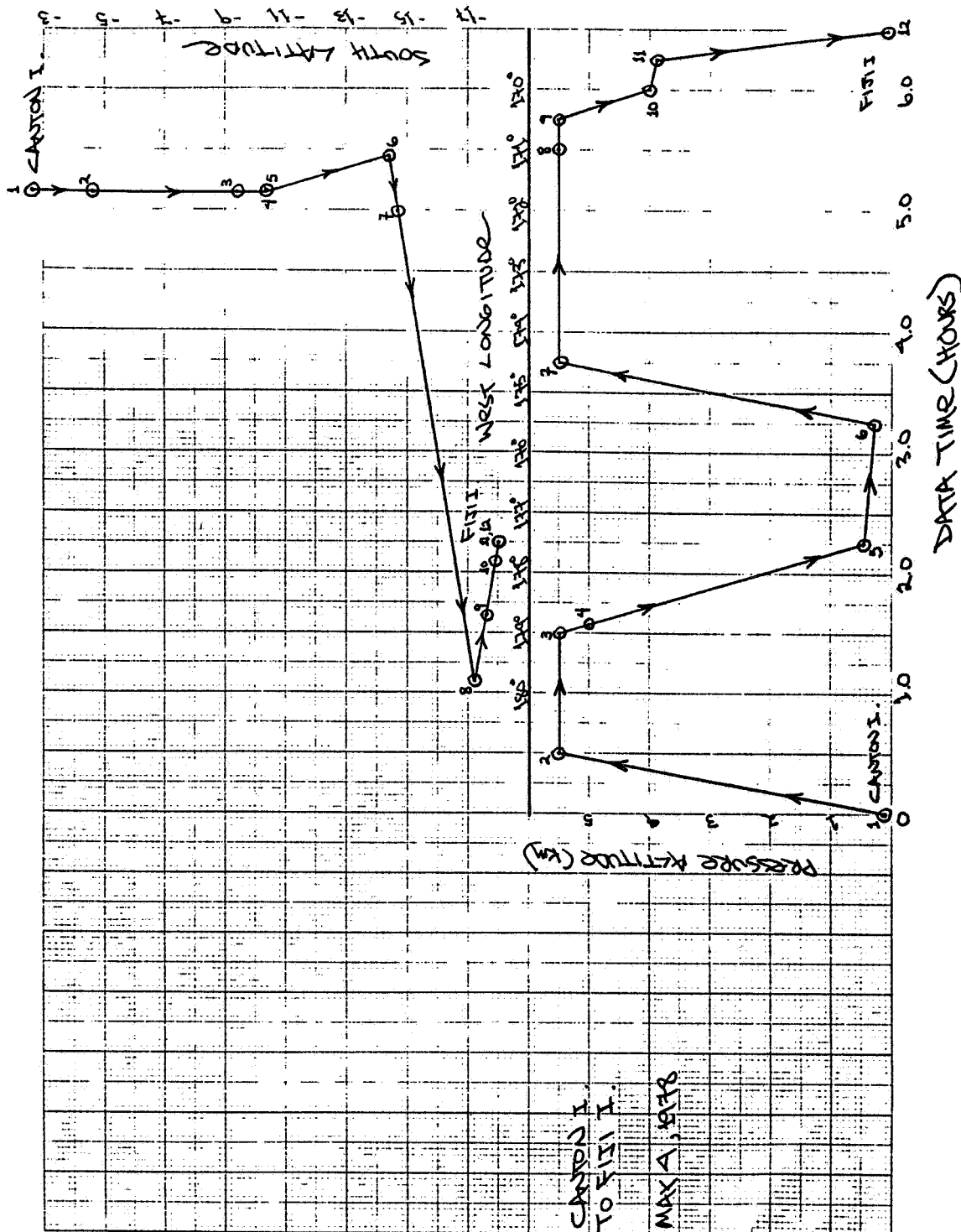


Fig. A13 (a). GAMETAG flight data for May 4, 1978.
Altitude and location flight track plotted as a
function of time after takeoff.

ORIGINAL PAGE IS
OF POOR QUALITY

Knollenberg Data
DATE=MAY 4, 1978

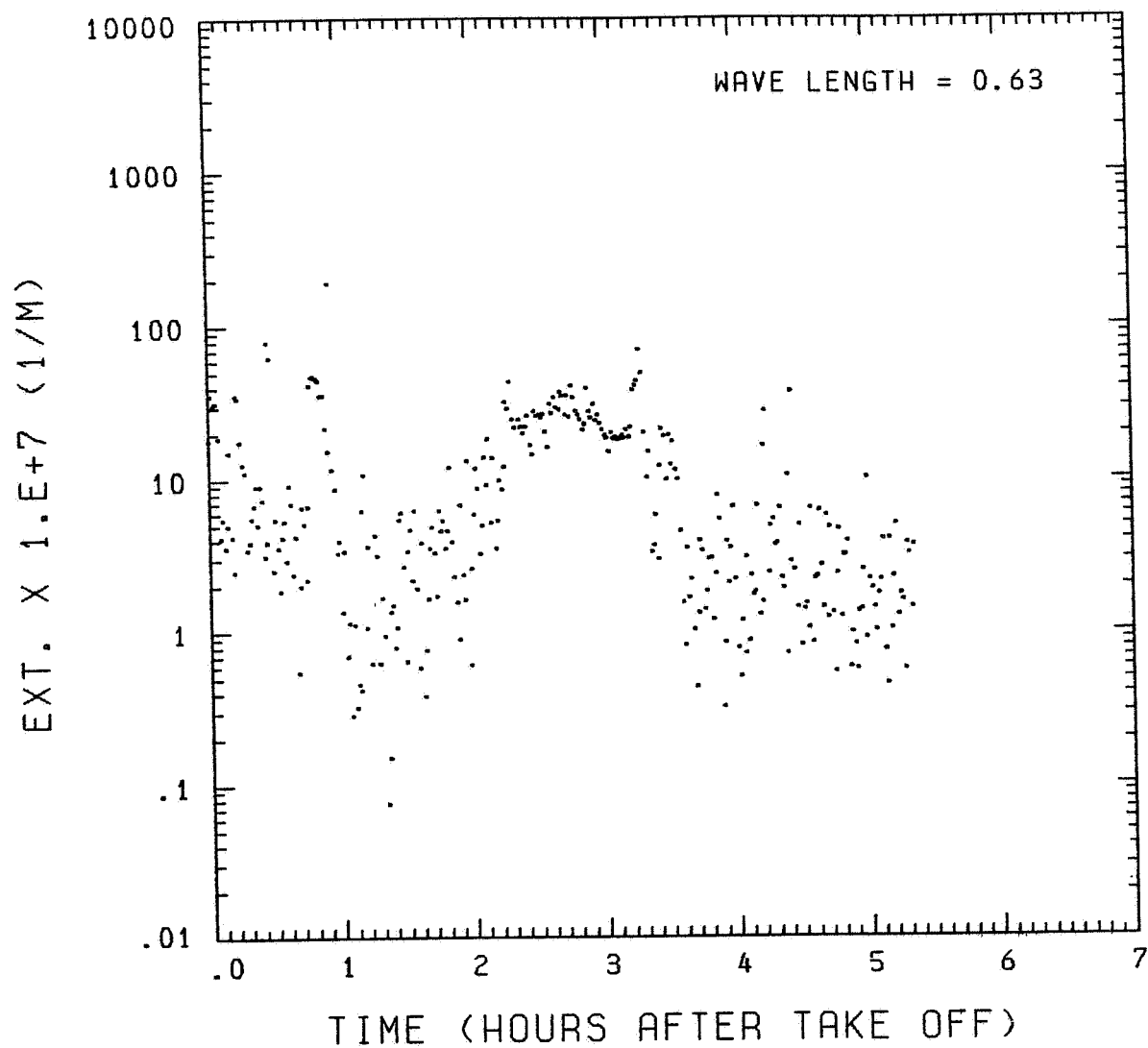


Fig. A13 (b). GAMETAG flight data for May 4, 1978.
Calculated particulate extinction along the flight
track for one-minute data sets for $\lambda = 0.63 \mu\text{m}$.

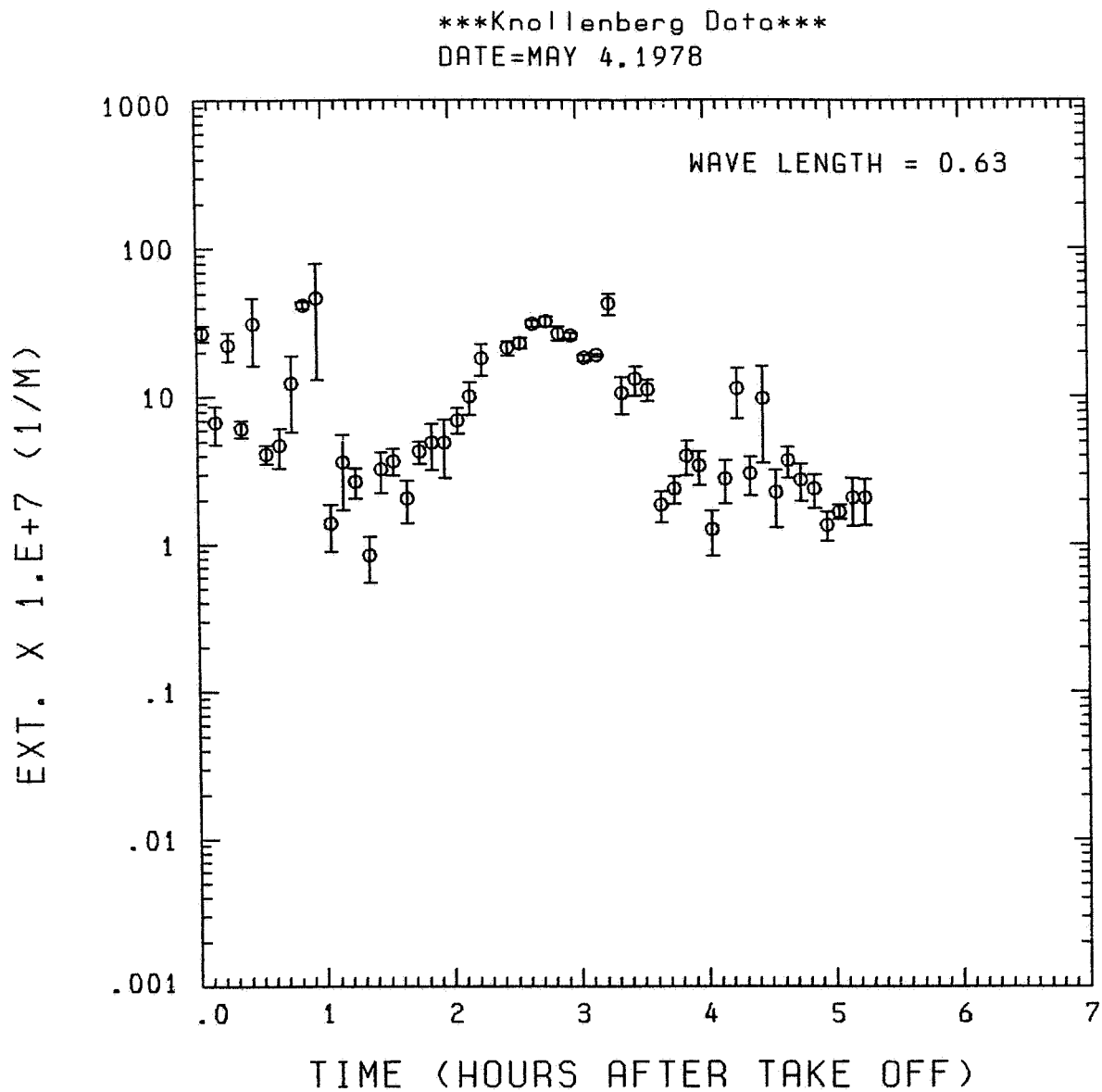


Fig. A13 (c). GAMETAG flight data for May 4, 1978.

Calculated particulate extinction along the flight track for five-minute data sets for $\lambda = 0.63 \mu\text{m}$.

ORIGINAL PAGE IS
OF POOR QUALITY

Knollenberg Data
DATE=MAY 4, 1978

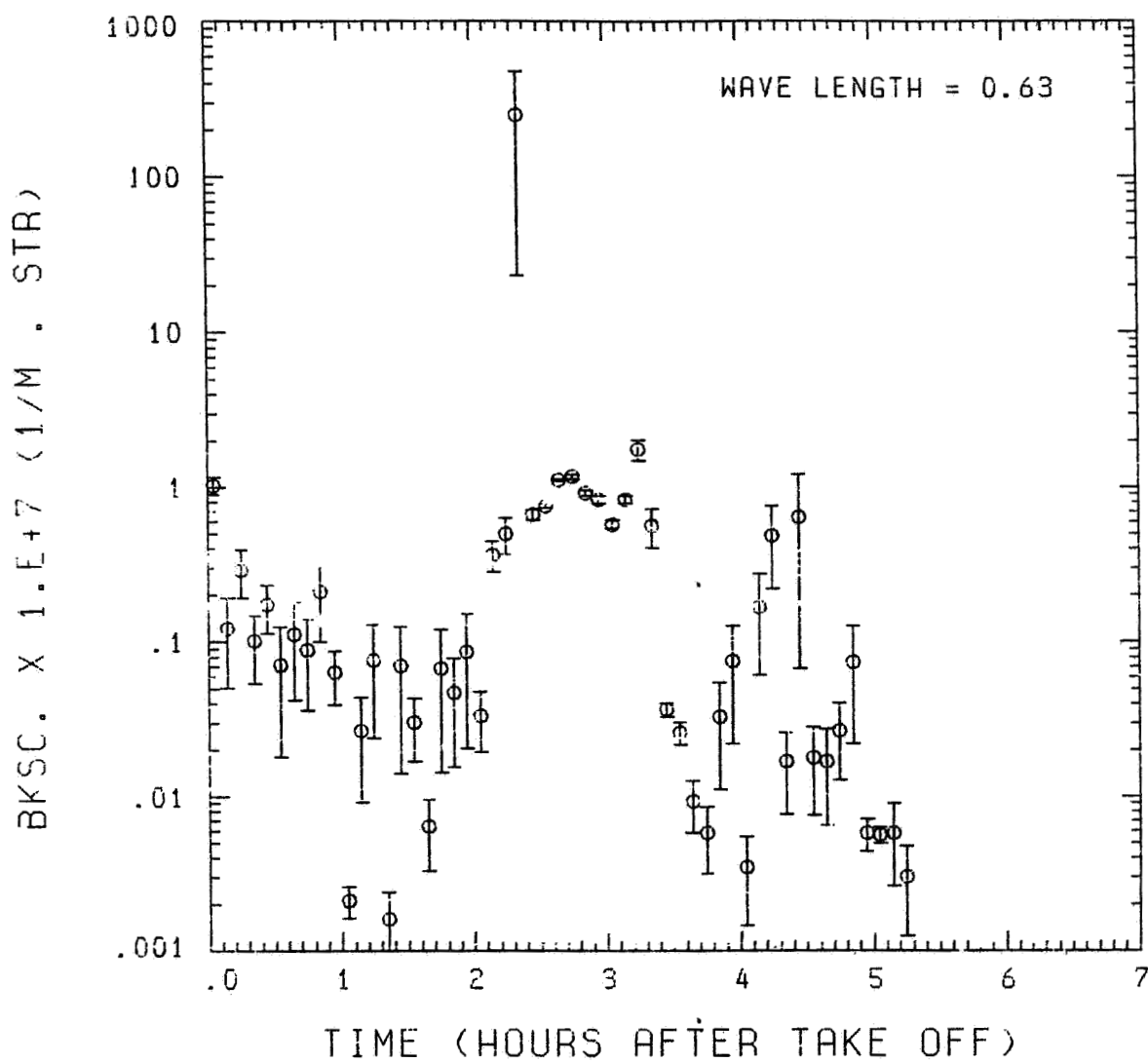


Fig. A13 (d). GAMETAG flight data for May 4, 1978.

Calculated backscatter coefficient along the flight
track for five-minute data sets for $\lambda = 0.63 \mu\text{m}$.

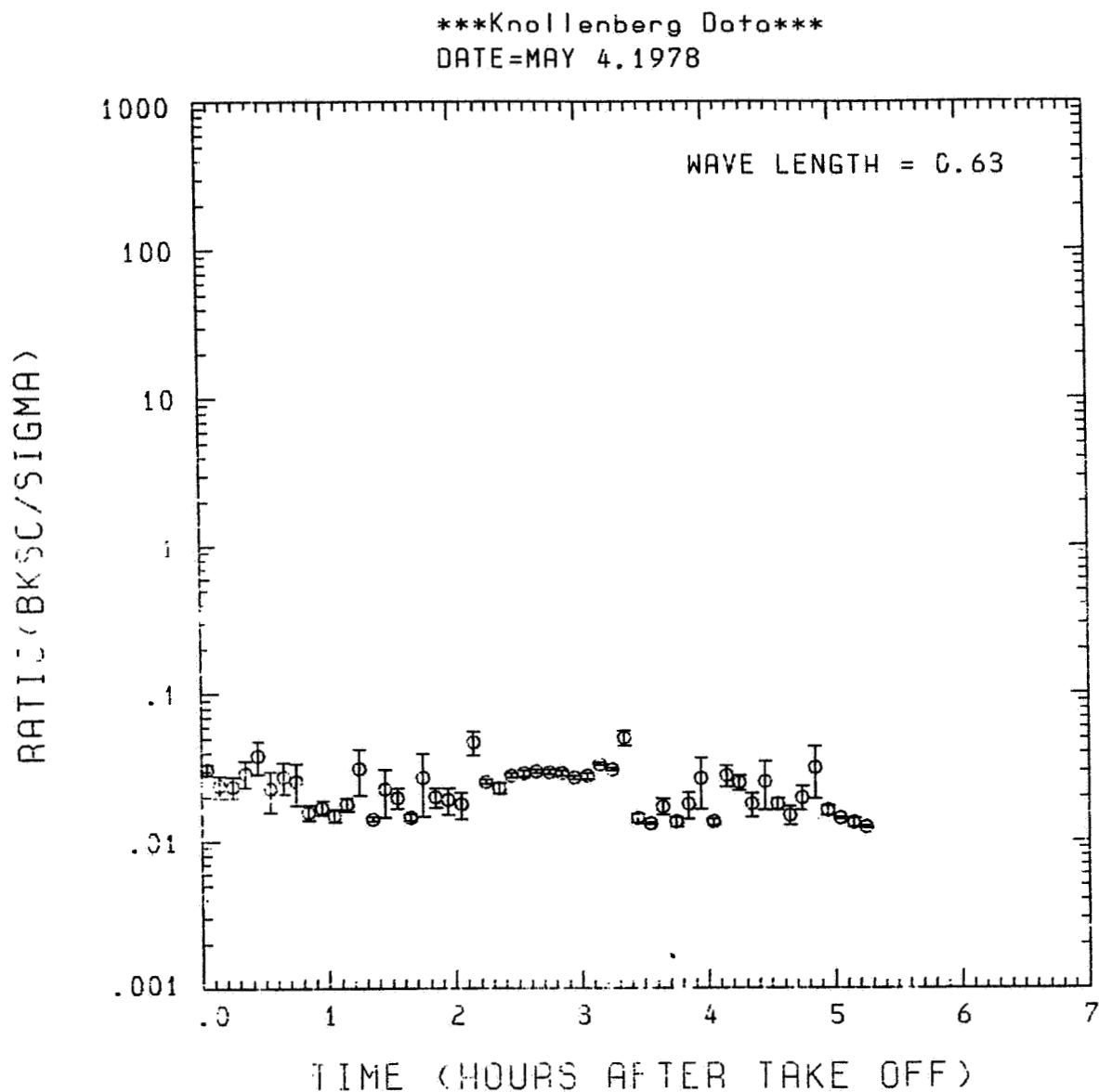


Fig. A13 (e). GAMETAG flight data for May 4, 1978.
Calculated ratios for backscatter to extinction for
five-minute data sets for $\lambda = 0.63 \mu\text{m}$.

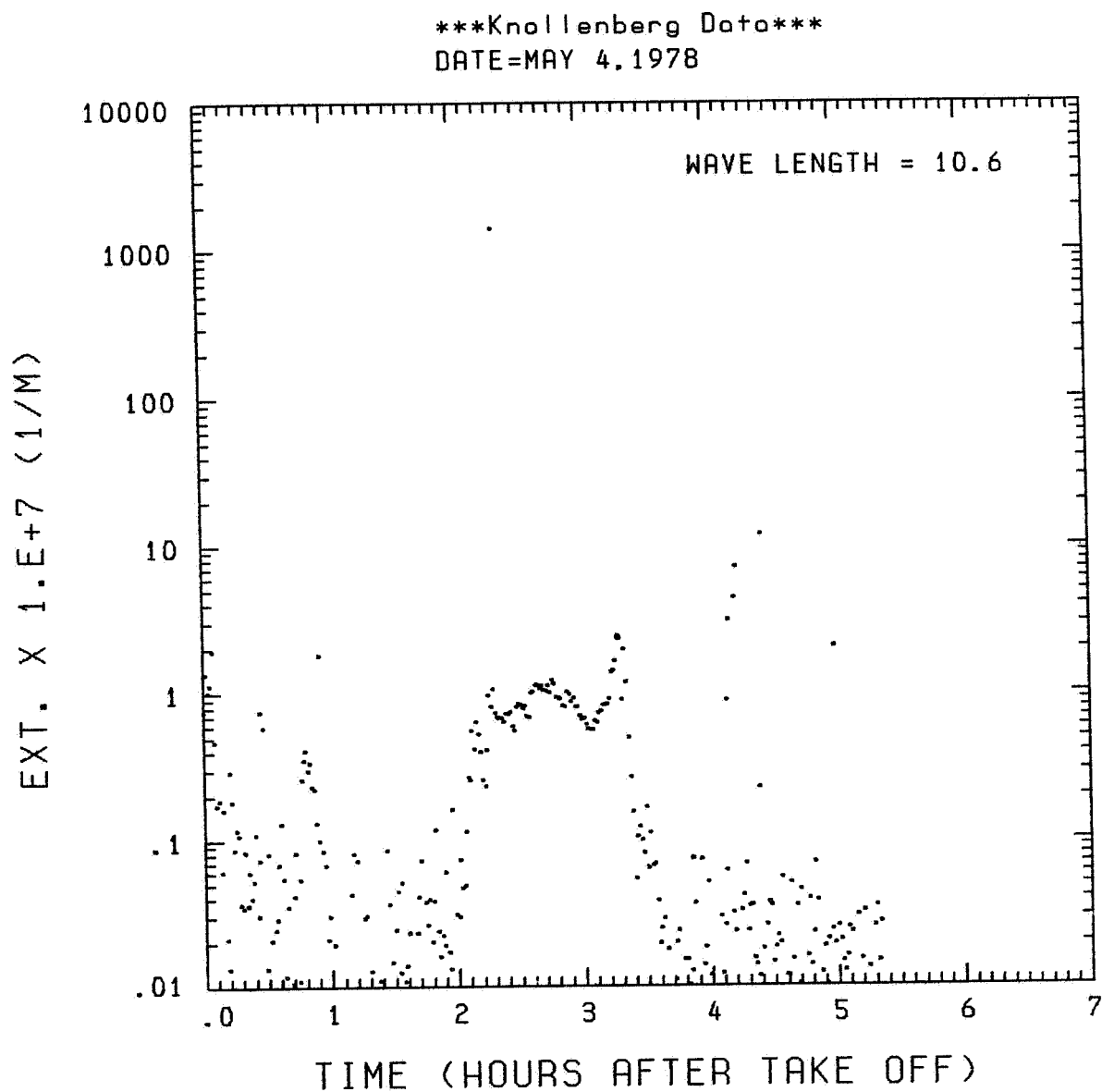


Fig. A13 (f). GAMETAG flight data for May 4, 1978.
Calculated particulate extinction along the flight
track for one-minute data sets for $\lambda = 10.6 \mu\text{m}$.

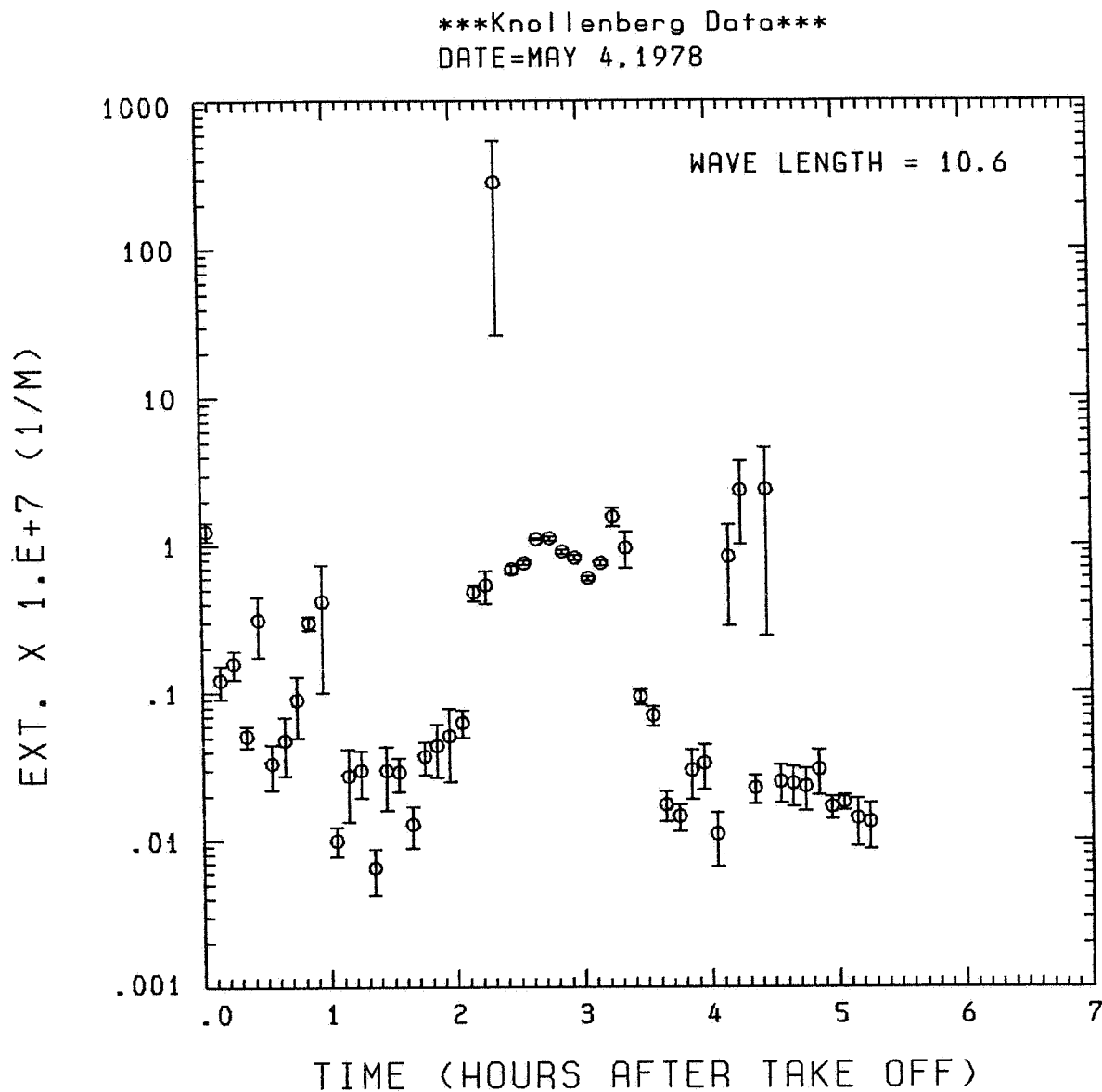


Fig. A13 (g). GAMETAG flight data for May 4, 1978.

Calculated particulate extinction along the flight track for five-minute data sets for $\lambda = 10.6 \mu\text{m}$.

Knollenberg Data
DATE=MAY 4, 1978

BKSC. X 10^{-4} (1/M · STR)

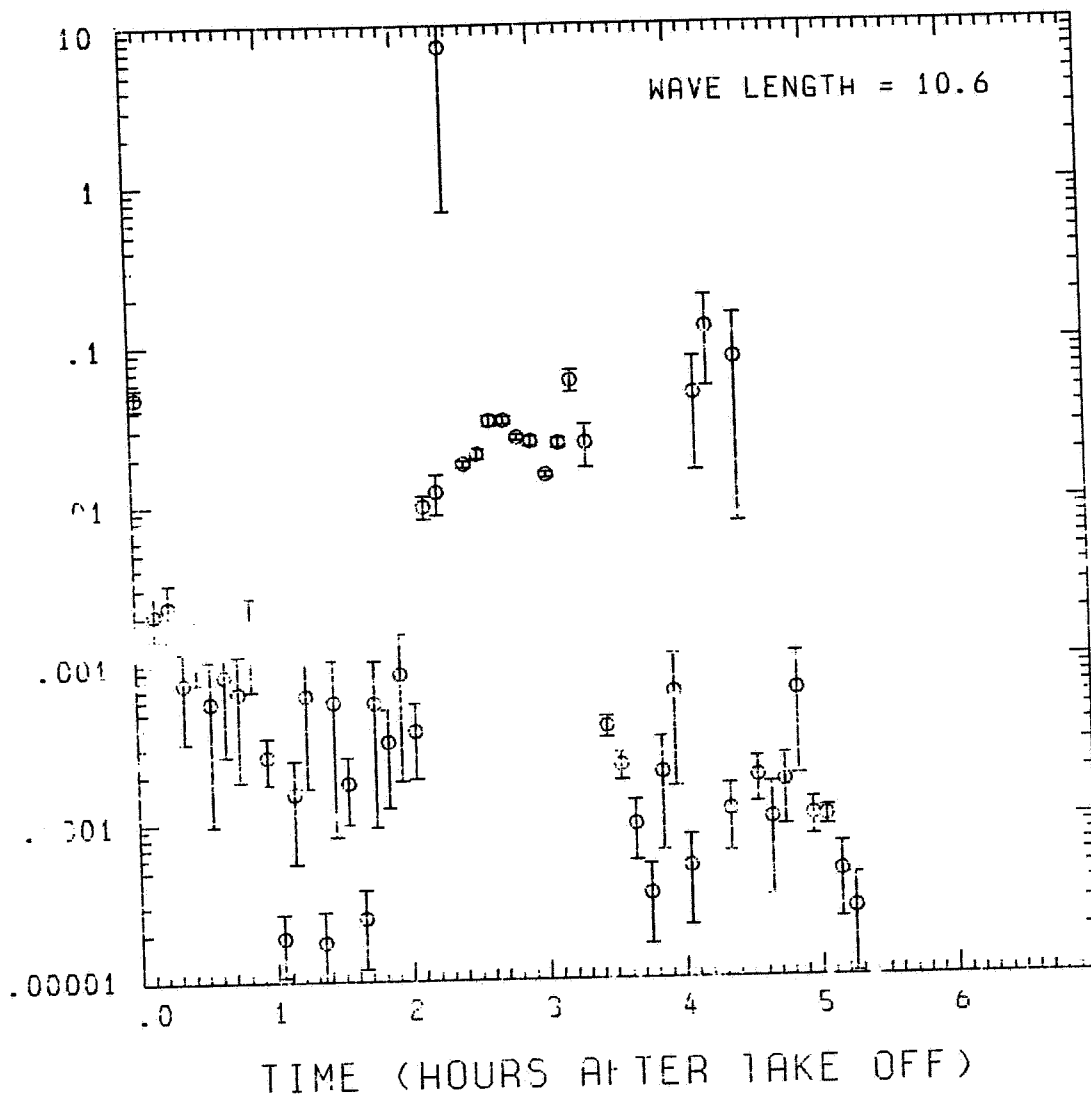


Fig. A13 (h). GAMETAG flight data for May 4, 1978.
Calculated backscatter coefficient along the flight
track for five-minute data sets for $\lambda = 10.6 \mu\text{m}$.

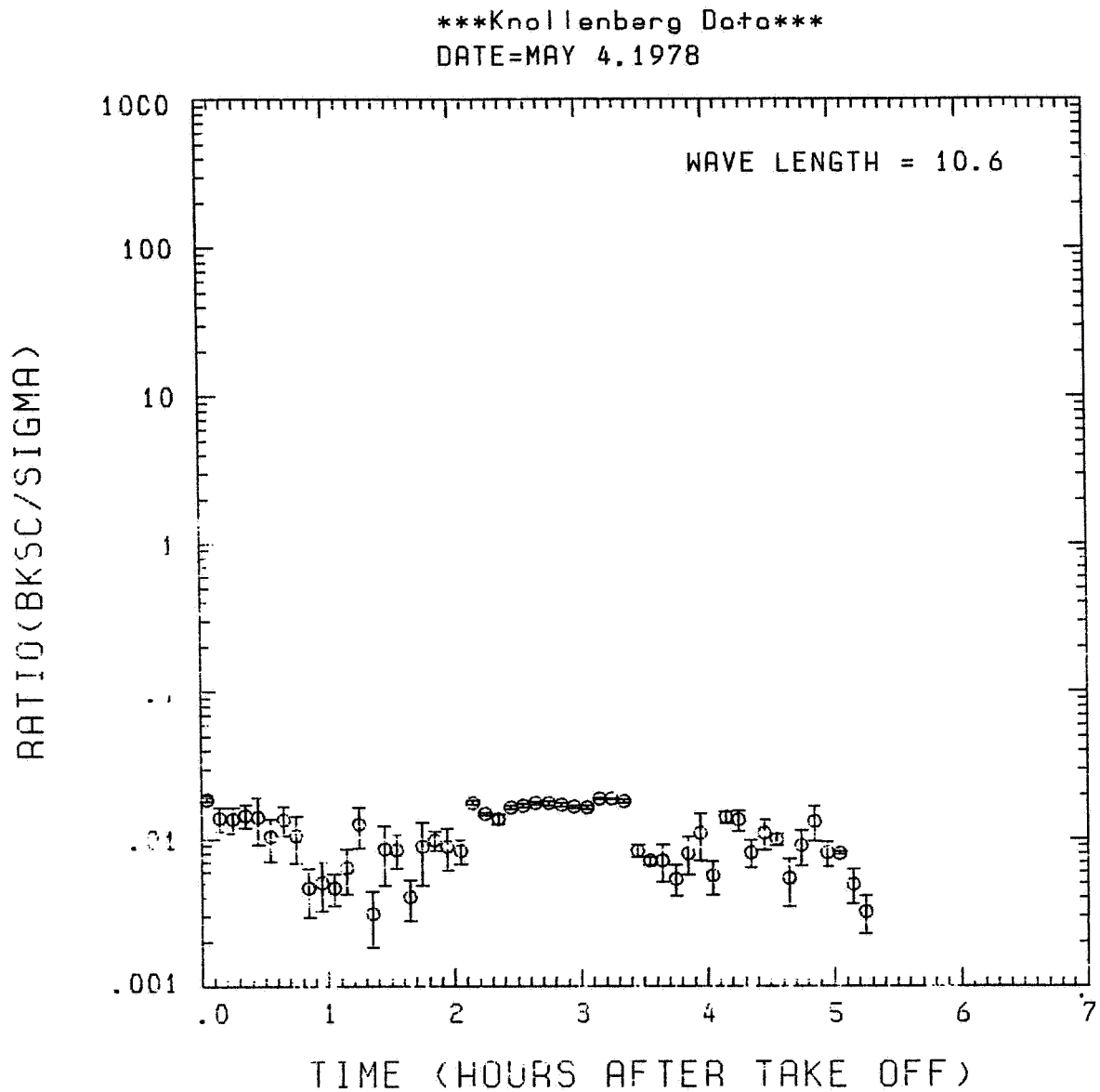


Fig. A13 (i). GAMETAG flight data for May 4, 1978.
Calculated ratios for backscatter to extinction for
five-minute data sets for $\lambda = 10.6 \mu\text{m}$.

Table A14. Significant times for May 10, 1978.
Christchurch, New Zealand to
Christchurch, New Zealand.

Significant Points

<u>#</u>	<u>TIME</u>	
1	22:08	Christchurch
2	22:35	
3	23:46	
4	0:01	
5	0:30	
6	1:04	
7	2:40	
8	3:18	
9	4:21	
10	4:28	
11	4:54	Christchurch

ORIGINAL PAGE IS
OF POOR QUALITY

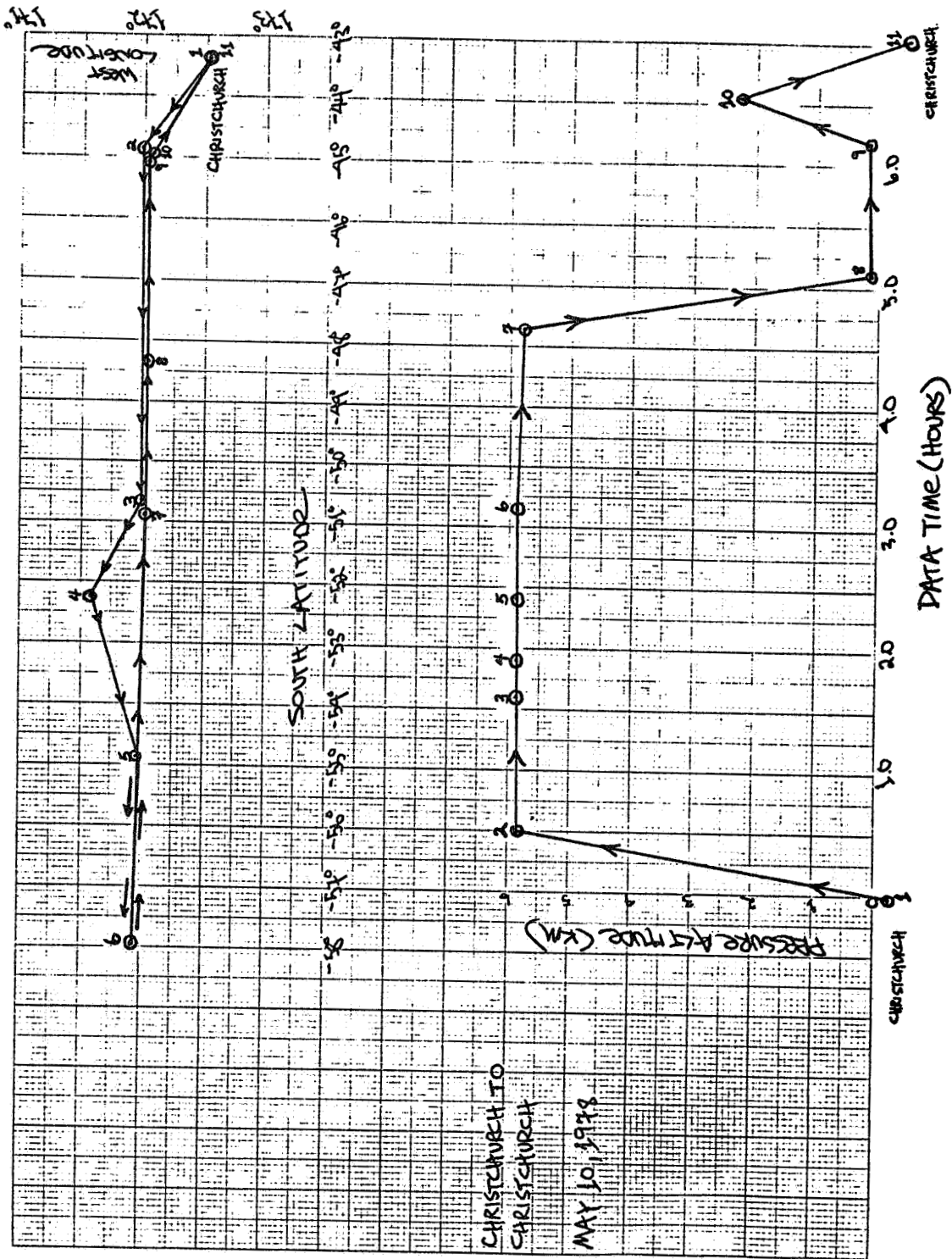


Fig. A 14 (a). GAMETAG flight data for May 10, 1978.
Altitude and location flight track plotted as a
function of time after takeoff.

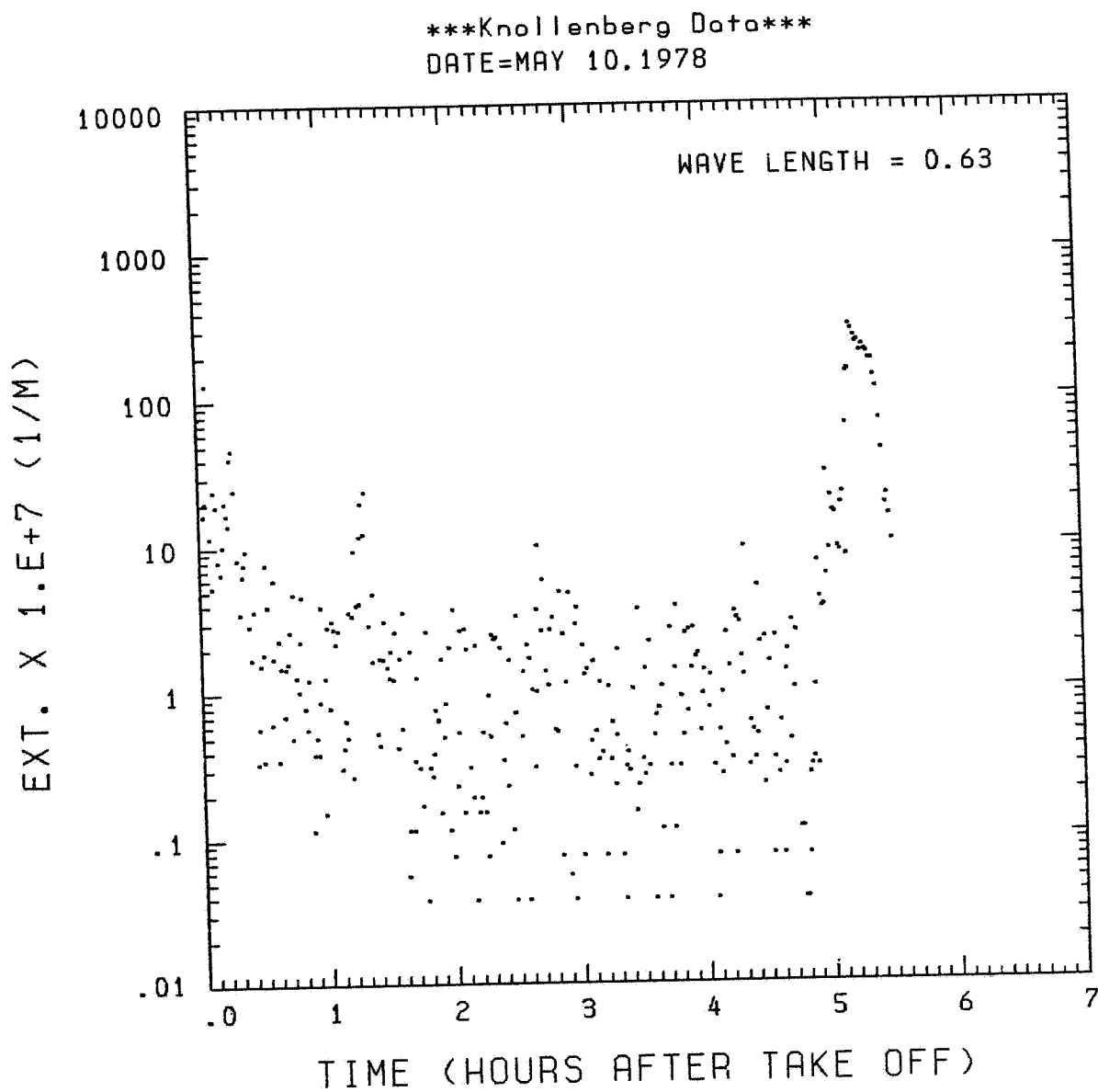


Fig. A14 (b). GAMETAG flight data for May 10, 1978.
Calculated particulate extinction along the flight
track for one-minute data sets for $\lambda = 0.63 \mu\text{m}$.

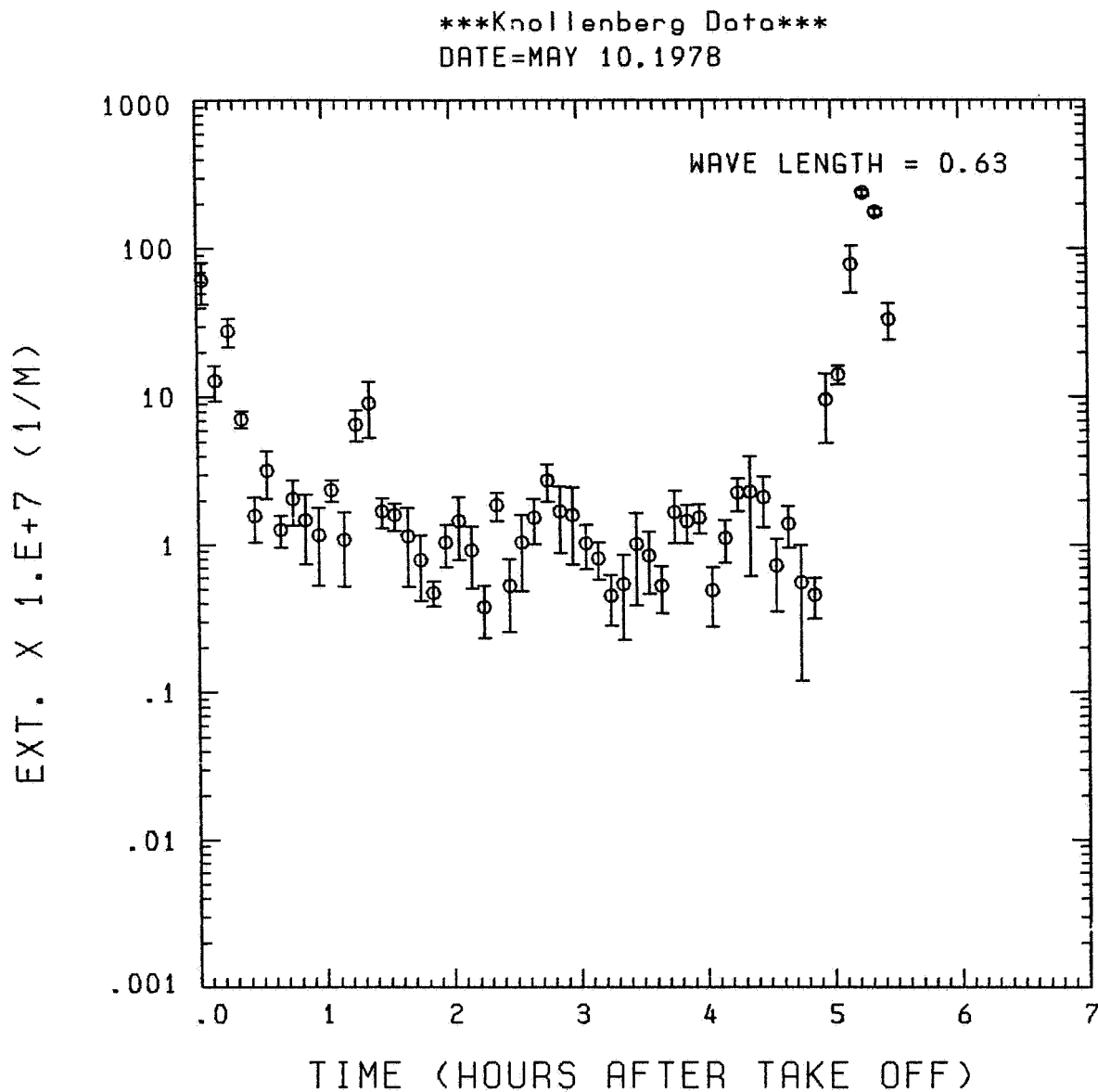


Fig. A14 (c). GAMETAG flight data for May 10, 1978.

Calculated particulate extinction along the flight track for five-minute data sets for $\lambda = 0.63 \mu\text{m}$.

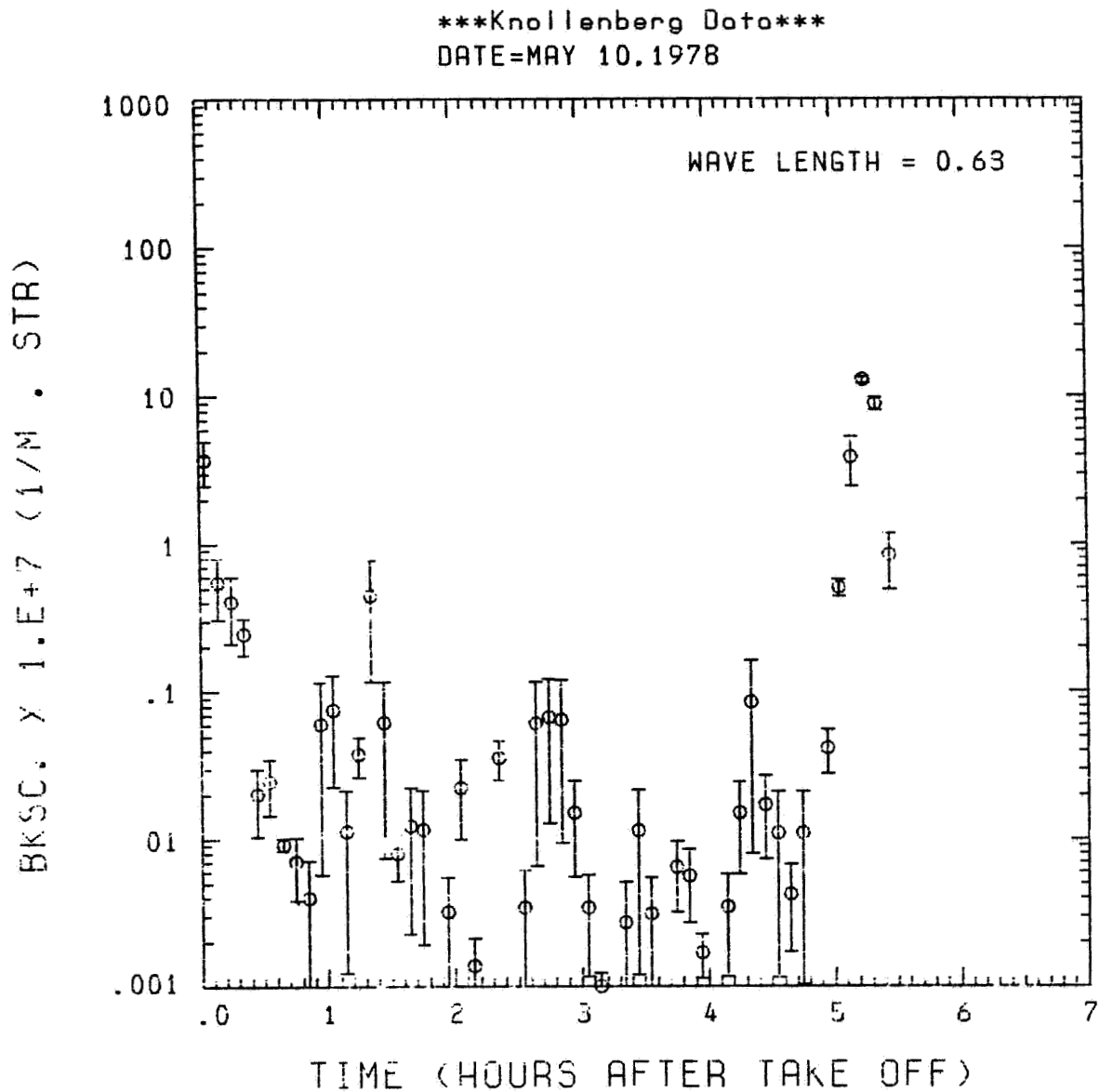


Fig. A14(d). GAMETAG flight data for May 10, 1978.

Calculated backscatter coefficient along the flight track for five-minute data sets for $\lambda = 0.63 \mu\text{m}$.

Knollenberg Data
 DATE= MAY 10, 1978

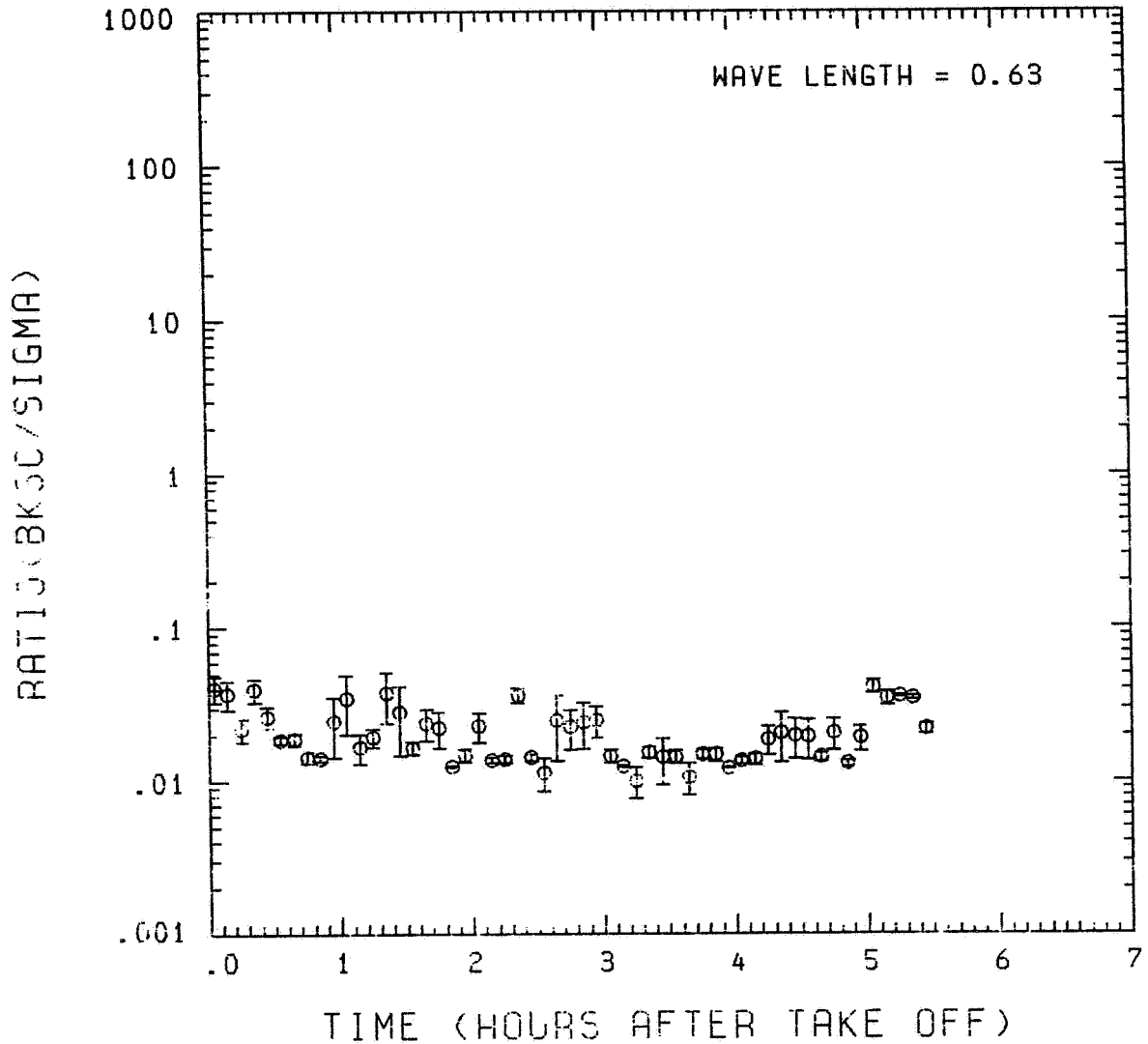


Fig. A 14(e). GAMETAG flight data for May 10, 1978.
 Calculated ratios for backscatter to extinction for
 five-minute data sets for $\lambda = 0.63 \mu\text{m}$.

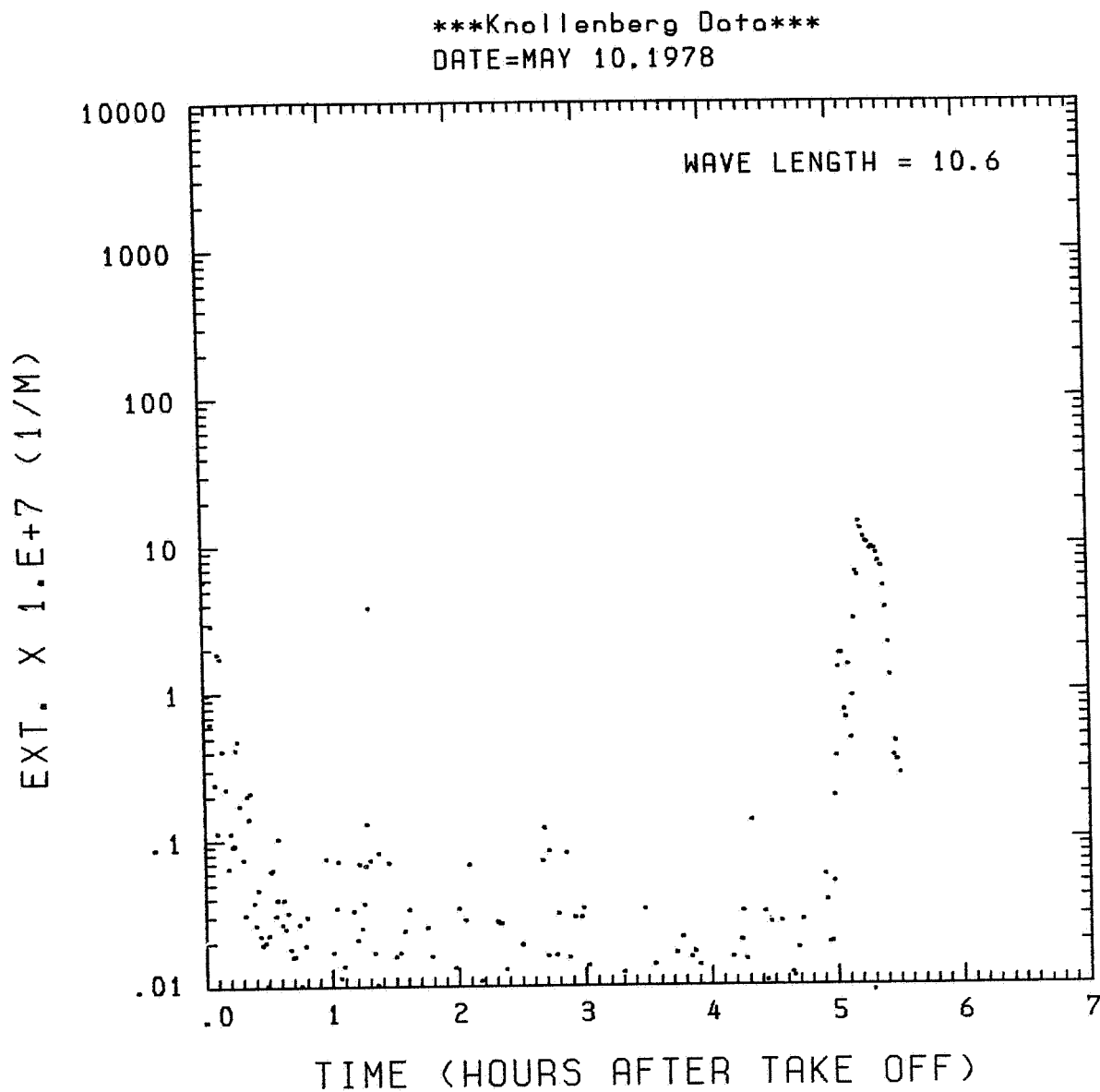


Fig. A 14(f). GAMETAG flight data for May 10, 1978.
Calculated particulate extinction along the flight
track for one-minute data sets for $\lambda = 10.6 \mu\text{m}$.

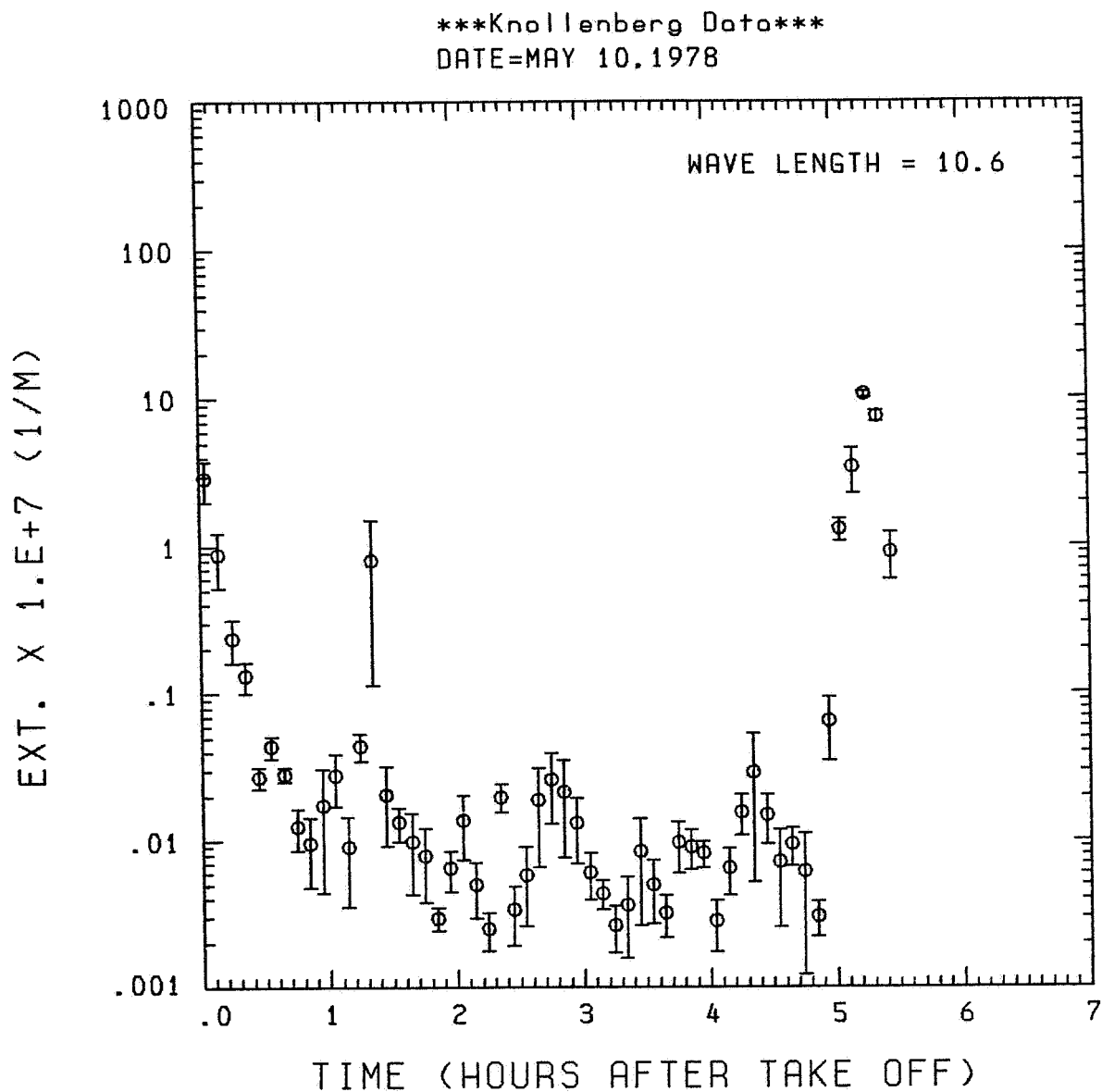


Fig. A14 (g). GAMETAG flight data for May 10, 1978.

Calculated particulate extinction along the flight track for five-minute data sets for $\lambda = 10.6 \mu\text{m}$.

ORIGINAL PAGE IS
OF POOR QUALITY

Knollenberg Data
DATE=MAY 10.1978

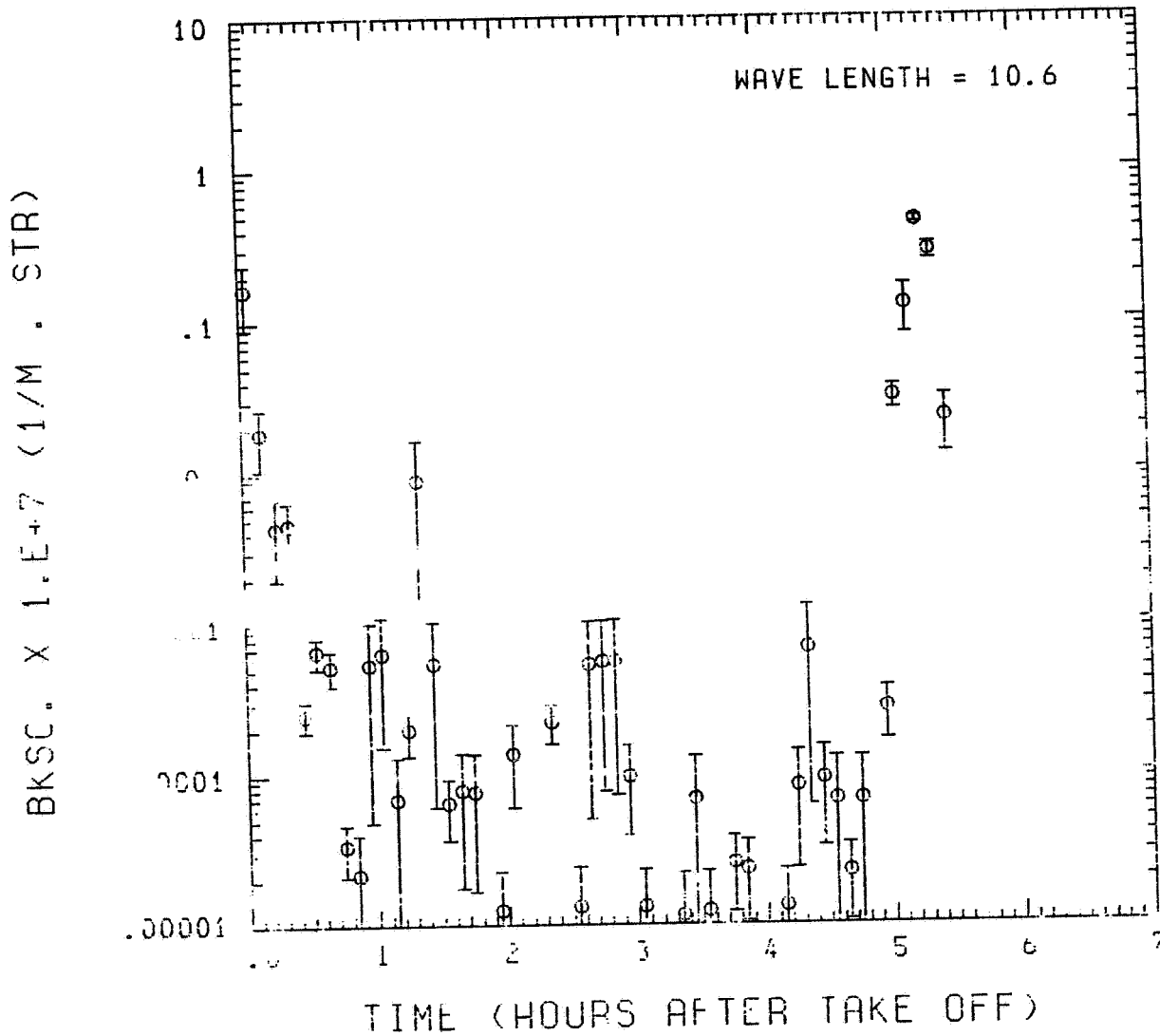


Fig. A14(h). GAMETAG flight data for May 10, 1978.

Calculated backscatter coefficient along the flight
track for five-minute data sets for $\lambda = 10.6 \mu\text{m}$.

Knollenberg Data

DATE=MAY 10,1978

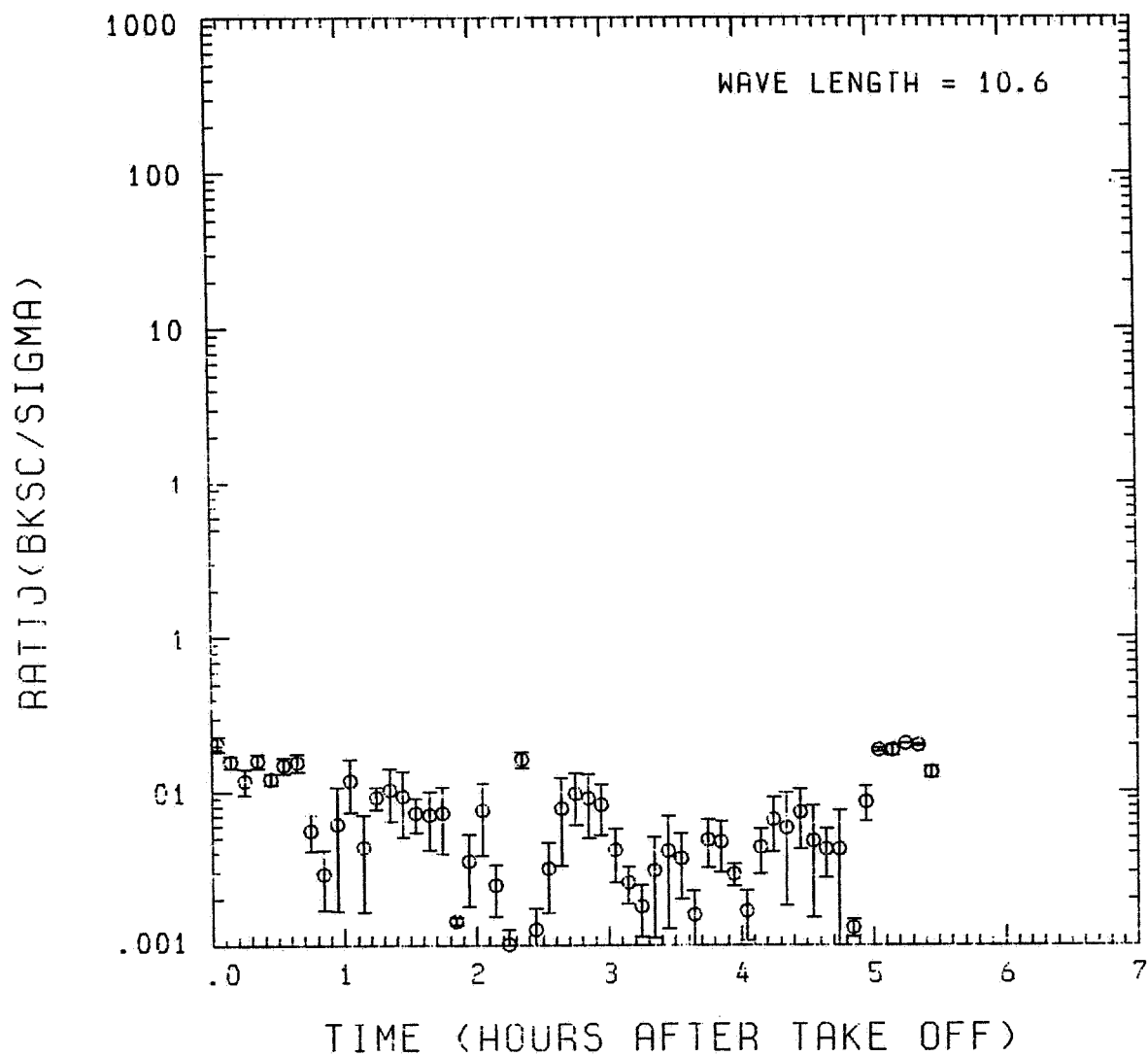


Fig. A 14 (i). GAMETAG flight data for May 10, 1978.

Calculated ratios for backscatter to extinction for five-minute data sets for $\lambda = 10.6 \mu\text{m}$.

Table A15. Significant times for May 11, 1978.
Christchurch, New Zealand to
Nandi, Fiji Islands

Significant Points

<u>#</u>	<u>TIME</u>	
*	Computer on out of Christchurch	
1	22:34	
2	22:52	
3	23:50	
4	00:27	(Alt.) = 00:30 (Long.)
5	01:12	
6	01:33	
7	03:39	
8	03:46	
9	04:03	
*	Data gap 04:04 - 04:11	
10	04:20	Nandi

ORIGINAL PAGE IS
OF POOR QUALITY

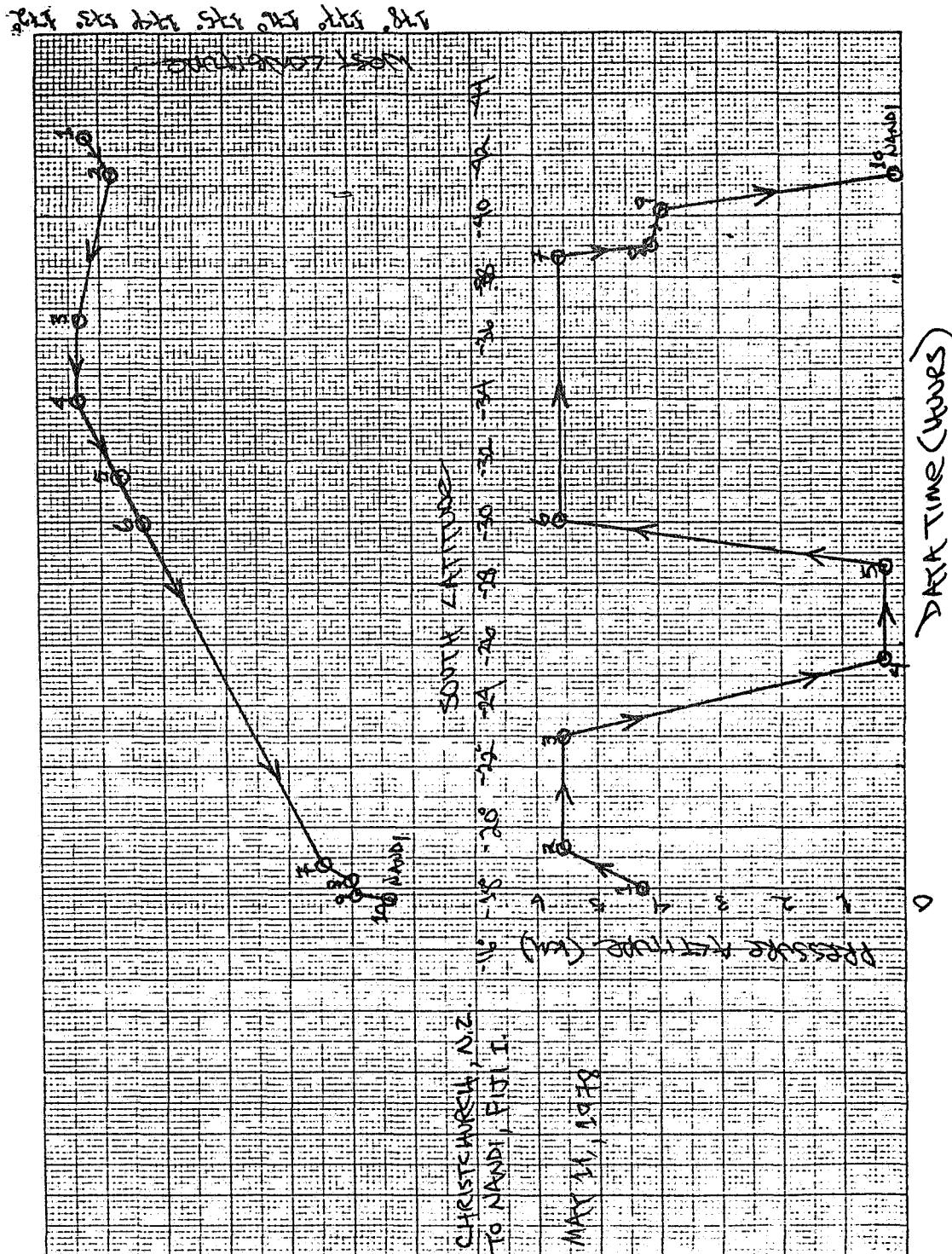


Fig. A15 (a). GAMETAG flight data for May 11, 1978.
Altitude and location flight track plotted as a
function of time after takeoff.

Knollenberg Data
DATE=MAY 11, 1978

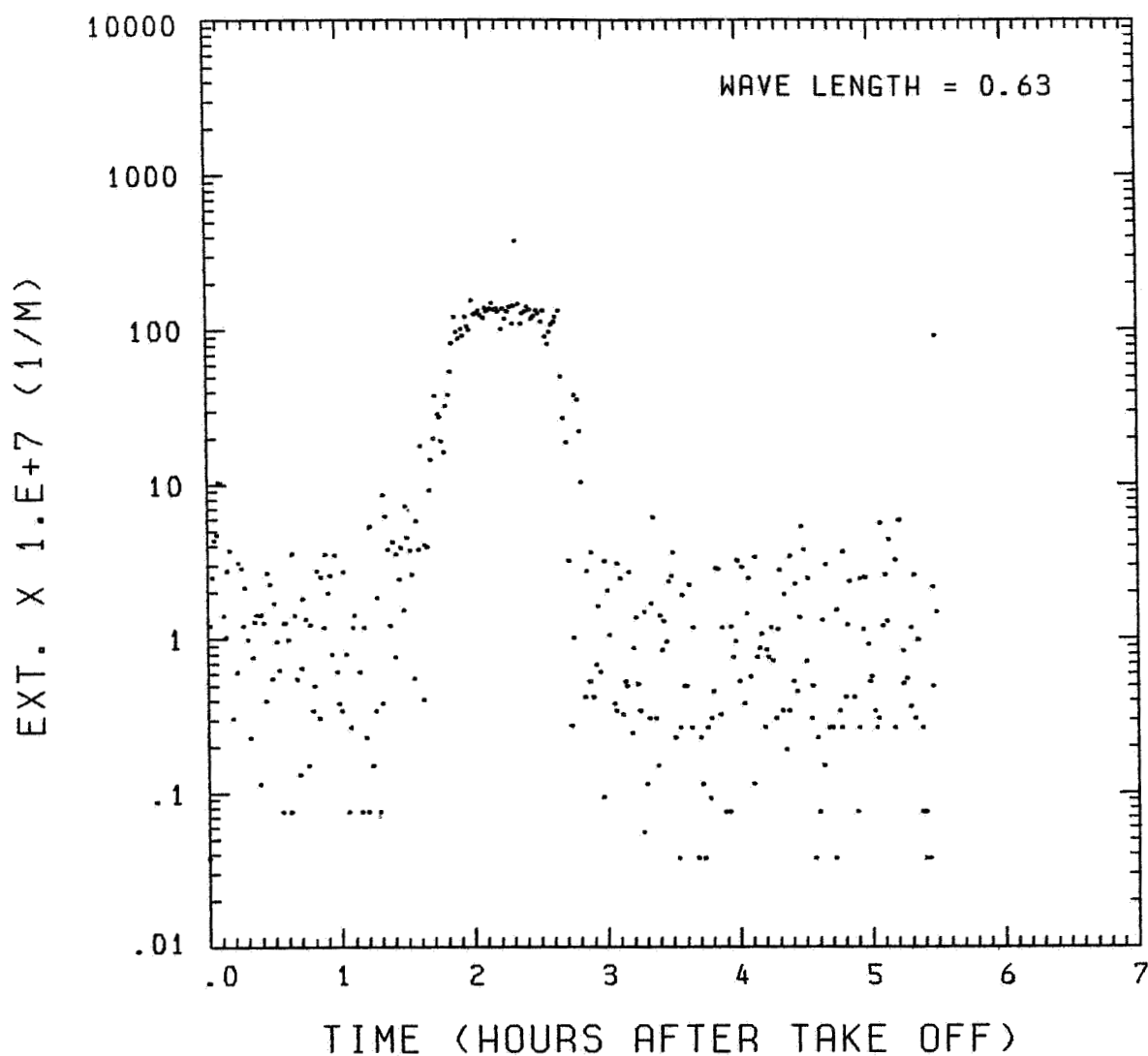


Fig. A15 (b). GAMETAG flight data for May 11, 1978.
Calculated particulate extinction along the flight
track for one-minute data sets for $\lambda = 0.63 \mu\text{m}$.

Knollenberg Data
 DATE=MAY 11, 1978

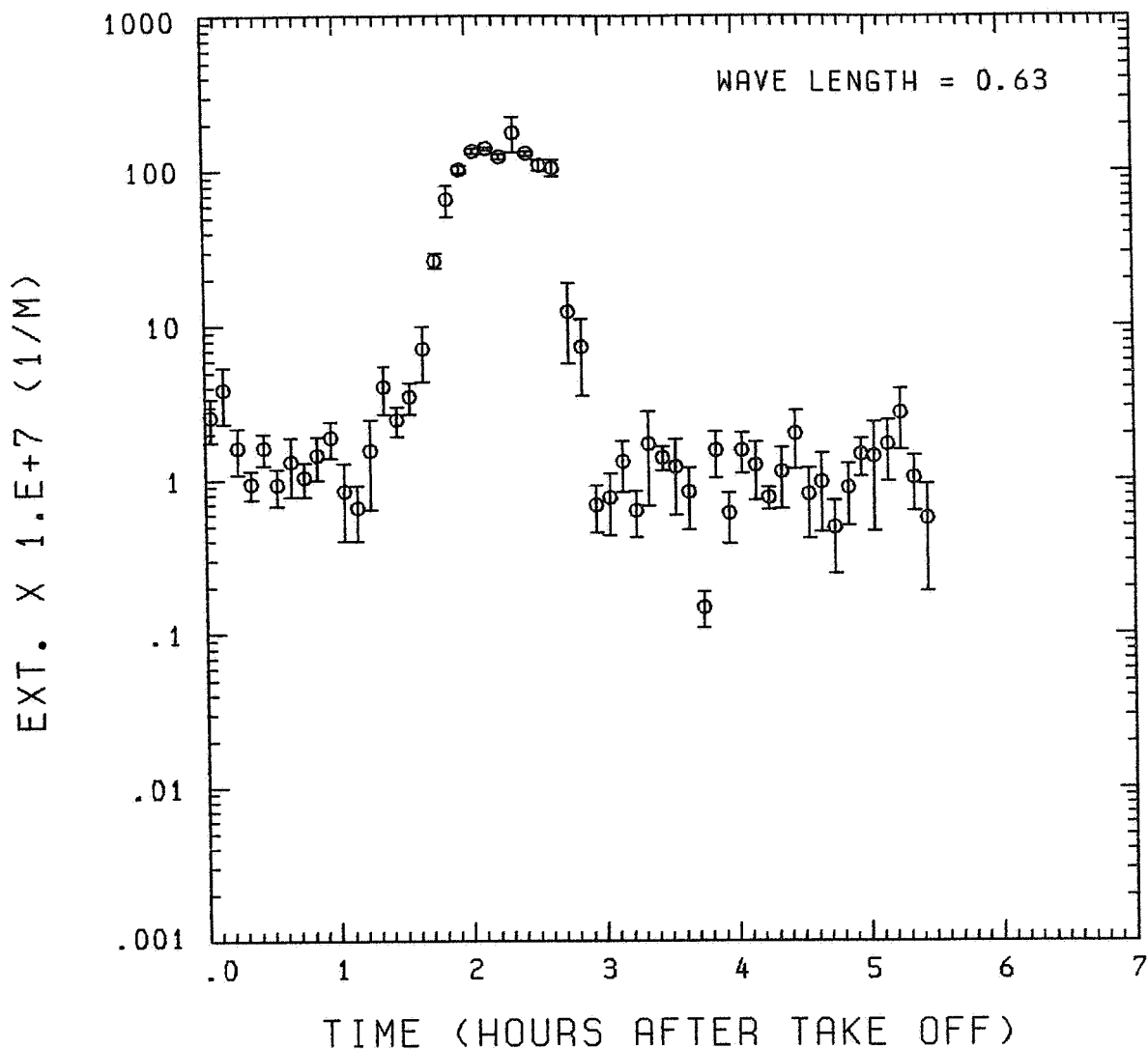


Fig. A15 (c). GAMETAG flight data for May 11, 1978.
 Calculated particulate extinction along the flight
 track for five-minute data sets for $\lambda = 0.63 \mu\text{m}$.

ORIGINAL PAGE IS
OF POOR QUALITY

Knollenberg Data
DATE=MAY 11, 1978

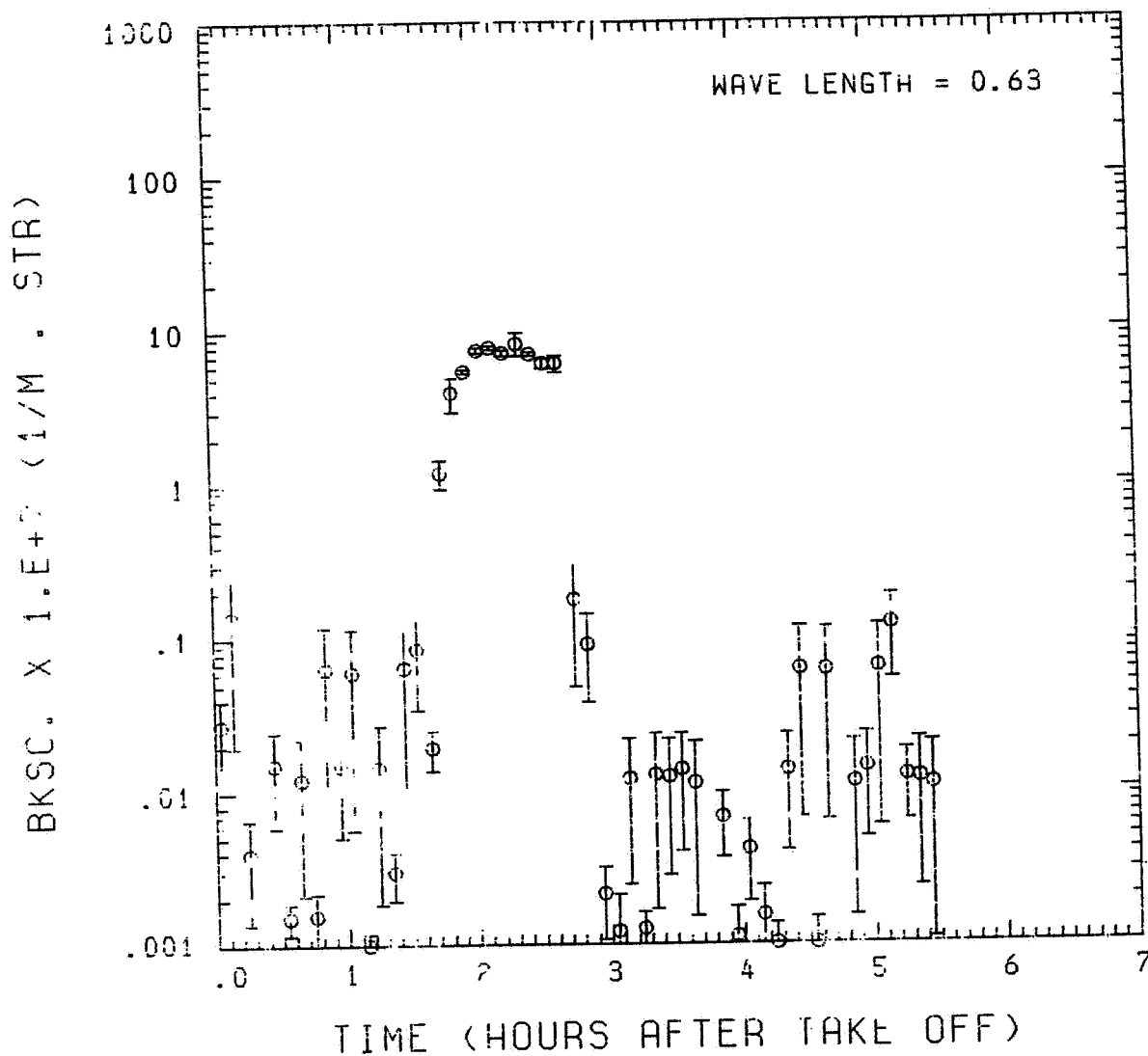


Fig. A15 (d). GAMETAG flight data for May 11, 1978.

Calculated backscatter coefficient along the flight
track for five-minute data sets for $\lambda = 0.63 \mu\text{m}$.

Knollenberg Data

DATE=MAY 11, 1978

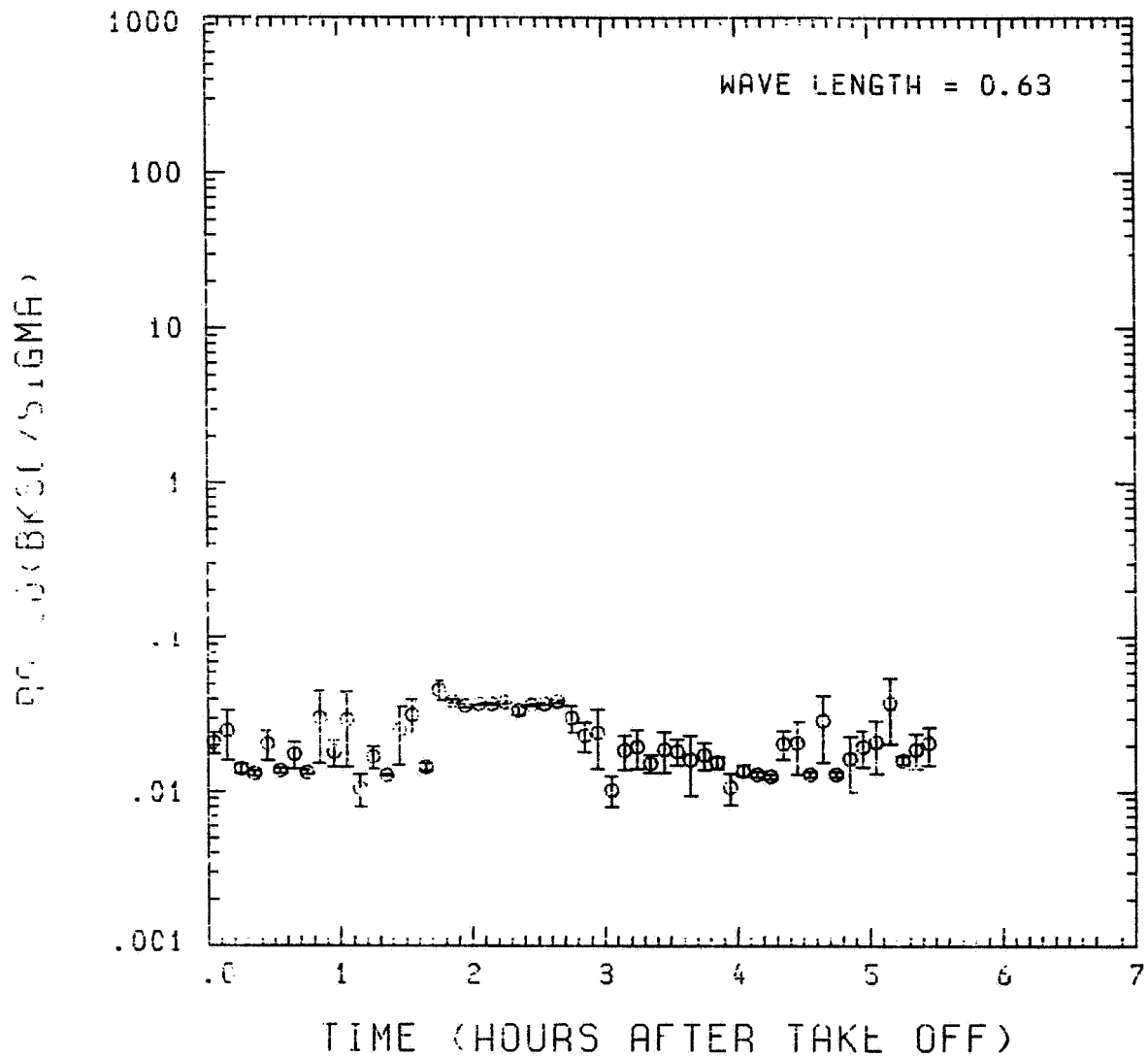


Fig. A15 (e). GAMETAG flight data for May 11, 1978.

Calculated ratios for backscatter to extinction for five-minute data sets for $\lambda = 0.63 \mu m$.

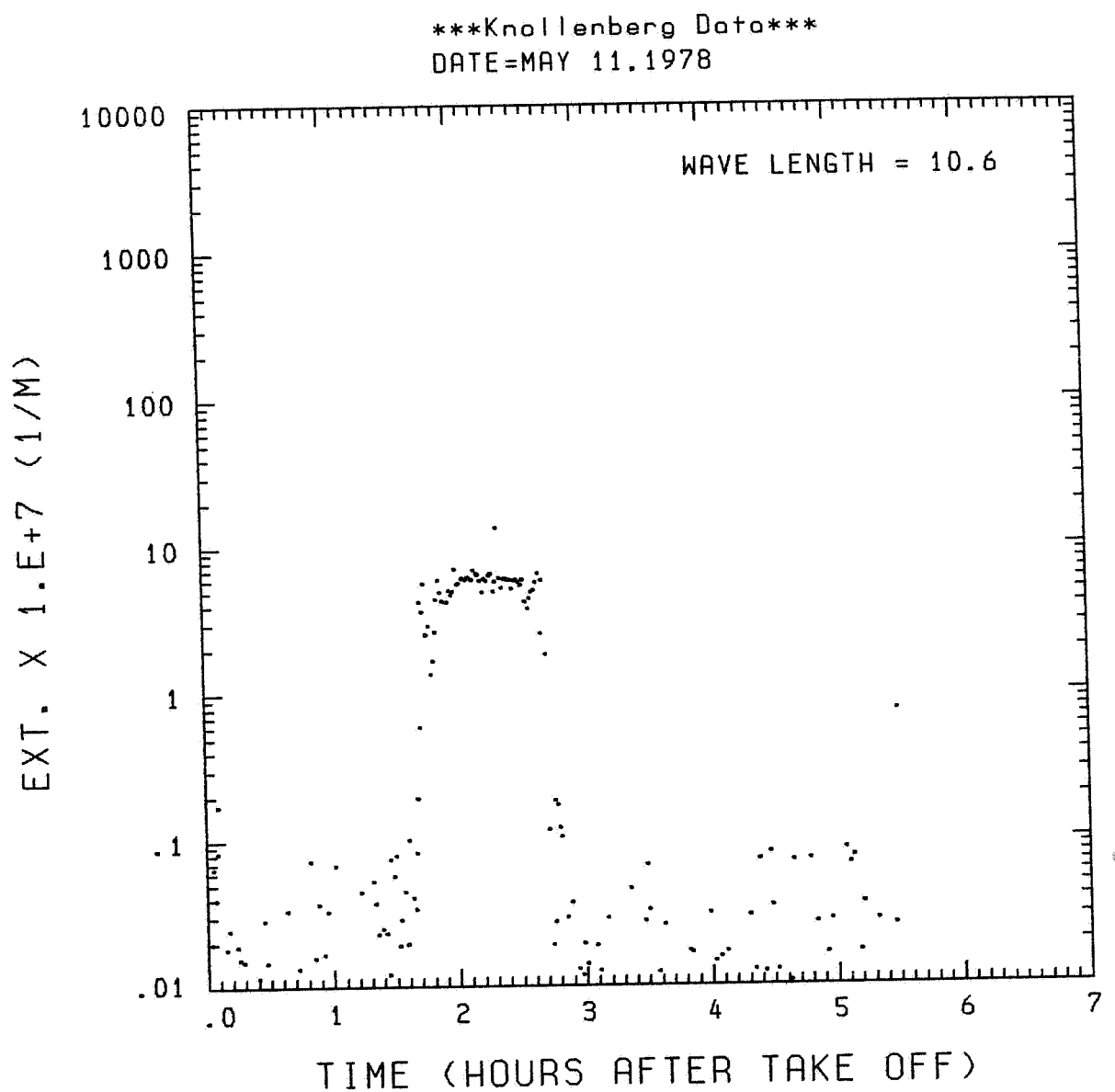


Fig. A15 (f). GAMETAG flight data for May 11, 1978.
Calculated particulate extinction along the flight
track for one-minute data sets for $\lambda = 10.6 \mu\text{m}$.

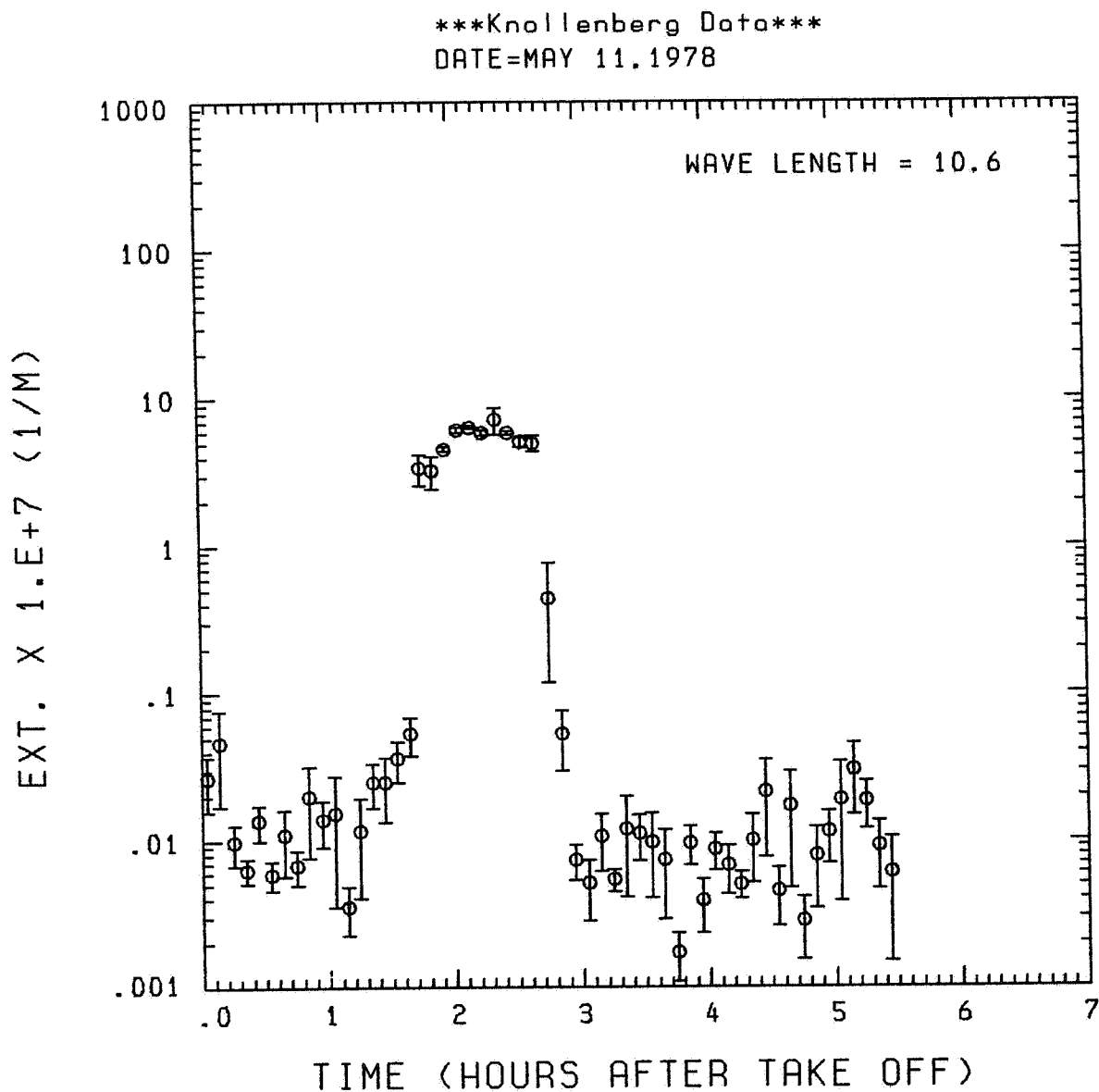


Fig. A15 (g). GAMETAG flight data for May 11, 1978.
Calculated particulate extinction along the flight
track for five-minute data sets for $\lambda = 10.6 \mu\text{m}$.

ORIGINAL PAGE IS
OF POOR QUALITY

Knollenberg Data
DATE=MAY 11, 1978

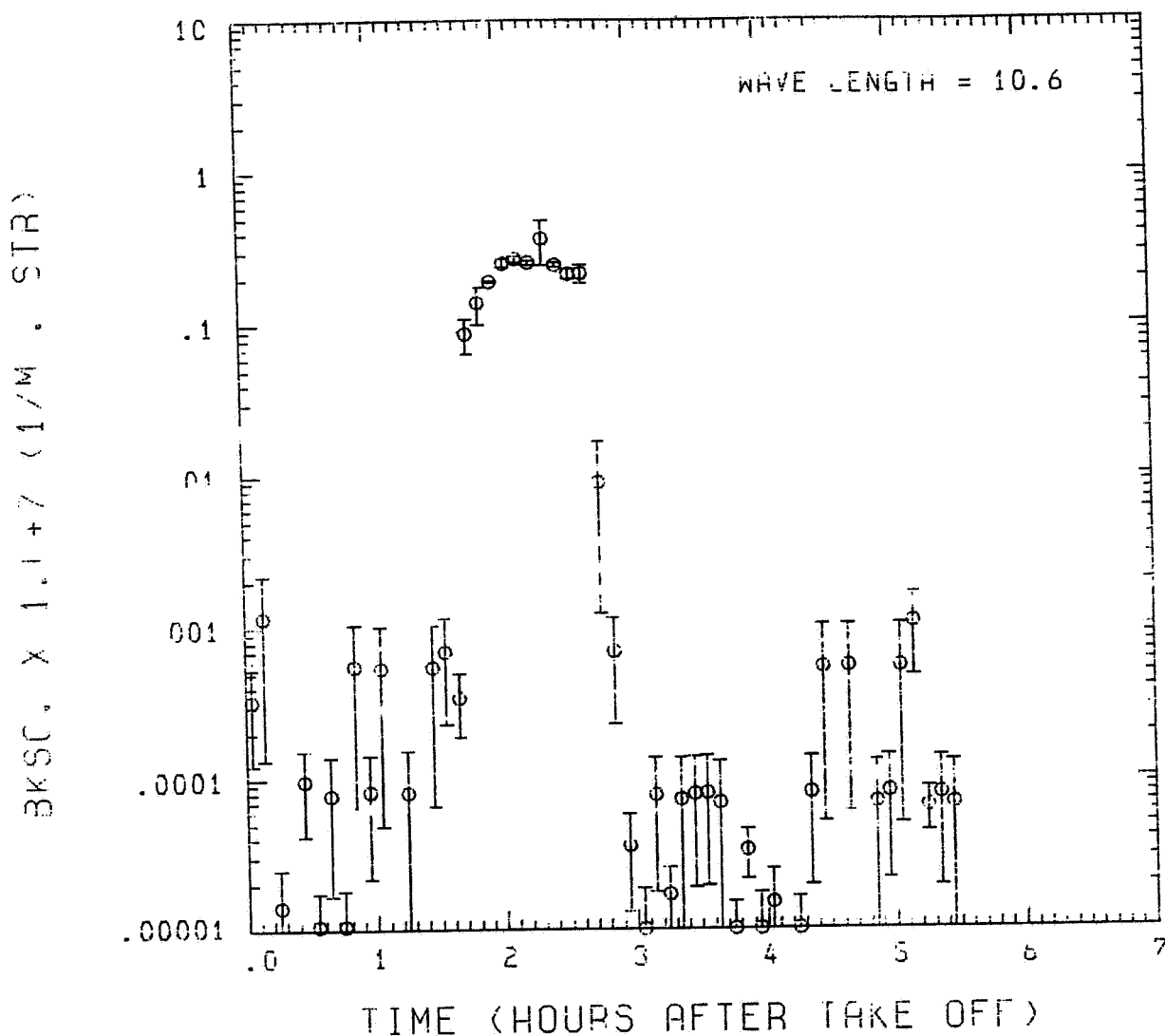


Fig. A15 (h). GAMETAG flight data for May 11, 1978.

Calculated backscatter coefficient along the flight
track for five-minute data sets for $\lambda = 10.6 \mu\text{m}$.

C-4

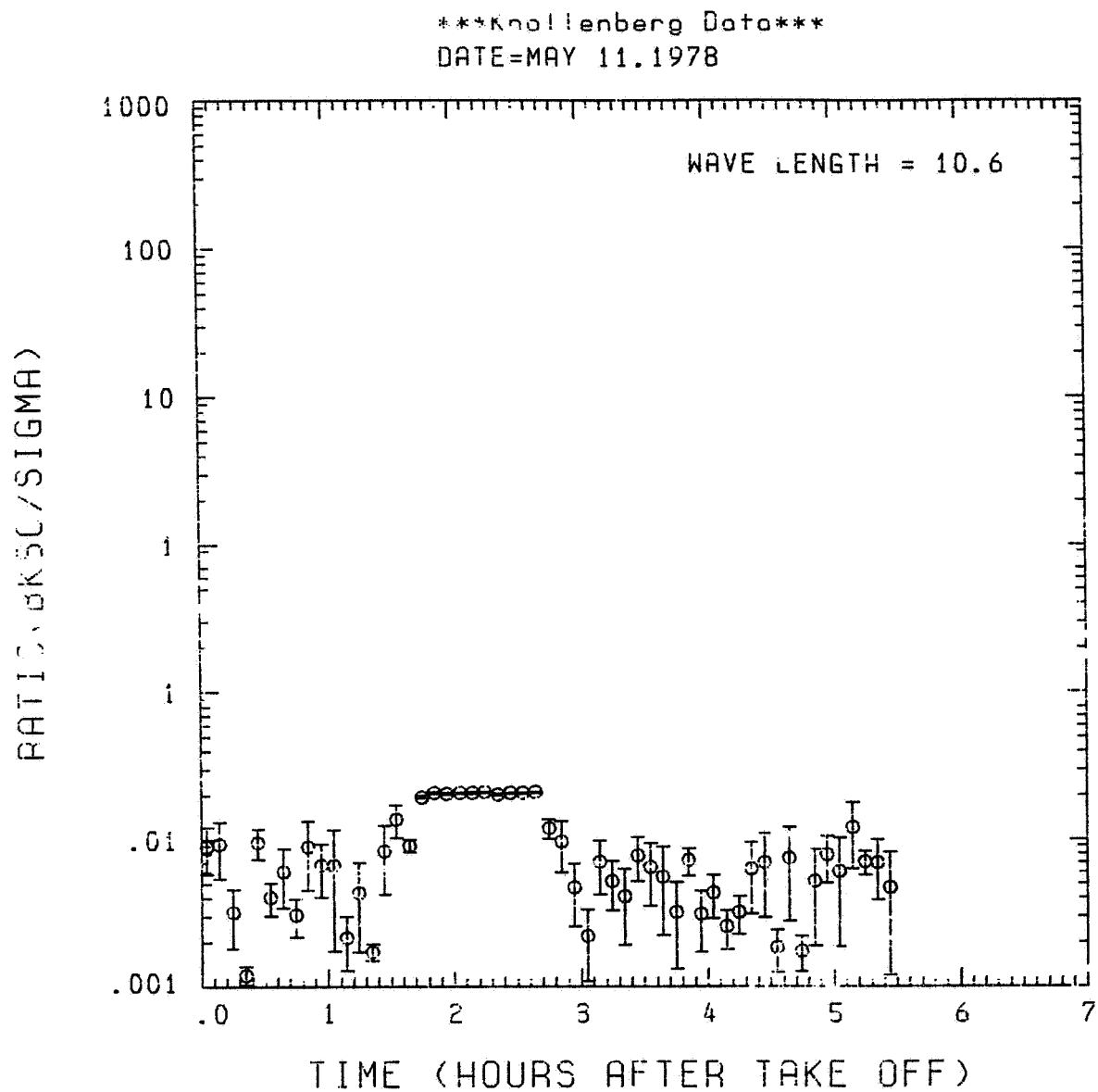


Fig. A15 (i). GAMETAG flight data for May 11, 1978.
Calculated ratios for backscatter to extinction for
five-minute data sets for $\lambda = 10.6 \mu\text{m}$.

Table A16. Significant times for May 12, 1978.
Nandi, Fiji Islands to Canton Island.

Significant Points

<u>#</u>	<u>TIME</u>	
1	21:50	Nandi
2	21:56	
3	22:10	
4	22:13	
5	23:11 (Alt.) - 23:36 (Long.)	
6	23:47	
7	0:25	
8	1:56	
9	2:30	
10	3:40	
11	3:45	Canton Island

ORIGINAL PAGE IS
OF POOR QUALITY

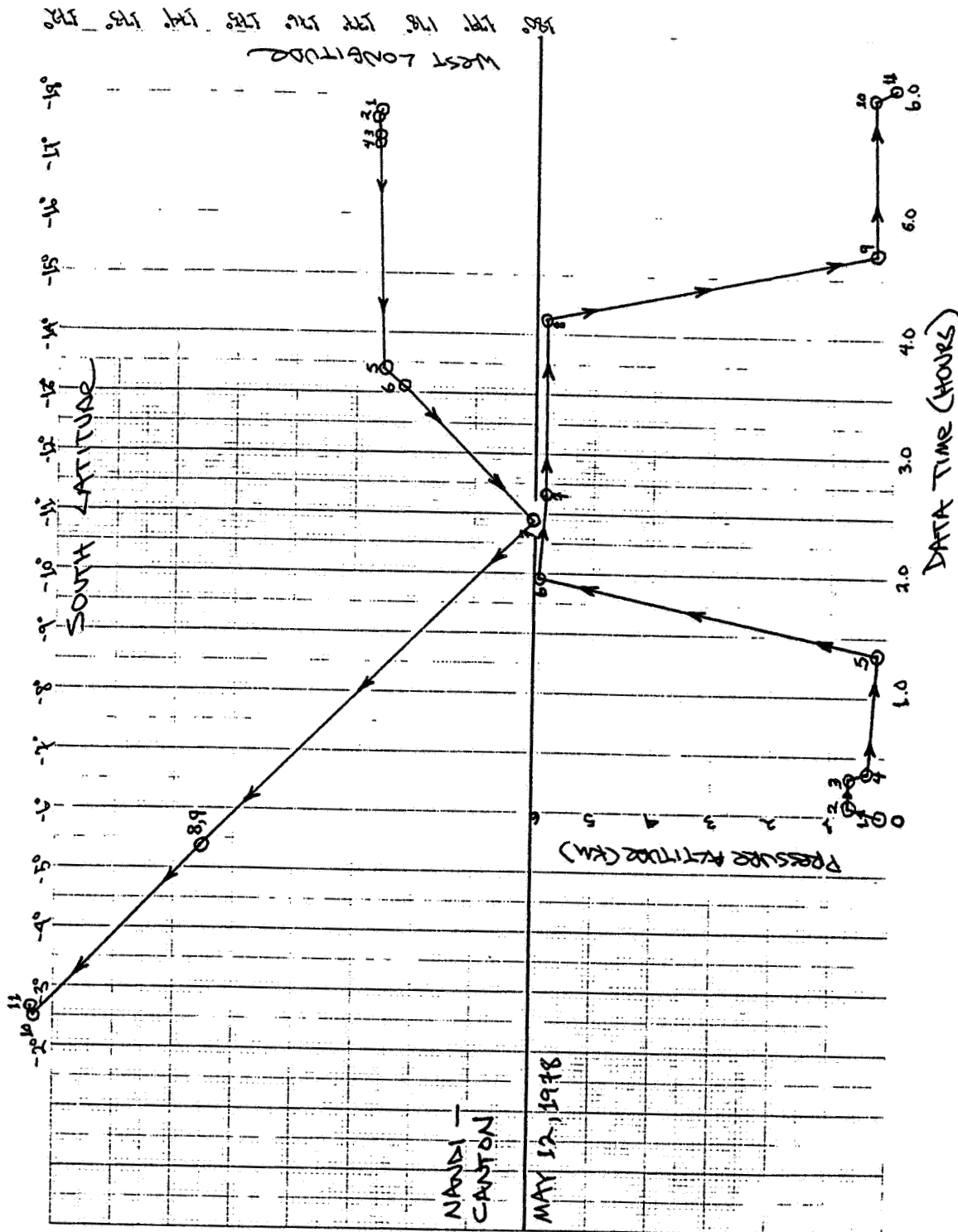


Fig. A16 (a). GAMETAG flight data for May 12, 1978.
Altitude and location flight track plotted as a
function of time after takeoff.

ORIGINAL PAGE IS
OF POOR QUALITY

Knollenberg Data

DATE=MAY 12, 1978

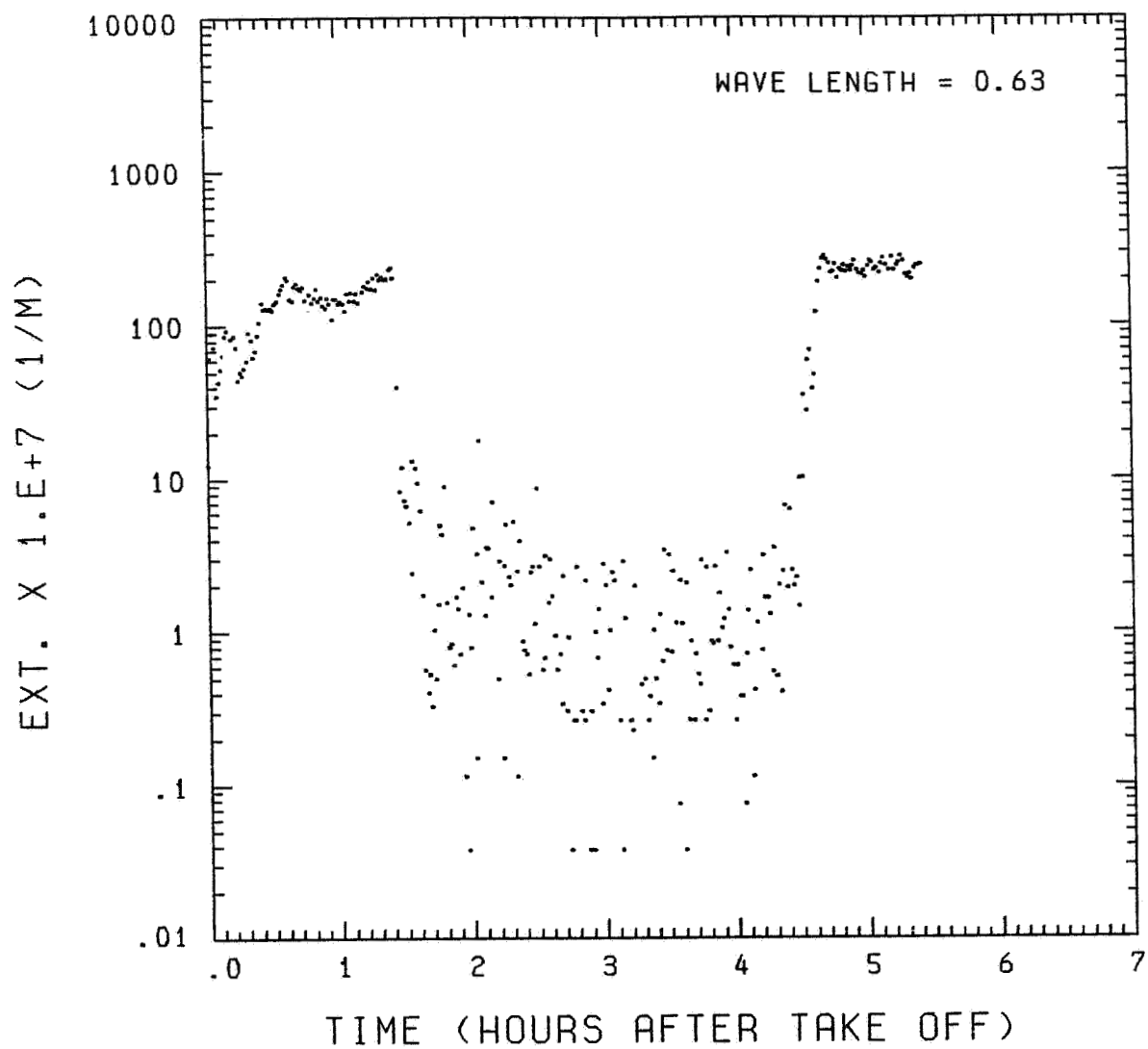


Fig. A16 (b). GAMETAG flight data for May 12, 1978.

Calculated particulate extinction along the flight
track for one-minute data sets for $\lambda = 0.63 \mu\text{m}$.

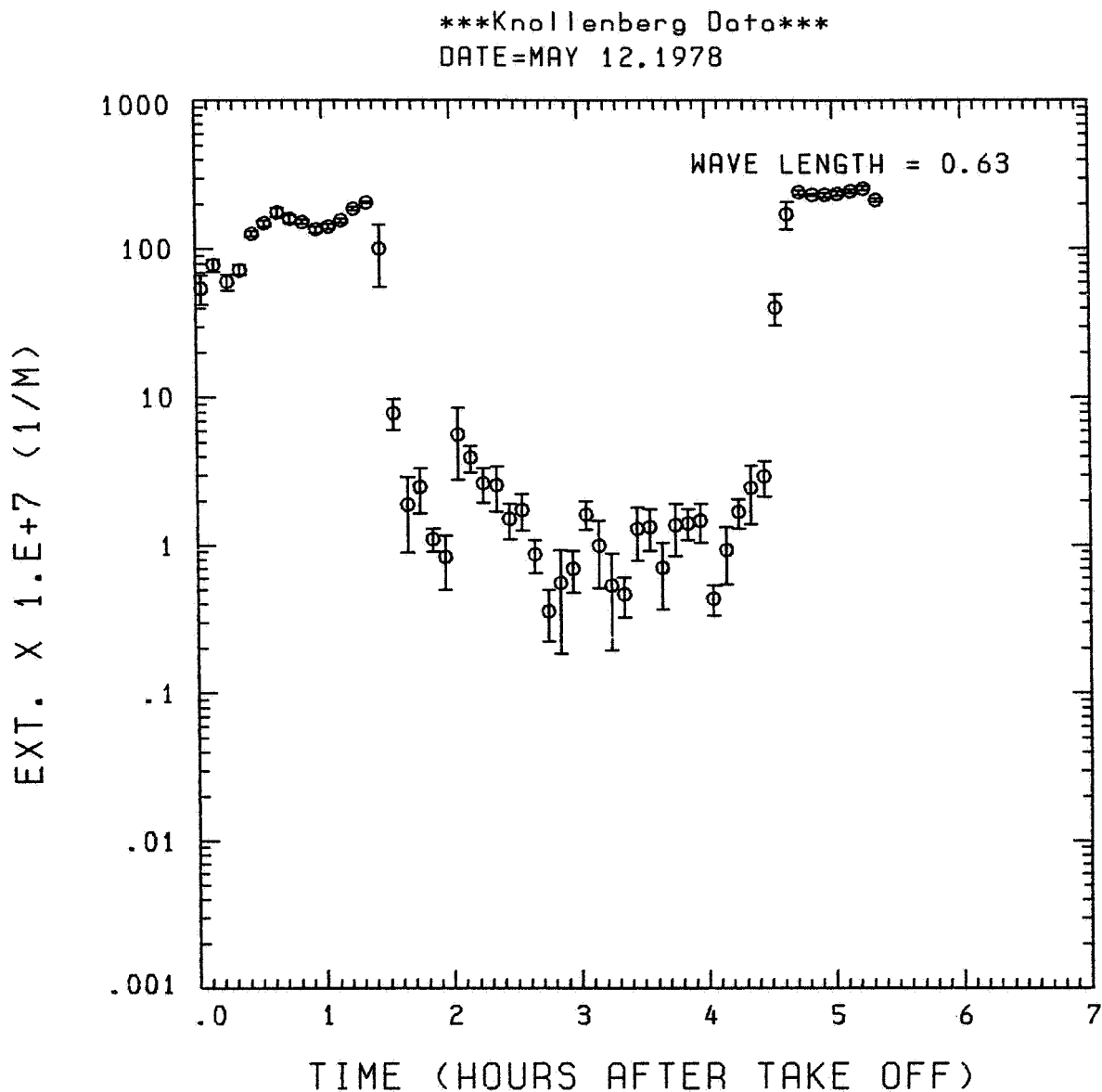


Fig. A16 (c). GAMETAG flight data for May 12, 1978.
Calculated particulate extinction along the flight
track for five-minute data sets for $\lambda = 0.63 \mu\text{m}$.

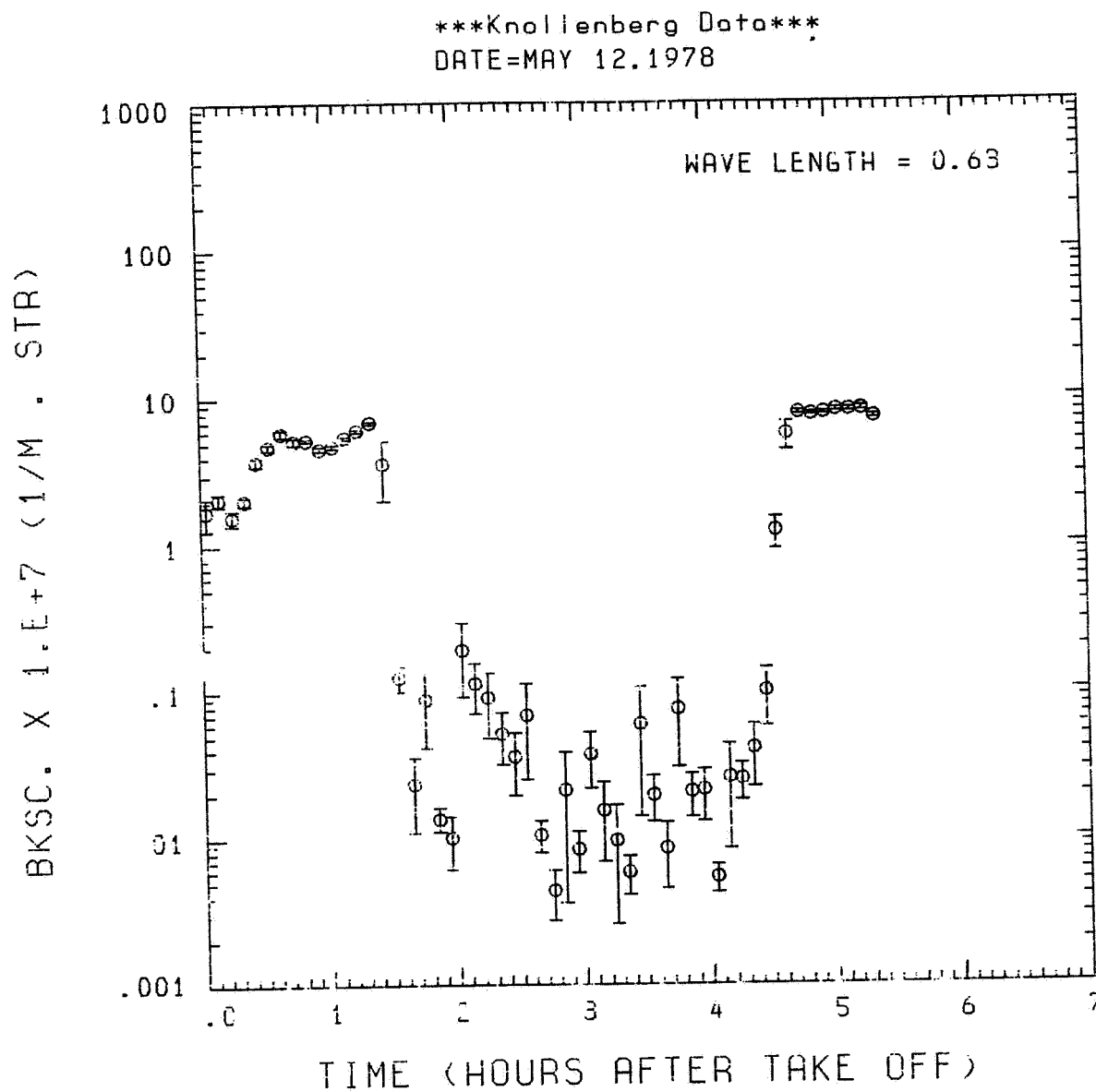


Fig. A16 (d). GAMETAG flight data for May 12, 1978.
Calculated backscatter coefficient along the flight
track for five-minute data sets for $\lambda = 0.63 \mu\text{m}$.

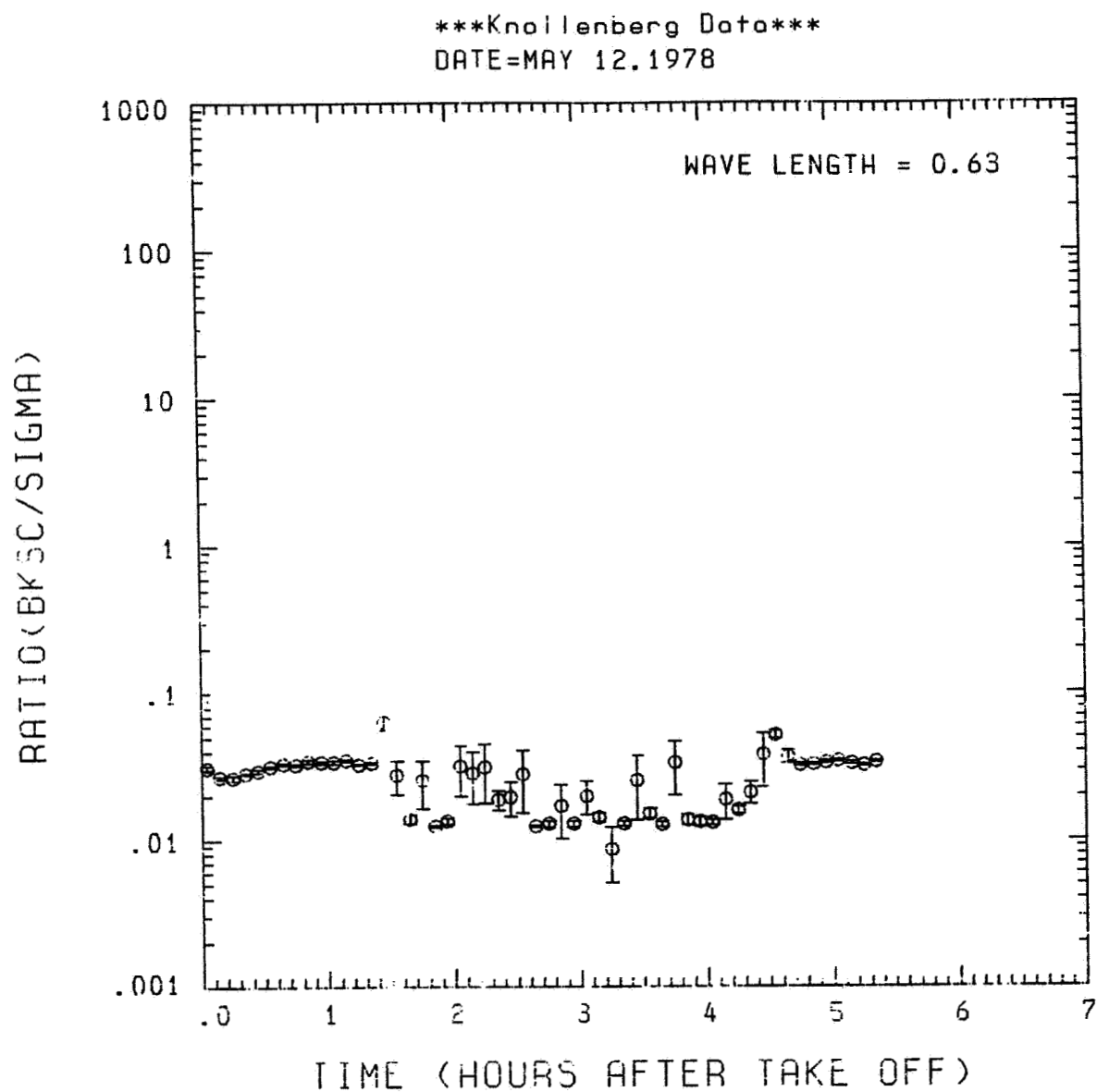


Fig. A16 (e). GAMETAG flight data for May 12, 1978.
Calculated ratios for backscatter to extinction for
five-minute data sets for $\lambda = 0.63 \mu\text{m}$.

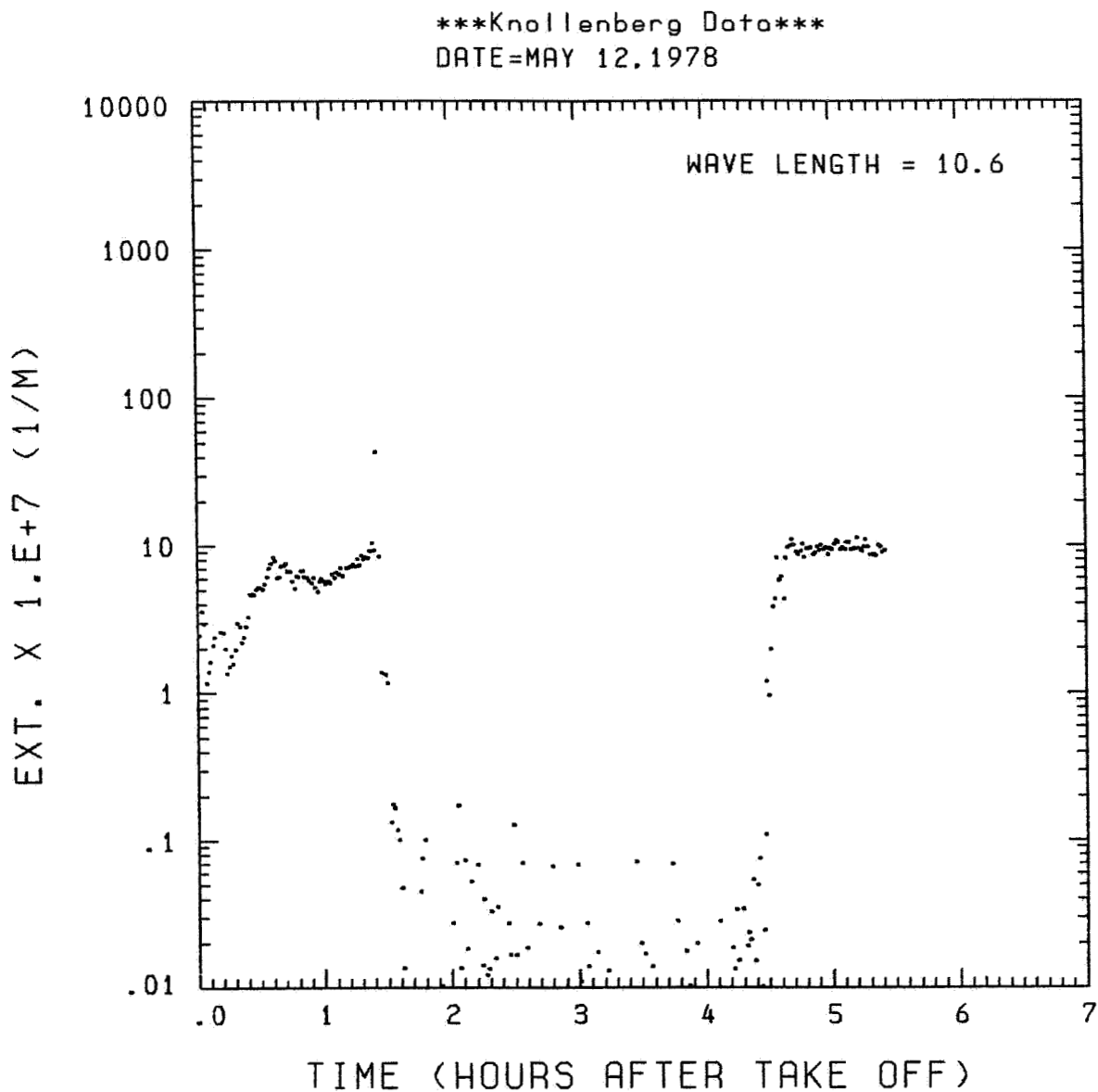


Fig. A16 (f). GAMETAG flight data for May 12, 1978.
Calculated particulate extinction along the flight
track for one-minute data sets for $\lambda = 10.6 \mu\text{m}$.

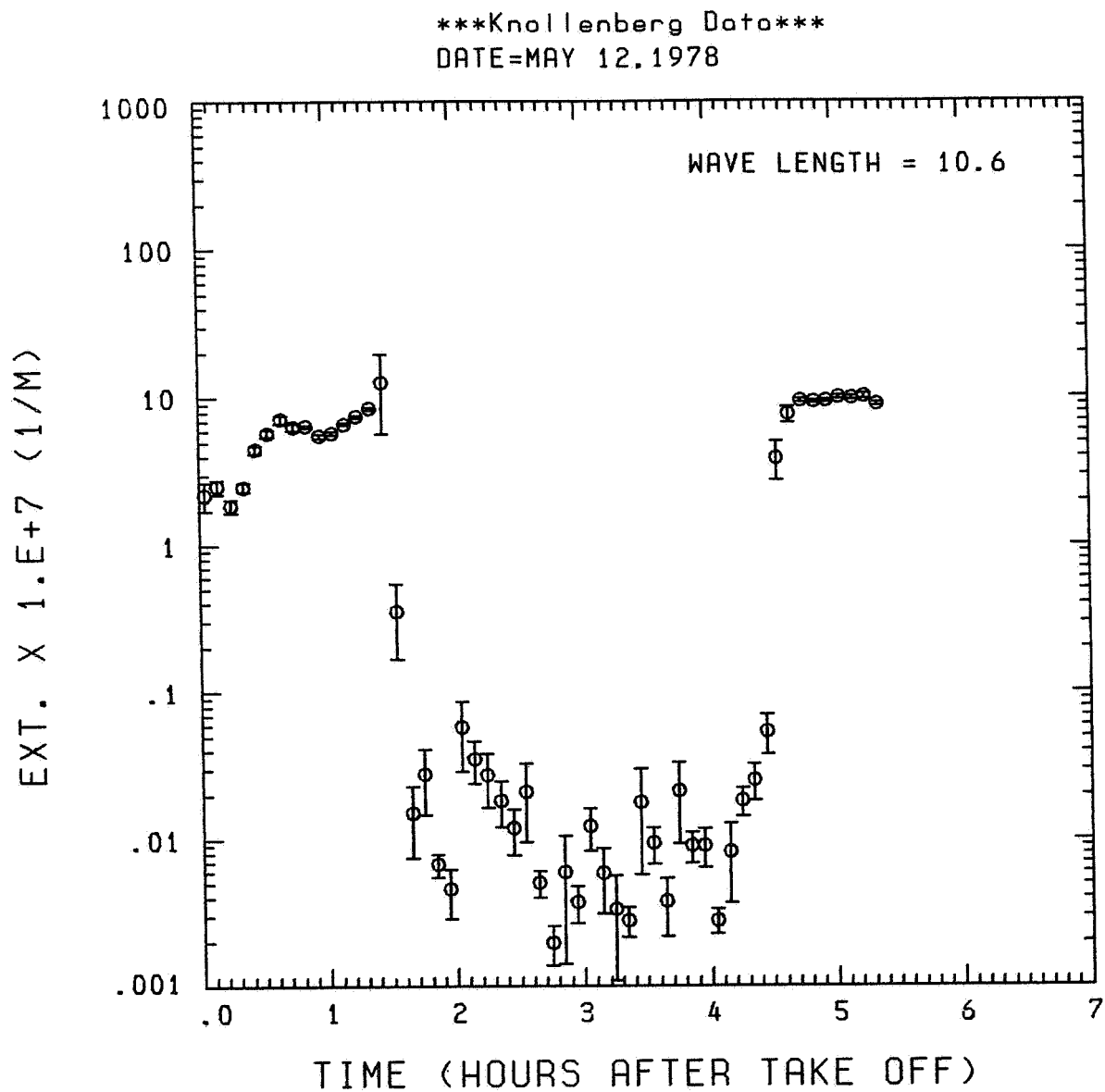


Fig. A16 (g). GAMETAG flight data for May 12, 1978.

Calculated particulate extinction along the flight track for five-minute data sets for $\lambda = 10.6 \mu\text{m}$.

Knollenberg Data
DATE=MAY 12, 1978

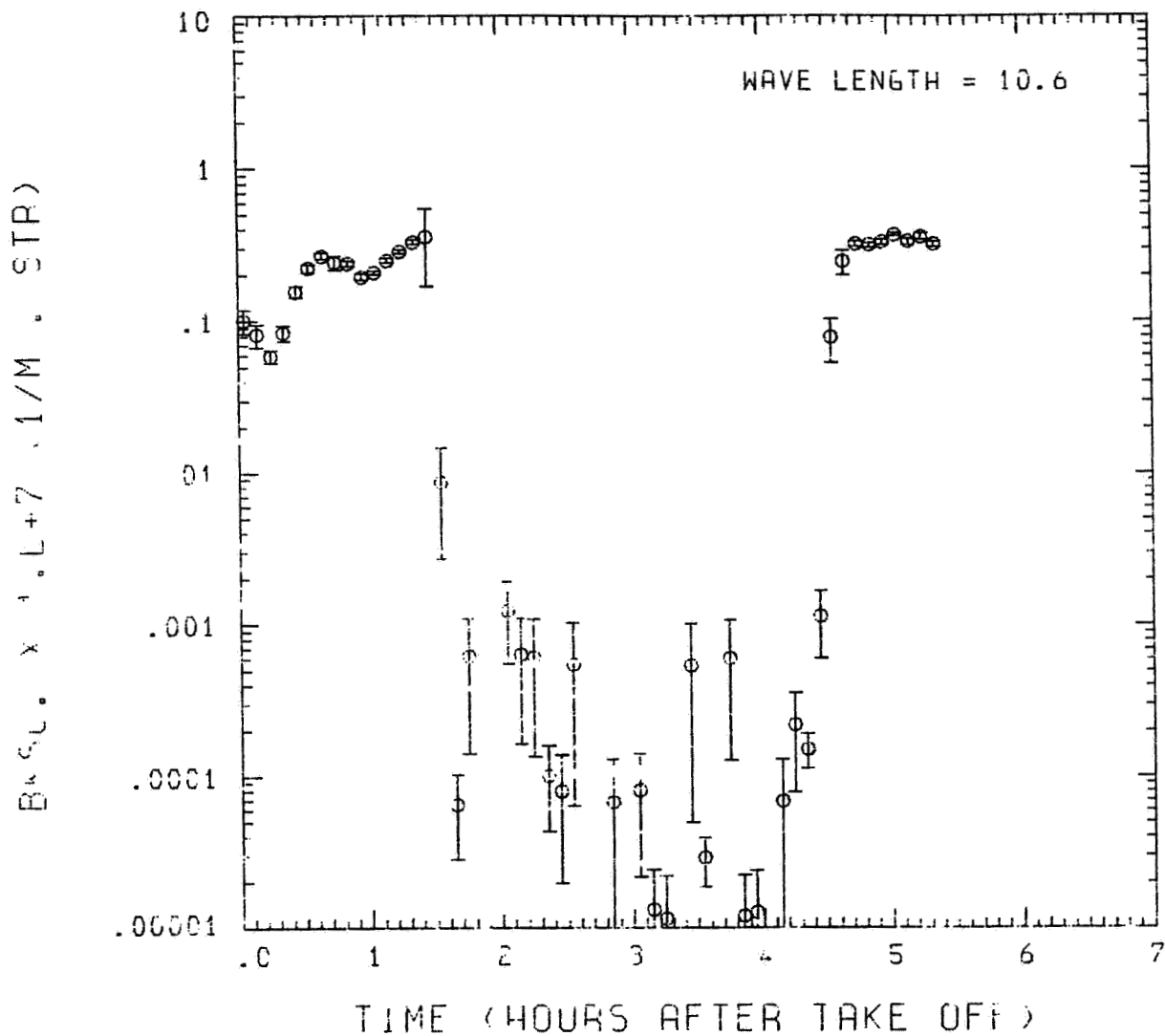


Fig. A16 (h). GAMETAG flight data for May 12, 1978.

Calculated backscatter coefficient along the flight
track for five-minute data sets for $\lambda = 10.6 \mu m$.

Knollenberg Data
 DATE=MAY 12.1978

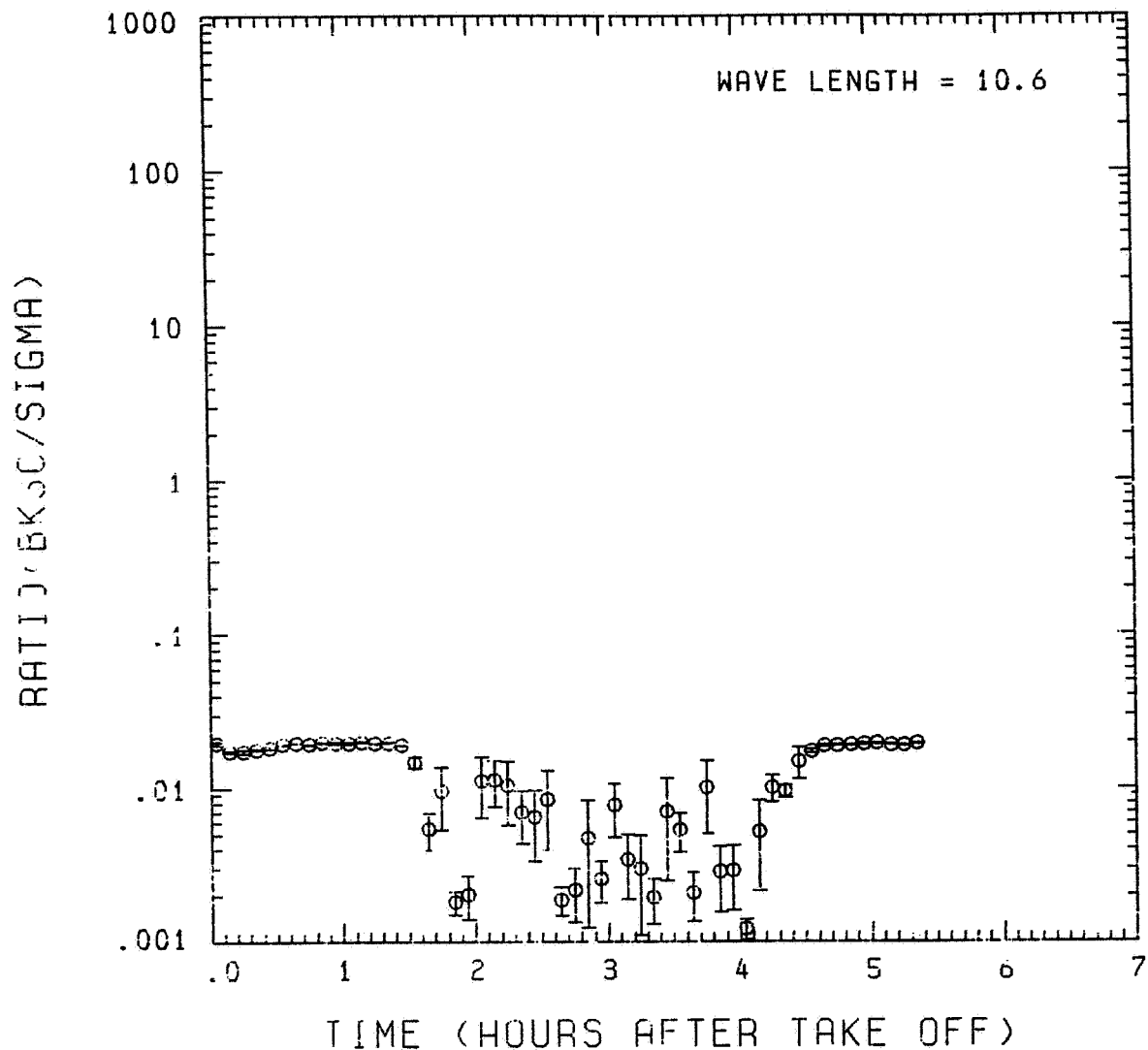


Fig. A16 (i). GAMETAG flight data for May 12, 1978.
 Calculated ratios for backscatter to extinction for
 five-minute data sets for $\lambda = 10.6 \mu\text{m}$.

Table A17. Significant times for May 14, 1978.
Johnston Atoll to Hilo, Hawaii.

Significant Points

<u>#</u>	<u>TIME</u>	
1	2:00	Johnston Atoll
2	2:32	
3	3:27	
4	3:37	
5	3:44	
6	4:05 (Alt.) - 4:03 (Long.)	
7	4:45	
8	4:54	
9	5:36	
10	6:32	
11	6:38	
12	7:01	
13	7:35	
14	7:45	
15	7:59	Hilo

ORIGINAL PAGE IS
OF POOR QUALITY

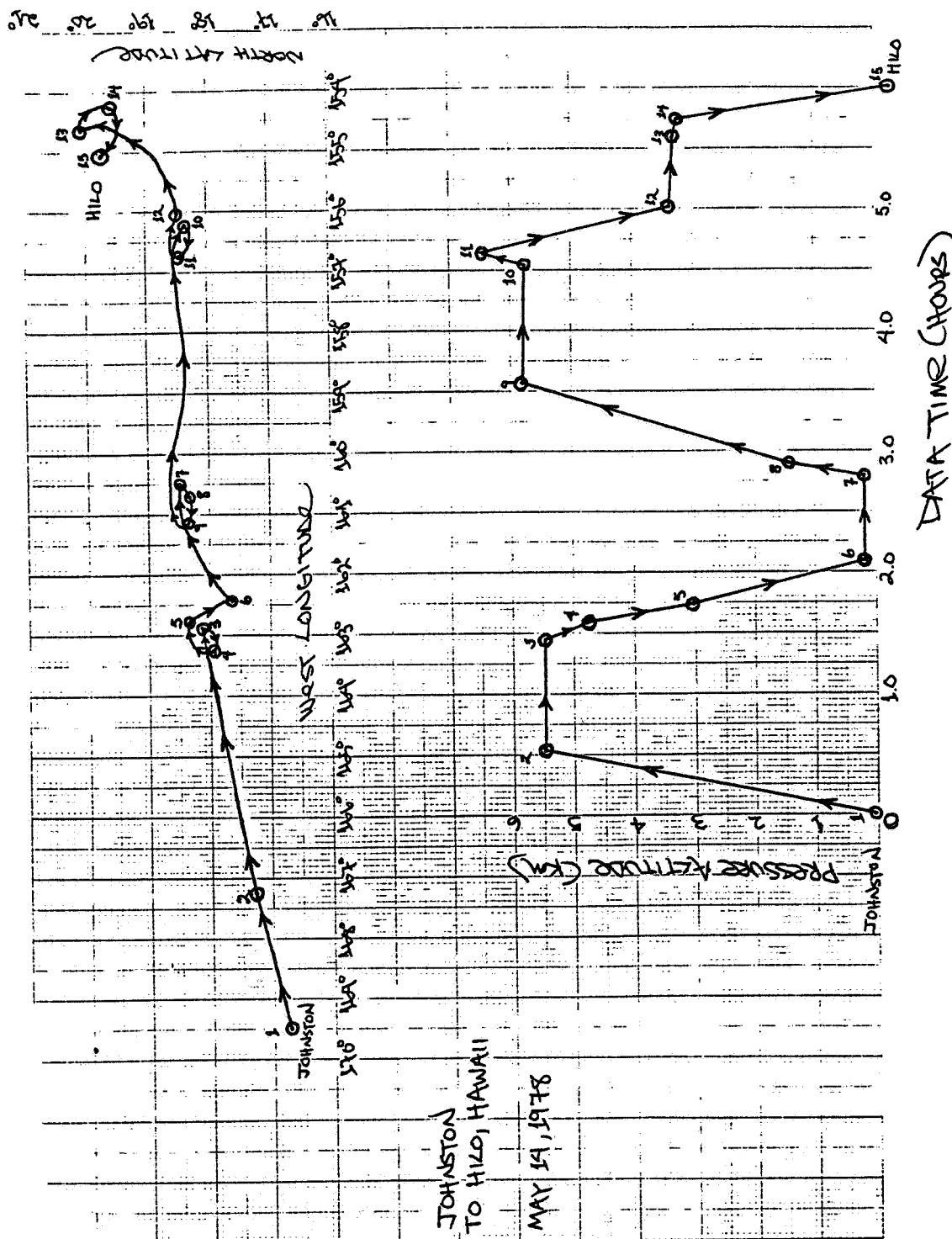


Fig. A17 (a). GAMETAG flight data for May 14, 1978.
Altitude and location flight track plotted as a
function of time after takeoff.

Knollenberg Data
DATE=MAY 14, 1978

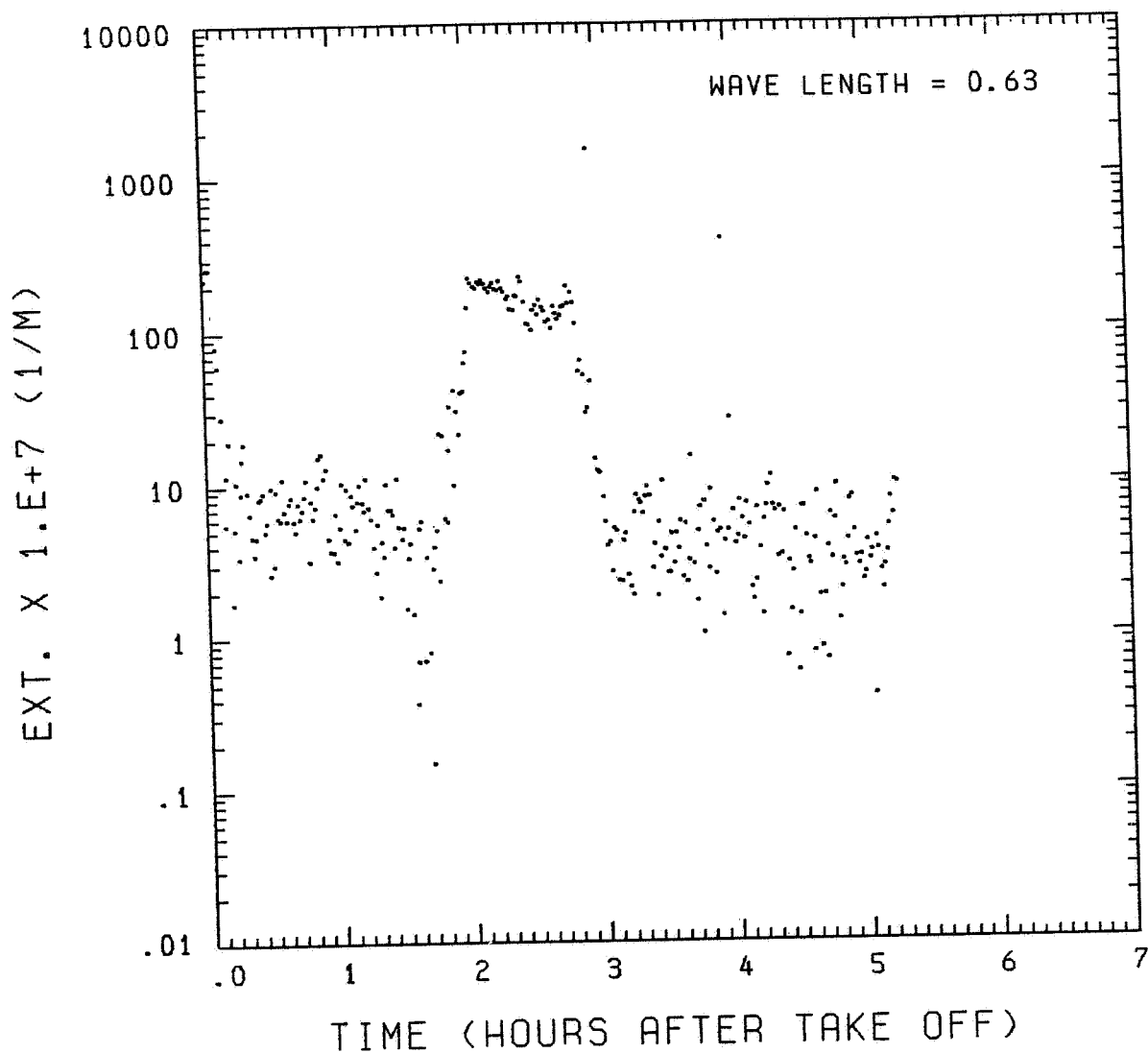


Fig. A17 (b). GAMETAG flight data for May 14, 1978.
Calculated particulate extinction along the flight
track for one-minute data sets for $\lambda = 0.63 \mu\text{m}$.

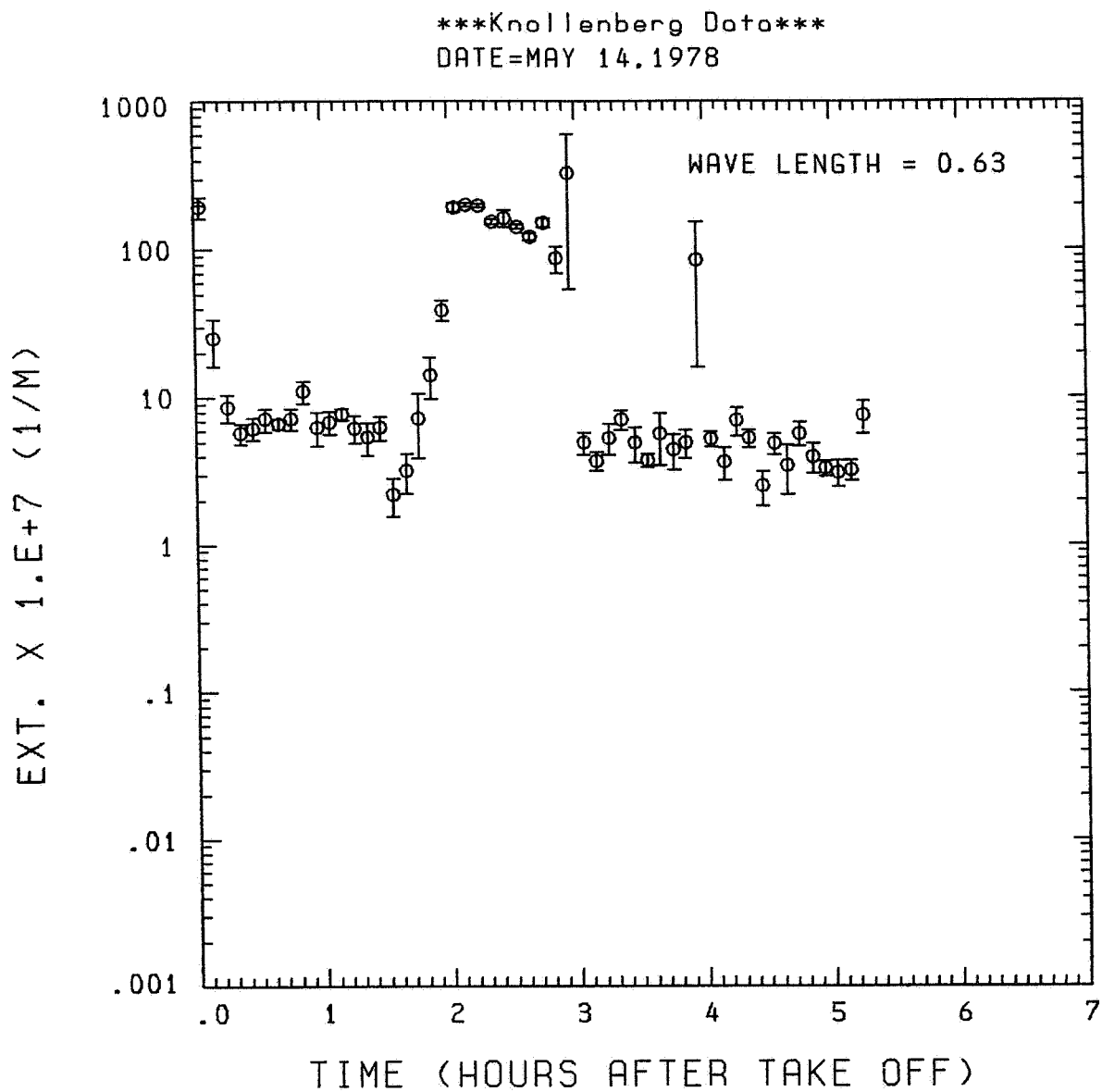


Fig. A17 (c). GAMETAG flight data for May 14, 1978.
Calculated particulate extinction along the flight
track for five-minute data sets for $\lambda = 0.63 \mu\text{m}$.

ORIGINAL PAGE IS
OF POOR QUALITY

Knollenberg Data
DATE=MAY 14, 1978

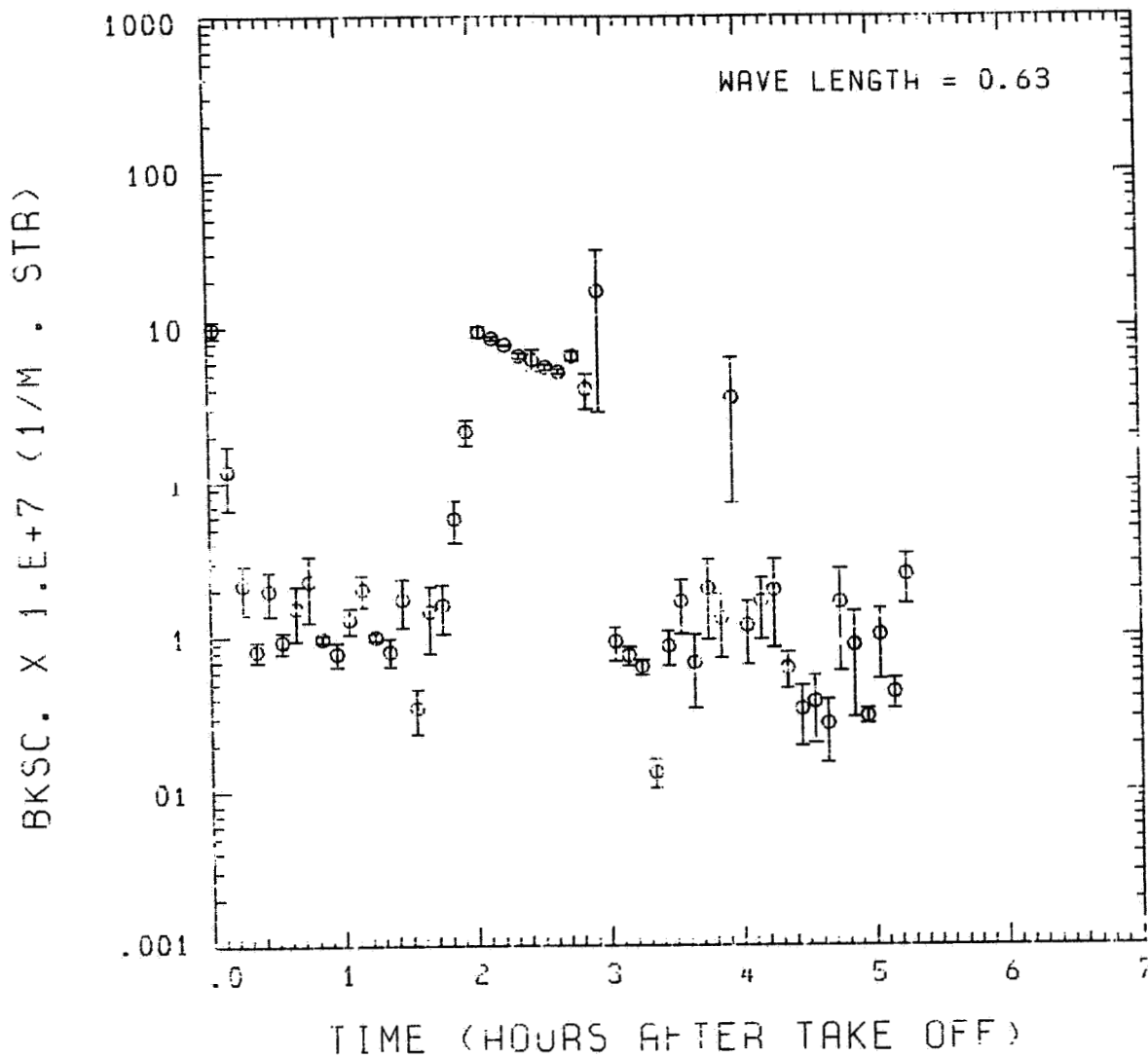


Fig. A17 (d). GAMETAG flight data for May 14, 1978.

Calculated backscatter coefficient along the flight
track for five-minute data sets for $\lambda = 0.63 \mu\text{m}$.

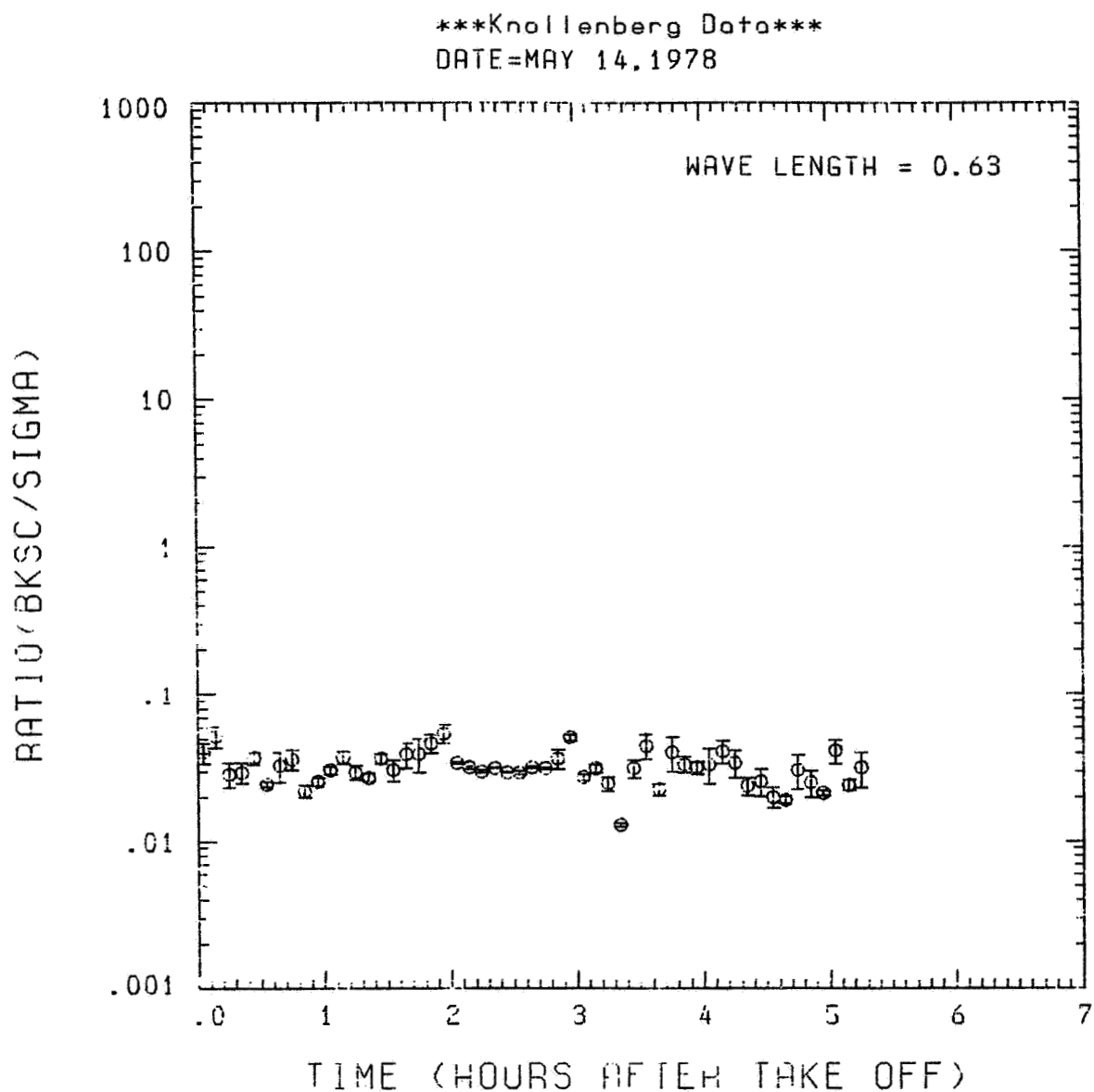


Fig. A17 (e). GAMETAG flight data for May 14, 1978.
Calculated ratios for backscatter to extinction for
five-minute data sets for $\lambda = 0.63 \mu\text{m}$.

ORIGINAL PAGE IS
OF POOR QUALITY

Knollenberg Data
DATE=MAY 14.1978

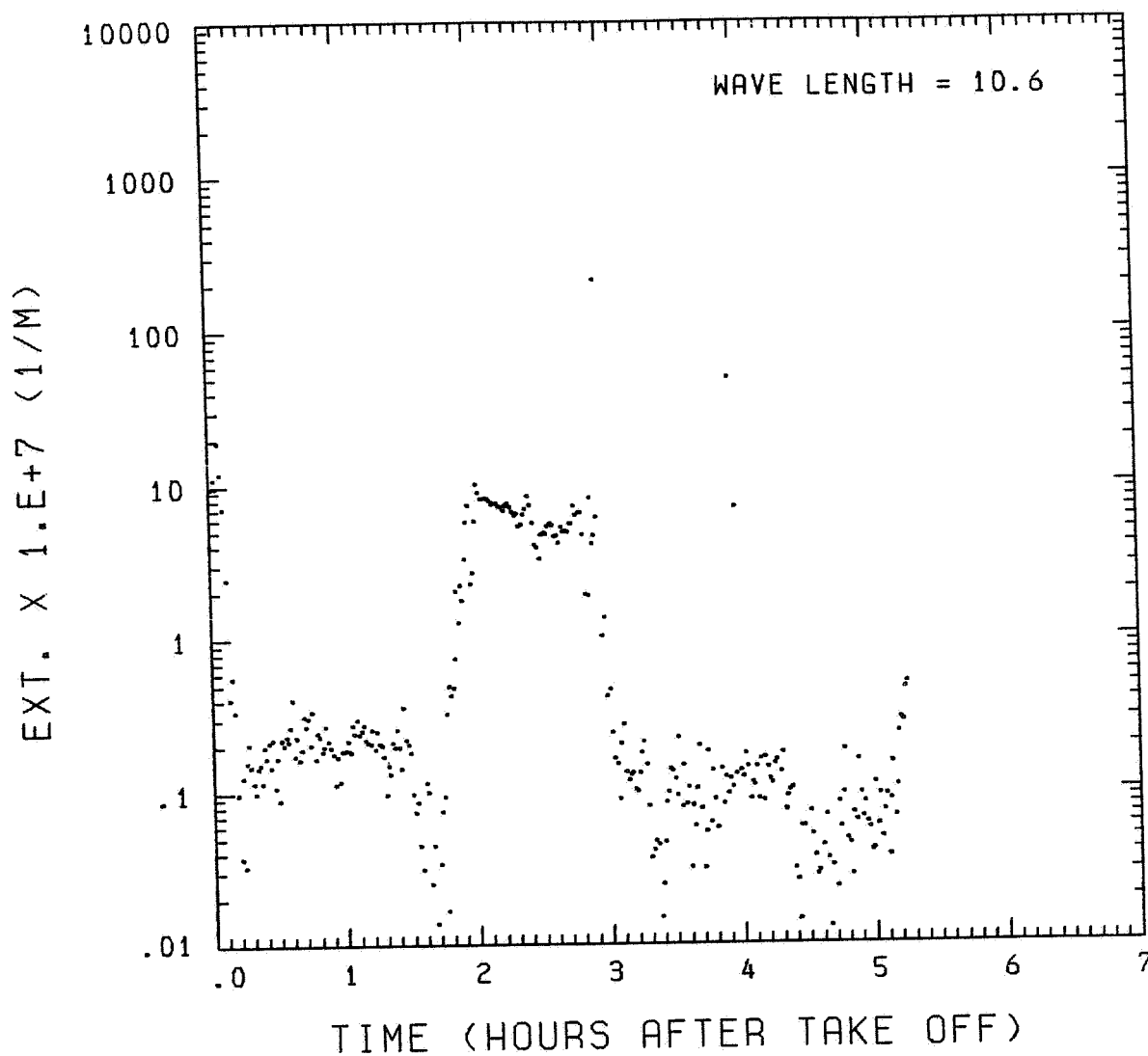


Fig. A17 (f). GAMETAG flight data for May 14, 1978.
Calculated particulate extinction along the flight
track for one-minute data sets for $\lambda = 10.6 \mu\text{m}$.

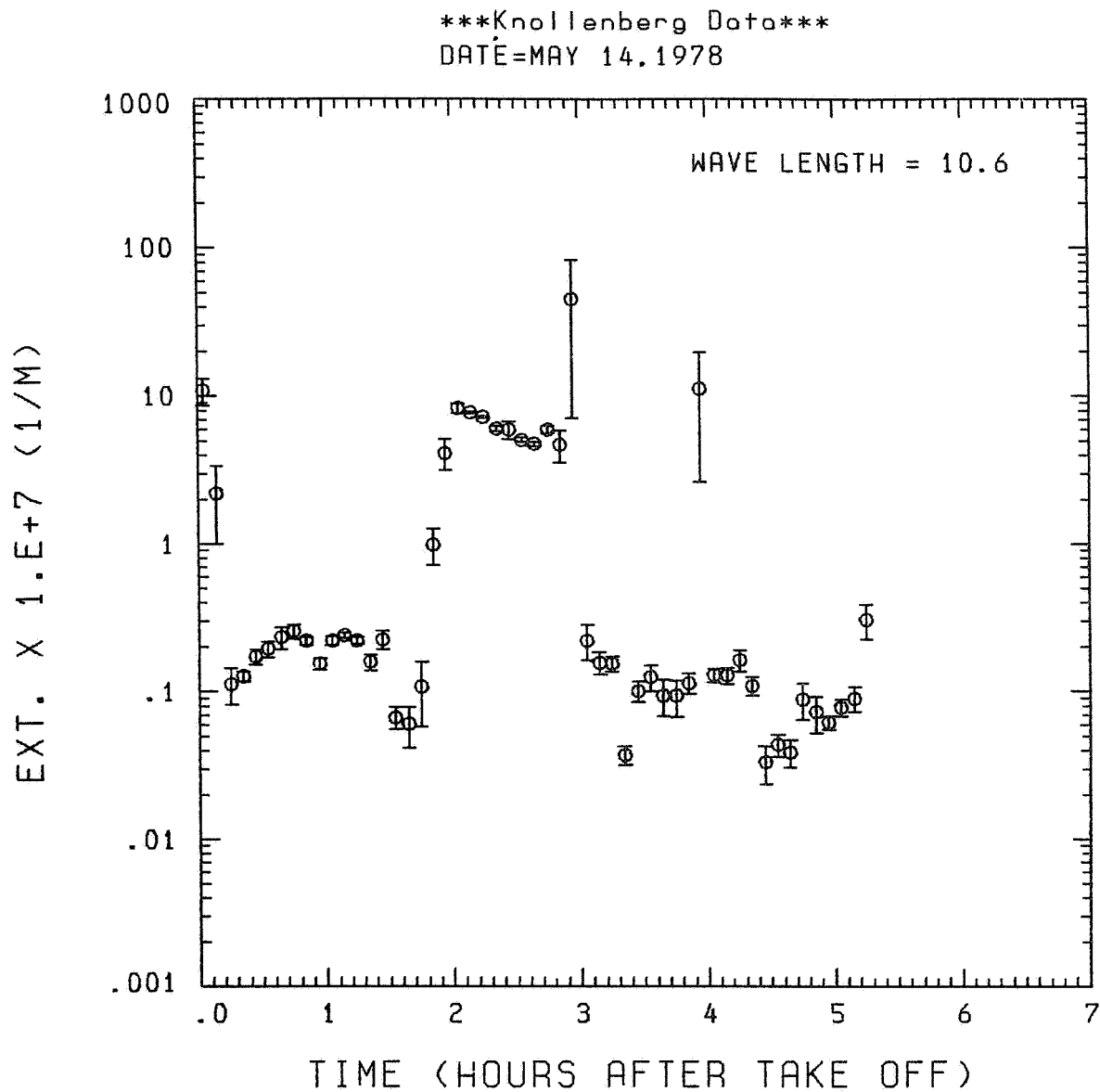


Fig. A17(g). GAMETAG flight data for May 14, 1978.

Calculated particulate extinction along the flight track for five-minute data sets for $\lambda = 10.6 \mu\text{m}$.

ORIGINAL PAGE IS
OF POOR QUALITY

Knollenberg Data
DATE=MAY 14, 1978

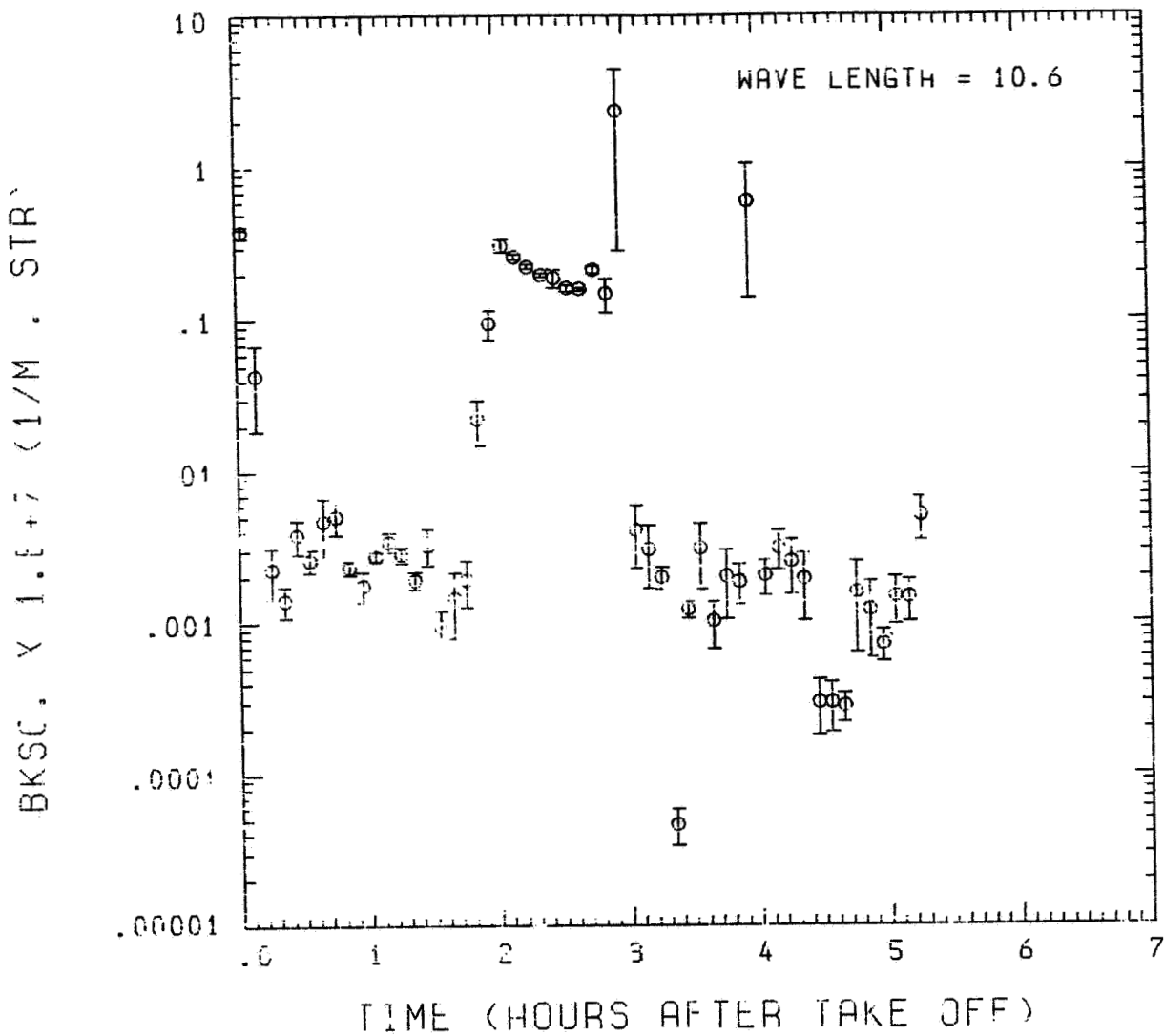


Fig. A17(h). GAMETAG flight data for May 14, 1978.
Calculated backscatter coefficient along the flight
track for five-minute data sets for $\lambda = 10.6 \mu m$.

Knollenberg Data

DATE=MAY 14.1978

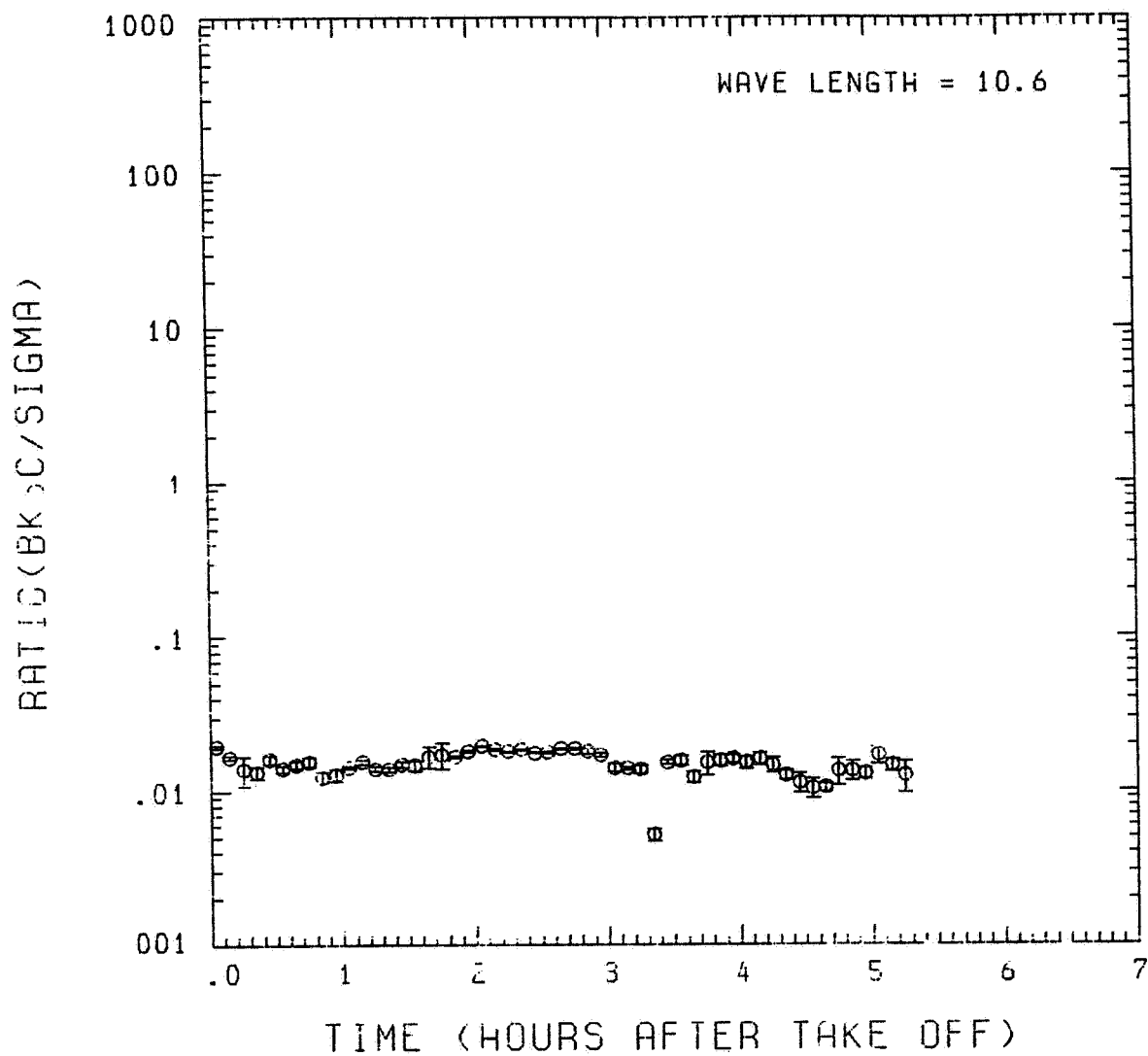


Fig. A 17 (i). GAMETAG flight data for May 14, 1978.

Calculated ratios for backscatter to extinction for
five-minute data sets for $\lambda = 10.6 \mu\text{m}$.

Table A18. Significant tiems for May 18, 1978.
Moffett Field, California to
Denver, Colorado.

Significant Points

<u>#</u>	TIME	
1	17:56	Moffett Field
2	18:21	
3	20:23	
4	20:40	
5	20:57	Denver

ORIGINAL PAGE IS
OF POOR QUALITY

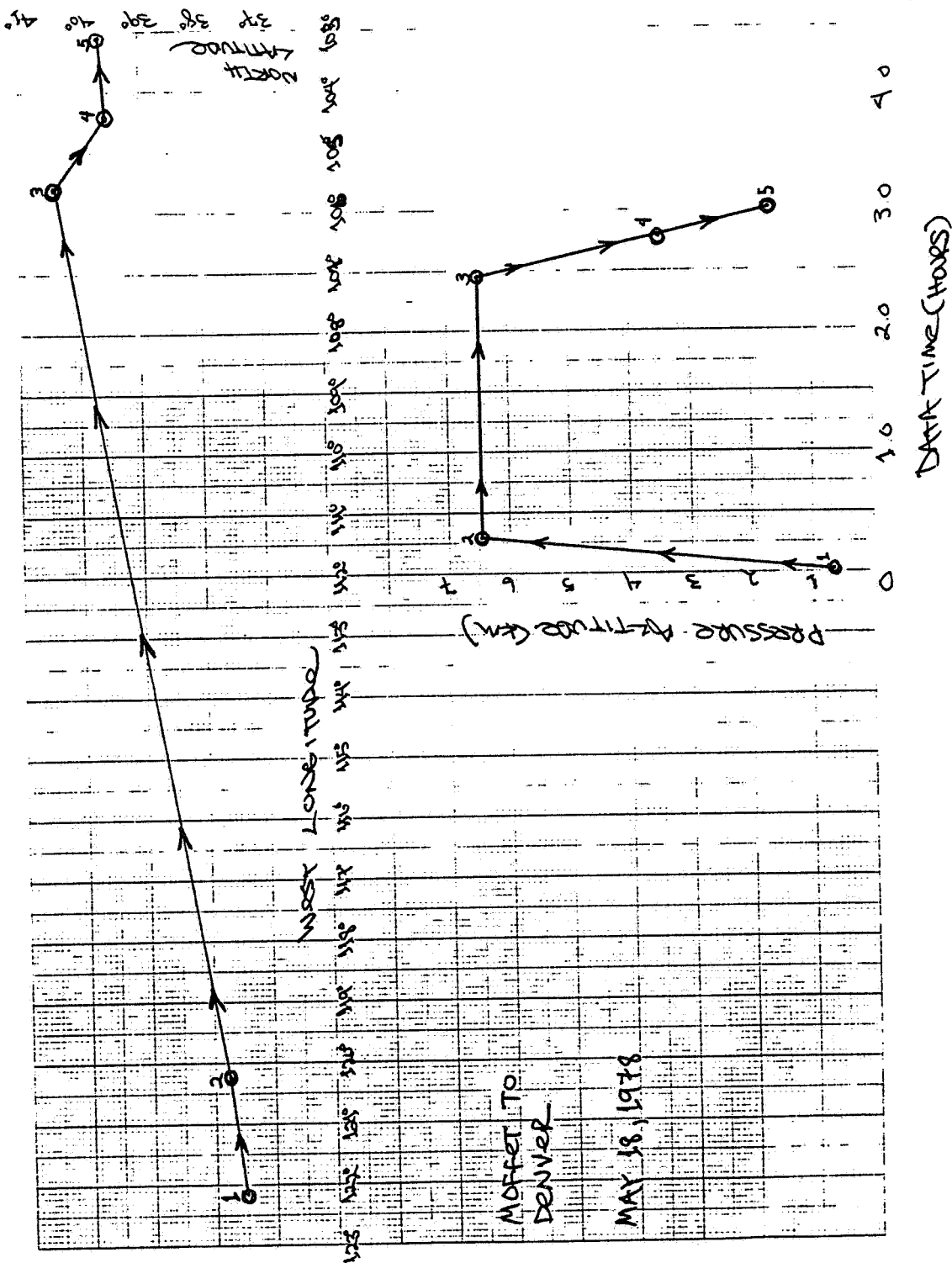


Fig. A 18 (a). GAMETAG flight data for May 18, 1978.
Altitude and location flight track plotted as a
function of time after takeoff.

Knollenberg Data
DATE=MAY 18, 1978

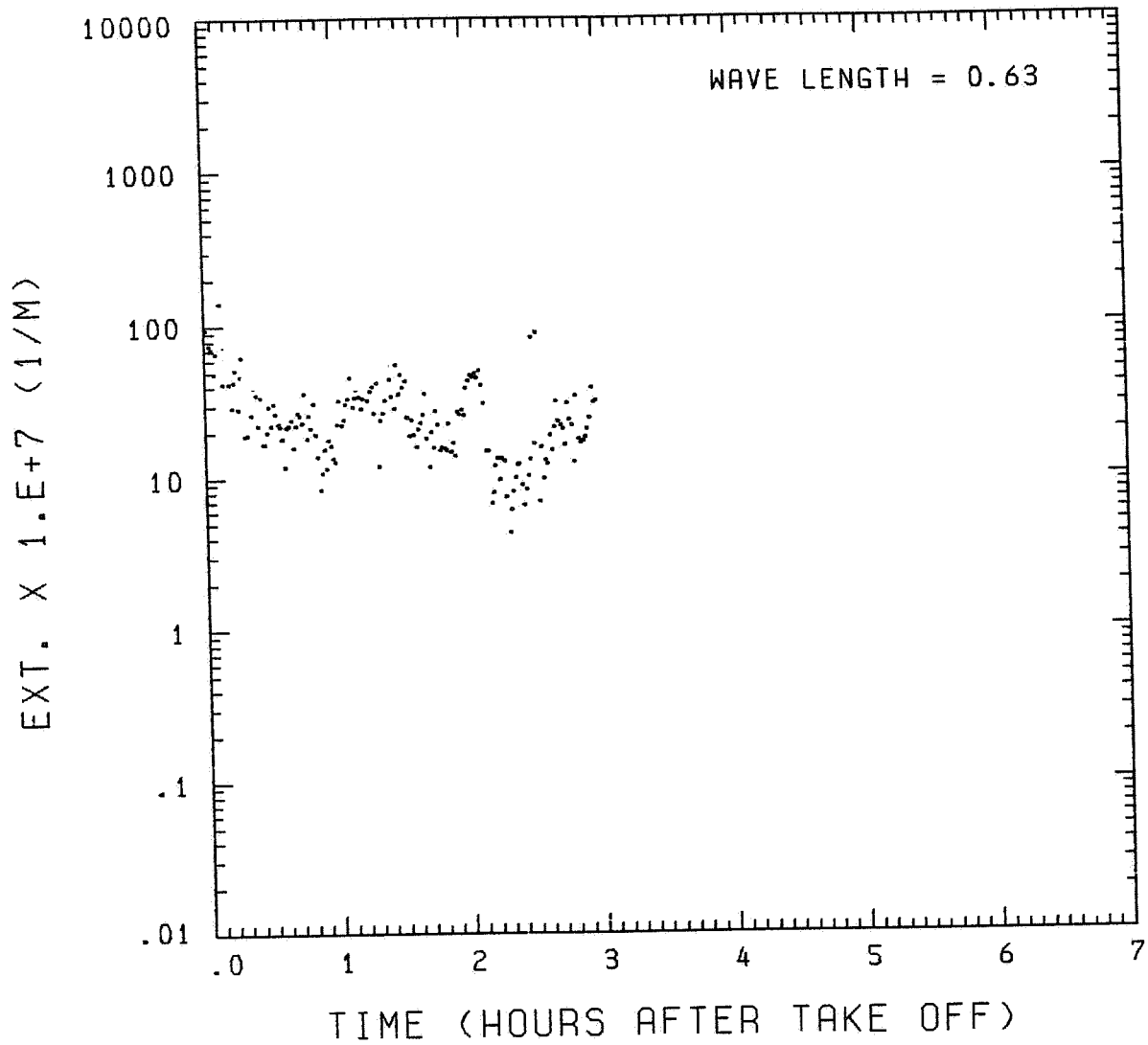


Fig. A18 (b). GAMETAG flight data for May 18, 1978.
Calculated particulate extinction along the flight
track for one-minute data sets for $\lambda = 0.63 \mu\text{m}$.

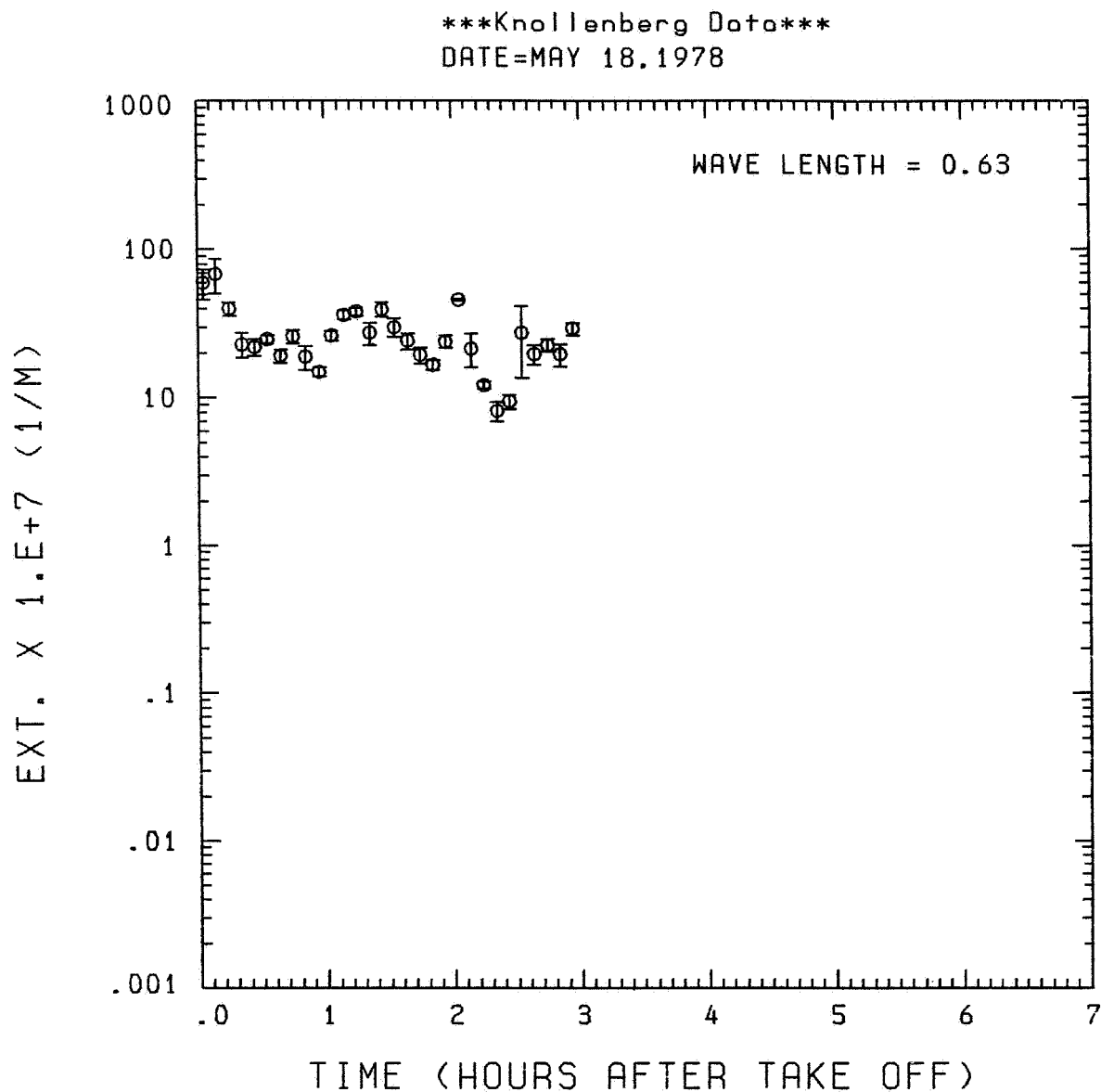


Fig. A18 (c). GAMETAG flight data for May 18, 1978.
Calculated particulate extinction along the flight
track for five-minute data sets for $\lambda = 0.63 \mu\text{m}$.

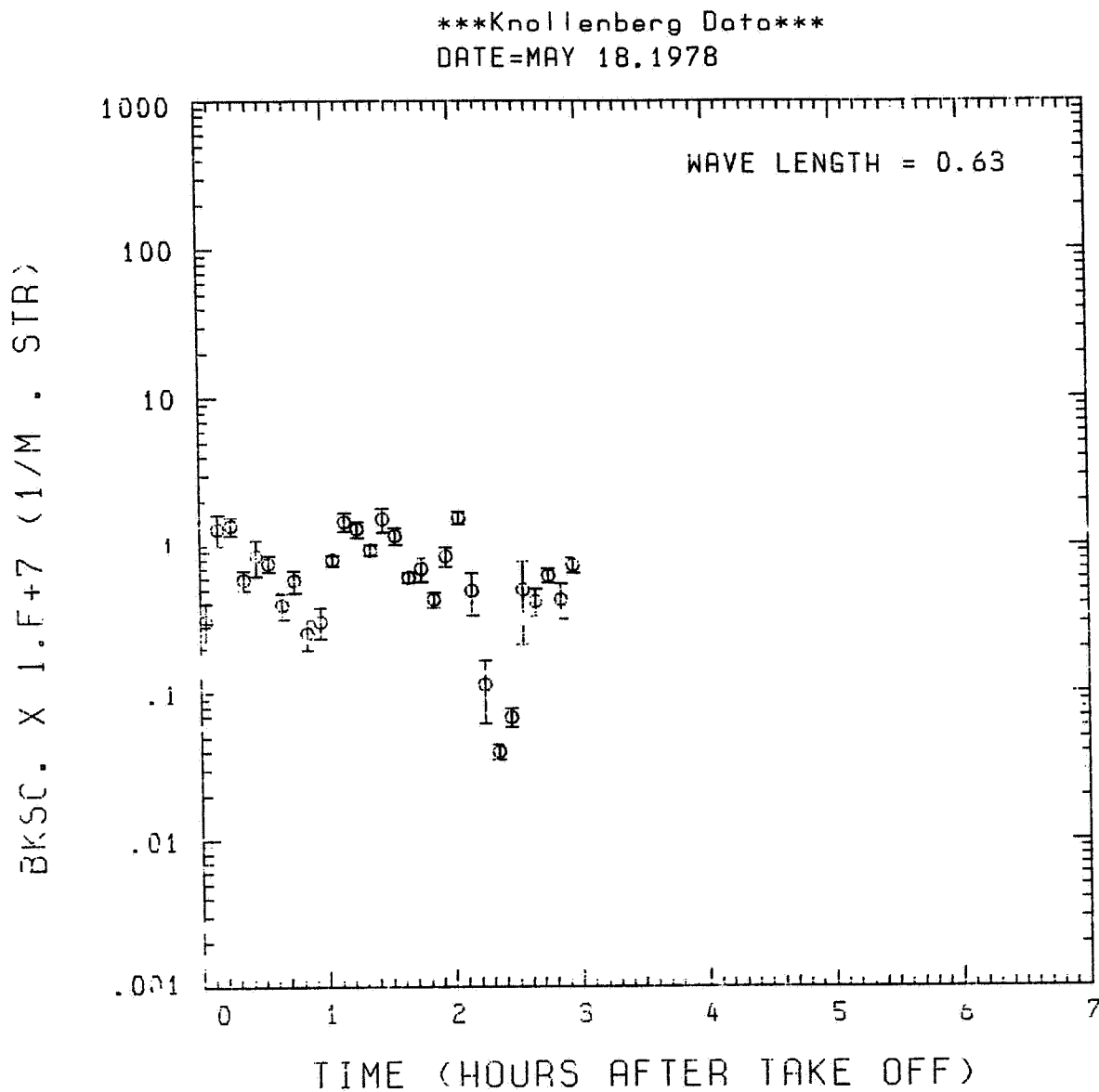


Fig. A18(d). GAMETAG flight data for May 18, 1978.
Calculated backscatter coefficient along the flight
track for five-minute data sets for $\lambda = 0.63 \mu\text{m}$.

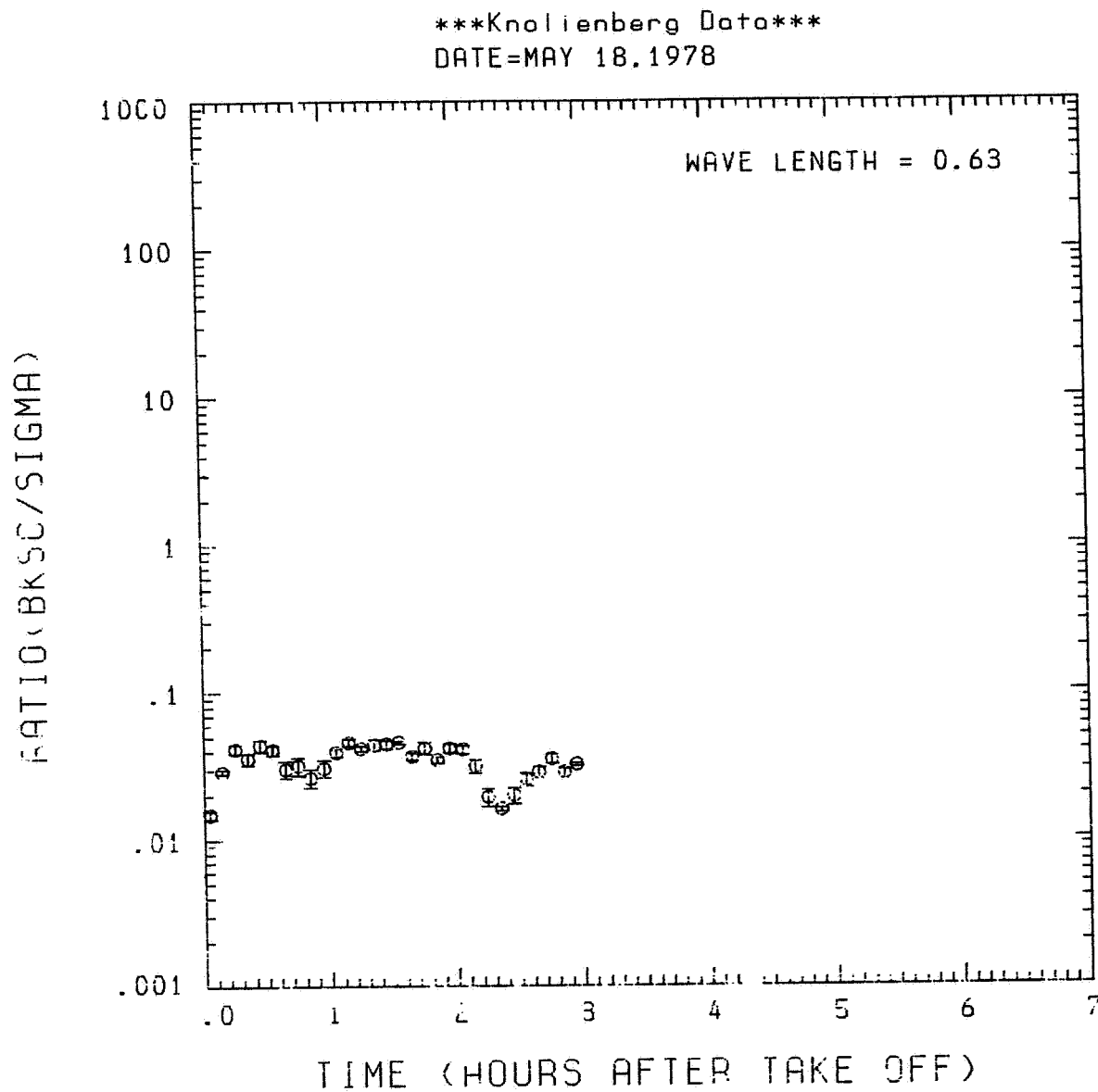


Fig. A 18(e). GAMETAG flight data for May 18, 1978.

Calculated ratios for backscatter to extinction for
five-minute data sets for $\lambda = 0.63 \mu\text{m}$.

Knollenberg Data
DATE=MAY 18,1978

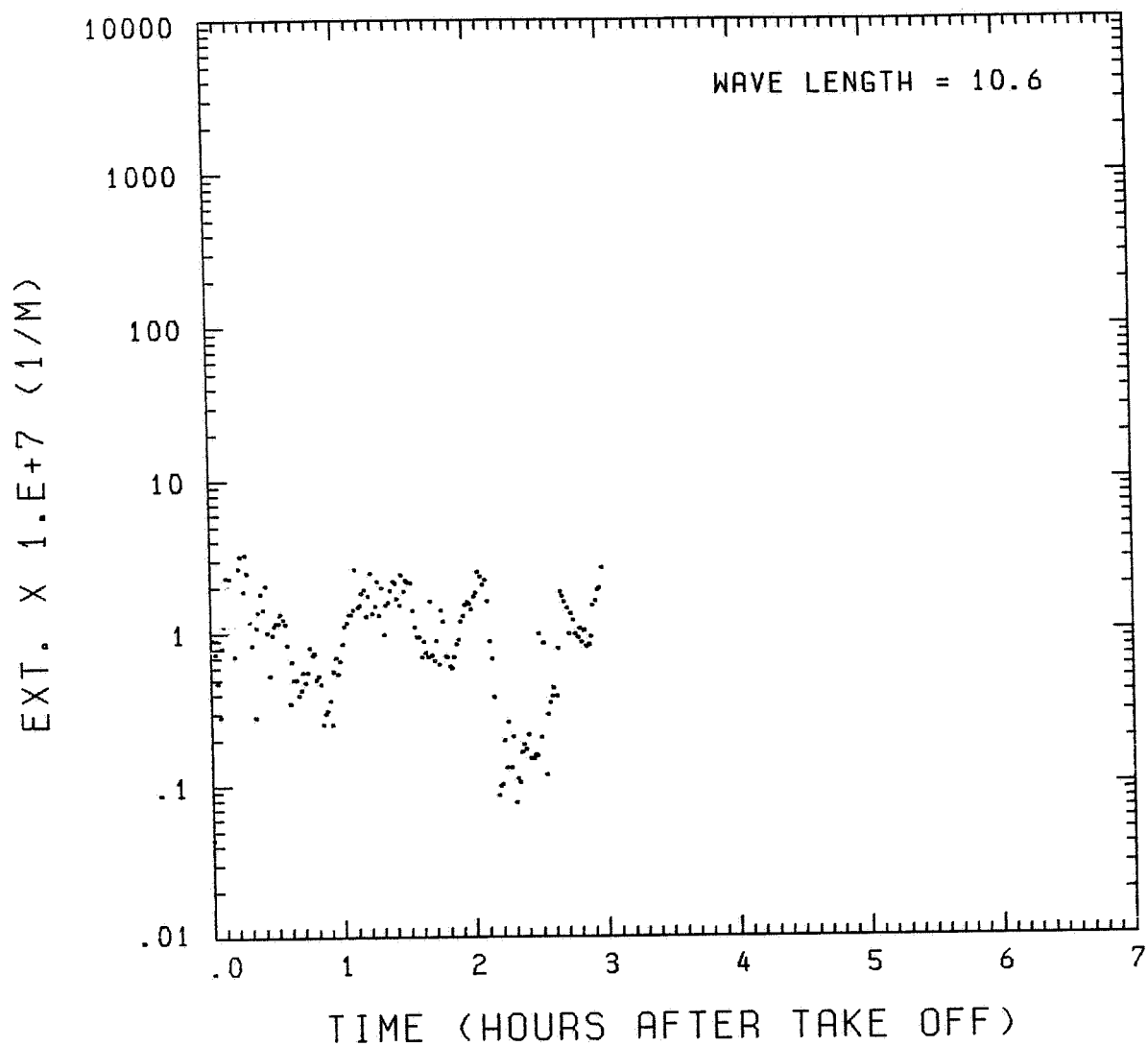


Fig. A 18(f). GAMETAG flight data for May 18, 1978.
Calculated particulate extinction along the flight
track for one-minute data sets for $\lambda = 10.6 \mu\text{m}$.

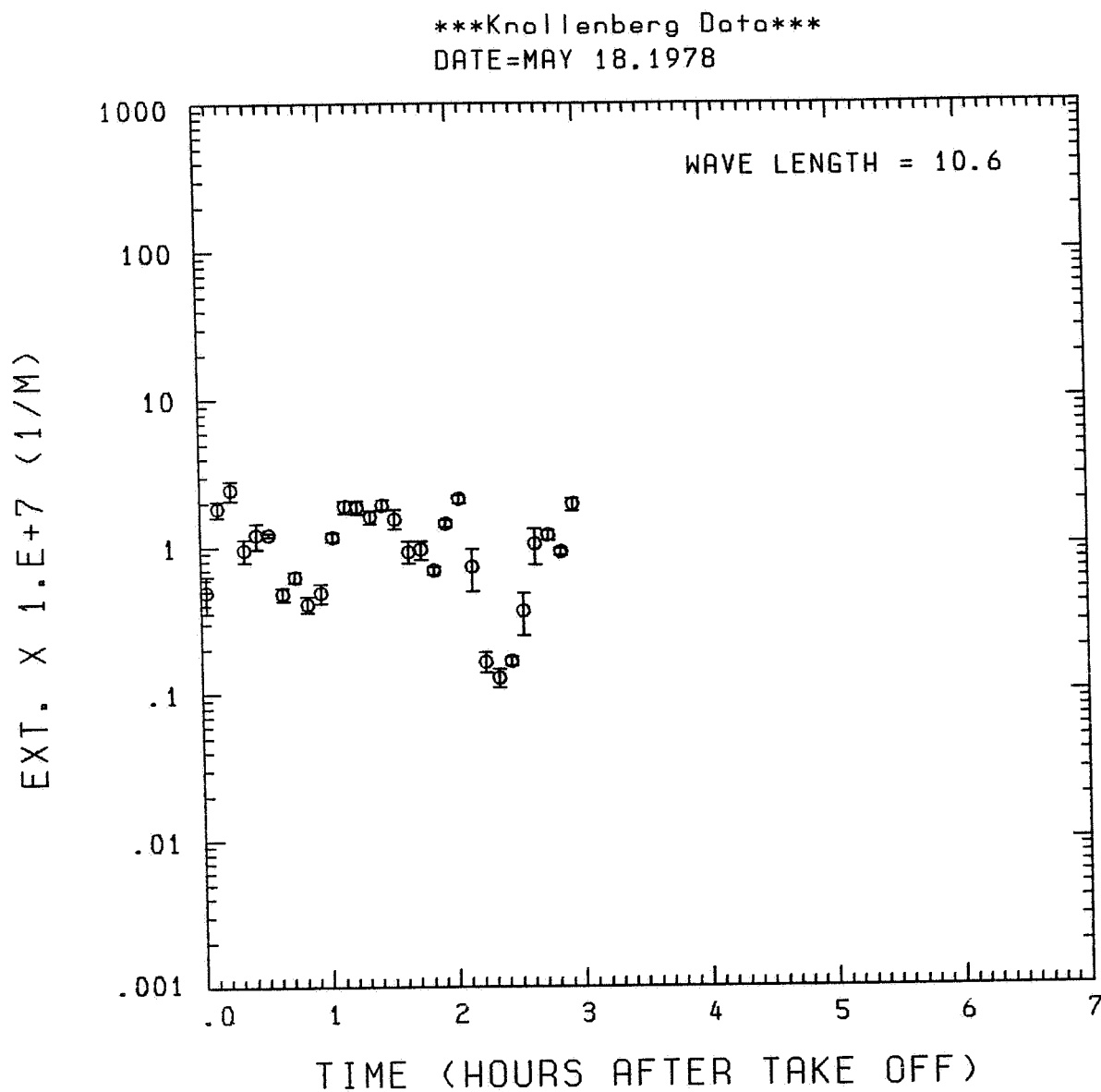


Fig. A 18(g). GAMETAG flight data for May 18, 1978.
Calculated particulate extinction along the flight
track for five-minute data sets for $\lambda = 10.6 \mu\text{m}$.

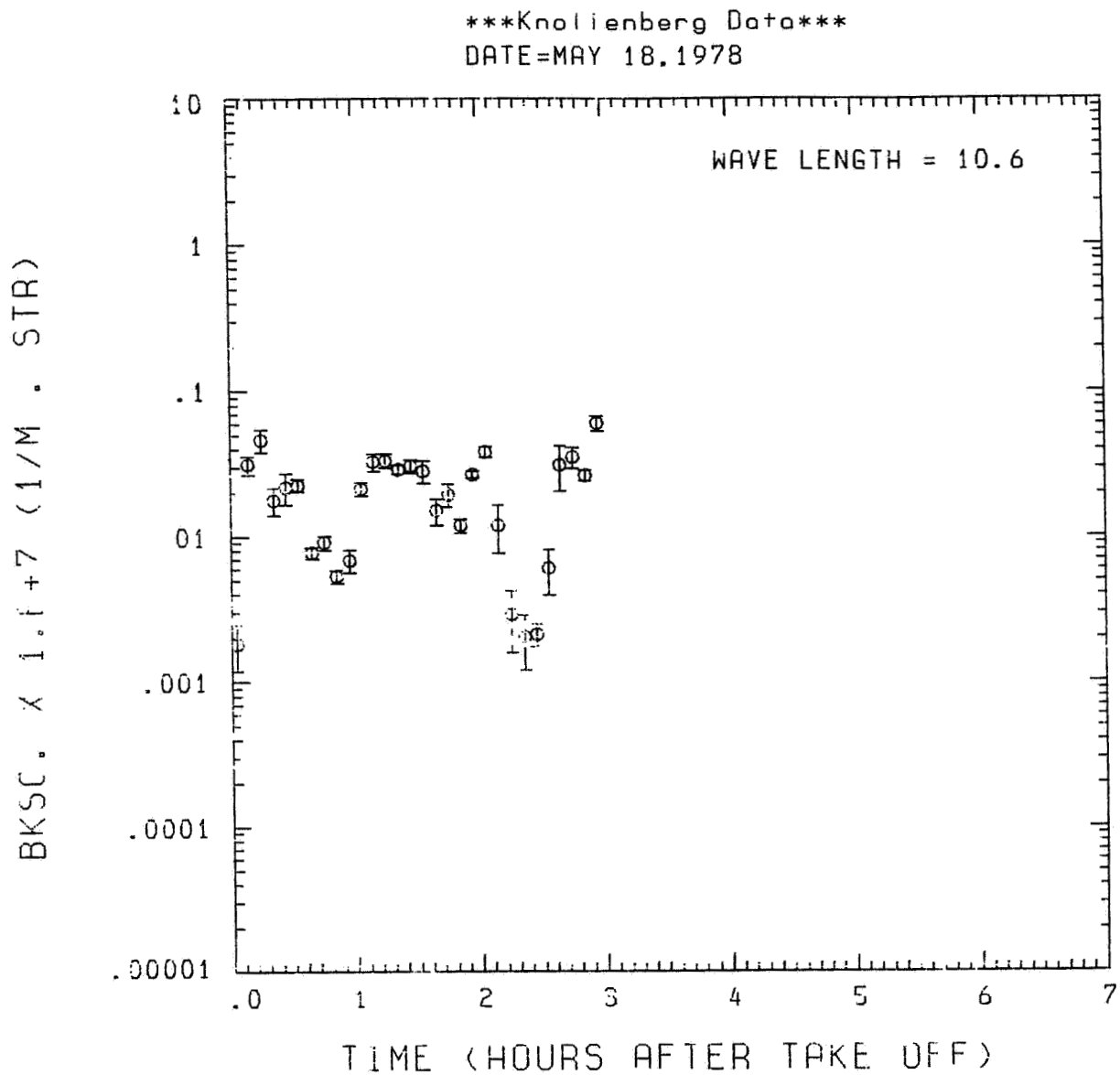


Fig. A 18(h). GAMETAG flight data for May 18, 1978.
Calculated backscatter coefficient along the flight track for five-minute data sets for $\lambda = 10.6 \mu\text{m}$.

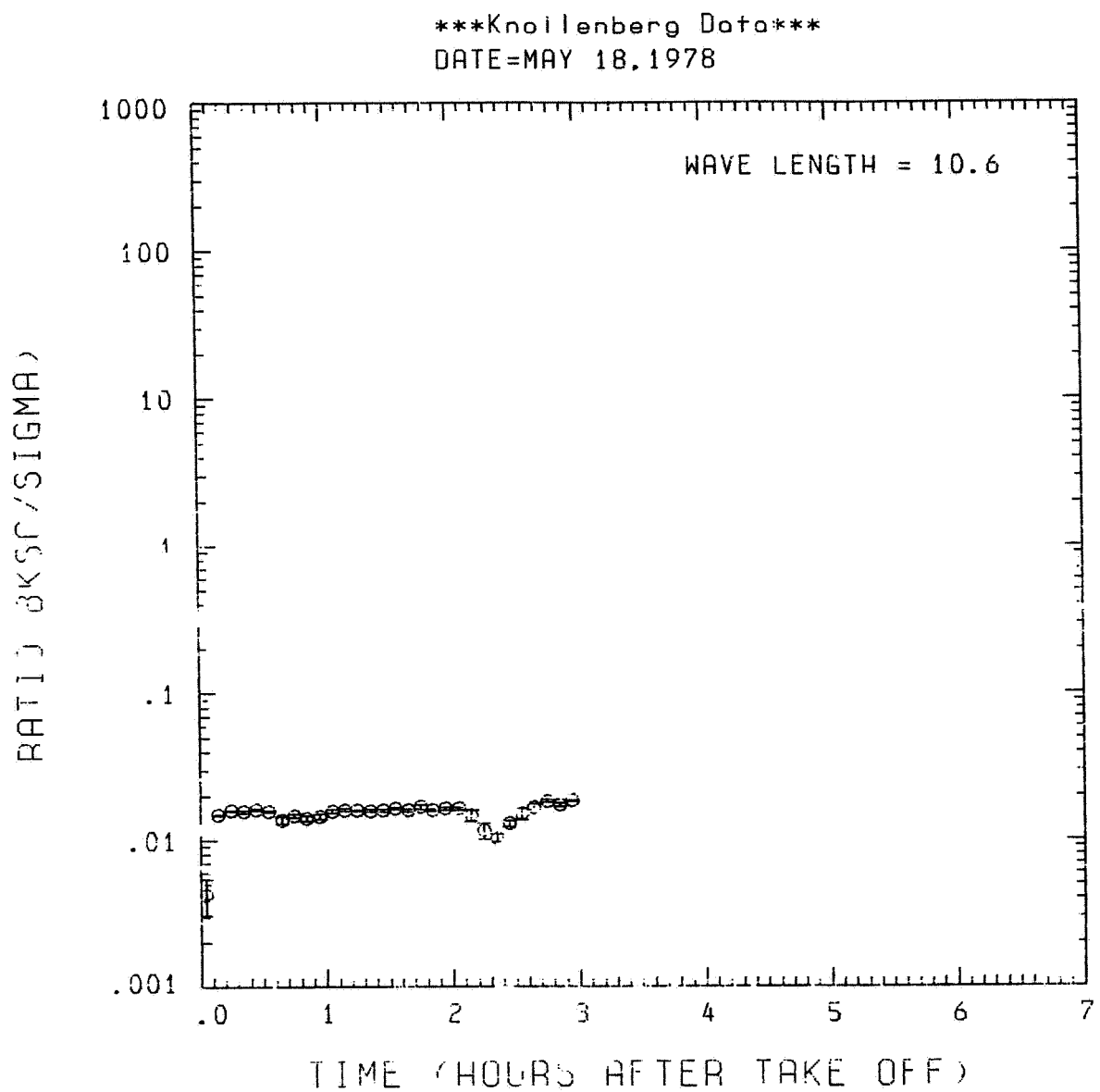


Fig. A 18 (i). GAMETAG flight data for May 18, 1978.
Calculated ratios for backscatter to extinction for
five-minute data sets for $\lambda = 10.6 \mu\text{m}$.

Table A19. Significant tiems for May 27, 1978.
 Denver, Colorado to Great Falls,
 Montana.

Significant Points

<u>#</u>	<u>TIME</u>	
1	22:04	Denver
2	22:44	
3	23:44	
4	0:00	
5	0:13	
6	0:21	Great Falls

ORIGINAL PAGE IS
OF POOR QUALITY

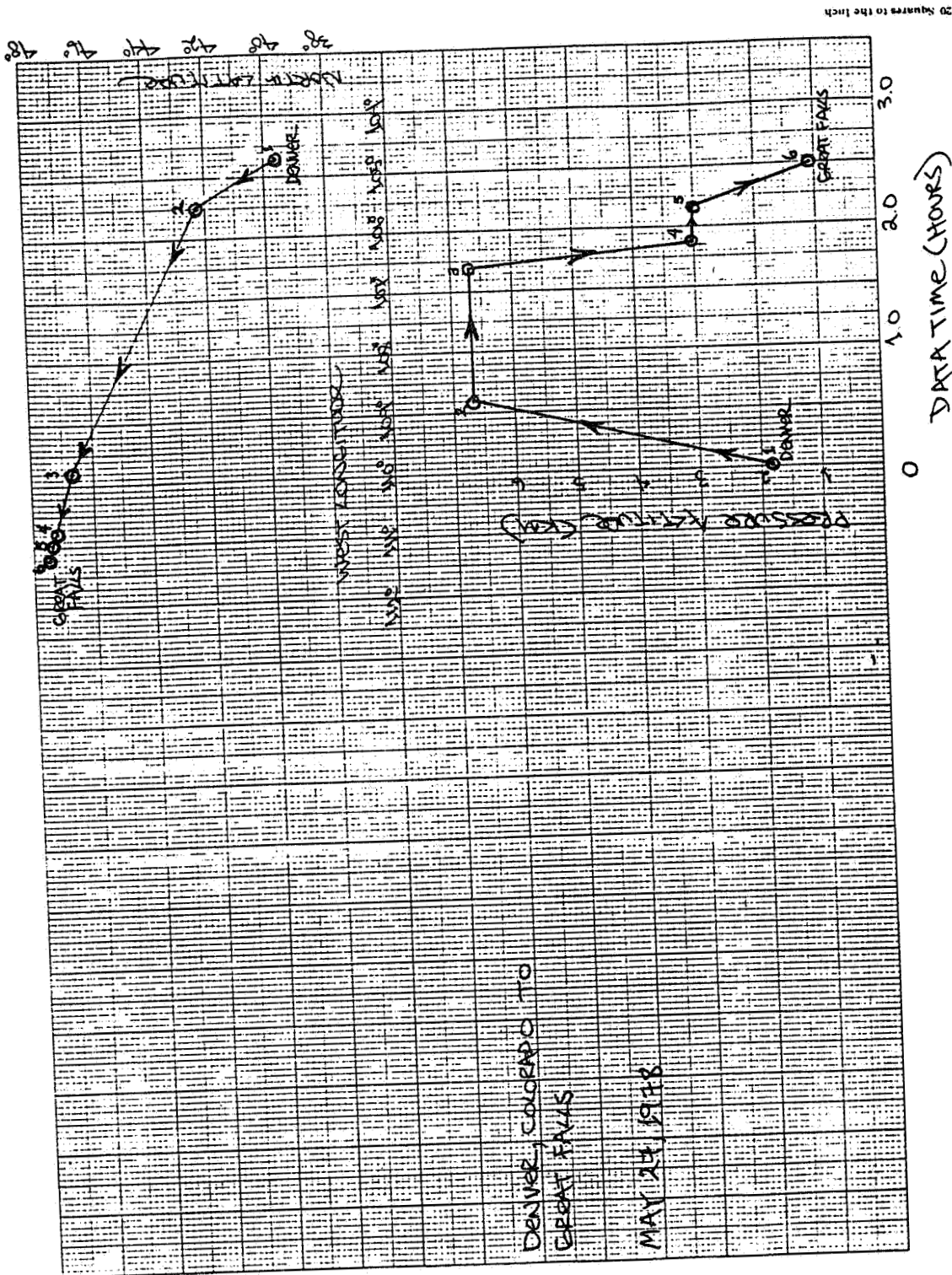


Fig. A 19 (a). GAMETAG flight data for May 27, 1978.
Altitude and location flight track plotted as a
function of time after takeoff.

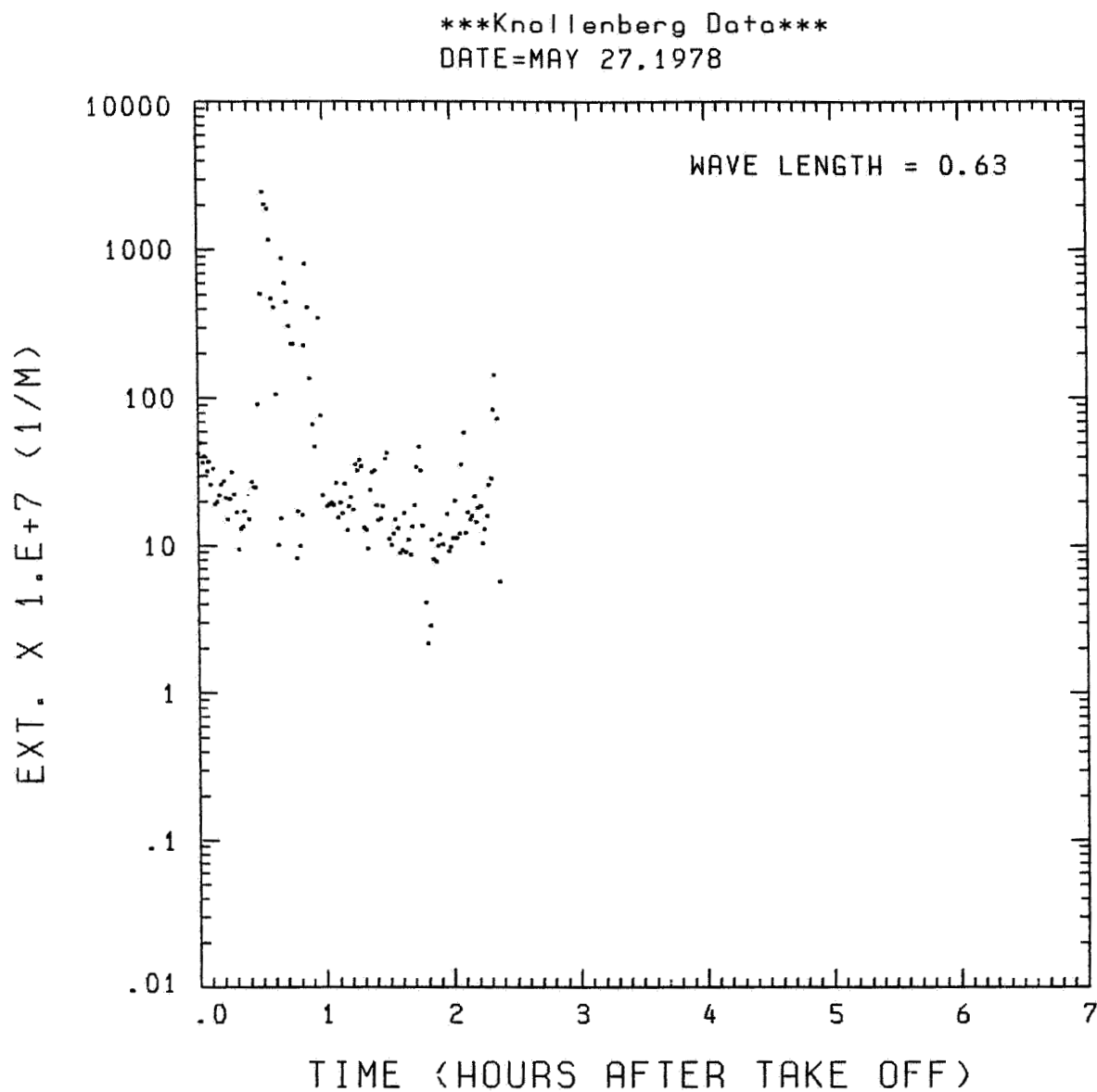


Fig. A 19 (b). GAMETAG flight data for May 27, 1978.
Calculated particulate extinction along the flight
track for one-minute data sets for $\lambda = 0.63 \mu\text{m}$.

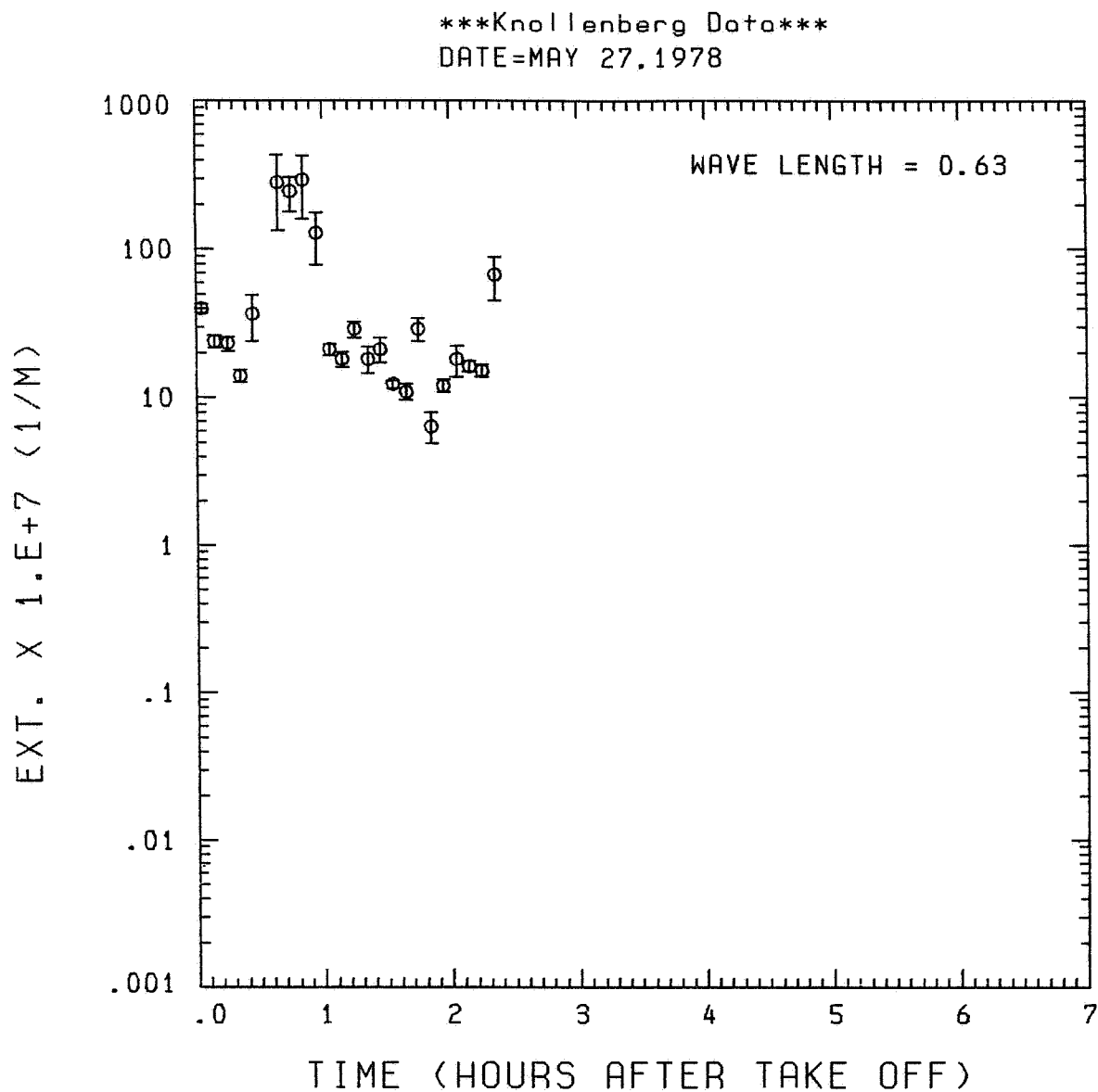


Fig. A19(c). GAMETAG flight data for May 27, 1978.

Calculated particulate extinction along the flight track for five-minute data sets for $\lambda = 0.63 \mu\text{m}$.

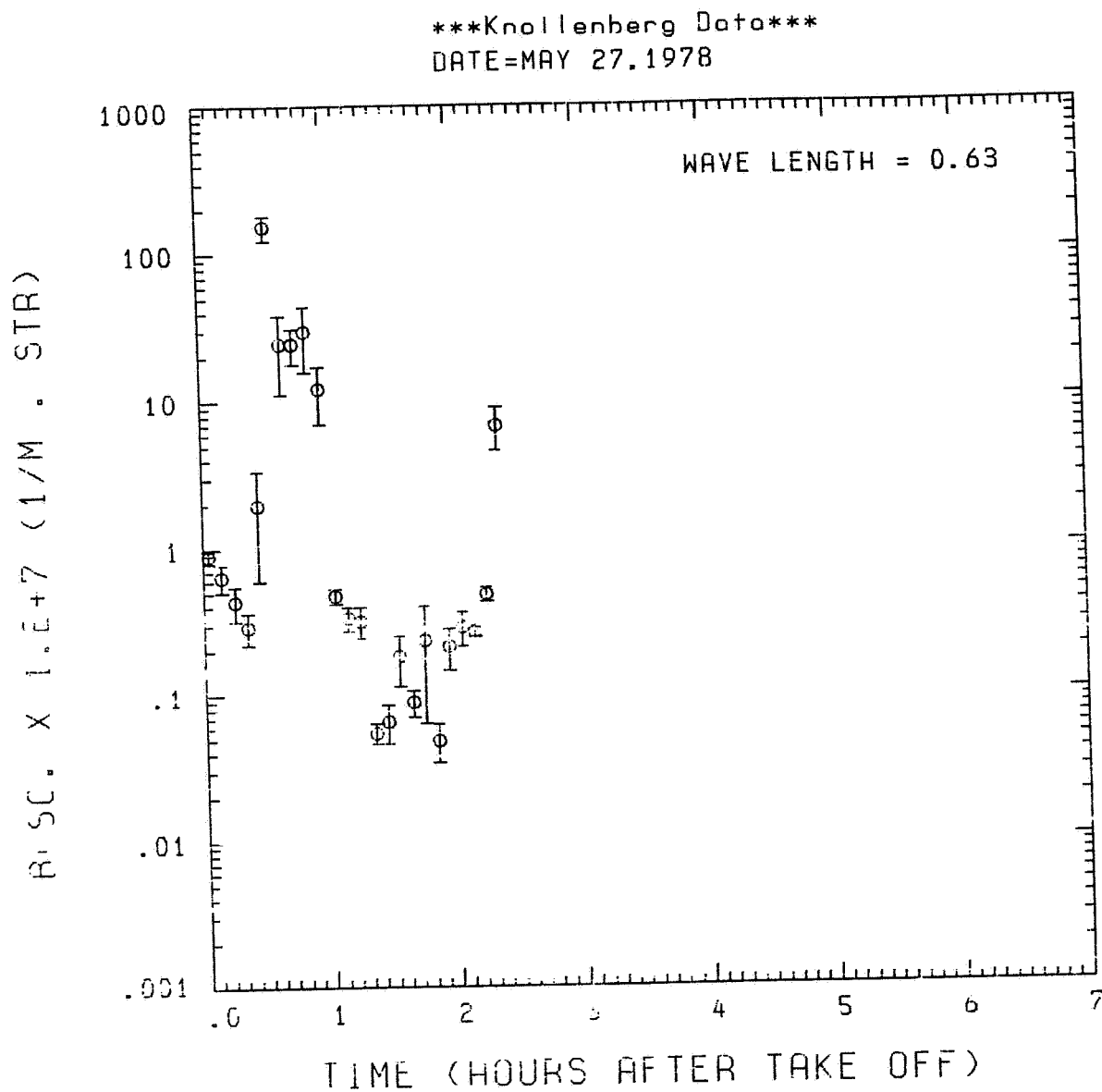


Fig. A19(d). GAMETAG flight data for May 27, 1978.
Calculated backscatter coefficient along the flight
track for five-minute data sets for $\lambda = 0.63 \mu\text{m}$.

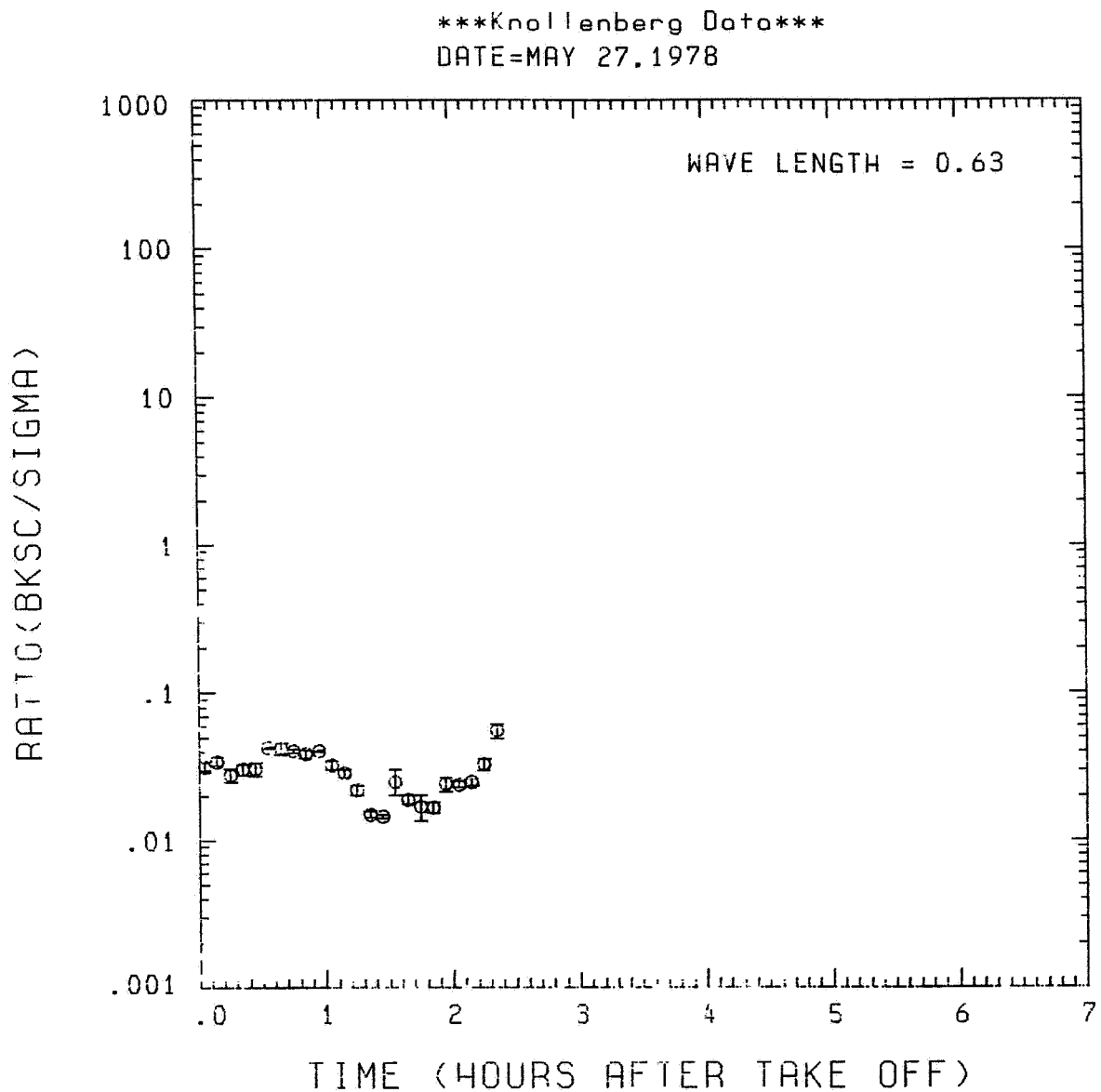


Fig. A19(e). GAMETAG flight data for May 27, 1978.

Calculated ratios for backscatter to extinction for
five-minute data sets for $\lambda = 0.63 \mu\text{m}$.

ORIGINAL PAGE IS
OF POOR QUALITY

Knollenberg Data
DATE=MAY 27.1978

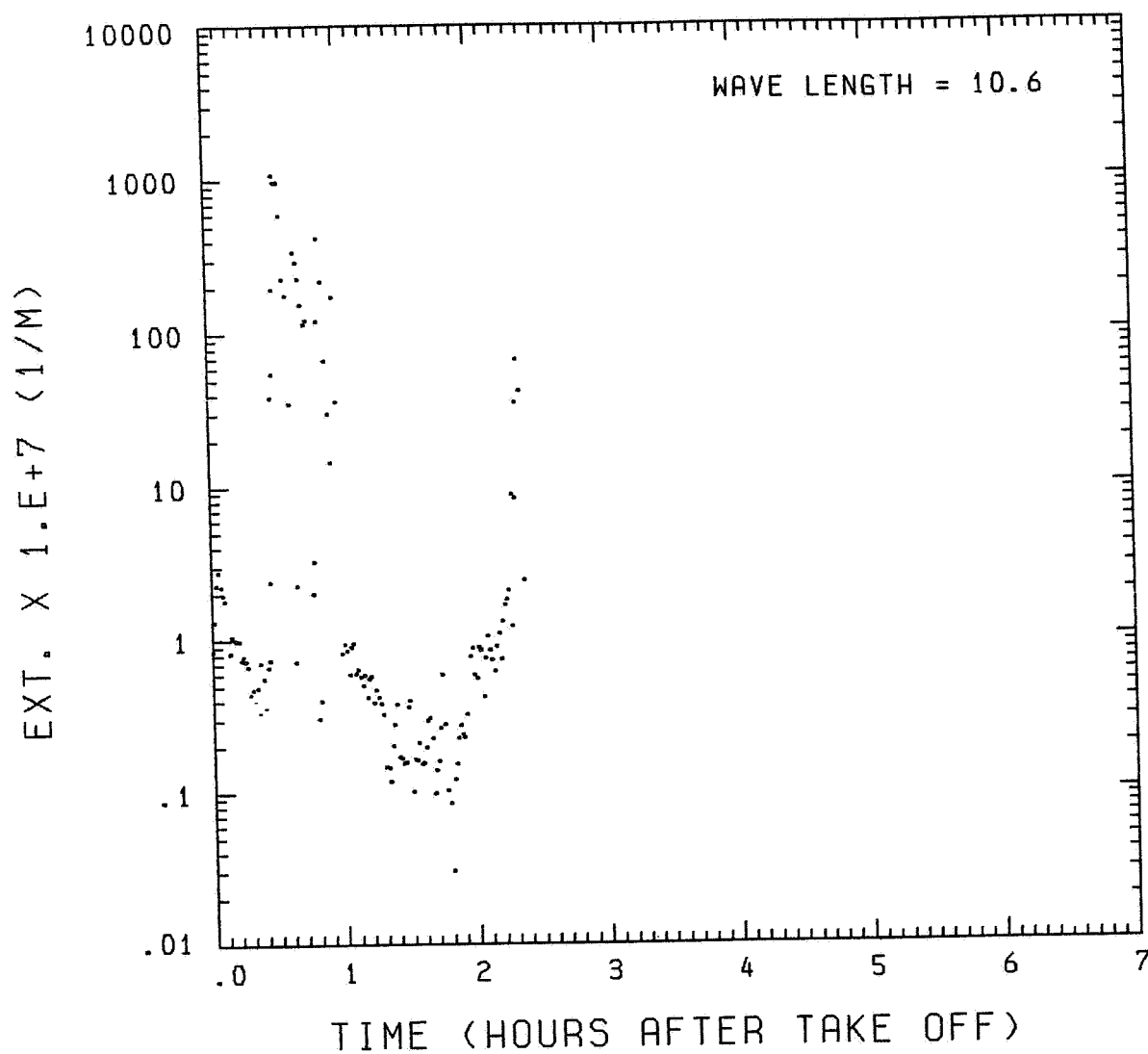


Fig. A 19 (f). GAMETAG flight data for May 27, 1978.
Calculated particulate extinction along the flight
track for one-minute data sets for $\lambda = 10.6 \mu\text{m}$.

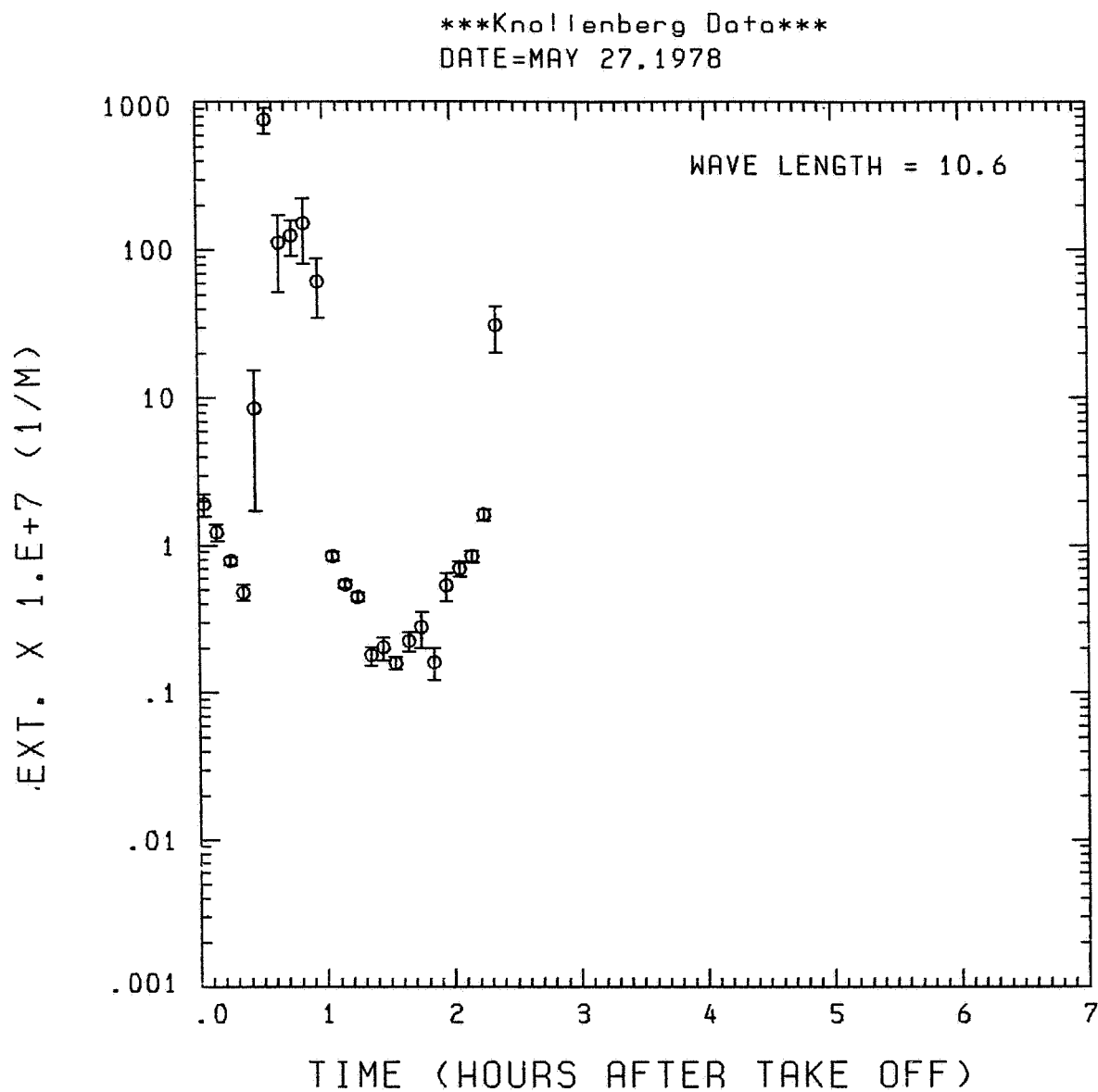


Fig. A 19(g). GAMETAG flight data for May 27, 1978.

Calculated particulate extinction along the flight track for five-minute data sets for $\lambda = 10.6 \mu\text{m}$.

Knollenberg Data
 DATE=MAY 27,1978

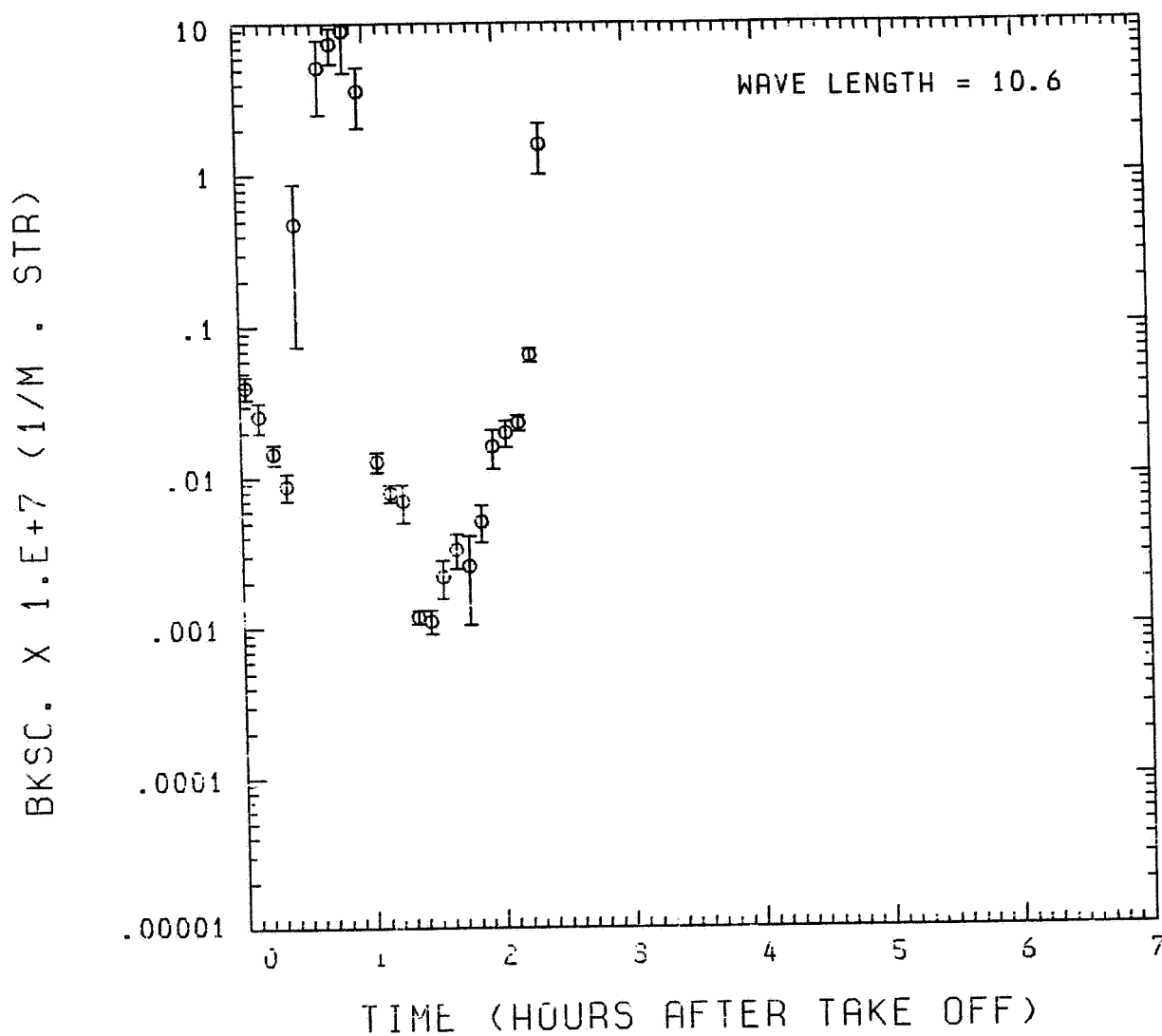


Fig. A19 (h). GAMETAG flight data for May 27, 1978.
 Calculated backscatter coefficient along the flight
 track for five-minute data sets for $\lambda = 10.6 \mu\text{m}$.

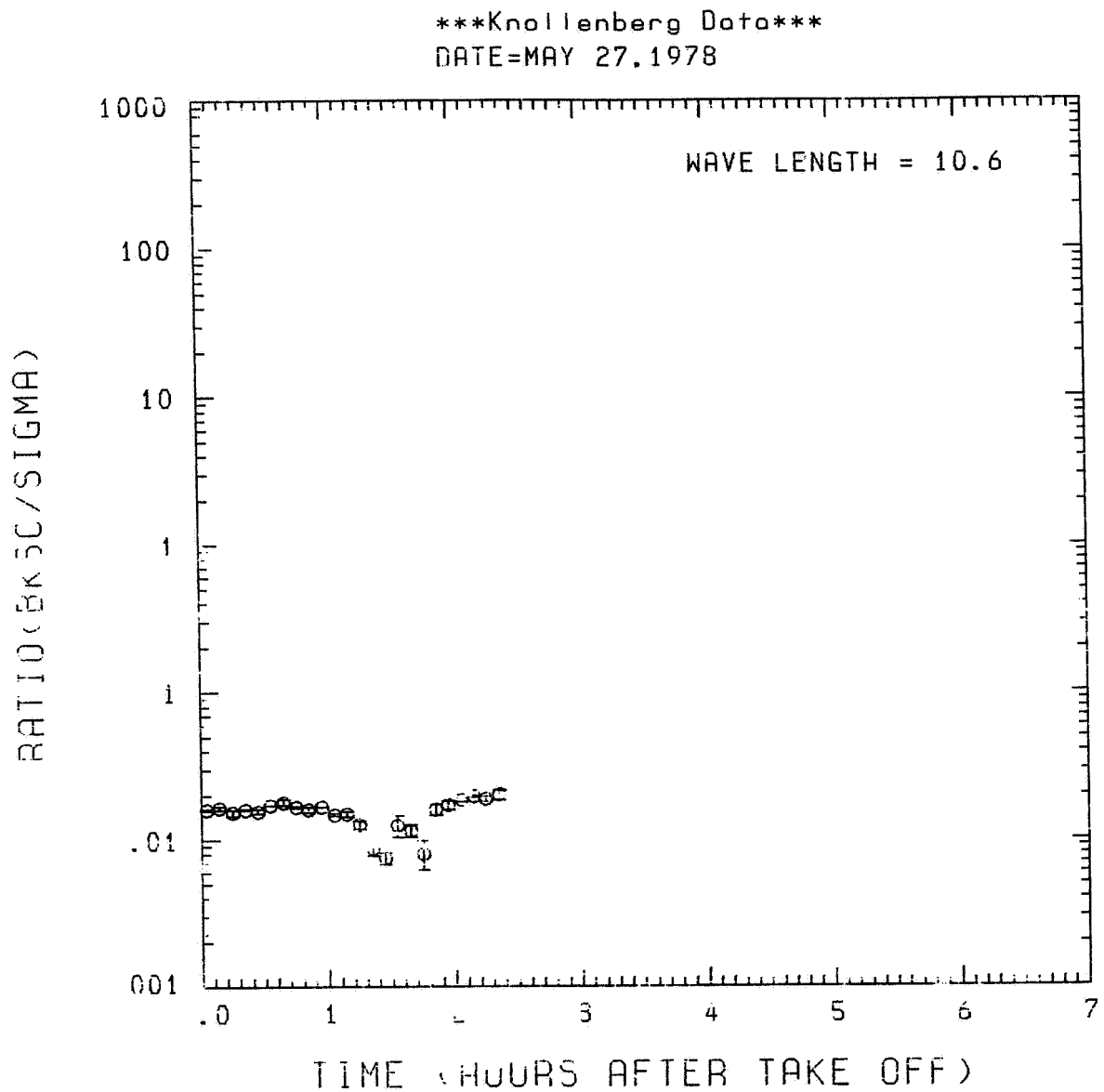


Fig. A 19(i). GAMETAG flight data for May 27, 1978.
Calculated ratios for backscatter to extinction for
five-minute data sets for $\lambda = 10.6 \mu\text{m}$.

Table A20. Significant times for May 28, 1978.
Great Falls, Montana to White Horse,
Canada.

Significant Points

<u>#</u>	<u>TIME</u>	
1	16:09	Great Falls
2	16:31	
3	17:05	
4	17:09	
5	17:22	
6	17:46	
7	18:45	
8	19:11	
9	19:52	
10	21:03	
11	21:22	White Horse

GRAFT FALLS TO WHITE HORSE
MAY 28, 1978

The map shows a flight path starting at Graft Falls (approx. 49°N, 114°W) and ending at White Horse (approx. 53°N, 100°W). The path is marked with numbered points 1 through 11. The map includes a latitude scale (47°N to 53°N) and a longitude scale (100°W to 130°W). A scale bar indicates distances in kilometers (0 to 100 km) and miles (0 to 100 miles). A compass rose shows the orientation of the map.

Point Number	Latitude (°N)	Longitude (°W)
1 (Start)	49.0	114.0
2	49.5	113.5
3	50.0	113.0
4	50.5	112.5
5	51.0	112.0
6	51.5	111.5
7	52.0	111.0
8	52.5	110.5
9	53.0	110.0
10	53.0	109.5
11 (End)	53.0	100.0

Fig. A20 (a). GAMETAG flight data for May 28, 1978. Altitude and location flight track plotted as a function of time after takeoff.

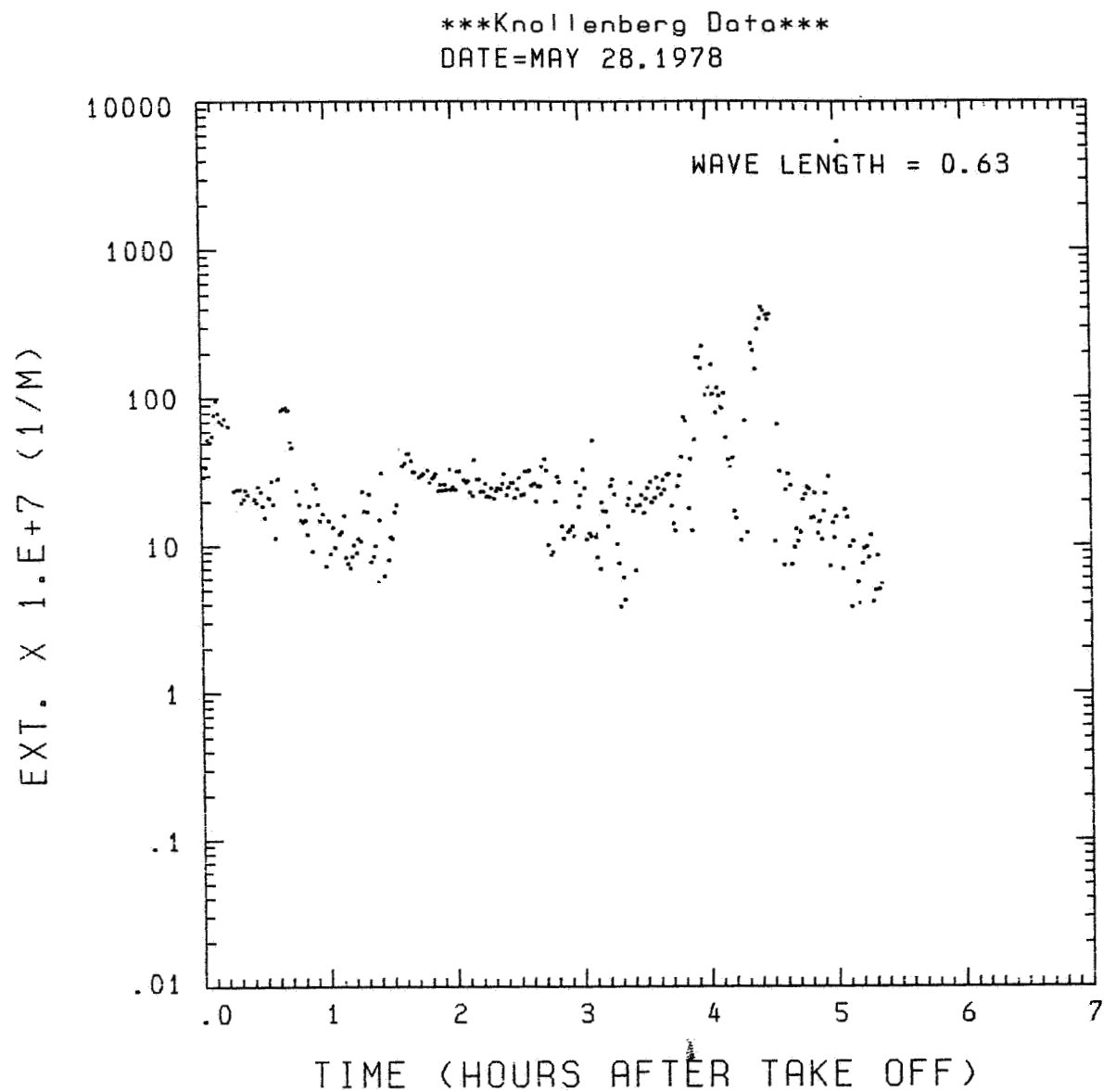


Fig. A20 (b). GAMETAG flight data for May 28, 1978.
Calculated particulate extinction along the flight
track for one-minute data sets for $\lambda = 0.63 \mu\text{m}$.

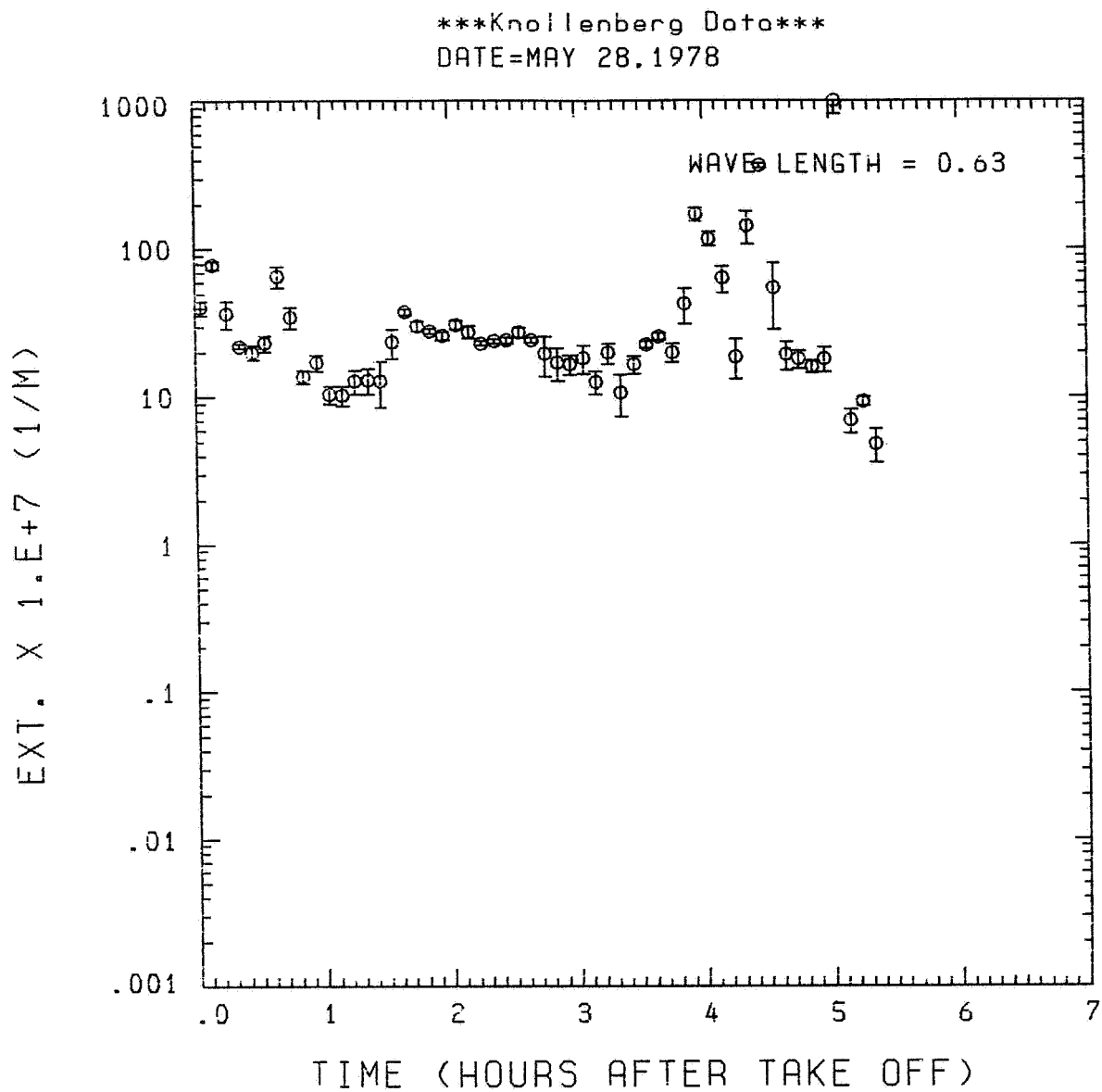


Fig. A20 (c). GAMETAG flight data for May 28, 1978.
Calculated particulate extinction along the flight
track for five-minute data sets for $\lambda = 0.63 \mu\text{m}$.

ORIGINAL PAGE IS
OF POOR QUALITY

Knollenberg Data
DATE=MAY 28,1978

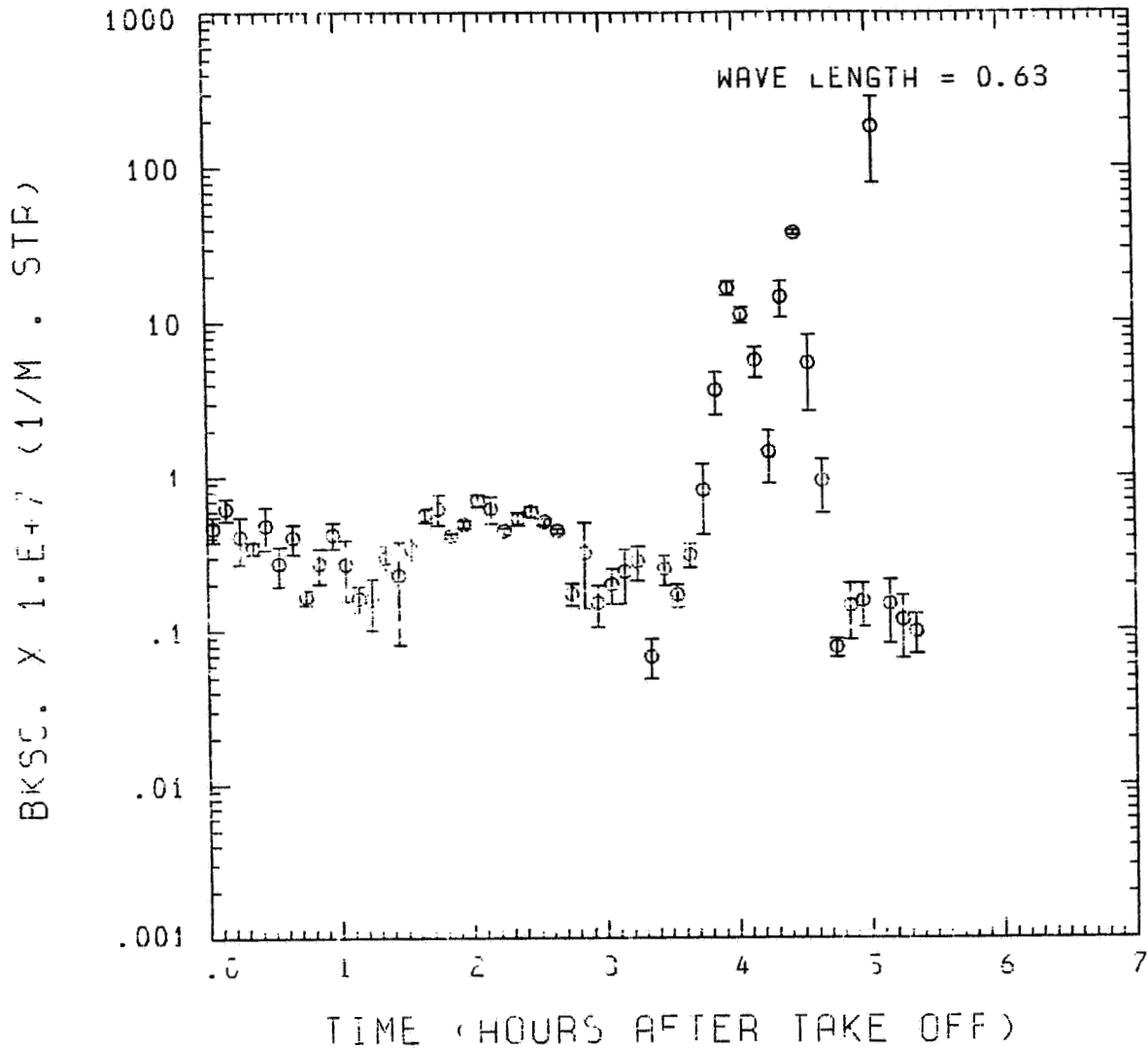


Fig. A20 (d). GAMETAG flight data for May 28, 1978.

Calculated backscatter coefficient along the flight
track for five-minute data sets for $\lambda = 0.63 \mu m$.

Knollenberg Data
 DATE=MAY 28.1978

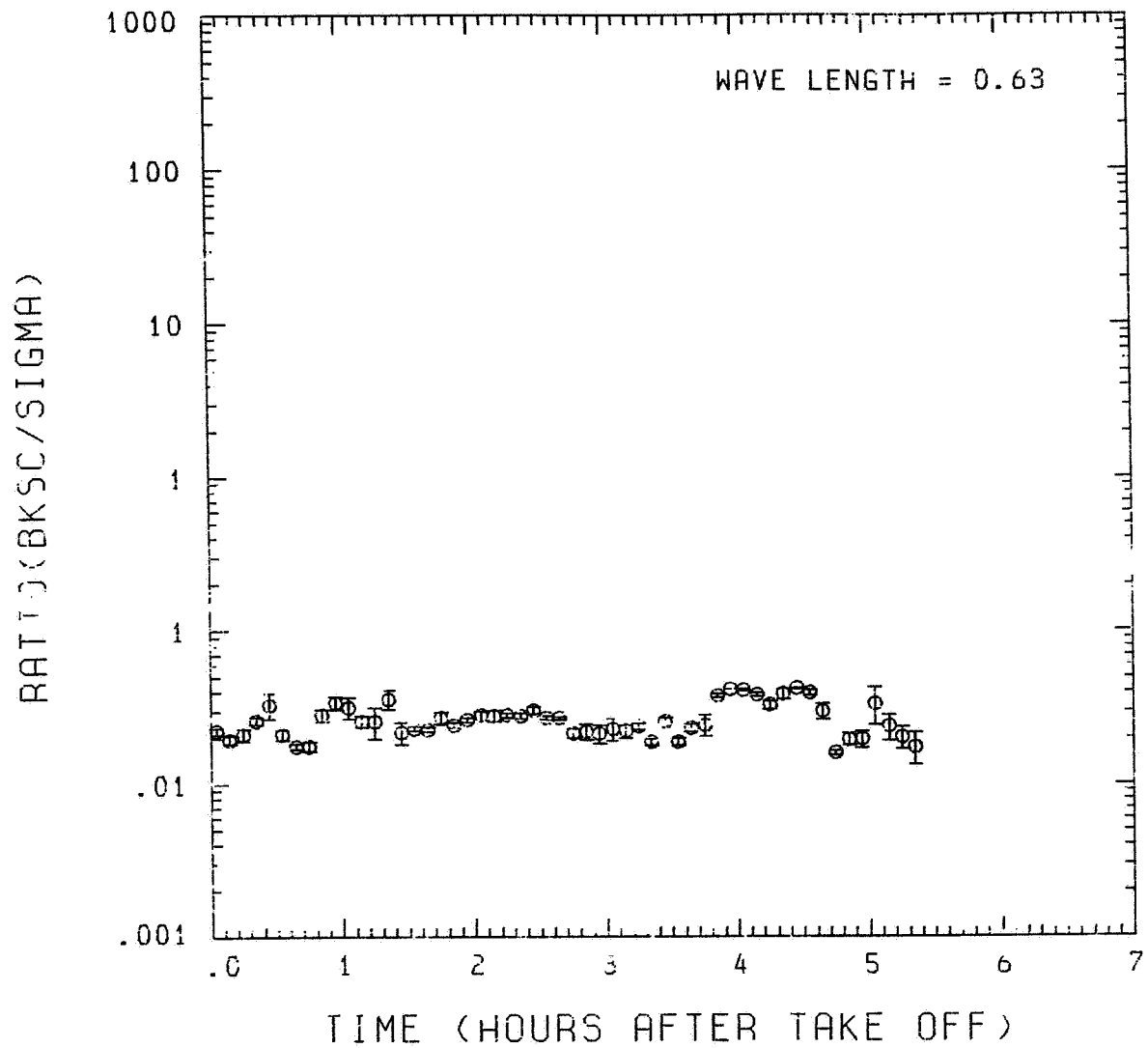


Fig. A20 (e). GAMETAG flight data for May 28, 1978.
 Calculated ratios for backscatter to extinction for
 five-minute data sets for $\lambda = 0.63 \mu\text{m}$.

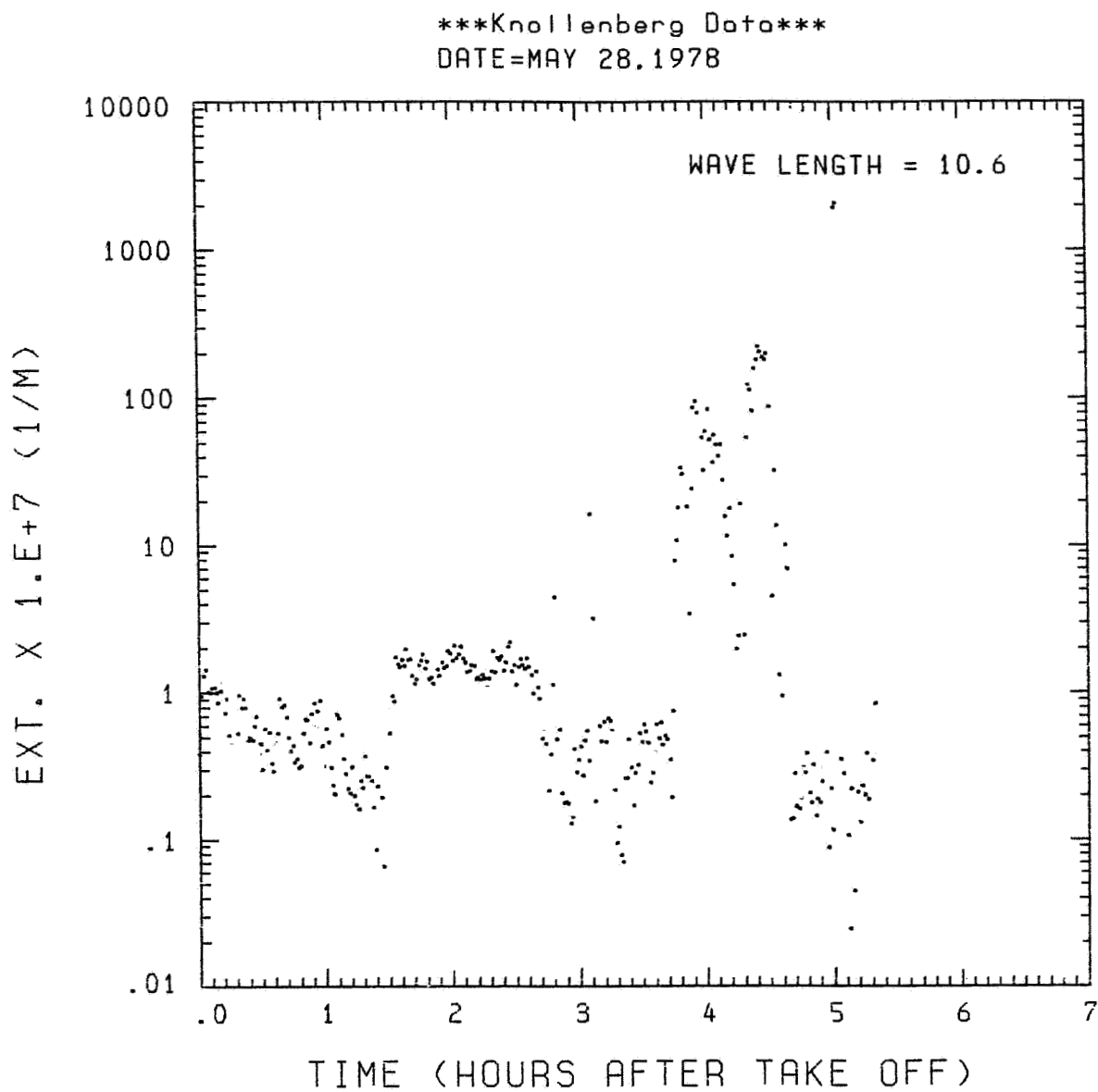


Fig. A20 (f). GAMETAG flight data for May 28, 1978.
Calculated particulate extinction along the flight
track for one-minute data sets for $\lambda = 10.6 \mu\text{m}$.

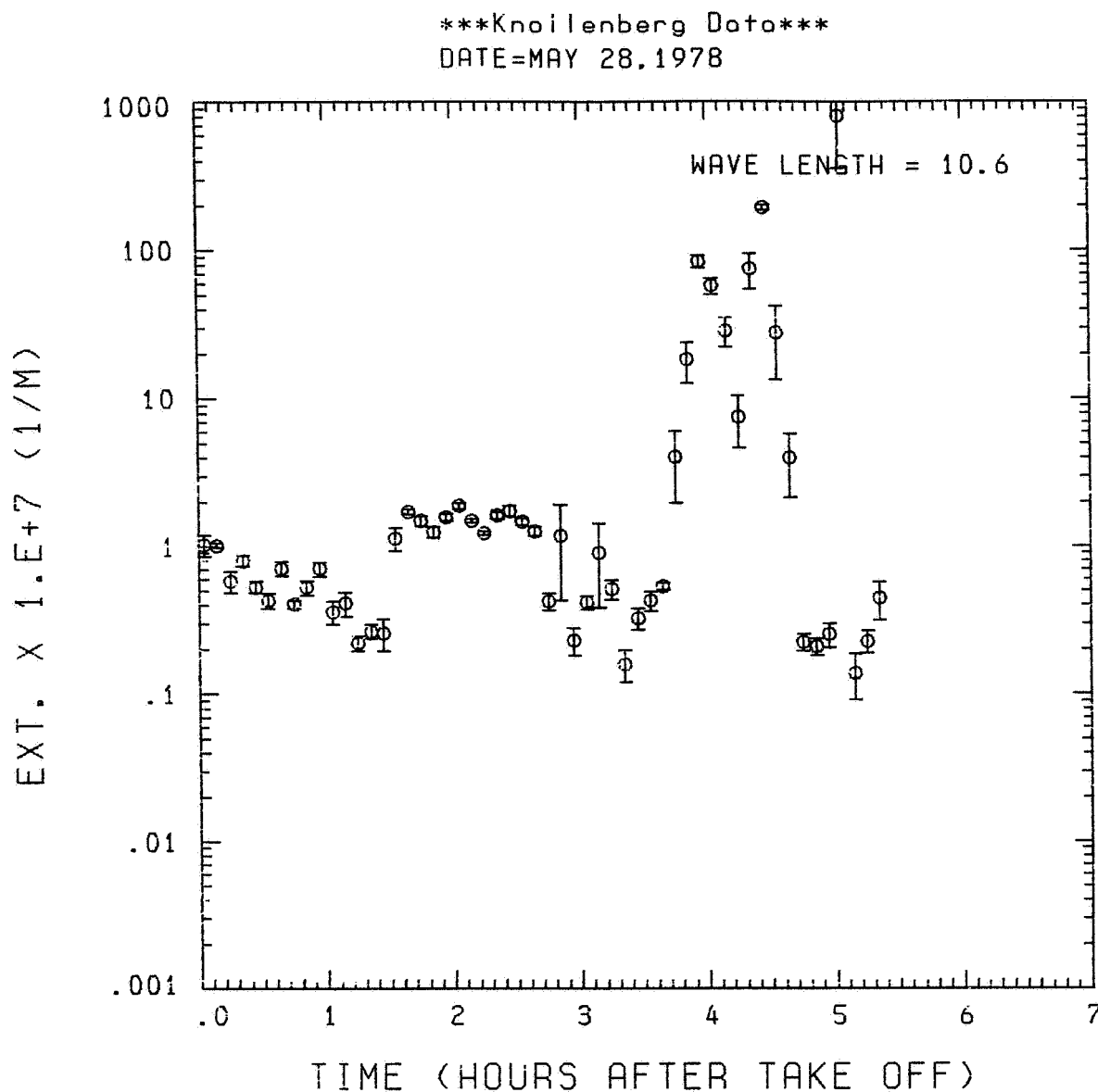


Fig. A20 (g). GAMETAG flight data for May 28, 1978.
Calculated particulate extinction along the flight
track for five-minute data sets for $\lambda = 10.6 \mu\text{m}$.

ORIGINAL PAGE IS
OF POOR QUALITY

Knollenberg Data
DATE=MAY 28, 1978

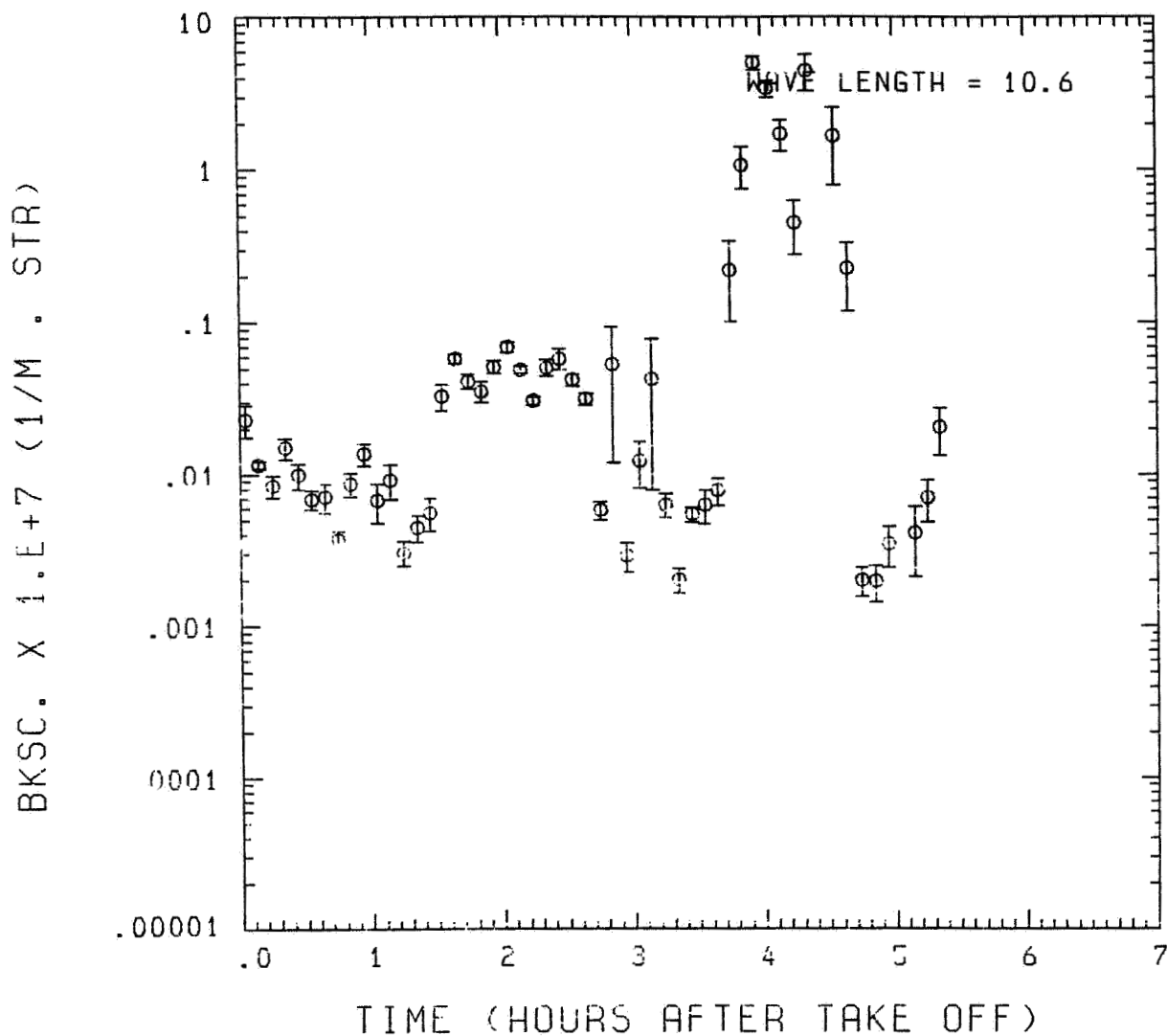


Fig. A20 (h). GAMETAG flight data for May 28, 1978.

Calculated backscatter coefficient along the flight
track for five-minute data sets for $\lambda = 10.6 \mu\text{m}$.

Knollenberg Data
 DATE=MAY 28.1978

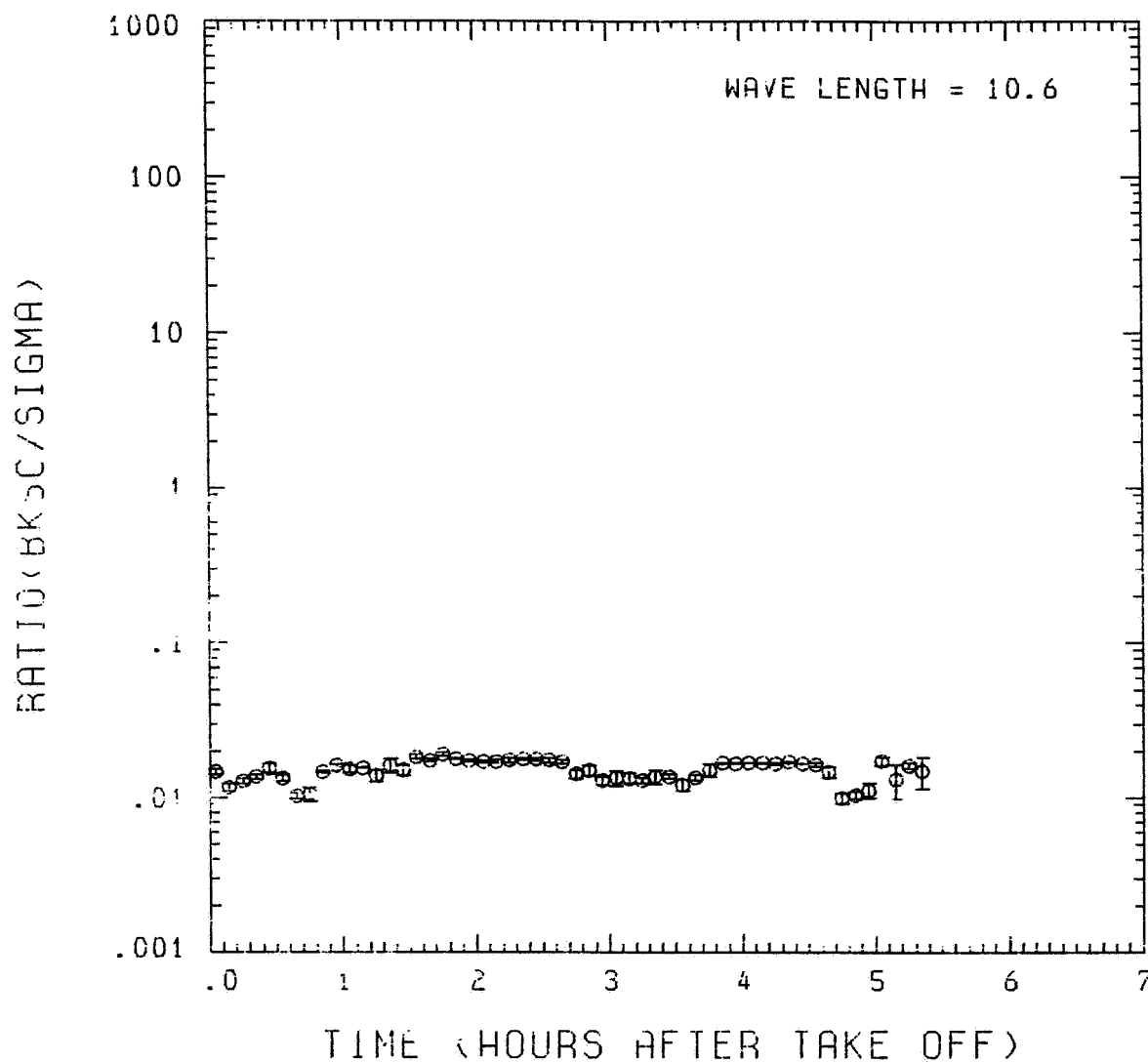


Fig. A20 (i). GAMETAG flight data for May 28, 1978.
 Calculated ratios for backscatter to extinction for
 five-minute data sets for $\lambda = 10.6 \mu\text{m}$.

Table A21. Significant tiems for May 31, 1978.
White Horse, Canada to Great Falls,
Montana.

Significant Points

<u>#</u>	<u>TIME</u>	
1	18:14	White Horse, Canada
2	18:41	
3	18:53	
4	19:21	
5	19:36	
6	20:09	
7	20:51	
8	21:04	
9	22:21	
10	22:43	Great Falls

ORIGINAL PAGE IS
OF POOR QUALITY

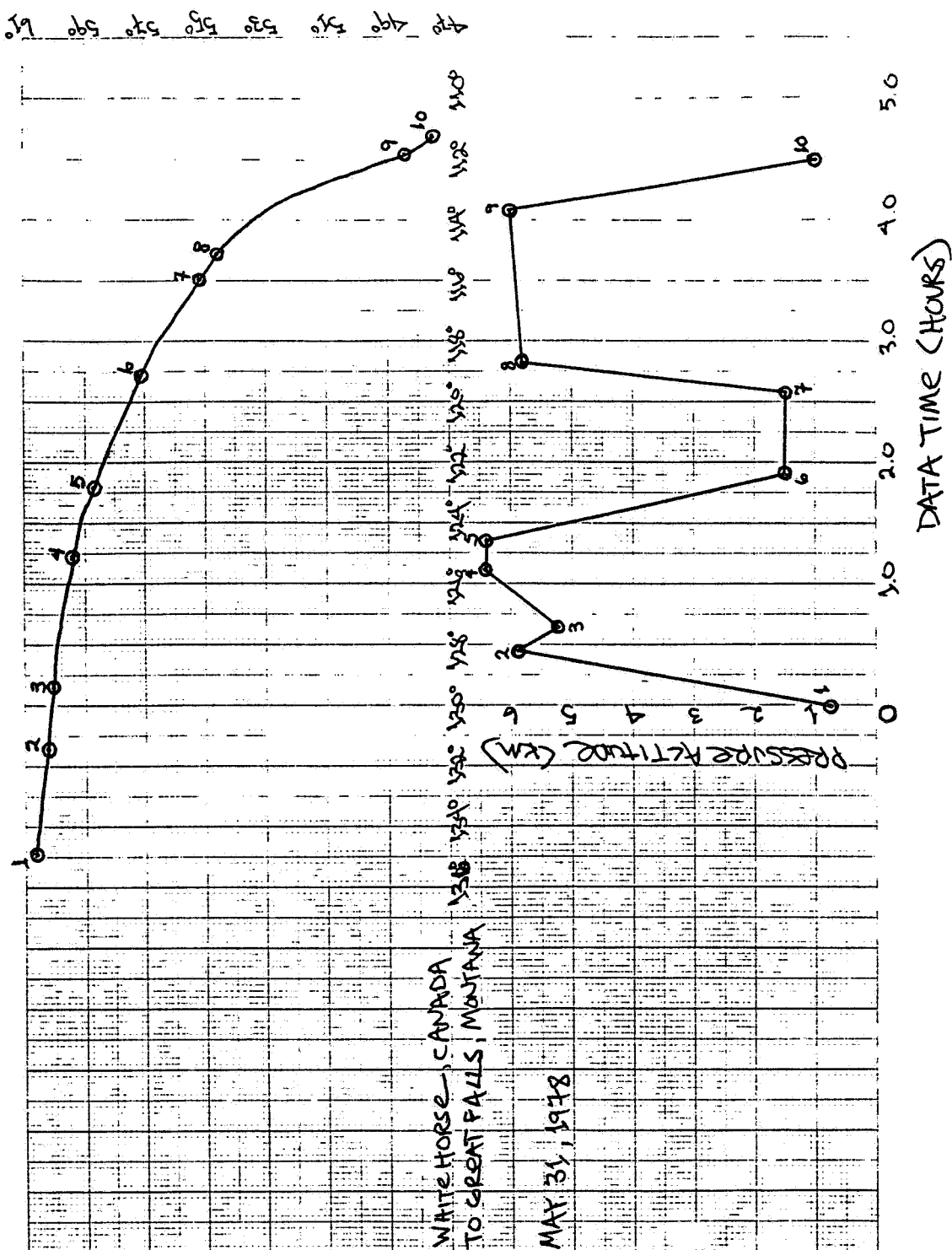


Fig. A21 (a). GAMETAG flight data for May 31, 1978.
Altitude and location flight track plotted as a
function of time after takeoff.

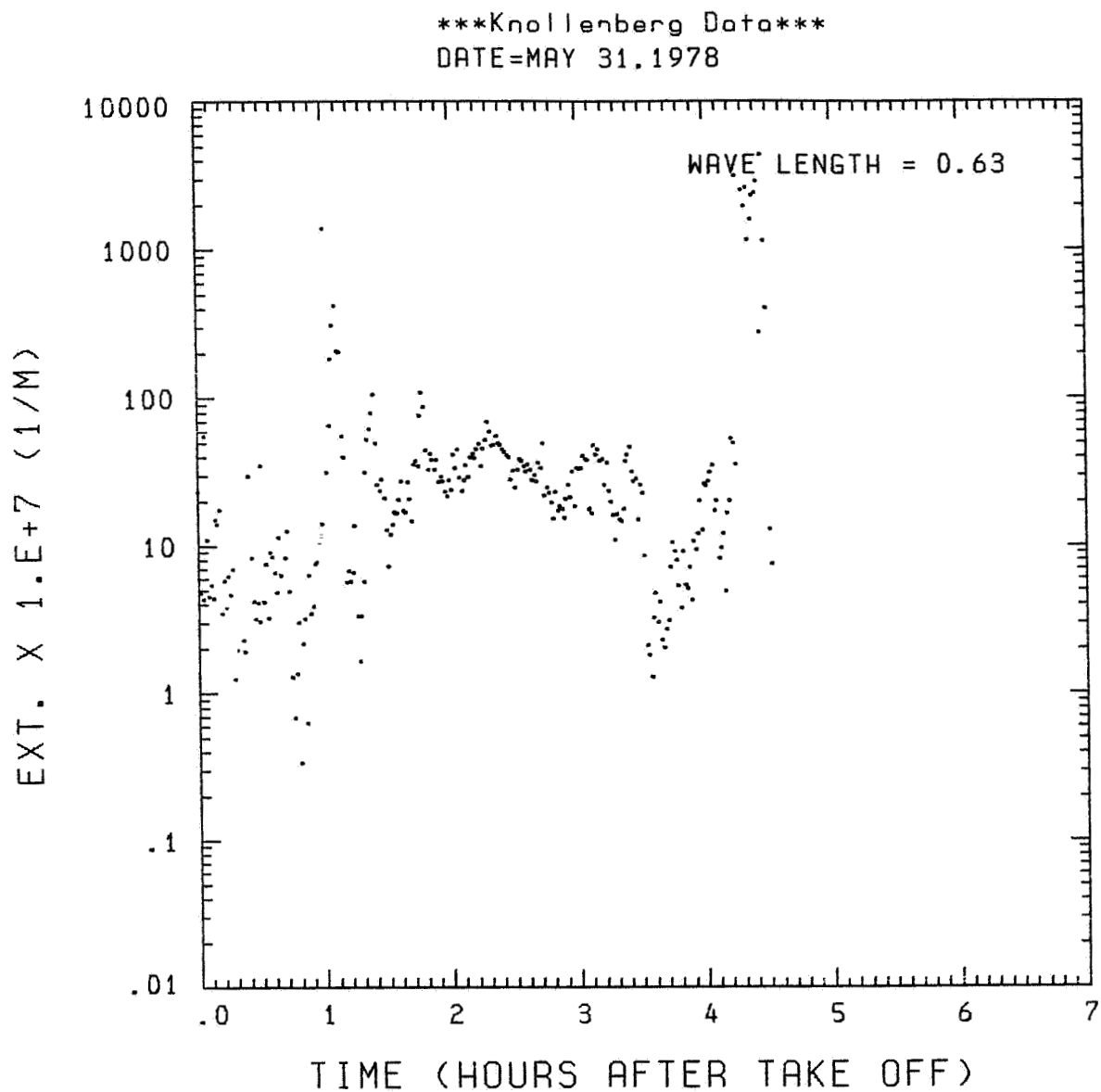


Fig. A21 (b). GAMETAG flight data for May 31, 1978.
Calculated particulate extinction along the flight
track for one-minute data sets for $\lambda = 0.63 \mu\text{m}$.

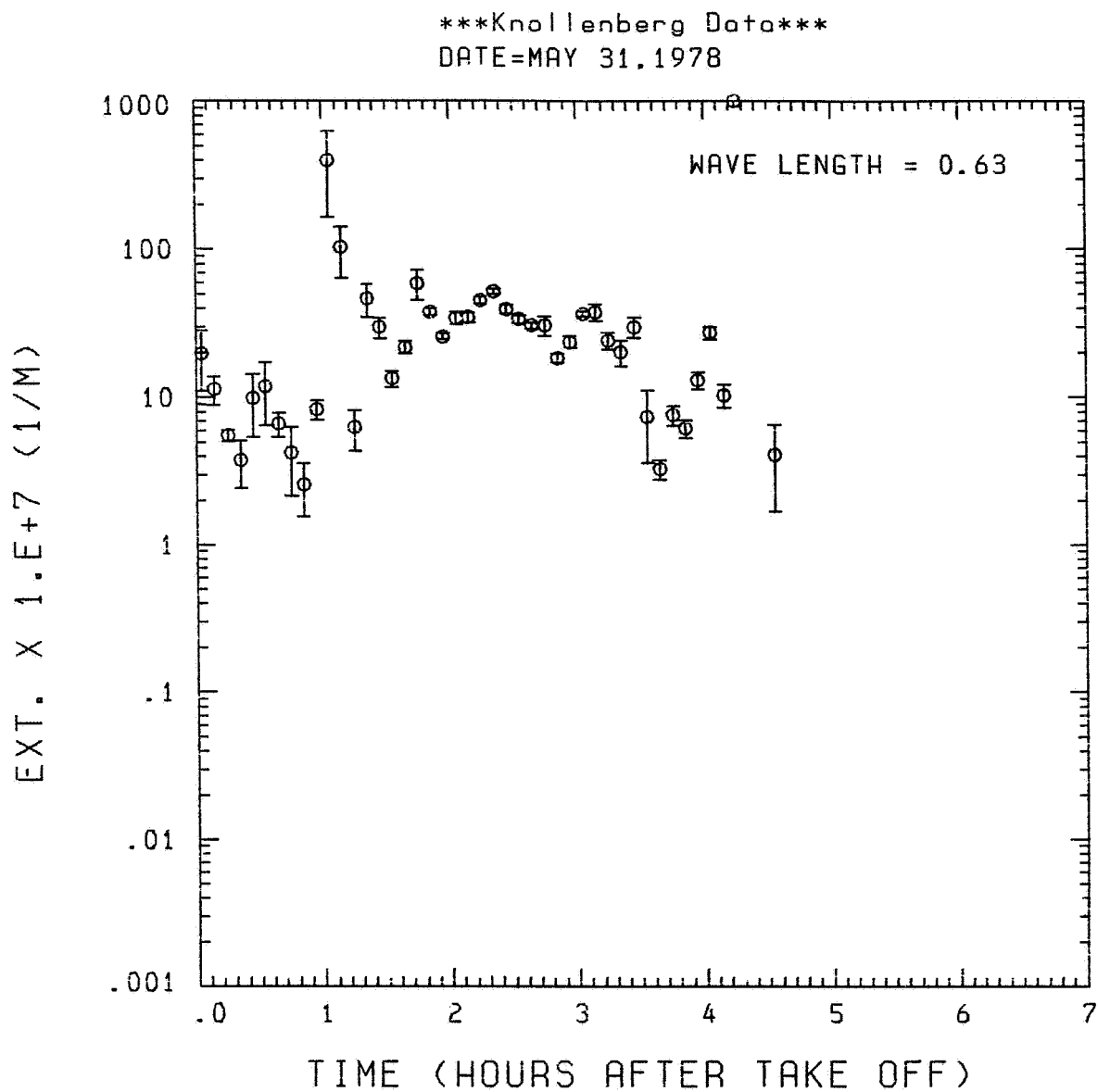


Fig. A21 (c). GAMETAG flight data for May 31, 1978.

Calculated particulate extinction along the flight track for five-minute data sets for $\lambda = 0.63 \mu\text{m}$.

ORIGINAL PAGE IS
OF POOR QUALITY

Knollenberg Data
DATE=MAY 31.1978

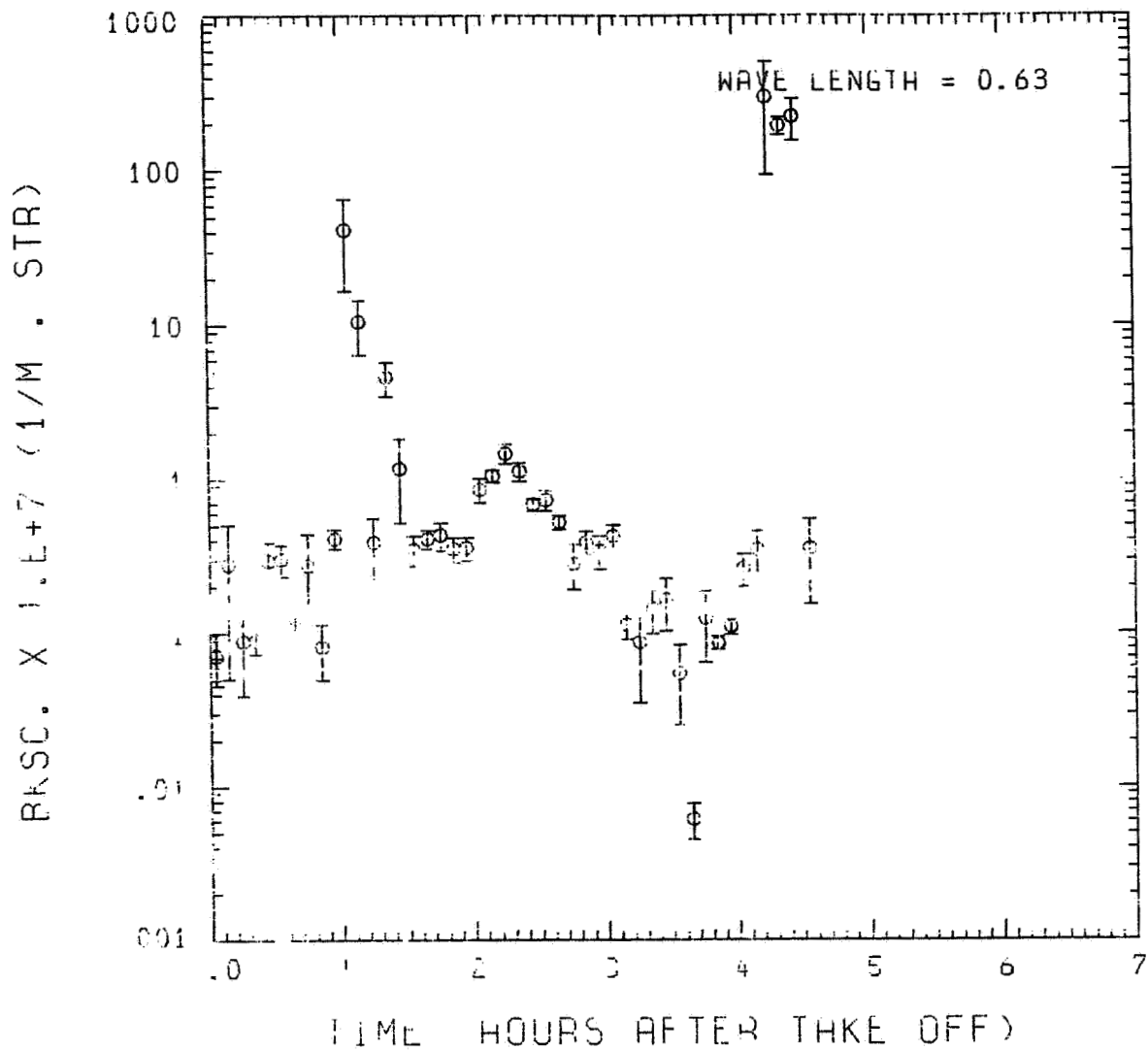


Fig. A21 (d). GAMETAG flight data for May 31, 1978.

Calculated backscatter coefficient along the flight
track for five-minute data sets for $\lambda = 0.63 \mu\text{m}$.

Knollenberg Data
DATE=MAY 31,1978

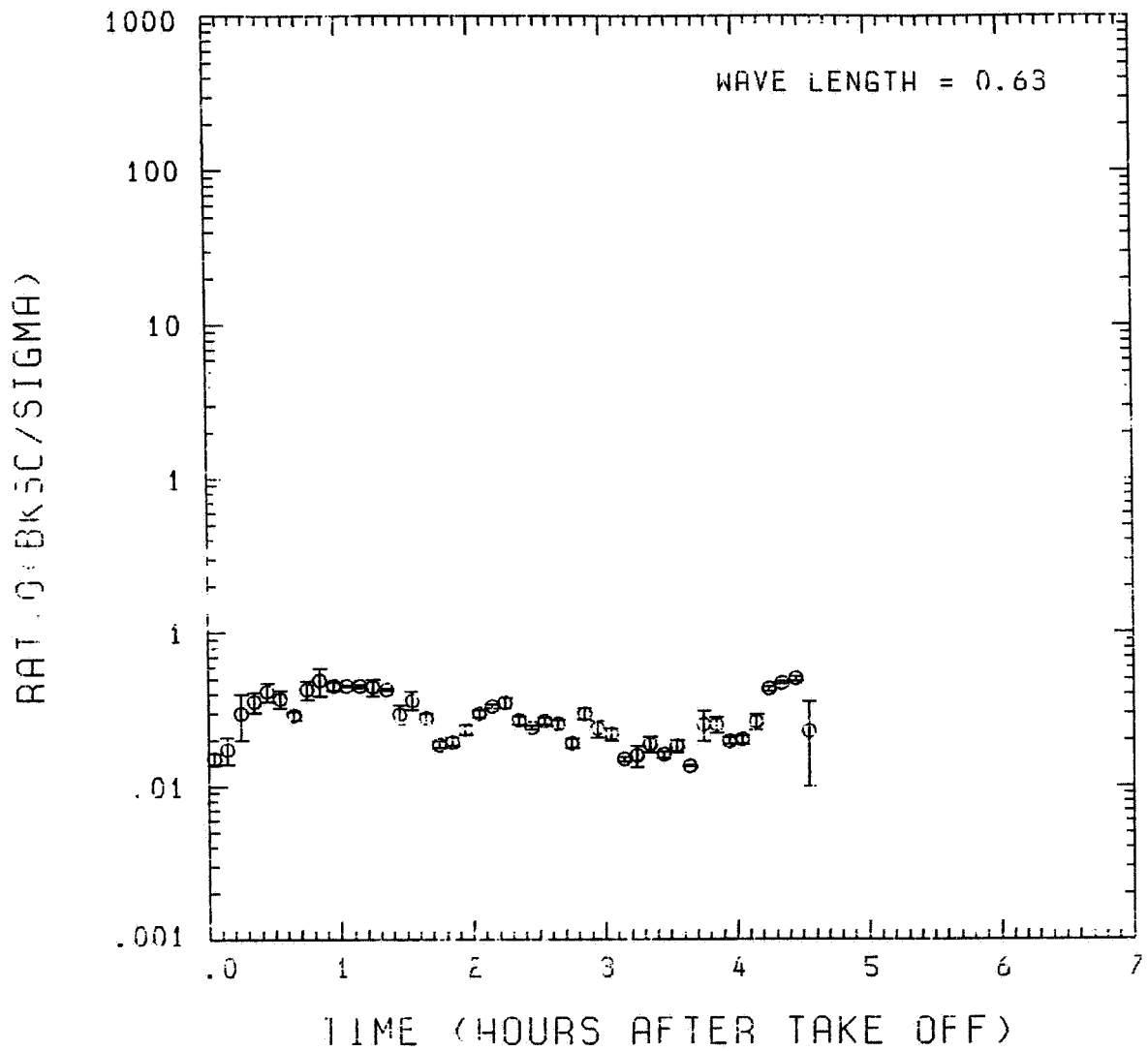


Fig. A21 (e). GAMETAG flight data for May 31, 1978.
Calculated ratios for backscatter to extinction for
five-minute data sets for $\lambda = 0.63 \mu\text{m}$.

ORIGINAL PAGE IS
OF POOR QUALITY

Knollenberg Data
DATE=MAY 31.1978

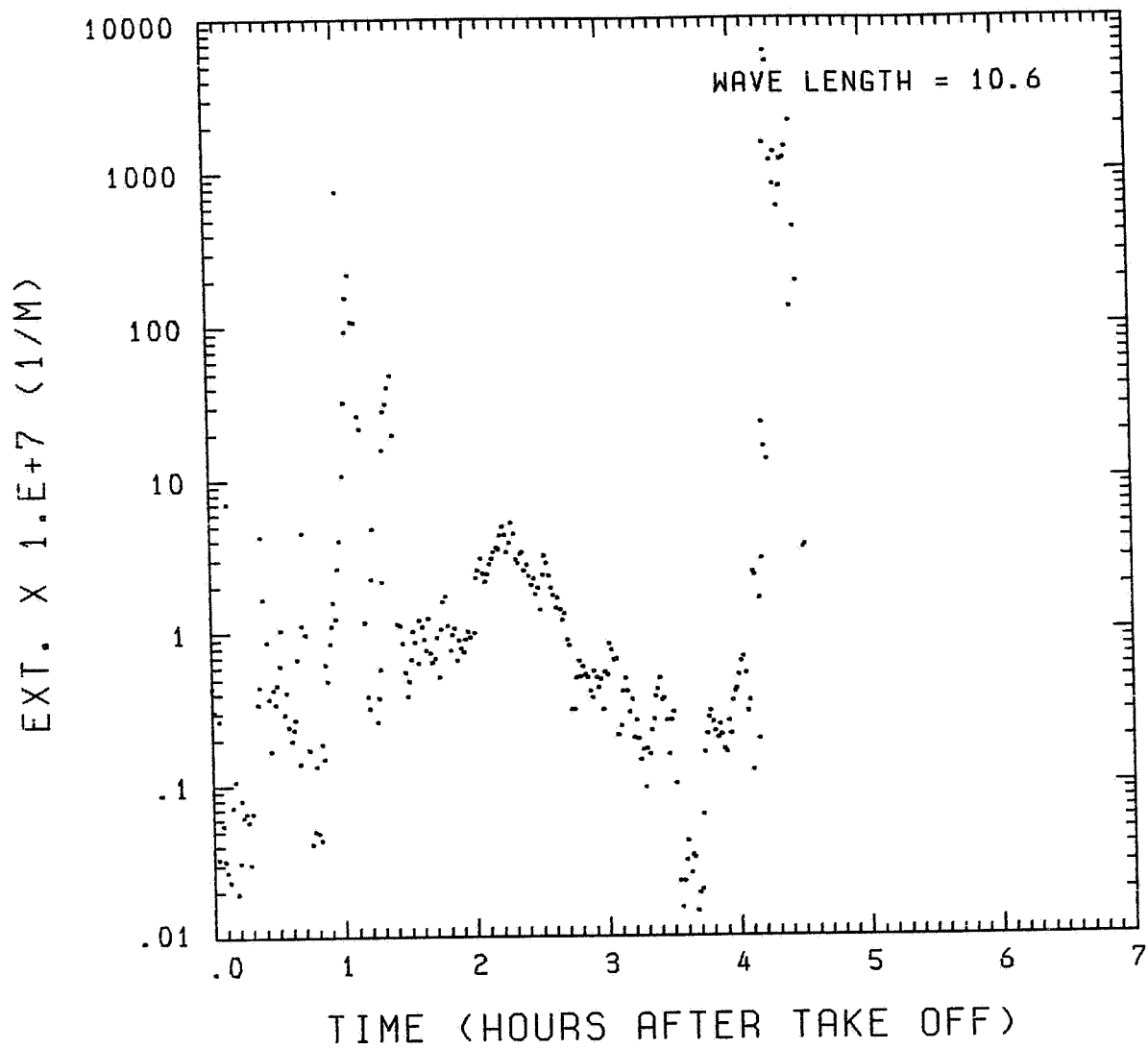


Fig. A21 (f). GAMETAG flight data for May 31, 1978.
Calculated particulate extinction along the flight
track for one-minute data sets for $\lambda = 10.6 \mu\text{m}$.

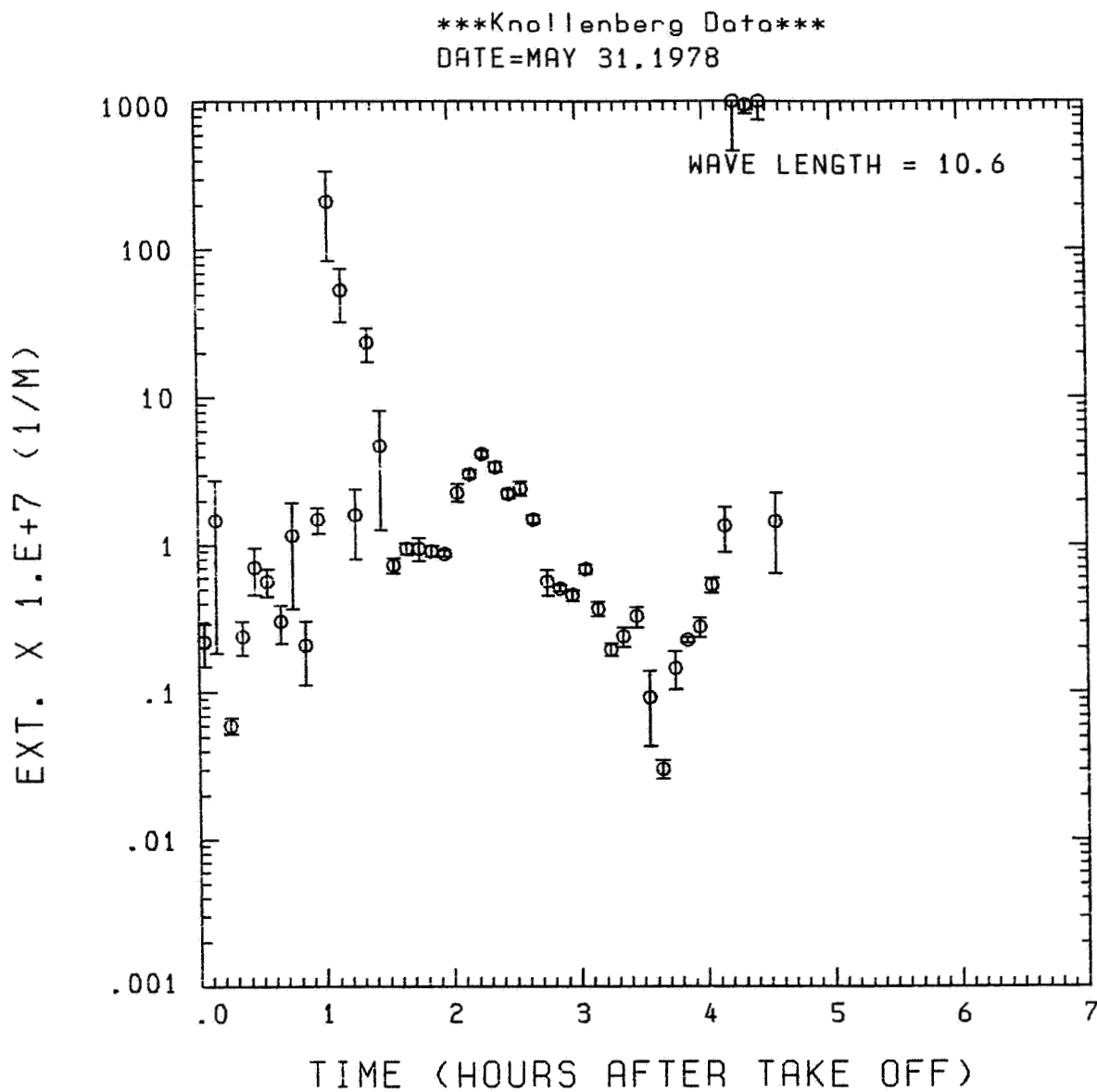


Fig. A21(g). GAMETAG flight data for May 31, 1978.

Calculated particulate extinction along the flight track for five-minute data sets for $\lambda = 10.6 \mu\text{m}$.

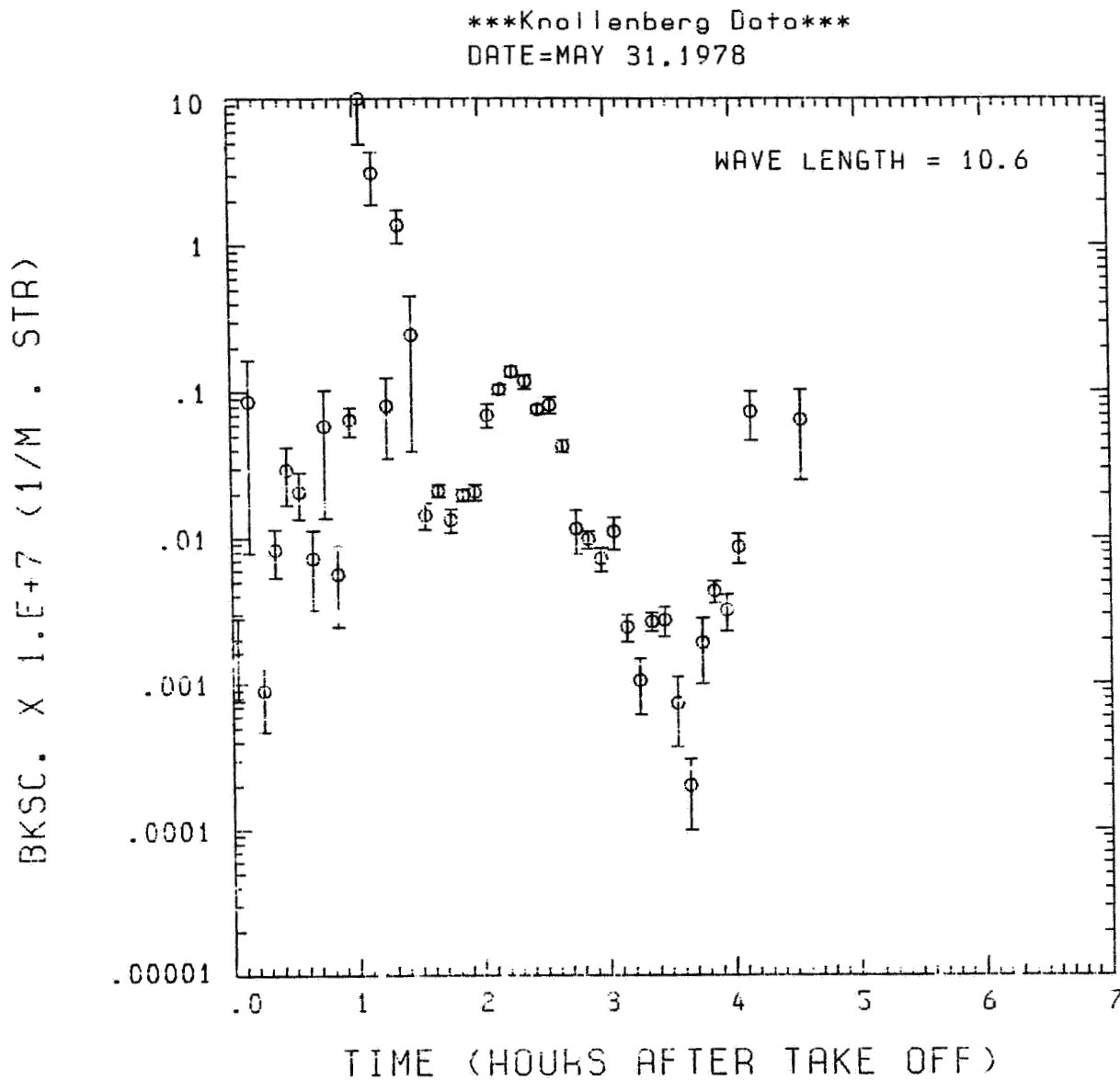


Fig. A21(h). GAMETAG flight data for May 31, 1978.

Calculated backscatter coefficient along the flight track for five-minute data sets for $\lambda = 10.6 \mu\text{m}$.

Knollenberg Data
 DATE=MAY 31.1978

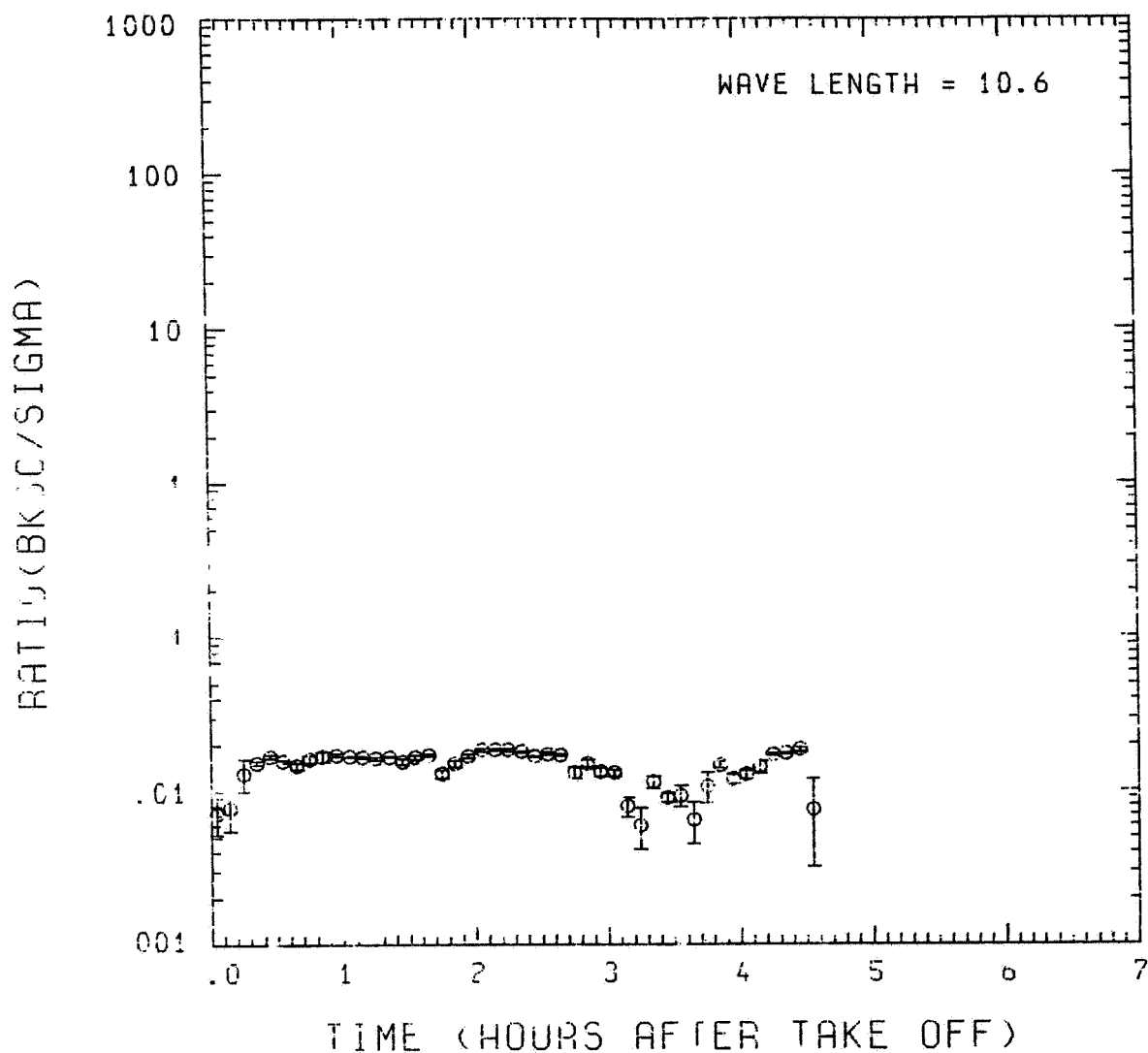


Fig. A21(i). GAMETAG flight data for May 31, 1978.
 Calculated ratios for backscatter to extinction for
 five-minute data sets for $\lambda = 10.6 \mu\text{m}$.

Table A22. Significant times for June 1, 1978.
Great Falls, Montana to Denver,
Colorado.

Significant Points

<u>#</u>	<u>TIME</u>	
1	15:50	Great Falls
2	16:05	
3	16:37	
4	16:44	
5	17:36	
6	17:45	Denver

ORIGINAL PAGE IS
OF POOR QUALITY

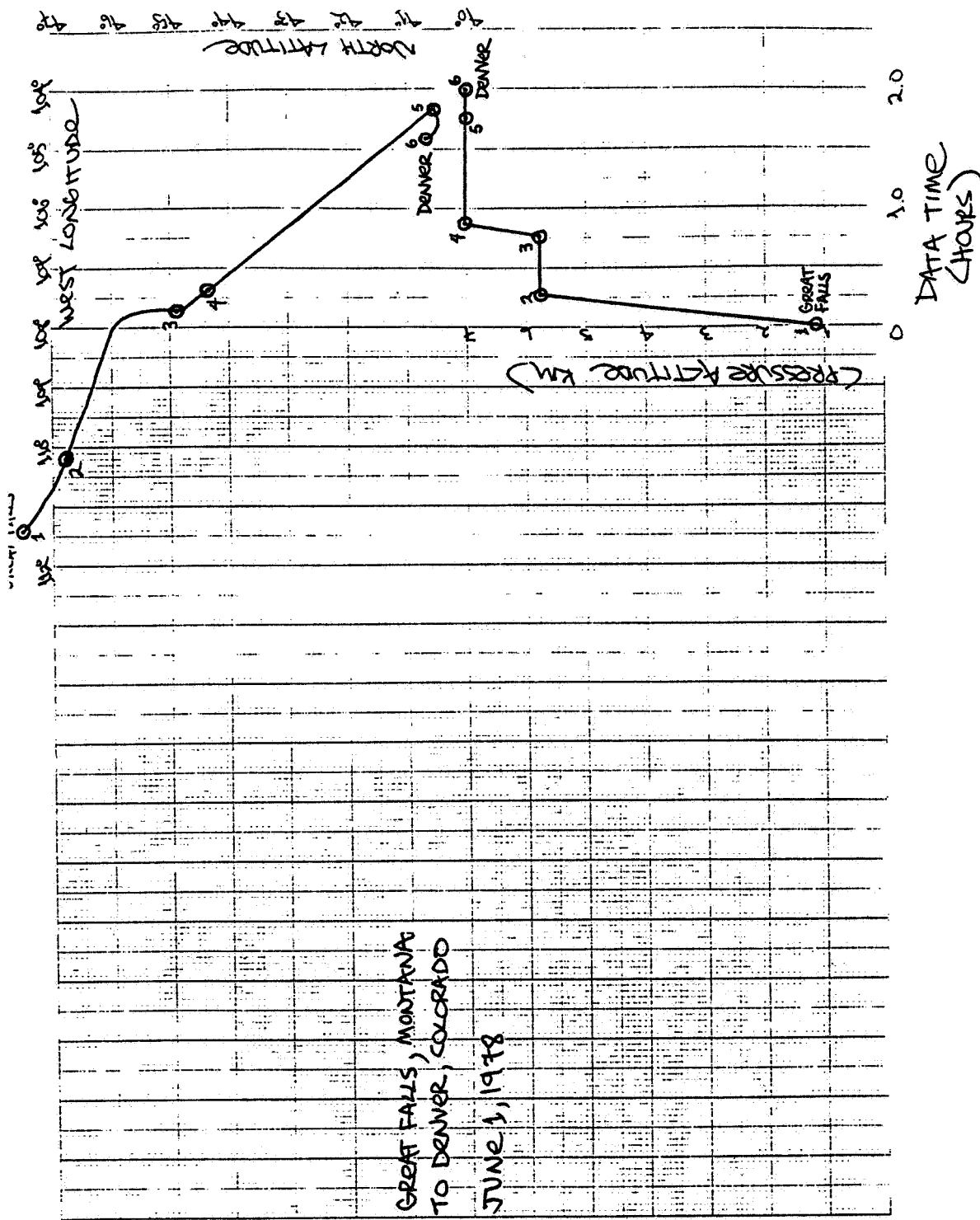


Fig. A22 (a). GAMETAG flight data for June 1, 1978.

Altitude and location flight track plotted as a function of time after takeoff.

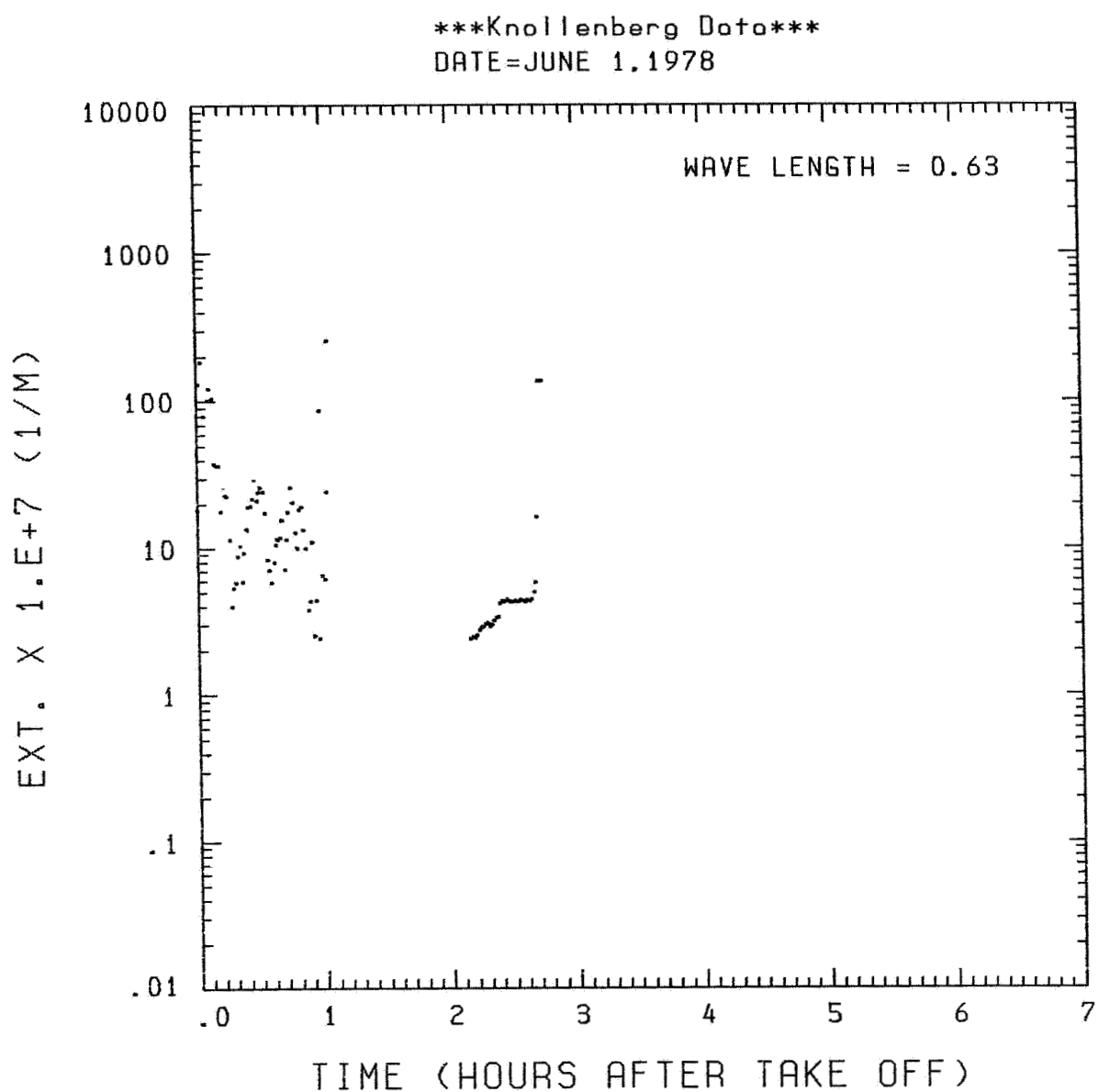


Fig. A22 (b). GAMETAG flight data for June 1, 1978.

Calculated particulate extinction along the flight track for one-minute data sets for $\lambda = 0.63 \mu\text{m}$.

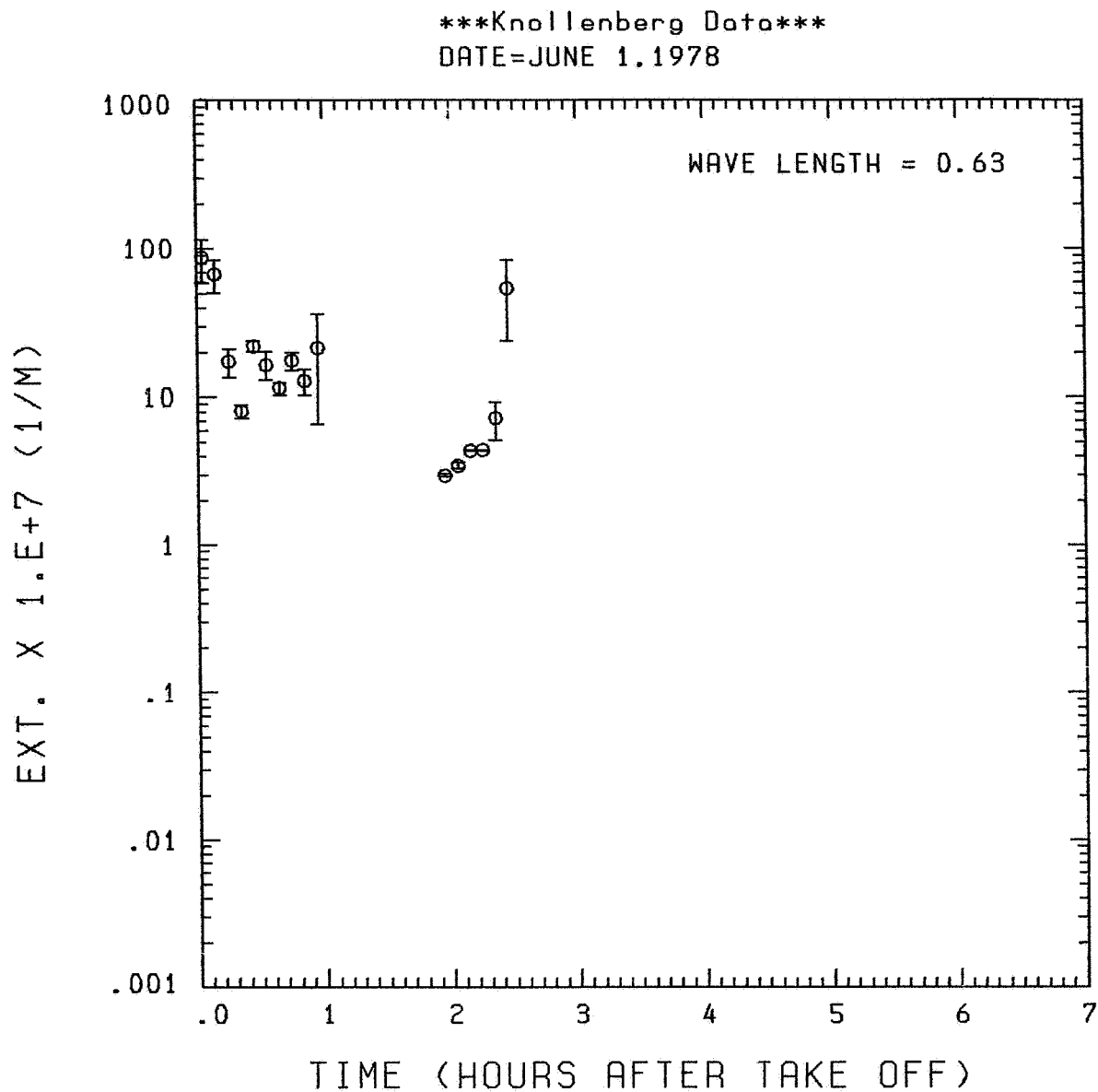


Fig. A22 (c). GAMETAG flight data for June 1, 1978.
Calculated particulate extinction along the flight
track for five-minute data sets for $\lambda = 0.63 \mu\text{m}$.

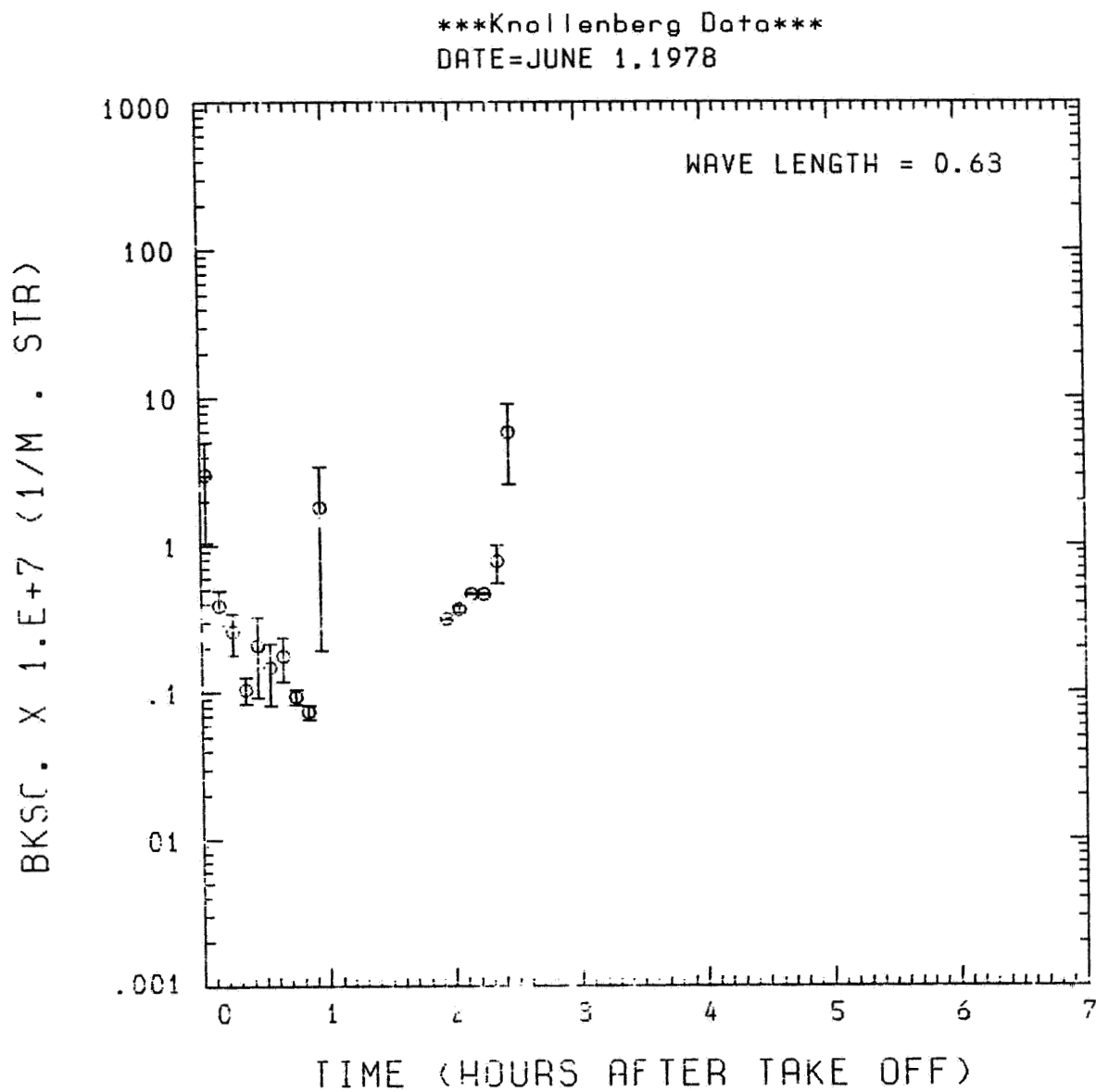


Fig. A22 (d). GAMETAG flight data for June 1, 1978.
Calculated backscatter coefficient along the flight
track for five-minute data sets for $\lambda = 0.63 \mu\text{m}$.

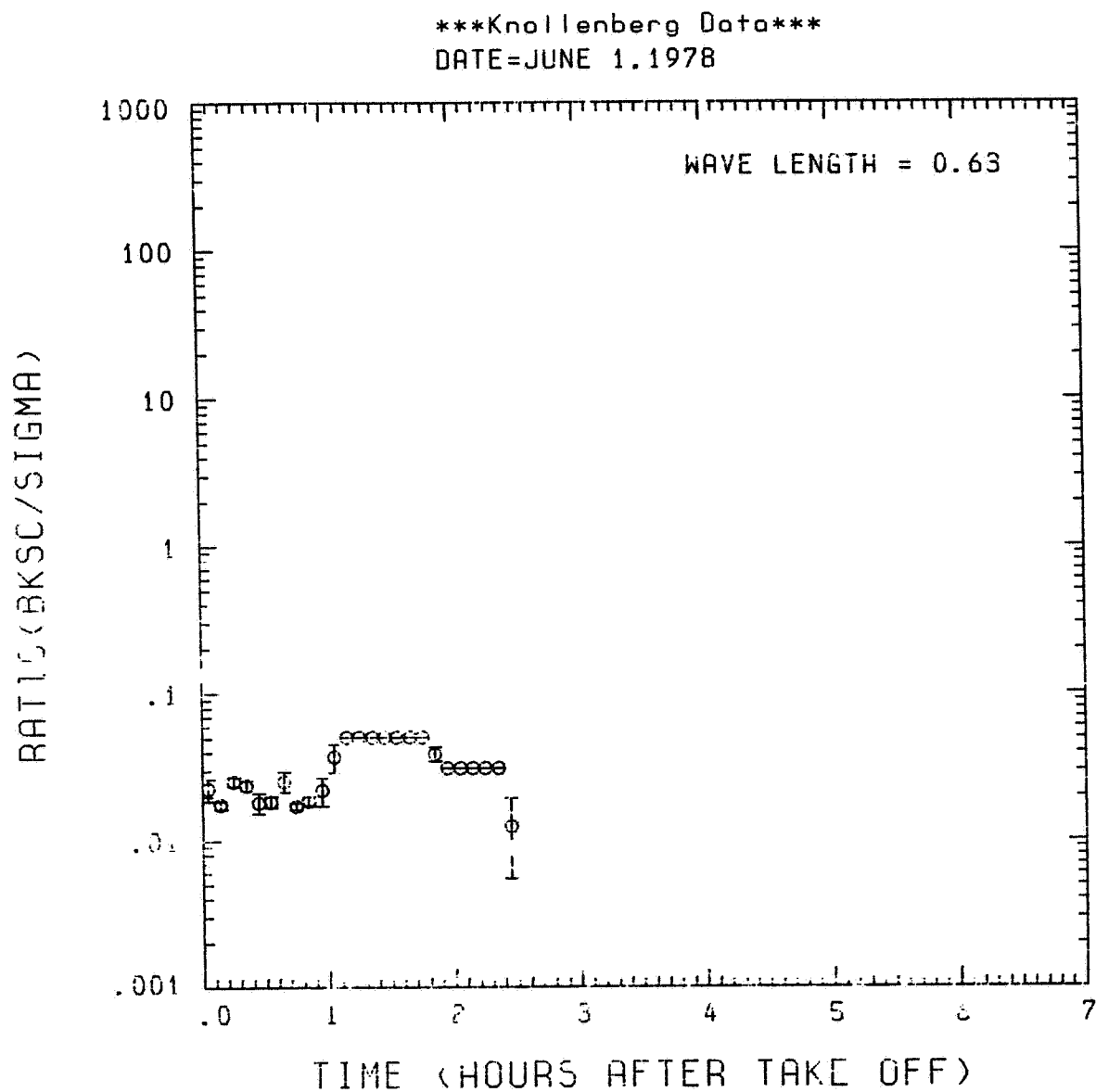


Fig. A22 (e). GAMETAG flight data for June 1, 1978.
Calculated ratios for backscatter to extinction for
five-minute data sets for $\lambda = 0.63 \mu\text{m}$.

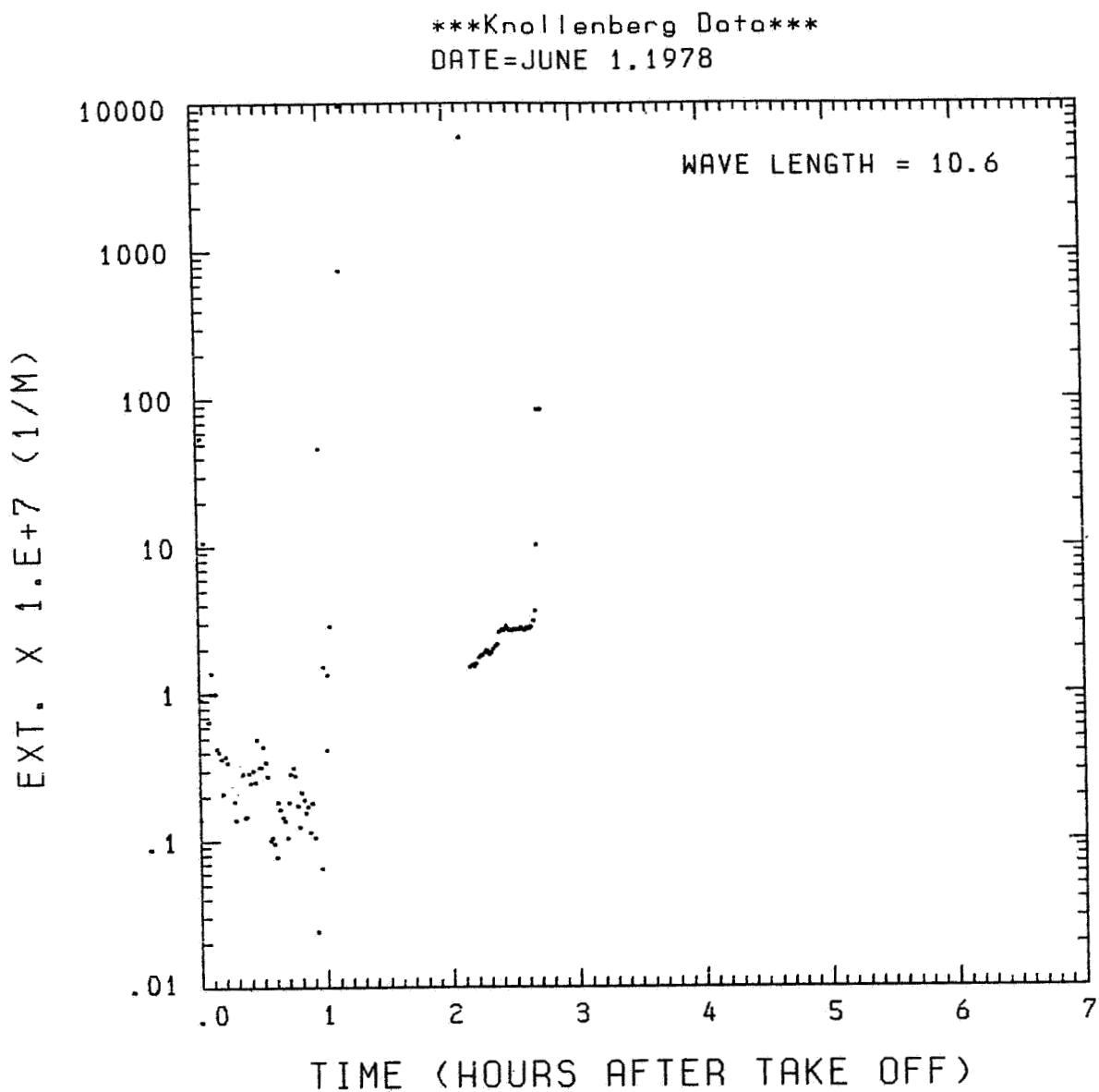


Fig. A22 (f). GAMETAG flight data for June 1, 1978.
Calculated particulate extinction along the flight
track for one-minute data sets for $\lambda = 10.6 \mu\text{m}$.

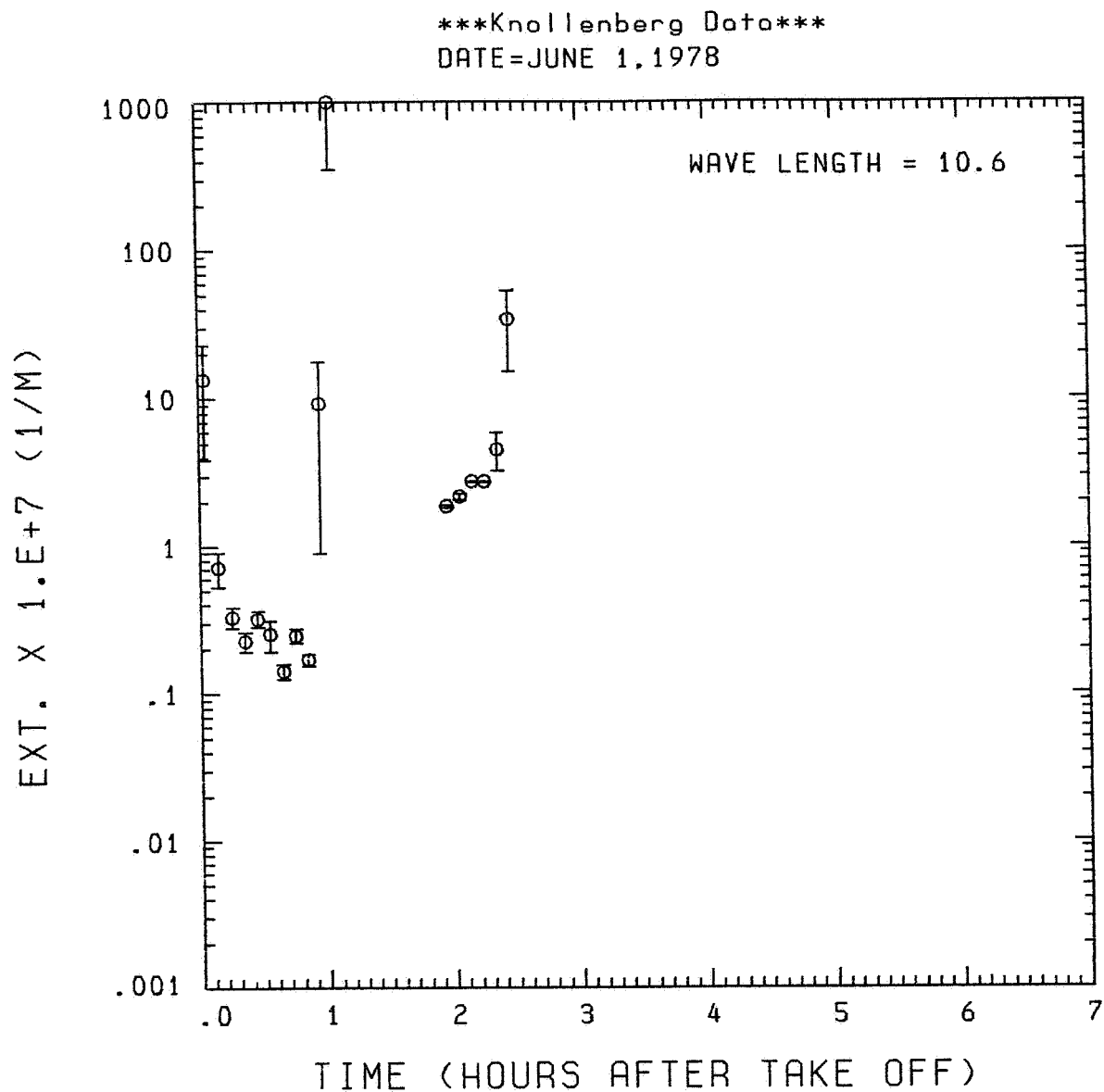


Fig. A22 (g). GAMETAG flight data for June 1, 1978.
Calculated particulate extinction along the flight
track for five-minute data sets for $\lambda = 10.6 \mu\text{m}$.

BKSC. $\times 1.E+7$ (1/M . STR)

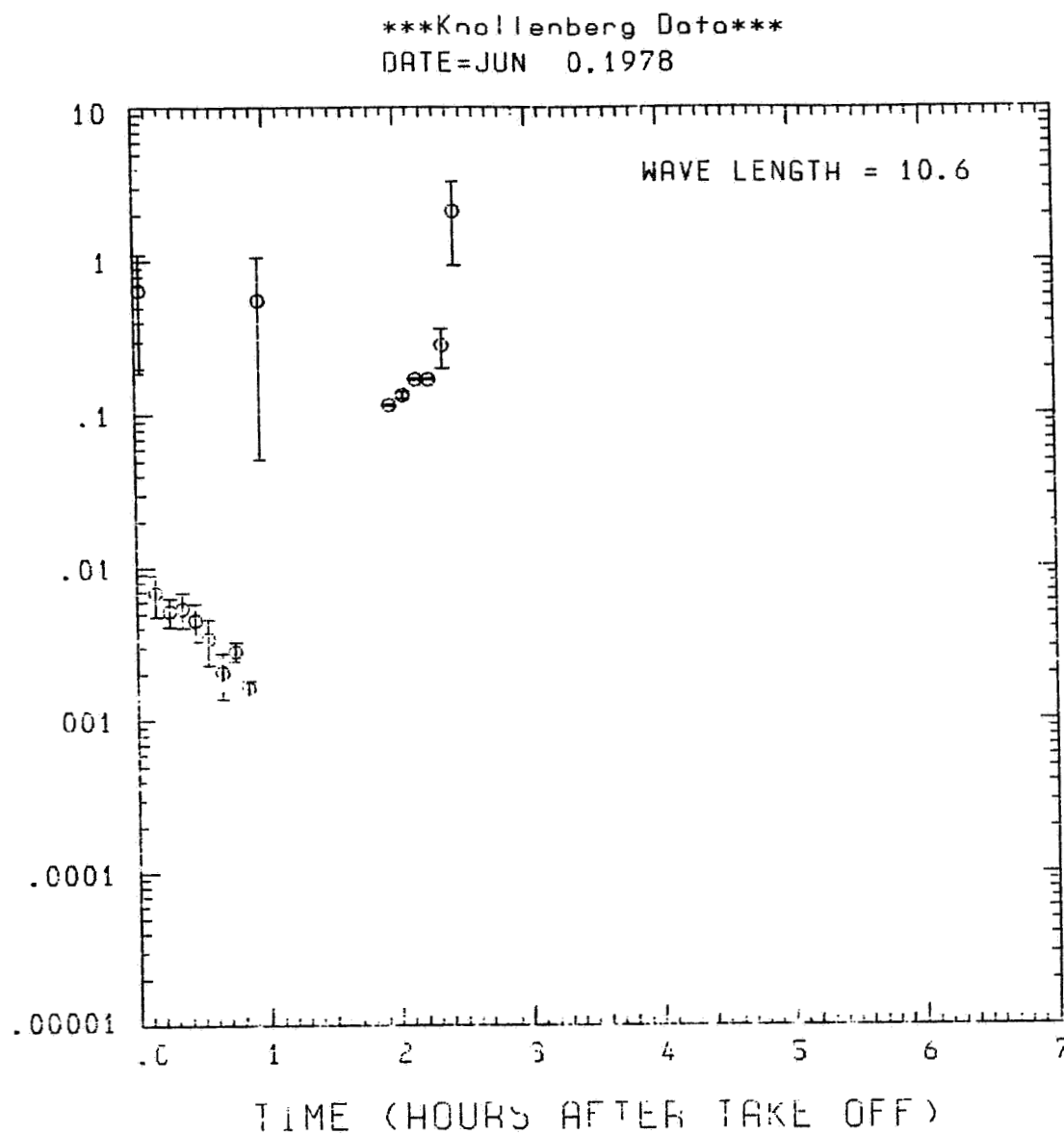


Fig. A22 (h). GAMETAG flight data for June 1, 1978.
Calculated backscatter coefficient along the flight
track for five-minute data sets for $\lambda = 10.6 \mu\text{m}$.

ORIGINAL PAGE IS
OF POOR QUALITY

Knolienberg Data
DATE=JUNE 1, 1978

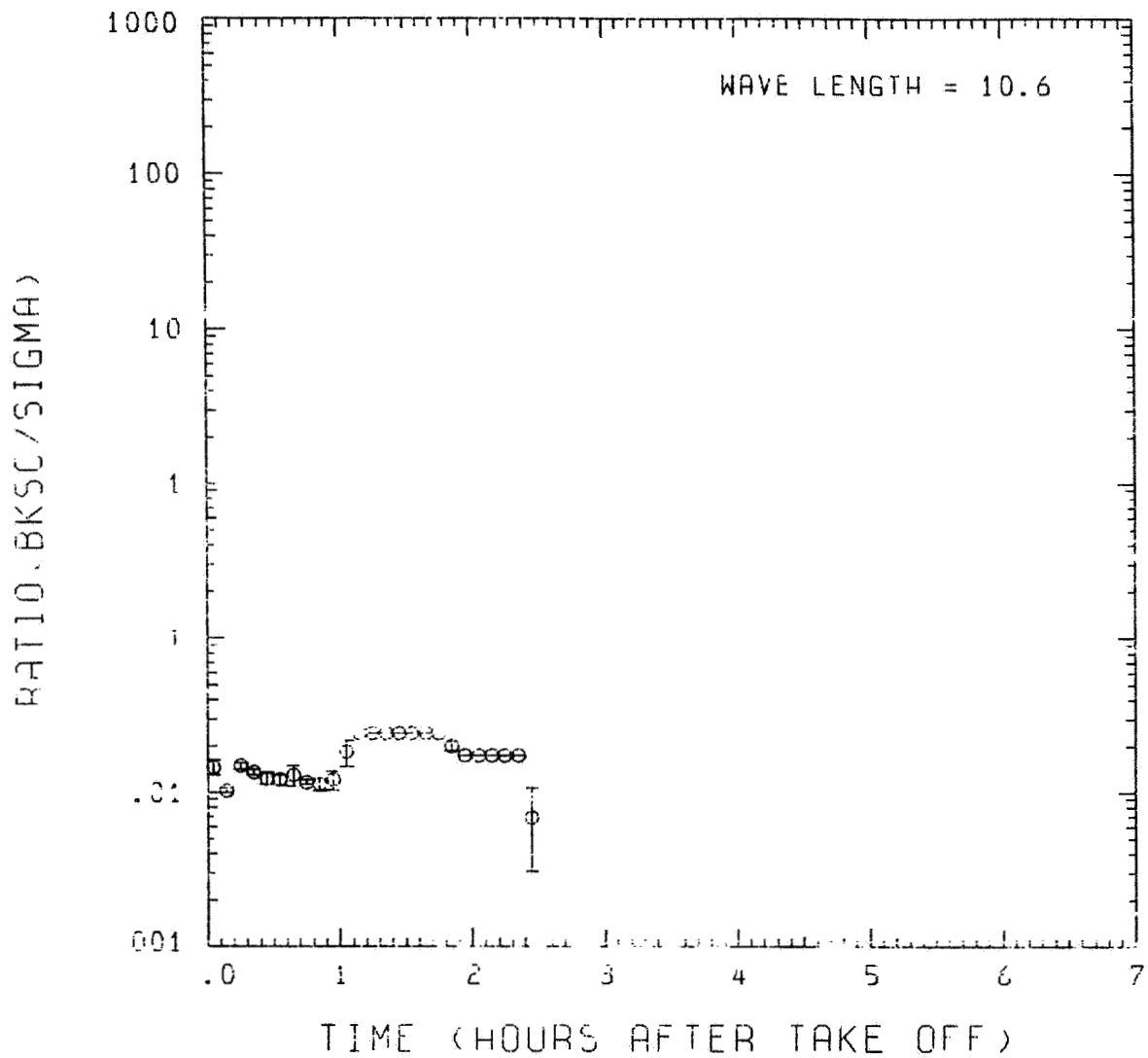


Fig. A22 (i). GAMETAG flight data for June 1, 1978.
Calculated ratios for backscatter to extinction for
five-minute data sets for $\lambda = 10.6 \mu\text{m}$.

APPENDIX B

LIST OF TABLES

Table B1.	Combined Size Ranges for GAMETAG Optical Particle Counter Data.	B1
Table B2.	Size Data (dn - cts/cm ³) for 1977 Flights.	B3
Table B3.	Size Data (dn - cts/cm ³) for 1978 Flights.	B13

PRECEDING PAGE BLANK NOT FILMED

PAGE B 11 INTENTIONALLY BLANK

**Table B1. Combined Size Ranges for GAMETAG
Optical Particle Counter Data**

1977			
Instrument	Range #	Radius Interval (μm)	Mean Radius (μm)
ASAS	1	0.126 - 0.170	0.146
ASAS	2	0.170 - 0.274	0.216
ASAS	3	0.274 - 0.385	0.325
ASAS	4	0.385 - 0.500	0.439
ASAS	5	0.500 - 0.625	0.521
ASAS	6	0.625 - 0.750	0.685
FSSP	7	0.750 - 1.104	0.91
FSSP	8	1.10 - 1.73	1.38
FSSP	9	1.73 - 2.34	2.01

1978			
ASAS - Same as 1977			
FSSP	7	0.25 - 0.75	0.43
FSSP	8	0.75 - 1.73	1.14
FSSP	9	1.73 - 2.34	2.01

STARTING TIME = 22:31:30						
DATA FILE = KQ.7.8						

STARTING TIME = 16:24:31						
ENDING TIME = 16:43:31						
DN = .973E 01	.167E 01	.109E 01	.577E 00	.345E 00	.347E 00	.102E 00 .351E-03

STARTING TIME = 16:45:31						
ENDING TIME = 17: 4:31						
DN = .507E 01	.278E 01	.605E 00	.259E 00	.119E 20	.565E 00	.213E 01 .520E-03

STARTING TIME = 17: 6:31						
ENDING TIME = 17:25:31						
DN = .133E 01	.577E 00	.103E 00	.710E-01	.643E-01	.509E-01	.123E-01 .447E-04

STARTING TIME = 17:27:31						
ENDING TIME = 17:45:31						
DN = .966E 01	.773E 00	.154E 00	.364E-01	.179E 00	.791E-01	.272E-01 .496E-03

STARTING TIME = 17:48:31						
ENDING TIME = 19: 7:31						
DN = .224E 02	.126E 01	.262E 20	.170E 00	.226E-01	.368E 00	.154E 00 .647E-02

STARTING TIME = 18:51:31						
ENDING TIME = 19:10:31						
DN = .136E 03	.788E 01	.337E 00	.297E 00	.163E 00	.674E 00	.175E 00 .607E-02

STARTING TIME = 19:12:31						
ENDING TIME = 19:31:31						
DN = .982E 01	.157E 01	.253E 00	.148E 00	.741E-01	.121E 01	.720E 01 .457E 01

STARTING TIME = 19:33:31						
ENDING TIME = 20 3:22:31						
DN = .267E 02	.265E 00	.448E-01	.463E-01	.525E-01	.447E 00	.894E 00 .482E 00

STARTING TIME = 20:54:31						
ENDING TIME = 20:13:31						
DN = .478E 00	.142E 00	.463E-01	.340E-01	.216E-01	.350E-01	.252E-02 .967E-04

STARTING TIME = 20:15:31						
ENDING TIME = 20:34:31						
DN = .103E 02	.577E 01	.226E-01	.494E-01	.278E-01	.113E 00	.277E-01 .495E-03

STARTING TIME = 20:36:31						
ENDING TIME = 20:56:31						
DN = .142E 02	.149E 01	.199E 00	.127E 00	.670E-01	.233E 00	.107E 00 .449E-02

STARTING TIME = 20:57:31						
ENDING TIME = 21:16:31						
DN = .300E 01	.222E 00	.525E-01	.401E-01	.154E-01	.202E 01	.839E 00 .116E 00

Table B2. Size Data (dn - cts/cm²) for 1977 Flights (continued)

Table B2. Size Data (dn - cts/cm³) for 1977 Flights (continued)

DATA FILE = K0.21.9									
STARTING TIME = 17:11:30									
DN = 165E 02	.148E 01	.327E 00	.267E 00	.170E 00	.000E 00	.000E 00	.000E 00	.000E 00	.000E 00
STARTING TIME = 17:52:30									
DN = 734E 01	.576E 00	.130E 00	.772E-01	.640E-01	.545E-01	.257E-02	.179E-04		
STARTING TIME = 18:11:30									
DN = 960E 00	.324E 00	.865E-01	.617E-01	.340E-01	.667E-01	.467E-02	.467E-04		
STARTING TIME = 18:14:30									
DN = 948E 00	.207E 00	.557E-01	.370E-01	.300E-01	.102E 00	.127E-01	.102E-03		
STARTING TIME = 18:55:30									
DN = 710E 00	.164E 00	.546E-01	.309E-01	.123E-01	.128E 00	.191E-01	.144E-03		
STARTING TIME = 19:16:30									
DN = 849E 00	.164E 00	.432E-01	.370E-01	.154E-01	.140E 00	.210E-01	.232E-03		
STARTING TIME = 19:37:30									
DN = 648E 00	.120E 00	.494E-01	.278E-01	.279E-01	.151E 00	.244E-01	.202E-03		
STARTING TIME = 20:17:30									
DN = 839E 00	.145E 00	.463E-01	.432E-01	.154E-01	.162E 00	.282E-01	.213E-03		
STARTING TIME = 20:38:30									
DN = 172E 01	.170E 00	.463E-01	.340E-01	.216E-01	.172E 00	.391E-01	.308E-03		
STARTING TIME = 20:40:30									
DN = 219E 02	.117E 00	.463E-01	.370E-01	.340E-01	.156E 00	.264E-01	.730E-01		
STARTING TIME = 21:1:30									
DN = 309E 01	.105E 00	.926E-02	.154E-01	.926E-02	.104E 00	.226E-02	.000E 00		
STARTING TIME = 21:22:30									
DN = 327E 00	.494E-01	.926E-02	.309E-01	.123E-01	.101E 00	.219E-02	.283E-04		
STARTING TIME = 21:43:30									
DN = 639E 00	.105E 00	.340E-01	.123E-01	.154E-01	.137E 00	.247E-02	.000E 00		
STARTING TIME = 22:4:30									
DN = 803E 01	.241E 00	.105E-01	.926E-02	.926E-02	.164E 00	.632E-02	.409E-04		
STARTING TIME = 22:25:30									
DN = 349E 00	.176E 00	.494E-01	.154E-01	.617E-02	.228E 00	.442E-01	.357E-03		

B6

1
2
3
4
5
6
7
8
9
10
11
12
13
14
15
16
17
18
19
20
21
22
23
24
25
26
27
28
29
30
31
32
33
34
35
36
37
38
39
40
41
42
43
44
45
46
47
48
49
50
51
52
53
54
55
56
57
58
59
60
61
62
63
64
65
66
67
68
69
70
71
72
73
74
75
76
77
78
79
80
81
82
83
84
85
86
87
88
89
90
91
92
93
94
95
96
97
98
99
100
101
102
103
104
105
106
107
108
109
110
111
112
113
114
115
116
117
118
119
120
121
122
123
124
125
126
127
128
129
130
131
132
133
134
135
136
137
138
139
140
141
142
143
144
145
146
147
148
149
150
151
152
153
154
155
156
157
158
159
160
161
162
163
164
165
166
167
168
169
170
171
172
173
174
175
176
177
178
179
180
181
182
183
184
185
186
187
188
189
190
191
192
193
194
195
196
197
198
199
200
201
202
203
204
205
206
207
208
209
210
211
212
213
214
215
216
217
218
219
220
221
222
223
224
225
226
227
228
229
230
231
232
233
234
235
236
237
238
239
240
241
242
243
244
245
246
247
248
249
250
251
252
253
254
255
256
257
258
259
260
261
262
263
264
265
266
267
268
269
270
271
272
273
274
275
276
277
278
279
280
281
282
283
284
285
286
287
288
289
290
291
292
293
294
295
296
297
298
299
300
301
302
303
304
305
306
307
308
309
310
311
312
313
314
315
316
317
318
319
320
321
322
323
324
325
326
327
328
329
330
331
332
333
334
335
336
337
338
339
340
341
342
343
344
345
346
347
348
349
350
351
352
353
354
355
356
357
358
359
360
361
362
363
364
365
366
367
368
369
370
371
372
373
374
375
376
377
378
379
380
381
382
383
384
385
386
387
388
389
390
391
392
393
394
395
396
397
398
399
400
401
402
403
404
405
406
407
408
409
410
411
412
413
414
415
416
417
418
419
420
421
422
423
424
425
426
427
428
429
430
431
432
433
434
435
436
437
438
439
440
441
442
443
444
445
446
447
448
449
450
451
452
453
454
455
456
457
458
459
460
461
462
463
464
465
466
467
468
469
470
471
472
473
474
475
476
477
478
479
480
481
482
483
484
485
486
487
488
489
490
491
492
493
494
495
496
497
498
499
500
501
502
503
504
505
506
507
508
509
510
511
512
513
514
515
516
517
518
519
520
521
522
523
524
525
526
527
528
529
530
531
532
533
534
535
536
537
538
539
540
541
542
543
544
545
546
547
548
549
550
551
552
553
554
555
556
557
558
559
560
561
562
563
564
565
566
567
568
569
570
571
572
573
574
575
576
577
578
579
580
581
582
583
584
585
586
587
588
589
590
591
592
593
594
595
596
597
598
599
600
601
602
603
604
605
606
607
608
609
610
611
612
613
614
615
616
617
618
619
620
621
622
623
624
625
626
627
628
629
630
631
632
633
634
635
636
637
638
639
640
641
642
643
644
645
646
647
648
649
650
651
652
653
654
655
656
657
658
659
660
661
662
663
664
665
666
667
668
669
670
671
672
673
674
675
676
677
678
679
680
681
682
683
684
685
686
687
688
689
690
691
692
693
694
695
696
697
698
699
700
701
702
703
704
705
706
707
708
709
710
711
712
713
714
715
716
717
718
719
720
721
722
723
724
725
726
727
728
729
730
731
732
733
734
735
736
737
738
739
740
741
742
743
744
745
746
747
748
749
750
751
752
753
754
755
756
757
758
759
760
761
762
763
764
765
766
767
768
769
770
771
772
773
774
775
776
777
778
779
780
781
782
783
784
785
786
787
788
789
790
791
792
793
794
795
796
797
798
799
800
801
802
803
804
805
806
807
808
809
810
811
812
813
814
815
816
817
818
819
820
821
822
823
824
825
826
827
828
829
830
831
832
833
834
835
836
837
838
839
840
84

B9

Table B2. Size Data (dn - cts/cm³) for 1977 Flights (continued)

Table B3. Size Data (dn - cts/cm³) for 1978 Flights.

DATA FILE = NK4.APD27									
STARTING TIME = 16:52: 0									
ENDING TIME = 17:11: 0									
DN = .117E 00	.117E 00	.455E-01	.000E 00	.370E-02	.079E 00	.299E 00	.179E 00		
STARTING TIME = 17:12: 0									
ENDING TIME = 17:31: 0									
DN = .136E 00	.117E 00	.149E-01	.149E-01	.189E-01	.416E-01	.276E-02	.439E-03		
STARTING TIME = 17:32: 0									
ENDING TIME = 17:51: 0									
DN = .632E 01	.849E 01	.294E 01	.251E 01	.214E 01	.506E-02	.251E-03	.900E 00		
STARTING TIME = 17:52: 0									
ENDING TIME = 19:11: 0									
DN = .096E 00	.085E-01	.189E-01	.758E-02	.114E-01	.169E-02	.863E-04	.000E 00		
STARTING TIME = 19:12: 0									
ENDING TIME = 19:31: 0									
DN = .028E 00	.067E-01	.227E-01	.759E-02	.753E-02	.131E-02	.147E-03	.000E 00		
STARTING TIME = 19:32: 0									
ENDING TIME = 19:51: 0									
DN = .659E 00	.759E-01	.114E-01	.152E-01	.114E-01	.073E-03	.147E-03	.149E-04		
STARTING TIME = 19:52: 0									
ENDING TIME = 19:11: 0									
DN = .111E 01	.644E-01	.265E-01	.149E-01	.227E-01	.121E-02	.175E-03	.144E-04		
STARTING TIME = 19:12: 0									
ENDING TIME = 19:31: 0									
DN = .129E 01	.102E 00	.341E-01	.114E-01	.753E-02	.121E-02	.173E-03	.143E-04		
STARTING TIME = 19:32: 0									
ENDING TIME = 19:51: 0									
DN = .419E 01	.326E 00	.682E-01	.971E-01	.604E-01	.515E-01	.799E-02	.568E-03		
STARTING TIME = 19:52: 0									
ENDING TIME = 20:11: 0									
DN = .029E 01	.156E 01	.495E 00	.352E 00	.247E 00	.479E 00	.804E-01	.936E-02		
STARTING TIME = 20:12: 0									
ENDING TIME = 20:31: 0									
DN = .870E 01	.107E 01	.214E 00	.197E 00	.985E-01	.240E 00	.336E-01	.406E-02		
STARTING TIME = 20:32: 0									
ENDING TIME = 20:51: 0									
DN = .104E 02	.122E 01	.258E 00	.159E 00	.129E 00	.225E 00	.309E-01	.368E-02		
STARTING TIME = 20:52: 0									
ENDING TIME = 21:11: 0									
DN = .332E 01	.496E 00	.121E 00	.945E-01	.341E-01	.969E-01	.855E-02	.954E-03		
STARTING TIME = 21:12: 0									
ENDING TIME = 21:31: 0									
DN = .326E 00	.110E 00	.303E-01	.227E-01	.152E-01	.709E-02	.238E-03	.000E 00		
STARTING TIME = 21:32: 0									
ENDING TIME = 21:51: 0									
DN = .136E 01	.539E 00	.205E 00	.102E 00	.642E-01	.979E-01	.647E-02	.528E-03		
STARTING TIME = 21:52: 0									
ENDING TIME = 22:13: 0									
DN = .493E 01	.130E 01	.381E 00	.314E 00	.250E 00	.237E 00	.153E-01	.129E-02		
STARTING TIME = 22:14: 0									

Table B3. Size Data (dn - cts/cm³) for 1978 Flights (continued).

DATA FILE = NKN.MAY2									
STARTING TIME = 20:31:0									
ENDING TIME = 20:22:0									
DN = .606E 01	.187E 01	.746E 00	.205E 00	.179E 00	.720E-01	.370E 00	.748E-01	.553E-02	
STARTING TIME = 20:23:0									
ENDING TIME = 20:42:0									
DN = .426E 01	.922E 00	.417E 00	.155E 00	.114E 00	.795E-01	.644E-01	.310E-02	.172E-03	
STARTING TIME = 20:43:0									
ENDING TIME = 21:02:0									
DN = .430E 01	.180E 00	.180E 00	.682E-01	.417E-01	.265E-01	.179E-01	.836E-03	.960E-04	
STARTING TIME = 21:03:0									
ENDING TIME = 21:22:0									
DN = .226E 01	.122E 01	.216E 00	.114E 00	.606E-01	.530E-01	.247E-01	.126E-02	.865E-04	
STARTING TIME = 21:23:0									
ENDING TIME = 21:42:0									
DN = .197E 01	.178E 01	.254E 00	.121E 00	.117E 00	.758E-01	.421E-01	.215E-02	.101E-03	
STARTING TIME = 21:43:0									
ENDING TIME = 22:02:0									
DN = .124E 01	.290E 00	.290E 00	.871E-01	.758E-01	.682E-01	.244E-01	.132E-02	.571E-04	
STARTING TIME = 22:03:0									
ENDING TIME = 22:22:0									
DN = .144E 01	.330E 00	.330E 00	.155E 00	.133E 00	.341E-01	.764E-01	.415E-02	.344E-03	
STARTING TIME = 22:23:0									
ENDING TIME = 22:42:0									
DN = .352E 01	.498E 00	.235E 00	.322E 00	.345E 00	.710E 00	.130E 00	.450E-02		
STARTING TIME = 22:43:0									
ENDING TIME = 23:02:0									
DN = .331E 01	.124E 01	.330E 00	.572E 00	.383E 00	.117E 01	.211E 00	.727E-02		
STARTING TIME = 23:03:0									
DATA FILE = NKN.MAY4									
STARTING TIME = 20:51:0									
ENDING TIME = 21:10:0									
DN = .126E 01	.439E 00	.530E-01	.199E-01	.227E-01	.355E 00	.112E 00	.203E-01		
STARTING TIME = 21:11:0									
ENDING TIME = 21:30:0									
DN = .265E 00	.179E 00	.303E-01	.265E-01	.227E-01	.820E-04	.000E 00	.000E 00		
STARTING TIME = 21:31:0									
ENDING TIME = 21:50:0									
DN = .362E 01	.174E 00	.341E-01	.227E-01	.227E-01	.433E-04	.000E 00	.000E 00		
STARTING TIME = 21:51:0									
ENDING TIME = 22:10:0									
DN = .223E 00	.606E-01	.341E-01	.114E-01	.370E-02	.115E-03	.000E 00	.000E 00		
STARTING TIME = 22:11:0									
ENDING TIME = 22:30:0									
DN = .510E 00	.492E-01	.199E-01	.114E-01	.370E-02	.115E-03	.000E 00	.000E 00		

✱

Table B3. Size Data (dn - cts/cm³) for 1978 Flights (continued).

DATA FILE = DM91.MAY10										
STARTING TIME = 23:5:0										
ENDING TIME = 23:24:0										
DN =	.155E 01	.572F 00	.909E-01	.985F-01	.606E-01	.714E-01	.325E-01		.246E-02	
STARTING TIME = 23:25:0										
ENDING TIME = 23:44:0										
DN =	.201E 00	.813F-01	.758E-02	.189F-01	.152F-01	.119F-02	.919E-04		.345E-04	
STARTING TIME = 23:45:0										
ENDING TIME = 23:4:0										
DN =	.178E 00	.341E-01	.114E-01	.000F 00	.379F-02	.132E-03	.000E 00		.000E 00	
STARTING TIME = 23:5:0										
ENDING TIME = 23:24:0										
DN =	.465E 00	.947E-01	.379E-01	.189F-01	.379F-02	.150F-01	.000E 00		.000E 00	
STARTING TIME = 23:25:0										
ENDING TIME = 23:44:0										
DN =	.386E 00	.455F-01	.114E-01	.379F-02	.758F-02	.101F-03	.000E 00		.000F 00	
STARTING TIME = 23:45:0										
ENDING TIME = 24:4:0										
DN =	.745E-01	.758E-02	.758E-02	.379F-02	.000F 00	.143F-04	.000F 00		.000E 00	
STARTING TIME = 24:5:0										
ENDING TIME = 24:24:0										
DN =	.606E-01	.189F-01	.000E 00	.152F-01	.379F-02	.000F 00	.000E 00		.000E 00	
STARTING TIME = 24:25:0										
ENDING TIME = 24:44:0										
DN =	.163E 00	.265E-01	.758E-02	.379F-02	.000F 00	.144E-04	.000F 00		.000E 00	
STARTING TIME = 24:45:0										
ENDING TIME = 25:4:0										
DN =	.167E 00	.668F-01	.152F-01	.152F-01	.152F-01	.574F-04	.000E 00		.000E 00	
STARTING TIME = 25:5:0										
ENDING TIME = 25:24:0										
DN =	.148E 00	.758F-01	.189F-01	.758F-02	.000F 00	.000E 00	.000F 00		.000F 00	
STARTING TIME = 25:25:0										
ENDING TIME = 25:44:0										
DN =	.170E 00	.114E-01	.379E-02	.379F-02	.000F 00	.142F-04	.000F 00		.000F 00	
STARTING TIME = 25:45:0										
ENDING TIME = 26:4:0										
DN =	.136E 00	.341E-01	.152F-01	.000F 00	.000F 00	.000F 00	.000F 00		.000F 00	
STARTING TIME = 26:6:0										
ENDING TIME = 26:25:0										
DN =	.102E 00	.341E-01	.114E-01	.114E-01	.379F-02	.000E 00	.000E 00		.000E 00	
STARTING TIME = 26:26:0										
ENDING TIME = 26:45:0										
DN =	.102E 00	.189E-01	.758E-02	.758F-02	.000F 00	.151F-04	.000F 00		.000E 00	
STARTING TIME = 26:46:0										
ENDING TIME = 27:5:0										
DN =	.179E 00	.163F 00	.152E-01	.152F-01	.000E 00	.765E-03	.136E-03		.000E 00	
STARTING TIME = 27:6:0										
ENDING TIME = 27:25:0										
DN =	.657E-01	.104E 01	.273E 00	.244E 00	.220E 00	.979F 00	.204F 00		.843E-02	
STARTING TIME = 27:26:0										

Table B3. Size Data (dn - cts/cm³) for 1978 Flights (continued).

DATA FILE = N4N.V4Y11									
STARTING TIME = 22:34:0									
ENDING TIME = 22:53:0									
DN = .227E 00	.492E-01	.152E-01	.149E-01	.758E-02	.648E-04	.167E-04	.000E 00		
STARTING TIME = 22:54:0									
ENDING TIME = 23:13:0									
DN = .121E 00	.303E-01	.379E-02	.758E-02	.000E 00	.577E-04	.000E 00	.000E 00		
STARTING TIME = 23:14:0									
ENDING TIME = 23:33:0									
DN = .341E 00	.303E-01	.758E-02	.758E-02	.379E-02	.718E-04	.000E 00	.000E 00		
STARTING TIME = 23:34:0									
ENDING TIME = 23:53:0									
DN = .174E 00	.227E-01	.379E-02	.379E-02	.379E-02	.000E 00	.000E 00	.000E 00		
STARTING TIME = 23:54:0									
ENDING TIME = 24:13:0									
DN = .265E 00	.167E 00	.114E-01	.114E-01	.758E-02	.234E-03	.000E 00	.000E 00		
STARTING TIME = 24:14:0									
ENDING TIME = 24:33:0									
DN = .666E 00	.602E 00	.833E-01	.120E 00	.947E-01	.463E 00	.984E-01	.405E-02		
STARTING TIME = 24:34:0									
ENDING TIME = 24:53:0									
DN = .159E 01	.841E 00	.205E 00	.307E 00	.239E 00	.104E 01	.229E 00	.791E-02		
STARTING TIME = 24:54:0									
ENDING TIME = 25:13:0									
DN = .240E 01	.107E 01	.289E 00	.330E 00	.277E 00	.948E 00	.211E 00	.128E-01		
STARTING TIME = 25:14:0									
ENDING TIME = 25:33:0									
DN = .295E 00	.432E 00	.227E-01	.152E-01	.379E-02	.433E-01	.736E-02	.271E-03		
STARTING TIME = 25:34:0									
ENDING TIME = 25:53:0									
DN = .202E-01	.265E-01	.379E-02	.379E-02	.000E 00	.717E-04	.000E 00	.000E 00		
STARTING TIME = 25:54:0									
ENDING TIME = 26:13:0									
DN = .193E 00	.379E-01	.379E-02	.152E-01	.379E-02	.145E-04	.000E 00	.000E 00		
STARTING TIME = 26:14:0									
ENDING TIME = 26:33:0									
DN = .417E-01	.227E-01	.758E-02	.379E-02	.000E 00	.429E-04	.000E 00	.000E 00		
STARTING TIME = 26:34:0									
ENDING TIME = 26:53:0									
DN = .117E 00	.379E-01	.379E-02	.379E-02	.000E 00	.143E-04	.000E 00	.000E 00		
STARTING TIME = 26:54:0									
ENDING TIME = 27:13:0									
DN = .114E 00	.303E-01	.379E-02	.379E-02	.114E-01	.144E-04	.000E 00	.000E 00		
STARTING TIME = 27:14:0									
ENDING TIME = 27:33:0									
DN = .606E-01	.189E-01	.379E-02	.758E-02	.379E-02	.000E 00	.000E 00	.000E 00		
STARTING TIME = 27:34:0									
ENDING TIME = 27:53:0									
DN = .114E 00	.379E-01	.189E-01	.379E-02	.114E-01	.514E-04	.000E 00	.000E 00		
STARTING TIME = 27:54:0									
ENDING TIME = 28:13:0									
DN = .114E 00	.379E-01	.189E-01	.379E-02	.114E-01	.514E-04	.000E 00	.000E 00		

Table B3. Size Data (dn - cts/cm³) for 1978 Flights (continued).

DATA FILE = 'KQV.WAV12'											
STARTING TIME = 21:50: 0											
ENDING TIME = 22: 9: 0											
DN = .237E 01	.750E 00	.307E 00	.220F 00	.136F 00	.394E 00	.593F-01	.305E-02				
STARTING TIME = 22:10: 0											
ENDING TIME = 22:29: 0											
DN = .429F 01	.989E 00	.322E 00	.447C 00	.337E 00	.925F 00	.167E 00	.619E-02				
STARTING TIME = 22:30: 0											
ENDING TIME = 22:49: 0											
DN = .501E 01	.105E 01	.371E 00	.383F 00	.333F 00	.116E 01	.210E 00	.691F-02				
STARTING TIME = 22:50: 0											
ENDING TIME = 23: 9: 0											
DN = .536F 01	.105E 01	.289F 00	.447E 00	.386F 00	.125E 01	.234F 00	.806E-02				
STARTING TIME = 23:10: 0											
ENDING TIME = 23:29: 0											
DN = .201E 01	.610E 00	.121F 00	.159F 00	.129F 00	.522E 00	.100E 00	.376E-02				
STARTING TIME = 23:30: 0											
ENDING TIME = 23:49: 0											
DN = .277F 00	.379F-01	.379E-02	.379F-02	.758F-02	.351F-04	.000E 00	.000E 00				
STARTING TIME = 23:50: 0											
ENDING TIME = 24: 9: 0											
DN = .270F 00	.947F-01	.227F-01	.152F-01	.157F-01	.144F-04	.000E 00	.000E 00				
STARTING TIME = 24:10: 0											
ENDING TIME = 24:29: 0											
DN = .196C 00	.152F-01	.152F-01	.152F-01	.758F-02	.000F 00	.000E 00	.000E 00				
STARTING TIME = 24:30: 0											
ENDING TIME = 24:49: 0											
DN = .568E-01	.114E-01	.000E 00	.758F-02	.758F-02	.000F 00	.000E 00	.000E 00				
STARTING TIME = 24:50: 0											
ENDING TIME = 25: 9: 0											
DN = .644E-01	.152E-01	.114E-01	.379F-02	.000F 00	.000E 00	.000E 00	.000E 00				
STARTING TIME = 25:10: 0											
ENDING TIME = 25:29: 0											
DN = .121E 00	.265F-01	.758E-02	.000E 00	.379F-02	.425F-04	.000E 00	.000E 00				
STARTING TIME = 25:30: 0											
ENDING TIME = 25:49: 0											
DN = .178E 00	.379F-02	.758F-02	.379F-02	.379F-02	.000F 00	.000E 00	.000E 00				
STARTING TIME = 25:50: 0											
ENDING TIME = 26: 9: 0											
DN = .102E 00	.303E-01	.758F-02	.379F-02	.000F 00	.187F-03	.177F-04	.000E 00				
STARTING TIME = 26:10: 0											
ENDING TIME = 26:29: 0											
DN = .277E 01	.731E 00	.557E 00	.125E 00	.117E 00	.909F-01	.299F 00	.451E-01	.115E-02			
STARTING TIME = 26:30: 0											
ENDING TIME = 26:49: 0											
DN = .408E 01	.146E 01	.523F 00	.644E 00	.531F 00	.188F 01	.305E 00	.790E-02				
STARTING TIME = 26:50: 0											
ENDING TIME = 27: 9: 0											
DN = .386E 01	.152F 01	.599E 00	.621E 00	.549E 00	.195E 01	.315F 00	.971E-02				
STARTING TIME = 27:10: 0											

Table B3. Size Data (dn - cts/cm³) for 1978 Flights (continued).

DATA FILE = NPN.MAY14											
STARTING TIME = 2:00	DN =	.137E 01	.633E 00	.144E 00	.220E 00	.170E 00	.413E 00	.669E-01	.355E-02		
ENDING TIME = 2:19	DN =	.367E 01									
STARTING TIME = 2:20	DN =	.299E 00	.163E 00	.417E-01	.265E-01	.149E-01	.437E-02	.423F-03	.324F-04		
ENDING TIME = 2:39	DN =	.152E 01									
STARTING TIME = 2:40	DN =	.682E 00	.159E 00	.341E-01	.189E-01	.114E-01	.100F-01	.402E-03	.322E-04		
ENDING TIME = 2:59	DN =	.287E 01									
STARTING TIME = 3:00	DN =	.344E 00	.144F 00	.417E-01	.379F-01	.379E-02	.117E-01	.352E-03	.162F-04		
ENDING TIME = 3:19	DN =	.136E 01									
STARTING TIME = 3:20	DN =	.223E 00	.871E-01	.341E-01	.227E-01	.114E-01	.677E-02	.240E-03	.000E 00		
ENDING TIME = 3:39	DN =	.109E 01									
STARTING TIME = 3:40	DN =	.492E 00	.473E 00	.379E-01	.758E-01	.568E-01	.112F 00	.129E-01	.534F-03		
ENDING TIME = 3:59	DN =	.146E 01									
STARTING TIME = 4:00	DN =	.401E 01	.137E 01	.394E 00	.553E 00	.477E 00	.155E 01	.220E 00	.738E-02		
ENDING TIME = 4:19	DN =	.127E 02									
STARTING TIME = 4:20	DN =	.533E 01	.955E 00	.330F 00	.367F 00	.375E 00	.107F 01	.149F 00	.506E-02		
ENDING TIME = 4:39	DN =	.144F 02									
STARTING TIME = 4:40	DN =	.531E 01	.180E 01	.648E 00	.652E 00	.572E 00	.749E 00	.149E 00	.282E-01		
ENDING TIME = 4:59	DN =	.107E 02									
STARTING TIME = 5:00	DN =	.133E 00	.201E 00	.152E-01	.759F-02	.009F 00	.825E-02	.303E-03	.361E-04		
ENDING TIME = 5:19	DN =	.731E 00									
STARTING TIME = 5:20	DN =	.892E 00	.133F 00	.265E-01	.227E-01	.754F-02	.353F-02	.979E-04	.154E-04		
ENDING TIME = 5:39	DN =	.216E 00									
STARTING TIME = 5:40	DN =	.101E 01	.530F 00	.180F 00	.833E-01	.705E-01	.234E-01	.151E-01	.620E-02		
ENDING TIME = 5:59	DN =	.140E 01									
STARTING TIME = 6:00	DN =	.326E 00	.117F 00	.303F-01	.149F-01	.227E-01	.570E-02	.154F-03	.284F-04		
ENDING TIME = 6:19	DN =	.111E 01									
STARTING TIME = 6:20	DN =	.201E 00	.833E-01	.303E-01	.265F-01	.000F 00	.145E-02	.143F-04	.000F 00		
ENDING TIME = 6:39	DN =	.762E 00									
STARTING TIME = 6:40	DN =	.174F 00	.000F-01	.455F-01	.758F-02	.114E-01	.244E-02	.661E-04	.000E 00		
ENDING TIME = 6:59	DN =	.000F 00									
STARTING TIME = 7:00	DN =										

Table B3. Size Data (dn - cts/cm³) for 1978 Flights (continued).

DATA FILE: = NKN. "AYLA

[illegible]DATA FILE = NKH.4AY27

	STARTING TIME = 21:58:00	.390E 00	.871E-01	.758E-01	.834F-01	.141E-01	.247E-02
	ENDING TIME = 22:17:00	.217E 01					
ON =	.473F 01						
	STARTING TIME = 22:18:00	.155E 01	.424E 00	.322E 00	.167E 00	.891E 00	.470E 00
	ENDING TIME = 22:37:00	.543E 01					
ON =	.555F 01						
	STARTING TIME = 22:38:00	.576E 00	.201E 00	.945E-01	.979F 00	.897E 00	.375E 00
	ENDING TIME = 22:57:00	.305E 01					
ON =	.242F 01						
	STARTING TIME = 22:58:00	.349E 00	.117E 00	.720E-01	.265E-01	.740E-01	.407E-01
	ENDING TIME = 23:17:00	.234E 01					
ON =	.236E 01						
	STARTING TIME = 23:18:00	.284F 00	.759E-01	.303F-01	.152F-01	.607E-02	.000F 00
	ENDING TIME = 23:37:00	.417E 01				.288F-C3	
ON =	.671C 01						

1

B19

Table B3. Size Data (dn - cts/cm³) for 1978 Flights (continued).

[illegible]

1. REPORT NO. NASA CR-3959	2. GOVERNMENT ACCESSION NO.	3. RECIPIENT'S CATALOG NO.	
4. TITLE AND SUBTITLE Development of a Global Model for Atmospheric Backscatter at CO ₂ Wavelengths		5. REPORT DATE February 1986	
		6. PERFORMING ORGANIZATION CODE	
7. AUTHOR(S) G. S. Kent, P. H. Wang, U. Farrukh, A. Deepak, and E. M. Patterson		8. PERFORMING ORGANIZATION REPORT #	
9. PERFORMING ORGANIZATION NAME AND ADDRESS Institute for Atmospheric Optics and Remote Sensing P.O. Box P Hampton, Virginia 23666		10. WORK UNIT NO. M-510	
		11. CONTRACT OR GRANT NO. NAS8-35594	
12. SPONSORING AGENCY NAME AND ADDRESS National Aeronautics and Space Administration Washington, D.C. 20546		13. TYPE OF REPORT & PERIOD COVERED Contractor Report December 7, 1983 - April 6, 1985	
		14. SPONSORING AGENCY CODE	
15. SUPPLEMENTARY NOTES G. S. Kent, P. H. Wang, U. Farrukh, and A. Deepak: Institute for Atmospheric Optics and Remote Sensing, Hampton, Virginia. E. M. Patterson: Georgia Technology Research Institute, Atlanta, Georgia. Technical Monitors: Daniel E. Fitzjarrauld and Margaret B. Alexander Prepared for the Atmospheric Sciences Division, Systems Dynamics Laboratory, Marshall Space Flight Center, Alabama 35812			
16. ABSTRACT The objective of this work was to improve our understanding of the variation of the aerosol backscattering at 10.6 μm within the free troposphere and to develop a model to describe this variation. The analysis combines theoretical modeling with the results contained within three independent data sets. The data sets used were obtained by the SAGE I/SAM II satellite experiments, the GAMETAG flight series, and by direct backscatter measurements. The theoretical work includes use of a bimodal, two component aerosol model, and the study of the microphysical and associated optical changes occurring within an aerosol plume. A consistent picture is obtained that describes the variation of the aerosol backscattering function in the free troposphere with altitude, latitude, and season.			
17. KEY WORDS Global Scale Processes Remote Sensing Aerosol Backscatter Troposphere Modeling		18. DISTRIBUTION STATEMENT Unclassified - Unlimited STAR Category: 47	
19. SECURITY CLASSIF. (of this report) Unclassified	20. SECURITY CLASSIF. (of this page) Unclassified	21. NO. OF PAGES 396	22. PRICE A17